



**EFFECTS OF ENVIRONMENT ON CREEP BEHAVIOR OF  
NEXTEL720/ALUMINA-MULLITE CERAMIC COMPOSITE  
WITH  $\pm 45^\circ$  FIBER ORIENTATION AT 1200°C  
THESIS**

Muzaffer OZER, First Lieutenant, TAAF

AFIT/GSS/ENY/09-M05

**DEPARTMENT OF THE AIR FORCE  
AIR UNIVERSITY**

**AIR FORCE INSTITUTE OF TECHNOLOGY**

**Wright-Patterson Air Force Base, Ohio**

APPROVED FOR PUBLIC RELEASE; DISTRIBUTION UNLIMITED

The views expressed in this thesis are those of the author and do not reflect the official policy or position of the United States Air Force, Department of Defense, or the United States Government.

AFIT/GSS/ENY/09-M05

EFFECTS OF ENVIRONMENT ON CREEP BEHAVIOR OF  
NEXTEL720/ALUMINA-MULLITE CERAMIC COMPOSITE  
WITH  $\pm 45^\circ$  FIBER ORIENTATION AT 1200°C

THESIS

Presented to the Faculty

Department of Aeronautics and Astronautics

Graduate School of Engineering and Management

Air Force Institute of Technology

Air University

Air Education and Training Command

In Partial Fulfillment of the Requirements for the

Degree of Master of Science (Space Systems)

Muzaffer OZER, B.S.

First Lieutenant, TAAF

March 2009

APPROVED FOR PUBLIC RELEASE; DISTRIBUTION UNLIMITED

AFIT/GSS/ENY/09-M05

EFFECTS OF ENVIRONMENT ON CREEP BEHAVIOR OF  
NEXTEL720/ALUMINA-MULLITE CERAMIC COMPOSITE  
WITH  $\pm 45^\circ$  FIBER ORIENTATION AT 1200°C

Muzaffer OZER, B.S.

First Lieutenant, TAAF

Approved:

/signed/

12 Mar 2009

\_\_\_\_\_  
Dr. Marina B. Ruggles-Wrenn (Chairman)

/signed/

\_\_\_\_\_  
Date

18 Mar 2009

\_\_\_\_\_  
Dr. Geoff E. Fair (Member)

/signed/

\_\_\_\_\_  
Date

13 Mar 2009

\_\_\_\_\_  
Dr. Randall S. Hay (Member)

\_\_\_\_\_  
Date

## **Abstract**

Aerospace components require structural materials that have superior long-term mechanical properties under severe environmental conditions, such as ultra-high temperature, high pressure, or water vapor. Ceramic matrix composites (CMCs), capable of maintaining excellent strength and fracture toughness at high temperatures continue to attract attention as candidate materials for aerospace turbine engine applications.

Previous studies by the advisor and graduate students investigated mechanical behavior of Nextel720/Alumina CMC consisting of N720 fibers in a porous alumina matrix. These studies revealed that while this CMC exhibits an exceptionally high fatigue limit at 1200°C, it also experiences substantial strain accumulation under sustained loading conditions. Furthermore, these earlier investigations revealed degrading effect of steam environments on material performance under both static and cyclic loadings. Additional matrix sintering was observed at 1200°C, which led to the loss of matrix porosity and deterioration of composite toughness. This degradation process was accelerated in the presence of steam. The present effort will investigate the off-axis creep behavior of the Nexte720/Alumina-Mullite CMC, a material system which relies on a porous alumina/mullite matrix for damage tolerance as compared to the pure alumina matrix in earlier studies.

This research evaluated the creep behavior of N720/AM with a  $\pm 45^\circ$  fiber orientation at  $1200^\circ\text{C}$  in: laboratory air, steam, and argon environments. Creep-rupture tests at the creep stress levels of: 32, 30, 26, and 20 MPa were conducted in each environment. Additionally 35 MPa stress level examined in air and 13 MPa stress level examined both in air and steam. The N720/AM with a  $\pm 45^\circ$  fiber orientation survived creep run-out (100 h of creep stress) for stress levels  $\leq 20$  MPa in all environments. Retained tensile strength was evaluated for all specimens achieving run-out. The creep-rupture results showed a decrease in creep life with increasing creep stress. The presence of steam had negative effect on the creep rates. Following the tests Optical and Scanning Electron Microscope (SEM) micrographs were used to examine damage zones.

## **Acknowledgments**

I would like to thank my faculty advisor, Dr. Marina B. Ruggles-Wrenn for her support, guidance and leadership throughout my work. I would also like to thank Mr. Barry Paige, Chris Zickefoose, John Hixenbaugh and Sean Miller for their help with the lab equipment. Also, I am very grateful for all of the help and companionship of 1<sup>st</sup> LT. Tufan YELESER who guided me during the initial phase of my study. Most of all I am thankful for my very supportive family, my wife and my son, and friends who were always there for me.

Muzaffer OZER

## Table of Contents

	Page
Abstract.....	iv
Acknowledgments.....	vi
Table of Contents .....	vii
List of Figures .....	ix
List of Tables.....	lxxi
I. Introduction.....	1
II. Background.....	3
2.1 Ceramic Matrix Composites .....	3
2.2 Previous Research Efforts.....	5
2.3 The N720/AM Ceramic Matrix Composite.....	7
2.4 Thesis Objective.....	9
III. Experimental Setup .....	10
3.1 Specimen Preparation .....	10
3.2 Mechanical Testing Equipment .....	11
3.3 Environmental Controls.....	14
3.4 Microstructural Characterization .....	16
3.5 Test Procedures.....	17
3.5.1 <i>Preparation of Mechanical Testing Equipment.</i> .....	17
3.5.2 <i>Temperature Calibration.</i> .....	18
3.5.3 <i>Monotonic Tensile Test.</i> .....	19
3.5.4 <i>Creep Test.</i> .....	20
3.5.5 <i>Tensile Tests at 0.0025 and 25 MPa/s</i> .....	21
IV. Results and Discussion.....	22
4.1 Section Summary .....	22
4.2 Thermal Expansion .....	23
4.3 Monotonic Tension .....	24
4.4 Creep-Rupture Tests .....	30
4.5 Composite Microstructure .....	56

V. Conclusions.....	80
Appendix: Additional SEM Micrographs .....	83
Bibliography.....	424
Vita .....	427

## List of Figures

Figure	Page
1. Common CMC damage tolerance mechanisms: (a) Weak fiber/matrix interface and (b) Porous matrix [Zok, Levi].....	5
2. Test Specimen, dimensions in mm. ....	10
3. N720/AM tensile specimen with tabs. ....	11
4. MTS 5 kip mechanical testing machine.....	12
5. 5 kip mechanical testing station.....	12
6. Extensometer platform with heat shield and cooling air. ....	13
7. Interior view of modified furnace insulation where heating elements and control thermocouple are visible. ....	14
8. Alumina susceptor and steam feeding tube on the 5 kip machine.....	15
9. Zeiss Stemi SV II optical microscope.....	16
10. FEI Quanta 200 Scanning Electron Microscope.....	17
11. Test specimen instrumented with thermocouples.....	18
12. Typical creep test procedure. ....	21
13. Tensile stress-strain curves for N720/AM ceramic composite at 1200°C in laboratory air. Data for 0°/90° fiber orientation from Genelin[21].....	26
14. Tensile stress-strain curves for N720/A ceramic composite at 1200°C in laboratory air. Data for N720/A from Siegert[16], Harlan [20].....	26
15. Tensile stress-strain curves for N720/AM composite with ±45° fiber orientation at 1200°C in laboratory air.....	28
16. Tensile stress-strain curves for N720/AM composite with ±45° fiber orientation at 1200°C in steam.....	30

Figure	Page
17. Creep vs. time curves for N720/A composite with $\pm 45^\circ$ fiber orientation obtained at 1200°C in laboratory air. Data for N720/A from Siegert [16], Ruggles-Wrenn et al [17].	33
18. Creep vs. time curves for N720/A composite with $\pm 45^\circ$ fiber orientation obtained at 1200°C in laboratory air. Data for N720/A from Siegert [16], Ruggles-Wrenn et al [17].	34
19. Creep vs. time curves for N720/AM composite with $\pm 45^\circ$ fiber orientation obtained at 1200°C in laboratory air.	34
20. Creep vs. time curves for N720/A composite with $\pm 45^\circ$ fiber orientation obtained at 1200°C in steam. Data for N720/A from Siegert [16], Ruggles-Wrenn et al [17].	37
21. Creep vs. time curves for N720/AM composite with $\pm 45^\circ$ fiber orientation obtained at 1200°C in steam.	38
22. Creep vs. time curves for N720/A composite with $\pm 45^\circ$ fiber orientation obtained at 1200°C in argon. Data for N720/A from Siegert [16], Ruggles-Wrenn et al [17].	41
23. Creep vs. time curves for N720/AM composite with $\pm 45^\circ$ fiber orientation obtained at 1200°C in argon.	42
24. Creep vs. time curves for N720/AM composite with $\pm 45^\circ$ fiber orientation obtained at 1200°C in argon.	43
25. Effect of prior creep at 1200°C in laboratory air, steam and argon on tensile stress-strain behavior of N720/A composite with $\pm 45^\circ$ fiber orientation. Data for N720/A from Siegert [16], Ruggles-Wrenn et al [17].	45
26. Effect of prior creep at 1200°C in laboratory air and in steam on tensile stress-strain behavior of N720/AM composite with $\pm 45^\circ$ fiber orientation.	45
27. Applied stress vs. time to failure for N720/A ceramic composites with $\pm 45^\circ$ fiber orientation at 1200°C in air, argon and steam. Data for N720/A from Siegert [16], Ruggles-Wrenn et al [17].	47
28. Applied stress vs. time to failure for N720/AM ceramic composites with $\pm 45^\circ$ fiber orientation at 1200°C in laboratory air, argon and steam.	47

Figure	Page
29. Secondary creep rate as a function of applied stress for N720/AM and N720/A composites with $\pm 45^\circ$ fiber orientation at $1200^\circ\text{C}$ in laboratory air, argon and steam. Data for N720/A from Siegert [16], Ruggles-Wrenn et al [17].....	49
30. Secondary creep rate as a function of applied stress for N720/AM composite with $\pm 45^\circ$ fiber orientation at $1200^\circ\text{C}$ in laboratory air, argon and steam.....	49
31. Creep strain vs. time obtained for creep stress of 13 MPa in laboratory air and steam environments at $1200^\circ\text{C}$ .....	50
32. Creep strain vs. time obtained for creep stress of 20 MPa in steam and argon environments at $1200^\circ\text{C}$ .....	51
33. Creep strain vs. time obtained for creep stress of 26 MPa in steam and argon environments at $1200^\circ\text{C}$ .....	51
34. Creep strain vs. time obtained for creep stress of 30 MPa in laboratory air, steam and argon environments at $1200^\circ\text{C}$ .....	52
35. Creep strain vs. time obtained for creep stress of 32 MPa in laboratory air, steam and argon environments at $1200^\circ\text{C}$ .....	52
36. Creep-stress vs. time to failure for N720/AM with $0^\circ/90^\circ$ and $\pm 45^\circ$ fiber orientations at $1200^\circ\text{C}$ in laboratory air, steam and argon. Data for N720/AM with $0^\circ/90^\circ$ fiber orientation from Genelin [21].....	54
37. Creep rate vs. creep-stress for N720/AM with $0^\circ/90^\circ$ and $\pm 45^\circ$ fiber orientations at $1200^\circ\text{C}$ in laboratory air, steam and argon. Data for N720/AM with $0^\circ/90^\circ$ fiber orientation from Genelin [21].....	54
38. Fracture surfaces of the N720/AM specimens with $\pm 45^\circ$ fiber orientation subjected to tensile test to failure following 100 h at $1200^\circ\text{C}$ in laboratory air at: (a)-(b) 13 MPa and (c)-(d) 32 MPa.....	57
39. Fracture surfaces of the N720/AM specimens with $\pm 45^\circ$ fiber orientation obtained in creep tests conducted at $1200^\circ\text{C}$ in steam at: (a)-(b) 13 MPa, $t_f = >100$ h; (c)-(d) 20 MPa, $t_f = >100$ h; (e)-(f) 30 MPa, $t_f = 1.08$ h and (g)-(h) 32 MPa, $t_f = 0.02$ h.....	58
40. Fracture surfaces of the N720/AM specimens with $\pm 45^\circ$ fiber orientation obtained in creep tests conducted at $1200^\circ\text{C}$ in argon at: (a)-(b) 20 MPa, $t_f = >100$ h; (c)-(d) 26 MPa, $t_f = 76$ h and (e)-(f) 32 MPa, $t_f = 0.08$ h.....	60

Figure	Page
41. Fracture surfaces of the N720/AM specimens with $\pm 45^\circ$ fiber orientation obtained from load controlled tensile tests at $1200^\circ\text{C}$ at $0.0025\text{ MPa/s}$ in: (a)-(b) laboratory air, $t_f = 4.76\text{ h}$ ; (c)-(d) steam, $t_f = 5.46\text{ h}$ .....	61
42. Fracture surfaces of the N720/AM specimens with $\pm 45^\circ$ fiber orientation obtained from load controlled tensile tests at $1200^\circ\text{C}$ at $25\text{ MPa/s}$ in: (a)-(b) laboratory air, $t_f = 0.0004\text{ h}$ ; (c)-(d) steam, $t_f = 0.00038\text{ h}$ .....	62
43. Fracture surface of the N720/AM specimen with $\pm 45^\circ$ fiber orientation subjected to displacement controlled ( $0.05\text{ mm/s}$ ) monotonic tensile test to failure at $1200^\circ\text{C}$ in laboratory air, $t_f = 0.0007\text{ h}$ .....	63
44. SEM micrograph of the fracture surface of the N720/AM with $\pm 45^\circ$ fiber orientation subjected to tensile test to failure at $1200^\circ\text{C}$ in laboratory air.....	64
45. SEM micrographs of fracture surfaces of N720/AM with $\pm 45^\circ$ fiber orientation produced in creep tests conducted in laboratory air at $1200^\circ\text{C}$ at: (a) - (b) $13\text{ MPa}$ , (c) $30\text{ MPa}$ and (d) $32\text{ MPa}$ .....	65
46. SEM micrographs of fracture surfaces of N720/AM with $\pm 45^\circ$ fiber orientation produced in creep tests conducted in steam at $1200^\circ\text{C}$ at: (a) - (b) $13\text{ MPa}$ , (c) $30\text{ MPa}$ and (d) $32\text{ MPa}$ .....	67
47. SEM micrographs of N720/AM fibers subjected to creep tests at $1200^\circ\text{C}$ conducted in: (a) laboratory air at $13\text{ MPa}$ and (b) steam at $32\text{ MPa}$ .....	68
48. SEM micrographs of N720/AM fiber bundles subjected to creep tests at $1200^\circ\text{C}$ conducted in: (a) laboratory air at $32\text{ MPa}$ , (b)-(c) steam at $13\text{ MPa}$ and (d) steam at $30\text{ MPa}$ .....	70
49. SEM micrographs of fracture surfaces of N720/AM with $\pm 45^\circ$ fiber orientation produced in creep tests conducted in argon at $1200^\circ\text{C}$ at: (a)-(b)-(c) $20\text{ MPa}$ and (d) $32\text{ MPa}$ .....	71
50. SEM micrographs of N720/AM fibers subjected to creep tests at $1200^\circ\text{C}$ conducted in argon at: (a) $20\text{ MPa}$ ( $t_f > 100\text{ h}$ ) and (b) $30\text{ MPa}$ ( $t_f = 3.42\text{ h}$ ).....	72
51. SEM micrographs of N720/AM fiber bundles subjected to creep tests at $1200^\circ\text{C}$ conducted in argon at: (a) $20\text{ MPa}$ ( $t_f > 100\text{ h}$ ) and (b) $32\text{ MPa}$ ( $t_f = 0.08\text{ h}$ ).....	73
52. SEM micrographs of fracture surfaces of N720/AM with $\pm 45^\circ$ fiber orientation produced in creep tests at $1200^\circ\text{C}$ conducted at $20\text{ MPa}$ in argon.....	74

Figure	Page
53. SEM micrograph of the fracture surface of the N720/AM specimen with $\pm 45^\circ$ fiber orientation subjected to tensile test to failure with a constant stress rate of 0.0025 MPa/s at 1200°C in laboratory air.....	75
54. SEM micrograph of the fracture surface of the N720/AM specimen with $\pm 45^\circ$ fiber orientation subjected to tensile test to failure with a constant stress rate of 25 MPa/s at 1200°C in laboratory air.....	76
55. SEM micrograph of the fracture surface of the N720/AM specimen with $\pm 45^\circ$ fiber orientation subjected to tensile test to failure with a constant stress rate of 0.0025 MPa/s at 1200°C in steam.....	77
56. SEM micrograph of the fracture surface of the N720/AM specimen with $\pm 45^\circ$ fiber orientation subjected to tensile test to failure with a constant stress rate of 25 MPa/s at 1200°C in steam.....	78
57. SEM micrograph of the fracture surface of the N720/AM specimen with $\pm 45^\circ$ fiber orientation subjected to displacement controlled (0.05 mm/s) monotonic tensile test to failure at 1200°C in laboratory air, $t_f = 0.0007$ h.....	79
58. SEM micrograph of the fracture surface of the N720/AM specimen subjected to tensile test to failure following 100 h at 13 MPa at 1200°C in laboratory air.....	83
59. SEM micrograph of the fracture surface of the N720/AM specimen subjected to tensile test to failure following 100 h at 13 MPa at 1200°C in laboratory air.....	83
60. SEM micrograph of the fracture surface of the N720/AM specimen subjected to tensile test to failure following 100 h at 13 MPa at 1200°C in laboratory air.....	84
61. SEM micrograph of the fracture surface of the N720/AM specimen subjected to tensile test to failure following 100 h at 13 MPa at 1200°C in laboratory air.....	84
62. SEM micrograph of the fracture surface of the N720/AM specimen subjected to tensile test to failure following 100 h at 13 MPa at 1200°C in laboratory air.....	85
63. SEM micrograph of the fracture surface of the N720/AM specimen subjected to tensile test to failure following 100 h at 13 MPa at 1200°C in laboratory air.....	85
64. SEM micrograph of the fracture surface of the N720/AM specimen subjected to tensile test to failure following 100 h at 13 MPa at 1200°C in laboratory air.....	86
65. SEM micrograph of the fracture surface of the N720/AM specimen subjected to tensile test to failure following 100 h at 13 MPa at 1200°C in laboratory air.....	86

Figure	Page
66. SEM micrograph of the fracture surface of the N720/AM specimen subjected to tensile test to failure following 100 h at 13 MPa at 1200°C in laboratory air.....	87
67. SEM micrograph of the fracture surface of the N720/AM specimen subjected to tensile test to failure following 100 h at 13 MPa at 1200°C in laboratory air.....	87
68. SEM micrograph of the fracture surface of the N720/AM specimen subjected to tensile test to failure following 100 h at 13 MPa at 1200°C in laboratory air.....	88
69. SEM micrograph of the fracture surface of the N720/AM specimen subjected to tensile test to failure following 100 h at 13 MPa at 1200°C in laboratory air.....	88
70. SEM micrograph of the fracture surface of the N720/AM specimen subjected to tensile test to failure following 100 h at 13 MPa at 1200°C in laboratory air.....	89
71. SEM micrograph of the fracture surface of the N720/AM specimen subjected to tensile test to failure following 100 h at 13 MPa at 1200°C in laboratory air.....	89
72. SEM micrograph of the fracture surface of the N720/AM specimen subjected to tensile test to failure following 100 h at 13 MPa at 1200°C in laboratory air.....	90
73. SEM micrograph of the fracture surface of the N720/AM specimen subjected to tensile test to failure following 100 h at 13 MPa at 1200°C in laboratory air.....	90
74. SEM micrograph of the fracture surface of the N720/AM specimen subjected to tensile test to failure following 100 h at 13 MPa at 1200°C in laboratory air.....	91
75. SEM micrograph of the fracture surface of the N720/AM specimen subjected to tensile test to failure following 100 h at 13 MPa at 1200°C in laboratory air.....	91
76. SEM micrograph of the fracture surface of the N720/AM specimen subjected to tensile test to failure following 100 h at 13 MPa at 1200°C in laboratory air.....	92
77. SEM micrograph of the fracture surface of the N720/AM specimen subjected to tensile test to failure following 100 h at 13 MPa at 1200°C in laboratory air.....	92
78. SEM micrograph of the fracture surface of the N720/AM specimen subjected to tensile test to failure following 100 h at 13 MPa at 1200°C in laboratory air.....	93
79. SEM micrograph of the fracture surface of the N720/AM specimen subjected to tensile test to failure following 100 h at 13 MPa at 1200°C in laboratory air.....	93

Figure	Page
80. SEM micrograph of the fracture surface of the N720/AM specimen subjected to tensile test to failure following 100 h at 13 MPa at 1200°C in laboratory air.....	94
81. SEM micrograph of the fracture surface of the N720/AM specimen subjected to tensile test to failure following 100 h at 13 MPa at 1200°C in laboratory air.....	94
82. SEM micrograph of the fracture surface of the N720/AM specimen subjected to tensile test to failure following 100 h at 30 MPa at 1200°C in laboratory air.....	95
83. SEM micrograph of the fracture surface of the N720/AM specimen subjected to tensile test to failure following 100 h at 30 MPa at 1200°C in laboratory air.....	95
84. SEM micrograph of the fracture surface of the N720/AM specimen subjected to tensile test to failure following 100 h at 30 MPa at 1200°C in laboratory air.....	96
85. SEM micrograph of the fracture surface of the N720/AM specimen subjected to tensile test to failure following 100 h at 30 MPa at 1200°C in laboratory air.....	96
86. SEM micrograph of the fracture surface of the N720/AM specimen subjected to tensile test to failure following 100 h at 30 MPa at 1200°C in laboratory air.....	97
87. SEM micrograph of the fracture surface of the N720/AM specimen subjected to tensile test to failure following 100 h at 30 MPa at 1200°C in laboratory air.....	97
88. SEM micrograph of the fracture surface of the N720/AM specimen subjected to tensile test to failure following 100 h at 30 MPa at 1200°C in laboratory air.....	98
89. SEM micrograph of the fracture surface of the N720/AM specimen subjected to tensile test to failure following 100 h at 30 MPa at 1200°C in laboratory air.....	98
90. SEM micrograph of the fracture surface of the N720/AM specimen subjected to tensile test to failure following 100 h at 30 MPa at 1200°C in laboratory air.....	99
91. SEM micrograph of the fracture surface of the N720/AM specimen subjected to tensile test to failure following 100 h at 30 MPa at 1200°C in laboratory air.....	99
92. SEM micrograph of the fracture surface of the N720/AM specimen subjected to tensile test to failure following 100 h at 30 MPa at 1200°C in laboratory air.....	100
93. SEM micrograph of the fracture surface of the N720/AM specimen subjected to tensile test to failure following 100 h at 30 MPa at 1200°C in laboratory air.....	100

Figure	Page
94. SEM micrograph of the fracture surface of the N720/AM specimen subjected to tensile test to failure following 100 h at 30 MPa at 1200°C in laboratory air.....	101
95. SEM micrograph of the fracture surface of the N720/AM specimen subjected to tensile test to failure following 100 h at 30 MPa at 1200°C in laboratory air.....	101
96. SEM micrograph of the fracture surface of the N720/AM specimen subjected to tensile test to failure following 100 h at 30 MPa at 1200°C in laboratory air.....	102
97. SEM micrograph of the fracture surface of the N720/AM specimen subjected to tensile test to failure following 100 h at 30 MPa at 1200°C in laboratory air.....	102
98. SEM micrograph of the fracture surface of the N720/AM specimen subjected to tensile test to failure following 100 h at 30 MPa at 1200°C in laboratory air.....	103
99. SEM micrograph of the fracture surface of the N720/AM specimen subjected to tensile test to failure following 100 h at 30 MPa at 1200°C in laboratory air.....	103
100. SEM micrograph of the fracture surface of the N720/AM specimen subjected to tensile test to failure following 100 h at 30 MPa at 1200°C in laboratory air.....	104
101. SEM micrograph of the fracture surface of the N720/AM specimen subjected to tensile test to failure following 100 h at 30 MPa at 1200°C in laboratory air.....	104
102. SEM micrograph of the fracture surface of the N720/AM specimen subjected to tensile test to failure following 100 h at 30 MPa at 1200°C in laboratory air.....	105
103. SEM micrograph of the fracture surface of the N720/AM specimen subjected to tensile test to failure following 100 h at 30 MPa at 1200°C in laboratory air.....	105
104. SEM micrograph of the fracture surface of the N720/AM specimen subjected to tensile test to failure following 100 h at 30 MPa at 1200°C in laboratory air.....	106
105. SEM micrograph of the fracture surface of the N720/AM specimen subjected to tensile test to failure following 100 h at 30 MPa at 1200°C in laboratory air.....	106
106. SEM micrograph of the fracture surface of the N720/AM specimen subjected to tensile test to failure following 100 h at 30 MPa at 1200°C in laboratory air.....	107
107. SEM micrograph of the fracture surface of the N720/AM specimen subjected to tensile test to failure following 100 h at 30 MPa at 1200°C in laboratory air.....	107

Figure	Page
108. SEM micrograph of the fracture surface of the N720/AM specimen subjected to tensile test to failure following 100 h at 30 MPa at 1200°C in laboratory air.....	108
109. SEM micrograph of the fracture surface of the N720/AM specimen subjected to tensile test to failure following 100 h at 30 MPa at 1200°C in laboratory air.....	108
110. SEM micrograph of the fracture surface of the N720/AM specimen subjected to tensile test to failure following 100 h at 30 MPa at 1200°C in laboratory air.....	109
111. SEM micrograph of the fracture surface of the N720/AM specimen subjected to tensile test to failure following 100 h at 30 MPa at 1200°C in laboratory air.....	109
112. SEM micrograph of the fracture surface of the N720/AM specimen subjected to tensile test to failure following 100 h at 30 MPa at 1200°C in laboratory air.....	110
113. SEM micrograph of the fracture surface of the N720/AM specimen subjected to tensile test to failure following 100 h at 30 MPa at 1200°C in laboratory air.....	110
114. SEM micrograph of the fracture surface of the N720/AM specimen subjected to tensile test to failure following 100 h at 30 MPa at 1200°C in laboratory air.....	111
115. SEM micrograph of the fracture surface of the N720/AM specimen subjected to tensile test to failure following 100 h at 30 MPa at 1200°C in laboratory air.....	111
116. SEM micrograph of the fracture surface of the N720/AM specimen subjected to tensile test to failure following 100 h at 30 MPa at 1200°C in laboratory air.....	112
117. SEM micrograph of the fracture surface of the N720/AM specimen subjected to tensile test to failure following 100 h at 30 MPa at 1200°C in laboratory air.....	112
118. SEM micrograph of the fracture surface of the N720/AM specimen subjected to tensile test to failure following 100 h at 30 MPa at 1200°C in laboratory air.....	113
119. SEM micrograph of the fracture surface of the N720/AM specimen subjected to tensile test to failure following 100 h at 30 MPa at 1200°C in laboratory air.....	113
120. SEM micrograph of the fracture surface of the N720/AM specimen subjected to tensile test to failure following 100 h at 32 MPa at 1200°C in laboratory air.....	114
121. SEM micrograph of the fracture surface of the N720/AM specimen subjected to tensile test to failure following 100 h at 32 MPa at 1200°C in laboratory air.....	114

Figure	Page
122. SEM micrograph of the fracture surface of the N720/AM specimen subjected to tensile test to failure following 100 h at 32 MPa at 1200°C in laboratory air.....	115
123. SEM micrograph of the fracture surface of the N720/AM specimen subjected to tensile test to failure following 100 h at 32 MPa at 1200°C in laboratory air.....	115
124. SEM micrograph of the fracture surface of the N720/AM specimen subjected to tensile test to failure following 100 h at 32 MPa at 1200°C in laboratory air.....	116
125. SEM micrograph of the fracture surface of the N720/AM specimen subjected to tensile test to failure following 100 h at 32 MPa at 1200°C in laboratory air.....	116
126. SEM micrograph of the fracture surface of the N720/AM specimen subjected to tensile test to failure following 100 h at 32 MPa at 1200°C in laboratory air.....	117
127. SEM micrograph of the fracture surface of the N720/AM specimen subjected to tensile test to failure following 100 h at 32 MPa at 1200°C in laboratory air.....	117
128. SEM micrograph of the fracture surface of the N720/AM specimen subjected to tensile test to failure following 100 h at 32 MPa at 1200°C in laboratory air.....	118
129. SEM micrograph of the fracture surface of the N720/AM specimen subjected to tensile test to failure following 100 h at 32 MPa at 1200°C in laboratory air.....	118
130. SEM micrograph of the fracture surface of the N720/AM specimen subjected to tensile test to failure following 100 h at 32 MPa at 1200°C in laboratory air.....	119
131. SEM micrograph of the fracture surface of the N720/AM specimen subjected to tensile test to failure following 100 h at 32 MPa at 1200°C in laboratory air.....	119
132. SEM micrograph of the fracture surface of the N720/AM specimen subjected to tensile test to failure following 100 h at 32 MPa at 1200°C in laboratory air.....	120
133. SEM micrograph of the fracture surface of the N720/AM specimen subjected to tensile test to failure following 100 h at 32 MPa at 1200°C in laboratory air.....	120
134. SEM micrograph of the fracture surface of the N720/AM specimen subjected to tensile test to failure following 100 h at 32 MPa at 1200°C in laboratory air.....	121
135. SEM micrograph of the fracture surface of the N720/AM specimen subjected to tensile test to failure following 100 h at 32 MPa at 1200°C in laboratory air.....	121

Figure	Page
136. SEM micrograph of the fracture surface of the N720/AM specimen subjected to tensile test to failure following 100 h at 32 MPa at 1200°C in laboratory air.....	122
137. SEM micrograph of the fracture surface of the N720/AM specimen subjected to tensile test to failure following 100 h at 32 MPa at 1200°C in laboratory air.....	122
138. SEM micrograph of the fracture surface of the N720/AM specimen subjected to tensile test to failure following 100 h at 32 MPa at 1200°C in laboratory air.....	123
139. SEM micrograph of the fracture surface of the N720/AM specimen subjected to tensile test to failure following 100 h at 32 MPa at 1200°C in laboratory air.....	123
140. SEM micrograph of the fracture surface of the N720/AM specimen subjected to tensile test to failure following 100 h at 32 MPa at 1200°C in laboratory air.....	124
141. SEM micrograph of the fracture surface of the N720/AM specimen subjected to tensile test to failure following 100 h at 32 MPa at 1200°C in laboratory air.....	124
142. SEM micrograph of the fracture surface of the N720/AM specimen subjected to tensile test to failure following 100 h at 32 MPa at 1200°C in laboratory air.....	125
143. SEM micrograph of the fracture surface of the N720/AM specimen subjected to tensile test to failure following 100 h at 32 MPa at 1200°C in laboratory air.....	125
144. SEM micrograph of the fracture surface of the N720/AM specimen subjected to tensile test to failure following 100 h at 32 MPa at 1200°C in laboratory air.....	126
145. SEM micrograph of the fracture surface of the N720/AM specimen subjected to tensile test to failure following 100 h at 32 MPa at 1200°C in laboratory air.....	126
146. SEM micrograph of the fracture surface of the N720/AM specimen subjected to tensile test to failure following 100 h at 32 MPa at 1200°C in laboratory air.....	127
147. SEM micrograph of the fracture surface of the N720/AM specimen subjected to tensile test to failure following 100 h at 32 MPa at 1200°C in laboratory air.....	127
148. SEM micrograph of the fracture surface of the N720/AM specimen subjected to tensile test to failure following 100 h at 32 MPa at 1200°C in laboratory air.....	128
149. SEM micrograph of the fracture surface of the N720/AM specimen subjected to tensile test to failure following 100 h at 32 MPa at 1200°C in laboratory air.....	128

Figure	Page
150. SEM micrograph of the fracture surface of the N720/AM specimen subjected to tensile test to failure following 100 h at 32 MPa at 1200°C in laboratory air.....	129
151. SEM micrograph of the fracture surface of the N720/AM specimen subjected to tensile test to failure following 100 h at 32 MPa at 1200°C in laboratory air.....	129
152. SEM micrograph of the fracture surface of the N720/AM specimen subjected to tensile test to failure following 100 h at 32 MPa at 1200°C in laboratory air.....	130
153. SEM micrograph of the fracture surface of the N720/AM specimen subjected to tensile test to failure following 100 h at 32 MPa at 1200°C in laboratory air.....	130
154. SEM micrograph of the fracture surface of the N720/AM specimen subjected to tensile test to failure following 100 h at 32 MPa at 1200°C in laboratory air.....	131
155. SEM micrograph of the fracture surface of the N720/AM specimen subjected to tensile test to failure following 100 h at 32 MPa at 1200°C in laboratory air.....	131
156. SEM micrograph of the fracture surface of the N720/AM specimen subjected to tensile test to failure following 100 h at 32 MPa at 1200°C in laboratory air.....	132
157. SEM micrograph of the fracture surface of the N720/AM specimen subjected to tensile test to failure following 100 h at 32 MPa at 1200°C in laboratory air.....	132
158. SEM micrograph of the fracture surface of the N720/AM specimen subjected to tensile test to failure following 100 h at 32 MPa at 1200°C in laboratory air.....	133
159. SEM micrograph of the fracture surface of the N720/AM specimen subjected to tensile test to failure following 100 h at 32 MPa at 1200°C in laboratory air.....	133
160. SEM micrograph of the fracture surface of the N720/AM specimen subjected to tensile test to failure following 100 h at 32 MPa at 1200°C in laboratory air.....	134
161. SEM micrograph of the fracture surface of the N720/AM specimen subjected to tensile test to failure following 100 h at 32 MPa at 1200°C in laboratory air.....	134
162. SEM micrograph of the fracture surface of the N720/AM specimen subjected to tensile test to failure following 100 h at 32 MPa at 1200°C in laboratory air.....	135
163. SEM micrograph of the fracture surface of the N720/AM specimen subjected to tensile test to failure following 100 h at 32 MPa at 1200°C in laboratory air.....	135

Figure	Page
164. SEM micrograph of the fracture surface of the N720/AM specimen subjected to tensile test to failure following 100 h at 32 MPa at 1200°C in laboratory air.....	136
165. SEM micrograph of the fracture surface of the N720/AM specimen subjected to tensile test to failure following 100 h at 32 MPa at 1200°C in laboratory air.....	136
166. SEM micrograph of the fracture surface of the N720/AM specimen subjected to tensile test to failure following 100 h at 32 MPa at 1200°C in laboratory air.....	137
167. SEM micrograph of the fracture surface of the N720/AM specimen subjected to tensile test to failure following 100 h at 32 MPa at 1200°C in laboratory air.....	137
168. SEM micrograph of the fracture surface of the N720/AM specimen subjected to tensile test to failure following 100 h at 32 MPa at 1200°C in laboratory air.....	138
169. SEM micrograph of the fracture surface of the N720/AM specimen subjected to tensile test to failure following 100 h at 32 MPa at 1200°C in laboratory air.....	138
170. SEM micrograph of the fracture surface of the N720/AM specimen subjected to tensile test to failure following 100 h at 32 MPa at 1200°C in laboratory air.....	139
171. SEM micrograph of the fracture surface of the N720/AM specimen subjected to tensile test to failure following 100 h at 32 MPa at 1200°C in laboratory air.....	139
172. SEM micrograph of the fracture surface of the N720/AM specimen subjected to tensile test to failure following 100 h at 32 MPa at 1200°C in laboratory air.....	140
173. SEM micrograph of the fracture surface of the N720/AM specimen subjected to tensile test to failure following 100 h at 32 MPa at 1200°C in laboratory air.....	140
174. SEM micrograph of the fracture surface of the N720/AM specimen subjected to tensile test to failure following 100 h at 13 MPa at 1200°C in steam.....	141
175. SEM micrograph of the fracture surface of the N720/AM specimen subjected to tensile test to failure following 100 h at 13 MPa at 1200°C in steam.....	141
176. SEM micrograph of the fracture surface of the N720/AM specimen subjected to tensile test to failure following 100 h at 13 MPa at 1200°C in steam.....	142
177. SEM micrograph of the fracture surface of the N720/AM specimen subjected to tensile test to failure following 100 h at 13 MPa at 1200°C in steam.....	142

Figure	Page
178. SEM micrograph of the fracture surface of the N720/AM specimen subjected to tensile test to failure following 100 h at 13 MPa at 1200°C in steam.....	143
179. SEM micrograph of the fracture surface of the N720/AM specimen subjected to tensile test to failure following 100 h at 13 MPa at 1200°C in steam.....	143
180. SEM micrograph of the fracture surface of the N720/AM specimen subjected to tensile test to failure following 100 h at 13 MPa at 1200°C in steam.....	144
181. SEM micrograph of the fracture surface of the N720/AM specimen subjected to tensile test to failure following 100 h at 13 MPa at 1200°C in steam.....	144
182. SEM micrograph of the fracture surface of the N720/AM specimen subjected to tensile test to failure following 100 h at 13 MPa at 1200°C in steam.....	145
183. SEM micrograph of the fracture surface of the N720/AM specimen subjected to tensile test to failure following 100 h at 13 MPa at 1200°C in steam.....	145
184. SEM micrograph of the fracture surface of the N720/AM specimen subjected to tensile test to failure following 100 h at 13 MPa at 1200°C in steam.....	146
185. SEM micrograph of the fracture surface of the N720/AM specimen subjected to tensile test to failure following 100 h at 13 MPa at 1200°C in steam.....	146
186. SEM micrograph of the fracture surface of the N720/AM specimen subjected to tensile test to failure following 100 h at 13 MPa at 1200°C in steam.....	147
187. SEM micrograph of the fracture surface of the N720/AM specimen subjected to tensile test to failure following 100 h at 13 MPa at 1200°C in steam.....	147
188. SEM micrograph of the fracture surface of the N720/AM specimen subjected to tensile test to failure following 100 h at 13 MPa at 1200°C in steam.....	148
189. SEM micrograph of the fracture surface of the N720/AM specimen subjected to tensile test to failure following 100 h at 13 MPa at 1200°C in steam.....	148
190. SEM micrograph of the fracture surface of the N720/AM specimen subjected to tensile test to failure following 100 h at 13 MPa at 1200°C in steam.....	149
191. SEM micrograph of the fracture surface of the N720/AM specimen subjected to tensile test to failure following 100 h at 13 MPa at 1200°C in steam.....	149

Figure	Page
192. SEM micrograph of the fracture surface of the N720/AM specimen subjected to tensile test to failure following 100 h at 13 MPa at 1200°C in steam.....	150
193. SEM micrograph of the fracture surface of the N720/AM specimen subjected to tensile test to failure following 100 h at 13 MPa at 1200°C in steam.....	150
194. SEM micrograph of the fracture surface of the N720/AM specimen subjected to tensile test to failure following 100 h at 13 MPa at 1200°C in steam.....	151
195. SEM micrograph of the fracture surface of the N720/AM specimen subjected to tensile test to failure following 100 h at 13 MPa at 1200°C in steam.....	151
196. SEM micrograph of the fracture surface of the N720/AM specimen subjected to tensile test to failure following 100 h at 13 MPa at 1200°C in steam.....	152
197. SEM micrograph of the fracture surface of the N720/AM specimen subjected to tensile test to failure following 100 h at 13 MPa at 1200°C in steam.....	152
198. SEM micrograph of the fracture surface of the N720/AM specimen subjected to tensile test to failure following 100 h at 13 MPa at 1200°C in steam.....	153
199. SEM micrograph of the fracture surface of the N720/AM specimen subjected to tensile test to failure following 100 h at 13 MPa at 1200°C in steam.....	153
200. SEM micrograph of the fracture surface of the N720/AM specimen subjected to tensile test to failure following 100 h at 13 MPa at 1200°C in steam.....	154
201. SEM micrograph of the fracture surface of the N720/AM specimen subjected to tensile test to failure following 100 h at 13 MPa at 1200°C in steam.....	154
202. SEM micrograph of the fracture surface of the N720/AM specimen subjected to tensile test to failure following 100 h at 13 MPa at 1200°C in steam.....	155
203. SEM micrograph of the fracture surface of the N720/AM specimen subjected to tensile test to failure following 100 h at 13 MPa at 1200°C in steam.....	155
204. SEM micrograph of the fracture surface of the N720/AM specimen subjected to tensile test to failure following 100 h at 13 MPa at 1200°C in steam.....	156
205. SEM micrograph of the fracture surface of the N720/AM specimen subjected to tensile test to failure following 100 h at 13 MPa at 1200°C in steam.....	156

Figure	Page
206. SEM micrograph of the fracture surface of the N720/AM specimen subjected to tensile test to failure following 100 h at 13 MPa at 1200°C in steam.....	157
207. SEM micrograph of the fracture surface of the N720/AM specimen subjected to tensile test to failure following 100 h at 13 MPa at 1200°C in steam.....	157
208. SEM micrograph of the fracture surface of the N720/AM specimen subjected to tensile test to failure following 100 h at 13 MPa at 1200°C in steam.....	158
209. SEM micrograph of the fracture surface of the N720/AM specimen subjected to tensile test to failure following 100 h at 13 MPa at 1200°C in steam.....	158
210. SEM micrograph of the fracture surface of the N720/AM specimen subjected to tensile test to failure following 100 h at 13 MPa at 1200°C in steam.....	159
211. SEM micrograph of the fracture surface of the N720/AM specimen subjected to tensile test to failure following 100 h at 13 MPa at 1200°C in steam.....	159
212. SEM micrograph of the fracture surface of the N720/AM specimen subjected to tensile test to failure following 100 h at 13 MPa at 1200°C in steam.....	160
213. SEM micrograph of the fracture surface of the N720/AM specimen subjected to tensile test to failure following 100 h at 13 MPa at 1200°C in steam.....	160
214. SEM micrograph of the fracture surface of the N720/AM specimen subjected to tensile test to failure following 100 h at 13 MPa at 1200°C in steam.....	161
215. SEM micrograph of the fracture surface of the N720/AM specimen subjected to tensile test to failure following 100 h at 13 MPa at 1200°C in steam.....	161
216. SEM micrograph of the fracture surface of the N720/AM specimen subjected to tensile test to failure following 100 h at 13 MPa at 1200°C in steam.....	162
217. SEM micrograph of the fracture surface of the N720/AM specimen subjected to tensile test to failure following 100 h at 13 MPa at 1200°C in steam.....	162
218. SEM micrograph of the fracture surface of the N720/AM specimen subjected to tensile test to failure following 100 h at 13 MPa at 1200°C in steam.....	163
219. SEM micrograph of the fracture surface of the N720/AM specimen subjected to tensile test to failure following 100 h at 13 MPa at 1200°C in steam.....	163

Figure	Page
220. SEM micrograph of the fracture surface of the N720/AM specimen subjected to tensile test to failure following 100 h at 13 MPa at 1200°C in steam.....	164
221. SEM micrograph of the fracture surface of the N720/AM specimen subjected to tensile test to failure following 100 h at 13 MPa at 1200°C in steam.....	164
222. SEM micrograph of the fracture surface of the N720/AM specimen subjected to tensile test to failure following 100 h at 13 MPa at 1200°C in steam.....	165
223. SEM micrograph of the fracture surface of the N720/AM specimen with $\pm 45^\circ$ fiber orientation obtained in creep test conducted at 30 MPa at 1200°C in steam. Creep lifetime $t_f = 1.08$ h.....	165
224. SEM micrograph of the fracture surface of the N720/AM specimen with $\pm 45^\circ$ fiber orientation obtained in creep test conducted at 30 MPa at 1200°C in steam. Creep lifetime $t_f = 1.08$ h.....	166
225. SEM micrograph of the fracture surface of the N720/AM specimen with $\pm 45^\circ$ fiber orientation obtained in creep test conducted at 30 MPa at 1200°C in steam. Creep lifetime $t_f = 1.08$ h.....	166
226. SEM micrograph of the fracture surface of the N720/AM specimen with $\pm 45^\circ$ fiber orientation obtained in creep test conducted at 30 MPa at 1200°C in steam. Creep lifetime $t_f = 1.08$ h.....	167
227. SEM micrograph of the fracture surface of the N720/AM specimen with $\pm 45^\circ$ fiber orientation obtained in creep test conducted at 30 MPa at 1200°C in steam. Creep lifetime $t_f = 1.08$ h.....	167
228. SEM micrograph of the fracture surface of the N720/AM specimen with $\pm 45^\circ$ fiber orientation obtained in creep test conducted at 30 MPa at 1200°C in steam. Creep lifetime $t_f = 1.08$ h.....	168
229. SEM micrograph of the fracture surface of the N720/AM specimen with $\pm 45^\circ$ fiber orientation obtained in creep test conducted at 30 MPa at 1200°C in steam. Creep lifetime $t_f = 1.08$ h.....	168
230. SEM micrograph of the fracture surface of the N720/AM specimen with $\pm 45^\circ$ fiber orientation obtained in creep test conducted at 30 MPa at 1200°C in steam. Creep lifetime $t_f = 1.08$ h.....	169

Figure	Page
231. SEM micrograph of the fracture surface of the N720/AM specimen with $\pm 45^\circ$ fiber orientation obtained in creep test conducted at 30 MPa at 1200°C in steam. Creep lifetime $t_f = 1.08$ h.....	169
232. SEM micrograph of the fracture surface of the N720/AM specimen with $\pm 45^\circ$ fiber orientation obtained in creep test conducted at 30 MPa at 1200°C in steam. Creep lifetime $t_f = 1.08$ h.....	170
233. SEM micrograph of the fracture surface of the N720/AM specimen with $\pm 45^\circ$ fiber orientation obtained in creep test conducted at 30 MPa at 1200°C in steam. Creep lifetime $t_f = 1.08$ h.....	170
234. SEM micrograph of the fracture surface of the N720/AM specimen with $\pm 45^\circ$ fiber orientation obtained in creep test conducted at 30 MPa at 1200°C in steam. Creep lifetime $t_f = 1.08$ h.....	171
235. SEM micrograph of the fracture surface of the N720/AM specimen with $\pm 45^\circ$ fiber orientation obtained in creep test conducted at 30 MPa at 1200°C in steam. Creep lifetime $t_f = 1.08$ h.....	171
236. SEM micrograph of the fracture surface of the N720/AM specimen with $\pm 45^\circ$ fiber orientation obtained in creep test conducted at 30 MPa at 1200°C in steam. Creep lifetime $t_f = 1.08$ h.....	172
237. SEM micrograph of the fracture surface of the N720/AM specimen with $\pm 45^\circ$ fiber orientation obtained in creep test conducted at 30 MPa at 1200°C in steam. Creep lifetime $t_f = 1.08$ h.....	172
238. SEM micrograph of the fracture surface of the N720/AM specimen with $\pm 45^\circ$ fiber orientation obtained in creep test conducted at 30 MPa at 1200°C in steam. Creep lifetime $t_f = 1.08$ h.....	173
239. SEM micrograph of the fracture surface of the N720/AM specimen with $\pm 45^\circ$ fiber orientation obtained in creep test conducted at 30 MPa at 1200°C in steam. Creep lifetime $t_f = 1.08$ h.....	173
240. SEM micrograph of the fracture surface of the N720/AM specimen with $\pm 45^\circ$ fiber orientation obtained in creep test conducted at 30 MPa at 1200°C in steam. Creep lifetime $t_f = 1.08$ h.....	174

Figure	Page
241. SEM micrograph of the fracture surface of the N720/AM specimen with $\pm 45^\circ$ fiber orientation obtained in creep test conducted at 30 MPa at 1200°C in steam. Creep lifetime $t_f = 1.08$ h.....	174
242. SEM micrograph of the fracture surface of the N720/AM specimen with $\pm 45^\circ$ fiber orientation obtained in creep test conducted at 30 MPa at 1200°C in steam. Creep lifetime $t_f = 1.08$ h.....	175
243. SEM micrograph of the fracture surface of the N720/AM specimen with $\pm 45^\circ$ fiber orientation obtained in creep test conducted at 30 MPa at 1200°C in steam. Creep lifetime $t_f = 1.08$ h.....	175
244. SEM micrograph of the fracture surface of the N720/AM specimen with $\pm 45^\circ$ fiber orientation obtained in creep test conducted at 30 MPa at 1200°C in steam. Creep lifetime $t_f = 1.08$ h.....	176
245. SEM micrograph of the fracture surface of the N720/AM specimen with $\pm 45^\circ$ fiber orientation obtained in creep test conducted at 30 MPa at 1200°C in steam. Creep lifetime $t_f = 1.08$ h.....	176
246. SEM micrograph of the fracture surface of the N720/AM specimen with $\pm 45^\circ$ fiber orientation obtained in creep test conducted at 30 MPa at 1200°C in steam. Creep lifetime $t_f = 1.08$ h.....	177
247. SEM micrograph of the fracture surface of the N720/AM specimen with $\pm 45^\circ$ fiber orientation obtained in creep test conducted at 30 MPa at 1200°C in steam. Creep lifetime $t_f = 1.08$ h.....	177
248. SEM micrograph of the fracture surface of the N720/AM specimen with $\pm 45^\circ$ fiber orientation obtained in creep test conducted at 30 MPa at 1200°C in steam. Creep lifetime $t_f = 1.08$ h.....	178
249. SEM micrograph of the fracture surface of the N720/AM specimen with $\pm 45^\circ$ fiber orientation obtained in creep test conducted at 30 MPa at 1200°C in steam. Creep lifetime $t_f = 1.08$ h.....	178
250. SEM micrograph of the fracture surface of the N720/AM specimen with $\pm 45^\circ$ fiber orientation obtained in creep test conducted at 30 MPa at 1200°C in steam. Creep lifetime $t_f = 1.08$ h.....	179

Figure	Page
251. SEM micrograph of the fracture surface of the N720/AM specimen with $\pm 45^\circ$ fiber orientation obtained in creep test conducted at 30 MPa at 1200°C in steam. Creep lifetime $t_f = 1.08$ h.....	179
252. SEM micrograph of the fracture surface of the N720/AM specimen with $\pm 45^\circ$ fiber orientation obtained in creep test conducted at 30 MPa at 1200°C in steam. Creep lifetime $t_f = 1.08$ h.....	180
253. SEM micrograph of the fracture surface of the N720/AM specimen with $\pm 45^\circ$ fiber orientation obtained in creep test conducted at 30 MPa at 1200°C in steam. Creep lifetime $t_f = 1.08$ h.....	180
254. SEM micrograph of the fracture surface of the N720/AM specimen with $\pm 45^\circ$ fiber orientation obtained in creep test conducted at 30 MPa at 1200°C in steam. Creep lifetime $t_f = 1.08$ h.....	181
255. SEM micrograph of the fracture surface of the N720/AM specimen with $\pm 45^\circ$ fiber orientation obtained in creep test conducted at 30 MPa at 1200°C in steam. Creep lifetime $t_f = 1.08$ h.....	181
256. SEM micrograph of the fracture surface of the N720/AM specimen with $\pm 45^\circ$ fiber orientation obtained in creep test conducted at 30 MPa at 1200°C in steam. Creep lifetime $t_f = 1.08$ h.....	182
257. SEM micrograph of the fracture surface of the N720/AM specimen with $\pm 45^\circ$ fiber orientation obtained in creep test conducted at 30 MPa at 1200°C in steam. Creep lifetime $t_f = 1.08$ h.....	182
258. SEM micrograph of the fracture surface of the N720/AM specimen with $\pm 45^\circ$ fiber orientation obtained in creep test conducted at 30 MPa at 1200°C in steam. Creep lifetime $t_f = 1.08$ h.....	183
259. SEM micrograph of the fracture surface of the N720/AM specimen with $\pm 45^\circ$ fiber orientation obtained in creep test conducted at 30 MPa at 1200°C in steam. Creep lifetime $t_f = 1.08$ h.....	183
260. SEM micrograph of the fracture surface of the N720/AM specimen with $\pm 45^\circ$ fiber orientation obtained in creep test conducted at 30 MPa at 1200°C in steam. Creep lifetime $t_f = 1.08$ h.....	184

Figure	Page
261. SEM micrograph of the fracture surface of the N720/AM specimen with $\pm 45^\circ$ fiber orientation obtained in creep test conducted at 30 MPa at 1200°C in steam. Creep lifetime $t_f = 1.08$ h.....	184
262. SEM micrograph of the fracture surface of the N720/AM specimen with $\pm 45^\circ$ fiber orientation obtained in creep test conducted at 30 MPa at 1200°C in steam. Creep lifetime $t_f = 1.08$ h.....	185
263. SEM micrograph of the fracture surface of the N720/AM specimen with $\pm 45^\circ$ fiber orientation obtained in creep test conducted at 32 MPa at 1200°C in steam. Creep lifetime $t_f = 0.02$ h.....	185
264. SEM micrograph of the fracture surface of the N720/AM specimen with $\pm 45^\circ$ fiber orientation obtained in creep test conducted at 32 MPa at 1200°C in steam. Creep lifetime $t_f = 0.02$ h.....	186
265. SEM micrograph of the fracture surface of the N720/AM specimen with $\pm 45^\circ$ fiber orientation obtained in creep test conducted at 32 MPa at 1200°C in steam. Creep lifetime $t_f = 0.02$ h.....	186
266. SEM micrograph of the fracture surface of the N720/AM specimen with $\pm 45^\circ$ fiber orientation obtained in creep test conducted at 32 MPa at 1200°C in steam. Creep lifetime $t_f = 0.02$ h.....	187
267. SEM micrograph of the fracture surface of the N720/AM specimen with $\pm 45^\circ$ fiber orientation obtained in creep test conducted at 32 MPa at 1200°C in steam. Creep lifetime $t_f = 0.02$ h.....	187
268. SEM micrograph of the fracture surface of the N720/AM specimen with $\pm 45^\circ$ fiber orientation obtained in creep test conducted at 32 MPa at 1200°C in steam. Creep lifetime $t_f = 0.02$ h.....	188
269. SEM micrograph of the fracture surface of the N720/AM specimen with $\pm 45^\circ$ fiber orientation obtained in creep test conducted at 32 MPa at 1200°C in steam. Creep lifetime $t_f = 0.02$ h.....	188
270. SEM micrograph of the fracture surface of the N720/AM specimen with $\pm 45^\circ$ fiber orientation obtained in creep test conducted at 32 MPa at 1200°C in steam. Creep lifetime $t_f = 0.02$ h.....	189

Figure	Page
271. SEM micrograph of the fracture surface of the N720/AM specimen with $\pm 45^\circ$ fiber orientation obtained in creep test conducted at 32 MPa at 1200°C in steam. Creep lifetime $t_f = 0.02$ h.....	189
272. SEM micrograph of the fracture surface of the N720/AM specimen with $\pm 45^\circ$ fiber orientation obtained in creep test conducted at 32 MPa at 1200°C in steam. Creep lifetime $t_f = 0.02$ h.....	190
273. SEM micrograph of the fracture surface of the N720/AM specimen with $\pm 45^\circ$ fiber orientation obtained in creep test conducted at 32 MPa at 1200°C in steam. Creep lifetime $t_f = 0.02$ h.....	190
274. SEM micrograph of the fracture surface of the N720/AM specimen with $\pm 45^\circ$ fiber orientation obtained in creep test conducted at 32 MPa at 1200°C in steam. Creep lifetime $t_f = 0.02$ h.....	191
275. SEM micrograph of the fracture surface of the N720/AM specimen with $\pm 45^\circ$ fiber orientation obtained in creep test conducted at 32 MPa at 1200°C in steam. Creep lifetime $t_f = 0.02$ h.....	191
276. SEM micrograph of the fracture surface of the N720/AM specimen with $\pm 45^\circ$ fiber orientation obtained in creep test conducted at 32 MPa at 1200°C in steam. Creep lifetime $t_f = 0.02$ h.....	192
277. SEM micrograph of the fracture surface of the N720/AM specimen with $\pm 45^\circ$ fiber orientation obtained in creep test conducted at 32 MPa at 1200°C in steam. Creep lifetime $t_f = 0.02$ h.....	192
278. SEM micrograph of the fracture surface of the N720/AM specimen with $\pm 45^\circ$ fiber orientation obtained in creep test conducted at 32 MPa at 1200°C in steam. Creep lifetime $t_f = 0.02$ h.....	193
279. SEM micrograph of the fracture surface of the N720/AM specimen with $\pm 45^\circ$ fiber orientation obtained in creep test conducted at 32 MPa at 1200°C in steam. Creep lifetime $t_f = 0.02$ h.....	193
280. SEM micrograph of the fracture surface of the N720/AM specimen with $\pm 45^\circ$ fiber orientation obtained in creep test conducted at 32 MPa at 1200°C in steam. Creep lifetime $t_f = 0.02$ h.....	194

Figure	Page
281. SEM micrograph of the fracture surface of the N720/AM specimen with $\pm 45^\circ$ fiber orientation obtained in creep test conducted at 32 MPa at 1200°C in steam. Creep lifetime $t_f = 0.02$ h.....	194
282. SEM micrograph of the fracture surface of the N720/AM specimen with $\pm 45^\circ$ fiber orientation obtained in creep test conducted at 32 MPa at 1200°C in steam. Creep lifetime $t_f = 0.02$ h.....	195
283. SEM micrograph of the fracture surface of the N720/AM specimen with $\pm 45^\circ$ fiber orientation obtained in creep test conducted at 32 MPa at 1200°C in steam. Creep lifetime $t_f = 0.02$ h.....	195
284. SEM micrograph of the fracture surface of the N720/AM specimen with $\pm 45^\circ$ fiber orientation obtained in creep test conducted at 32 MPa at 1200°C in steam. Creep lifetime $t_f = 0.02$ h.....	196
285. SEM micrograph of the fracture surface of the N720/AM specimen with $\pm 45^\circ$ fiber orientation obtained in creep test conducted at 32 MPa at 1200°C in steam. Creep lifetime $t_f = 0.02$ h.....	196
286. SEM micrograph of the fracture surface of the N720/AM specimen with $\pm 45^\circ$ fiber orientation obtained in creep test conducted at 32 MPa at 1200°C in steam. Creep lifetime $t_f = 0.02$ h.....	197
287. SEM micrograph of the fracture surface of the N720/AM specimen with $\pm 45^\circ$ fiber orientation obtained in creep test conducted at 32 MPa at 1200°C in steam. Creep lifetime $t_f = 0.02$ h.....	197
288. SEM micrograph of the fracture surface of the N720/AM specimen with $\pm 45^\circ$ fiber orientation obtained in creep test conducted at 32 MPa at 1200°C in steam. Creep lifetime $t_f = 0.02$ h.....	198
289. SEM micrograph of the fracture surface of the N720/AM specimen with $\pm 45^\circ$ fiber orientation obtained in creep test conducted at 32 MPa at 1200°C in steam. Creep lifetime $t_f = 0.02$ h.....	198
290. SEM micrograph of the fracture surface of the N720/AM specimen with $\pm 45^\circ$ fiber orientation obtained in creep test conducted at 32 MPa at 1200°C in steam. Creep lifetime $t_f = 0.02$ h.....	199

Figure	Page
291. SEM micrograph of the fracture surface of the N720/AM specimen with $\pm 45^\circ$ fiber orientation obtained in creep test conducted at 32 MPa at 1200°C in steam. Creep lifetime $t_f = 0.02$ h.....	199
292. SEM micrograph of the fracture surface of the N720/AM specimen with $\pm 45^\circ$ fiber orientation obtained in creep test conducted at 32 MPa at 1200°C in steam. Creep lifetime $t_f = 0.02$ h.....	200
293. SEM micrograph of the fracture surface of the N720/AM specimen with $\pm 45^\circ$ fiber orientation obtained in creep test conducted at 32 MPa at 1200°C in steam. Creep lifetime $t_f = 0.02$ h.....	200
294. SEM micrograph of the fracture surface of the N720/AM specimen with $\pm 45^\circ$ fiber orientation obtained in creep test conducted at 32 MPa at 1200°C in steam. Creep lifetime $t_f = 0.02$ h.....	201
295. SEM micrograph of the fracture surface of the N720/AM specimen with $\pm 45^\circ$ fiber orientation obtained in creep test conducted at 32 MPa at 1200°C in steam. Creep lifetime $t_f = 0.02$ h.....	201
296. SEM micrograph of the fracture surface of the N720/AM specimen with $\pm 45^\circ$ fiber orientation obtained in creep test conducted at 32 MPa at 1200°C in steam. Creep lifetime $t_f = 0.02$ h.....	202
297. SEM micrograph of the fracture surface of the N720/AM specimen with $\pm 45^\circ$ fiber orientation obtained in creep test conducted at 32 MPa at 1200°C in steam. Creep lifetime $t_f = 0.02$ h.....	202
298. SEM micrograph of the fracture surface of the N720/AM specimen with $\pm 45^\circ$ fiber orientation obtained in creep test conducted at 32 MPa at 1200°C in steam. Creep lifetime $t_f = 0.02$ h.....	203
299. SEM micrograph of the fracture surface of the N720/AM specimen with $\pm 45^\circ$ fiber orientation obtained in creep test conducted at 32 MPa at 1200°C in steam. Creep lifetime $t_f = 0.02$ h.....	203
300. SEM micrograph of the fracture surface of the N720/AM specimen with $\pm 45^\circ$ fiber orientation obtained in creep test conducted at 32 MPa at 1200°C in steam. Creep lifetime $t_f = 0.02$ h.....	204

Figure	Page
301. SEM micrograph of the fracture surface of the N720/AM specimen with $\pm 45^\circ$ fiber orientation obtained in creep test conducted at 32 MPa at 1200°C in steam. Creep lifetime $t_f = 0.02$ h.....	204
302. SEM micrograph of the fracture surface of the N720/AM specimen with $\pm 45^\circ$ fiber orientation obtained in creep test conducted at 32 MPa at 1200°C in steam. Creep lifetime $t_f = 0.02$ h.....	205
303. SEM micrograph of the fracture surface of the N720/AM specimen with $\pm 45^\circ$ fiber orientation obtained in creep test conducted at 32 MPa at 1200°C in steam. Creep lifetime $t_f = 0.02$ h.....	205
304. SEM micrograph of the fracture surface of the N720/AM specimen with $\pm 45^\circ$ fiber orientation obtained in creep test conducted at 32 MPa at 1200°C in steam. Creep lifetime $t_f = 0.02$ h.....	206
305. SEM micrograph of the fracture surface of the N720/AM specimen with $\pm 45^\circ$ fiber orientation obtained in creep test conducted at 32 MPa at 1200°C in steam. Creep lifetime $t_f = 0.02$ h.....	206
306. SEM micrograph of the fracture surface of the N720/AM specimen with $\pm 45^\circ$ fiber orientation obtained in creep test conducted at 32 MPa at 1200°C in steam. Creep lifetime $t_f = 0.02$ h.....	207
307. SEM micrograph of the fracture surface of the N720/AM specimen with $\pm 45^\circ$ fiber orientation obtained in creep test conducted at 32 MPa at 1200°C in steam. Creep lifetime $t_f = 0.02$ h.....	207
308. SEM micrograph of the fracture surface of the N720/AM specimen with $\pm 45^\circ$ fiber orientation obtained in creep test conducted at 32 MPa at 1200°C in steam. Creep lifetime $t_f = 0.02$ h.....	208
309. SEM micrograph of the fracture surface of the N720/AM specimen subjected to tensile test to failure following 100 h at 20 MPa at 1200°C in argon.....	208
310. SEM micrograph of the fracture surface of the N720/AM specimen subjected to tensile test to failure following 100 h at 20 MPa at 1200°C in argon.....	209
311. SEM micrograph of the fracture surface of the N720/AM specimen subjected to tensile test to failure following 100 h at 20 MPa at 1200°C in argon.....	209

Figure	Page
312. SEM micrograph of the fracture surface of the N720/AM specimen subjected to tensile test to failure following 100 h at 20 MPa at 1200°C in argon.....	210
313. SEM micrograph of the fracture surface of the N720/AM specimen subjected to tensile test to failure following 100 h at 20 MPa at 1200°C in argon.....	210
314. SEM micrograph of the fracture surface of the N720/AM specimen subjected to tensile test to failure following 100 h at 20 MPa at 1200°C in argon.....	211
315. SEM micrograph of the fracture surface of the N720/AM specimen subjected to tensile test to failure following 100 h at 20 MPa at 1200°C in argon.....	211
316. SEM micrograph of the fracture surface of the N720/AM specimen subjected to tensile test to failure following 100 h at 20 MPa at 1200°C in argon.....	212
317. SEM micrograph of the fracture surface of the N720/AM specimen subjected to tensile test to failure following 100 h at 20 MPa at 1200°C in argon.....	212
318. SEM micrograph of the fracture surface of the N720/AM specimen subjected to tensile test to failure following 100 h at 20 MPa at 1200°C in argon.....	213
319. SEM micrograph of the fracture surface of the N720/AM specimen subjected to tensile test to failure following 100 h at 20 MPa at 1200°C in argon.....	213
320. SEM micrograph of the fracture surface of the N720/AM specimen subjected to tensile test to failure following 100 h at 20 MPa at 1200°C in argon.....	214
321. SEM micrograph of the fracture surface of the N720/AM specimen subjected to tensile test to failure following 100 h at 20 MPa at 1200°C in argon.....	214
322. SEM micrograph of the fracture surface of the N720/AM specimen subjected to tensile test to failure following 100 h at 20 MPa at 1200°C in argon.....	215
323. SEM micrograph of the fracture surface of the N720/AM specimen subjected to tensile test to failure following 100 h at 20 MPa at 1200°C in argon.....	215
324. SEM micrograph of the fracture surface of the N720/AM specimen subjected to tensile test to failure following 100 h at 20 MPa at 1200°C in argon.....	216
325. SEM micrograph of the fracture surface of the N720/AM specimen subjected to tensile test to failure following 100 h at 20 MPa at 1200°C in argon.....	216

Figure	Page
326. SEM micrograph of the fracture surface of the N720/AM specimen subjected to tensile test to failure following 100 h at 20 MPa at 1200°C in argon.....	217
327. SEM micrograph of the fracture surface of the N720/AM specimen subjected to tensile test to failure following 100 h at 20 MPa at 1200°C in argon.....	217
328. SEM micrograph of the fracture surface of the N720/AM specimen subjected to tensile test to failure following 100 h at 20 MPa at 1200°C in argon.....	218
329. SEM micrograph of the fracture surface of the N720/AM specimen subjected to tensile test to failure following 100 h at 20 MPa at 1200°C in argon.....	218
330. SEM micrograph of the fracture surface of the N720/AM specimen subjected to tensile test to failure following 100 h at 20 MPa at 1200°C in argon.....	219
331. SEM micrograph of the fracture surface of the N720/AM specimen subjected to tensile test to failure following 100 h at 20 MPa at 1200°C in argon.....	219
332. SEM micrograph of the fracture surface of the N720/AM specimen subjected to tensile test to failure following 100 h at 20 MPa at 1200°C in argon.....	220
333. SEM micrograph of the fracture surface of the N720/AM specimen subjected to tensile test to failure following 100 h at 20 MPa at 1200°C in argon.....	220
334. SEM micrograph of the fracture surface of the N720/AM specimen subjected to tensile test to failure following 100 h at 20 MPa at 1200°C in argon.....	221
335. SEM micrograph of the fracture surface of the N720/AM specimen subjected to tensile test to failure following 100 h at 20 MPa at 1200°C in argon.....	221
336. SEM micrograph of the fracture surface of the N720/AM specimen subjected to tensile test to failure following 100 h at 20 MPa at 1200°C in argon.....	222
337. SEM micrograph of the fracture surface of the N720/AM specimen subjected to tensile test to failure following 100 h at 20 MPa at 1200°C in argon.....	222
338. SEM micrograph of the fracture surface of the N720/AM specimen subjected to tensile test to failure following 100 h at 20 MPa at 1200°C in argon.....	223
339. SEM micrograph of the fracture surface of the N720/AM specimen subjected to tensile test to failure following 100 h at 20 MPa at 1200°C in argon.....	223

Figure	Page
340. SEM micrograph of the fracture surface of the N720/AM specimen subjected to tensile test to failure following 100 h at 20 MPa at 1200°C in argon.....	224
341. SEM micrograph of the fracture surface of the N720/AM specimen subjected to tensile test to failure following 100 h at 20 MPa at 1200°C in argon.....	224
342. SEM micrograph of the fracture surface of the N720/AM specimen subjected to tensile test to failure following 100 h at 20 MPa at 1200°C in argon.....	225
343. SEM micrograph of the fracture surface of the N720/AM specimen subjected to tensile test to failure following 100 h at 20 MPa at 1200°C in argon.....	225
344. SEM micrograph of the fracture surface of the N720/AM specimen subjected to tensile test to failure following 100 h at 20 MPa at 1200°C in argon.....	226
345. SEM micrograph of the fracture surface of the N720/AM specimen subjected to tensile test to failure following 100 h at 20 MPa at 1200°C in argon.....	226
346. SEM micrograph of the fracture surface of the N720/AM specimen subjected to tensile test to failure following 100 h at 20 MPa at 1200°C in argon.....	227
347. SEM micrograph of the fracture surface of the N720/AM specimen subjected to tensile test to failure following 100 h at 20 MPa at 1200°C in argon.....	227
348. SEM micrograph of the fracture surface of the N720/AM specimen subjected to tensile test to failure following 100 h at 20 MPa at 1200°C in argon.....	228
349. SEM micrograph of the fracture surface of the N720/AM specimen subjected to tensile test to failure following 100 h at 20 MPa at 1200°C in argon.....	228
350. SEM micrograph of the fracture surface of the N720/AM specimen subjected to tensile test to failure following 100 h at 20 MPa at 1200°C in argon.....	229
351. SEM micrograph of the fracture surface of the N720/AM specimen subjected to tensile test to failure following 100 h at 20 MPa at 1200°C in argon.....	229
352. SEM micrograph of the fracture surface of the N720/AM specimen subjected to tensile test to failure following 100 h at 20 MPa at 1200°C in argon.....	230
353. SEM micrograph of the fracture surface of the N720/AM specimen subjected to tensile test to failure following 100 h at 20 MPa at 1200°C in argon.....	230

Figure	Page
354. SEM micrograph of the fracture surface of the N720/AM specimen subjected to tensile test to failure following 100 h at 20 MPa at 1200°C in argon.....	231
355. SEM micrograph of the fracture surface of the N720/AM specimen subjected to tensile test to failure following 100 h at 20 MPa at 1200°C in argon.....	231
356. SEM micrograph of the fracture surface of the N720/AM specimen subjected to tensile test to failure following 100 h at 20 MPa at 1200°C in argon.....	232
357. SEM micrograph of the fracture surface of the N720/AM specimen subjected to tensile test to failure following 100 h at 20 MPa at 1200°C in argon.....	232
358. SEM micrograph of the fracture surface of the N720/AM specimen subjected to tensile test to failure following 100 h at 20 MPa at 1200°C in argon.....	233
359. SEM micrograph of the fracture surface of the N720/AM specimen subjected to tensile test to failure following 100 h at 20 MPa at 1200°C in argon.....	233
360. SEM micrograph of the fracture surface of the N720/AM specimen subjected to tensile test to failure following 100 h at 20 MPa at 1200°C in argon.....	234
361. SEM micrograph of the fracture surface of the N720/AM specimen subjected to tensile test to failure following 100 h at 20 MPa at 1200°C in argon.....	234
362. SEM micrograph of the fracture surface of the N720/AM specimen subjected to tensile test to failure following 100 h at 20 MPa at 1200°C in argon.....	235
363. SEM micrograph of the fracture surface of the N720/AM specimen subjected to tensile test to failure following 100 h at 20 MPa at 1200°C in argon.....	235
364. SEM micrograph of the fracture surface of the N720/AM specimen subjected to tensile test to failure following 100 h at 20 MPa at 1200°C in argon.....	236
365. SEM micrograph of the fracture surface of the N720/AM specimen with $\pm 45^\circ$ fiber orientation obtained in creep test conducted at 30 MPa at 1200°C in argon. Creep lifetime $t_f = 3.42$ h.....	236
366. SEM micrograph of the fracture surface of the N720/AM specimen with $\pm 45^\circ$ fiber orientation obtained in creep test conducted at 30 MPa at 1200°C in argon. Creep lifetime $t_f = 3.42$ h.....	237

Figure	Page
367. SEM micrograph of the fracture surface of the N720/AM specimen with $\pm 45^\circ$ fiber orientation obtained in creep test conducted at 30 MPa at 1200°C in argon. Creep lifetime $t_f = 3.42$ h.....	237
368. SEM micrograph of the fracture surface of the N720/AM specimen with $\pm 45^\circ$ fiber orientation obtained in creep test conducted at 30 MPa at 1200°C in argon. Creep lifetime $t_f = 3.42$ h.....	238
369. SEM micrograph of the fracture surface of the N720/AM specimen with $\pm 45^\circ$ fiber orientation obtained in creep test conducted at 30 MPa at 1200°C in argon. Creep lifetime $t_f = 3.42$ h.....	238
370. SEM micrograph of the fracture surface of the N720/AM specimen with $\pm 45^\circ$ fiber orientation obtained in creep test conducted at 30 MPa at 1200°C in argon. Creep lifetime $t_f = 3.42$ h.....	239
371. SEM micrograph of the fracture surface of the N720/AM specimen with $\pm 45^\circ$ fiber orientation obtained in creep test conducted at 30 MPa at 1200°C in argon. Creep lifetime $t_f = 3.42$ h.....	239
372. SEM micrograph of the fracture surface of the N720/AM specimen with $\pm 45^\circ$ fiber orientation obtained in creep test conducted at 30 MPa at 1200°C in argon. Creep lifetime $t_f = 3.42$ h.....	240
373. SEM micrograph of the fracture surface of the N720/AM specimen with $\pm 45^\circ$ fiber orientation obtained in creep test conducted at 30 MPa at 1200°C in argon. Creep lifetime $t_f = 3.42$ h.....	240
374. SEM micrograph of the fracture surface of the N720/AM specimen with $\pm 45^\circ$ fiber orientation obtained in creep test conducted at 30 MPa at 1200°C in argon. Creep lifetime $t_f = 3.42$ h.....	241
375. SEM micrograph of the fracture surface of the N720/AM specimen with $\pm 45^\circ$ fiber orientation obtained in creep test conducted at 30 MPa at 1200°C in argon. Creep lifetime $t_f = 3.42$ h.....	241
376. SEM micrograph of the fracture surface of the N720/AM specimen with $\pm 45^\circ$ fiber orientation obtained in creep test conducted at 30 MPa at 1200°C in argon. Creep lifetime $t_f = 3.42$ h.....	242

Figure	Page
377. SEM micrograph of the fracture surface of the N720/AM specimen with $\pm 45^\circ$ fiber orientation obtained in creep test conducted at 30 MPa at 1200°C in argon. Creep lifetime $t_f = 3.42$ h.....	242
378. SEM micrograph of the fracture surface of the N720/AM specimen with $\pm 45^\circ$ fiber orientation obtained in creep test conducted at 30 MPa at 1200°C in argon. Creep lifetime $t_f = 3.42$ h.....	243
379. SEM micrograph of the fracture surface of the N720/AM specimen with $\pm 45^\circ$ fiber orientation obtained in creep test conducted at 30 MPa at 1200°C in argon. Creep lifetime $t_f = 3.42$ h.....	243
380. SEM micrograph of the fracture surface of the N720/AM specimen with $\pm 45^\circ$ fiber orientation obtained in creep test conducted at 30 MPa at 1200°C in argon. Creep lifetime $t_f = 3.42$ h.....	244
381. SEM micrograph of the fracture surface of the N720/AM specimen with $\pm 45^\circ$ fiber orientation obtained in creep test conducted at 30 MPa at 1200°C in argon. Creep lifetime $t_f = 3.42$ h.....	244
382. SEM micrograph of the fracture surface of the N720/AM specimen with $\pm 45^\circ$ fiber orientation obtained in creep test conducted at 30 MPa at 1200°C in argon. Creep lifetime $t_f = 3.42$ h.....	245
383. SEM micrograph of the fracture surface of the N720/AM specimen with $\pm 45^\circ$ fiber orientation obtained in creep test conducted at 30 MPa at 1200°C in argon. Creep lifetime $t_f = 3.42$ h.....	245
384. SEM micrograph of the fracture surface of the N720/AM specimen with $\pm 45^\circ$ fiber orientation obtained in creep test conducted at 30 MPa at 1200°C in argon. Creep lifetime $t_f = 3.42$ h.....	246
385. SEM micrograph of the fracture surface of the N720/AM specimen with $\pm 45^\circ$ fiber orientation obtained in creep test conducted at 30 MPa at 1200°C in argon. Creep lifetime $t_f = 3.42$ h.....	246
386. SEM micrograph of the fracture surface of the N720/AM specimen with $\pm 45^\circ$ fiber orientation obtained in creep test conducted at 30 MPa at 1200°C in argon. Creep lifetime $t_f = 3.42$ h.....	247

Figure	Page
387. SEM micrograph of the fracture surface of the N720/AM specimen with $\pm 45^\circ$ fiber orientation obtained in creep test conducted at 30 MPa at 1200°C in argon. Creep lifetime $t_f = 3.42$ h.....	247
388. SEM micrograph of the fracture surface of the N720/AM specimen with $\pm 45^\circ$ fiber orientation obtained in creep test conducted at 30 MPa at 1200°C in argon. Creep lifetime $t_f = 3.42$ h.....	248
389. SEM micrograph of the fracture surface of the N720/AM specimen with $\pm 45^\circ$ fiber orientation obtained in creep test conducted at 30 MPa at 1200°C in argon. Creep lifetime $t_f = 3.42$ h.....	248
390. SEM micrograph of the fracture surface of the N720/AM specimen with $\pm 45^\circ$ fiber orientation obtained in creep test conducted at 30 MPa at 1200°C in argon. Creep lifetime $t_f = 3.42$ h.....	249
391. SEM micrograph of the fracture surface of the N720/AM specimen with $\pm 45^\circ$ fiber orientation obtained in creep test conducted at 30 MPa at 1200°C in argon. Creep lifetime $t_f = 3.42$ h.....	249
392. SEM micrograph of the fracture surface of the N720/AM specimen with $\pm 45^\circ$ fiber orientation obtained in creep test conducted at 30 MPa at 1200°C in argon. Creep lifetime $t_f = 3.42$ h.....	250
393. SEM micrograph of the fracture surface of the N720/AM specimen with $\pm 45^\circ$ fiber orientation obtained in creep test conducted at 30 MPa at 1200°C in argon. Creep lifetime $t_f = 3.42$ h.....	250
394. SEM micrograph of the fracture surface of the N720/AM specimen with $\pm 45^\circ$ fiber orientation obtained in creep test conducted at 30 MPa at 1200°C in argon. Creep lifetime $t_f = 3.42$ h.....	251
395. SEM micrograph of the fracture surface of the N720/AM specimen with $\pm 45^\circ$ fiber orientation obtained in creep test conducted at 30 MPa at 1200°C in argon. Creep lifetime $t_f = 3.42$ h.....	251
396. SEM micrograph of the fracture surface of the N720/AM specimen with $\pm 45^\circ$ fiber orientation obtained in creep test conducted at 30 MPa at 1200°C in argon. Creep lifetime $t_f = 3.42$ h.....	252

Figure	Page
397. SEM micrograph of the fracture surface of the N720/AM specimen with $\pm 45^\circ$ fiber orientation obtained in creep test conducted at 30 MPa at 1200°C in argon. Creep lifetime $t_f = 3.42$ h.....	252
398. SEM micrograph of the fracture surface of the N720/AM specimen with $\pm 45^\circ$ fiber orientation obtained in creep test conducted at 30 MPa at 1200°C in argon. Creep lifetime $t_f = 3.42$ h.....	253
399. SEM micrograph of the fracture surface of the N720/AM specimen with $\pm 45^\circ$ fiber orientation obtained in creep test conducted at 30 MPa at 1200°C in argon. Creep lifetime $t_f = 3.42$ h.....	253
400. SEM micrograph of the fracture surface of the N720/AM specimen with $\pm 45^\circ$ fiber orientation obtained in creep test conducted at 30 MPa at 1200°C in argon. Creep lifetime $t_f = 3.42$ h.....	254
401. SEM micrograph of the fracture surface of the N720/AM specimen with $\pm 45^\circ$ fiber orientation obtained in creep test conducted at 30 MPa at 1200°C in argon. Creep lifetime $t_f = 3.42$ h.....	254
402. SEM micrograph of the fracture surface of the N720/AM specimen with $\pm 45^\circ$ fiber orientation obtained in creep test conducted at 30 MPa at 1200°C in argon. Creep lifetime $t_f = 3.42$ h.....	255
403. SEM micrograph of the fracture surface of the N720/AM specimen with $\pm 45^\circ$ fiber orientation obtained in creep test conducted at 30 MPa at 1200°C in argon. Creep lifetime $t_f = 3.42$ h.....	255
404. SEM micrograph of the fracture surface of the N720/AM specimen with $\pm 45^\circ$ fiber orientation obtained in creep test conducted at 30 MPa at 1200°C in argon. Creep lifetime $t_f = 3.42$ h.....	256
405. SEM micrograph of the fracture surface of the N720/AM specimen with $\pm 45^\circ$ fiber orientation obtained in creep test conducted at 30 MPa at 1200°C in argon. Creep lifetime $t_f = 3.42$ h.....	256
406. SEM micrograph of the fracture surface of the N720/AM specimen with $\pm 45^\circ$ fiber orientation obtained in creep test conducted at 30 MPa at 1200°C in argon. Creep lifetime $t_f = 3.42$ h.....	257

Figure	Page
407. SEM micrograph of the fracture surface of the N720/AM specimen with $\pm 45^\circ$ fiber orientation obtained in creep test conducted at 30 MPa at 1200°C in argon. Creep lifetime $t_f = 3.42$ h.....	257
408. SEM micrograph of the fracture surface of the N720/AM specimen with $\pm 45^\circ$ fiber orientation obtained in creep test conducted at 30 MPa at 1200°C in argon. Creep lifetime $t_f = 3.42$ h.....	258
409. SEM micrograph of the fracture surface of the N720/AM specimen with $\pm 45^\circ$ fiber orientation obtained in creep test conducted at 30 MPa at 1200°C in argon. Creep lifetime $t_f = 3.42$ h.....	258
410. SEM micrograph of the fracture surface of the N720/AM specimen with $\pm 45^\circ$ fiber orientation obtained in creep test conducted at 30 MPa at 1200°C in argon. Creep lifetime $t_f = 3.42$ h.....	259
411. SEM micrograph of the fracture surface of the N720/AM specimen with $\pm 45^\circ$ fiber orientation obtained in creep test conducted at 30 MPa at 1200°C in argon. Creep lifetime $t_f = 3.42$ h.....	259
412. SEM micrograph of the fracture surface of the N720/AM specimen with $\pm 45^\circ$ fiber orientation obtained in creep test conducted at 30 MPa at 1200°C in argon. Creep lifetime $t_f = 3.42$ h.....	260
413. SEM micrograph of the fracture surface of the N720/AM specimen with $\pm 45^\circ$ fiber orientation obtained in creep test conducted at 30 MPa at 1200°C in argon. Creep lifetime $t_f = 3.42$ h.....	260
414. SEM micrograph of the fracture surface of the N720/AM specimen with $\pm 45^\circ$ fiber orientation obtained in creep test conducted at 30 MPa at 1200°C in argon. Creep lifetime $t_f = 3.42$ h.....	261
415. SEM micrograph of the fracture surface of the N720/AM specimen with $\pm 45^\circ$ fiber orientation obtained in creep test conducted at 30 MPa at 1200°C in argon. Creep lifetime $t_f = 3.42$ h.....	261
416. SEM micrograph of the fracture surface of the N720/AM specimen with $\pm 45^\circ$ fiber orientation obtained in creep test conducted at 30 MPa at 1200°C in argon. Creep lifetime $t_f = 3.42$ h.....	262

Figure	Page
417. SEM micrograph of the fracture surface of the N720/AM specimen with $\pm 45^\circ$ fiber orientation obtained in creep test conducted at 30 MPa at 1200°C in argon. Creep lifetime $t_f = 3.42$ h.....	262
418. SEM micrograph of the fracture surface of the N720/AM specimen with $\pm 45^\circ$ fiber orientation obtained in creep test conducted at 30 MPa at 1200°C in argon. Creep lifetime $t_f = 3.42$ h.....	263
419. SEM micrograph of the fracture surface of the N720/AM specimen with $\pm 45^\circ$ fiber orientation obtained in creep test conducted at 30 MPa at 1200°C in argon. Creep lifetime $t_f = 3.42$ h.....	263
420. SEM micrograph of the fracture surface of the N720/AM specimen with $\pm 45^\circ$ fiber orientation obtained in creep test conducted at 30 MPa at 1200°C in argon. Creep lifetime $t_f = 3.42$ h.....	264
421. SEM micrograph of the fracture surface of the N720/AM specimen with $\pm 45^\circ$ fiber orientation obtained in creep test conducted at 30 MPa at 1200°C in argon. Creep lifetime $t_f = 3.42$ h.....	264
422. SEM micrograph of the fracture surface of the N720/AM specimen with $\pm 45^\circ$ fiber orientation obtained in creep test conducted at 30 MPa at 1200°C in argon. Creep lifetime $t_f = 3.42$ h.....	265
423. SEM micrograph of the fracture surface of the N720/AM specimen with $\pm 45^\circ$ fiber orientation obtained in creep test conducted at 30 MPa at 1200°C in argon. Creep lifetime $t_f = 3.42$ h.....	265
424. SEM micrograph of the fracture surface of the N720/AM specimen with $\pm 45^\circ$ fiber orientation obtained in creep test conducted at 30 MPa at 1200°C in argon. Creep lifetime $t_f = 3.42$ h.....	266
425. SEM micrograph of the fracture surface of the N720/AM specimen with $\pm 45^\circ$ fiber orientation obtained in creep test conducted at 30 MPa at 1200°C in argon. Creep lifetime $t_f = 3.42$ h.....	266
426. SEM micrograph of the fracture surface of the N720/AM specimen with $\pm 45^\circ$ fiber orientation obtained in creep test conducted at 30 MPa at 1200°C in argon. Creep lifetime $t_f = 3.42$ h.....	267

Figure	Page
427. SEM micrograph of the fracture surface of the N720/AM specimen with $\pm 45^\circ$ fiber orientation obtained in creep test conducted at 32 MPa at 1200°C in argon. Creep lifetime $t_f = 0.08$ h.....	267
428. SEM micrograph of the fracture surface of the N720/AM specimen with $\pm 45^\circ$ fiber orientation obtained in creep test conducted at 32 MPa at 1200°C in argon. Creep lifetime $t_f = 0.08$ h.....	268
429. SEM micrograph of the fracture surface of the N720/AM specimen with $\pm 45^\circ$ fiber orientation obtained in creep test conducted at 32 MPa at 1200°C in argon. Creep lifetime $t_f = 0.08$ h.....	268
430. SEM micrograph of the fracture surface of the N720/AM specimen with $\pm 45^\circ$ fiber orientation obtained in creep test conducted at 32 MPa at 1200°C in argon. Creep lifetime $t_f = 0.08$ h.....	269
431. SEM micrograph of the fracture surface of the N720/AM specimen with $\pm 45^\circ$ fiber orientation obtained in creep test conducted at 32 MPa at 1200°C in argon. Creep lifetime $t_f = 0.08$ h.....	269
432. SEM micrograph of the fracture surface of the N720/AM specimen with $\pm 45^\circ$ fiber orientation obtained in creep test conducted at 32 MPa at 1200°C in argon. Creep lifetime $t_f = 0.08$ h.....	270
433. SEM micrograph of the fracture surface of the N720/AM specimen with $\pm 45^\circ$ fiber orientation obtained in creep test conducted at 32 MPa at 1200°C in argon. Creep lifetime $t_f = 0.08$ h.....	270
434. SEM micrograph of the fracture surface of the N720/AM specimen with $\pm 45^\circ$ fiber orientation obtained in creep test conducted at 32 MPa at 1200°C in argon. Creep lifetime $t_f = 0.08$ h.....	271
435. SEM micrograph of the fracture surface of the N720/AM specimen with $\pm 45^\circ$ fiber orientation obtained in creep test conducted at 32 MPa at 1200°C in argon. Creep lifetime $t_f = 0.08$ h.....	271
436. SEM micrograph of the fracture surface of the N720/AM specimen with $\pm 45^\circ$ fiber orientation obtained in creep test conducted at 32 MPa at 1200°C in argon. Creep lifetime $t_f = 0.08$ h.....	272

Figure	Page
437. SEM micrograph of the fracture surface of the N720/AM specimen with $\pm 45^\circ$ fiber orientation obtained in creep test conducted at 32 MPa at 1200°C in argon. Creep lifetime $t_f = 0.08$ h.....	272
438. SEM micrograph of the fracture surface of the N720/AM specimen with $\pm 45^\circ$ fiber orientation obtained in creep test conducted at 32 MPa at 1200°C in argon. Creep lifetime $t_f = 0.08$ h.....	273
439. SEM micrograph of the fracture surface of the N720/AM specimen with $\pm 45^\circ$ fiber orientation obtained in creep test conducted at 32 MPa at 1200°C in argon. Creep lifetime $t_f = 0.08$ h.....	273
440. SEM micrograph of the fracture surface of the N720/AM specimen with $\pm 45^\circ$ fiber orientation obtained in creep test conducted at 32 MPa at 1200°C in argon. Creep lifetime $t_f = 0.08$ h.....	274
441. SEM micrograph of the fracture surface of the N720/AM specimen with $\pm 45^\circ$ fiber orientation obtained in creep test conducted at 32 MPa at 1200°C in argon. Creep lifetime $t_f = 0.08$ h.....	274
442. SEM micrograph of the fracture surface of the N720/AM specimen with $\pm 45^\circ$ fiber orientation obtained in creep test conducted at 32 MPa at 1200°C in argon. Creep lifetime $t_f = 0.08$ h.....	275
443. SEM micrograph of the fracture surface of the N720/AM specimen with $\pm 45^\circ$ fiber orientation obtained in creep test conducted at 32 MPa at 1200°C in argon. Creep lifetime $t_f = 0.08$ h.....	275
444. SEM micrograph of the fracture surface of the N720/AM specimen with $\pm 45^\circ$ fiber orientation obtained in creep test conducted at 32 MPa at 1200°C in argon. Creep lifetime $t_f = 0.08$ h.....	276
445. SEM micrograph of the fracture surface of the N720/AM specimen with $\pm 45^\circ$ fiber orientation obtained in creep test conducted at 32 MPa at 1200°C in argon. Creep lifetime $t_f = 0.08$ h.....	276
446. SEM micrograph of the fracture surface of the N720/AM specimen with $\pm 45^\circ$ fiber orientation obtained in creep test conducted at 32 MPa at 1200°C in argon. Creep lifetime $t_f = 0.08$ h.....	277

Figure	Page
447. SEM micrograph of the fracture surface of the N720/AM specimen with $\pm 45^\circ$ fiber orientation obtained in creep test conducted at 32 MPa at 1200°C in argon. Creep lifetime $t_f = 0.08$ h.....	277
448. SEM micrograph of the fracture surface of the N720/AM specimen with $\pm 45^\circ$ fiber orientation obtained in creep test conducted at 32 MPa at 1200°C in argon. Creep lifetime $t_f = 0.08$ h.....	278
449. SEM micrograph of the fracture surface of the N720/AM specimen with $\pm 45^\circ$ fiber orientation obtained in creep test conducted at 32 MPa at 1200°C in argon. Creep lifetime $t_f = 0.08$ h.....	278
450. SEM micrograph of the fracture surface of the N720/AM specimen with $\pm 45^\circ$ fiber orientation obtained in creep test conducted at 32 MPa at 1200°C in argon. Creep lifetime $t_f = 0.08$ h.....	279
451. SEM micrograph of the fracture surface of the N720/AM specimen with $\pm 45^\circ$ fiber orientation obtained in creep test conducted at 32 MPa at 1200°C in argon. Creep lifetime $t_f = 0.08$ h.....	279
452. SEM micrograph of the fracture surface of the N720/AM specimen with $\pm 45^\circ$ fiber orientation obtained in creep test conducted at 32 MPa at 1200°C in argon. Creep lifetime $t_f = 0.08$ h.....	280
453. SEM micrograph of the fracture surface of the N720/AM specimen with $\pm 45^\circ$ fiber orientation obtained in creep test conducted at 32 MPa at 1200°C in argon. Creep lifetime $t_f = 0.08$ h.....	280
454. SEM micrograph of the fracture surface of the N720/AM specimen with $\pm 45^\circ$ fiber orientation obtained in creep test conducted at 32 MPa at 1200°C in argon. Creep lifetime $t_f = 0.08$ h.....	281
455. SEM micrograph of the fracture surface of the N720/AM specimen with $\pm 45^\circ$ fiber orientation obtained in creep test conducted at 32 MPa at 1200°C in argon. Creep lifetime $t_f = 0.08$ h.....	281
456. SEM micrograph of the fracture surface of the N720/AM specimen with $\pm 45^\circ$ fiber orientation obtained in creep test conducted at 32 MPa at 1200°C in argon. Creep lifetime $t_f = 0.08$ h.....	282

Figure	Page
457. SEM micrograph of the fracture surface of the N720/AM specimen with $\pm 45^\circ$ fiber orientation obtained in creep test conducted at 32 MPa at 1200°C in argon. Creep lifetime $t_f = 0.08$ h.....	282
458. SEM micrograph of the fracture surface of the N720/AM specimen with $\pm 45^\circ$ fiber orientation obtained in creep test conducted at 32 MPa at 1200°C in argon. Creep lifetime $t_f = 0.08$ h.....	283
459. SEM micrograph of the fracture surface of the N720/AM specimen with $\pm 45^\circ$ fiber orientation obtained in creep test conducted at 32 MPa at 1200°C in argon. Creep lifetime $t_f = 0.08$ h.....	283
460. SEM micrograph of the fracture surface of the N720/AM specimen with $\pm 45^\circ$ fiber orientation obtained in creep test conducted at 32 MPa at 1200°C in argon. Creep lifetime $t_f = 0.08$ h.....	284
461. SEM micrograph of the fracture surface of the N720/AM specimen with $\pm 45^\circ$ fiber orientation obtained in creep test conducted at 32 MPa at 1200°C in argon. Creep lifetime $t_f = 0.08$ h.....	284
462. SEM micrograph of the fracture surface of the N720/AM specimen with $\pm 45^\circ$ fiber orientation obtained in creep test conducted at 32 MPa at 1200°C in argon. Creep lifetime $t_f = 0.08$ h.....	285
463. SEM micrograph of the fracture surface of the N720/AM specimen with $\pm 45^\circ$ fiber orientation obtained in creep test conducted at 32 MPa at 1200°C in argon. Creep lifetime $t_f = 0.08$ h.....	285
464. SEM micrograph of the fracture surface of the N720/AM specimen with $\pm 45^\circ$ fiber orientation obtained in creep test conducted at 32 MPa at 1200°C in argon. Creep lifetime $t_f = 0.08$ h.....	286
465. SEM micrograph of the fracture surface of the N720/AM specimen with $\pm 45^\circ$ fiber orientation obtained in creep test conducted at 32 MPa at 1200°C in argon. Creep lifetime $t_f = 0.08$ h.....	286
466. SEM micrograph of the fracture surface of the N720/AM specimen with $\pm 45^\circ$ fiber orientation obtained in creep test conducted at 32 MPa at 1200°C in argon. Creep lifetime $t_f = 0.08$ h.....	287

Figure	Page
467. SEM micrograph of the fracture surface of the N720/AM specimen with $\pm 45^\circ$ fiber orientation obtained in creep test conducted at 32 MPa at 1200°C in argon. Creep lifetime $t_f = 0.08$ h.....	287
468. SEM micrograph of the fracture surface of the N720/AM specimen with $\pm 45^\circ$ fiber orientation obtained in creep test conducted at 32 MPa at 1200°C in argon. Creep lifetime $t_f = 0.08$ h.....	288
469. SEM micrograph of the fracture surface of the N720/AM specimen with $\pm 45^\circ$ fiber orientation obtained in creep test conducted at 32 MPa at 1200°C in argon. Creep lifetime $t_f = 0.08$ h.....	288
470. SEM micrograph of the fracture surface of the N720/AM specimen with $\pm 45^\circ$ fiber orientation obtained in creep test conducted at 32 MPa at 1200°C in argon. Creep lifetime $t_f = 0.08$ h.....	289
471. SEM micrograph of the fracture surface of the N720/AM specimen with $\pm 45^\circ$ fiber orientation obtained in creep test conducted at 32 MPa at 1200°C in argon. Creep lifetime $t_f = 0.08$ h.....	289
472. SEM micrograph of the fracture surface of the N720/AM specimen with $\pm 45^\circ$ fiber orientation obtained in creep test conducted at 32 MPa at 1200°C in argon. Creep lifetime $t_f = 0.08$ h.....	290
473. SEM micrograph of the fracture surface of the N720/AM specimen subjected to tensile test to failure with a constant stress rate of 0.0025 MPa/s at 1200°C in laboratory air.....	290
474. SEM micrograph of the fracture surface of the N720/AM specimen subjected to tensile test to failure with a constant stress rate of 0.0025 MPa/s at 1200°C in laboratory air.....	291
475. SEM micrograph of the fracture surface of the N720/AM specimen subjected to tensile test to failure with a constant stress rate of 0.0025 MPa/s at 1200°C in laboratory air.....	291
476. SEM micrograph of the fracture surface of the N720/AM specimen subjected to tensile test to failure with a constant stress rate of 0.0025 MPa/s at 1200°C in laboratory air.....	292

Figure	Page
477. SEM micrograph of the fracture surface of the N720/AM specimen subjected to tensile test to failure with a constant stress rate of 0.0025 MPa/s at 1200°C in laboratory air.....	292
478. SEM micrograph of the fracture surface of the N720/AM specimen subjected to tensile test to failure with a constant stress rate of 0.0025 MPa/s at 1200°C in laboratory air.....	293
479. SEM micrograph of the fracture surface of the N720/AM specimen subjected to tensile test to failure with a constant stress rate of 0.0025 MPa/s at 1200°C in laboratory air.....	293
480. SEM micrograph of the fracture surface of the N720/AM specimen subjected to tensile test to failure with a constant stress rate of 0.0025 MPa/s at 1200°C in laboratory air.....	294
481. SEM micrograph of the fracture surface of the N720/AM specimen subjected to tensile test to failure with a constant stress rate of 0.0025 MPa/s at 1200°C in laboratory air.....	294
482. SEM micrograph of the fracture surface of the N720/AM specimen subjected to tensile test to failure with a constant stress rate of 0.0025 MPa/s at 1200°C in laboratory air.....	295
483. SEM micrograph of the fracture surface of the N720/AM specimen subjected to tensile test to failure with a constant stress rate of 0.0025 MPa/s at 1200°C in laboratory air.....	295
484. SEM micrograph of the fracture surface of the N720/AM specimen subjected to tensile test to failure with a constant stress rate of 0.0025 MPa/s at 1200°C in laboratory air.....	296
485. SEM micrograph of the fracture surface of the N720/AM specimen subjected to tensile test to failure with a constant stress rate of 0.0025 MPa/s at 1200°C in laboratory air.....	296
486. SEM micrograph of the fracture surface of the N720/AM specimen subjected to tensile test to failure with a constant stress rate of 0.0025 MPa/s at 1200°C in laboratory air.....	297

Figure	Page
487. SEM micrograph of the fracture surface of the N720/AM specimen subjected to tensile test to failure with a constant stress rate of 0.0025 MPa/s at 1200°C in laboratory air.....	297
488. SEM micrograph of the fracture surface of the N720/AM specimen subjected to tensile test to failure with a constant stress rate of 0.0025 MPa/s at 1200°C in laboratory air.....	298
489. SEM micrograph of the fracture surface of the N720/AM specimen subjected to tensile test to failure with a constant stress rate of 0.0025 MPa/s at 1200°C in laboratory air.....	298
490. SEM micrograph of the fracture surface of the N720/AM specimen subjected to tensile test to failure with a constant stress rate of 0.0025 MPa/s at 1200°C in laboratory air.....	299
491. SEM micrograph of the fracture surface of the N720/AM specimen subjected to tensile test to failure with a constant stress rate of 0.0025 MPa/s at 1200°C in laboratory air.....	299
492. SEM micrograph of the fracture surface of the N720/AM specimen subjected to tensile test to failure with a constant stress rate of 0.0025 MPa/s at 1200°C in laboratory air.....	300
493. SEM micrograph of the fracture surface of the N720/AM specimen subjected to tensile test to failure with a constant stress rate of 0.0025 MPa/s at 1200°C in laboratory air.....	300
494. SEM micrograph of the fracture surface of the N720/AM specimen subjected to tensile test to failure with a constant stress rate of 0.0025 MPa/s at 1200°C in laboratory air.....	301
495. SEM micrograph of the fracture surface of the N720/AM specimen subjected to tensile test to failure with a constant stress rate of 0.0025 MPa/s at 1200°C in laboratory air.....	301
496. SEM micrograph of the fracture surface of the N720/AM specimen subjected to tensile test to failure with a constant stress rate of 0.0025 MPa/s at 1200°C in laboratory air.....	302

Figure	Page
497. SEM micrograph of the fracture surface of the N720/AM specimen subjected to tensile test to failure with a constant stress rate of 0.0025 MPa/s at 1200°C in laboratory air.....	302
498. SEM micrograph of the fracture surface of the N720/AM specimen subjected to tensile test to failure with a constant stress rate of 0.0025 MPa/s at 1200°C in laboratory air.....	303
499. SEM micrograph of the fracture surface of the N720/AM specimen subjected to tensile test to failure with a constant stress rate of 0.0025 MPa/s at 1200°C in laboratory air.....	303
500. SEM micrograph of the fracture surface of the N720/AM specimen subjected to tensile test to failure with a constant stress rate of 0.0025 MPa/s at 1200°C in laboratory air.....	304
501. SEM micrograph of the fracture surface of the N720/AM specimen subjected to tensile test to failure with a constant stress rate of 0.0025 MPa/s at 1200°C in laboratory air.....	304
502. SEM micrograph of the fracture surface of the N720/AM specimen subjected to tensile test to failure with a constant stress rate of 0.0025 MPa/s at 1200°C in laboratory air.....	305
503. SEM micrograph of the fracture surface of the N720/AM specimen subjected to tensile test to failure with a constant stress rate of 0.0025 MPa/s at 1200°C in laboratory air.....	305
504. SEM micrograph of the fracture surface of the N720/AM specimen subjected to tensile test to failure with a constant stress rate of 0.0025 MPa/s at 1200°C in laboratory air.....	306
505. SEM micrograph of the fracture surface of the N720/AM specimen subjected to tensile test to failure with a constant stress rate of 0.0025 MPa/s at 1200°C in laboratory air.....	306
506. SEM micrograph of the fracture surface of the N720/AM specimen subjected to tensile test to failure with a constant stress rate of 0.0025 MPa/s at 1200°C in laboratory air.....	307

Figure	Page
507. SEM micrograph of the fracture surface of the N720/AM specimen subjected to tensile test to failure with a constant stress rate of 0.0025 MPa/s at 1200°C in laboratory air.....	307
508. SEM micrograph of the fracture surface of the N720/AM specimen subjected to tensile test to failure with a constant stress rate of 0.0025 MPa/s at 1200°C in laboratory air.....	308
509. SEM micrograph of the fracture surface of the N720/AM specimen subjected to tensile test to failure with a constant stress rate of 0.0025 MPa/s at 1200°C in laboratory air.....	308
510. SEM micrograph of the fracture surface of the N720/AM specimen subjected to tensile test to failure with a constant stress rate of 0.0025 MPa/s at 1200°C in laboratory air.....	309
511. SEM micrograph of the fracture surface of the N720/AM specimen subjected to tensile test to failure with a constant stress rate of 0.0025 MPa/s at 1200°C in laboratory air.....	309
512. SEM micrograph of the fracture surface of the N720/AM specimen subjected to tensile test to failure with a constant stress rate of 0.0025 MPa/s at 1200°C in laboratory air.....	310
513. SEM micrograph of the fracture surface of the N720/AM specimen subjected to tensile test to failure with a constant stress rate of 0.0025 MPa/s at 1200°C in laboratory air.....	310
514. SEM micrograph of the fracture surface of the N720/AM specimen subjected to tensile test to failure with a constant stress rate of 0.0025 MPa/s at 1200°C in laboratory air.....	311
515. SEM micrograph of the fracture surface of the N720/AM specimen subjected to tensile test to failure with a constant stress rate of 0.0025 MPa/s at 1200°C in steam.....	311
516. SEM micrograph of the fracture surface of the N720/AM specimen subjected to tensile test to failure with a constant stress rate of 0.0025 MPa/s at 1200°C in steam.....	312

Figure	Page
517. SEM micrograph of the fracture surface of the N720/AM specimen subjected to tensile test to failure with a constant stress rate of 0.0025 MPa/s at 1200°C in steam.....	312
518. SEM micrograph of the fracture surface of the N720/AM specimen subjected to tensile test to failure with a constant stress rate of 0.0025 MPa/s at 1200°C in steam.....	313
519. SEM micrograph of the fracture surface of the N720/AM specimen subjected to tensile test to failure with a constant stress rate of 0.0025 MPa/s at 1200°C in steam.....	313
520. SEM micrograph of the fracture surface of the N720/AM specimen subjected to tensile test to failure with a constant stress rate of 0.0025 MPa/s at 1200°C in steam.....	314
521. SEM micrograph of the fracture surface of the N720/AM specimen subjected to tensile test to failure with a constant stress rate of 0.0025 MPa/s at 1200°C in steam.....	314
522. SEM micrograph of the fracture surface of the N720/AM specimen subjected to tensile test to failure with a constant stress rate of 0.0025 MPa/s at 1200°C in steam.....	315
523. SEM micrograph of the fracture surface of the N720/AM specimen subjected to tensile test to failure with a constant stress rate of 0.0025 MPa/s at 1200°C in steam.....	315
524. SEM micrograph of the fracture surface of the N720/AM specimen subjected to tensile test to failure with a constant stress rate of 0.0025 MPa/s at 1200°C in steam.....	316
525. SEM micrograph of the fracture surface of the N720/AM specimen subjected to tensile test to failure with a constant stress rate of 0.0025 MPa/s at 1200°C in steam.....	316
526. SEM micrograph of the fracture surface of the N720/AM specimen subjected to tensile test to failure with a constant stress rate of 0.0025 MPa/s at 1200°C in steam.....	317

Figure	Page
527. SEM micrograph of the fracture surface of the N720/AM specimen subjected to tensile test to failure with a constant stress rate of 0.0025 MPa/s at 1200°C in steam.....	317
528. SEM micrograph of the fracture surface of the N720/AM specimen subjected to tensile test to failure with a constant stress rate of 0.0025 MPa/s at 1200°C in steam.....	318
529. SEM micrograph of the fracture surface of the N720/AM specimen subjected to tensile test to failure with a constant stress rate of 0.0025 MPa/s at 1200°C in steam.....	318
530. SEM micrograph of the fracture surface of the N720/AM specimen subjected to tensile test to failure with a constant stress rate of 0.0025 MPa/s at 1200°C in steam.....	319
531. SEM micrograph of the fracture surface of the N720/AM specimen subjected to tensile test to failure with a constant stress rate of 0.0025 MPa/s at 1200°C in steam.....	319
532. SEM micrograph of the fracture surface of the N720/AM specimen subjected to tensile test to failure with a constant stress rate of 0.0025 MPa/s at 1200°C in steam.....	320
533. SEM micrograph of the fracture surface of the N720/AM specimen subjected to tensile test to failure with a constant stress rate of 0.0025 MPa/s at 1200°C in steam.....	320
534. SEM micrograph of the fracture surface of the N720/AM specimen subjected to tensile test to failure with a constant stress rate of 0.0025 MPa/s at 1200°C in steam.....	321
535. SEM micrograph of the fracture surface of the N720/AM specimen subjected to tensile test to failure with a constant stress rate of 0.0025 MPa/s at 1200°C in steam.....	321
536. SEM micrograph of the fracture surface of the N720/AM specimen subjected to tensile test to failure with a constant stress rate of 0.0025 MPa/s at 1200°C in steam.....	322

Figure	Page
537. SEM micrograph of the fracture surface of the N720/AM specimen subjected to tensile test to failure with a constant stress rate of 0.0025 MPa/s at 1200°C in steam.....	322
538. SEM micrograph of the fracture surface of the N720/AM specimen subjected to tensile test to failure with a constant stress rate of 0.0025 MPa/s at 1200°C in steam.....	323
539. SEM micrograph of the fracture surface of the N720/AM specimen subjected to tensile test to failure with a constant stress rate of 0.0025 MPa/s at 1200°C in steam.....	323
540. SEM micrograph of the fracture surface of the N720/AM specimen subjected to tensile test to failure with a constant stress rate of 0.0025 MPa/s at 1200°C in steam.....	324
541. SEM micrograph of the fracture surface of the N720/AM specimen subjected to tensile test to failure with a constant stress rate of 0.0025 MPa/s at 1200°C in steam.....	324
542. SEM micrograph of the fracture surface of the N720/AM specimen subjected to tensile test to failure with a constant stress rate of 0.0025 MPa/s at 1200°C in steam.....	325
543. SEM micrograph of the fracture surface of the N720/AM specimen subjected to tensile test to failure with a constant stress rate of 0.0025 MPa/s at 1200°C in steam.....	325
544. SEM micrograph of the fracture surface of the N720/AM specimen subjected to tensile test to failure with a constant stress rate of 0.0025 MPa/s at 1200°C in steam.....	326
545. SEM micrograph of the fracture surface of the N720/AM specimen subjected to tensile test to failure with a constant stress rate of 0.0025 MPa/s at 1200°C in steam.....	326
546. SEM micrograph of the fracture surface of the N720/AM specimen subjected to tensile test to failure with a constant stress rate of 0.0025 MPa/s at 1200°C in steam.....	327

Figure	Page
547. SEM micrograph of the fracture surface of the N720/AM specimen subjected to tensile test to failure with a constant stress rate of 0.0025 MPa/s at 1200°C in steam.....	327
548. SEM micrograph of the fracture surface of the N720/AM specimen subjected to tensile test to failure with a constant stress rate of 0.0025 MPa/s at 1200°C in steam.....	328
549. SEM micrograph of the fracture surface of the N720/AM specimen subjected to tensile test to failure with a constant stress rate of 0.0025 MPa/s at 1200°C in steam.....	328
550. SEM micrograph of the fracture surface of the N720/AM specimen subjected to tensile test to failure with a constant stress rate of 0.0025 MPa/s at 1200°C in steam.....	329
551. SEM micrograph of the fracture surface of the N720/AM specimen subjected to tensile test to failure with a constant stress rate of 0.0025 MPa/s at 1200°C in steam.....	329
552. SEM micrograph of the fracture surface of the N720/AM specimen subjected to tensile test to failure with a constant stress rate of 0.0025 MPa/s at 1200°C in steam.....	330
553. SEM micrograph of the fracture surface of the N720/AM specimen subjected to tensile test to failure with a constant stress rate of 0.0025 MPa/s at 1200°C in steam.....	330
554. SEM micrograph of the fracture surface of the N720/AM specimen subjected to tensile test to failure with a constant stress rate of 0.0025 MPa/s at 1200°C in steam.....	331
555. SEM micrograph of the fracture surface of the N720/AM specimen subjected to tensile test to failure with a constant stress rate of 0.0025 MPa/s at 1200°C in steam.....	331
556. SEM micrograph of the fracture surface of the N720/AM specimen subjected to tensile test to failure with a constant stress rate of 0.0025 MPa/s at 1200°C in steam.....	332

Figure	Page
557. SEM micrograph of the fracture surface of the N720/AM specimen subjected to tensile test to failure with a constant stress rate of 0.0025 MPa/s at 1200°C in steam.....	332
558. SEM micrograph of the fracture surface of the N720/AM specimen subjected to tensile test to failure with a constant stress rate of 0.0025 MPa/s at 1200°C in steam.....	333
559. SEM micrograph of the fracture surface of the N720/AM specimen subjected to tensile test to failure with a constant stress rate of 0.0025 MPa/s at 1200°C in steam.....	333
560. SEM micrograph of the fracture surface of the N720/AM specimen subjected to tensile test to failure with a constant stress rate of 0.0025 MPa/s at 1200°C in steam.....	334
561. SEM micrograph of the fracture surface of the N720/AM specimen subjected to tensile test to failure with a constant stress rate of 0.0025 MPa/s at 1200°C in steam.....	334
562. SEM micrograph of the fracture surface of the N720/AM specimen subjected to tensile test to failure with a constant stress rate of 25 MPa/s at 1200°C in laboratory air.....	335
563. SEM micrograph of the fracture surface of the N720/AM specimen subjected to tensile test to failure with a constant stress rate of 25 MPa/s at 1200°C in laboratory air.....	335
564. SEM micrograph of the fracture surface of the N720/AM specimen subjected to tensile test to failure with a constant stress rate of 25 MPa/s at 1200°C in laboratory air.....	336
565. SEM micrograph of the fracture surface of the N720/AM specimen subjected to tensile test to failure with a constant stress rate of 25 MPa/s at 1200°C in laboratory air.....	336
566. SEM micrograph of the fracture surface of the N720/AM specimen subjected to tensile test to failure with a constant stress rate of 25 MPa/s at 1200°C in laboratory air.....	337

Figure	Page
567. SEM micrograph of the fracture surface of the N720/AM specimen subjected to tensile test to failure with a constant stress rate of 25 MPa/s at 1200°C in laboratory air.....	337
568. SEM micrograph of the fracture surface of the N720/AM specimen subjected to tensile test to failure with a constant stress rate of 25 MPa/s at 1200°C in laboratory air.....	338
569. SEM micrograph of the fracture surface of the N720/AM specimen subjected to tensile test to failure with a constant stress rate of 25 MPa/s at 1200°C in laboratory air.....	338
570. SEM micrograph of the fracture surface of the N720/AM specimen subjected to tensile test to failure with a constant stress rate of 25 MPa/s at 1200°C in laboratory air.....	339
571. SEM micrograph of the fracture surface of the N720/AM specimen subjected to tensile test to failure with a constant stress rate of 25 MPa/s at 1200°C in laboratory air.....	339
572. SEM micrograph of the fracture surface of the N720/AM specimen subjected to tensile test to failure with a constant stress rate of 25 MPa/s at 1200°C in laboratory air.....	340
573. SEM micrograph of the fracture surface of the N720/AM specimen subjected to tensile test to failure with a constant stress rate of 25 MPa/s at 1200°C in laboratory air.....	340
574. SEM micrograph of the fracture surface of the N720/AM specimen subjected to tensile test to failure with a constant stress rate of 25 MPa/s at 1200°C in laboratory air.....	341
575. SEM micrograph of the fracture surface of the N720/AM specimen subjected to tensile test to failure with a constant stress rate of 25 MPa/s at 1200°C in laboratory air.....	341
576. SEM micrograph of the fracture surface of the N720/AM specimen subjected to tensile test to failure with a constant stress rate of 25 MPa/s at 1200°C in laboratory air.....	342

Figure	Page
577. SEM micrograph of the fracture surface of the N720/AM specimen subjected to tensile test to failure with a constant stress rate of 25 MPa/s at 1200°C in laboratory air.....	342
578. SEM micrograph of the fracture surface of the N720/AM specimen subjected to tensile test to failure with a constant stress rate of 25 MPa/s at 1200°C in laboratory air.....	343
579. SEM micrograph of the fracture surface of the N720/AM specimen subjected to tensile test to failure with a constant stress rate of 25 MPa/s at 1200°C in laboratory air.....	343
580. SEM micrograph of the fracture surface of the N720/AM specimen subjected to tensile test to failure with a constant stress rate of 25 MPa/s at 1200°C in laboratory air.....	344
581. SEM micrograph of the fracture surface of the N720/AM specimen subjected to tensile test to failure with a constant stress rate of 25 MPa/s at 1200°C in laboratory air.....	344
582. SEM micrograph of the fracture surface of the N720/AM specimen subjected to tensile test to failure with a constant stress rate of 25 MPa/s at 1200°C in laboratory air.....	345
583. SEM micrograph of the fracture surface of the N720/AM specimen subjected to tensile test to failure with a constant stress rate of 25 MPa/s at 1200°C in laboratory air.....	345
584. SEM micrograph of the fracture surface of the N720/AM specimen subjected to tensile test to failure with a constant stress rate of 25 MPa/s at 1200°C in laboratory air.....	346
585. SEM micrograph of the fracture surface of the N720/AM specimen subjected to tensile test to failure with a constant stress rate of 25 MPa/s at 1200°C in laboratory air.....	346
586. SEM micrograph of the fracture surface of the N720/AM specimen subjected to tensile test to failure with a constant stress rate of 25 MPa/s at 1200°C in laboratory air.....	347

Figure	Page
587. SEM micrograph of the fracture surface of the N720/AM specimen subjected to tensile test to failure with a constant stress rate of 25 MPa/s at 1200°C in laboratory air.....	347
588. SEM micrograph of the fracture surface of the N720/AM specimen subjected to tensile test to failure with a constant stress rate of 25 MPa/s at 1200°C in laboratory air.....	348
589. SEM micrograph of the fracture surface of the N720/AM specimen subjected to tensile test to failure with a constant stress rate of 25 MPa/s at 1200°C in laboratory air.....	348
590. SEM micrograph of the fracture surface of the N720/AM specimen subjected to tensile test to failure with a constant stress rate of 25 MPa/s at 1200°C in laboratory air.....	349
591. SEM micrograph of the fracture surface of the N720/AM specimen subjected to tensile test to failure with a constant stress rate of 25 MPa/s at 1200°C in laboratory air.....	349
592. SEM micrograph of the fracture surface of the N720/AM specimen subjected to tensile test to failure with a constant stress rate of 25 MPa/s at 1200°C in laboratory air.....	350
593. SEM micrograph of the fracture surface of the N720/AM specimen subjected to tensile test to failure with a constant stress rate of 25 MPa/s at 1200°C in laboratory air.....	350
594. SEM micrograph of the fracture surface of the N720/AM specimen subjected to tensile test to failure with a constant stress rate of 25 MPa/s at 1200°C in laboratory air.....	351
595. SEM micrograph of the fracture surface of the N720/AM specimen subjected to tensile test to failure with a constant stress rate of 25 MPa/s at 1200°C in laboratory air.....	351
596. SEM micrograph of the fracture surface of the N720/AM specimen subjected to tensile test to failure with a constant stress rate of 25 MPa/s at 1200°C in laboratory air.....	352

Figure	Page
597. SEM micrograph of the fracture surface of the N720/AM specimen subjected to tensile test to failure with a constant stress rate of 25 MPa/s at 1200°C in steam.....	352
598. SEM micrograph of the fracture surface of the N720/AM specimen subjected to tensile test to failure with a constant stress rate of 25 MPa/s at 1200°C in steam.....	353
599. SEM micrograph of the fracture surface of the N720/AM specimen subjected to tensile test to failure with a constant stress rate of 25 MPa/s at 1200°C in steam.....	353
600. SEM micrograph of the fracture surface of the N720/AM specimen subjected to tensile test to failure with a constant stress rate of 25 MPa/s at 1200°C in steam.....	354
601. SEM micrograph of the fracture surface of the N720/AM specimen subjected to tensile test to failure with a constant stress rate of 25 MPa/s at 1200°C in steam.....	354
602. SEM micrograph of the fracture surface of the N720/AM specimen subjected to tensile test to failure with a constant stress rate of 25 MPa/s at 1200°C in steam.....	355
603. SEM micrograph of the fracture surface of the N720/AM specimen subjected to tensile test to failure with a constant stress rate of 25 MPa/s at 1200°C in steam.....	355
604. SEM micrograph of the fracture surface of the N720/AM specimen subjected to tensile test to failure with a constant stress rate of 25 MPa/s at 1200°C in steam.....	356
605. SEM micrograph of the fracture surface of the N720/AM specimen subjected to tensile test to failure with a constant stress rate of 25 MPa/s at 1200°C in steam.....	356
606. SEM micrograph of the fracture surface of the N720/AM specimen subjected to tensile test to failure with a constant stress rate of 25 MPa/s at 1200°C in steam.....	357

Figure	Page
607. SEM micrograph of the fracture surface of the N720/AM specimen subjected to tensile test to failure with a constant stress rate of 25 MPa/s at 1200°C in steam.....	357
608. SEM micrograph of the fracture surface of the N720/AM specimen subjected to tensile test to failure with a constant stress rate of 25 MPa/s at 1200°C in steam.....	358
609. SEM micrograph of the fracture surface of the N720/AM specimen subjected to tensile test to failure with a constant stress rate of 25 MPa/s at 1200°C in steam.....	358
610. SEM micrograph of the fracture surface of the N720/AM specimen subjected to tensile test to failure with a constant stress rate of 25 MPa/s at 1200°C in steam.....	359
611. SEM micrograph of the fracture surface of the N720/AM specimen subjected to tensile test to failure with a constant stress rate of 25 MPa/s at 1200°C in steam.....	359
612. SEM micrograph of the fracture surface of the N720/AM specimen subjected to tensile test to failure with a constant stress rate of 25 MPa/s at 1200°C in steam.....	360
613. SEM micrograph of the fracture surface of the N720/AM specimen subjected to tensile test to failure with a constant stress rate of 25 MPa/s at 1200°C in steam.....	360
614. SEM micrograph of the fracture surface of the N720/AM specimen subjected to tensile test to failure with a constant stress rate of 25 MPa/s at 1200°C in steam.....	361
615. SEM micrograph of the fracture surface of the N720/AM specimen subjected to tensile test to failure with a constant stress rate of 25 MPa/s at 1200°C in steam.....	361
616. SEM micrograph of the fracture surface of the N720/AM specimen subjected to tensile test to failure with a constant stress rate of 25 MPa/s at 1200°C in steam.....	362

Figure	Page
617. SEM micrograph of the fracture surface of the N720/AM specimen subjected to tensile test to failure with a constant stress rate of 25 MPa/s at 1200°C in steam.....	362
618. SEM micrograph of the fracture surface of the N720/AM specimen subjected to tensile test to failure with a constant stress rate of 25 MPa/s at 1200°C in steam.....	363
619. SEM micrograph of the fracture surface of the N720/AM specimen subjected to tensile test to failure with a constant stress rate of 25 MPa/s at 1200°C in steam.....	363
620. SEM micrograph of the fracture surface of the N720/AM specimen subjected to tensile test to failure with a constant stress rate of 25 MPa/s at 1200°C in steam.....	364
621. SEM micrograph of the fracture surface of the N720/AM specimen subjected to tensile test to failure with a constant stress rate of 25 MPa/s at 1200°C in steam.....	364
622. SEM micrograph of the fracture surface of the N720/AM specimen subjected to tensile test to failure with a constant stress rate of 25 MPa/s at 1200°C in steam.....	365
623. SEM micrograph of the fracture surface of the N720/AM specimen subjected to tensile test to failure with a constant stress rate of 25 MPa/s at 1200°C in steam.....	365
624. SEM micrograph of the fracture surface of the N720/AM specimen subjected to tensile test to failure with a constant stress rate of 25 MPa/s at 1200°C in steam.....	366
625. SEM micrograph of the fracture surface of the N720/AM specimen subjected to tensile test to failure with a constant stress rate of 25 MPa/s at 1200°C in steam.....	366
626. SEM micrograph of the fracture surface of the N720/AM specimen subjected to tensile test to failure with a constant stress rate of 25 MPa/s at 1200°C in steam.....	367

Figure	Page
627. SEM micrograph of the fracture surface of the N720/AM specimen subjected to tensile test to failure with a constant stress rate of 25 MPa/s at 1200°C in steam.....	367
628. SEM micrograph of the fracture surface of the N720/AM specimen subjected to tensile test to failure with a constant stress rate of 25 MPa/s at 1200°C in steam.....	368
629. SEM micrograph of the fracture surface of the N720/AM specimen subjected to tensile test to failure with a constant stress rate of 25 MPa/s at 1200°C in steam.....	368
630. SEM micrograph of the fracture surface of the N720/AM specimen subjected to tensile test to failure with a constant stress rate of 25 MPa/s at 1200°C in steam.....	369
631. SEM micrograph of the fracture surface of the N720/AM specimen subjected to tensile test to failure with a constant stress rate of 25 MPa/s at 1200°C in steam.....	369
632. SEM micrograph of the fracture surface of the N720/AM specimen subjected to tensile test to failure with a constant stress rate of 25 MPa/s at 1200°C in steam.....	370
633. SEM micrograph of the fracture surface of the N720/AM specimen subjected to tensile test to failure with a constant stress rate of 25 MPa/s at 1200°C in steam.....	370
634. SEM micrograph of the fracture surface of the N720/AM specimen subjected to tensile test to failure with a constant stress rate of 25 MPa/s at 1200°C in steam.....	371
635. SEM micrograph of the fracture surface of the N720/AM specimen subjected to tensile test to failure with a constant stress rate of 25 MPa/s at 1200°C in steam.....	371
636. SEM micrograph of the fracture surface of the N720/AM specimen subjected to tensile test to failure with a constant stress rate of 25 MPa/s at 1200°C in steam.....	372

Figure	Page
637. SEM micrograph of the fracture surface of the N720/AM specimen subjected to monotonic tensile test to failure at 1200°C in laboratory air.....	372
638. SEM micrograph of the fracture surface of the N720/AM specimen subjected to monotonic tensile test to failure at 1200°C in laboratory air.....	373
639. SEM micrograph of the fracture surface of the N720/AM specimen subjected to monotonic tensile test to failure at 1200°C in laboratory air.....	373
640. SEM micrograph of the fracture surface of the N720/AM specimen subjected to monotonic tensile test to failure at 1200°C in laboratory air.....	374
641. SEM micrograph of the fracture surface of the N720/AM specimen subjected to monotonic tensile test to failure at 1200°C in laboratory air.....	374
642. SEM micrograph of the fracture surface of the N720/AM specimen subjected to monotonic tensile test to failure at 1200°C in laboratory air.....	375
643. SEM micrograph of the fracture surface of the N720/AM specimen subjected to monotonic tensile test to failure at 1200°C in laboratory air.....	375
644. SEM micrograph of the fracture surface of the N720/AM specimen subjected to monotonic tensile test to failure at 1200°C in laboratory air.....	376
645. SEM micrograph of the fracture surface of the N720/AM specimen subjected to monotonic tensile test to failure at 1200°C in laboratory air.....	376
646. SEM micrograph of the fracture surface of the N720/AM specimen subjected to monotonic tensile test to failure at 1200°C in laboratory air.....	377
647. SEM micrograph of the fracture surface of the N720/AM specimen subjected to monotonic tensile test to failure at 1200°C in laboratory air.....	377
648. SEM micrograph of the fracture surface of the N720/AM specimen subjected to monotonic tensile test to failure at 1200°C in laboratory air.....	378
649. SEM micrograph of the fracture surface of the N720/AM specimen subjected to monotonic tensile test to failure at 1200°C in laboratory air.....	378
650. SEM micrograph of the fracture surface of the N720/AM specimen subjected to monotonic tensile test to failure at 1200°C in laboratory air.....	379

Figure	Page
651. SEM micrograph of the fracture surface of the N720/AM specimen subjected to monotonic tensile test to failure at 1200°C in laboratory air.....	379
652. SEM micrograph of the fracture surface of the N720/AM specimen subjected to monotonic tensile test to failure at 1200°C in laboratory air.....	380
653. SEM micrograph of the fracture surface of the N720/AM specimen subjected to monotonic tensile test to failure at 1200°C in laboratory air.....	380
654. SEM micrograph of the fracture surface of the N720/AM specimen subjected to monotonic tensile test to failure at 1200°C in laboratory air.....	381
655. SEM micrograph of the fracture surface of the N720/AM specimen subjected to monotonic tensile test to failure at 1200°C in laboratory air.....	381
656. SEM micrograph of the fracture surface of the N720/AM specimen subjected to monotonic tensile test to failure at 1200°C in laboratory air.....	382
657. SEM micrograph of the fracture surface of the N720/AM specimen subjected to monotonic tensile test to failure at 1200°C in laboratory air.....	382
658. SEM micrograph of the fracture surface of the N720/AM specimen subjected to monotonic tensile test to failure at 1200°C in laboratory air.....	383
659. SEM micrograph of the fracture surface of the N720/AM specimen subjected to monotonic tensile test to failure at 1200°C in laboratory air.....	383
660. SEM micrograph of the fracture surface of the N720/AM specimen subjected to monotonic tensile test to failure at 1200°C in laboratory air.....	384
661. SEM micrograph of the fracture surface of the N720/AM specimen subjected to monotonic tensile test to failure at 1200°C in laboratory air.....	384
662. SEM micrograph of the fracture surface of the N720/AM specimen subjected to monotonic tensile test to failure at 1200°C in laboratory air.....	385
663. SEM micrograph of the fracture surface of the N720/AM specimen subjected to monotonic tensile test to failure at 1200°C in laboratory air.....	385
664. Fracture surface of the N720/AM specimen subjected to tensile test to failure following 100 h at 13 MPa at 1200°C in laboratory air.(a)-(c):front view, (b)-(d):side view.....	386

Figure	Page
665. Fracture surface of the N720/AM specimen subjected to tensile test to failure following 100 h at 13 MPa at 1200°C in laboratory air.(e)-(g):front view, (f)-(h):side view.....	387
666. Fracture surface of the N720/AM specimen subjected to tensile test to failure following 100 h at 30 MPa at 1200°C in laboratory air.(a)-(c):front view, (b)-(d):side view.....	388
667. Fracture surface of the N720/AM specimen subjected to tensile test to failure following 100 h at 30 MPa at 1200°C in laboratory air. (e)-(g):front view, (f)-(h):side view .....	389
668. Fracture surface of the N720/AM specimen subjected to tensile test to failure following 100 h at 32 MPa at 1200°C in laboratory air.(a)-(c):front view, (b)-(d):side view.....	390
669. Fracture surface of the N720/AM specimen subjected to tensile test to failure following 100 h at 32 MPa at 1200°C in laboratory air. (e)-(g):front view, (f)-(h):side view .....	391
670. Fracture surface of the N720/AM specimen subjected to tensile test to failure following 100 h at 13 MPa at 1200°C in steam.(a)-(c):front view, (b)-(d):side view.....	392
671. Fracture surface of the N720/AM specimen subjected to tensile test to failure following 100 h at 13 MPa at 1200°C in steam.(e)-(g):front view, (f)-(h):side view.....	393
672. Fracture surface of the N720/AM specimen subjected to tensile test to failure following 100 h at 20 MPa at 1200°C in steam.(a)-(c):front view, (b)-(d):side view.....	394
673. Fracture surface of the N720/AM specimen subjected to tensile test to failure following 100 h at 20 MPa at 1200°C in steam.(e)-(g):front view, (f)-(h):side view.....	395
674. Fracture surface of the N720/AM specimen with $\pm 45^\circ$ fiber orientation obtained in creep test conducted at 26 MPa at 1200°C in steam. Creep lifetime $t_f = 99.4$ h. (a)-(c): front view, (b)-(d): side view.....	396

Figure	Page
675. Fracture surface of the N720/AM specimen with $\pm 45^\circ$ fiber orientation obtained in creep test conducted at 26 MPa at 1200°C in steam. Creep lifetime $t_f = 99.4$ h. (e)-(g): front view, (f)-(h): side view.....	397
676. Fracture surface of the N720/AM specimen with $\pm 45^\circ$ fiber orientation obtained in creep test conducted at 30 MPa at 1200°C in steam. Creep lifetime $t_f = 1.08$ h. (a)-(c): front view, (b)-(d): side view.....	398
677. Fracture surface of the N720/AM specimen with $\pm 45^\circ$ fiber orientation obtained in creep test conducted at 30 MPa at 1200°C in steam. Creep lifetime $t_f = 1.08$ h. (e)-(g): front view, (f)-(h): side view.....	399
678. Fracture surface of the N720/AM specimen with $\pm 45^\circ$ fiber orientation obtained in creep test conducted at 32 MPa at 1200°C in steam. Creep lifetime $t_f = 0.02$ h. (a)-(c): front view, (b)-(d): side view.....	400
679. Fracture surface of the N720/AM specimen with $\pm 45^\circ$ fiber orientation obtained in creep test conducted at 32 MPa at 1200°C in steam. Creep lifetime $t_f = 0.02$ h. (e)-(g): front view, (f)-(h): side view.....	401
680. Fracture surface of the N720/AM specimen subjected to tensile test to failure following 100 h at 20 MPa at 1200°C in argon. (a)-(c): front view, (b)-(d): side view.....	402
681. Fracture surface of the N720/AM specimen subjected to tensile test to failure following 100 h at 20 MPa at 1200°C in argon. (a)-(c): front view, (b)-(d): side view.....	403
682. Fracture surface of the N720/AM specimen with $\pm 45^\circ$ fiber orientation obtained in creep test conducted at 26 MPa at 1200°C in argon. Creep lifetime $t_f = 76$ h. (a)-(c): front view, (b)-(d): side view.....	404
683. Fracture surface of the N720/AM specimen with $\pm 45^\circ$ fiber orientation obtained in creep test conducted at 26 MPa at 1200°C in argon. Creep lifetime $t_f = 76$ h. (e)-(g): front view, (f)-(h): side view.....	405
684. Fracture surface of the N720/AM specimen with $\pm 45^\circ$ fiber orientation obtained in creep test conducted at 30 MPa at 1200°C in argon. Creep lifetime $t_f = 3.42$ h. (a)-(c): front view, (b)-(d): side view.....	406

Figure	Page
685. Fracture surface of the N720/AM specimen with $\pm 45^\circ$ fiber orientation obtained in creep test conducted at 30 MPa at 1200°C in argon. Creep lifetime $t_f = 3.42$ h. (e)-(g): front view, (f)-(h): side view.....	407
686. Fracture surface of the N720/AM specimen with $\pm 45^\circ$ fiber orientation obtained in creep test conducted at 32 MPa at 1200°C in argon. Creep lifetime $t_f = 0.08$ h. (a)-(c): front view, (b)-(d): side view.....	408
687. Fracture surface of the N720/AM specimen with $\pm 45^\circ$ fiber orientation obtained in creep test conducted at 32 MPa at 1200°C in argon. Creep lifetime $t_f = 0.08$ h. (e)-(g): front view, (f)-(h): side view.....	409
688. Fracture surface of the N720/AM specimen subjected to tensile test to failure with a constant stress rate of 0.0025 MPa/s at 1200°C in laboratory air. (a)-(c): front view, (b)-(d): side view.....	410
689. Fracture surface of the N720/AM specimen subjected to tensile test to failure with a constant stress rate of 0.0025 MPa/s at 1200°C in laboratory air. (e)-(g): front view, (f)-(h): side view.....	411
690. Fracture surface of the N720/AM specimen subjected to tensile test to failure with a constant stress rate of 0.0025 MPa/s at 1200°C in laboratory air. (a)-(c): front view, (b)-(d): side view.....	412
691. Fracture surface of the N720/AM specimen subjected to tensile test to failure with a constant stress rate of 0.0025 MPa/s at 1200°C in laboratory air. (e)-(g): front view, (f)-(h): side view.....	413
692. Fracture surface of the N720/AM specimen subjected to tensile test to failure with a constant stress rate of 0.0025 MPa/s at 1200°C in laboratory air. (a)-(c): front view, (b)-(d): side view.....	414
693. Fracture surface of the N720/AM specimen subjected to tensile test to failure with a constant stress rate of 0.0025 MPa/s at 1200°C in laboratory air. (e)-(g): front view, (f)-(h): side view.....	415
694. Fracture surface of the N720/AM specimen subjected to tensile test to failure with a constant stress rate of 0.0025 MPa/s at 1200°C in laboratory air. (a)-(c): front view, (b)-(d): side view.....	416

Figure	Page
695. Fracture surface of the N720/AM specimen subjected to tensile test to failure with a constant stress rate of 0.0025 MPa/s at 1200°C in laboratory air. (e)-(g): front view, (f)-(h): side view.....	417
696. Fracture surface of the N720/AM specimen subjected to monotonic tensile test to failure at 1200°C in laboratory air. (a)-(c): front view, (b)-(d): side view.....	418
697. Fracture surface of the N720/AM specimen subjected to monotonic tensile test to failure at 1200°C in laboratory air. (a)-(c): front view, (b)-(d): side view.....	419
698. Fracture surface of the N720/AM specimen subjected to monotonic tensile test to failure at 1200°C in laboratory air. (a)-(c): front view, (b)-(d): side view.....	420
699. Fracture surface of the N720/AM specimen subjected to monotonic tensile test to failure at 1200°C in laboratory air. (a)-(c): front view, (b)-(d): side view.....	421
700. Fracture surface of the N720/AM specimen subjected to monotonic tensile test to failure at 1200°C in laboratory air. (a)-(c): front view, (b)-(d): side view.....	422
701. Fracture surface of the N720/AM specimen subjected to monotonic tensile test to failure at 1200°C in laboratory air. (a)-(c): front view, (b)-(d): side view.....	423

## List of Tables

Table	Page
1. Physical properties of the N720/AM CMC test panel provided by COI.....	9
2. Temperature calibration set points.....	19
3. Summary of creep tests conducted at 1200°C.....	20
4. Summary of tensile data.....	22
5. Summary of creep data.....	23
6. Summary of retained properties for specimens achieving creep run-out of 100 h.....	23
7. Average thermal strains produced by N720/A and N720/AM CMCs with $\pm 45^\circ$ fiber orientation due to temperature rise from 23 to 1200°C. Data for N720/A from Siegert [16].....	24
8. Average tensile properties for N720/A and N720/AM with $\pm 45^\circ$ fiber orientation at 1200°C in laboratory air. Data for N720/A from Siegert [16] and Ruggles-Wrenn et al [17].....	25
9. Summary of tensile properties of N720/AM composite with $\pm 45^\circ$ fiber orientation at 1200°C in laboratory air obtained in stress controlled tensile tests.....	27
10. Summary of tensile properties of N720/AM composite with $\pm 45^\circ$ fiber orientation at 1200°C in steam obtained in stress controlled tensile test.....	28
11. Average modulus of elasticity of N720/AM specimens with $\pm 45^\circ$ fiber orientation tested in creep at 1200°C.....	31
12. Average modulus of elasticity of N720/A specimens with $\pm 45^\circ$ fiber orientation tested in creep at 1200°C. Data for N720/A from Siegert [16].....	31
13. Creep results for the N720/A and N720/AM composites with $\pm 45^\circ$ fiber orientation tested in laboratory air. Data for N720/A from Siegert [16] and Ruggles-Wrenn et al [17].....	32
14. Creep results for the N720/A and N720/AM composites with $\pm 45^\circ$ fiber orientation tested in steam. Data for N720/A from Siegert [16] and Ruggles-Wrenn et al [17].....	35

Table	Page
15. Creep results for the N720/A and N720/AM composites with $\pm 45^\circ$ fiber orientation tested in argon. Data for N720/A from Siegert [16] and Ruggles-Wrenn et al [17].	39
16. Retained properties of the N720/A and N720/AM specimens with $\pm 45^\circ$ fiber orientation subjected to prior creep at $1200^\circ\text{C}$ in laboratory air, steam and argon environments. Data for N720/A from Siegert [16], Ruggles-Wrenn et al [17].	44

EFFECT OF ENVIRONMENT ON CREEP BEHAVIOR OF  
NEXTEL720/ALUMINA-MULLITE CERAMIC COMPOSITE  
WITH  $\pm 45^\circ$  FIBER ORIENTATION AT 1200°C

## **I. Introduction**

Material is the main body for all engineering wonders. Every structure we see around is composed of some material. When we talk about the strength of the whole structure, actually we are talking about the strength of the constitutive material(s) properties. The increase of the man's expectations from the structures increased the need for the material that has essential properties. The researches exposed a new way of producing materials that man needed: "composites".

A composite is "... a material system consisting of two or more phases on a macroscopic scale, whose mechanical performance and properties are designed to be superior to those of the constituent materials acting independently" [1:1]. Composite materials made their appearance in commercial airplanes with the introduction of the Boeing 707 in the 1950s. Today, composites make up a large percentage of aircraft structural components. Composites comprise 9% of the aircraft structural weight in the Boeing 777. Boeing is predicting that 50% of the material used on the 787 Dreamliner, scheduled for delivery in 2010, will be composites [2]. Ceramic matrix composites (CMCs), capable of maintaining excellent strength and fracture toughness at high temperatures continue to attract attention as candidate materials for aerospace turbine engine applications. Higher material operating temperatures and decreased cooling air

requirement are the significant advantages that CMCs offer to the aerospace engine design community. Advanced reusable space launch vehicles will likely incorporate fiber reinforced CMCs in critical propulsion components. Before ceramic matrix composites can be widely used in high-temperature aerospace engine applications, their structural integrity and long-term environmental durability must be assured. Characterization of the mechanical behavior of the candidate CMCs in relevant engine environments is required for design of structural components with these materials.

The next chapter discusses background information of Ceramic Matrix Composites and their applications. In addition, some comments are made related to the creep-rupture behavior of CMCs, as well as factors affecting the creep performance of these materials. Past work on CMCs is also discussed. Experimental setup used in this research is discussed in detail. Results are presented and discussed. Finally, conclusions and recommendations for future work are offered.

## II. Background

### 2.1 Ceramic Matrix Composites

Advances in technology bring new demands to the structures arena. New designs for aircraft engines, rockets and hypersonic missiles and flight vehicles require materials that exhibit excellent strength and fracture toughness and retained properties under high temperature and varying environmental factors. The majority of research efforts are focused on continuous-fiber reinforced ceramic composites (CFCC) with a variety of SiC and Carbon based material systems. These composites have been proven to effectively endure the effects of high temperatures but exhibited poor on long term durability in oxidizing environments such as air and steam.

Fibers used in ceramic matrix composites exhibit high strength and stiffness at high temperatures. The fibers provide the backbone for reinforcing ceramic materials [3:45]. Reinforcements can be either continuous or discontinuous fibers based on their size, which can range from smaller multifiber tows (5-15 $\mu$ m diameter) to larger monofilaments (50-100 $\mu$ m). Discontinuous fibers are very short, while continuous fibers are longer and are laid out in bundles. At present both non-oxide and oxide fibers are available. Non-oxide fibers are generally based on silicon carbide (SiC). Oxide fibers are traditionally composed of alumina ( $Al_2O_3$ ) and/or mullite ( $3Al_2O_3 \cdot 2SiO_2$ ) [3:12].

While the fibers serve as a backbone supporting a composite material, matrix plays an important role as well. The matrix protects the fibers from the surrounding

environment allowing the CMC to withstand extremely high temperatures. In the case of the composite with  $\pm 45^\circ$  fiber orientation studied in this research effort, the matrix also provides some of the load-bearing capability. In designing a CMC, choice of matrix material is as important as the choice of fiber reinforcement. A suitable ceramic matrix material should be able to infiltrate a bundle of fibers, form a mechanical or frictional bond with the reinforcement (fibers), while not reacting chemically with the fiber reinforcement during fabrication or service, and not physically damage the fibers. Furthermore, matrix material must have good creep and fatigue resistance, and be chemically stable [3:40]. A chemically stable matrix is impermeable to moisture and resistant to oxidation. The need for the environmentally stable composites motivated the development of CMCs based on environmentally stable oxide constituents [4-9].

Despite the many attractive properties of ceramics, damage tolerance is an issue that degrades their usage scope. There are two methods used to improve the damage tolerance in continuous fiber-reinforced ceramic composites [Figure 1]. The first method relies on fiber coating or interphase to mechanically separate the fiber reinforcement from the matrix. The weak interface between fiber and matrix allows cracks to propagate through the matrix, but around the fibers. The disadvantage of this approach is the complexity of producing coated fibers. The second approach involves the use of a porous matrix with low fracture toughness to achieve the crack deflection. The porous matrix composites may be less costly to manufacture, but they have their unique challenges. The porous matrix of composites must be weak enough to deflect cracks around the fiber reinforcement, but also strong enough to withstand the off-axis loading [10].

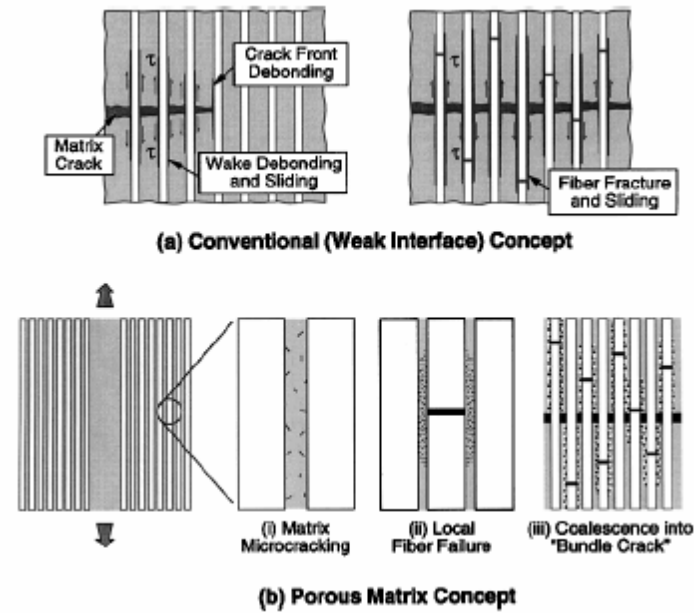


**Figure 1. Common CMC damage tolerance mechanisms: (a) Weak fiber/matrix interface and (b) Porous matrix [10]**

## 2.2 Previous Research Efforts

Previous research efforts on ceramic matrix composites at AFIT explored mechanical behavior of the N720/A composite [11-20]. The material consisted of Nextel 720 mullite-alumina fibers and relied on a porous alumina matrix for damage tolerance. Harlan [20] studied the creep-rupture behavior of the material with 0/90° fiber orientation in both air and steam environments at 1200 and 1330°C. The results showed that while the material performed well during creep testing in air, creep performance in steam was severely degraded. Creep performance at 1330°C was poor in air and was further degraded by the presence of steam. Harlan concluded that fiber fracture was the main failure mechanism of the material in all environments.

Braun [13] investigated the creep rupture behavior of the N720/A composite in laboratory air and in steam, at 1000 and 1100 °C. At 1000°C the accumulated creep strains were less than 2% and all specimens achieved a 100 h creep run-out. At 1100°C, creep performance was reduced in both environments with a greater reduction in creep performance observed in steam.

Braun observed a clear correlation between the appearance of fracture surfaces, creep lifetimes and test environment. Specimens tested in steam had much flatter fracture surfaces and shorter fracture zones than samples tested in air at the same temperature. Variations in temperature also affected the fracture surface. Fracture surfaces obtained at lower temperatures exhibited more fiber pull-out than those obtained at higher temperatures. Braun found that as creep life increased, so did the amount of fiber pull-out. It was concluded that creep testing at higher temperatures resulted in additional matrix sintering and decreased matrix porosity which in turn resulted in a less damage tolerant composite.

Siegert [16] studied the creep behavior of the N720/A composite, with  $\pm 45^\circ$  fiber orientations. In Siegert's research effort, specimens were tested in air and steam as well as argon, a non-oxidizing environment. The results showed that specimens tested in air produced lower creep rates than specimens tested at the same stress levels in argon and steam. Specimens tested in argon had higher creep rates than those tested in steam. However, creep lifetimes in argon were similar to those in steam.

The only study reporting on effects of environment on the mechanical behavior of Nextel720/alumina-mullite (N720/AM) CMC to-date is that by Genelin [21]. The objective

of that study was to assess the creep-rupture behavior of the Nextel 720/AM ceramic matrix composite at 1200°C in laboratory air, argon and steam. Genelin observed that the tensile modulus of N720/AM CMC is slightly higher, while the UTS is somewhat below the corresponding values for the N720/A composite. The tensile stress-strain curve departs from linearity at the stresses between 20 and 30 MPa. However, the nonlinearity is not strongly pronounced. Such stress-strain behavior is qualitatively similar to that exhibited by the N720/A composite at 1200 °C [12-14, 19-20]. In air, the creep rates of N720/AM were 5 times lower than those of the N720/A composite. However, in steam the creep rates produced by N720/AM CMC were two times those obtained for the N720/A. While the presence of argon had a minimal effect on the creep rate of N720/A, in the case of the N720/AM composite the effect of argon on the secondary creep rate was nearly as degrading as that of the steam environment. The creep rates of the N720/AM in argon were at least an order of magnitude higher than those in air and similar to those obtained in steam.

### **2.3 The N720/AM Ceramic Matrix Composite**

The N720/AM composite is a continuous fiber oxide-oxide ceramic matrix composite consisting of Nextel™ 720 mullite-alumina fibers and a porous alumina-mullite matrix with no fiber coating. The composite relies on the porosity of its matrix for crack deflection.

The Nextel 720 fiber is produced by Minnesota Mining and Manufacturing (3M) for use in high temperature composites. The two phase mullite-alumina fiber was designed to operate at temperatures in excess of 1100°C and the manufacturer claims a

reduction in creep rate of three orders of magnitude when compared to its predecessor the Nextel 610 single alumina phase fiber. The fiber is manufactured using a sol-gel process and has a diameter of 12.5  $\mu\text{m}$ . The fiber is made up of 85%  $\text{Al}_2\text{O}_3$  and 15%  $\text{SiO}_2$  by weight, has a single filament tensile strength of 2100 MPa and a Young's modulus of 260 GPa. Comprised of oxides, these fibers have also been shown to be resistant to the effects of environment. Previous research also showed that the fibers exhibit linear elastic behavior and brittle failure [22].

Previous research has shown that the main failure mechanism of composites such as these has been densification of the porous matrix due to additional sintering at high temperatures. Because of its slow sintering kinetics up to 1300°C and excellent creep resistance, mullite was added to the matrix of the N720/AM composite as a means of limiting shrinkage associated with the sintering of a pure alumina matrix [23,24]. The low fracture toughness and elastic modulus make mullite ideal for crack deflection in a porous matrix, but these same properties hinder its effectiveness against shear, off-axis and compressive loading. As a result, a mixture of both alumina and mullite create a more operationally capable matrix [25].

The material studied was Nextel<sup>TM</sup>720/alumina-mullite (N720/AM), an oxide-oxide ceramic composite consisting of a porous alumina-mullite matrix reinforced with Nextel<sup>TM</sup>720 fibers. The composite, manufactured by COI Ceramics (San Diego, CA), was supplied in a form of a 3.2 mm thick plate, comprised of 12 0°/90° woven layers, with a density of  $\sim 2.57 \text{ g/cm}^3$  and a fiber volume of approximately 40%. Composite porosity was  $\sim 28.3\%$ . The laminate was fabricated following the procedure described

elsewhere [26]. No coating was applied to the fibers. The damage tolerance of the N720/AM composite is enabled by a porous matrix.

Physical properties of the panel tested over the course of this research were provided by COI and can be seen in Table 1. The volume percent of mullite in the matrix did not exceed 13%.

**Table 1. Physical properties of the N720/AM CMC test panel provided by COI**

<b>Panel #</b>	<b>Thickness (mm)</b>	<b>Fabric (% Volume)</b>	<b>Matrix (% Volume)</b>	<b>Porosity (% Volume)</b>	<b>Density (g/cc)</b>
7693-1	3.18	40.0	31.7	28.3	2.57

## **2.4 Thesis Objective**

The objective of this research is to assess the creep rupture behavior of Nextel<sup>TM</sup> 720/AM ceramic matrix composite with  $\pm 45^\circ$  fiber orientation at 1200°C in laboratory air, in argon and in steam. Testing of specimens with a  $\pm 45^\circ$  fiber orientation permits evaluation of the matrix-dominated response of the composite. Multiple tests are conducted in all three environments at varying levels of creep stress. This data can then be compared to data from previous research efforts on the N720/A CMC with a  $\pm 45^\circ$  fiber orientation, a similar composite with a pure alumina matrix.

### III. Experimental Setup

#### 3.1 Specimen Preparation

The specimens used for this study were cut from a single composite panel by the AFIT machine shop using a high pressure waterjet. Average thickness of the panel was 3.18 mm. Standard dogbone-shaped specimens were used in all tests. Specimen geometry is shown in Figure 2.

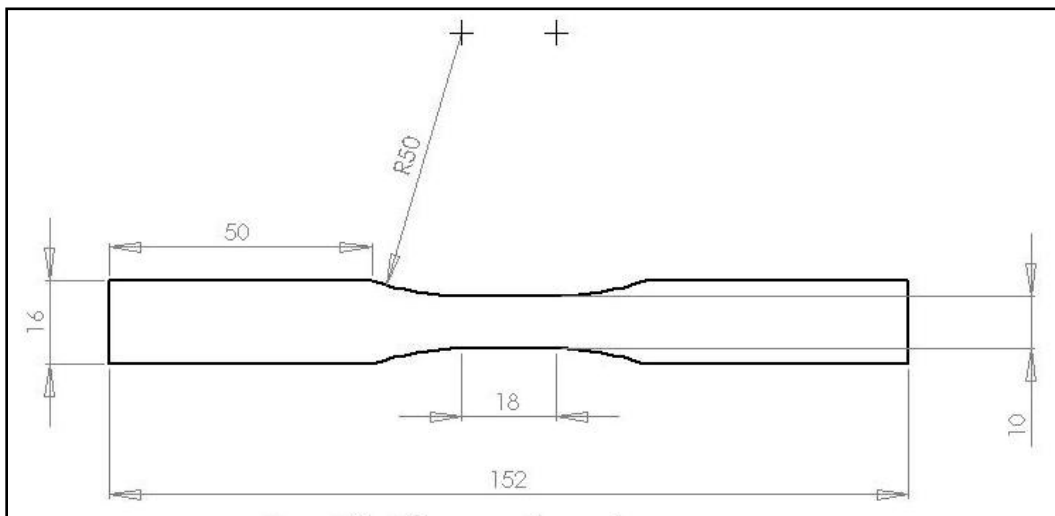


**Figure 2. Test Specimen, dimensions in mm**

After machining, the specimens were cleaned to remove any debris created during the cutting process. The specimens were first rinsed with alcohol, and then placed in an ultrasonic cleaner for 20 min. Once removed from the ultrasonic bath, the specimens were soaked in alcohol for 20 min and finally dried in an oven for 2 h at 250°C.

As the last step to prepare the specimens for testing, fiber glass tabs were attached to the gripping sections. The tabs were attached to the specimens using M-Bond 200 adhesive. A specimen with tabs can be seen in Figure 3.

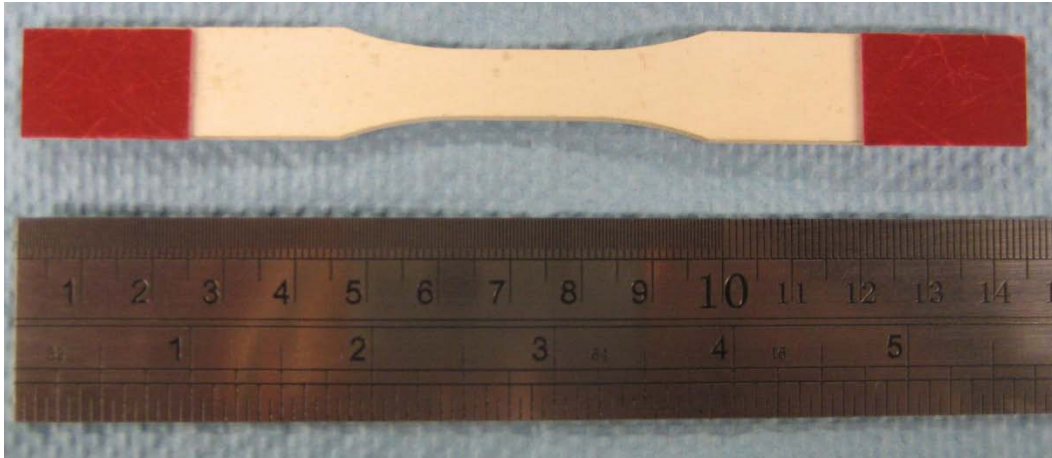


**Figure 3. N720/AM tensile specimen with tabs [21]**

### **3.2 Mechanical Testing Equipment**

An MTS Corporation model 810 servo-hydraulic testing machine with the load capacity of 5.5 kip (25 kN) was used for all mechanical testing for this research. The machine was equipped with MTS 647 hydraulic wedge grips. In order to prevent the slippage of a specimen, each wedge was coated with a layer of surf alloy. The grips were water cooled down to 15°C by a NESLAB model HX-75 chiller. Grip pressure of 8 MPa was used in all tests. The machine was equipped with an MTS Teststar II digital controller to generate input signals and acquire data. The MTS Multipurpose Testware (MPT) software was used for the programming of automated test routines and data collection.

The 5 kip mechanical testing machine and 5 kip mechanical testing station can be seen in Figures 4 and 5, respectively.



**Figure 4. MTS 5 kip mechanical testing machine**



**Figure 5. 5 kip mechanical testing station**

Strain measurements were performed with an MTS high temperature low contact force extensometer with a 12.77 mm gage length. A heat shield and an air cooling system were used to protect the extensometer from the high temperatures required for this research. The extensometer was calibrated to measure tensile strains between -5% to 20% (see Figure 6).

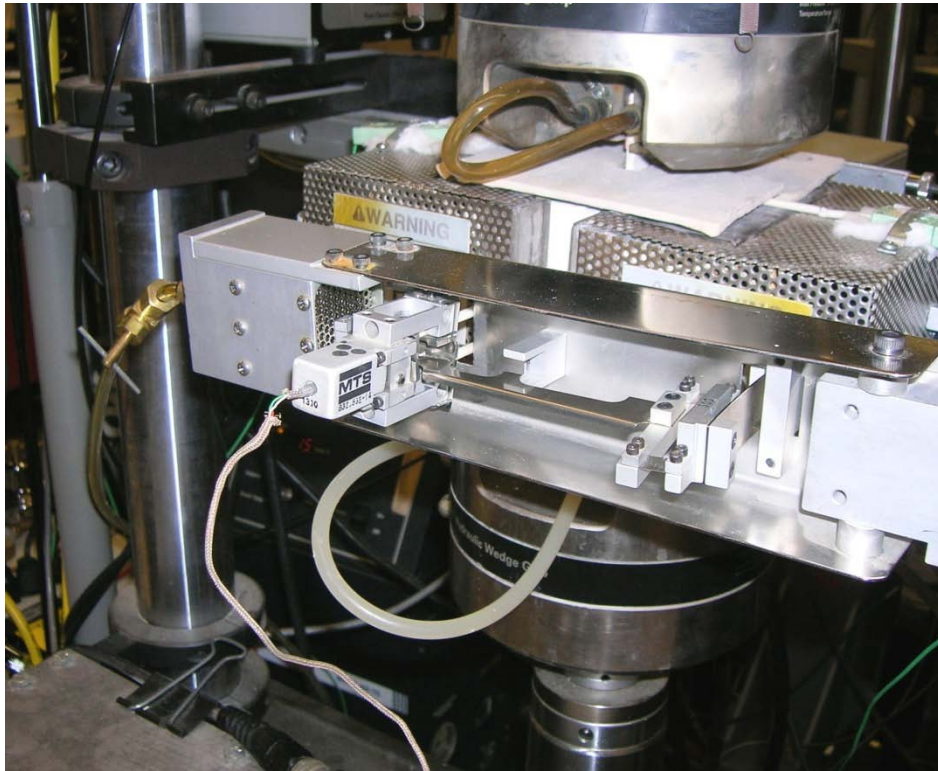


**Figure 6. Extensometer platform with heat shield and cooling air**

### 3.3 Environmental Controls

The 5 kip machine was equipped with a two zone Amteco Hot Rail Furnace System for the elevated temperature testing. The furnace included two heating elements per zone and was internally insulated with alumina. The insulation was shaped to allow the furnace to close around the specimen without any interference. A small hole in the back and slots in the front were cut for gas feeding tube and the extensometer rods, respectively. A ceramic sheet was placed on top of the furnaces for insulation (see Figure 7). The furnace zones were controlled using MTS 409 Temperature Controllers. Two R-type thermocouples were used to provide feedback to the controllers.

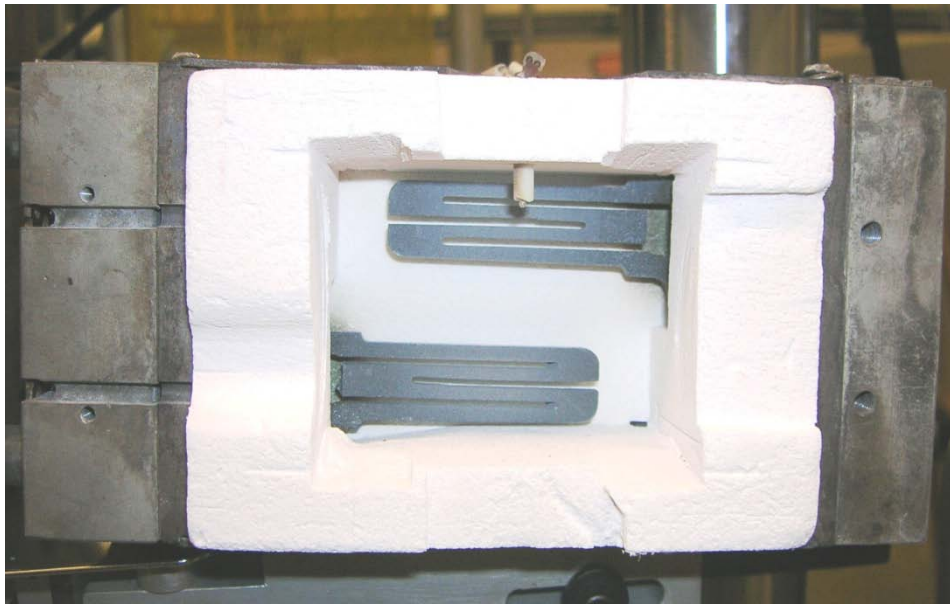


**Figure 7. Interior view of modified furnace insulation where heating elements and control thermocouple are visible**

An alumina susceptor was used for testing in both argon and steam environments. An AMTECO HRFS-STMGEN steam generation system using deionized water was used to generate steam. The steam was pumped to the back of the susceptor at approximately 30 mL/h flow rate. Temperature control on the steam generator was set to 273°F. During the tests in argon environment, ultra high purity argon (99.999% pure) was pumped into the susceptor. Flow was regulated using an Omega Mass Flow Controller set to 40.8 mL/hr. This flow rate was chosen to ensure all air would be evacuated from the susceptor creating a near 100% argon environment. The specimen with a susceptor and gas feeding tube can be seen in Figure 8.



**Figure 8. Alumina susceptor and steam feeding tube on the 5 kip machine**

### 3.4 Microstructural Characterization

After the completion of mechanical testing, fracture surfaces were examined using both an optical microscope and a scanning electron microscope (SEM). A Zeiss Stemi SV II optical microscope equipped with a Zeiss AxioCam HRC digital camera and Axiovision version 4.4 software (see Figure 9) was used. The specimens were also examined using an FEI Quanta 200 SEM shown in Figure 10.



**Figure 9. Zeiss Stemi SV II optical microscope**

The N720/AM CMC is a non-conductive material. Therefore in order to view the fracture surfaces of the samples under the SEM, they were first coated with a thin layer of carbon using an SPI-Module Sputter Coater. Micrographs were taken at several different magnifications in order to examine the details of microstructure and fracture surfaces.



**Figure 10. FEI Quanta 200 Scanning Electron Microscope**

### **3.5 Test Procedures**

#### ***3.5.1 Preparation of Mechanical Testing Equipment.***

Prior to every test, the testing machine was warmed up to ensure the hydraulic fluid was at operating temperature and fluid lines were cleared. The MTS function generator was used to cycle the actuator in displacement control for a minimum of 1 hour. The function generator was programmed in displacement control using a square wave function at a frequency of 3 Hz and amplitude of .001 inches. Prior to every test, the cooling water for the grips was checked and its temperature was set to 15°C. Cooling air for the extensometer was also checked.

### ***3.5.2 Temperature Calibration***

All tests were conducted at 1200°C. To calibrate the furnace controllers, a specimen from the same CMC panel was instrumented with two R-type thermocouples. The thermocouples were attached to the specimen by sandwiching them between the specimen and scrap pieces of N720/AM on each side. The assembly was then wired together with piano wire to secure the thermocouples in place. This calibration specimen could then be used to calibrate the ovens to achieve a temperature of 1200°C on the surface of the specimen (see Figure 11).

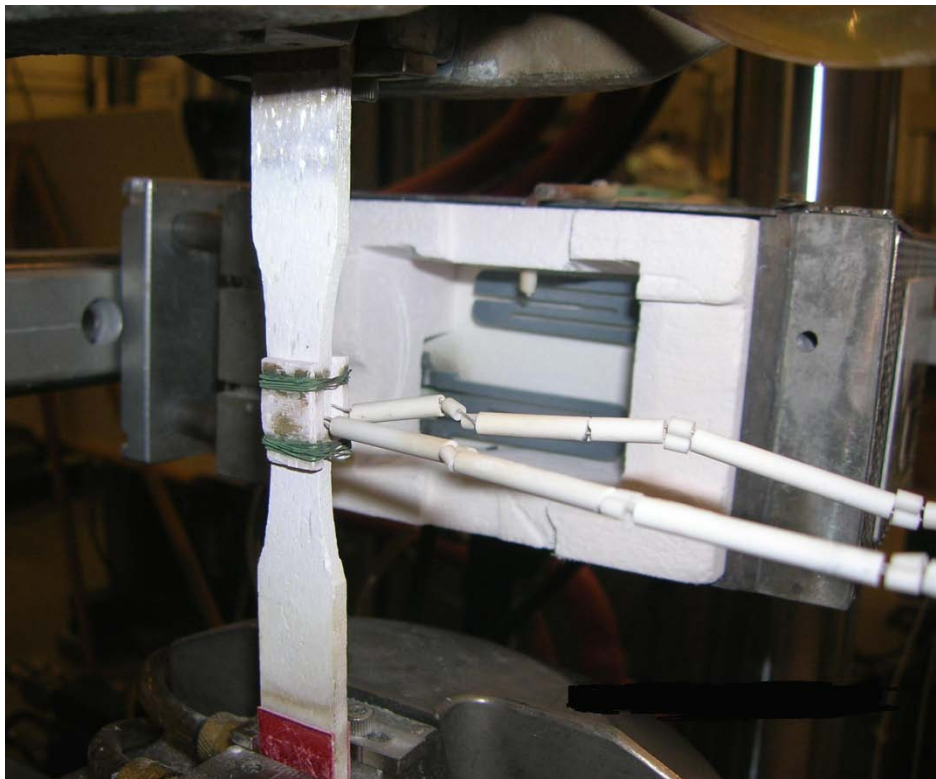


**Figure 11. Test specimen instrumented with thermocouples**

The sample was first gripped under displacement control in the top grip. Then the load cell was zeroed out and control mode was switched to force before the bottom grip was closed. Then the ovens were closed around the specimen and the temperature was raised to 1050°C at a rate of 1°C/s. While the thermocouple temperature readings were closely monitored, the oven temperature was manually increased to achieve the desired temperature on the test specimen.

When both thermocouples were reading within  $\pm 5^\circ\text{C}$  of the desired temperature, at least a 2 hour elapsed dwell time were started. This calibration procedure was repeated on a periodic basis to ensure the temperature of the test specimen was consistently at 1200°C. The temperature controller settings obtained for each heating zone are given in Table 2 for testing in laboratory air, steam and argon environments.

**Table 2. Temperature calibration set points**

<b>Environment</b>	<b>Right Set Point (°C)</b>	<b>Left Set Point (°C)</b>
<b>AIR</b>	1157	1183
<b>STEAM</b>	1232	1237
<b>ARGON</b>	1200	1250

### **3.5.3 Monotonic Tensile Test.**

Two monotonic tensile tests to failure were conducted for this research in displacement control and one tensile test to failure was performed in load control. These tensile tests were carried out at 1200°C in laboratory air.

The temperature were increased under zero load from 23 °C to 1200°C at the rate of 1°C/s and held at 1200°C for 20 min. During this phase of testing, force, strain, displacement, oven temperature and time were recorded every second. After the 20

minutes of dwell time, mechanical loading was applied. Displacement-controlled tests were performed at a constant rate of 0.05mm/s. For this phase of the tensile test, data was recorded every 0.05 s. The load-controlled test was performed at a constant rate of 15 MPa/s.

#### **3.5.4 Creep Test.**

Creep tests were conducted at 1200°C in air, steam and argon environments. The summary of creep tests can be seen in Table 3.

**Table 3. Summary of creep tests conducted at 1200°C**

<b>Specimen #</b>	<b>Test Environment</b>	<b>Creep Stress (MPa)</b>
<b>S04</b>	Air	13
<b>S05</b>	Air	30
<b>S06</b>	Air	35
<b>L01</b>	Air	32
<b>L02</b>	Steam	32
<b>L03</b>	Steam	13
<b>L04</b>	Steam	26
<b>L05</b>	Steam	30
<b>L06</b>	Steam	20
<b>L07</b>	Argon	30
<b>L08</b>	Argon	20
<b>L09</b>	Argon	32
<b>L10</b>	Argon	26
<b>L15</b>	Steam	26

Creep tests were conducted in force control. Specimens were loaded to the creep stress at the rate of 15 MPa/s. During load up, data was recorded every 0.05 s. After the desired stress level was reached, the data recording intervals were altered according to the creep time. Creep run-out was set to 100 h. If the specimen achieved a run-out, the load was ramped down to zero at 15 MPa/s and then a tensile test to failure was conducted at

1200°C to measure retained properties. An example of a typical creep test procedure is shown in Figure 12.

Type	Name	Start	Interrupt
	Upper/Lower Disp Limits	<Procedure>.Start	
	Record Warm Up	<Procedure>.Start	Warm Up/Hold Ovens.Done
	Warm Up/Hold Ovens	<Procedure>.Start	Upper/Lower Disp Limits.Done
	Record Load Up	Warm Up/Hold Ovens.Done	Ramp Up (Load Ctrl).Done
	Ramp Up (Load Ctrl)	Warm Up/Hold Ovens.Done	Upper/Lower Disp Limits.Done
	Record Creep (0-5 min)	Ramp Up (Load Ctrl).Done	
	Record Creep (5-10 min)	Record Creep (0-5 min).Done	
	Record Creep (10 min -1 hr)	Record Creep (5-10 min).Done	
	Record Creep (1-3 hr)	Record Creep (10 min -1 hr).Done	
	Record Creep (3-5 hr)	Record Creep (1-3 hr).Done	
	Record Creep (5-25 hr)	Record Creep (3-5 hr).Done	
	Record Creep (25-100 hr)	Record Creep (5-25 hr).Done	Hold Load 100 Hrs (Load Ctrl).Done
	Hold Load 100 Hrs (Load Ctrl)	Ramp Up (Load Ctrl).Done	Upper/Lower Disp Limits.Done
	Record Ramp Down	Hold Load 100 Hrs (Load Ctrl).Done	Ramp Down (Load Ctrl).Done
	Ramp Down (Load Ctrl)	Hold Load 100 Hrs (Load Ctrl).Done	Upper/Lower Disp Limits.Done
	Record Tensile Test	Ramp Down (Load Ctrl).Done	Tensile Test (Dsp Ctrl).Done
	Tensile Test (Dsp Ctrl)	Ramp Down (Load Ctrl).Done	Upper/Lower Disp Limits.Done
	Shut Down Ovens	Tensile Test (Dsp Ctrl).Done	

Procedure is done when Shut Down Ovens.Done

**Figure 12. Typical creep test procedure**

### 3.5.5 Tensile Tests at 0.0025 and 25 MPa/s

Five tensile tests were conducted to explore the hypothesis that slow crack growth is the primary failure mechanism for the N720/AM CMC with  $\pm 45^\circ$  fiber orientation. These tests were conducted at constant stress rates of 0.0025 and 25 MPa/s in force control at 1200°C in laboratory air and in steam.

## IV. Results and Discussion

### 4.1 Section Summary

This chapter reports the detailed findings of this research. Complete summaries of experimental data are given in Tables 4-6 below. The section begins with a discussion of thermal properties of the N720/AM composite with  $\pm 45^\circ$  fiber orientation. Results of the monotonic tensile tests and creep rupture tests are then presented and compared to results for the N720/A composite from earlier studies. Following, analysis of the optical micrographs and results of the SEM observations will be discussed. All tests in this research effort were conducted using specimens from a single panel, number 7693-1.

**Table 4. Summary of tensile data**

<b>Specimen #</b>	<b>Environment</b>	<b>Loading Rate</b>	<b>Thermal Strain (%)</b>	<b>E (GPa)</b>	<b>UTS (MPa)</b>
<b>S01</b>	Air	0.05 mm/s	0.78	42.5	38.58
<b>S02</b>	Air	0.05 mm/s	0.76	40.8	37.01
<b>S06*</b>	Air	15 MPa/s	0.74	41.9	34.62
<b>Average</b>				<b>41.7</b>	<b>36.74</b>

\*Test conducted in load control

**Table 5. Summary of creep data**

Specimen #	Environment	Thermal Strain (%)	E (GPa)	Creep Stress (MPa)	Creep Life (h)	Creep Strain (%)
S04	Air	0.77	41.9	13	>100	0.785
S05	Air	0.77	42.1	30	>100	4.101
L01	Air	0.72	41.6	32	>100	4.354
L02	Steam	0.80	39.8	32	0.02	0.642
L03	Steam	0.79	42.4	13	>100	4.275
L05	Steam	0.84	39.3	30	1.08	5.682
L06	Steam	0.84	36.4	20	>100	12.48
L15	Steam	0.90	39.8	26	99.4	18.25
L07	Argon	0.90	45.0	30	3.42	12.97
L08	Argon	0.92	39.5	20	>100	16.72
L09	Argon	0.91	36.3	32	0.08	2.444
L10	Argon	0.88	41.2	26	76.0	19.25

**Table 6. Summary of retained properties for specimens achieving creep run-out of 100 h**

Specimen #	Environment	Prior Creep Stress (MPa)	Control Method	Retained E (GPa)	Retained UTS (MPa)
S04	Air	13	0.05 mm/s	51.0	44.3
S05	Air	30	0.05 mm/s	49.1	48.1
L01	Air	32	0.05 mm/s	49.5	48.5
L03	Steam	13	0.05 mm/s	46.0	48.8
L06	Steam	20	0.05 mm/s	40.6	57.5
L08	Argon	20	0.05 mm/s	46.1	54.5

## 4.2 Thermal Expansion

Thermal strain was recorded during the ramp-up to test temperature. Then, the thermal strain values were used to calculate the coefficient of thermal expansion (CTE),

$\alpha_t$ , by using the equation:  $\alpha_t = \frac{\varepsilon_t}{\Delta T}$  where  $\varepsilon_t$  is the thermal strain in m/m and  $\Delta T$  is the change in temperature in degrees Kelvin.

For the 21 specimens tested, thermal strains varied between 0.74 and 0.92%. The calculated coefficient of linear thermal expansion for the N720/AM CMC with  $\pm 45^\circ$  fiber orientation was  $7.09 \cdot 10^{-6} \text{K}^{-1}$ , which was slightly higher than that for the N720/A composite with  $\pm 45^\circ$  fiber orientation which utilized the same fibers, but had a pure alumina matrix. Thermal strain measurements and coefficients of linear thermal expansion are summarized in Table 7.

**Table 7. Average thermal strains produced by N720/A and N720/AM CMCs with  $\pm 45^\circ$  fiber orientation due to temperature rise from 23 to 1200°C.**

**Data for N720/A from Siegert [16].**

Author	Material	Specimens	Average Thermal Strain (%)	Coefficient of Thermal Expansion ( $10^{-6} \text{K}^{-1}$ )
Siegert [16]	N720/A	16	0.65	6.00
Current Research	N720/AM	21	0.84	7.09

### 4.3 Monotonic Tension

Three tensile tests to failure were performed to determine the ultimate tensile strength (UTS) and the modulus of elasticity (E) of the N720/AM specimens with a  $\pm 45^\circ$  fiber orientation at 1200 °C in laboratory air. The test performed in displacement control was conducted at the rate of 0.05 mm/s and the load-controlled tensile test was conducted at the rate of 15 MPa/s. For the N720/AM composite with  $\pm 45^\circ$  fiber orientation, the average ultimate tensile strength (UTS) was 36.7 MPa, the average elastic modulus was 41.7 GPa and average failure strain was 0.24%. From the previous study [16,17] we

know that for the N720/A composite with  $\pm 45^\circ$  fiber orientation, the average UTS was 54.9 MPa, the average elastic modulus was 46 GPa and failure strain was 0.27%.

Representative stress-strain curves for both composites with  $\pm 45^\circ$  fiber orientation are shown in Figure 13 and Figure 14, where data for N720/A composite with  $\pm 45^\circ$  fiber orientation is from Siegert [16], Ruggles-Wrenn et al [17].

**Table 8. Average tensile properties for N720/A and N720/AM with  $\pm 45^\circ$  fiber orientation at 1200°C in laboratory air. Data for N720/A from Siegert [16], Ruggles-Wrenn et al [17].**

N720/A $\pm 45^\circ$ fiber orientation			N720/AM $\pm 45^\circ$ fiber orientation		
UTS (MPa)	E (GPa)	$\epsilon_f$ (%)	UTS (MPa)	E (GPa)	$\epsilon_f$ (%)
54.9	46	0.27	36.7	41.7	0.24

In Figure 13, a tensile stress-strain curve obtained at 1200°C for N720/AM with  $\pm 45^\circ$  fiber orientation is shown together with the stress-strain curve for N720/AM with  $0/90^\circ$  fiber orientation from prior work [21]. As seen in Figure 13, the stress-strain curve for the  $0^\circ/90^\circ$  fiber orientation is nearly linear to failure. However, the stress-strain curve for the  $\pm 45^\circ$  cross-ply exhibits a short linear region and then departs from linearity. Note that the tensile curve for the  $\pm 45^\circ$  cross-ply is equivalent to a shear stress-strain curve of the  $0^\circ/90^\circ$  cross-ply. Note that the stress-strain curves for N720/AM with both  $0^\circ/90^\circ$  and  $\pm 45^\circ$  fiber orientations are qualitatively similar to the corresponding stress-strain curves reported by Siegert [16] for the N720/A CMC (Figure 14).

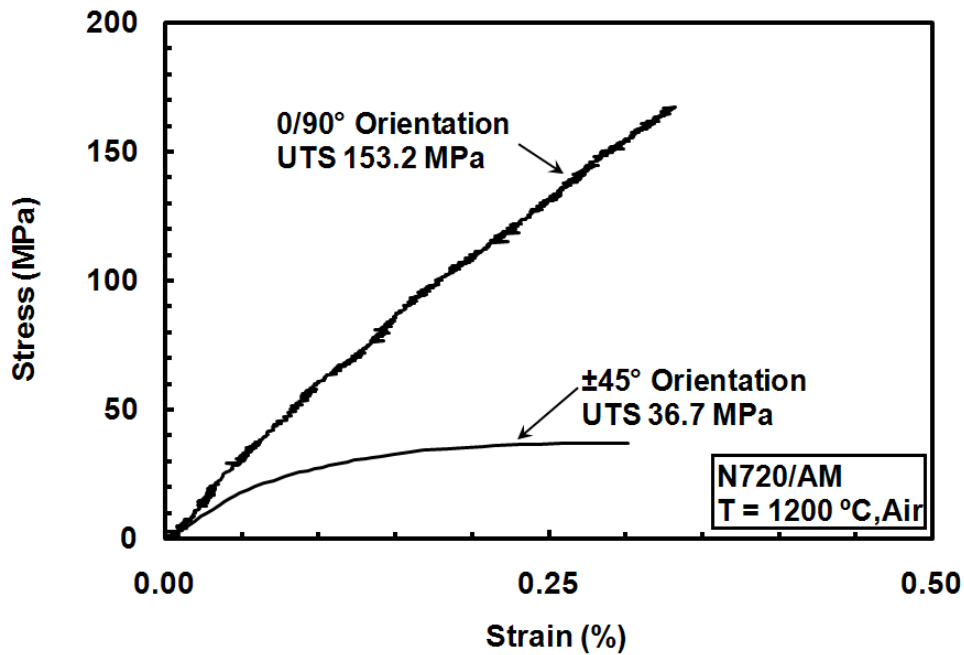


Figure 13. Tensile stress-strain curves for N720/AM ceramic composite at 1200°C in laboratory air. Data for 0°/90° fiber orientation from Genelin [21].

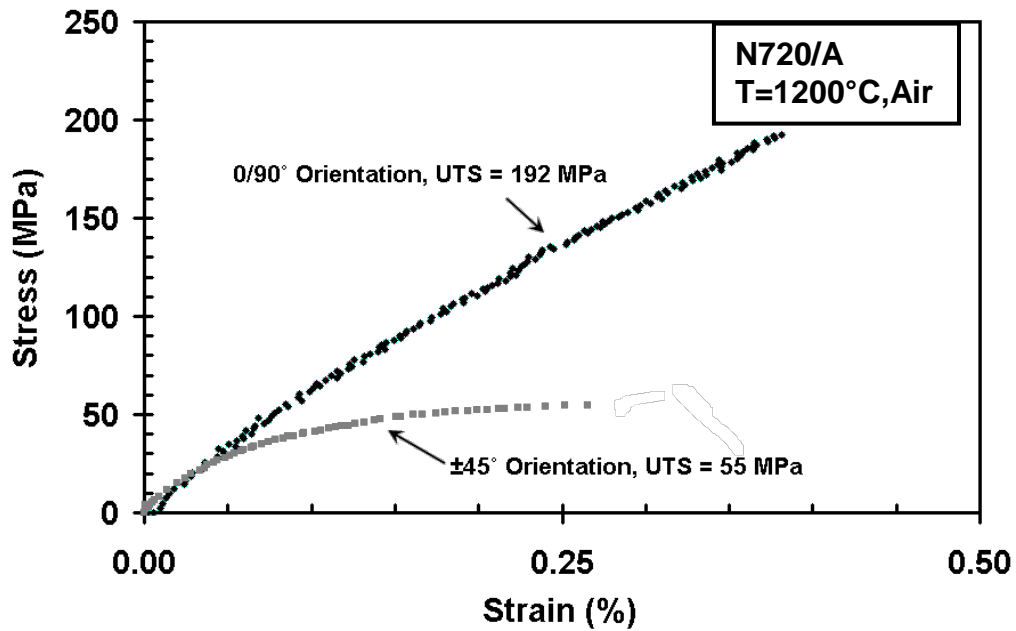


Figure 14. Tensile stress-strain curves for N720/A ceramic composite at 1200°C in laboratory air. Data for N720/A from Siegert [16], Harlan [20].

Five N720/AM specimens with  $\pm 45^\circ$  fiber orientation were also tested in tension to failure in load control at  $1200^\circ\text{C}$  in laboratory air and steam to investigate the effect of stress rate on tensile properties. The stress controlled tensile tests were conducted at constant stress rates of 0.0025 and 25 MPa/s. Modulus, ultimate tensile strength, failure strain and time to failure are presented in Table 9 and Table 10 for each test in laboratory air and in steam, respectively. Stress-strain curves produced at each stress rate are typified in Figure 15 and Figure 16.

**Table 9. Summary of tensile properties of N720/AM composite with  $\pm 45^\circ$  fiber orientation at  $1200^\circ\text{C}$  in laboratory air obtained in stress controlled tensile tests**

<b>Stress Rate</b>	<b>E</b>	<b>UTS</b>	<b>Failure Strain</b>	<b>Time to Failure</b>
<b>(MPa/s)</b>	<b>(GPa)</b>	<b>(MPa)</b>	<b>(%)</b>	<b>(h)</b>
<b>0.0025</b>	11.9	42.7	2.17	4.76
<b>25</b>	42.0	35.3	0.23	0.0004

As can be seen in Figure 15, in the 25 MPa/s constant stress rate test the N720/AM composite with  $\pm 45^\circ$  fiber orientation produced an elastic modulus of 42.0 GPa which is similar to the average modulus observed in displacement-controlled tensile tests in laboratory air at  $1200^\circ\text{C}$  (41.7 GPa). Furthermore, the ultimate tensile strength was 35.3 MPa, which is also similar to the average UTS observed in displacement-controlled tensile tests in air at  $1200^\circ\text{C}$  (36.7 MPa). Failure strain was close to that obtained in displacement-controlled tensile tests in laboratory air.

At 0.0025 MPa/s, the stress-strain behavior changes dramatically. The elastic modulus was 11.9 GPa, which is 72% lower than that obtained in the 25 MPa/s test. As

stress levels increase, the slope of the stress-strain curve drops and considerable inelastic strain develops. The UTS was 42.7 MPa, which is 20% higher than that produced in the 25 MPa/s test. Failure strain obtained in the 0.0025 MPa/s test is nearly 10 times that produced in the 25 MPa/s test.

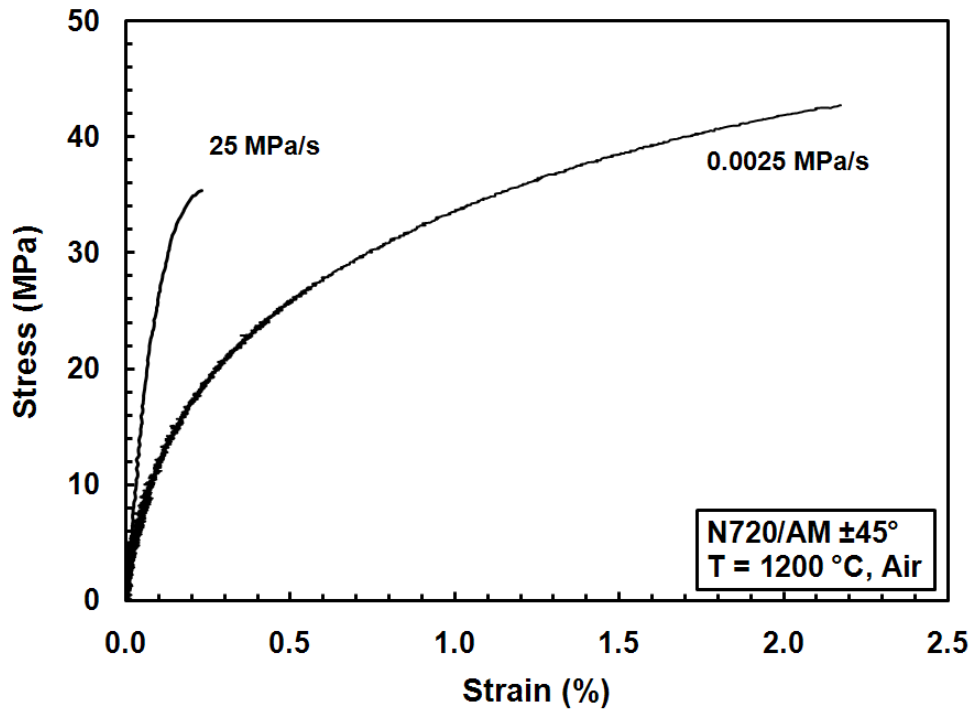


**Figure 15. Tensile stress-strain curves for N720/AM composite with  $\pm 45^\circ$  fiber orientation at  $1200^\circ\text{C}$  in laboratory air. Dependence of stress-strain behavior and tensile properties on stress rate is evident.**

**Table 10. Summary of tensile properties of N720/AM composite with  $\pm 45^\circ$  fiber orientation at  $1200^\circ\text{C}$  in steam obtained in stress controlled tensile tests**

Stress Rate (MPa/s)	E (GPa)	UTS (MPa)	Failure Strain (%)	Time to Failure (h)
0.0025	4.47	46.0	10.2	5.12
0.0025	3.95	49.2	8.76	5.46
25	40.9	33.3	0.23	0.00038

Results in Figure 16 and Table 10 reveal that the tensile properties produced at 0.0025 MPa/s and at 25 MPa/s in steam were similar to those obtained in corresponding tests in laboratory air. For 25 MPa/s test the ultimate tensile strength was 33.3 MPa, which represents a 9% reduction compared to the average UTS observed in displacement-controlled tensile tests in laboratory air at 1200°C (36.7 MPa) and a 5% reduction compared to UTS obtained in the 25MPa/s test performed in laboratory air at 1200°C (35.3 MPa). The modulus obtained in the 25MPa/s test in steam (40.9 GPa) was slightly lower than the average modulus produced in displacement-controlled tensile tests conducted in laboratory air at 1200°C (41.7 GPa). The failure strain was 0.23%.

Two tests were conducted at 0.0025 MPa/s in steam for confirmation purposes. The two tests produced similar results and similar stress-strain curves. The stress-strain curves obtained in steam were similar to the stress-strain curves obtained at 0.0025MPa/s in air. The average modulus was 4.21 GPa, which represents a reduction of nearly 90% compared to the average modulus obtained at 1200°C in laboratory air at a displacement rate of 0.05 mm/s (41.7 GPa). The UTS values were 46.0 MPa and 49.2 MPa.

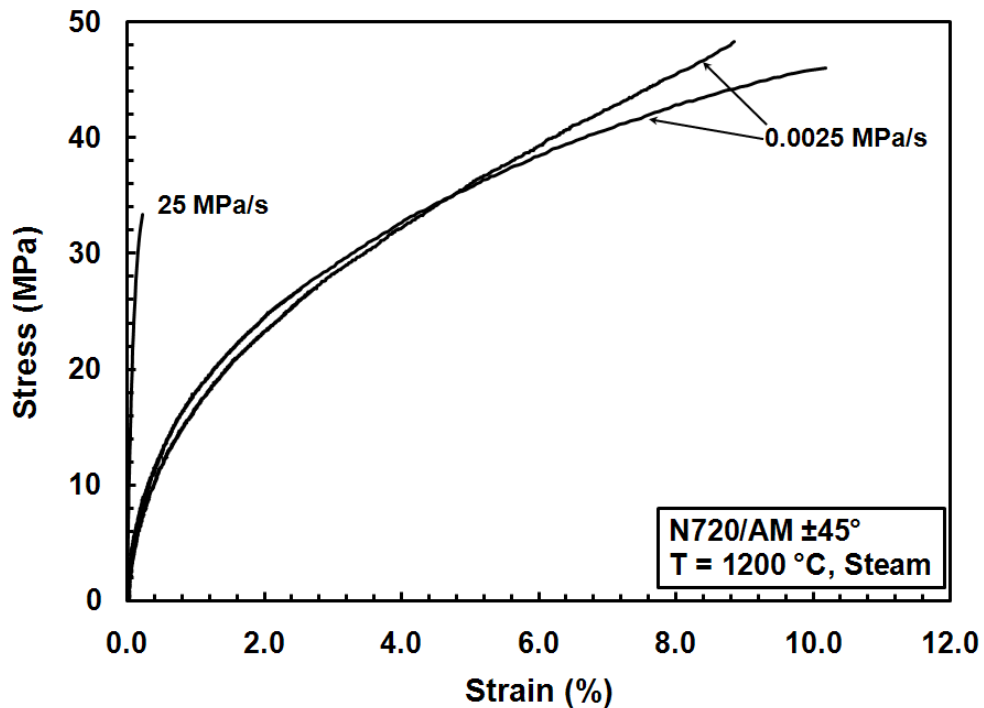


**Figure 16. Tensile stress-strain curves for N720/AM composite with  $\pm 45^\circ$  fiber orientation at  $1200^\circ\text{C}$  in steam. Dependence of stress-strain behavior and tensile properties on stress rate is evident.**

#### 4.4 Creep-Rupture Tests

Creep tests at 13, 30 and 32 MPa were carried out at  $1200^\circ\text{C}$  in laboratory air and in steam. In addition, creep tests at 20 and 26 MPa were also performed in steam. In argon, creep tests were carried out at 20, 26, 30 and 32 MPa. Results of the creep tests produced in laboratory air, in steam and in argon for the N720/A and N720/AM composites are presented in Table 5.

The modulus of elasticity,  $E$ , was calculated for each specimen. The average  $E$  for each load and environment can be seen in Table 11 and Table 12 for N720/AM and N720/A specimens with  $\pm 45^\circ$  fiber orientation, respectively.

**Table 11. Average modulus of elasticity of N720/AM specimens with  $\pm 45^\circ$  fiber orientation tested in creep at 1200°C**

Average E (GPa)	Creep Stress (MPa)					Environment		
	32	30	26	20	13	Air	Steam	Argon
	39.23	42.13	40.50	37.95	42.15	41.87	39.54	40.50

**Table 12. Average modulus of elasticity of N720/A specimens with  $\pm 45^\circ$  fiber orientation tested in creep at 1200°C. Data for N720/A from Siegert [16].**

Average E (GPa)	Load (MPa)				Environment		
	45	40	35	15	Air	Steam	Argon
	45.05	45.43	45.6	46.57	46.48	43.65	46.41

In all environments, N720/A specimens have higher average modulus values than N720/AM specimens. Note that the N720/A specimens also exhibit higher UTS values. I want to mention that the composite porosity of the N720/AM CMC was  $\sim 28.3\%$  and the matrix porosity of the N720/A CMC was  $\sim 24\%$ .

The results obtained from the creep tests conducted at 1200°C in laboratory air both for N720/AM and N720/A specimens with  $\pm 45^\circ$  fiber orientation are summarized in Table 13.

**Table 13. Creep results for the N720/A and N720/AM composites with  $\pm 45^\circ$  fiber orientation tested in laboratory air. Data for N720/A from Siegert [16], Ruggles-Wrenn et al [17].**

<b>Material</b>	<b>Creep Stress (MPa)</b>	<b>Creep Life (h)</b>	<b>Creep Strain (%)</b>
<b>N720/AM</b>	13	>100	0.785
<b>N720/AM</b>	30	>100	4.101
<b>N720/AM</b>	32	>100	4.354
<b>N720/A</b>	15	>100	3.38
<b>N720/A</b>	35	>100	13.3
<b>N720/A</b>	40	23.72	11.9
<b>N720/A</b>	45	0.033	1.48

All the creep tests performed in laboratory air achieved run-out and were subsequently subjected to a tensile test to failure in order to determine the retained strength and stiffness. As the creep stress level increased, accumulated creep strain also increased. The largest amount of creep strain (4.354%) was accumulated in the 32 MPa test. The reported results also show that the creep run-out stress for laboratory air environment is 32 MPa. Creep strains at all creep stress levels were higher than the failure strains obtained in tension tests.

For both materials creep tests performed at two lowest stress levels (13 and 30 MPa for N720/AM and 15 and 35 MPa for N720/A) achieved run-out. It is noteworthy that for all creep stress levels N720/A specimens with  $\pm 45^\circ$  fiber orientation accumulated higher strains than the N720/AM specimens with  $\pm 45^\circ$  fiber orientation.

Creep vs. time curves from prior work [16,17] obtained for N720/A composites with  $\pm 45^\circ$  fiber orientation in laboratory air at 1200°C are shown in Figures 17 and 18. In

all the tests in Figure 18, primary creep rapidly transitions into secondary creep. In the case of the 45 MPa test, secondary creep transitions into tertiary creep. For the creep stress levels  $\leq 40$  MPa, secondary creep persists until failure or to run-out.

Creep vs. time curves for N720/AM specimens with  $\pm 45^\circ$  fiber orientation obtained in laboratory air at  $1200^\circ\text{C}$  are shown in Figure 19. Primary creep and secondary creep regimes, but no tertiary creep are observed for all stress levels. Secondary creep continues until run-out is achieved for all stress levels. For the lower creep stress levels, the transition from primary to secondary creep regimes occurs earlier in the creep life.

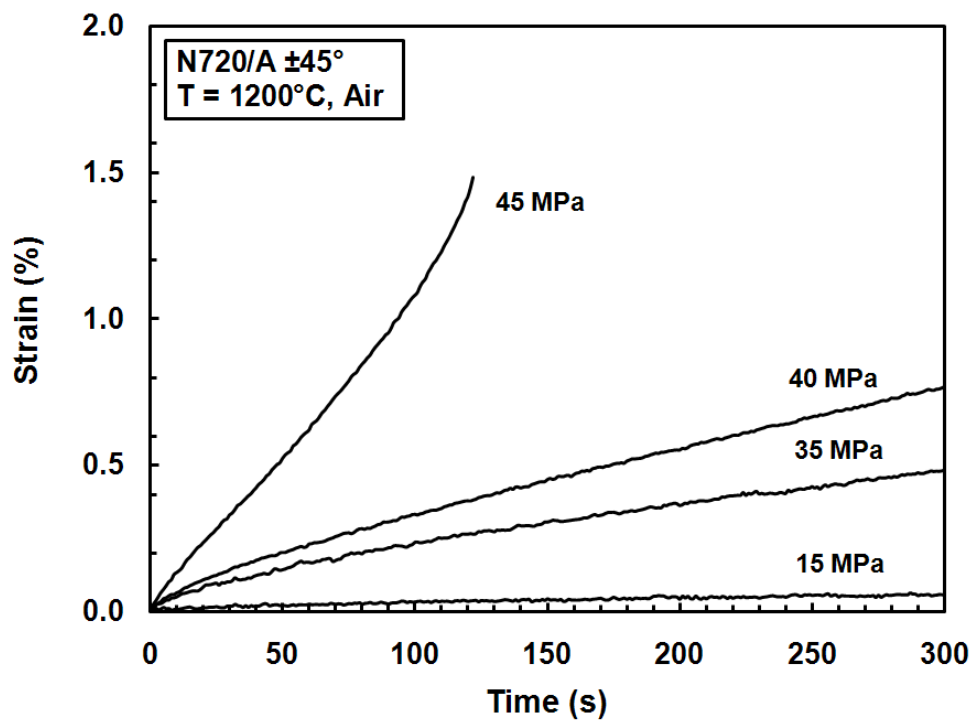


**Figure 17. Creep vs. time curves for N720/A composite with  $\pm 45^\circ$  fiber orientation obtained at  $1200^\circ\text{C}$  in laboratory air. Data for N720/A from Siegert [16], Ruggles-Wrenn et al [17].**

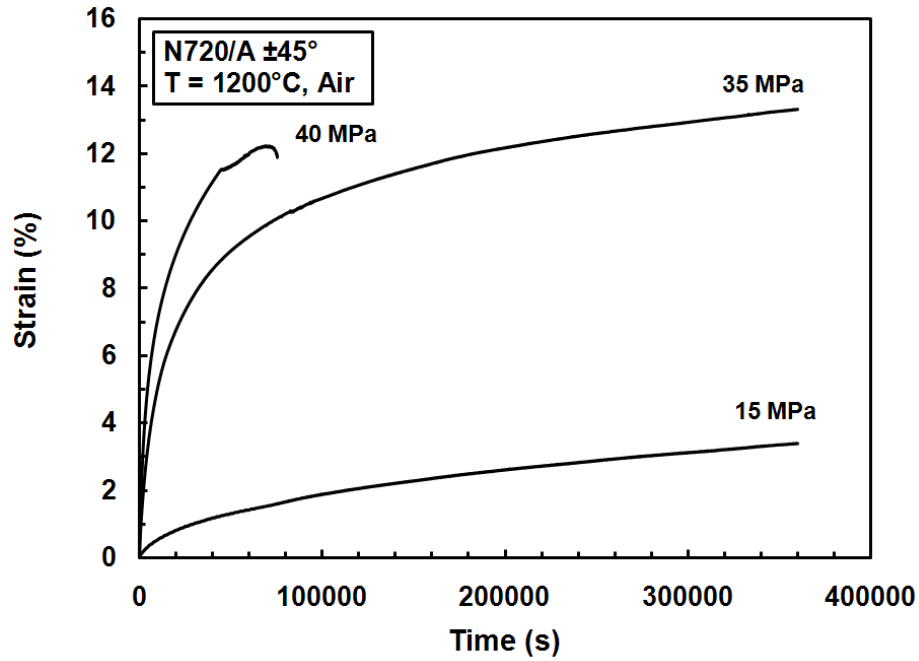


Figure 18. Creep vs. time curves for N720/A composite with  $\pm 45^\circ$  fiber orientation obtained at  $1200^\circ\text{C}$  in laboratory air. Data for N720/A from Siegert [16], Ruggles-Wrenn et al [17].

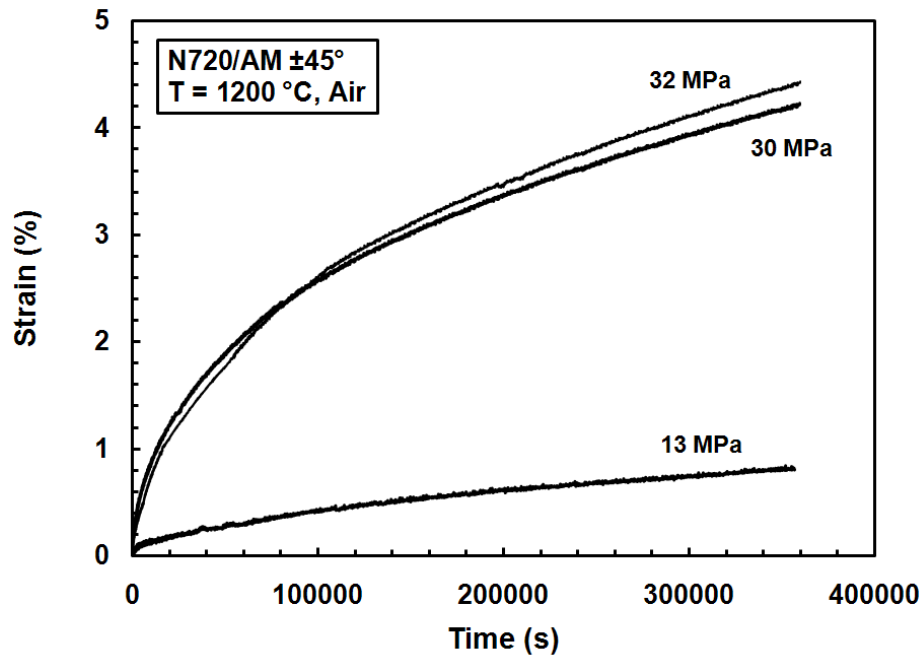


Figure 19. Creep vs. time curves for N720/AM composite with  $\pm 45^\circ$  fiber orientation obtained at  $1200^\circ\text{C}$  in laboratory air

Results of the creep tests conducted at 1200°C in steam for both materials are summarized in Table 14. Results for N720/A composite from Siegert [16], Ruggles-Wrenn et al [17] are included for comparison.

**Table 14. Creep results for the N720/A and N720/AM composites with  $\pm 45^\circ$  fiber orientation tested in steam. Data for N720/A from Siegert [16], Ruggles-Wrenn et al [17].**

<b>Material</b>	<b>Creep Stress (MPa)</b>	<b>Creep Life (h)</b>	<b>Creep Strain (%)</b>
<b>N720/AM</b>	13	>100	4.275
<b>N720/AM</b>	20	>100	12.48
<b>N720/AM</b>	26	99.4	18.25
<b>N720/AM</b>	30	1.08	5.682
<b>N720/AM</b>	32	0.02	0.642
<b>N720/A</b>	15	100	4.80
<b>N720/A</b>	35	100	17.8
<b>N720/A</b>	40	0.733	4.92
<b>N720/A</b>	45	0.016	0.65

The creep curves obtained at 1200 °C in steam for N720/AM specimens with  $\pm 45^\circ$  fiber orientation are presented in Figure 21. Creep curves for the N720/A from Siegert [16] and Ruggles-Wrenn et al [17] are shown in Figure 20 for comparison. The

creep curves obtained in steam environment for the N720/AM specimens with  $\pm 45^\circ$  fiber orientation had nearly the same appearance as those obtained in laboratory air. All creep curves had short primary creep followed by secondary creep, which persisted to the failure or run-out. Siegert [16] reported that in steam at 45 MPa, the N720/A specimens exhibited short primary and secondary creep regimes, but also early developed tertiary creep. Conversely for the N720/AM specimens no tertiary creep was observed (see Figure 21).

Creep strain accumulated at 13 MPa in steam was nearly 5 times that accumulated at 13 MPa in air. At 30 MPa, creep strain accumulated in steam was only  $\sim 1.4$  times that accumulated in air. At 32 MPa, the presence of steam resulted in a drastic decrease in creep strain as well as in creep lifetime. In steam run-out was achieved only at 13 and 20 MPa. Creep test conducted at 26 MPa in steam approached, but did not achieve a run-out. At 30 MPa creep lifetime in steam was 1.08 h and at 32 MPa creep lifetime in steam was merely 0.02 h. Recall that creep run-out was achieved at 30 and 32 MPa in laboratory air. These results demonstrate that the presence of steam degrades creep lifetime and creep performance of the N720/AM composite with  $\pm 45^\circ$  fiber orientation.

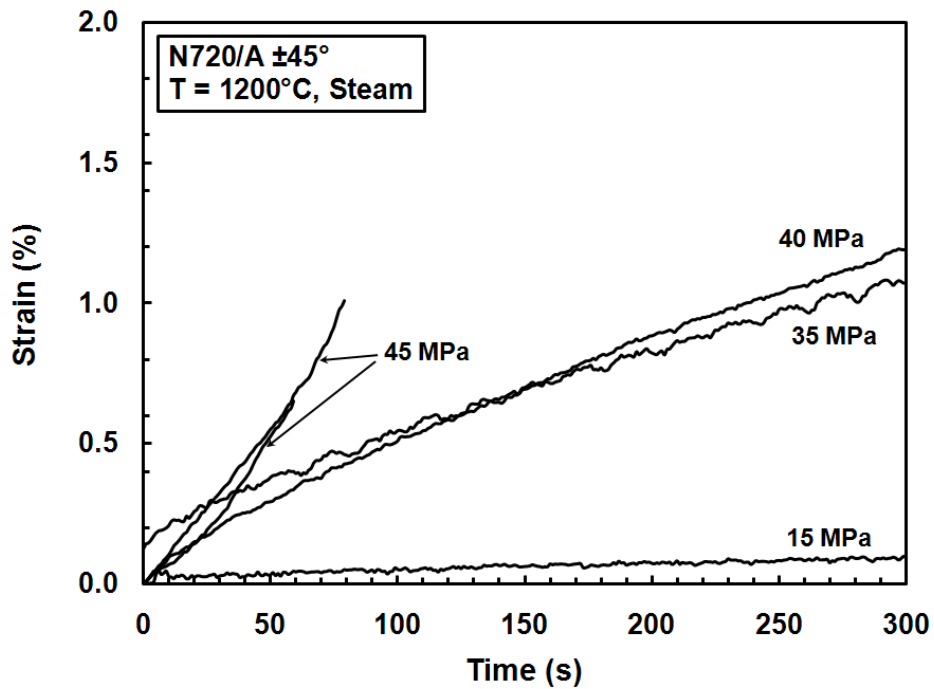
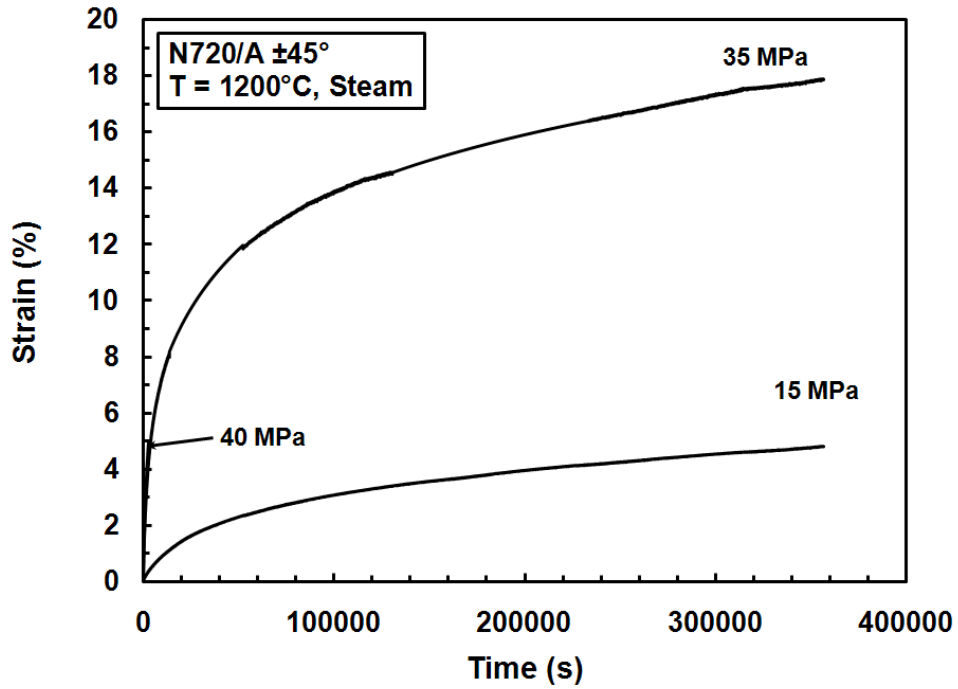


Figure 20. Creep vs. time curves for N720/A composite with  $\pm 45^\circ$  fiber orientation obtained at 1200°C in steam. Data for N720/A from Siegert [16], Ruggles-Wrenn et al [17].

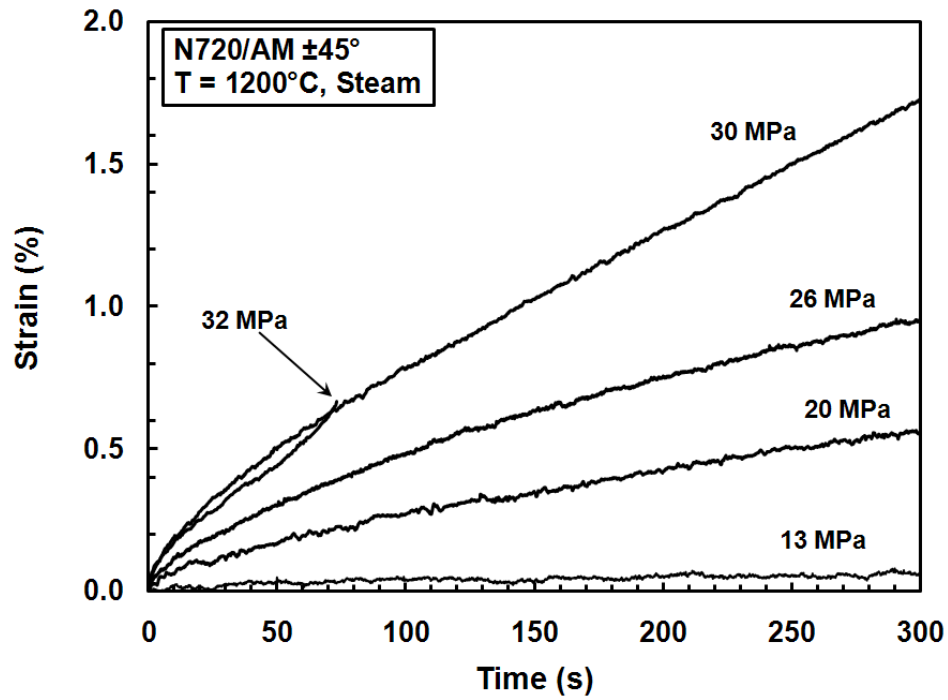
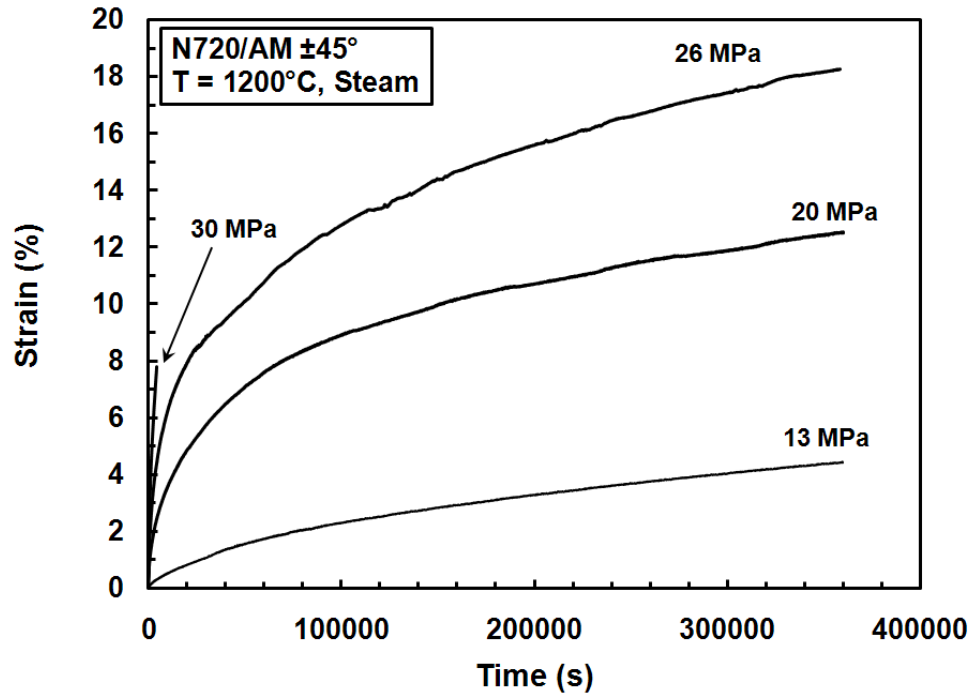


Figure 21. Creep vs. time curves for N720/AM composite with  $\pm 45^\circ$  fiber orientation obtained at 1200°C in steam

The results of creep tests conducted in argon environment are summarized in Table 15 for both N720/AM and N720/AM specimens. Data for N720/A composite are from Siegert [16], Ruggles-Wrenn et al [17].

**Table 15. Creep results for the N720/A and N720/AM composites with  $\pm 45^\circ$  fiber orientation tested in argon. Data for N720/A from Siegert [16], Ruggles-Wrenn et al [17].**

<b>Material</b>	<b>Creep Stress (MPa)</b>	<b>Creep Life (h)</b>	<b>Creep Strain (%)</b>
<b>N720/AM</b>	20	>100	16.72
<b>N720/AM</b>	26	76	19.25
<b>N720/AM</b>	30	3.42	12.97
<b>N720/AM</b>	32	0.08	2.444
<b>N720/A</b>	15	100	7.05
<b>N720/A</b>	30*	NA	4.46
<b>N720/A</b>	35	100	20.5
<b>N720/A</b>	40	0.014	3.36
<b>N720/A</b>	40	0.018	3.58
<b>N720/A</b>	45	0.004	3.55
<b>N720/A</b>	45	0.006	4.12

\*Test interrupted due to machine malfunction

As we know, argon environment is a non-oxidizing environment. Therefore it was expected that the presence of argon would not degrade creep performance of oxide/oxide CMCs like N720/AM. In argon, the 20 MPa creep test achieved run-out. But the 26 MPa test had a creep lifetime of 76 h. Recall that in steam creep lifetime at 26 MPa was 99.4 h. This was an unexpected result. On the other hand, presence of argon improved the creep lifetimes at 30 MPa and the 32 MPa. Furthermore, creep strains accumulated in argon were higher than the creep strains accumulated in air or in steam for the same stress level.

It is noteworthy that creep vs. time curves obtained at stress levels >20 MPa in argon environment exhibited tertiary creep regime. At 20 MPa in argon, only primary and secondary creep regimes were observed.

Results in Figures 22-24 permit comparison between creep curves produced at 30 MPa in argon by N720/A and N720/AM composites. It is seen that the creep curve produced by the N720/A specimens with  $\pm 45^\circ$  fiber orientation exhibits primary and secondary creep regimes and is also very close to the 15 MPa creep curve. On the other hand, N720/AM specimens with  $\pm 45^\circ$  fiber orientation accumulated considerably larger strain during primary and secondary creep regimes. Furthermore, tertiary creep was also observed. Note that in the 30 MPa test conducted in argon the N720/A specimen accumulated only 4.46 % strain after 50 h. Conversely, N720/AM specimens accumulated strain of 12.97% in 3.42 h.

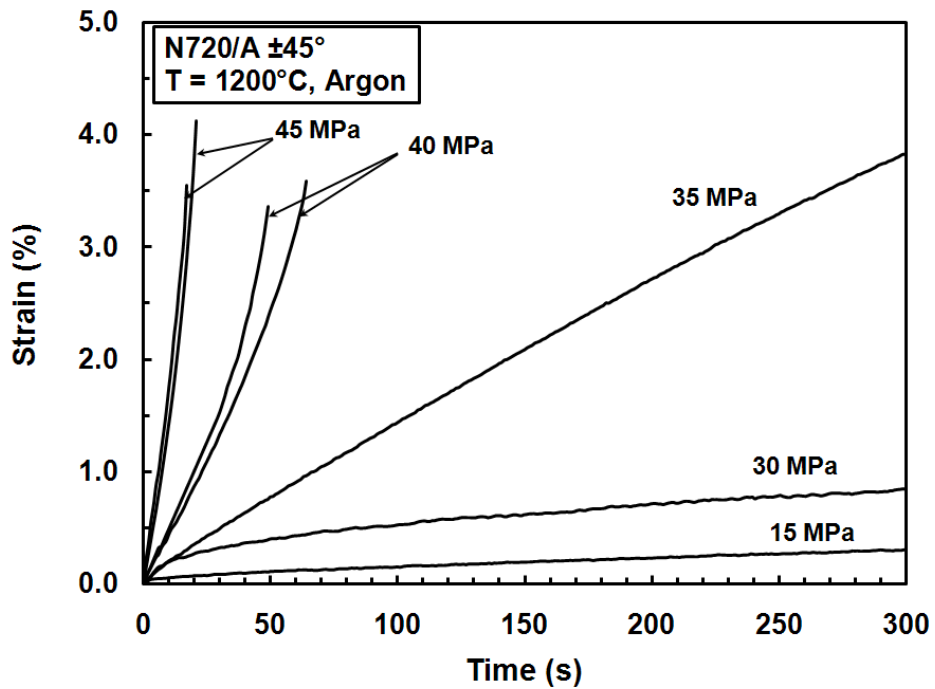
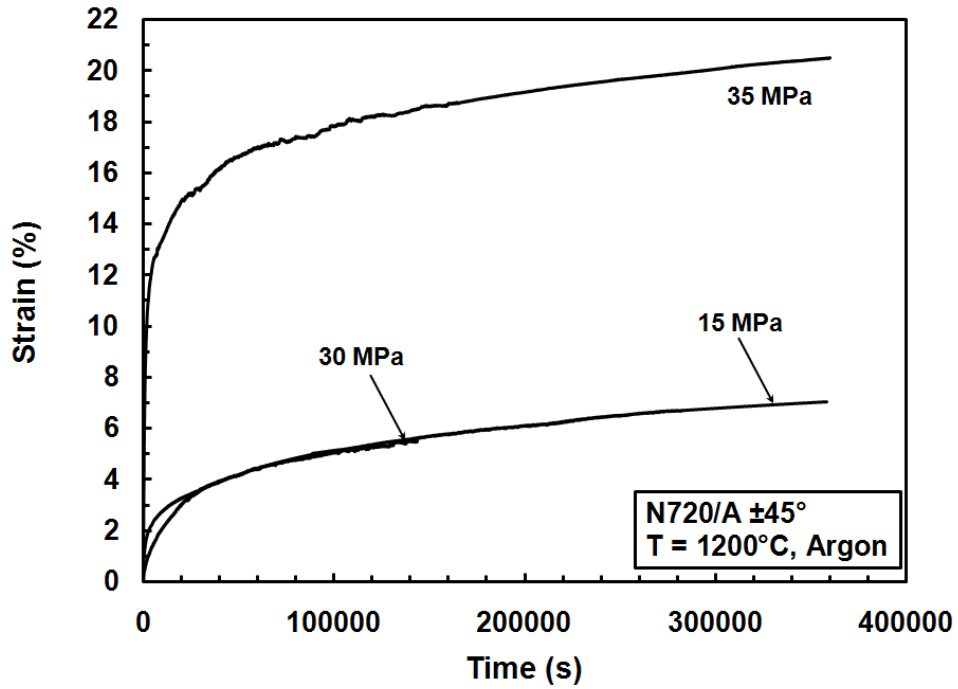


Figure 22. Creep vs. time curves for N720/A composite with  $\pm 45^\circ$  fiber orientation obtained at 1200°C in argon. Data for N720/A from Siegert [16], Ruggles-Wrenn et al [17].

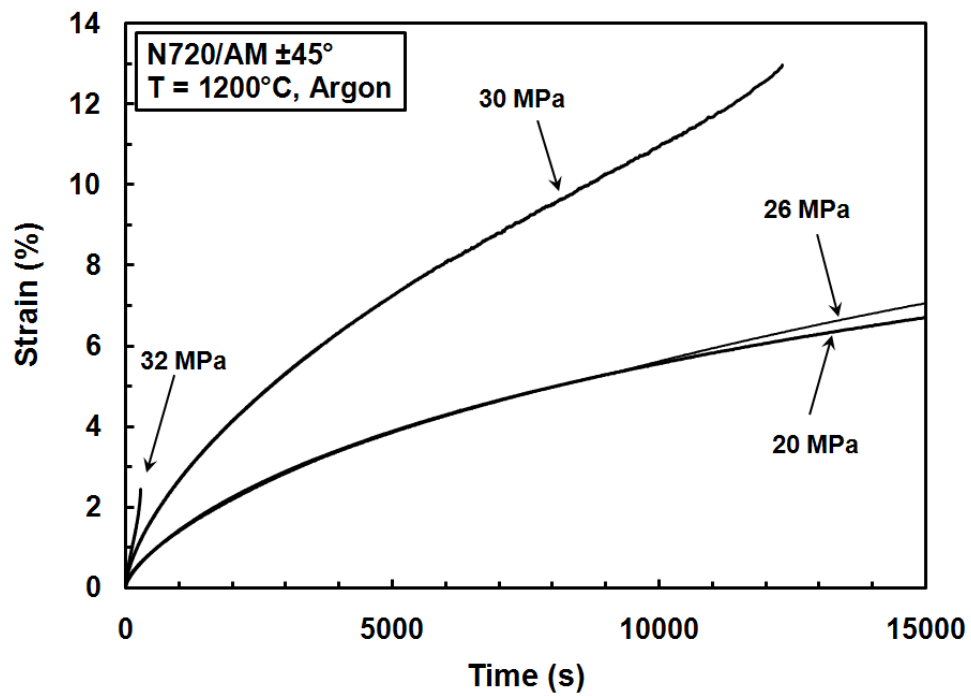
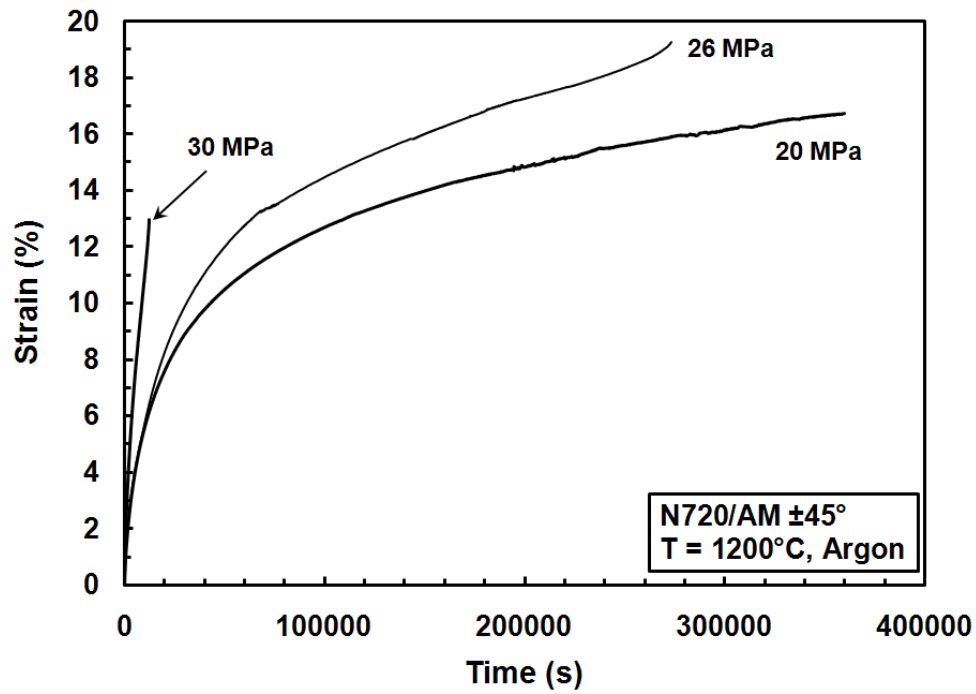
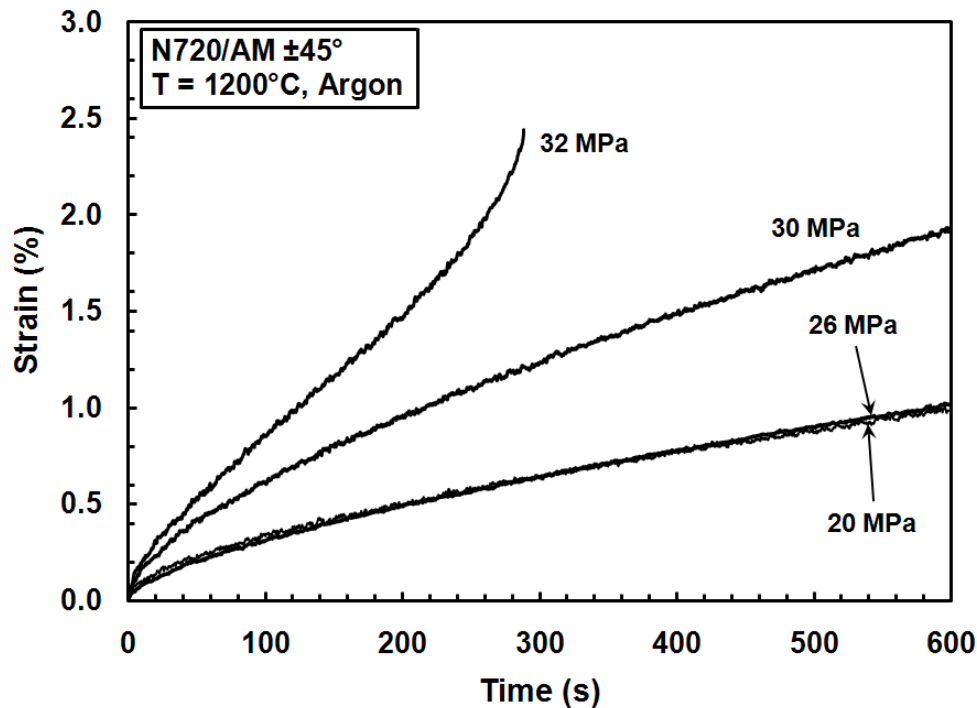


Figure 23. Creep vs. time curves for N720/AM composite with  $\pm 45^\circ$  fiber orientation obtained at 1200°C in argon



**Figure 24. Creep vs. time curves for N720/AM composite with  $\pm 45^\circ$  fiber orientation obtained at  $1200^\circ\text{C}$  in argon**

Retained strength and modulus of the specimens that achieved run-out in creep tests are summarized in Table 16. Data for N720/A from Siegert [16], Ruggles-Wrenn et al [17] are included for comparison. In the case of the N720/A, each specimen retained over 89% of its tensile strength, with most retaining over 100% of their tensile strength. The modulus retention was also close to or over 100%. Prior creep had minimal effect on the failure strain [16,17]. The N720/AM specimens retained over 100% of their tensile strength, with most retaining over 156% of the UTS following creep in steam environment. The modulus varied between 109% and 122%. Prior creep in air, steam

and argon environments had similar effects on the retained properties. For N720/AM specimens subjected to prior creep in air and steam environments, the failure strain values were nearly the same and noticeably lower than the failure strain obtained in tensile test for the as-processed CMC. However, the N720/AM specimen pre-crept in argon produced a considerably higher failure strain of 0.57%, which is more than 3 times the failure strain produced by specimens pre-crept in air and in steam. Figure 26 shows that prior creep in air and in steam caused reduction in the failure strain of the N720/AM specimens with  $\pm 45^\circ$  fiber orientation, but improved the tensile.

**Table 16. Retained properties of the N720/A and N720/AM specimens with  $\pm 45^\circ$  fiber orientation subjected to prior creep at 1200°C in laboratory air, steam and argon environments. Data for N720/A from Siegert [16], Ruggles-Wrenn et al [17].**

Material	Environment	Creep Stress (MPa)	Retained Strength (MPa)	Strength Retention (%)	Retained Modulus (GPa)	Modulus Retention (%)	Failure Strain (%)
N720/AM	Air	13	44.2	120	51.0	122	0.14
N720/AM	Air	30	48.1	130	49.1	117	0.17
N720/AM	Air	32	48.5	132	49.5	119	0.17
N720/AM	Steam	13	48.8	132	46.0	109	0.15
N720/AM	Steam	20	57.5	156	40.6	112	0.17
N720/AM	Argon	20	54.5	148	46.1	117	0.57
N720/A	Air	15	61.1	111	64.5	113.81	0.15
N720/A	Air	35	58.3	110	48.4	98.68	0.14
N720/A	Steam	15	67.0	121	63.4	103.49	0.17
N720/A	Steam	35	53.4	97	58.3	114.04	0.07
N720/A	Argon	15	73.0	132	68.8	102.21	0.14
N720/A	Argon	35	49.4	89	55.3	104.61	0.09

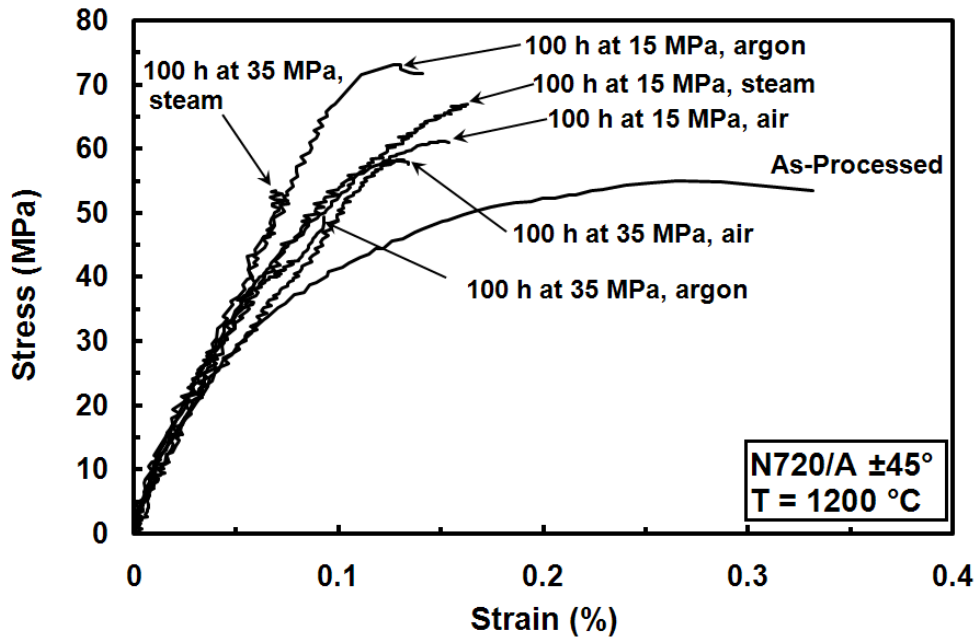


Figure 25. Effect of prior creep at  $1200^\circ\text{C}$  in laboratory air, steam and argon on tensile stress-strain behavior of N720/A composite with  $\pm 45^\circ$  fiber orientation. Data for N720/A from Siegert [16], Ruggles-Wrenn et al [17].

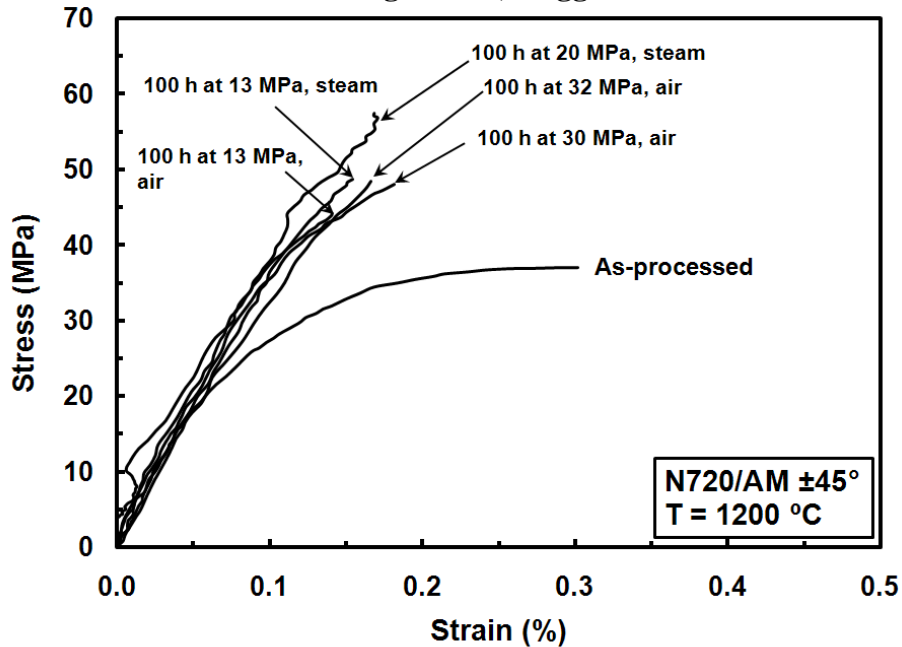
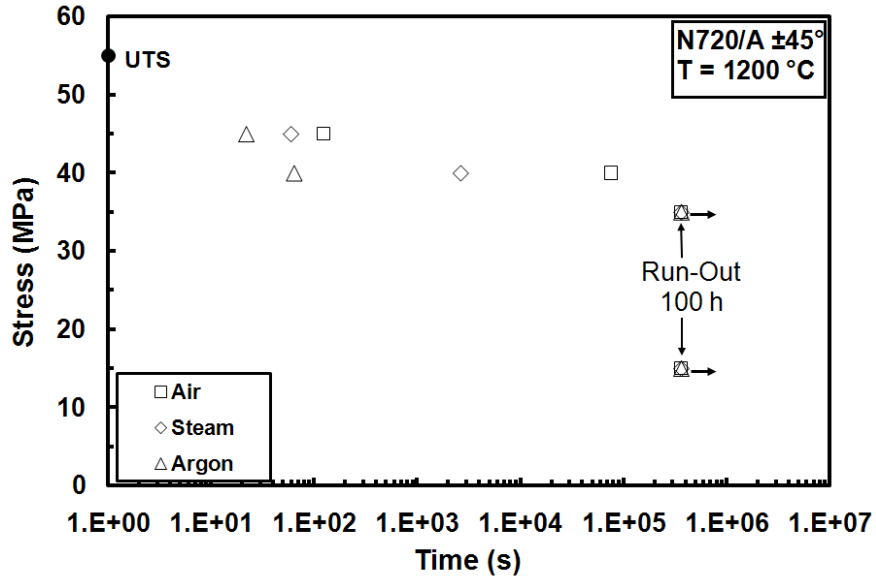


Figure 26. Effect of prior creep at  $1200^\circ\text{C}$  in laboratory air and in steam on tensile stress-strain behavior of N720/AM composite with  $\pm 45^\circ$  fiber orientation

It was reported that prior creep had no qualitative effect on tensile stress-strain behavior of the N720/A composite with  $\pm 45^\circ$  fiber orientation [16,17]. It is seen in Figure 26 that prior creep in air and in steam decreases the capacity of the N720/AM composite for inelastic straining.

The objective of this research was to assess the creep rupture behavior of Nextel<sup>TM</sup> 720/AM ceramic matrix composite at 1200°C in laboratory air, in argon and in steam. Stress-rupture behavior of N720/A and N720/AM composites is summarized in Figure 27 and Figure 28, respectively. Results for N720/A are from Siegert [16], Ruggles-Wrenn et al [17]. Test results demonstrate that in all test environments creep life decreased with increasing creep stress. It can be seen that for stress levels  $\leq 20$  MPa, run-out was achieved in all test environments. Recall that, all tests conducted in laboratory air achieved run-out. At creep stress levels above 20 MPa, specimens tested in air exhibited the longest creep lives followed by those tested in argon with the exception of 26 MPa test. Surprisingly the 26 MPa test conducted in steam produced a longer creep lifetime than the 26 MPa test conducted in argon. Results from prior work [16,17] in Figure 27 reveal that for stress levels  $\leq 35$  MPa, run-out was achieved in all test environments. However, at creep stress levels above 35 MPa, specimens tested in air exhibited the longest creep lives followed by those tested in steam. Specimens tested in argon at creep stress levels above 35 MPa exhibited the shortest creep lives [16,17]. Argon had no beneficial effect on creep lifetimes for both composites. For the N720/AM CMC, the reduction in creep life was at least 0.6% due to steam and at least 24% due to argon for

applied stress level of 26 MPa. For N720/AM for stress levels  $\geq 26$  MPa, the loss of creep life due to the presence of steam and argon was greater than 96%.



**Figure 27. Applied stress vs. time to failure for N720/A ceramic composites with  $\pm 45^\circ$  fiber orientation at  $1200^\circ\text{C}$  in air, argon and steam. Data for N720/A from Siegert [16], Ruggles-Wrenn et al [17].**

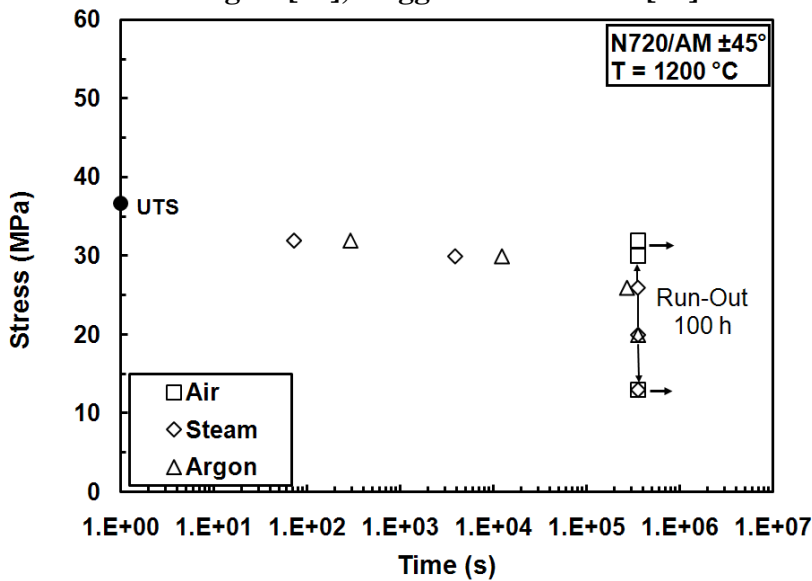


**Figure 28. Applied stress vs. time to failure for N720/AM ceramic composites with  $\pm 45^\circ$  fiber orientation at  $1200^\circ\text{C}$  in laboratory air, argon and steam**

Minimum creep strain rate was reached in all tests. Creep rate as a function of applied stress for N720/AM composites with  $\pm 45^\circ$  fiber orientation is presented in Figure 30. Results in Figure 30 reveal that the lowest creep rates were produced in laboratory air. Creep rate produced at 13 MPa in steam is only slightly higher than that produced in air. However for stress levels  $\geq 30$  MPa, creep rates produced in steam are 3 orders of magnitude higher than those in air. Note that creep rates obtained in argon are similar to those obtained in steam.

To facilitate comparison between the secondary creep rates obtained for N720/AM and those for N720/A CMC reported previously [16,17], creep rates for both composites are plotted as a function of applied stress in Figure 29. Note that in Figure 29 the applied stress is given in terms of %UTS. Results in Figure 29 reveal that creep rate of N720/A in air environment can be 1000 times higher than the creep rate of N720/AM. In steam, creep rate of N720/A can be 10 times higher than the creep rate of N720/AM. Finally, in argon creep rate of N720/A can be 100 times higher than the creep rate of N720/AM.

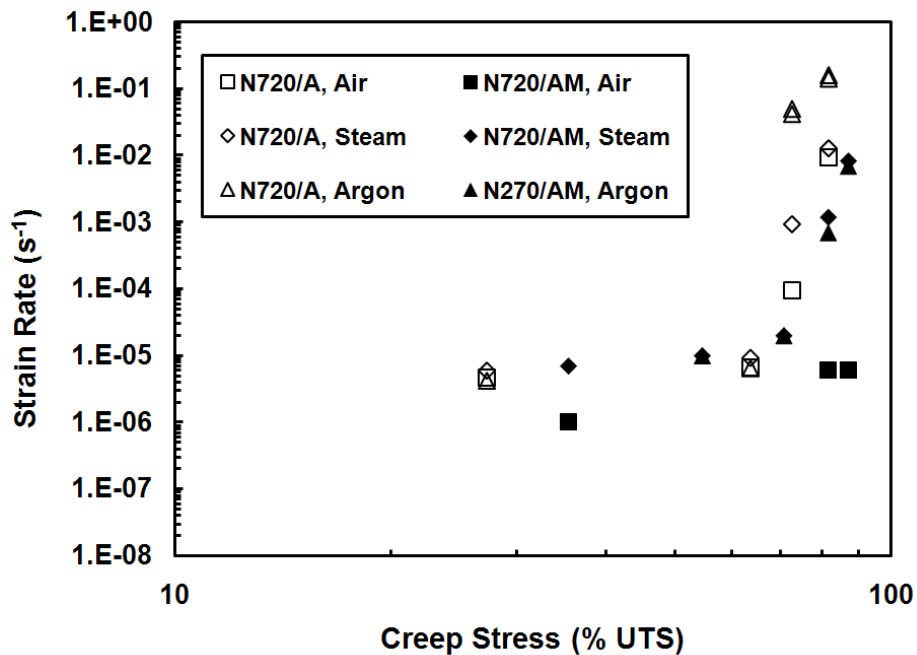


Figure 29. Secondary creep rate as a function of applied stress for N720/AM and N720/A composites with  $\pm 45^\circ$  fiber orientation at  $1200^\circ\text{C}$  in laboratory air, argon and steam. Data for N720/A from Siegert [16], Ruggles-Wrenn et al [17].

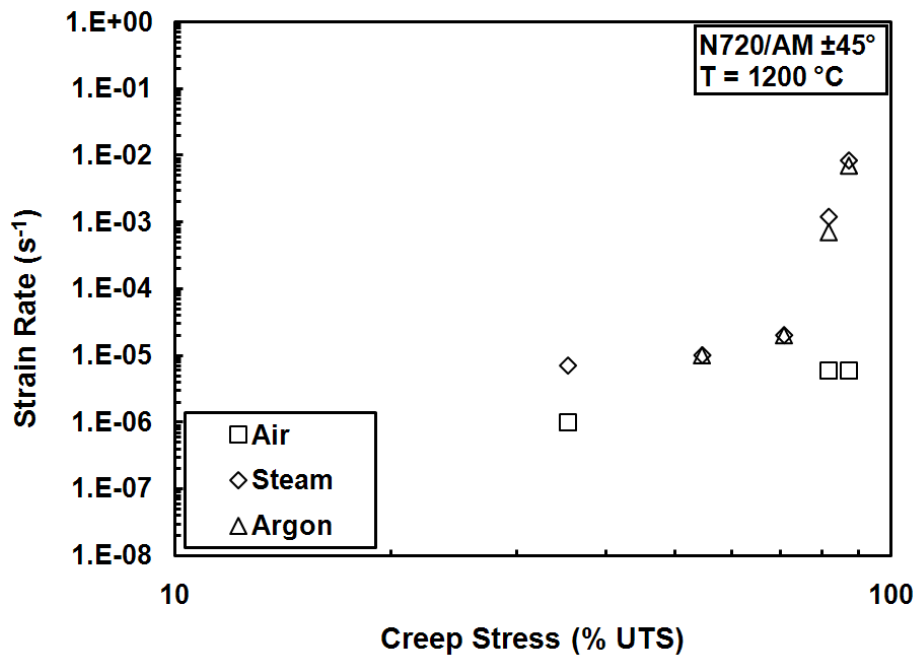
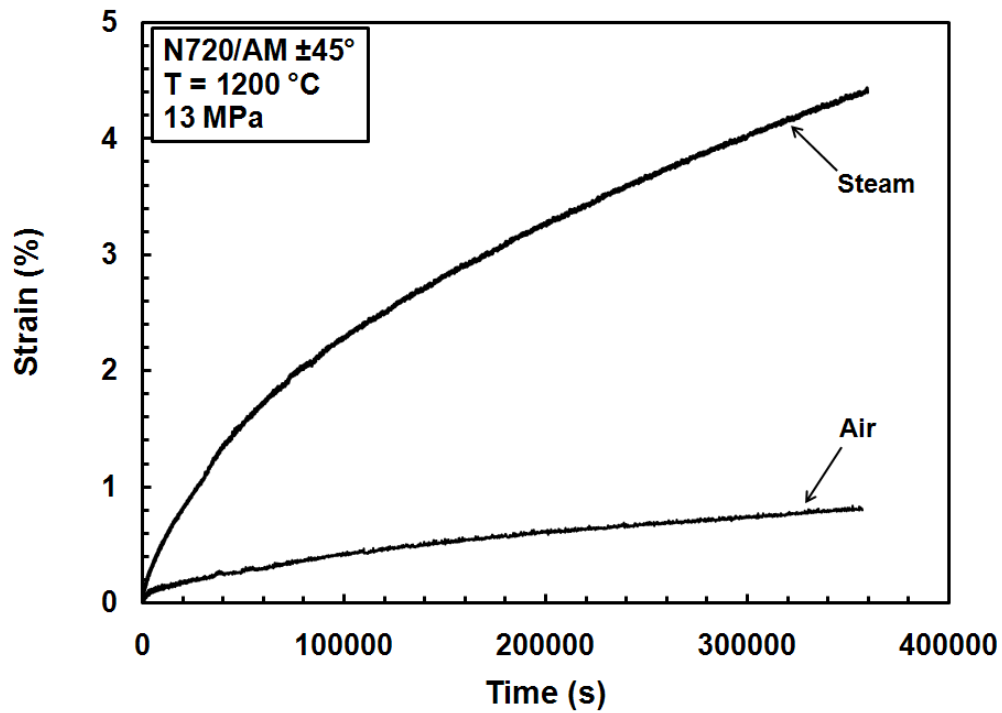


Figure 30. Secondary creep rate as a function of applied stress for N720/AM composite with  $\pm 45^\circ$  fiber orientation at  $1200^\circ\text{C}$  in laboratory air, argon and steam

To gain a better understanding of the effect of the environment on creep strain for N720/AM at 1200 °C, creep curves produced at a given applied stress level in air, steam and argon are presented in Figures 31-35. Results show that at all applied stresses, the largest creep strains are accumulated in argon, followed by those accumulated in steam. The lowest creep strains are produced in air.



**Figure 31. Creep strain vs. time obtained for creep stress of 13 MPa in laboratory air and steam environments at 1200°C**

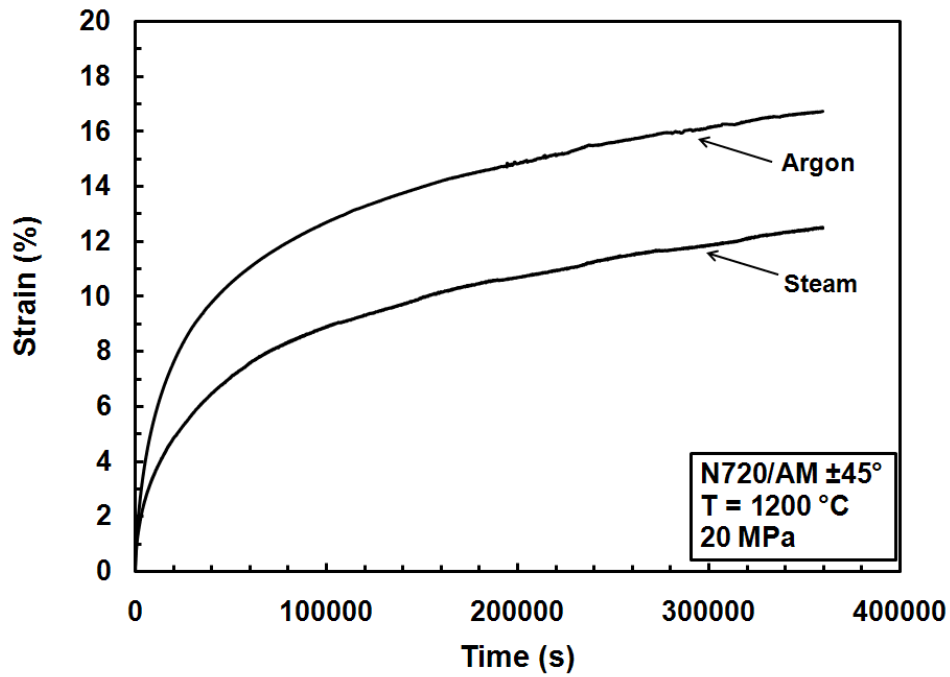


Figure 32. Creep strain vs. time obtained for creep stress of 20 MPa in steam and argon environments at 1200°C

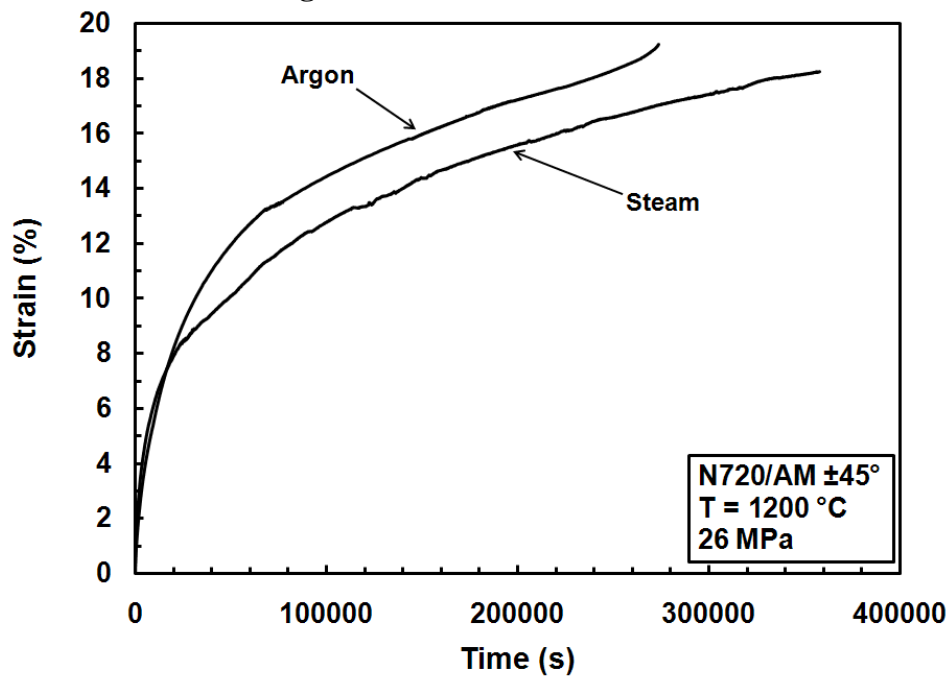


Figure 33. Creep strain vs. time obtained for creep stress of 26 MPa in steam and argon environments at 1200°C

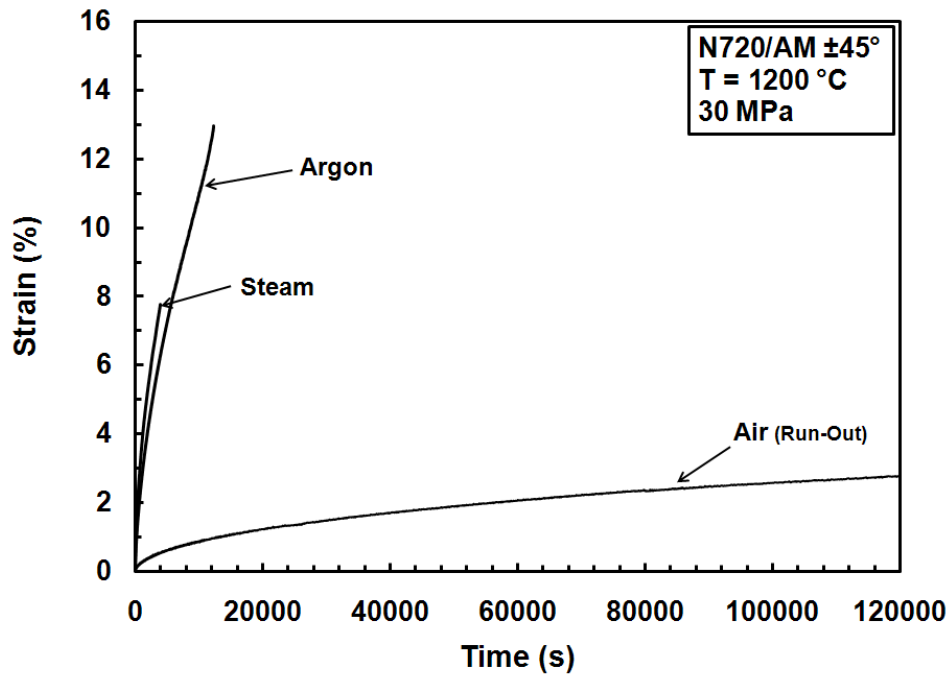


Figure 34. Creep strain vs. time obtained for creep stress of 30 MPa in laboratory air, steam and argon environments at 1200°C

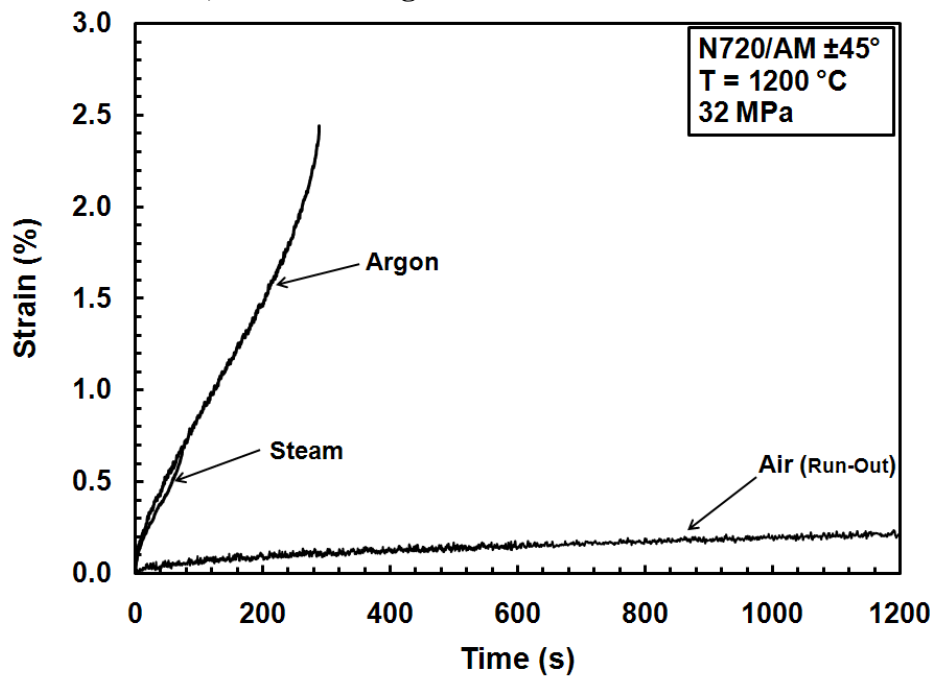


Figure 35. Creep strain vs. time obtained for creep stress of 32 MPa in laboratory air, steam and argon environments at 1200°C

Figure 31 through 35 also confirm that none of the specimens tested in air and steam exhibit tertiary creep. Only the creep tests conducted in argon produced tertiary creep. As was the case for the N720/A composite, for N720/AM composite with  $\pm 45^\circ$  fiber orientation the largest creep strains were accumulated in argon, followed by those accumulated in steam and air [16,17].

In an earlier study, Genelin [21] assessed the creep performance of N720/AM with  $0^\circ/90^\circ$  fiber orientation in laboratory air, steam and argon. Composite with  $0^\circ/90^\circ$  fiber orientation exhibits typical fiber-dominated behavior with fibers carrying most of the load. Therefore, composites with  $0^\circ/90^\circ$  fiber orientation exhibit much higher tensile strengths than those with the  $\pm 45^\circ$  fiber orientation. Behavior of the composite with  $\pm 45^\circ$  fiber orientation is matrix dominated, with only a small fraction of the load being carried by fibers. With weaker matrix carrying most of the load,  $\pm 45^\circ$  cross-ply exhibits a lower tensile strength than its  $0^\circ/90^\circ$  counterpart. The UTS for the N720/AM specimens with  $0^\circ/90^\circ$  fiber orientation was 153.2 MPa, while the UTS for the  $\pm 45^\circ$  specimens with  $\pm 45^\circ$  fiber orientation was only 36.7 MPa. In real-world applications, the composites would not be loaded strictly along the fiber direction all the time. For this reason, it is important to identify the effects of fiber orientation on performance of the CMC. In Figure 36, applied stress vs. rupture time curves obtained in laboratory air, steam and argon environments at  $1200^\circ\text{C}$  for the N720/AM composite with  $\pm 45^\circ$  fiber orientation are plotted together with the results for the N720/AM CMC with  $0^\circ/90^\circ$  fiber orientation from prior work [21].

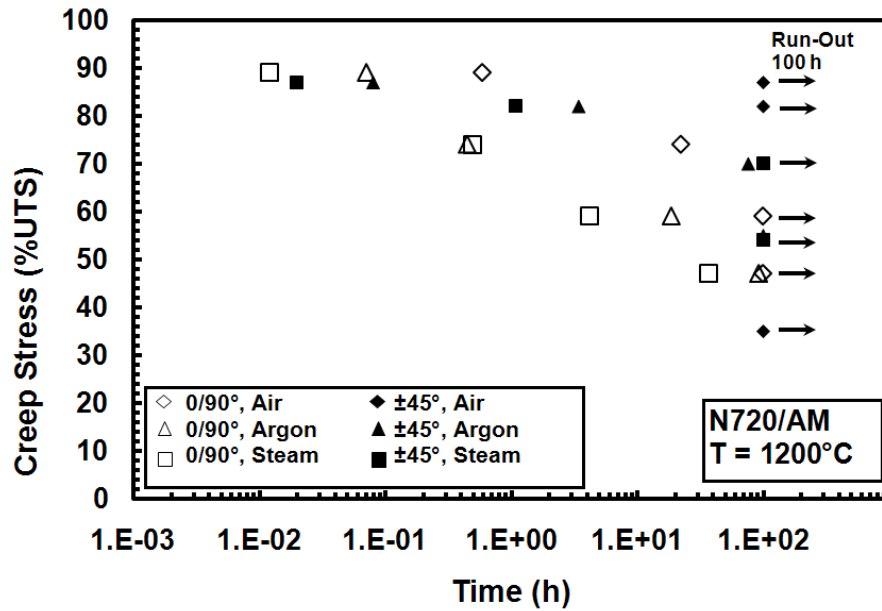


Figure 36. Creep-stress vs. time to failure for N720/AM with 0°/90° and ±45° fiber orientations at 1200°C in laboratory air, steam and argon. Data for N720/AM with 0°/90° fiber orientation from Genelin [21].

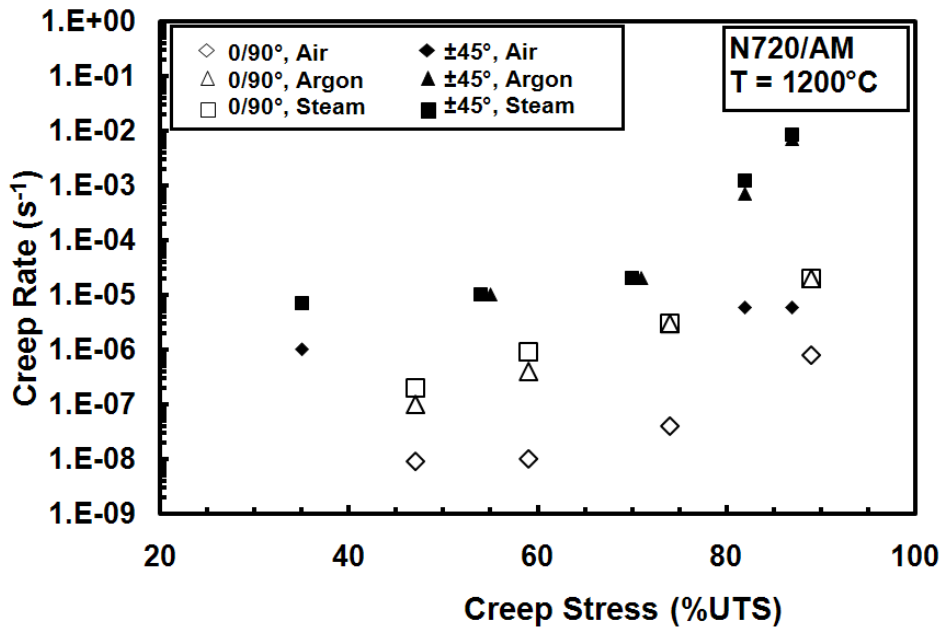


Figure 37. Creep rate vs. creep-stress for N720/AM with 0°/90° and ±45° fiber orientations at 1200°C in laboratory air, steam and argon. Data for N720/AM with 0°/90° fiber orientation from Genelin [21].

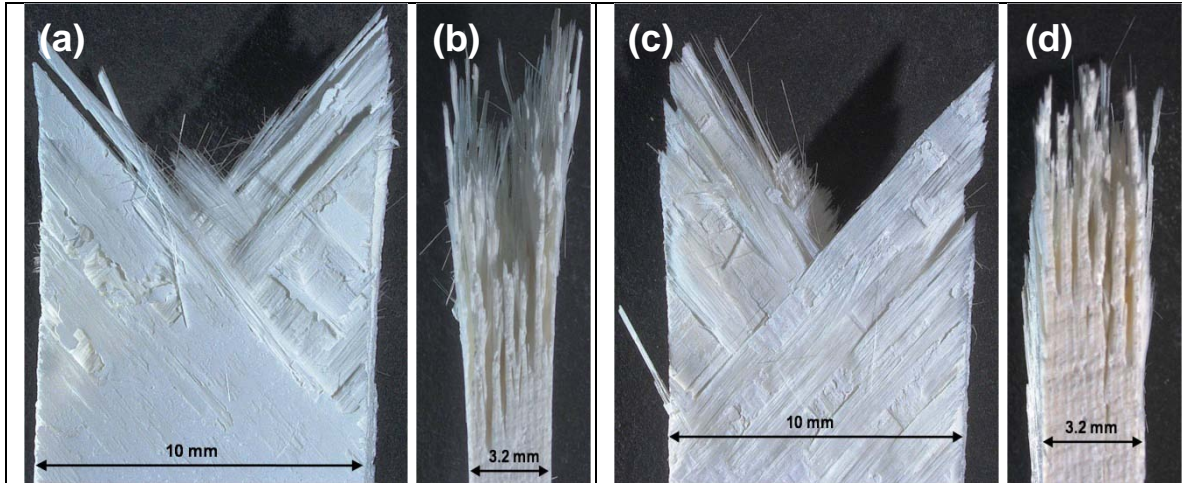
Due to the fiber-dominated behavior of the composites with  $0^\circ/90^\circ$  fiber orientation, N720/AM with  $0^\circ/90^\circ$  fiber orientation can operate at larger creep-stresses than the  $\pm 45^\circ$  cross-ply. For the N720/AM composite, the UTS of the  $0^\circ/90^\circ$  cross-ply is approximately 4.2 times that of the  $\pm 45^\circ$  cross-ply. Furthermore, Figure 36 reveals that N720/AM with  $0^\circ/90^\circ$  fiber orientation is more vulnerable to environmental degradation when operating in steam or argon environments than the  $\pm 45^\circ$  cross-ply. Figure 37 shows the creep strain rates versus the creep stress for both fiber orientations. It is seen that the creep rate increases with increasing stress regardless of fiber orientation. Results in Figure 37 also reveal that the presence of steam or argon accelerates creep of the both fiber orientations at all stress levels investigated. As expected, the  $\pm 45^\circ$  cross-ply exhibits higher overall creep rates than the  $0^\circ/90^\circ$  cross-ply. Similar observations were reported for the N720/A composite [16,17].

#### 4.5 Composite Microstructure

In this section, the microstructure of N720/AM specimens with  $\pm 45^\circ$  fiber orientation will be discussed. An optical microscope and a scanning electron microscope (SEM) were used to analyze the specimens following the mechanical testing.

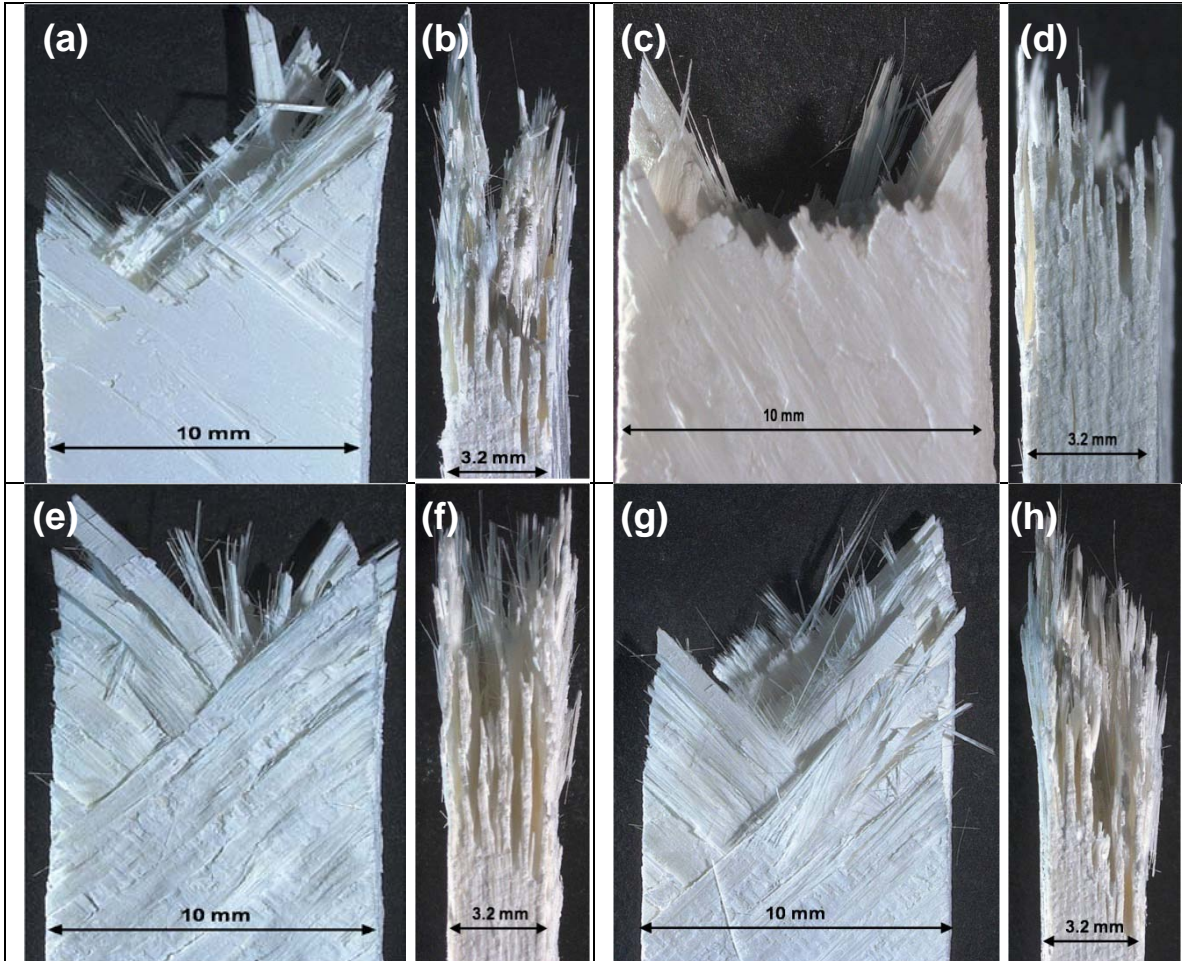
The fracture surfaces of all specimens were observed with an optical microscope. For each specimen multiple pictures were taken with the main objective of observing the complete fracture surface. Both frontal and side views of each specimen were examined. For each specimen, the nominal width was 10 mm and the nominal thickness was 3.2 mm.

Optical micrographs of all fracture surfaces produced in creep tests are shown in Figures 38-40. The optical micrographs reveal that all of the fracture surfaces, with the exception of that produced in the 20 MPa test conducted in steam, were V-shaped. Regardless of the test environment, fracture surfaces of the specimens retained the V shape. Micrographs of the fracture surfaces in Figure 38 show individual fiber pullout as well as coordinated fracture of fiber bundles. Notably, there was no discernable increase in the size of the damage zone with increasing creep stress. As mentioned above, the specimen tested at 20 MPa in steam represents an exception. The 20 MPa test conducted in steam achieved a run-out and the specimen was subjected to tension test to failure in order to measure retained strength and stiffness. The fracture surface shown in Figure 39 (c) and (d) has a flat appearance as opposed to the V shape. Micrographs in Figure 40 show the noticeable increase in the damage zone found in specimens tested in argon compared to those tested in air and steam.



**Figure 38. Fracture surfaces of the N720/AM specimens with  $\pm 45^\circ$  fiber orientation subjected to tensile test to failure following 100 h at  $1200^\circ\text{C}$  in laboratory air at: (a)-(b) 13 MPa and (c)-(d) 32 MPa**

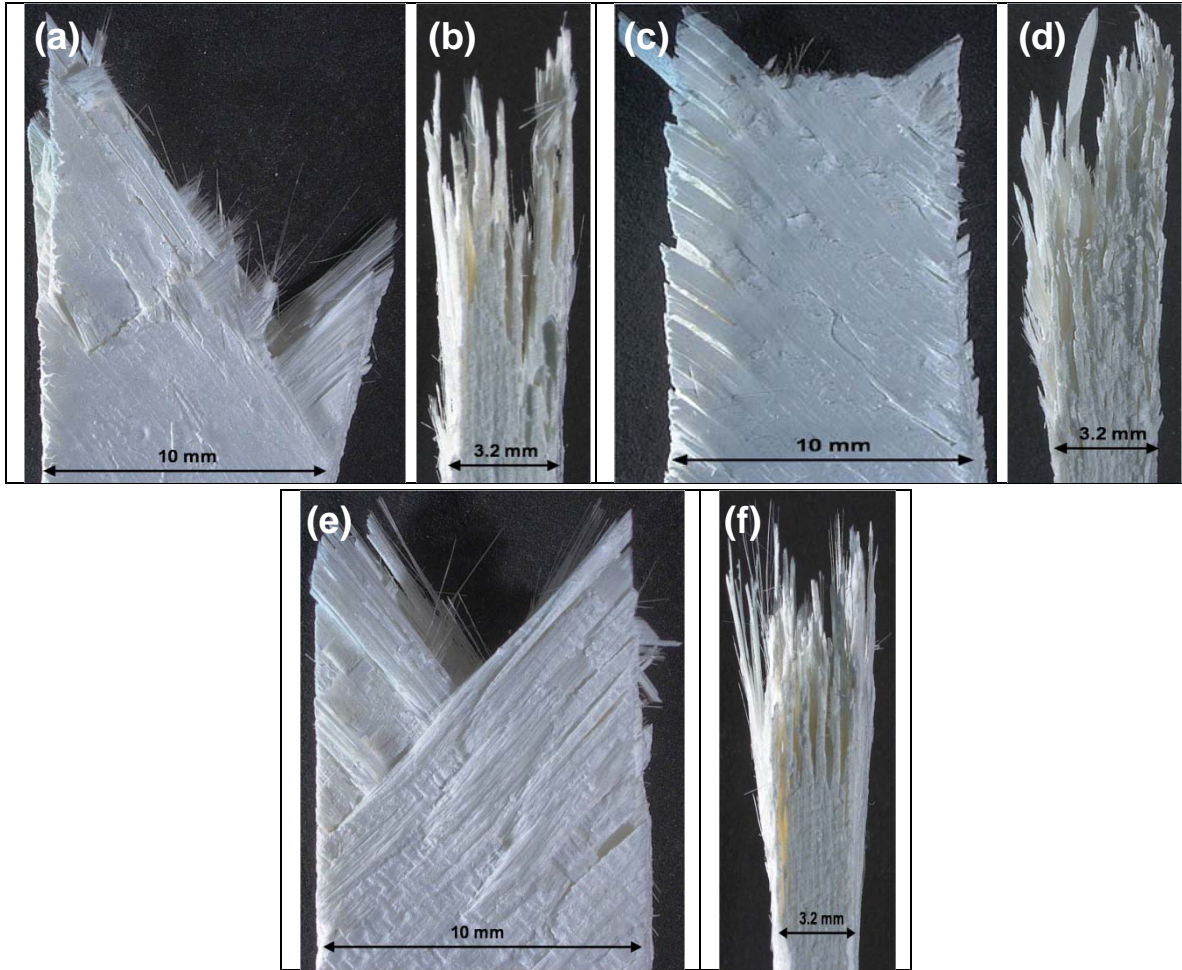
Micrographs in Figure 38 show that the fracture surfaces obtained in creep tests with different stress levels have the same V shape and the same size of the damage zone. Apparently the increase in stress has little effect on the shape of the fracture surface. The fracture surfaces of the specimens tested in laboratory air are fibrous. The side views in Figure 38 show that the specimen tested in air at 32 MPa produced a somewhat less brushy fracture surface than the specimen tested at 13 MPa in air.



**Figure 39. Fracture surfaces of the N720/AM specimens with  $\pm 45^\circ$  fiber orientation obtained in creep tests conducted at  $1200^\circ\text{C}$  in steam at: (a)-(b) 13 MPa,  $t_f = >100$  h; (c)-(d) 20 MPa,  $t_f = >100$  h; (e)-(f) 30 MPa,  $t_f = 1.08$  h and (g)-(h) 32 MPa,  $t_f = 0.02$ h**

Figure 39 shows optical micrographs of four specimens tested in steam at different creep stress levels. Specimens tested at 13 and 20 MPa achieved run-out and failed in a subsequent displacement controlled tension test. The fracture surfaces of the specimens tested at 13 MPa, 30 MPa and 32 MPa have V shape typical for the specimens with the  $\pm 45^\circ$  fiber orientation. On the contrary, the specimen tested at 20 MPa exhibits a

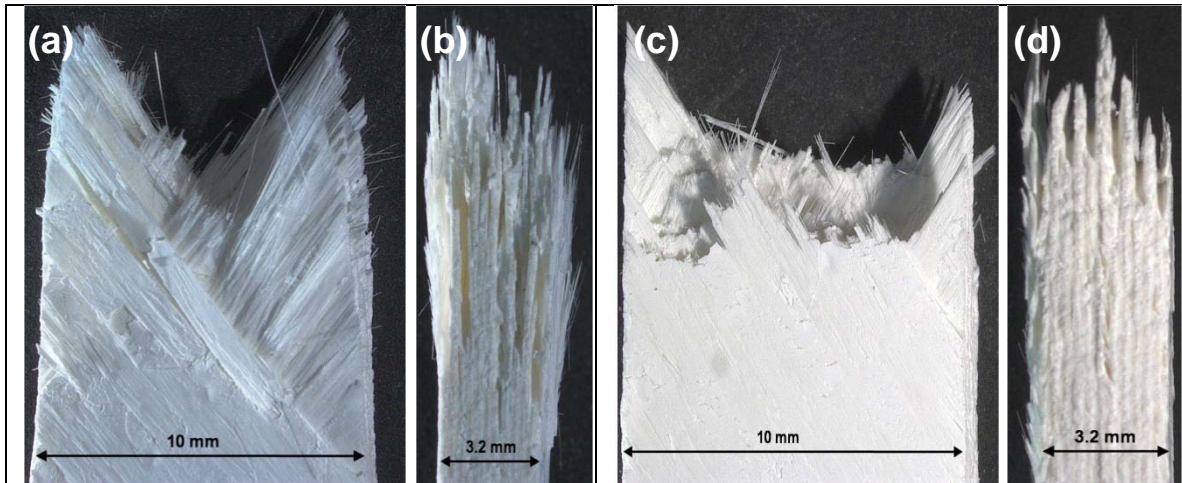
more planar fracture, which is likely due to the long exposure to steam. While the size of the damage zones for the specimens with the V-shaped fracture surfaces stayed nearly the same, the damage zone of the specimen tested at 20 MPa produced a nearly planar fracture surface. Micrographs in Figure 39 reveal the effect of prolonged exposure to steam at 1200°C on the appearance of the fracture surface. It is seen that the specimens subjected to shorter exposure in steam (Figure 39 (e)-(h)) produced more fibrous fracture surfaces than the specimens that achieved a 100-h creep run-out in steam and were then subjected to tension to failure. Note that the fracture surfaces of the specimens that were subjected to steam environment for 100 h or longer (Figures 39 (a)-(d)) are less fibrous and show a considerably larger degree of fiber breakage.



**Figure 40. Fracture surfaces of the N720/AM specimens with  $\pm 45^\circ$  fiber orientation obtained in creep tests conducted at  $1200^\circ\text{C}$  in argon at: (a)-(b) 20 MPa,  $t_f = >100$  h; (c)-(d) 26 MPa,  $t_f = 76$  h and (e)-(f) 32 MPa,  $t_f = 0.08$  h**

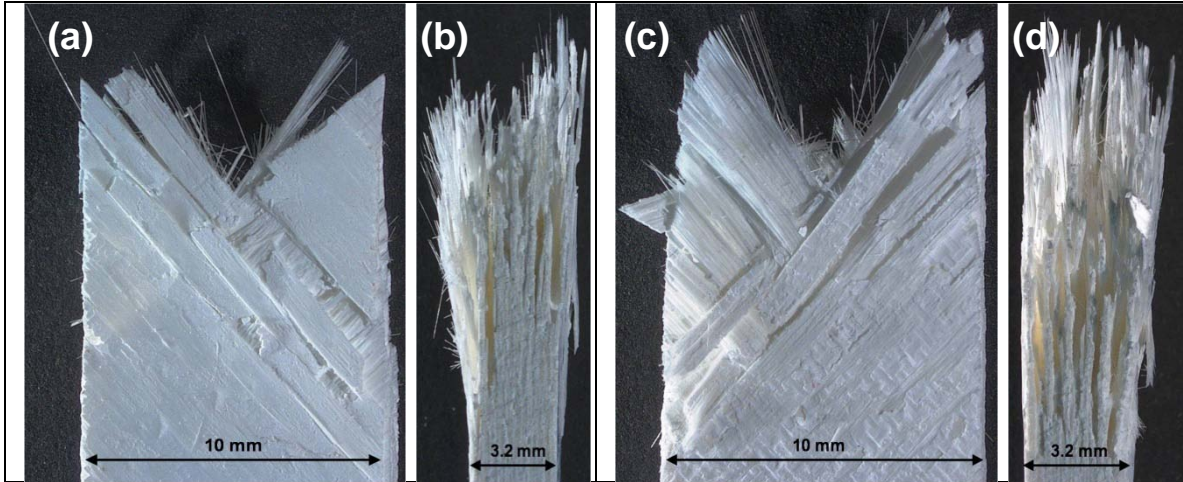
As mentioned earlier, the specimens tested in argon had longer damage zones compared to those tested in laboratory air and in steam. Nevertheless, specimens tested in argon produced V-shaped fracture surface (with the exception of the specimen tested at 26 MPa). Nearly planar fracture surface produced in argon at 26 MPa is shown in Figure 40 (c) and (d). As the time of exposure to argon decreased, the fracture surfaces became brushier and showed less fiber breakage. The length of the damage zone

produced in the 26 MPa test conducted in argon was nearly 1.5 times longer than the damage zones produced by other specimens tested in argon.



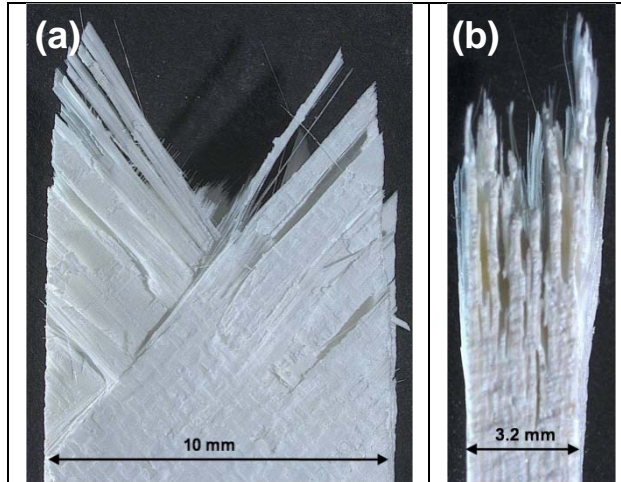
**Figure 41. Fracture surfaces of the N720/AM specimens with  $\pm 45^\circ$  fiber orientation obtained from load controlled tensile tests at  $1200^\circ\text{C}$  at  $0.0025\text{ MPa/s}$  in: (a)-(b) laboratory air,  $t_f = 4.76\text{ h}$ ; (c)-(d) steam,  $t_f = 5.46\text{ h}$**

Figure 41 shows optical micrographs of the two N720/AM specimens subjected to load controlled monotonic tensile tests conducted at a constant rate of  $0.0025\text{ MPa/s}$  at  $1200^\circ\text{C}$ . The specimen in Figure 41 (a) and (b) was tested in laboratory air. The damage zone appears to have the same brushy appearance as the damage zones of other specimens tested in air. In contrast, Figure 41 (c) and (d) shows the fracture surface of the specimen tested in steam environment. The fracture surface is nearly planar and shows significant fiber breakage. These features of the fracture surface are attributed to prolonged exposure to steam at  $1200^\circ\text{C}$  under load. Note that the sample tested in laboratory air failed after  $4.76\text{ h}$  while the sample tested in steam failed after  $5.46\text{ h}$ .



**Figure 42. Fracture surfaces of the N720/AM specimens with  $\pm 45^\circ$  fiber orientation obtained from load controlled tensile tests at  $1200^\circ\text{C}$  at  $25\text{ MPa/s}$  in: (a)-(b) laboratory air,  $t_f = 0.0004\text{ h}$ ; (c)-(d) steam,  $t_f = 0.00038\text{ h}$**

The micrographs in Figure 42 show the fracture surfaces of the specimens tested in load control at  $25\text{ MPa/s}$ . The fracture surfaces obtained in steam are similar to those produced in air. Apparently the short duration of the test did not afford sufficient time for the degrading affects of steam environment to develop. Both specimens produced the V-shaped fracture surfaces, although the fracture surfaces of the specimens tested in steam is somewhat less brushy than the fracture surface of the specimen tested in air. Note that the specimens tested at  $0.0025$  and at  $25\text{ MPa/s}$  in air produced similar fracture surfaces. Conversely, the fracture surfaces obtained at  $0.0025$  and at  $25\text{ MPa/s}$  in steam had markedly different appearance.



**Figure 43. Fracture surface of the N720/AM specimen with  $\pm 45^\circ$  fiber orientation subjected to displacement controlled (0.05 mm/s) monotonic tensile test to failure at  $1200^\circ\text{C}$  in laboratory air,  $t_f = 0.0007$  h**

The fracture surface of the specimen subjected to displacement controlled monotonic tensile test to failure shows all the characteristics of the fracture surfaces of the specimens tested in laboratory air, it has the V shape and is fibrous. There is little difference between the fracture surface produced in the load-controlled tensile test at 25 MPa/s in air and the fracture surfaces obtained in displacement control at 0.05 mm/s.

The use of optical microscopy permits some understanding of the overall structure of the specimen's fracture. However, an SEM affords the capability of examining every aspect of the microstructural damage and failure mechanisms at much higher magnification. This section will present the results of the SEM examinations. First, the post-test microstructure of specimens tested under different loading conditions and different environments will be compared. Then the typical damage characteristics observed in load-controlled tensile tests conducted in laboratory air and steam will be discussed. Figure 44 shows a typical fracture surface obtained in tests conducted with N720/AM specimens with  $\pm 45^\circ$  fiber orientation.



**Figure 44. SEM micrograph of the fracture surface of the N720/AM with  $\pm 45^\circ$  fiber orientation subjected to tensile test to failure at  $1200^\circ\text{C}$  in laboratory air**

Figure 45 shows the fracture surfaces of the N720/AM specimens with  $\pm 45^\circ$  fiber orientation subjected to creep tests conducted at  $1200^\circ\text{C}$  in laboratory air at 13, 30 and 32 MPa. As mentioned earlier, all specimens tested in creep in air achieved a run-out. Following the 100 h of creep lifetime, these specimens were subjected to a displacement controlled tensile test to failure. It is apparent that the fracture surfaces are predominantly brushy.

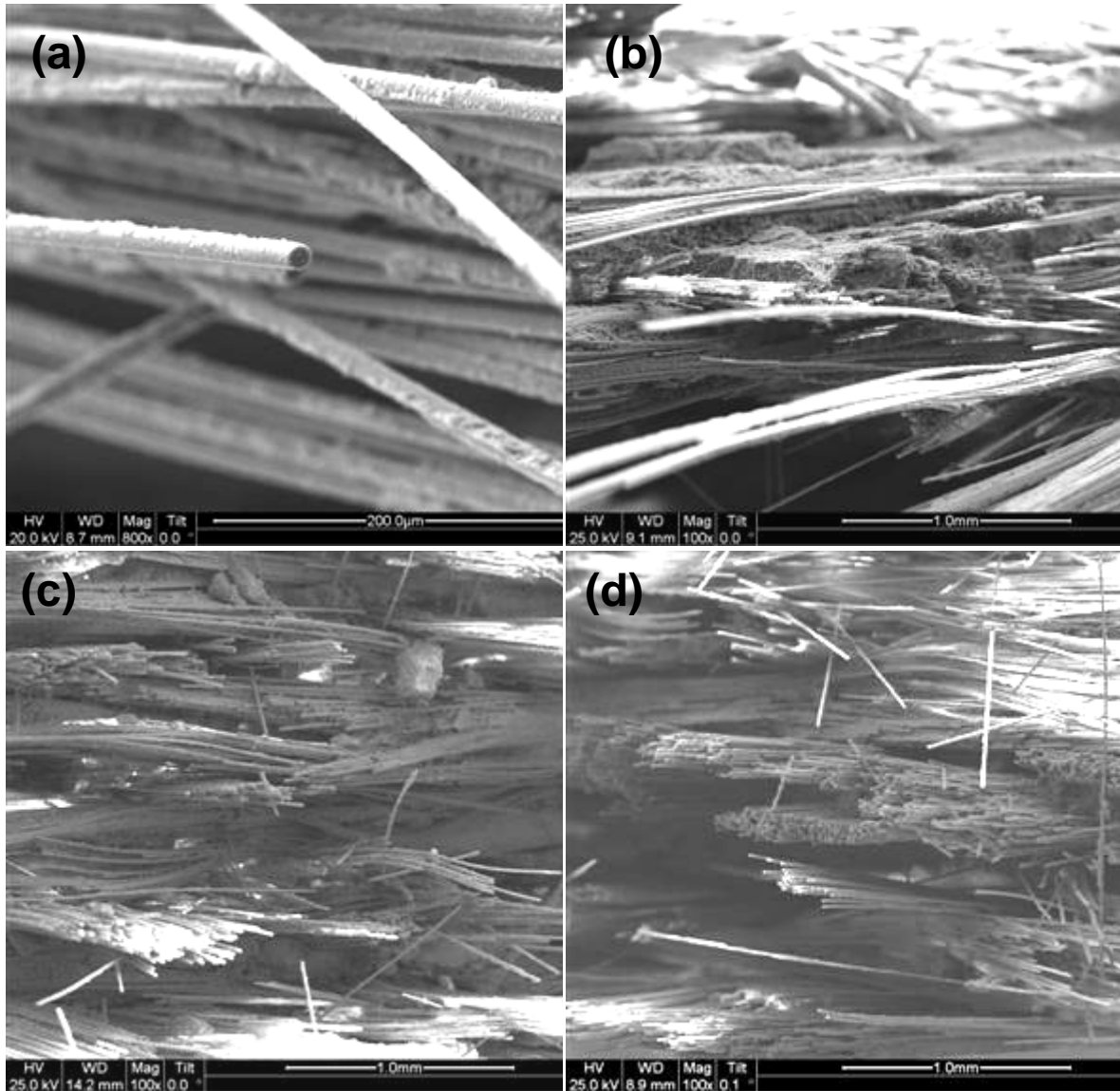


**Figure 45. SEM micrographs of fracture surfaces of N720/AM with  $\pm 45^\circ$  fiber orientation produced in creep tests conducted in laboratory air at  $1200^\circ\text{C}$  at: (a) - (b) 13 MPa, (c) 30 MPa and (d) 32 MPa**

In air environment, the alumina-mullite matrix did not strongly bond with the fibers, as evidenced by the fibrous fracture surfaces. This is further confirmed by SEM micrograph in Figure 45 (a), which shows only small amounts of matrix bonded to the fibers. Figures 45 (b), (c) and (d) show the fracture surfaces of the specimens tested at 13,

30 and 32 MPa, respectively. Individual fibers are discernible in these micrographs. Moreover, there is no distinctive difference between the SEM micrographs in Figures 45 (b), (c), and (d). This suggests that there is no discrete correlation between the topography of the fracture surface and the applied stress level.

Figure 46 shows the fracture surfaces of the N720/AM specimens with  $\pm 45^\circ$  fiber orientation subjected to creep tests at  $1200^\circ\text{C}$  in steam. Recall that the 13 and 20 MPa tests achieved run-out in steam. Following 100 h of creep, the run-out specimens were subjected to a displacement controlled tensile test to failure. The fracture surfaces obtained in steam exhibit different characteristics from those obtained in air. As seen in Figure 46 (b), the fracture surface of the specimen tested in creep at 13 MPa shows fiber bundles bonded together by matrix material. Conversely, the fracture surfaces of the specimens tested in creep at 30 and 32 MPa (see Figures 46 (c) and (d)), which had a much shorter exposure in steam, exhibit a lesser degree of bonding between fibers and matrix.

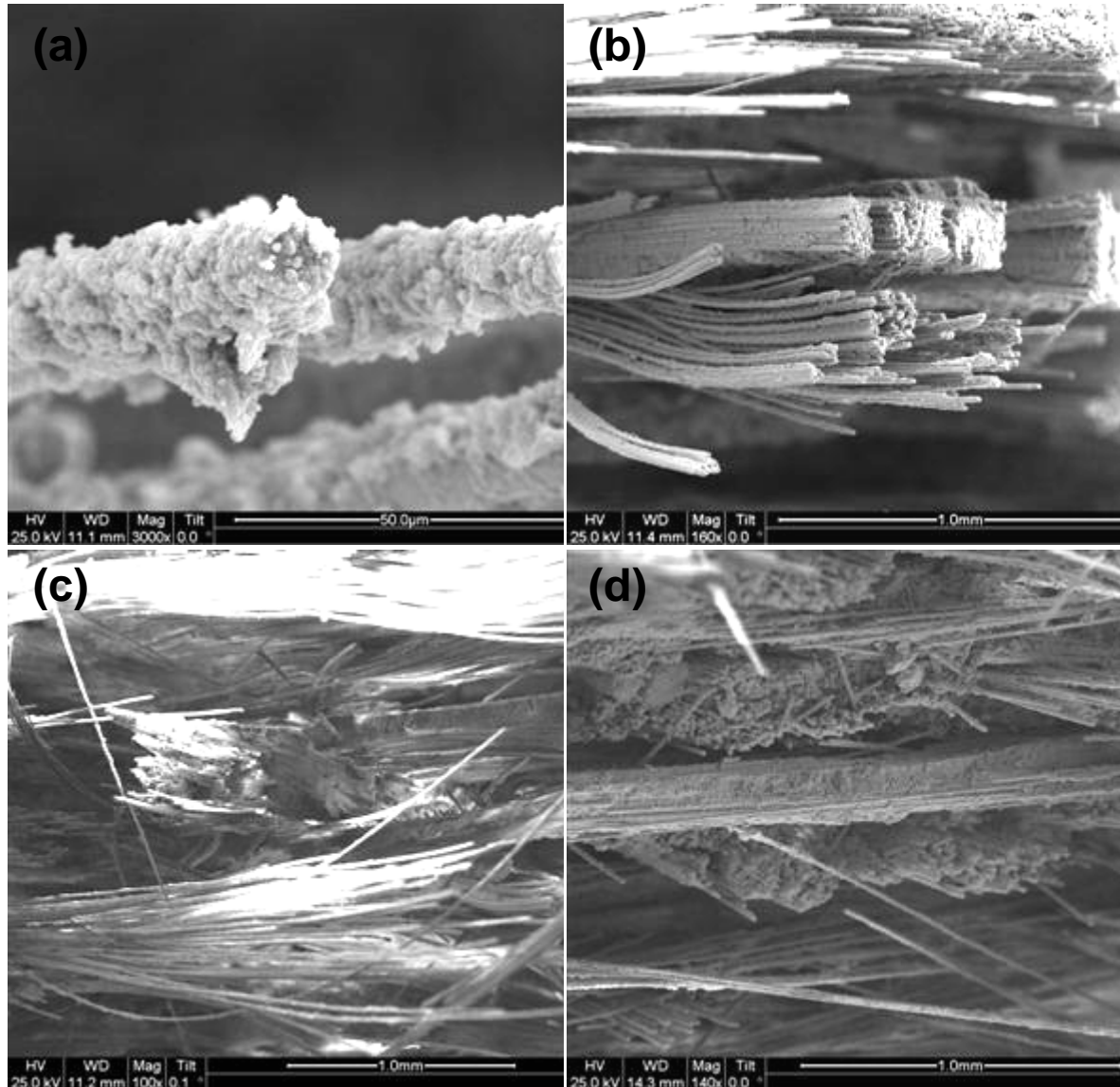


**Figure 46. SEM micrographs of fracture surfaces of N720/AM with  $\pm 45^\circ$  fiber orientation produced in creep tests conducted in steam at  $1200^\circ\text{C}$  at: (a) - (b) 13 MPa, (c) 30 MPa and (d) 32 MPa**

In steam environment, the amount of matrix material bonded to the fibers increases with longer exposure times to steam. Figure 46 (a) shows the micrograph of a fiber covered with a thick layer of matrix particles. This specimen was exposed to steam under load for 100 h or longer. Consider micrographs in Figures 47 (a) and (b).

Micrograph in Figure 47 (a) shows a fragment of the fracture surface of the specimen that achieved a 100-h run-out at 13 MPa in air. Figure 47 (b) presents a fracture surface of the specimen tested in creep at 32 MPa in steam, which failed after only 0.02 h. Yet even this short exposure to steam under load resulted in fiber-matrix bonding. We see a larger amount of matrix bonded to the fibers in the specimen tested in steam (Figure 47 (b)) than in the specimen tested in air (Figure 47 (a)). Note that the specimen in Figure 47 (b) had the shortest creep lifetime and therefore the least amount of matrix bonded to the fibers among the specimens tested in steam.

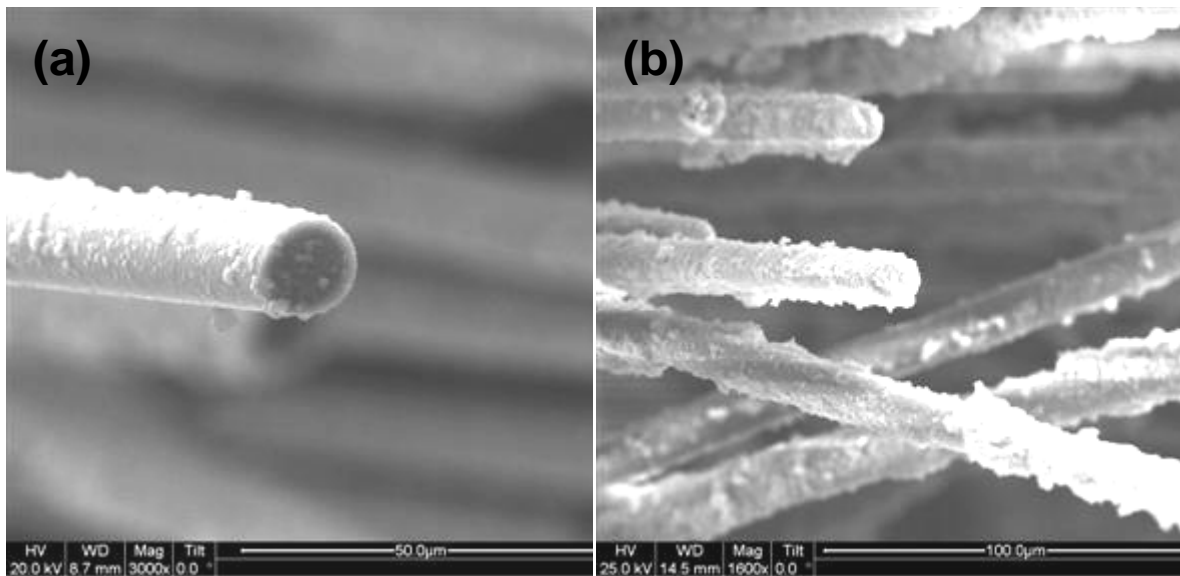
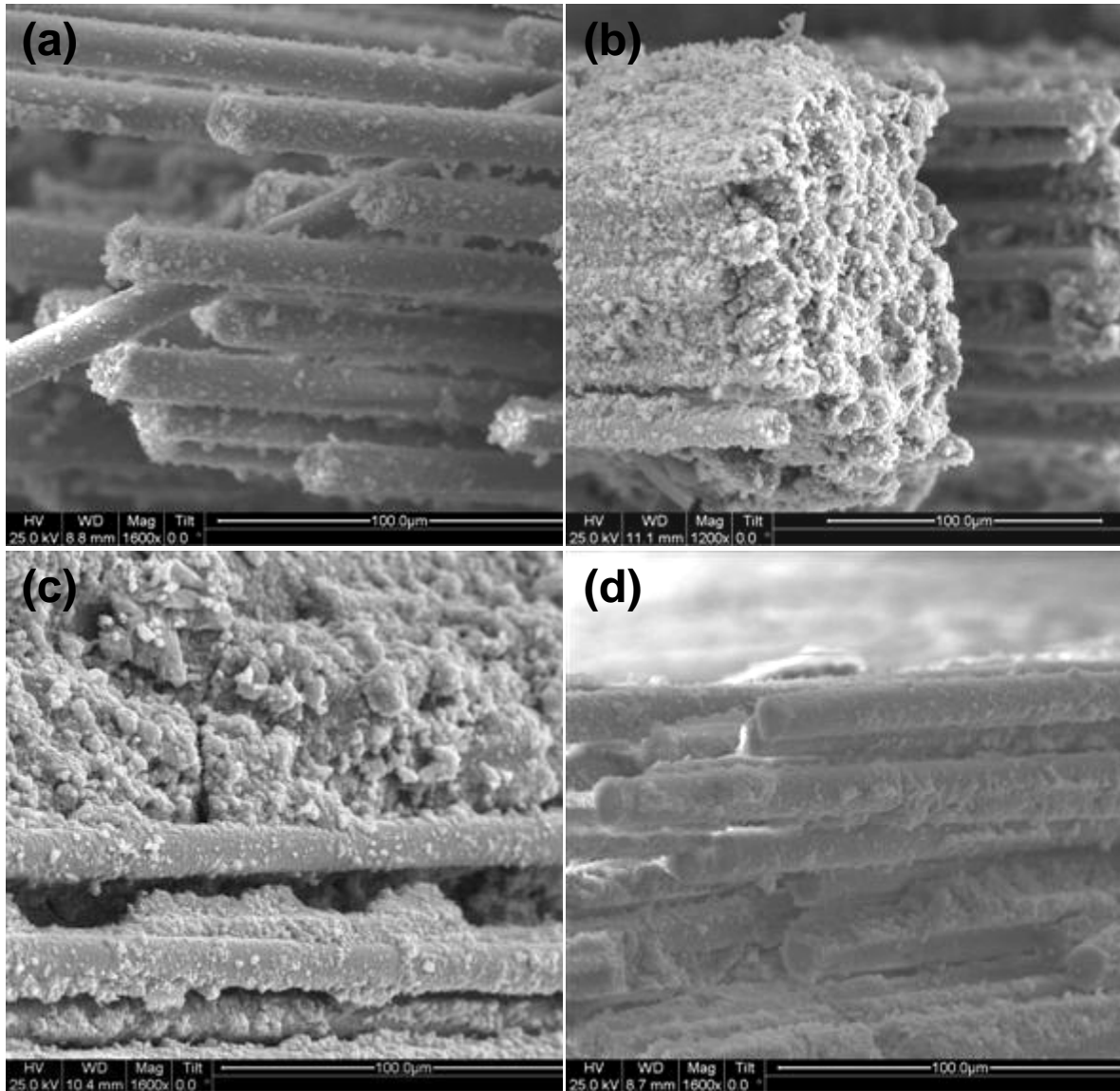


**Figure 47. SEM micrographs of N720/AM fibers subjected to creep tests at 1200°C conducted in: (a) laboratory air at 13 MPa and (b) steam at 32 MPa**

It is recognized that the N720/AM composite relies on matrix porosity for crack deflection, which allows the cracks to propagate around instead of through the fibers. Previous work [23,27] has shown that one of the failure mechanisms of porous-matrix

composites like N720/AM is densification of the porous matrix due to additional sintering at high temperatures. Because of its slow sintering kinetics at temperatures up to 1300°C and excellent creep resistance, mullite was added to the matrix of the N720/AM composite as a means of limiting shrinkage associated with the sintering of a pure alumina matrix. The low fracture toughness and elastic modulus make mullite ideal for crack deflection in a porous matrix, but these same properties hinder its effectiveness against shear, off-axis and compressive loading. As a result, a mixture of both alumina and mullite create more operationally capable matrix [25].

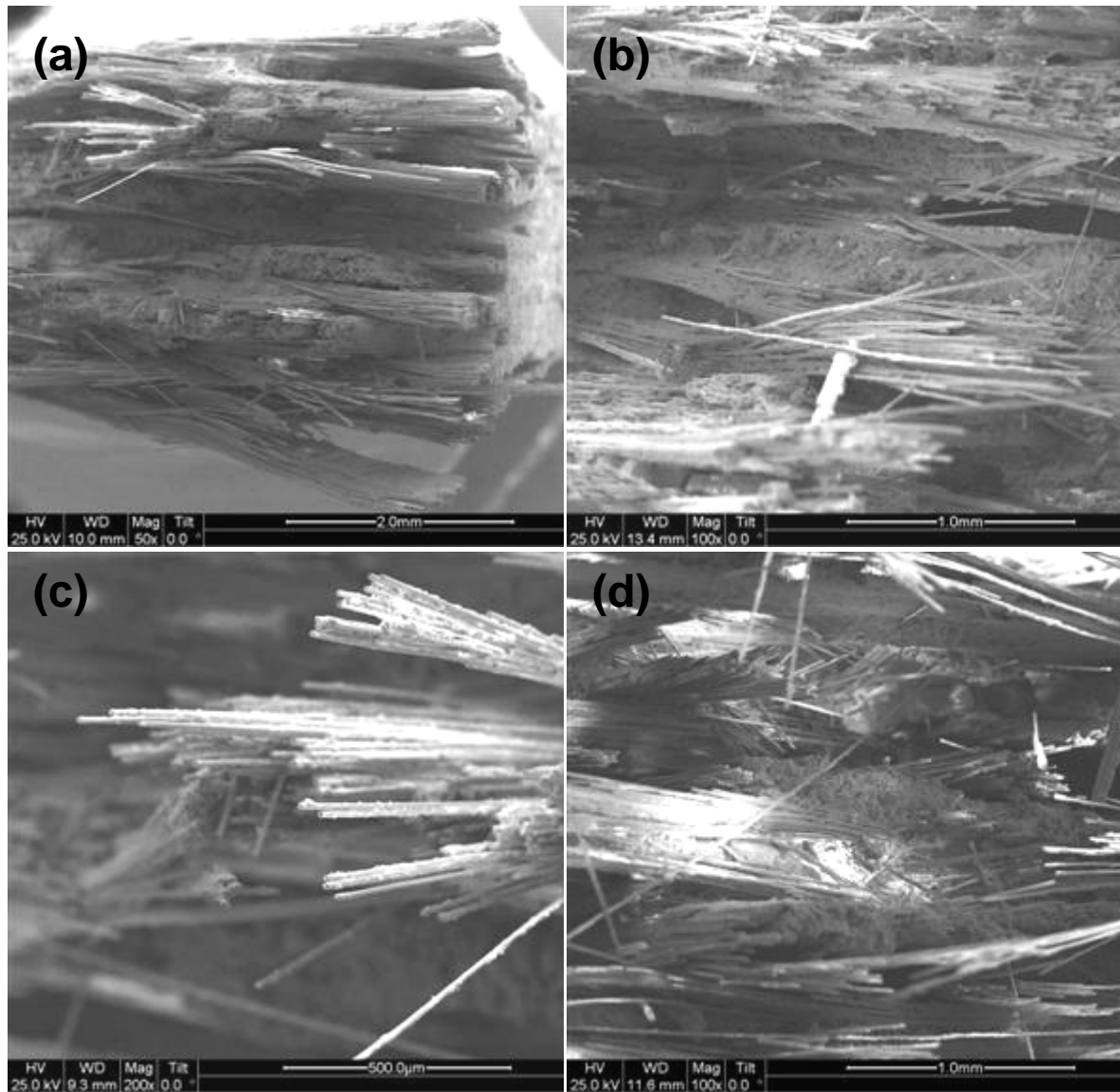
Figure 48 presents micrographs of the fracture surfaces obtained in air and in steam. Fracture surface in Figure 48 (a) was obtained in tensile test following 100 h of creep at 32 MPa in air. Note that this specimen shows the greatest degree of fiber-matrix bonding among the specimens tested in air. Figures 48 (b)-(c) present the fracture surface produced in tensile test following 100 h of creep at 13 MPa in steam. Figure 48 (d) show the fracture surface of the specimen that survived only 1.08 h in creep at 30 MPa in steam. It is seen that the least amount of matrix material bonded to fibers is observed in specimen tested in air. Conversely, the specimen exposed under load in steam for 100 h exhibits a very pronounced fiber-matrix bonding. Fiber bundles in Figure 48 (b) appear to be “glued” together by the matrix material. The specimen subjected to a shorter 1-h exposure in steam under load (Figure 48 (d)) also exhibits considerable degree of fiber-matrix bonding. However due to a shorter exposure time, the amount of matrix material bonded to fibers in this case is somewhat lower than in the case of the specimen exposed in steam under load for over 100 h.



**Figure 48. SEM micrographs of N720/AM fiber bundles subjected to creep tests at 1200°C conducted in: (a) laboratory air at 32 MPa , (b)-(c) steam at 13 MPa and (d) steam at 30 MPa**

As stated earlier, argon presence is a non-oxidizing environment. It was expected that the presence of argon would improve the creep resistance of the material but this was not the case for N720/AM specimens with  $\pm 45^\circ$  fiber orientation. Figure 49 presents

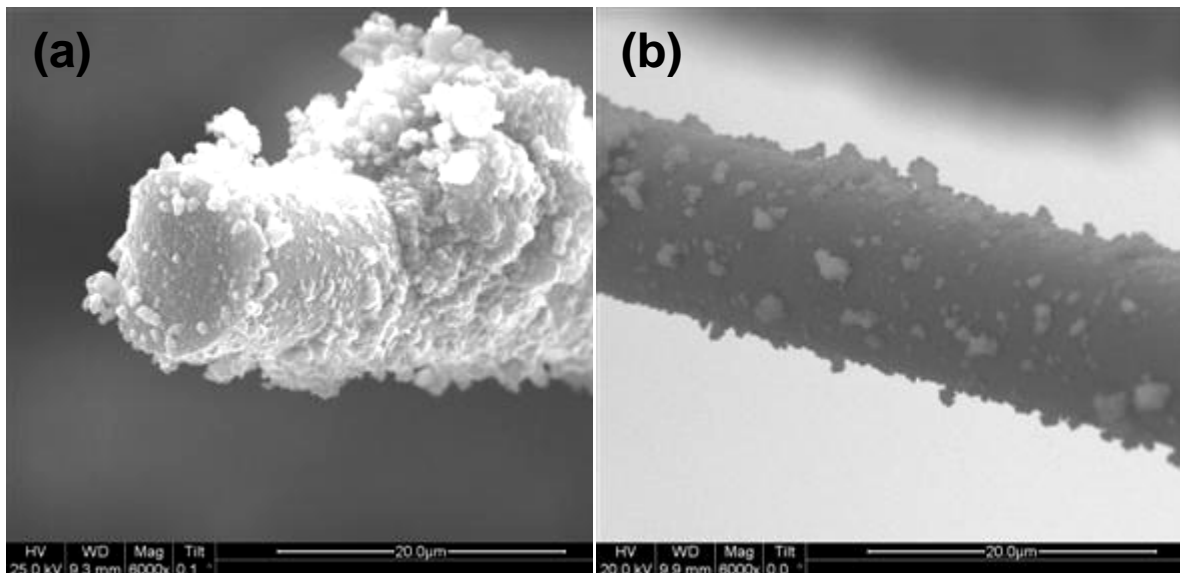
micrographs of the fracture surface of the specimens tested in argon. Recall that in argon creep run-out stress was 20 MPa.



**Figure 49. SEM micrographs of fracture surfaces of N720/AM with  $\pm 45^\circ$  fiber orientation produced in creep tests conducted in argon at  $1200^\circ\text{C}$  at: (a)-(b)-(c) 20MPa and (d) 32 MPa**

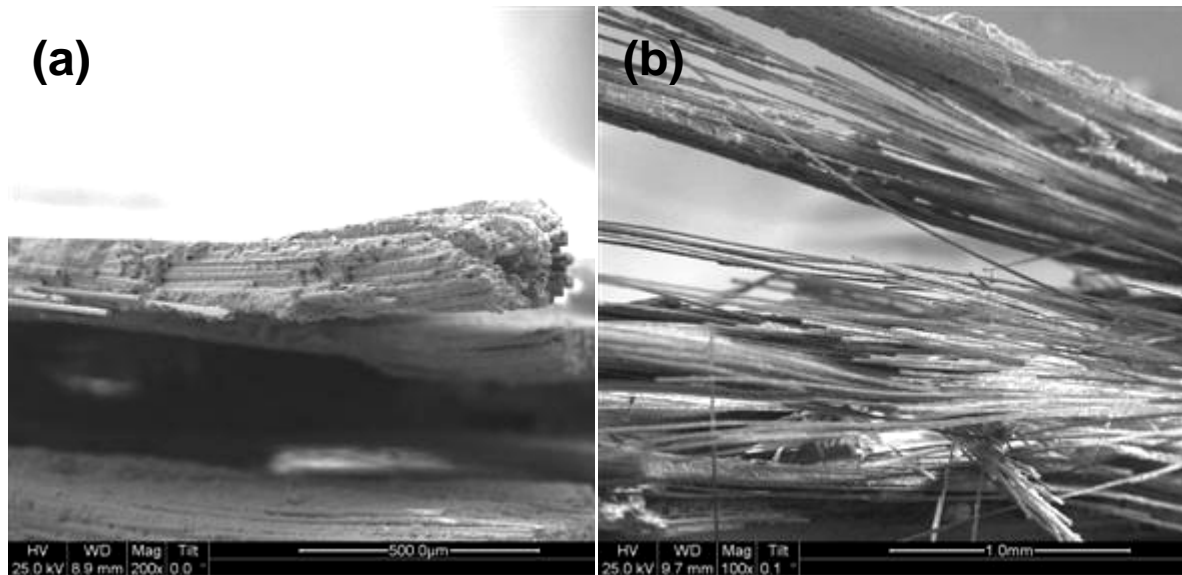
As was the case with the fracture surfaces produced in steam, the fracture surfaces produced in argon exhibit bonding between the alumina-mullite matrix and the fibers. The degree of fiber-matrix bonding is reduced in the case of the 32 MPa test, where exposure to argon under load was limited to 0.08 h. In contrast, the fracture surface obtained in argon in the 20 MPa test (exposure >100 h) is similar to that produced in the 20 MPa test in steam, showing large amounts of matrix bonded to the fibers.

Figure 50 (a) shows the micrograph of a fiber covered with matrix particles due to 100-h exposure under 20 MPa stress in argon. Figure 50 (b) shows an element of the fracture surface obtained in creep test at 30 MPa in argon with a lifetime of 3.42 h. In this case, shorter test duration results in a lower amount of matrix remaining bonded to the fiber. It appears that the presence of either steam or argon promotes matrix densification and fiber-matrix bonding.



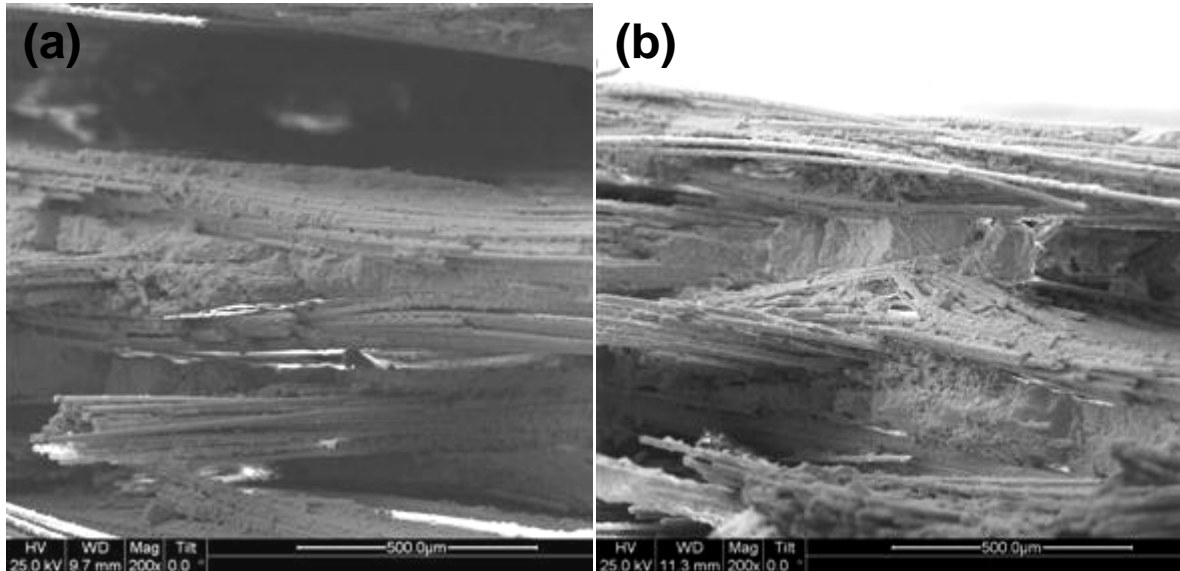
**Figure 50. SEM micrographs of N720/AM fibers subjected to creep tests at 1200°C conducted in argon at: (a) 20 MPa ( $t_f >100$  h) and (b) 30 MPa ( $t_f = 3.42$  h)**

This observation is further illustrated in Figure 51 (a) and (b). Fiber bundles in the specimen subjected to 100 h in argon under 20 MPa stress appear to be bonded together with the matrix material (see Figure 51 (a)). Contrastingly, fiber bundles in a specimen exposed in argon under 32 MPa-stress for only 0.08 h are relatively free of matrix. In this case, single filaments are visible (Figure 51 (b)).



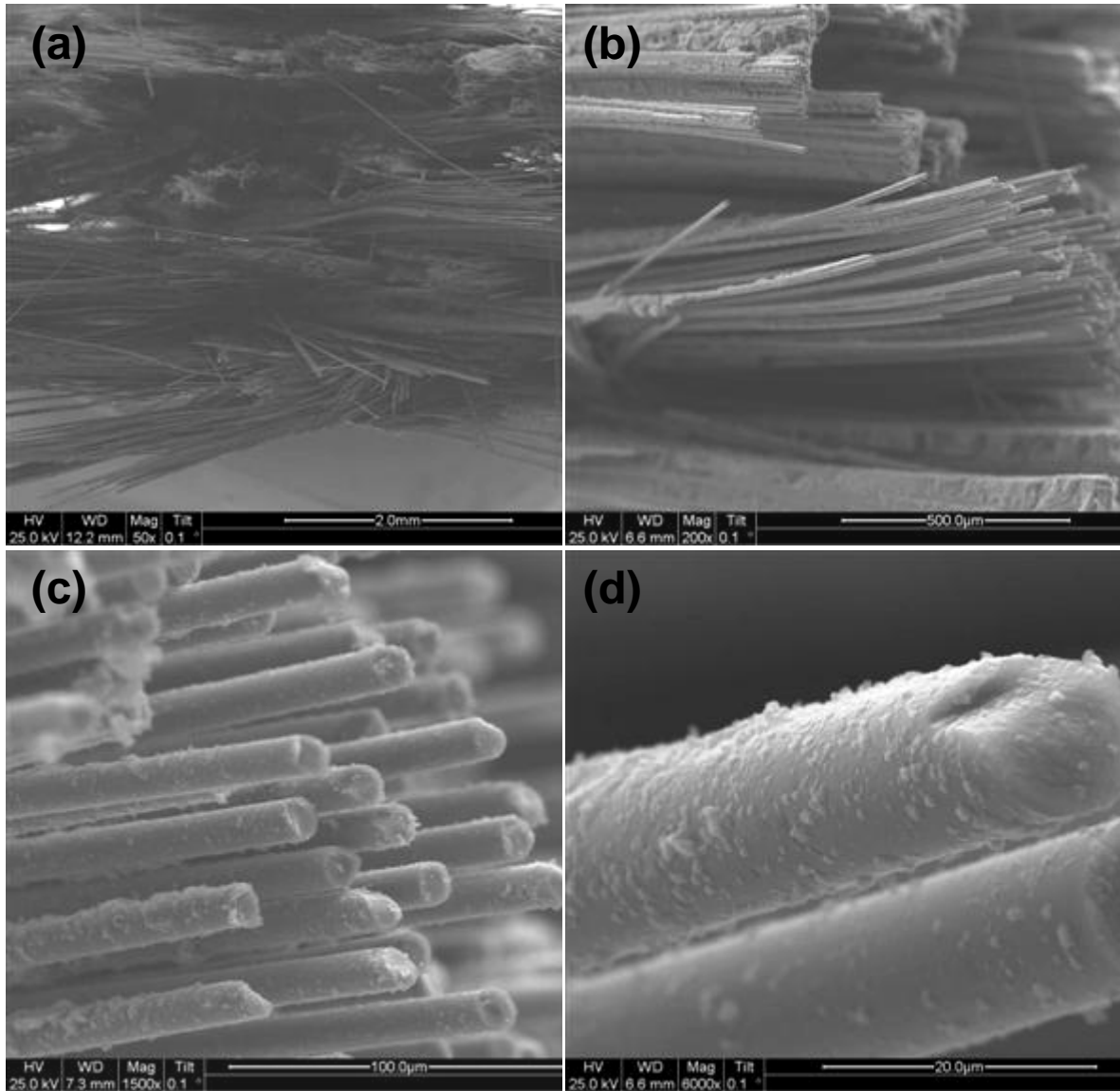
**Figure 51. SEM micrographs of N720/AM fiber bundles subjected to creep tests at 1200°C conducted in argon at: (a) 20 MPa ( $t_f > 100$  h) and (b) 32 MPa ( $t_f = 0.08$  h)**

The presence of argon promotes matrix densification and fiber-matrix bonding. Micrographs in Figure 52 (a) and (b) reveal that the initially porous matrix forms a denser aggregate after exposure to argon under stress. The matrix-rich areas appear as blocks; matrix does not disintegrate and fall away as would be expected for a porous-matrix.



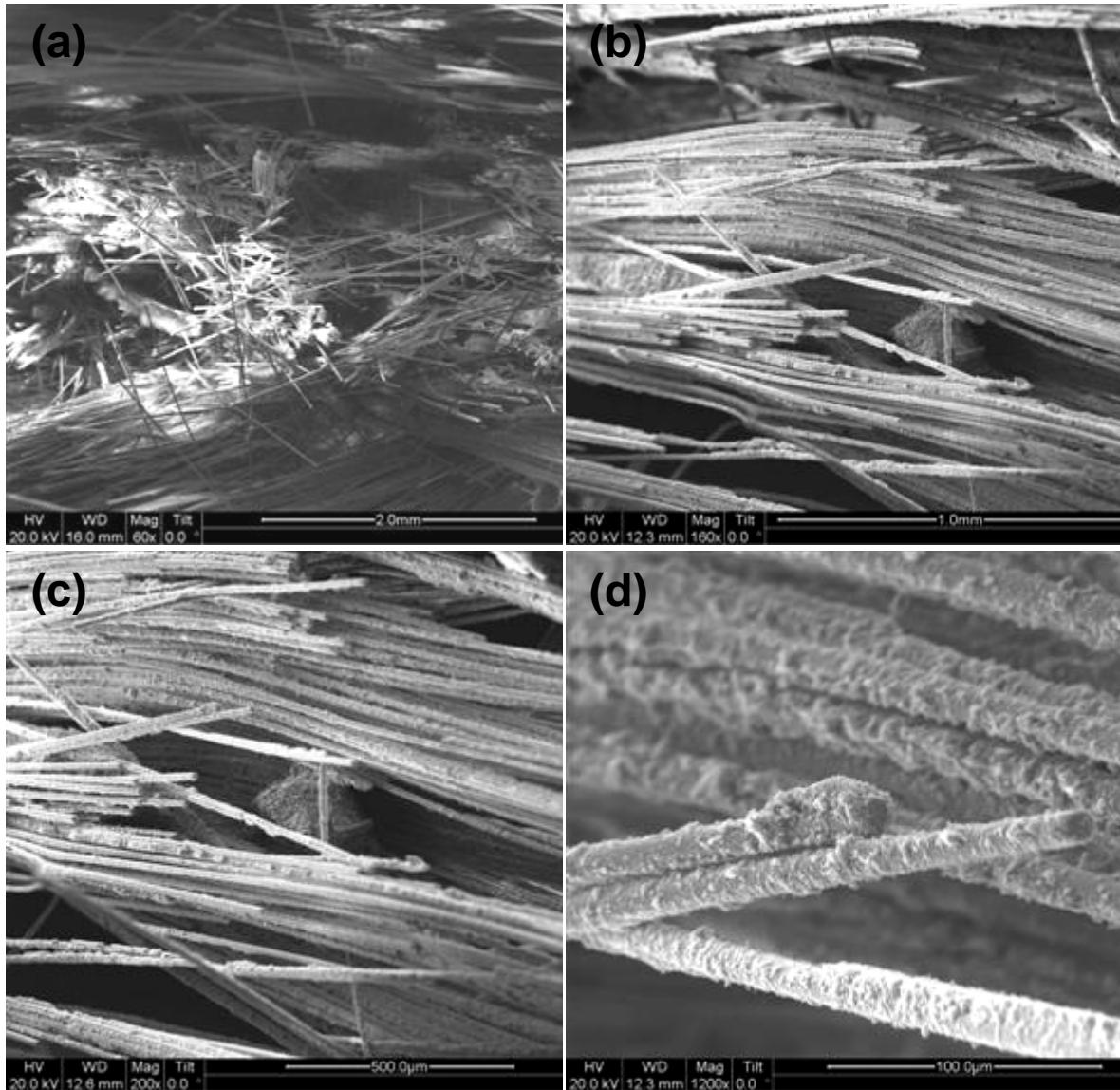
**Figure 52. SEM micrographs of fracture surfaces of N720/AM with  $\pm 45^\circ$  fiber orientation produced in creep tests at  $1200^\circ\text{C}$  conducted at 20 MPa in argon**

Micrographs in Figure 53-57 show the fracture surfaces of the N720/AM specimens with  $\pm 45^\circ$  fiber orientation obtained in tensile test to failure with a constant stress rate conducted in laboratory air and steam. Figure 53 shows the SEM micrographs of the test conducted with constant rate of 0.0025 MPa/s in laboratory air. The test duration was 4.76 h. When compared to the fracture surfaces of the specimens subjected to 100 h of prior creep in laboratory air, the microstructures are very similar (see Figures 53 (a), (b) and (c)). The fracture surface is brushy, individual fibers are clearly visible.



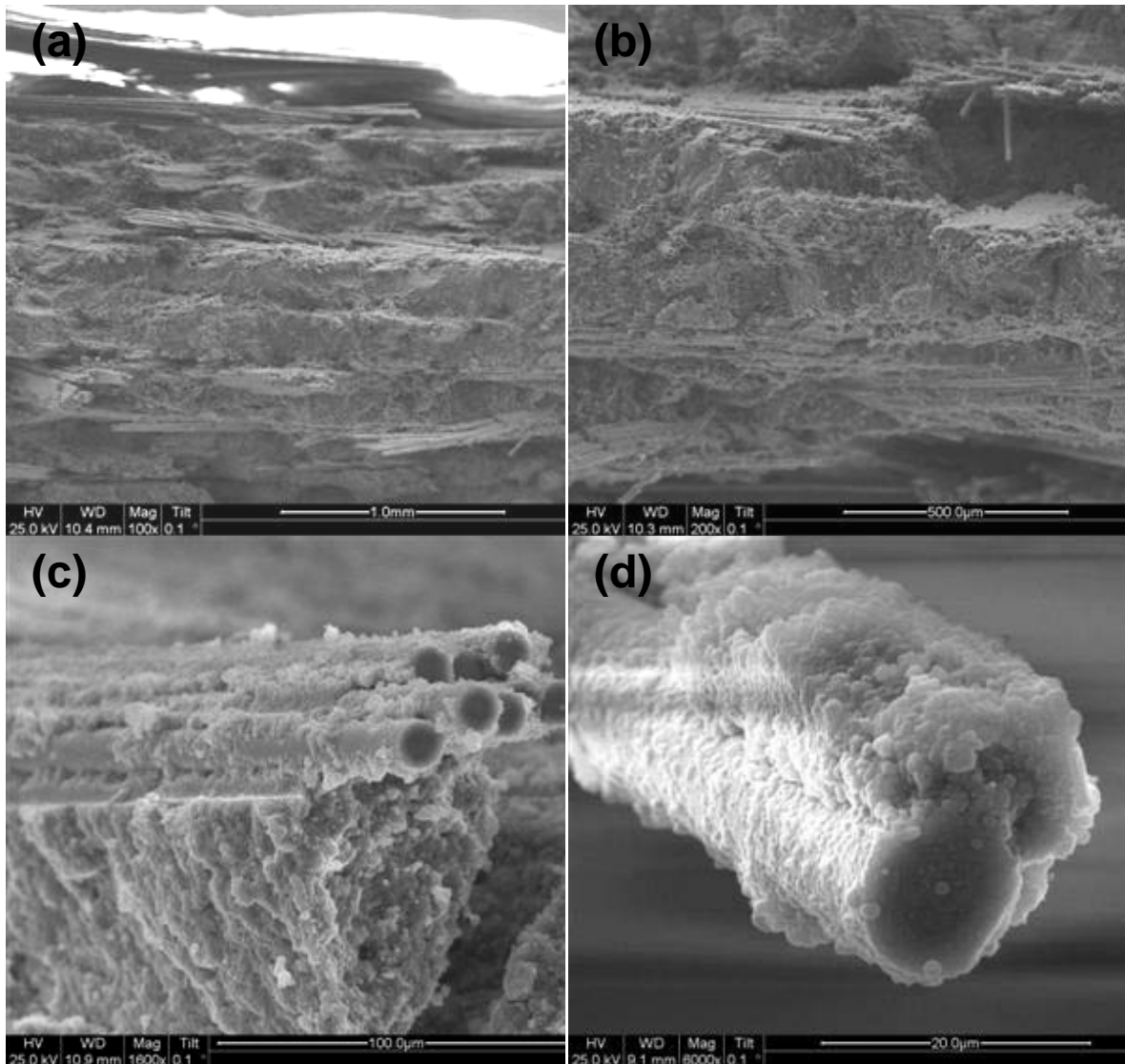
**Figure 53. SEM micrograph of the fracture surface of the N720/AM specimen with  $\pm 45^\circ$  fiber orientation subjected to tensile test to failure with a constant stress rate of 0.0025 MPa/s at 1200°C in laboratory air**

Fracture surfaces produced at a faster rate of 25 MPa/s in air are considerably more fibrous (see Figures 54 (a)-(b)). However, Figure 54 (d) shows a considerable amount of matrix bonded to the fibers. Similar degree of fiber-matrix bonding was observed in specimens subjected to the 30 and 32 MPa creep tests in laboratory air.



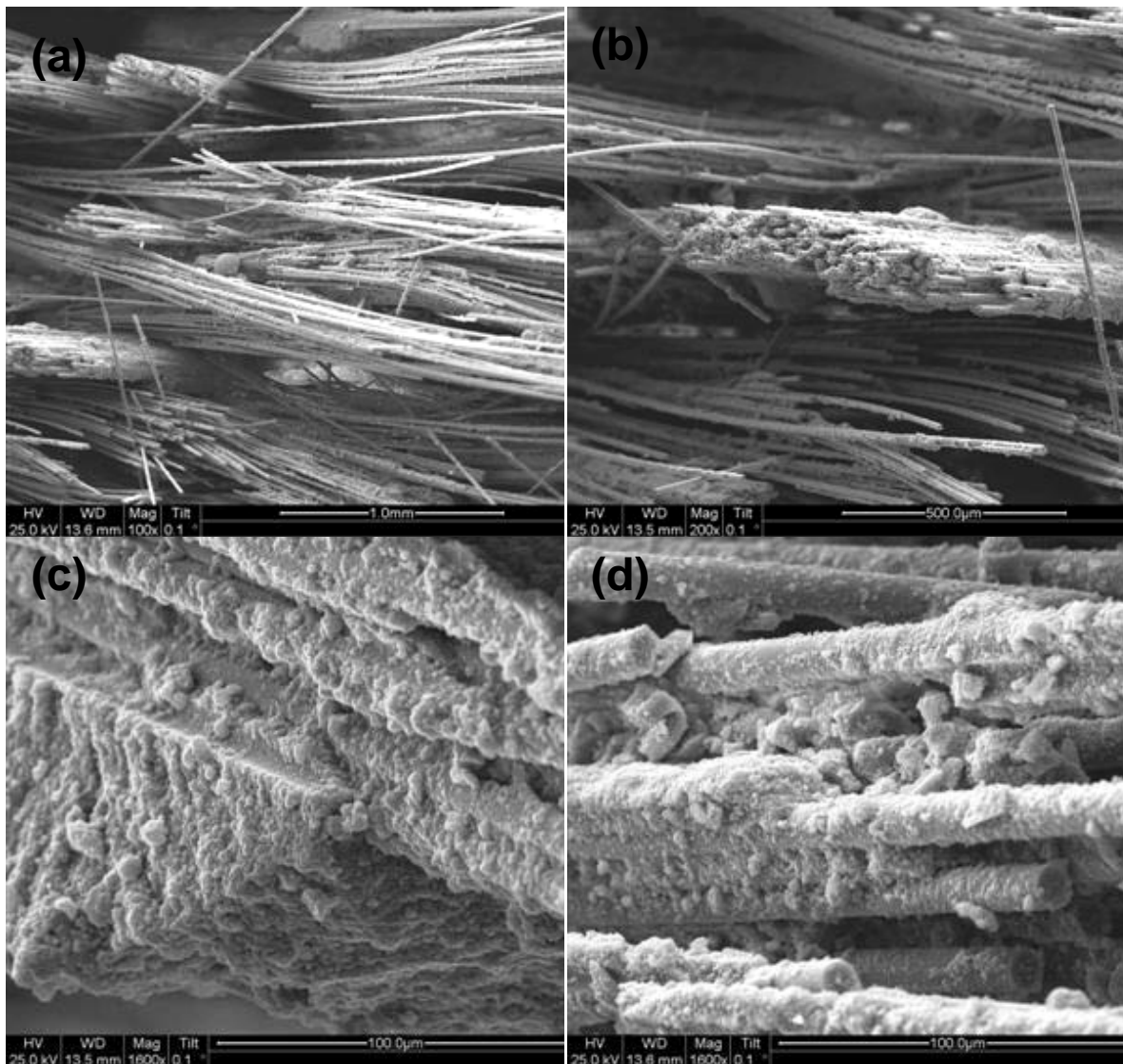
**Figure 54. SEM micrograph of the fracture surface of the N720/AM specimen with  $\pm 45^\circ$  fiber orientation subjected to tensile test to failure with a constant stress rate of 25 MPa/s at 1200°C in laboratory air.**

The fracture surface of the specimen subjected to tensile test to failure at 0.0025 MPa/s in steam is shown in Figure 55. The effect of steam environment on the matrix can be seen in these micrographs. Note that this specimen had 5.46 h of exposure to steam under increasing load. Matrix densification takes place, as evidenced by large chunks of matrix attached to the fibers throughout the fracture surfaces.



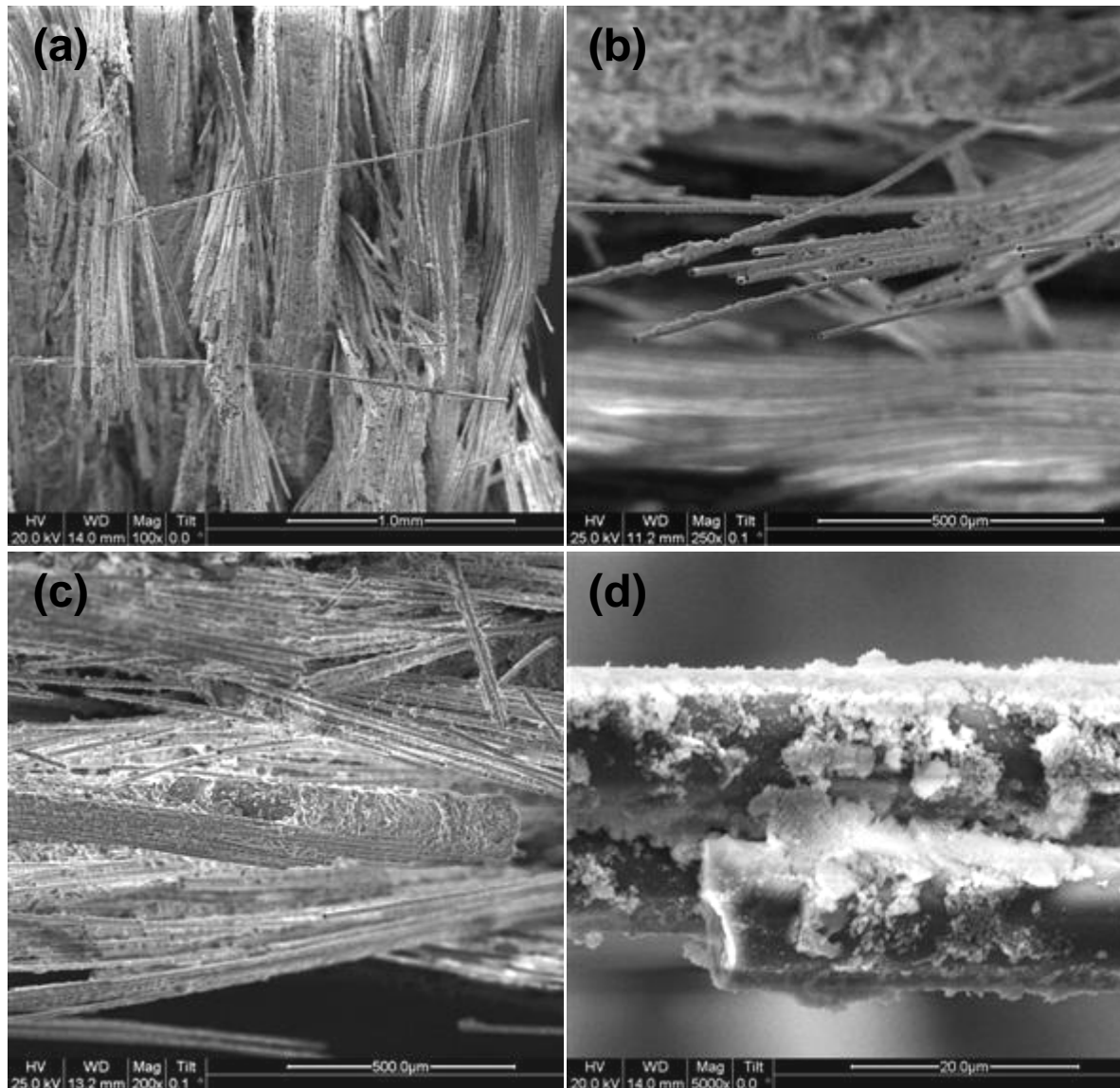
**Figure 55. SEM micrograph of the fracture surface of the N720/AM specimen with  $\pm 45^\circ$  fiber orientation subjected to tensile test to failure with a constant stress rate of 0.0025 MPa/s at 1200°C in steam.**

Figure 56 shows the micrographs of the fracture surface of the specimen subjected to tensile test to failure performed with a constant stress rate of 25 MPa/s in steam. Fracture surface produced at 25 MPa/s in steam exhibits characteristics similar to those produced at creep tests of short duration performed in steam(see Figures 46 (c) and (d)).



**Figure 56. SEM micrograph of the fracture surface of the N720/AM specimen with  $\pm 45^\circ$  fiber orientation subjected to tensile test to failure with a constant stress rate of 25 MPa/s at 1200°C in steam.**

Finally, we will have a look at the micrographs of the N720/AM specimen subjected to a monotonic tensile test to failure (conducted in displacement control) shown in Figure 57. The appearance of the fracture surface reveals the same characteristics as the tensile test to failure in air at constant rate of 25 MPa/s (see Figure 54).



**Figure 57. SEM micrograph of the fracture surface of the N720/AM specimen with  $\pm 45^\circ$  fiber orientation subjected to displacement controlled (0.05 mm/s) monotonic tensile test to failure at 1200°C in laboratory air,  $t_f = 0.0007$  h.**

## V. Conclusions

The tensile stress-strain behavior of the N720/AM composite with a  $\pm 45^\circ$  fiber orientation was investigated and the tensile properties measured at 1200 °C in laboratory air. The average tensile modulus was 41.7 GPa and the average tensile strength was 36.74 MPa. It is noteworthy that both the tensile modulus and the UTS of N720/AM CMC with a  $\pm 45^\circ$  fiber orientation are below the corresponding values for the N720/A composite with a  $\pm 45^\circ$  fiber orientation [16,17]. The tensile stress-strain curve exhibits a short linear region and departs from linearity at the stresses between 15 and 20 MPa. Such stress-strain behavior is qualitatively similar to that exhibited by the N720/A composite with a  $\pm 45^\circ$  fiber orientation at 1200 °C [16,17]. As expected, the tensile modulus and the UTS of N720/AM CMC with  $\pm 45^\circ$  fiber orientation are significantly lower than the corresponding values for the  $0^\circ/90^\circ$  fiber orientation [21].

The effects of the loading rate on tensile properties were examined in constant stress-rate tests conducted at 25 and 0.0025 MPa/s at 1200 °C in laboratory air and in steam. Tensile strength and modulus are influenced by the loading rate in both environments. In laboratory air, as the loading rate decreases by four orders of magnitude, tensile modulus drops by 72% while tensile strength increases by 20%. At 0.0025 MPa/s as the stress levels increase, the slope of the stress-strain curve drops and considerable inelastic strain develops. The failure strain produced at 0.0025 MPa/s is ten times that obtained in 25 MPa/s. In steam, the stress-strain curves produced at 25 and 0.0025 MPa/s are qualitatively similar to those obtained in laboratory air at the same loading rate. The tensile modulus obtained at 0.0025 MPa/s is 90% lower than that

produced at 25 MPa/s. In steam, the decrease in loading rate from 25 to 0.0025 MPa/s caused a 45 % increase in UTS.

The creep-rupture behavior was evaluated for stress levels ranging from 13 MPa to 32 MPa at 1200 °C in laboratory air, argon and steam. In laboratory air and in steam the N720/AM composite with a  $\pm 45^\circ$  fiber orientation exhibits primary and secondary creep regimes. In argon, primary, secondary and tertiary creep regimes were observed. The creep strains accumulated at all stress levels were higher than the failure strain obtained in tensile tests. For a given applied stress creep strain accumulation is highest in argon, followed by that in steam and in laboratory air. The 32 MPa creep test in air represents an exception with the creep strain accumulation of 4.43 % being the highest of all. In the case of the N720/A composite with a  $\pm 45^\circ$  fiber orientation, the correlation between creep strain accumulation and test environments was similar to that reported for the N720/AM composite with a  $\pm 45^\circ$  fiber orientation [17].

As reported in a previous study [16,17], environment has little effect on the creep lifetimes (up to 100 h) for applied stresses  $\leq 35$  MPa. For stresses  $\geq 40$  MPa, creep lifetimes can be reduced by as much as an order of magnitude in the presence of steam. An even greater reduction in creep life is seen in the presence of argon. The presence of an oxidizing environment, such as steam, dramatically reduced creep lifetimes of N720/AM composite with a  $\pm 45^\circ$  fiber orientation. The presence of argon also had a detrimental effect on the creep performance of N720/AM with a  $\pm 45^\circ$  fiber orientation. At higher stress levels creep lifetimes were reduced by over 96 % in the presence of steam or argon.

Creep run-out of 100 h was achieved in all tests performed in air. In steam and in argon creep run-out stress was 20 MPa. Prior creep in air, steam and argon environments had similar effects on the retained properties of the N720/AM specimens with a  $\pm 45^\circ$  fiber orientation. The N720/AM specimens retained over 120% of their tensile strength and their modulus increased by at least 9%.

Minimum creep rate was reached in all tests. At 1200 °C, creep strain rates range from  $1.0 \times 10^{-6}$  to  $6.0 \times 10^{-6} \text{ s}^{-1}$  in laboratory air, from  $1.0 \times 10^{-5}$  to  $7.0 \times 10^{-3} \text{ s}^{-1}$  in argon, and from  $7.0 \times 10^{-6}$  to  $8.4 \times 10^{-3} \text{ s}^{-1}$  in steam. The creep rates of the N720/AM in argon were at least an order of magnitude higher than those in air and similar to those obtained in steam. In air, the creep rate of N720/AM with a  $\pm 45^\circ$  fiber orientation was 1000 times lower than those of the N720/A composite with a  $\pm 45^\circ$  fiber orientation. In steam, the creep rate produced by N720/AM CMC with a  $\pm 45^\circ$  fiber orientation was 10 times lower than those obtained for the N720/A composite with a  $\pm 45^\circ$  fiber orientation. Finally in argon, the creep rate of N720/AM CMC with a  $\pm 45^\circ$  fiber orientation was 100 times lower than those obtained for the N720/A composite with a  $\pm 45^\circ$  fiber orientation.

Post-test microstructure was examined using an optical microscope and an SEM. In all tests conducted in air, the failure occurs primarily through matrix damage and interply delamination, with minimal fiber fracture. The same failure mechanisms prevail in tests of less than 75 h duration conducted in steam or in argon. For tests more than 75 h duration performed in steam or in argon, the failure mechanism is dominated by fiber fracture. It appears that the matrix undergoes additional sintering and consequently densification during the long-term tests. Increased fiber-matrix bonding is also apparent.

## Appendix: Additional SEM Micrographs

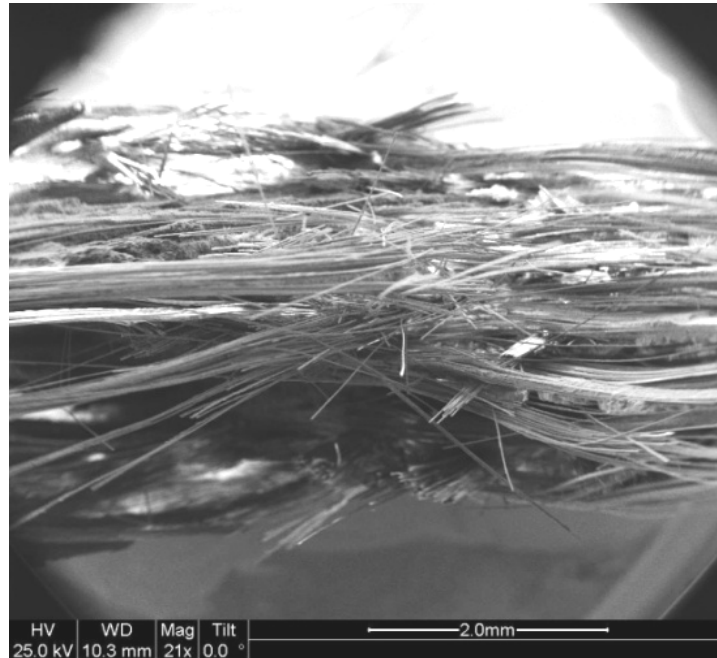


Figure 58. SEM micrograph of the fracture surface of the N720/AM specimen subjected to tensile test to failure following 100 h at 13 MPa at 1200°C in laboratory air.

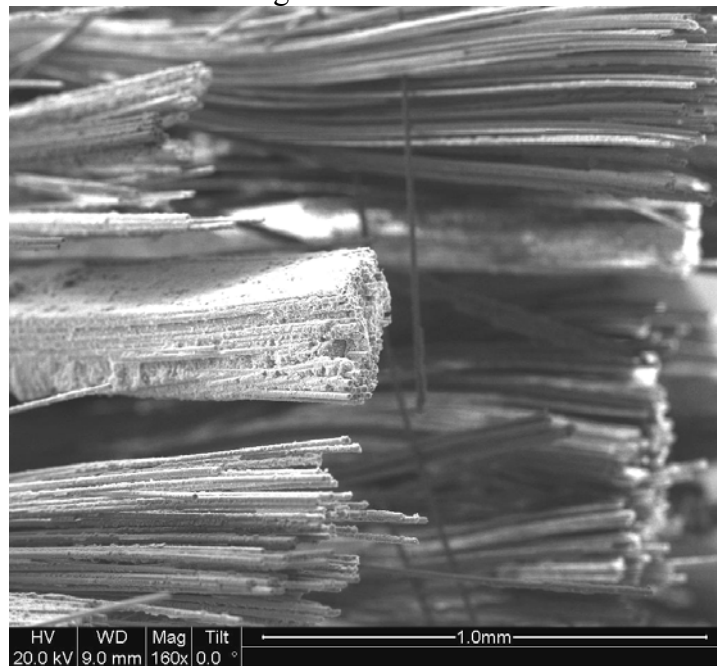


Figure 59. SEM micrograph of the fracture surface of the N720/AM specimen subjected to tensile test to failure following 100 h at 13 MPa at 1200°C in laboratory air.

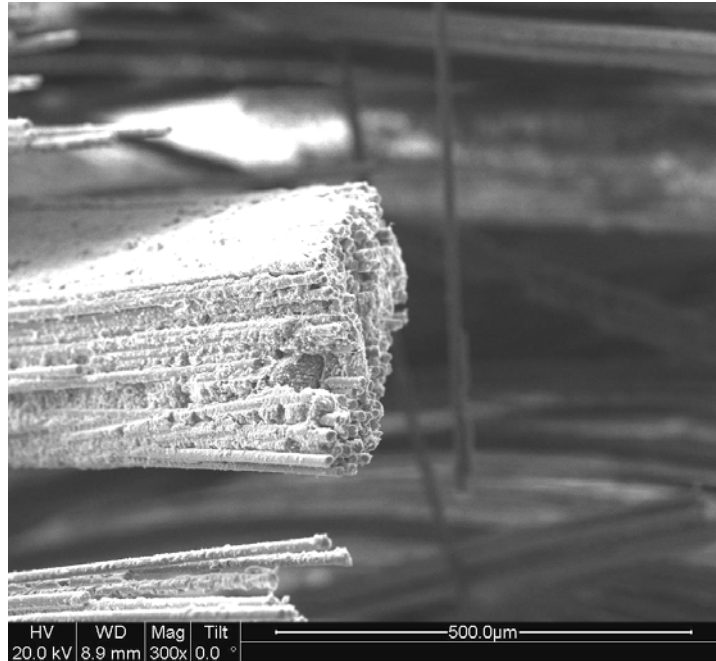


Figure 60. SEM micrograph of the fracture surface of the N720/AM specimen subjected to tensile test to failure following 100 h at 13 MPa at 1200°C in laboratory air.

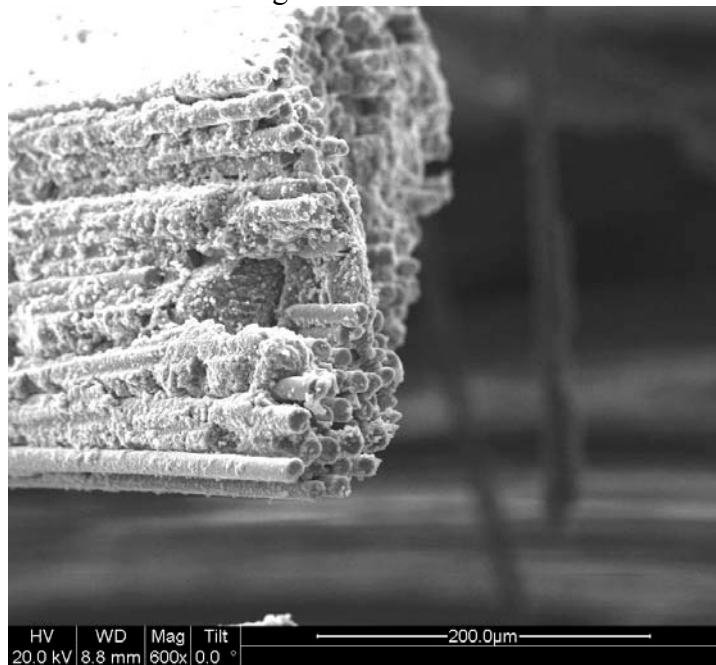


Figure 61. SEM micrograph of the fracture surface of the N720/AM specimen subjected to tensile test to failure following 100 h at 13 MPa at 1200°C in laboratory air.

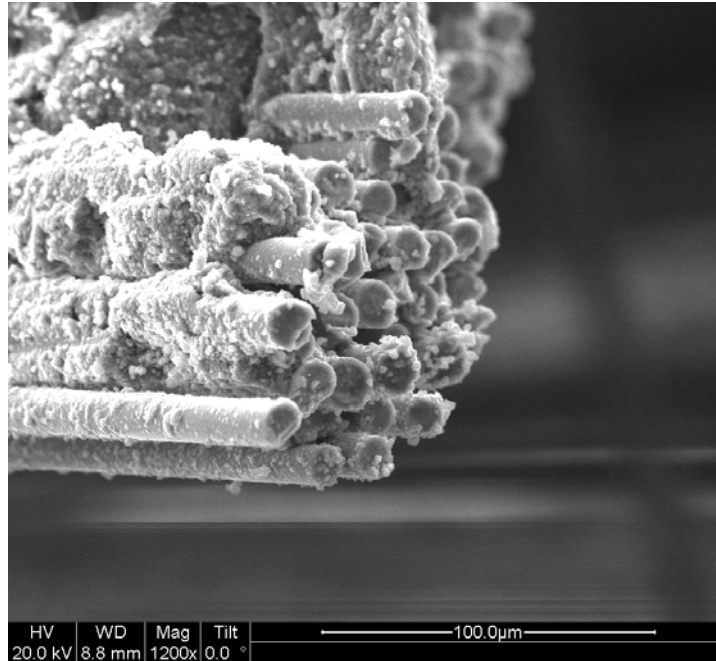


Figure 62. SEM micrograph of the fracture surface of the N720/AM specimen subjected to tensile test to failure following 100 h at 13 MPa at 1200°C in laboratory air.



Figure 63. SEM micrograph of the fracture surface of the N720/AM specimen subjected to tensile test to failure following 100 h at 13 MPa at 1200°C in laboratory air.

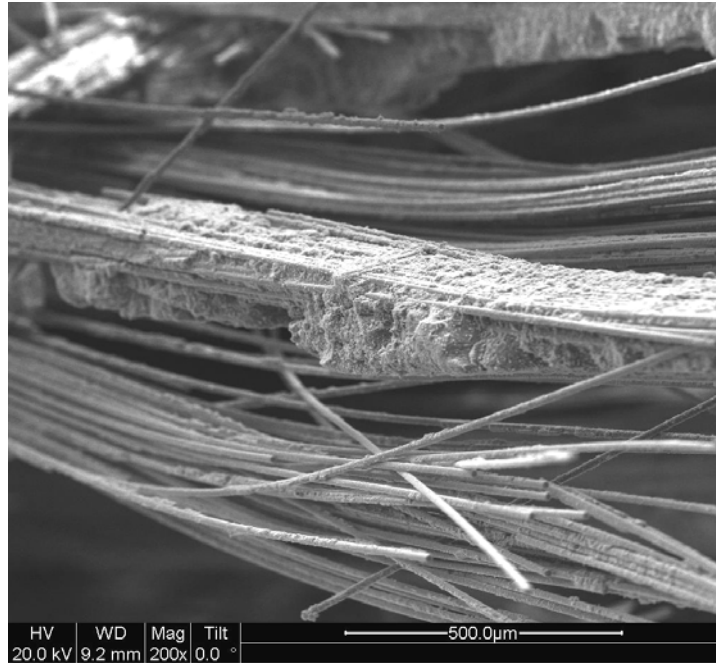


Figure 64. SEM micrograph of the fracture surface of the N720/AM specimen subjected to tensile test to failure following 100 h at 13 MPa at 1200°C in laboratory air.

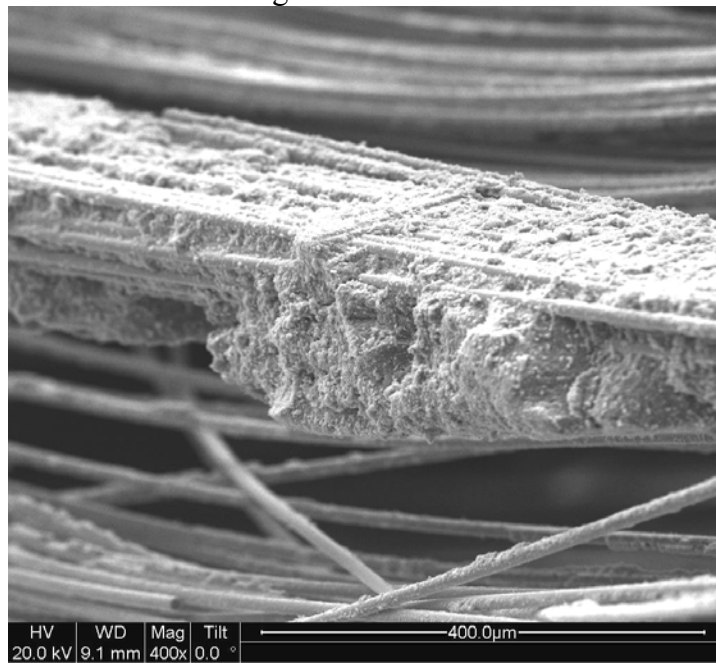


Figure 65. SEM micrograph of the fracture surface of the N720/AM specimen subjected to tensile test to failure following 100 h at 13 MPa at 1200°C in laboratory air.

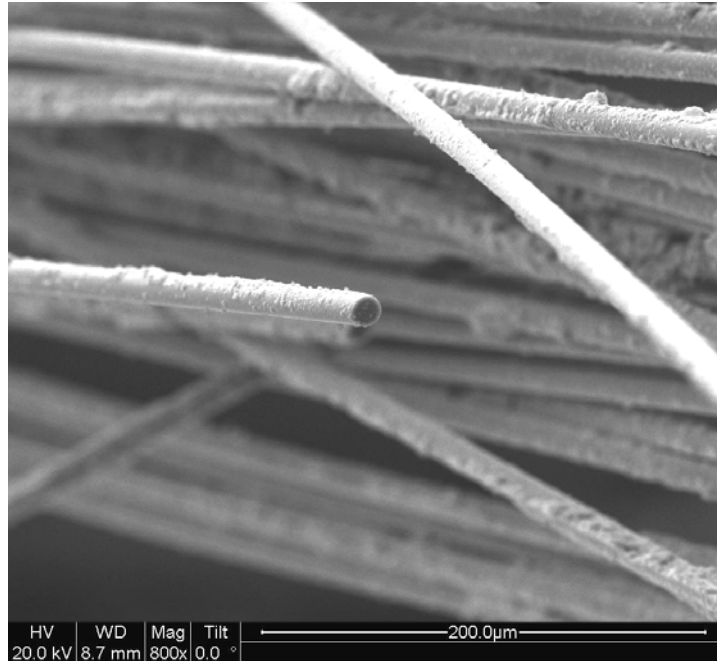


Figure 66. SEM micrograph of the fracture surface of the N720/AM specimen subjected to tensile test to failure following 100 h at 13 MPa at 1200°C in laboratory air.

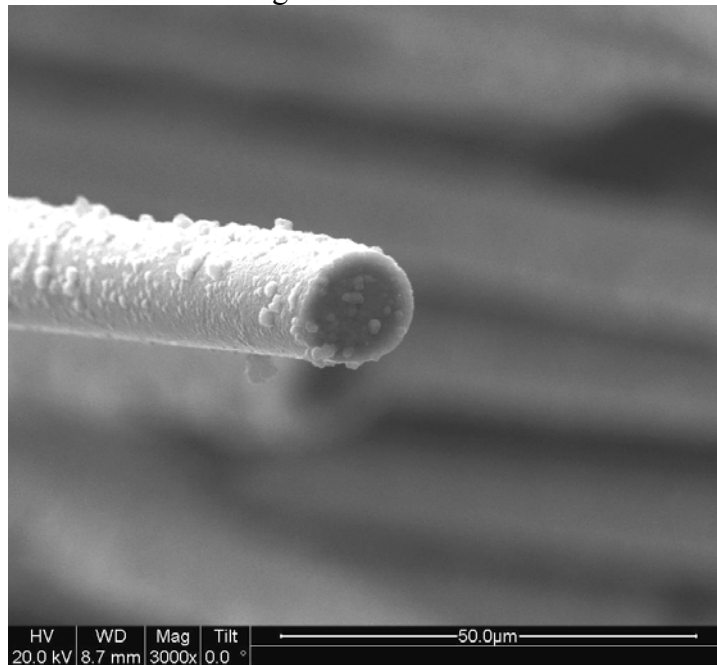


Figure 67. SEM micrograph of the fracture surface of the N720/AM specimen subjected to tensile test to failure following 100 h at 13 MPa at 1200°C in laboratory air.

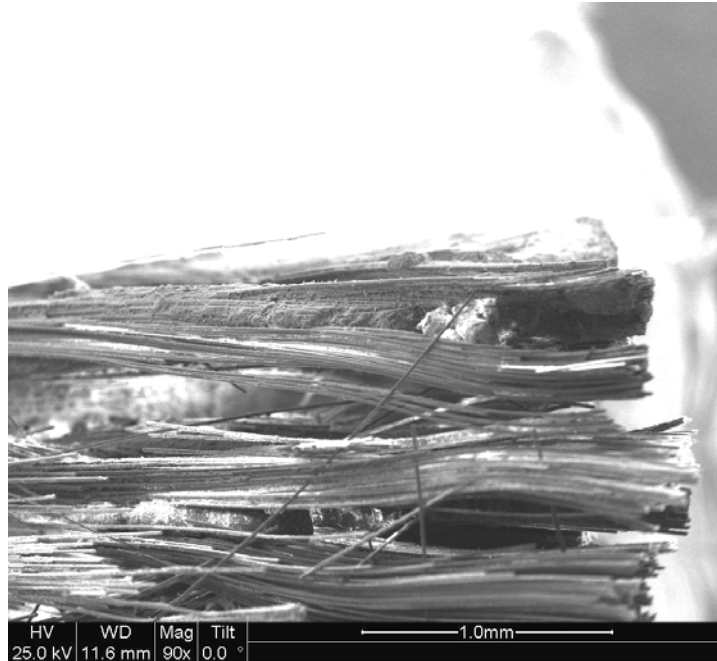


Figure 68. SEM micrograph of the fracture surface of the N720/AM specimen subjected to tensile test to failure following 100 h at 13 MPa at 1200°C in laboratory air.

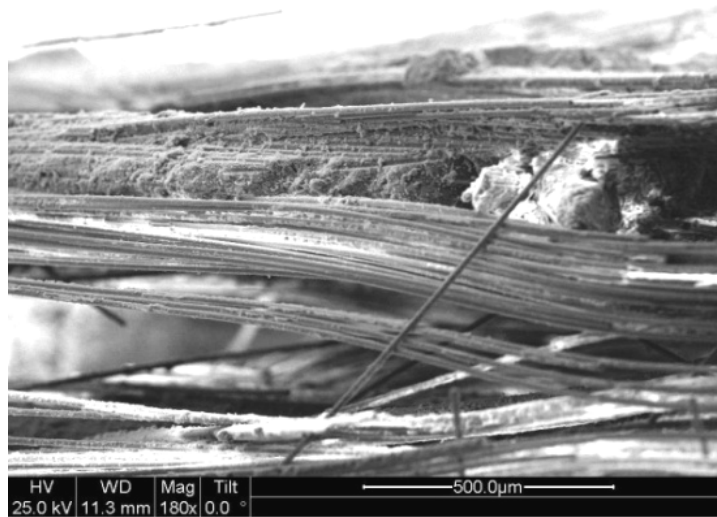


Figure 69. SEM micrograph of the fracture surface of the N720/AM specimen subjected to tensile test to failure following 100 h at 13 MPa at 1200°C in laboratory air.

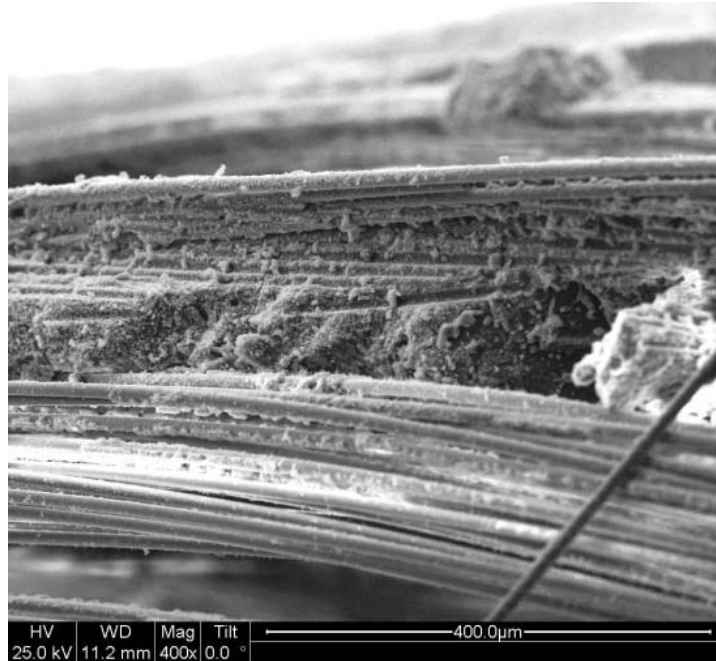


Figure 70. SEM micrograph of the fracture surface of the N720/AM specimen subjected to tensile test to failure following 100 h at 13 MPa at 1200°C in laboratory air.



Figure 71. SEM micrograph of the fracture surface of the N720/AM specimen subjected to tensile test to failure following 100 h at 13 MPa at 1200°C in laboratory air.

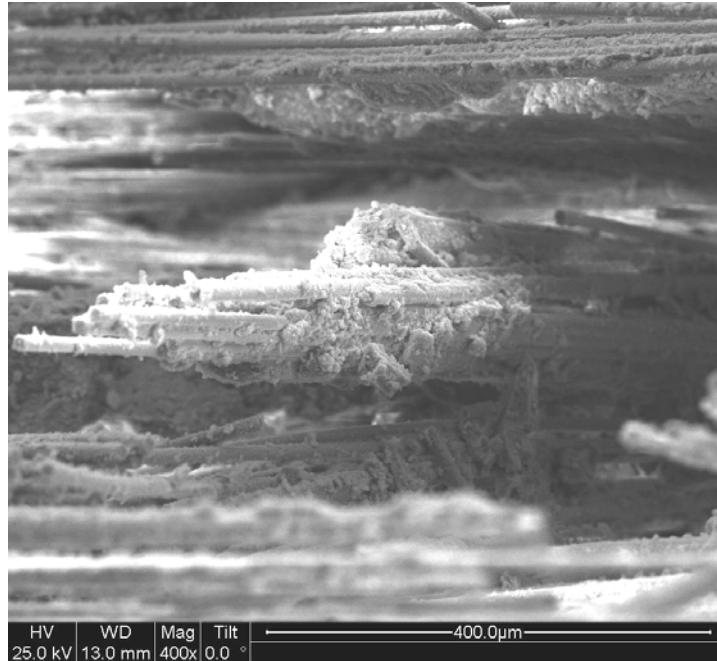


Figure 72. SEM micrograph of the fracture surface of the N720/AM specimen subjected to tensile test to failure following 100 h at 13 MPa at 1200°C in laboratory air.

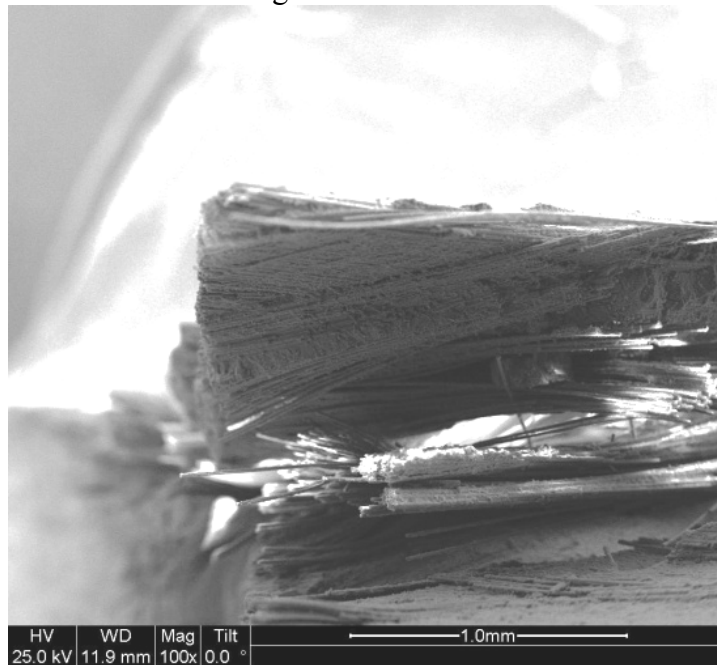


Figure 73. SEM micrograph of the fracture surface of the N720/AM specimen subjected to tensile test to failure following 100 h at 13 MPa at 1200°C in laboratory air.

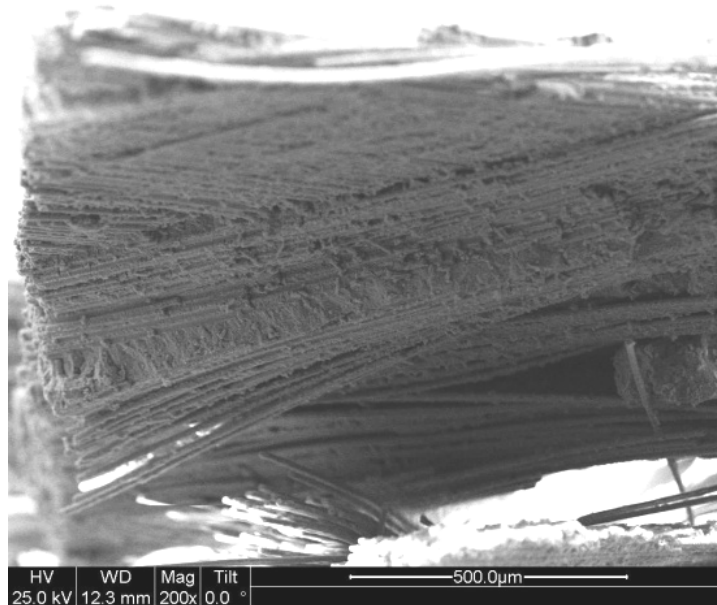


Figure 74. SEM micrograph of the fracture surface of the N720/AM specimen subjected to tensile test to failure following 100 h at 13 MPa at 1200°C in laboratory air.

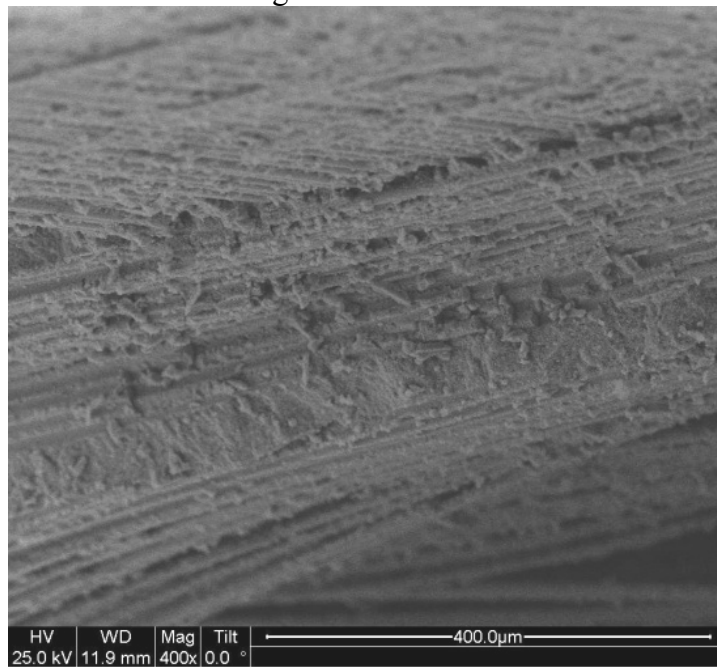


Figure 75. SEM micrograph of the fracture surface of the N720/AM specimen subjected to tensile test to failure following 100 h at 13 MPa at 1200°C in laboratory air.

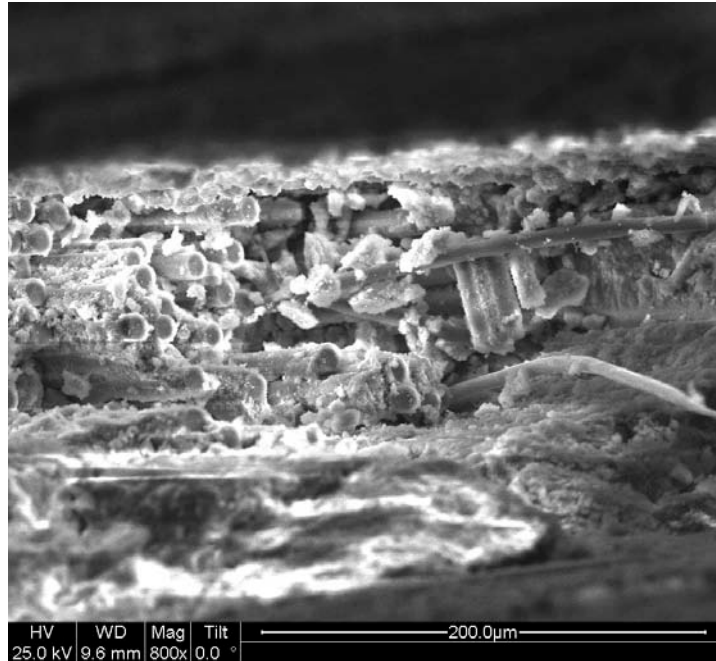


Figure 76. SEM micrograph of the fracture surface of the N720/AM specimen subjected to tensile test to failure following 100 h at 13 MPa at 1200°C in laboratory air.

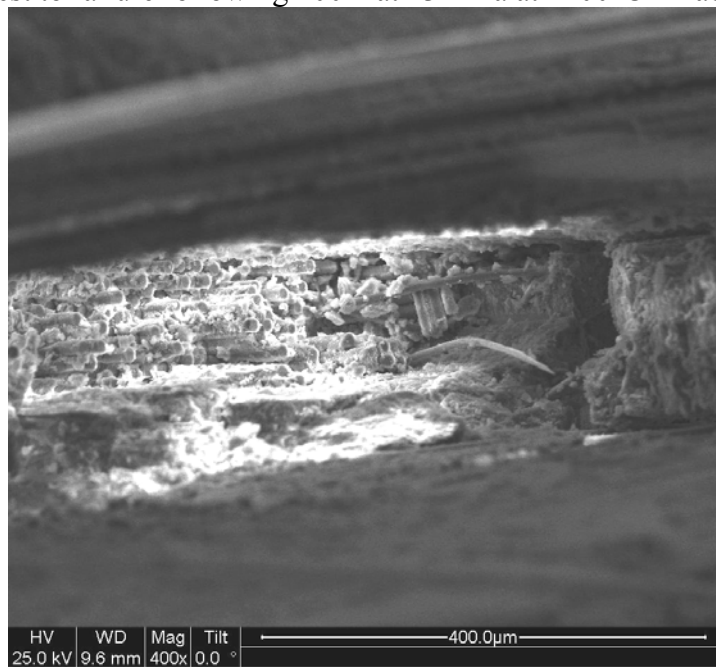


Figure 77. SEM micrograph of the fracture surface of the N720/AM specimen subjected to tensile test to failure following 100 h at 13 MPa at 1200°C in laboratory air.

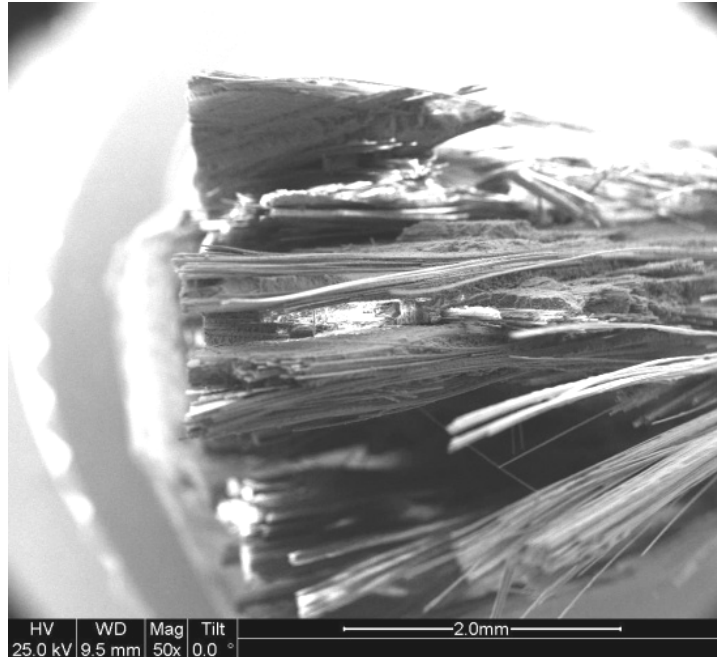


Figure 78. SEM micrograph of the fracture surface of the N720/AM specimen subjected to tensile test to failure following 100 h at 13 MPa at 1200°C in laboratory air.

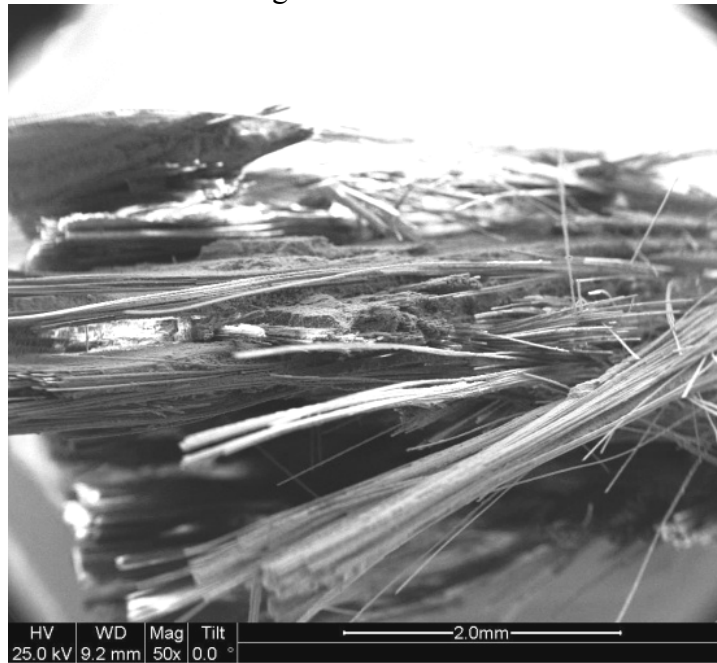


Figure 79. SEM micrograph of the fracture surface of the N720/AM specimen subjected to tensile test to failure following 100 h at 13 MPa at 1200°C in laboratory air.

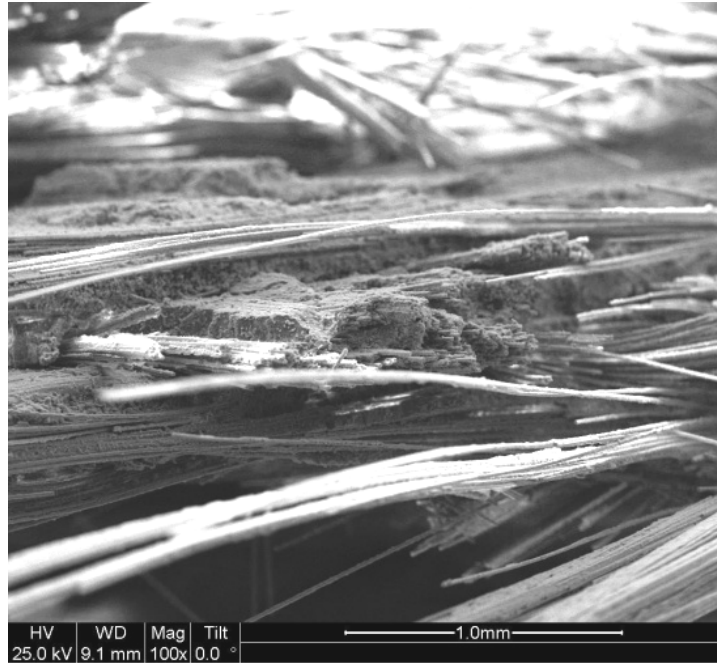


Figure 80. SEM micrograph of the fracture surface of the N720/AM specimen subjected to tensile test to failure following 100 h at 13 MPa at 1200°C in laboratory air.

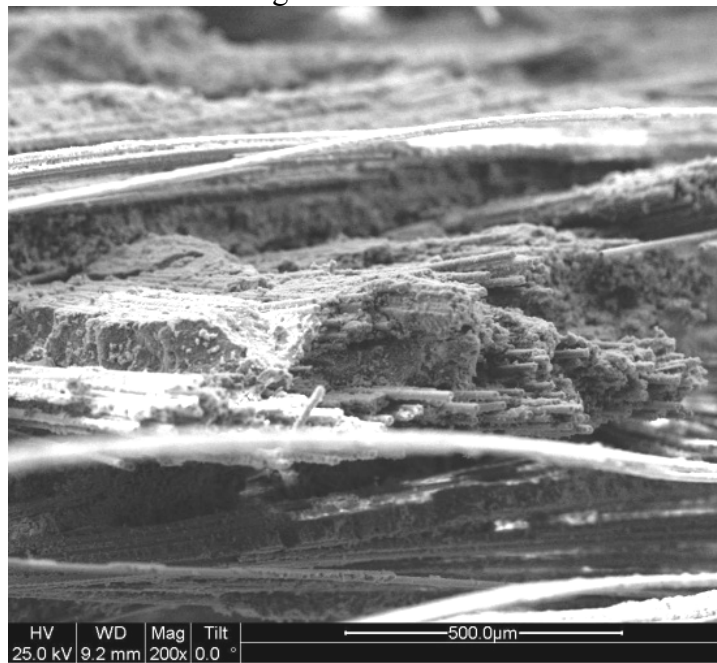


Figure 81. SEM micrograph of the fracture surface of the N720/AM specimen subjected to tensile test to failure following 100 h at 13 MPa at 1200°C in laboratory air.

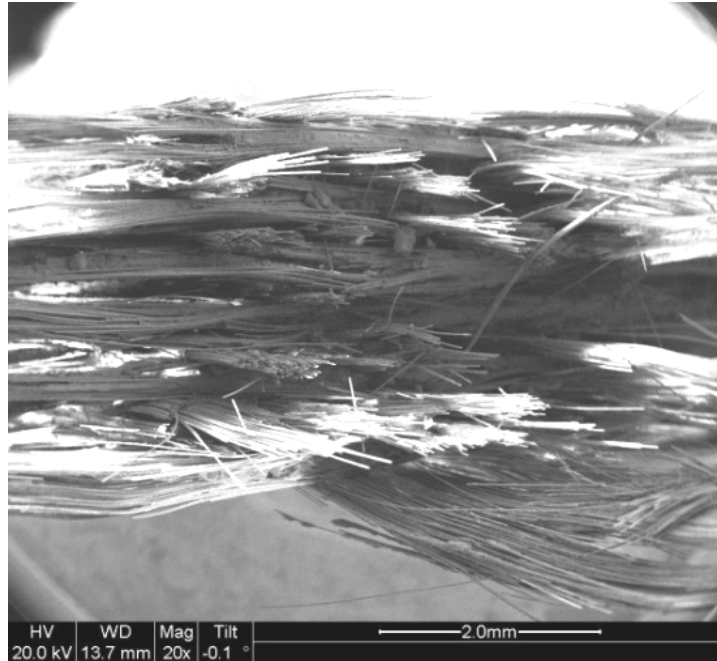


Figure 82. SEM micrograph of the fracture surface of the N720/AM specimen subjected to tensile test to failure following 100 h at 30 MPa at 1200°C in laboratory air.

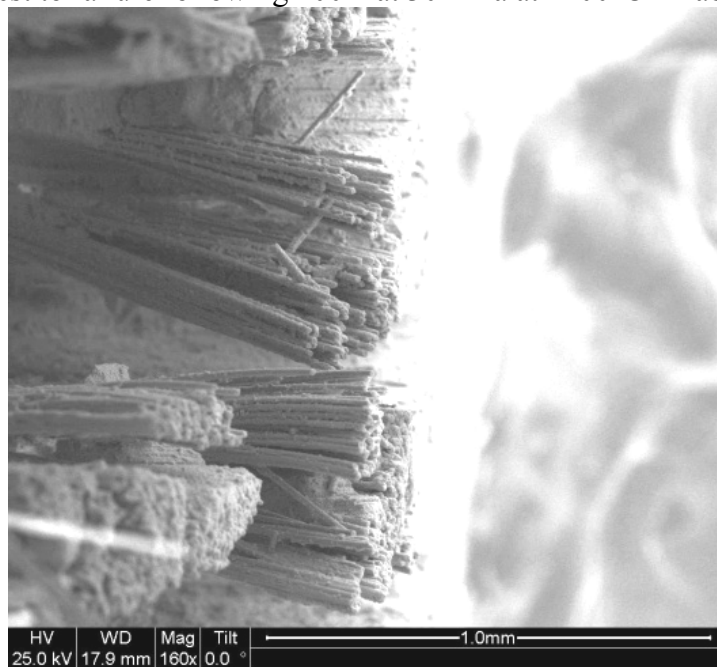


Figure 83. SEM micrograph of the fracture surface of the N720/AM specimen subjected to tensile test to failure following 100 h at 30 MPa at 1200°C in laboratory air.

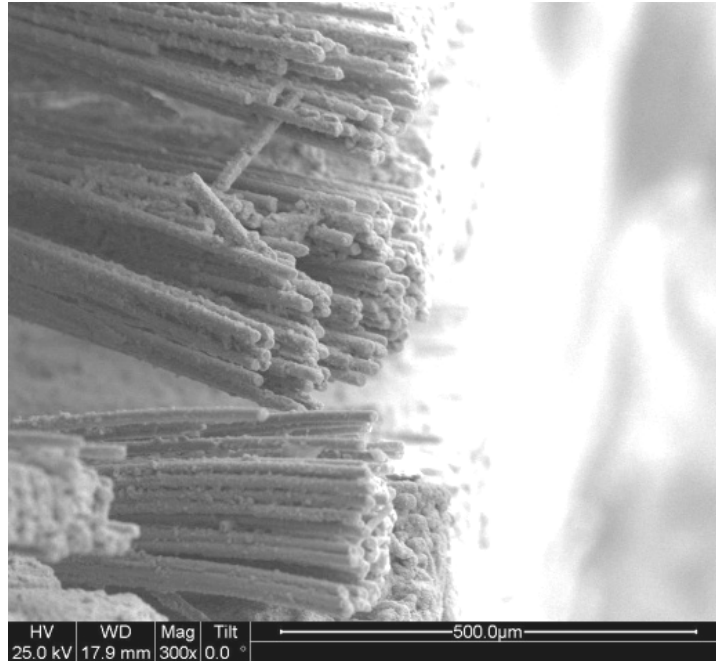


Figure 84. SEM micrograph of the fracture surface of the N720/AM specimen subjected to tensile test to failure following 100 h at 30 MPa at 1200°C in laboratory air.

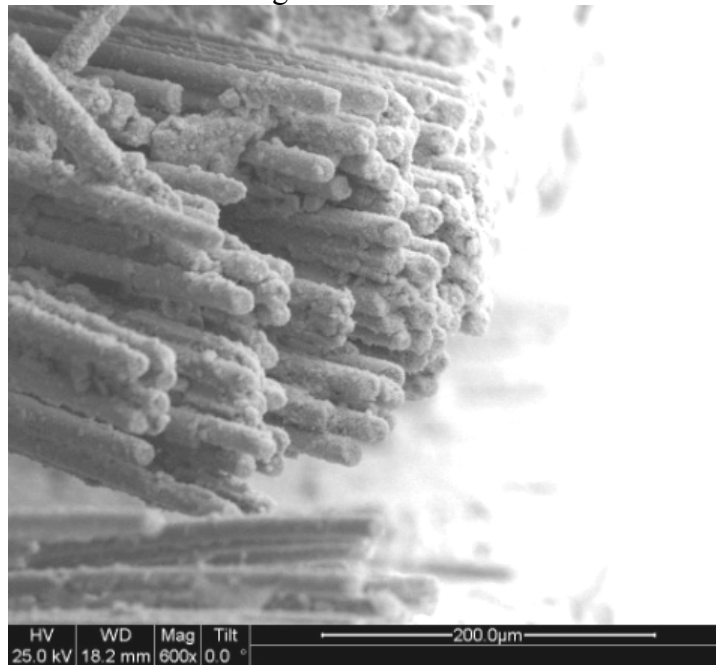


Figure 85. SEM micrograph of the fracture surface of the N720/AM specimen subjected to tensile test to failure following 100 h at 30 MPa at 1200°C in laboratory air.

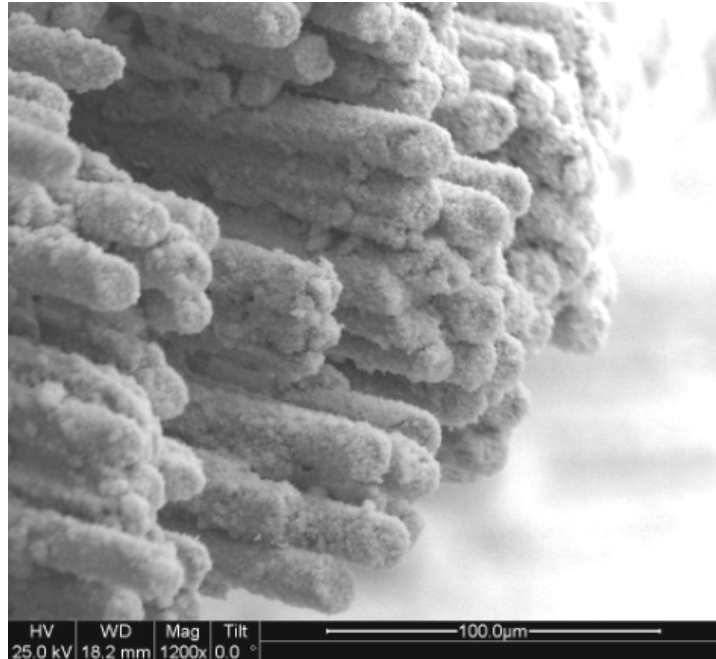


Figure 86. SEM micrograph of the fracture surface of the N720/AM specimen subjected to tensile test to failure following 100 h at 30 MPa at 1200°C in laboratory air.

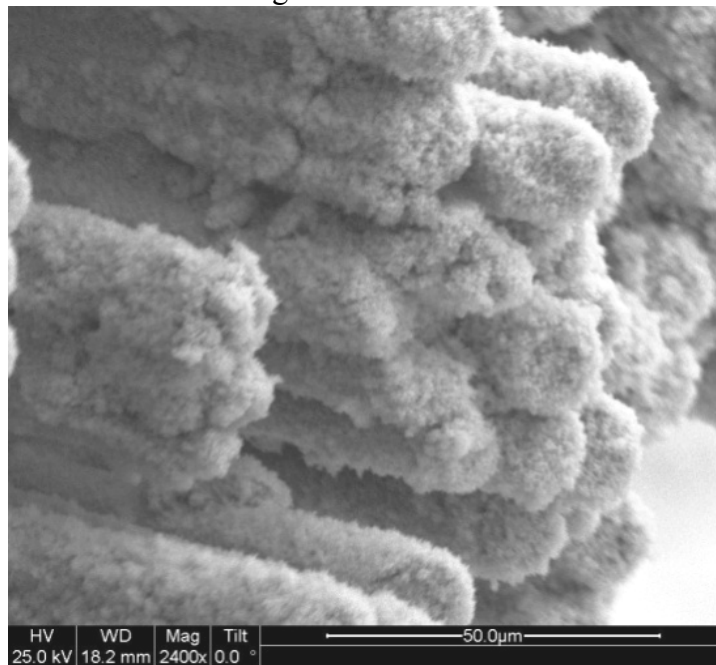


Figure 87. SEM micrograph of the fracture surface of the N720/AM specimen subjected to tensile test to failure following 100 h at 30 MPa at 1200°C in laboratory air.

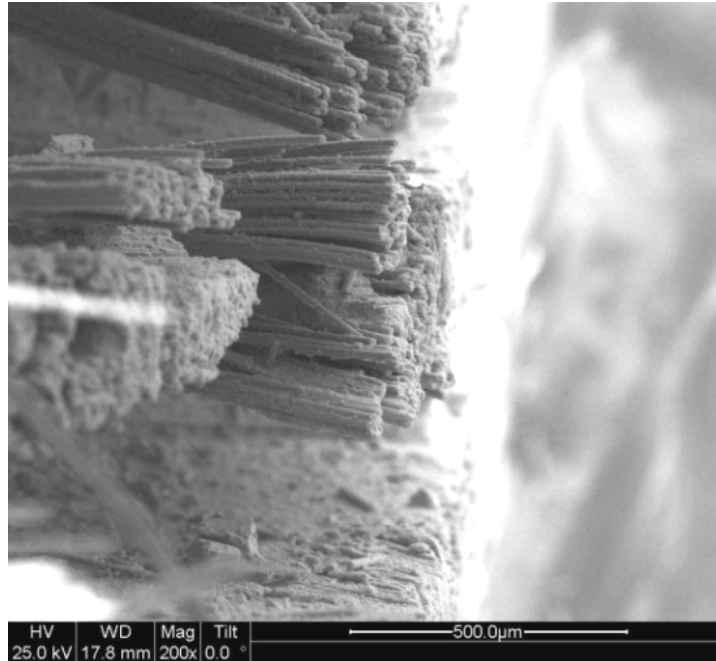


Figure 88. SEM micrograph of the fracture surface of the N720/AM specimen subjected to tensile test to failure following 100 h at 30 MPa at 1200°C in laboratory air.

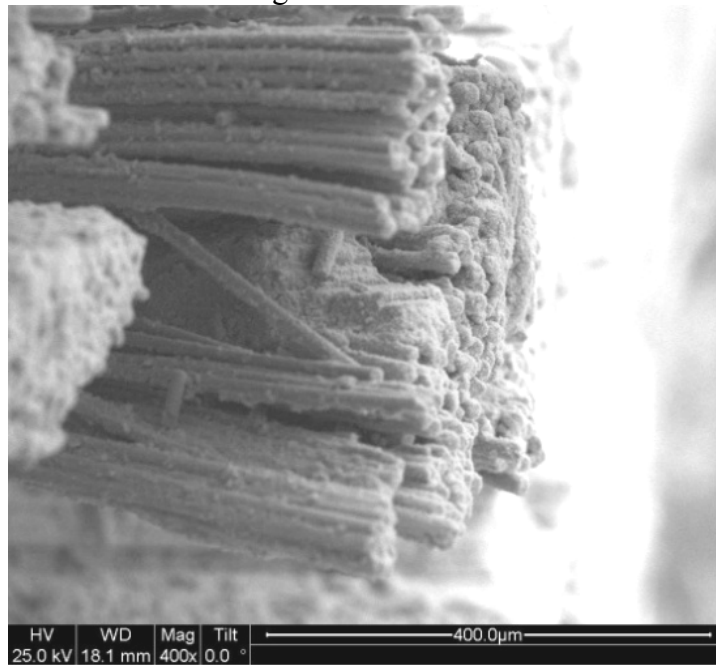


Figure 89. SEM micrograph of the fracture surface of the N720/AM specimen subjected to tensile test to failure following 100 h at 30 MPa at 1200°C in laboratory air.

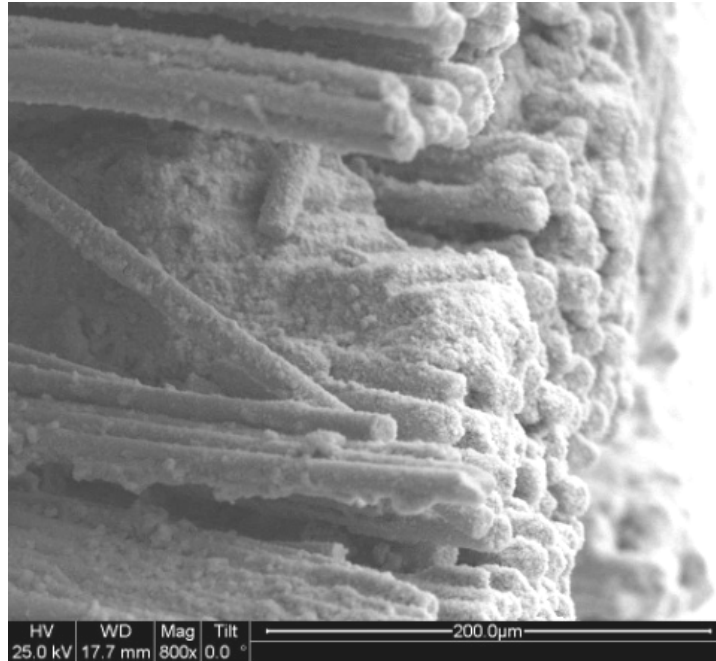


Figure 90. SEM micrograph of the fracture surface of the N720/AM specimen subjected to tensile test to failure following 100 h at 30 MPa at 1200°C in laboratory air.

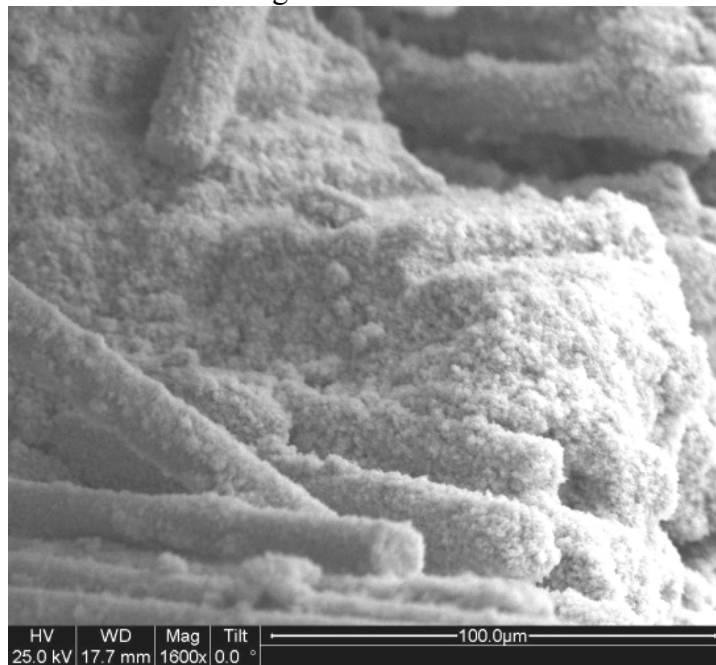


Figure 91. SEM micrograph of the fracture surface of the N720/AM specimen subjected to tensile test to failure following 100 h at 30 MPa at 1200°C in laboratory air.

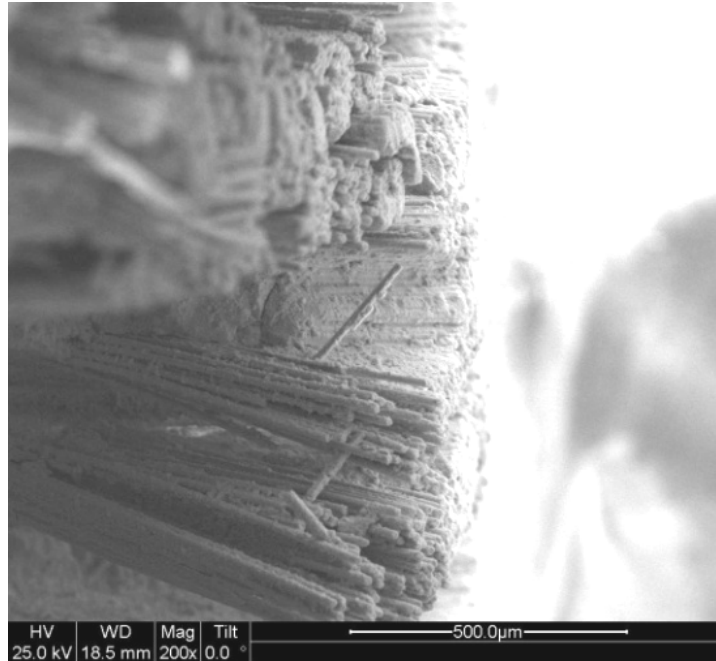


Figure 92. SEM micrograph of the fracture surface of the N720/AM specimen subjected to tensile test to failure following 100 h at 30 MPa at 1200°C in laboratory air.

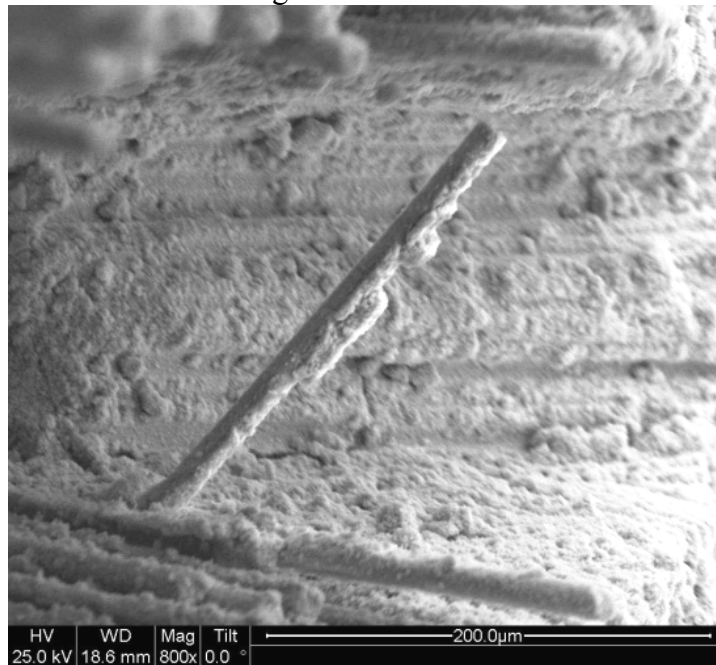


Figure 93. SEM micrograph of the fracture surface of the N720/AM specimen subjected to tensile test to failure following 100 h at 30 MPa at 1200°C in laboratory air.

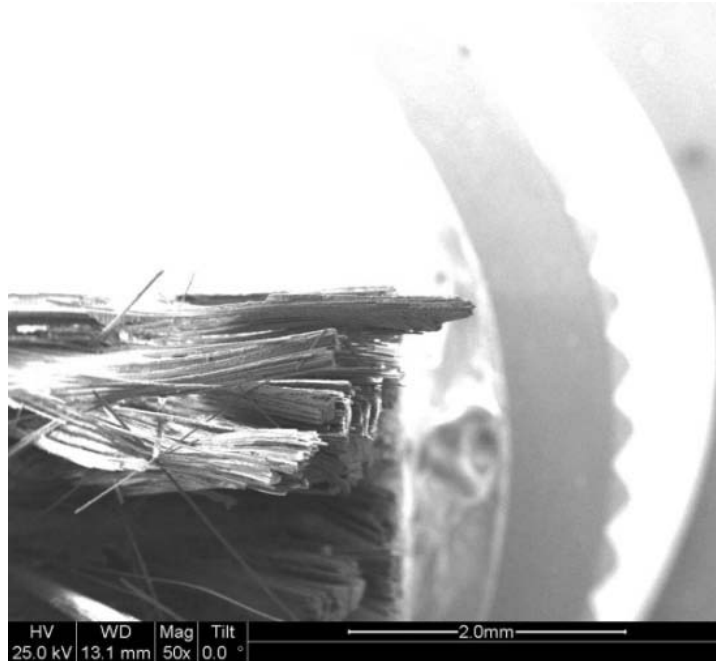


Figure 94. SEM micrograph of the fracture surface of the N720/AM specimen subjected to tensile test to failure following 100 h at 30 MPa at 1200°C in laboratory air.

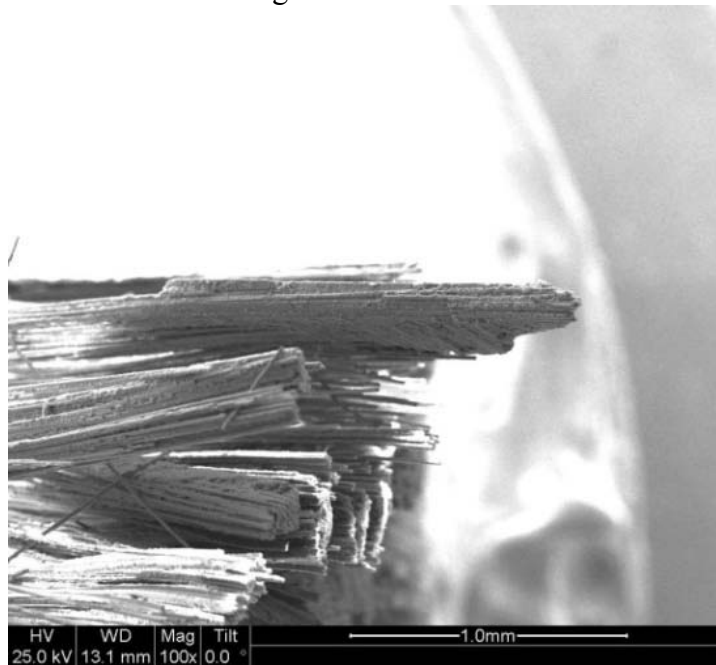


Figure 95. SEM micrograph of the fracture surface of the N720/AM specimen subjected to tensile test to failure following 100 h at 30 MPa at 1200°C in laboratory air.

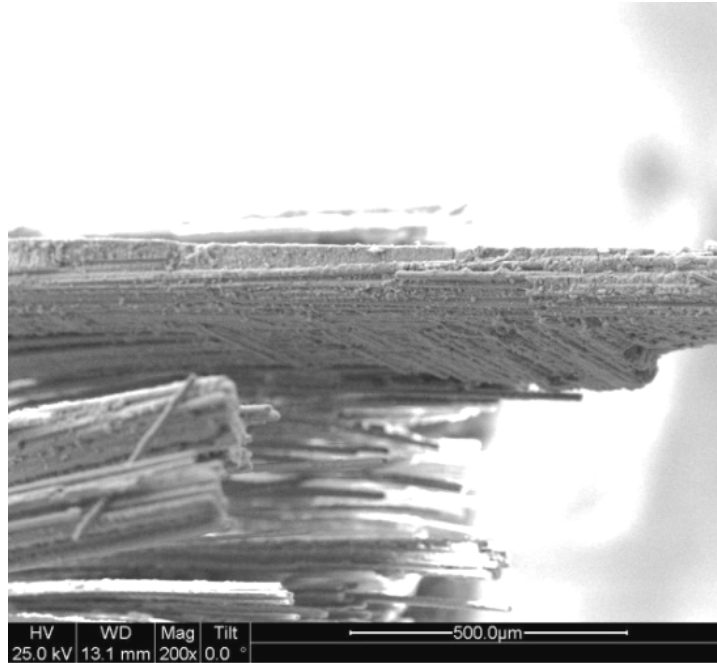


Figure 96. SEM micrograph of the fracture surface of the N720/AM specimen subjected to tensile test to failure following 100 h at 30 MPa at 1200°C in laboratory air.

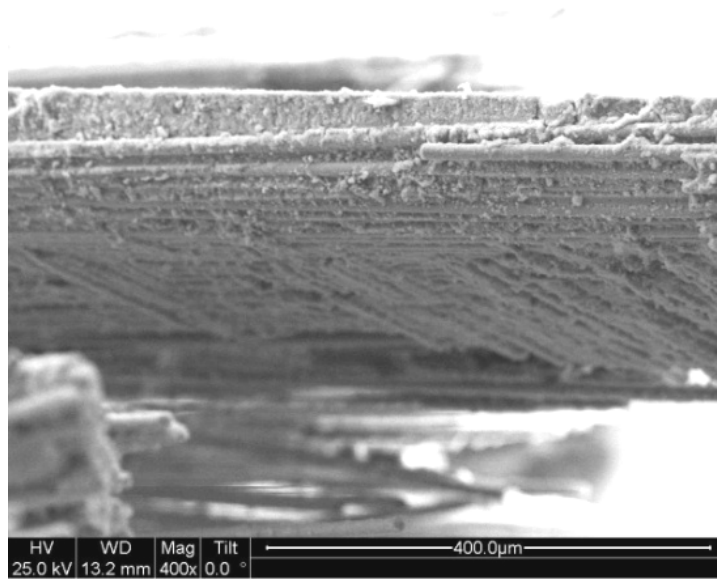


Figure 97. SEM micrograph of the fracture surface of the N720/AM specimen subjected to tensile test to failure following 100 h at 30 MPa at 1200°C in laboratory air.

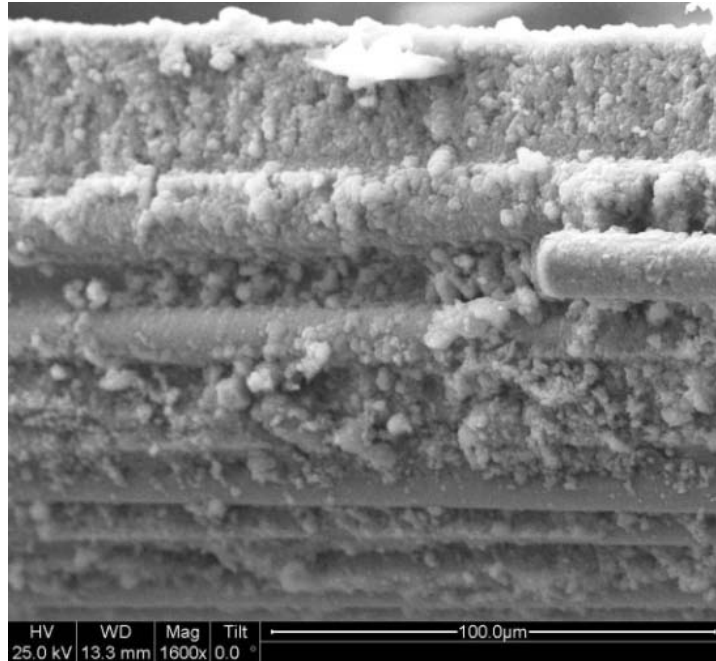


Figure 98. SEM micrograph of the fracture surface of the N720/AM specimen subjected to tensile test to failure following 100 h at 30 MPa at 1200°C in laboratory air.

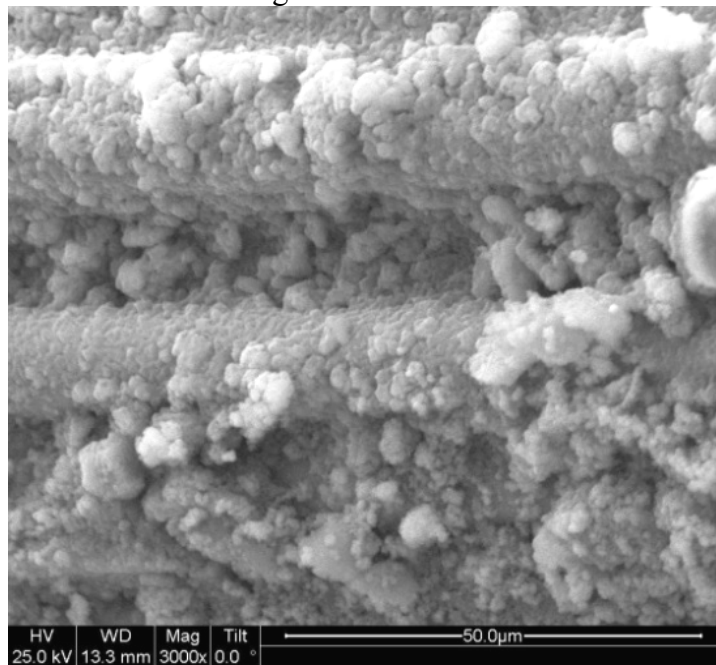


Figure 99. SEM micrograph of the fracture surface of the N720/AM specimen subjected to tensile test to failure following 100 h at 30 MPa at 1200°C in laboratory air.

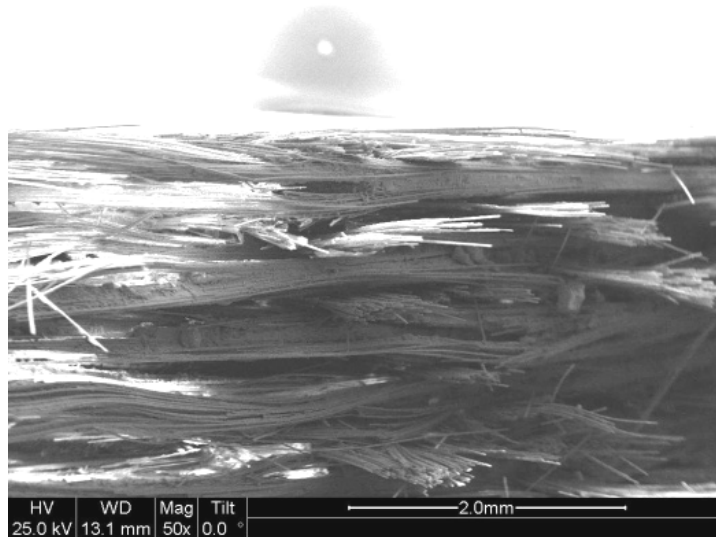


Figure 100. SEM micrograph of the fracture surface of the N720/AM specimen subjected to tensile test to failure following 100 h at 30 MPa at 1200°C in laboratory air.

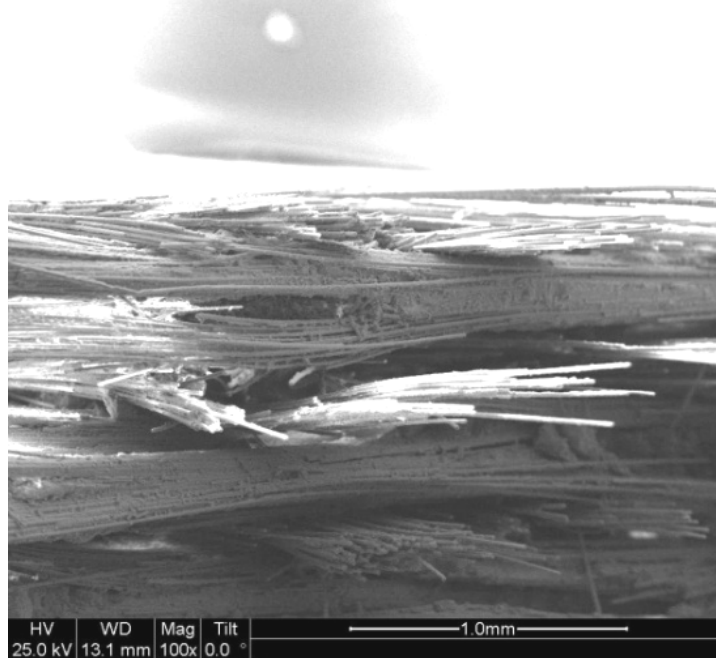


Figure 101. SEM micrograph of the fracture surface of the N720/AM specimen subjected to tensile test to failure following 100 h at 30 MPa at 1200°C in laboratory air.



Figure 102. SEM micrograph of the fracture surface of the N720/AM specimen subjected to tensile test to failure following 100 h at 30 MPa at 1200°C in laboratory air.

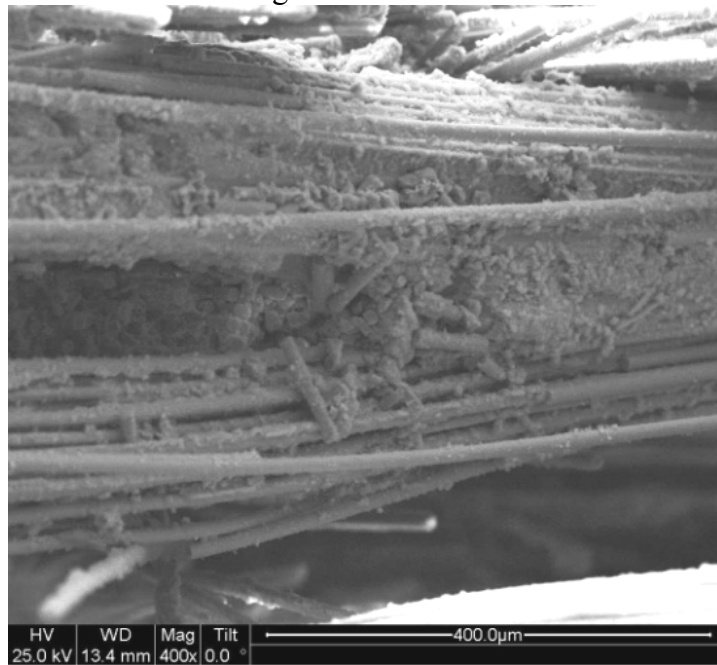


Figure 103. SEM micrograph of the fracture surface of the N720/AM specimen subjected to tensile test to failure following 100 h at 30 MPa at 1200°C in laboratory air.

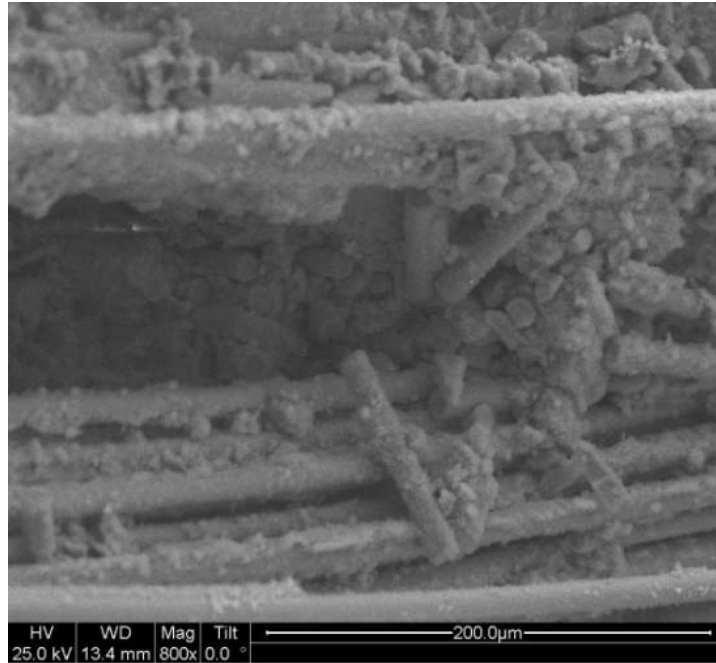


Figure 104. SEM micrograph of the fracture surface of the N720/AM specimen subjected to tensile test to failure following 100 h at 30 MPa at 1200°C in laboratory air.

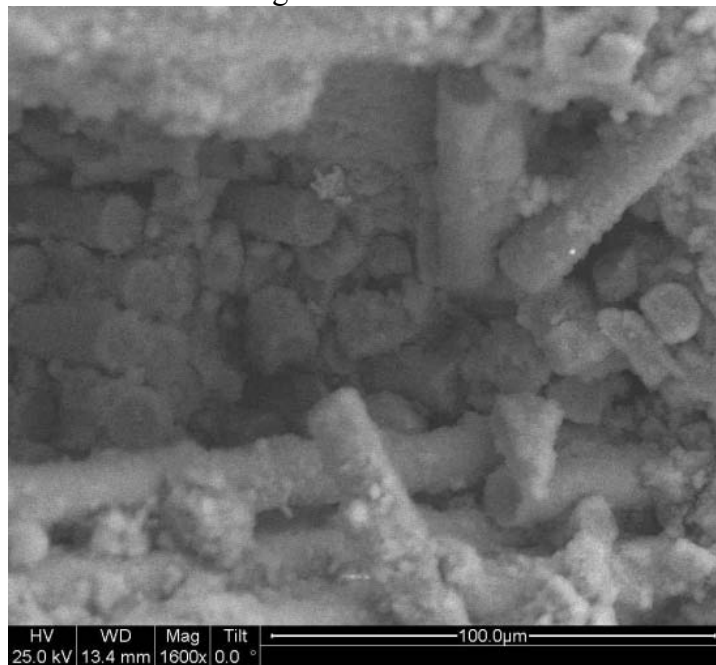


Figure 105. SEM micrograph of the fracture surface of the N720/AM specimen subjected to tensile test to failure following 100 h at 30 MPa at 1200°C in laboratory air.

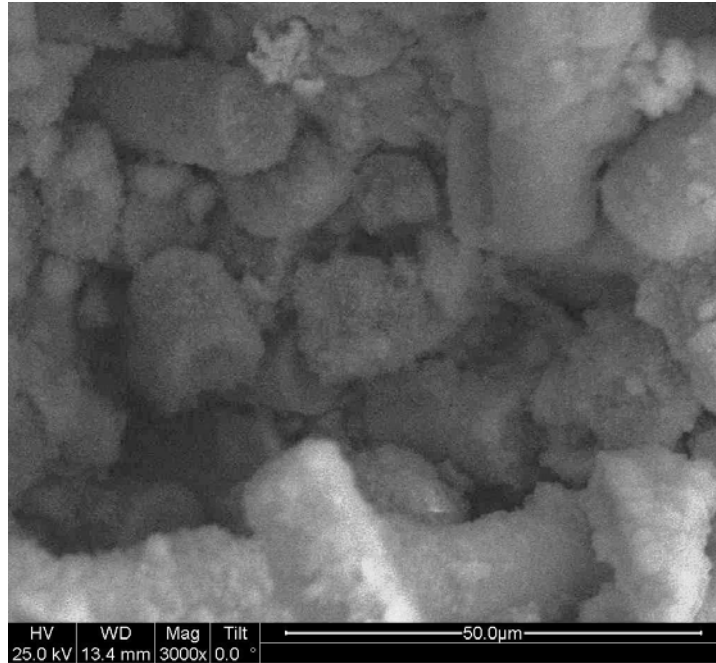


Figure 106. SEM micrograph of the fracture surface of the N720/AM specimen subjected to tensile test to failure following 100 h at 30 MPa at 1200°C in laboratory air.

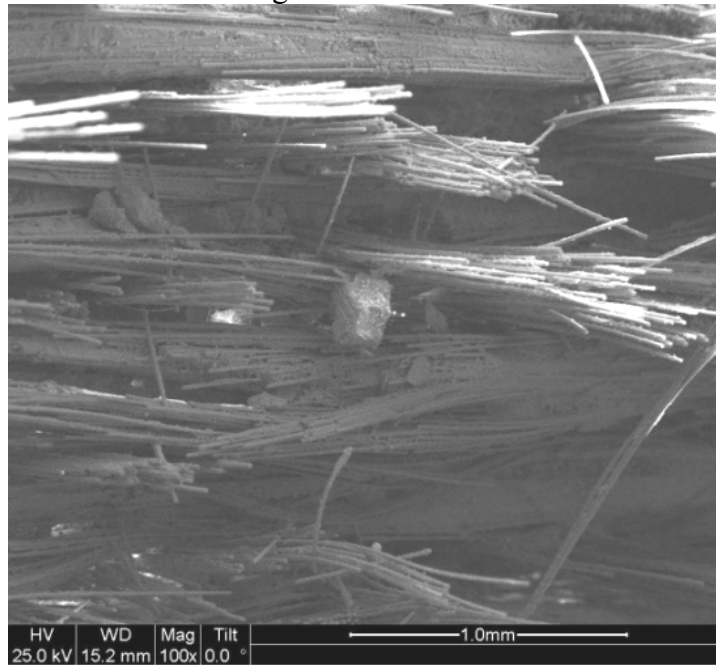


Figure 107. SEM micrograph of the fracture surface of the N720/AM specimen subjected to tensile test to failure following 100 h at 30 MPa at 1200°C in laboratory air.

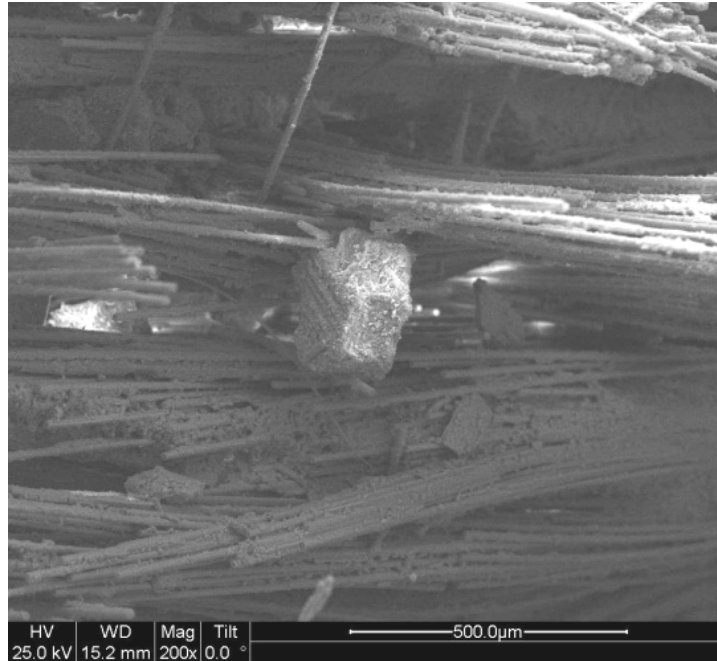


Figure 108. SEM micrograph of the fracture surface of the N720/AM specimen subjected to tensile test to failure following 100 h at 30 MPa at 1200°C in laboratory air.

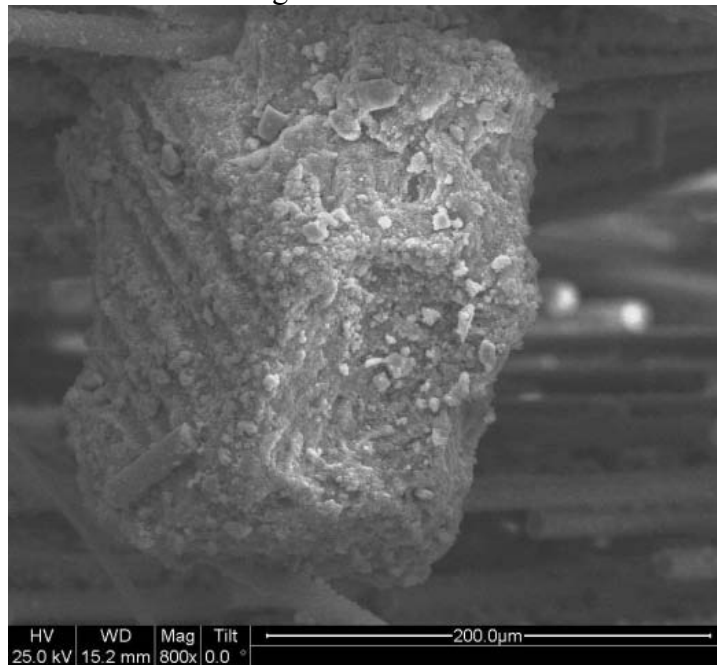


Figure 109. SEM micrograph of the fracture surface of the N720/AM specimen subjected to tensile test to failure following 100 h at 30 MPa at 1200°C in laboratory air.

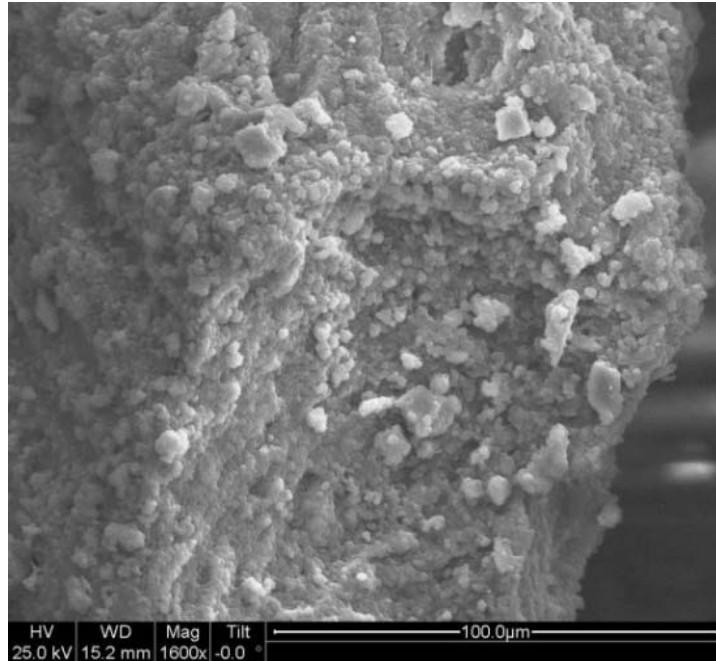


Figure 110. SEM micrograph of the fracture surface of the N720/AM specimen subjected to tensile test to failure following 100 h at 30 MPa at 1200°C in laboratory air.

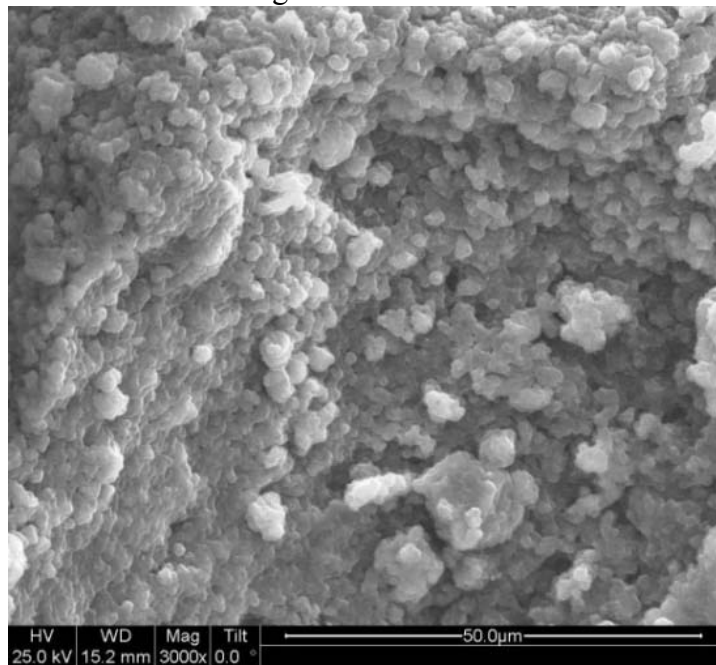


Figure 111. SEM micrograph of the fracture surface of the N720/AM specimen subjected to tensile test to failure following 100 h at 30 MPa at 1200°C in laboratory air.

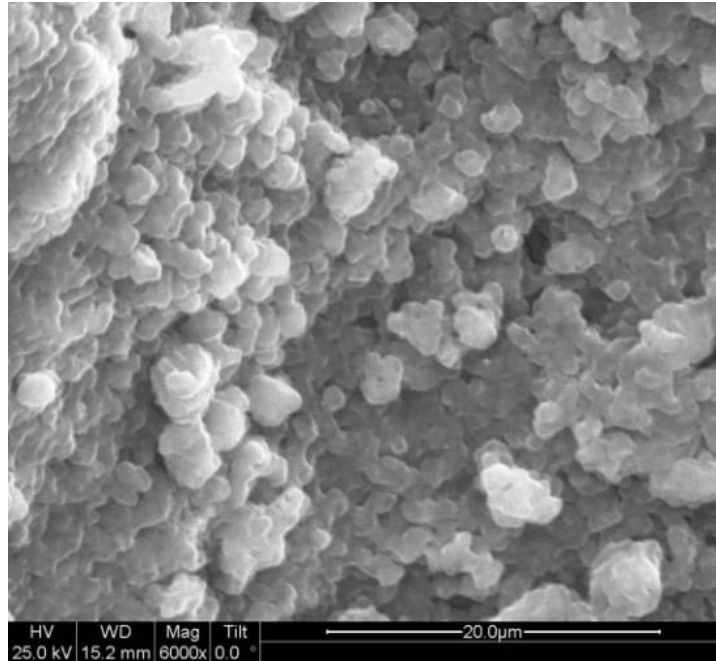


Figure 112. SEM micrograph of the fracture surface of the N720/AM specimen subjected to tensile test to failure following 100 h at 30 MPa at 1200°C in laboratory air.

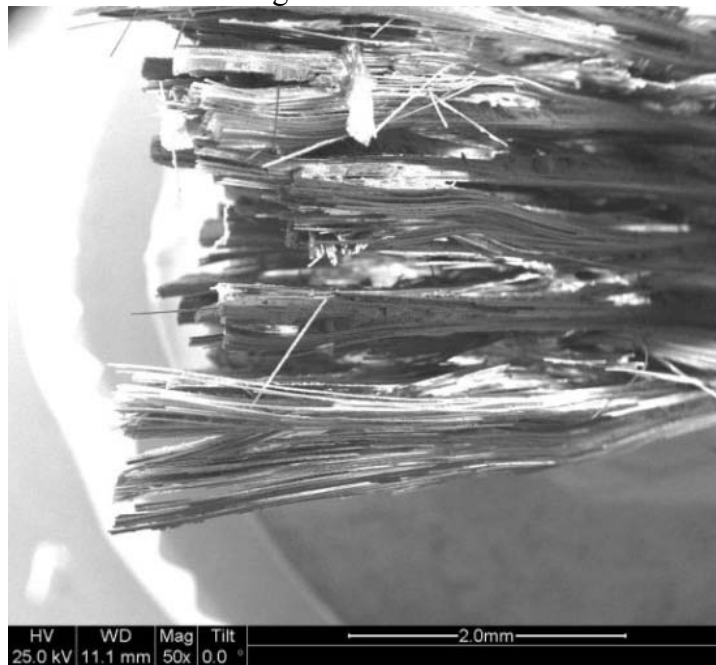


Figure 113. SEM micrograph of the fracture surface of the N720/AM specimen subjected to tensile test to failure following 100 h at 30 MPa at 1200°C in laboratory air.

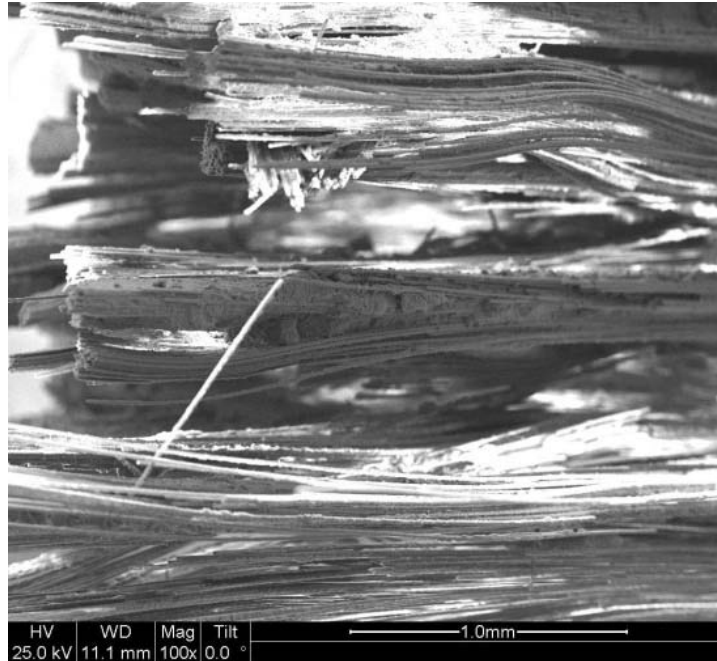


Figure 114. SEM micrograph of the fracture surface of the N720/AM specimen subjected to tensile test to failure following 100 h at 30 MPa at 1200°C in laboratory air.

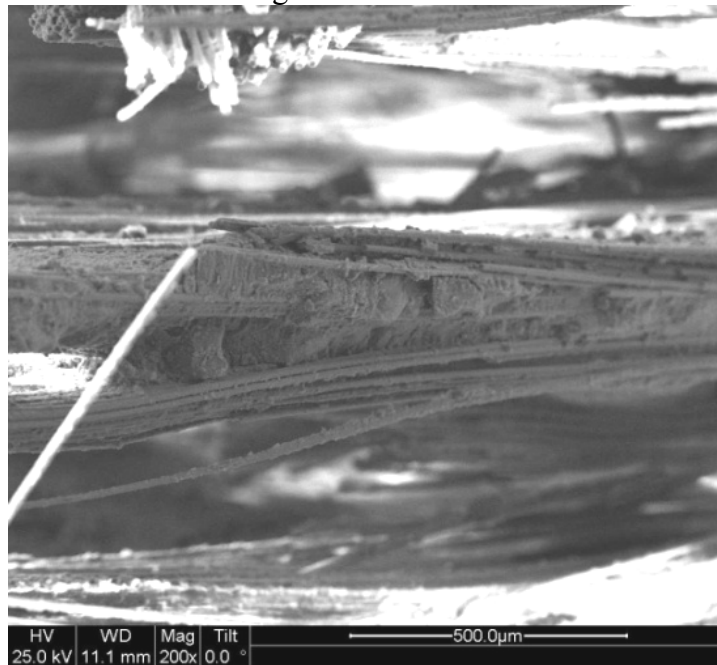


Figure 115. SEM micrograph of the fracture surface of the N720/AM specimen subjected to tensile test to failure following 100 h at 30 MPa at 1200°C in laboratory air.

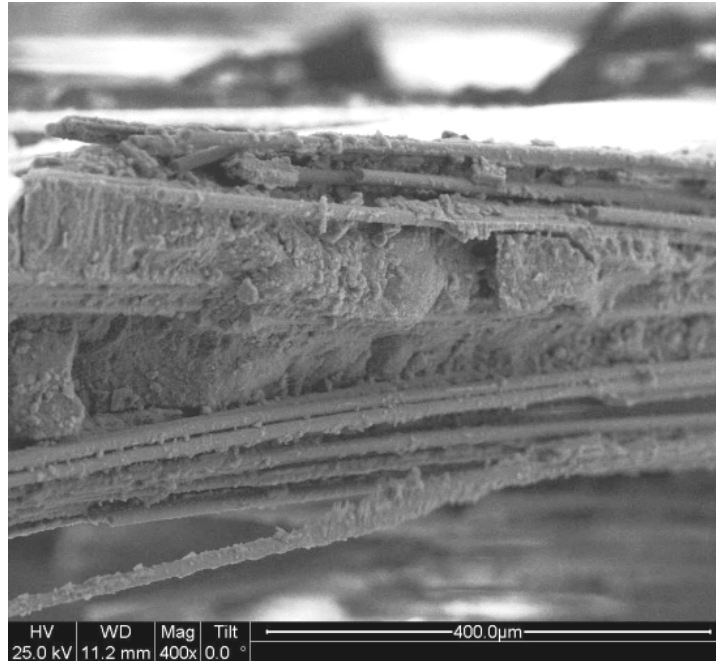


Figure 116. SEM micrograph of the fracture surface of the N720/AM specimen subjected to tensile test to failure following 100 h at 30 MPa at 1200°C in laboratory air.

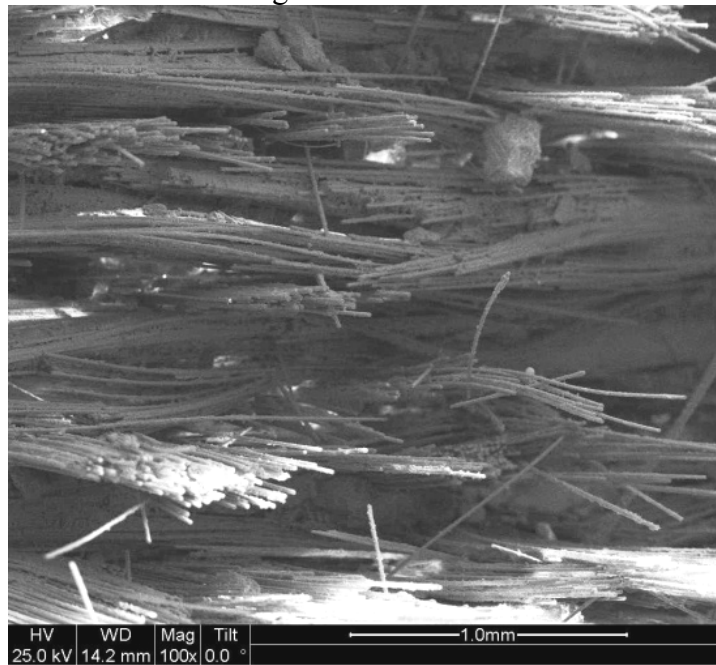


Figure 117. SEM micrograph of the fracture surface of the N720/AM specimen subjected to tensile test to failure following 100 h at 30 MPa at 1200°C in laboratory air.

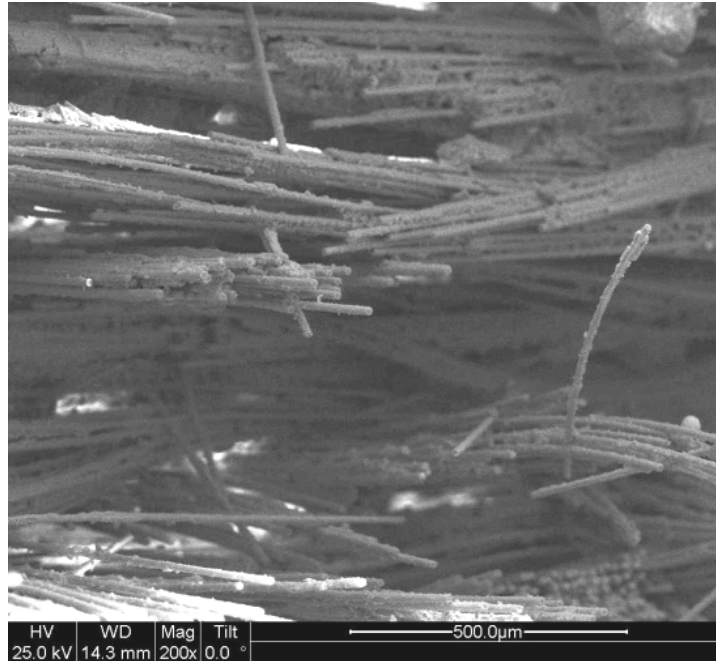


Figure 118. SEM micrograph of the fracture surface of the N720/AM specimen subjected to tensile test to failure following 100 h at 30 MPa at 1200°C in laboratory air.

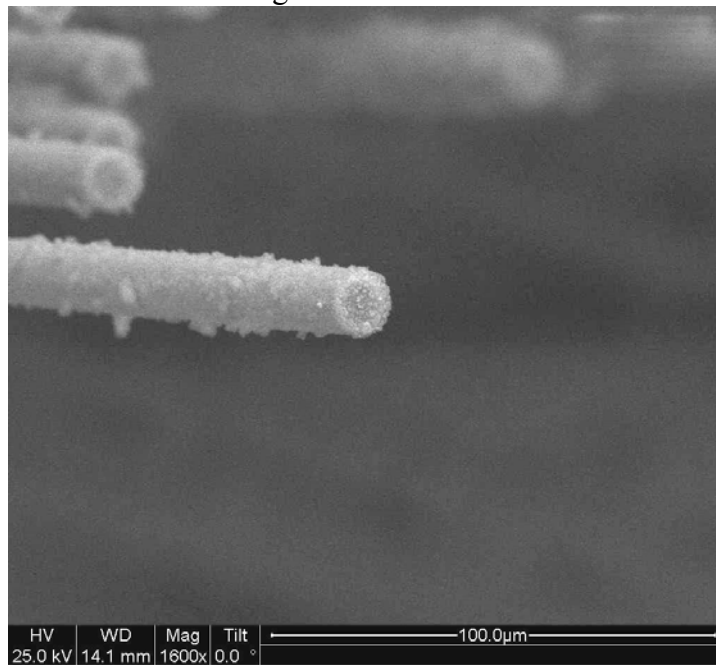


Figure 119. SEM micrograph of the fracture surface of the N720/AM specimen subjected to tensile test to failure following 100 h at 30 MPa at 1200°C in laboratory air.

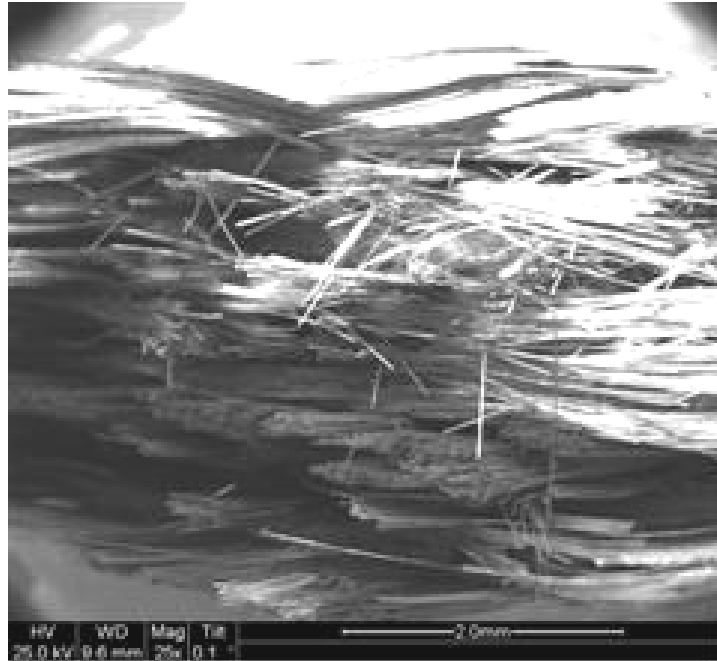


Figure 120. SEM micrograph of the fracture surface of the N720/AM specimen subjected to tensile test to failure following 100 h at 32 MPa at 1200°C in laboratory air.

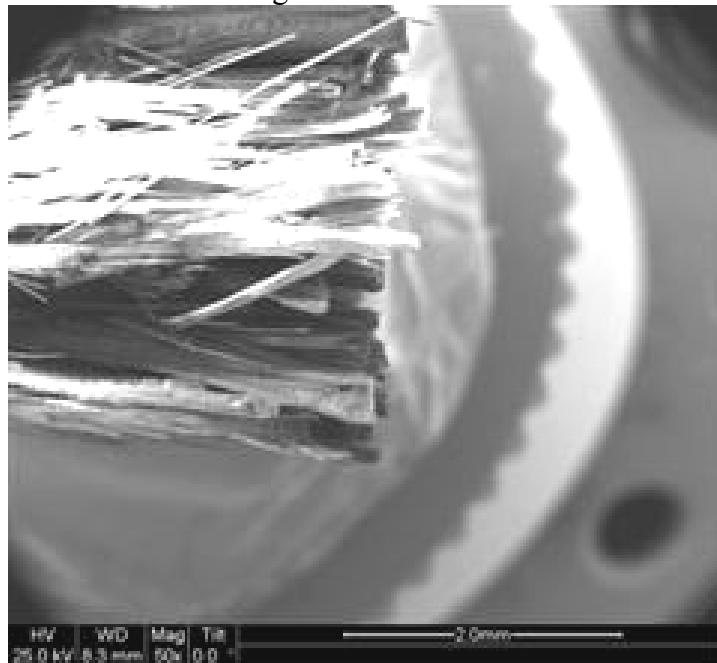


Figure 121. SEM micrograph of the fracture surface of the N720/AM specimen subjected to tensile test to failure following 100 h at 32 MPa at 1200°C in laboratory air.

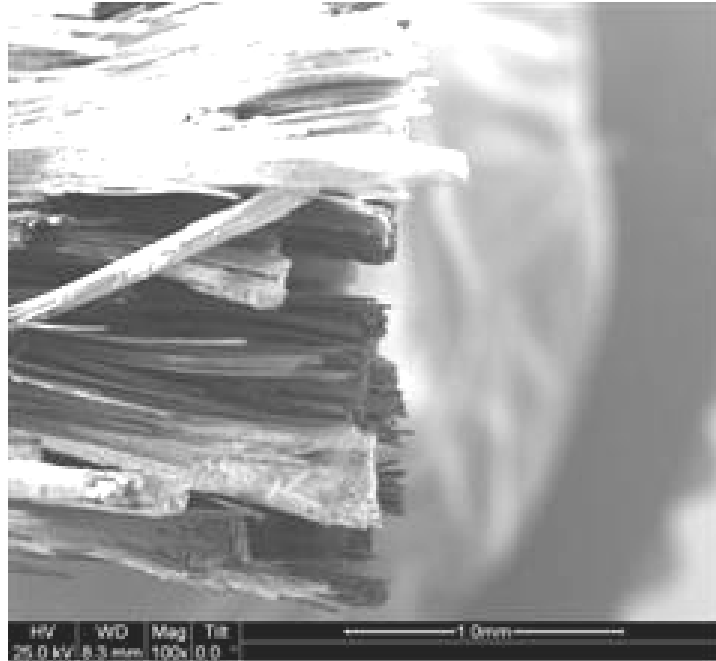


Figure 122. SEM micrograph of the fracture surface of the N720/AM specimen subjected to tensile test to failure following 100 h at 32 MPa at 1200°C in laboratory air.

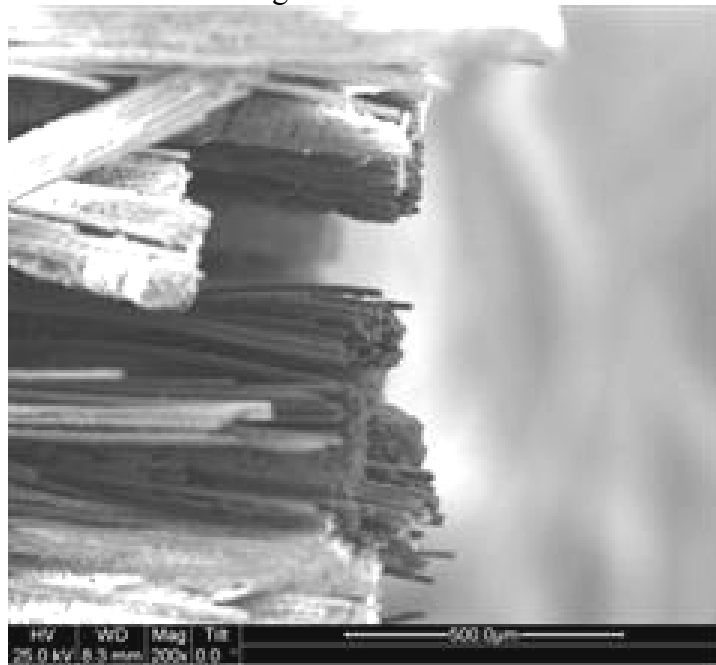


Figure 123. SEM micrograph of the fracture surface of the N720/AM specimen subjected to tensile test to failure following 100 h at 32 MPa at 1200°C in laboratory air.

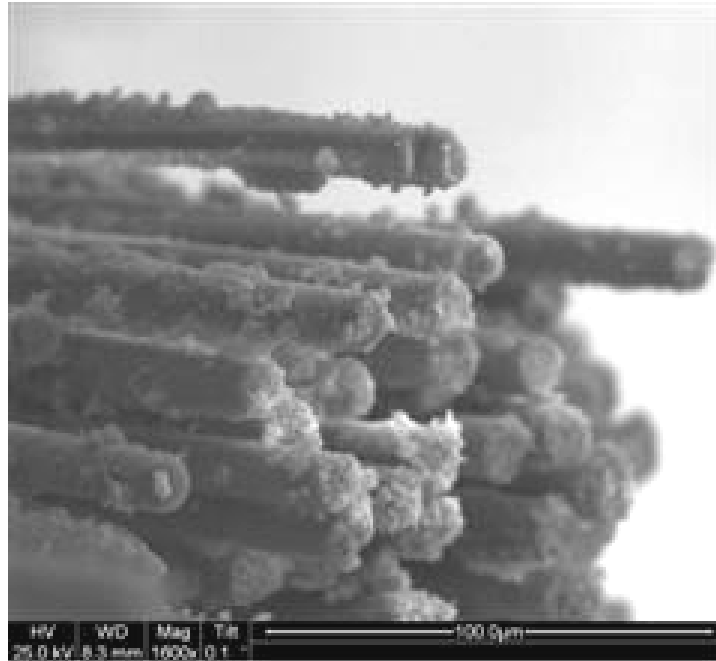


Figure 124. SEM micrograph of the fracture surface of the N720/AM specimen subjected to tensile test to failure following 100 h at 32 MPa at 1200°C in laboratory air.

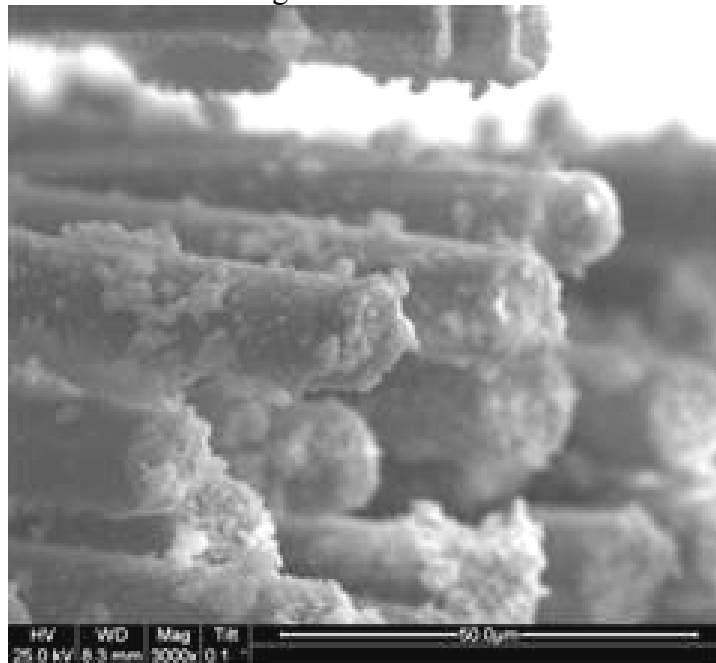


Figure 125. SEM micrograph of the fracture surface of the N720/AM specimen subjected to tensile test to failure following 100 h at 32 MPa at 1200°C in laboratory air.

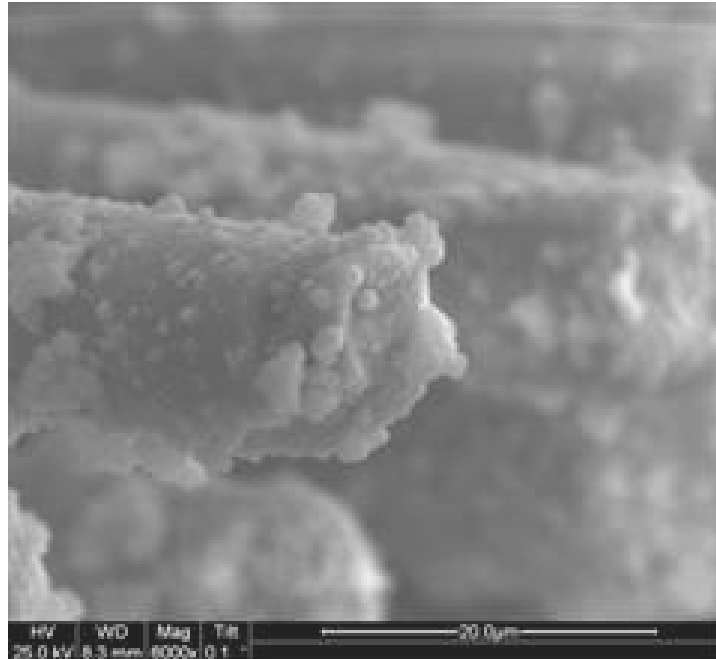


Figure 126. SEM micrograph of the fracture surface of the N720/AM specimen subjected to tensile test to failure following 100 h at 32 MPa at 1200°C in laboratory air.

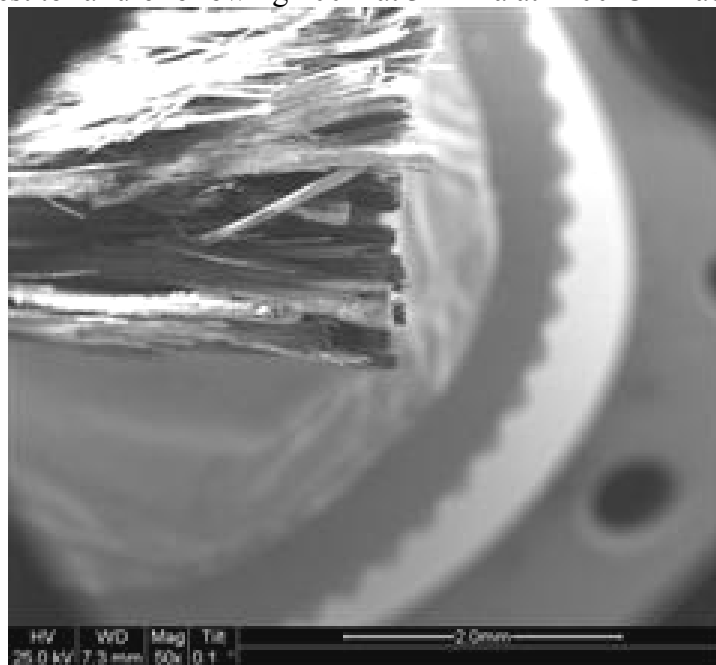


Figure 127. SEM micrograph of the fracture surface of the N720/AM specimen subjected to tensile test to failure following 100 h at 32 MPa at 1200°C in laboratory air.

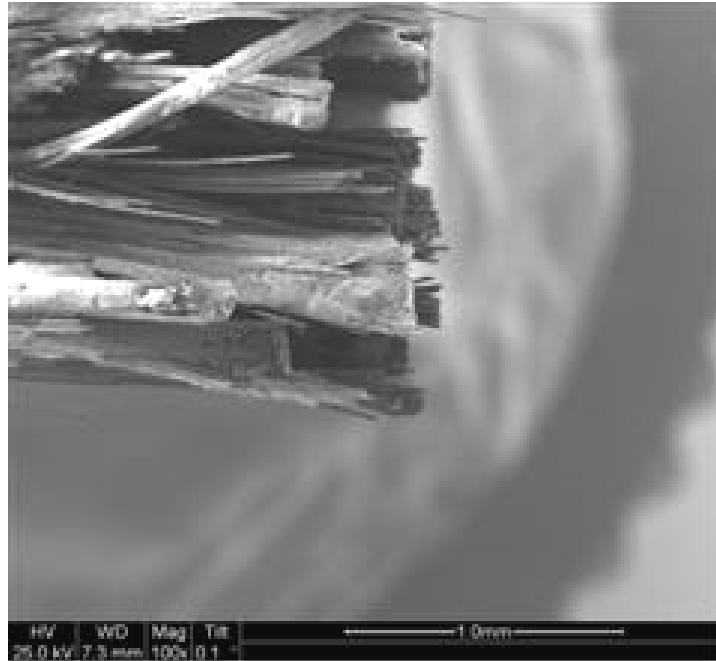


Figure 128. SEM micrograph of the fracture surface of the N720/AM specimen subjected to tensile test to failure following 100 h at 32 MPa at 1200°C in laboratory air.

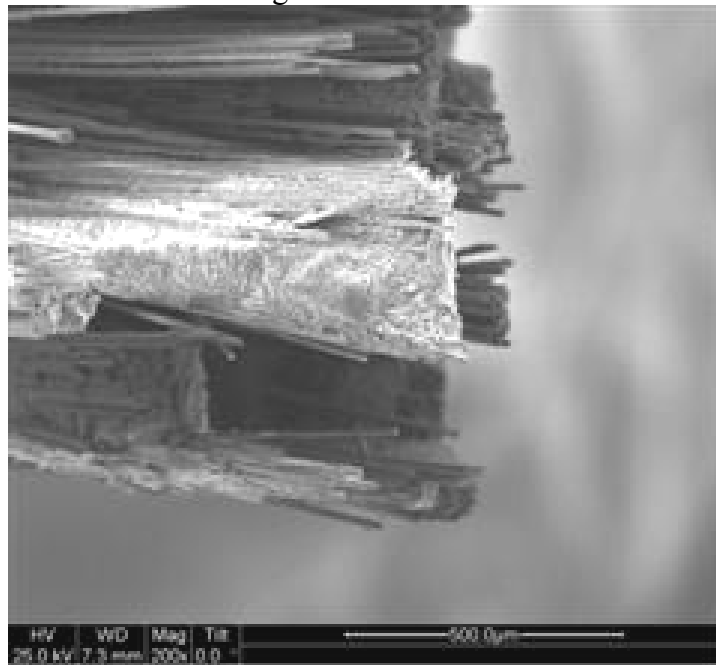


Figure 129. SEM micrograph of the fracture surface of the N720/AM specimen subjected to tensile test to failure following 100 h at 32 MPa at 1200°C in laboratory air.

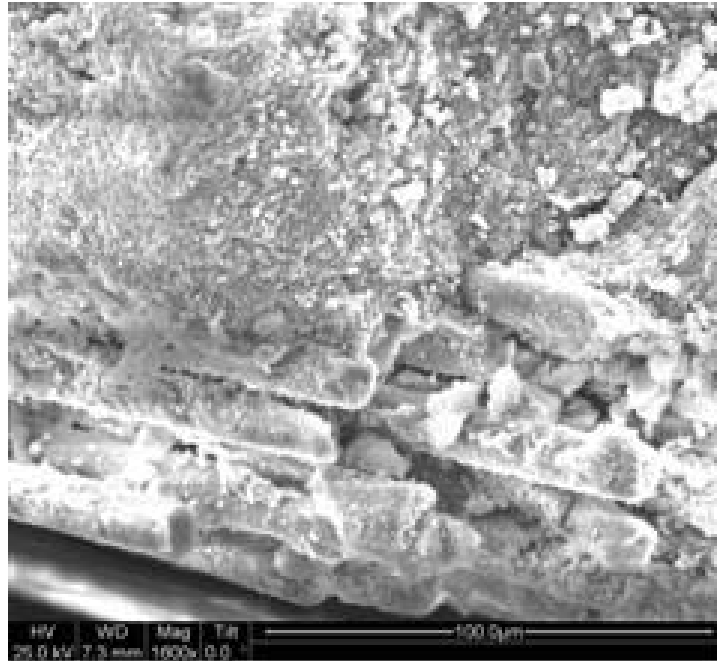


Figure 130. SEM micrograph of the fracture surface of the N720/AM specimen subjected to tensile test to failure following 100 h at 32 MPa at 1200°C in laboratory air.

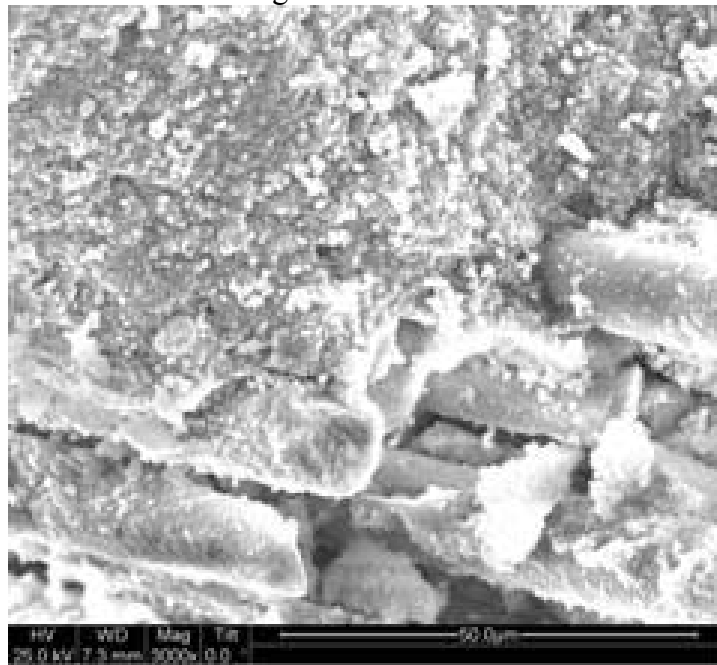


Figure 131. SEM micrograph of the fracture surface of the N720/AM specimen subjected to tensile test to failure following 100 h at 32 MPa at 1200°C in laboratory air.

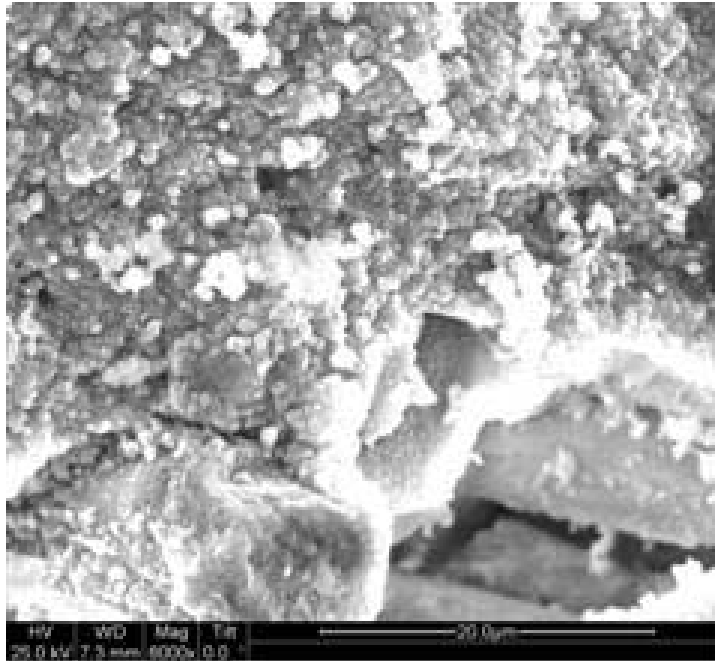


Figure 132. SEM micrograph of the fracture surface of the N720/AM specimen subjected to tensile test to failure following 100 h at 32 MPa at 1200°C in laboratory air.

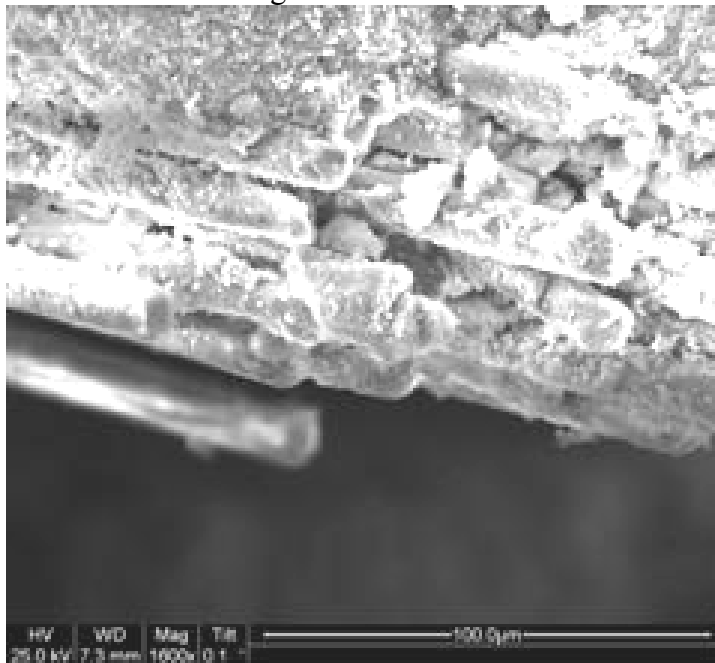


Figure 133. SEM micrograph of the fracture surface of the N720/AM specimen subjected to tensile test to failure following 100 h at 32 MPa at 1200°C in laboratory air.

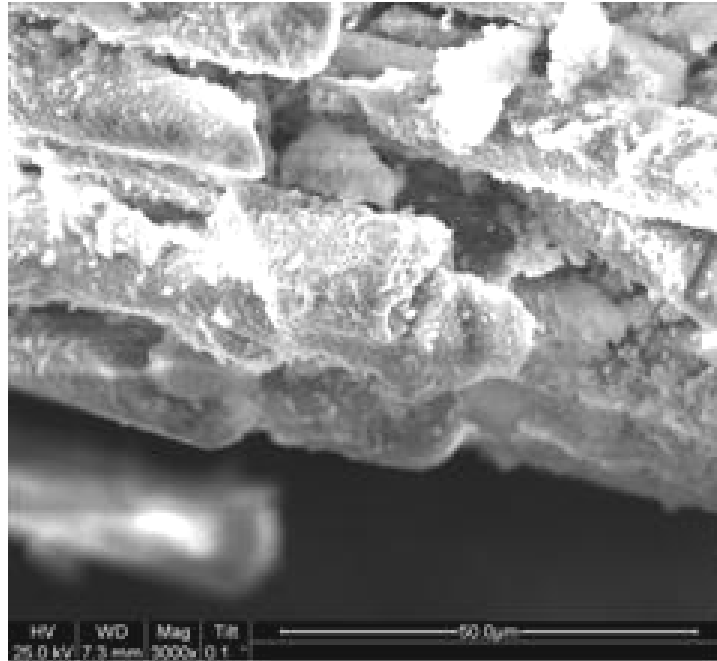


Figure 134. SEM micrograph of the fracture surface of the N720/AM specimen subjected to tensile test to failure following 100 h at 32 MPa at 1200°C in laboratory air.

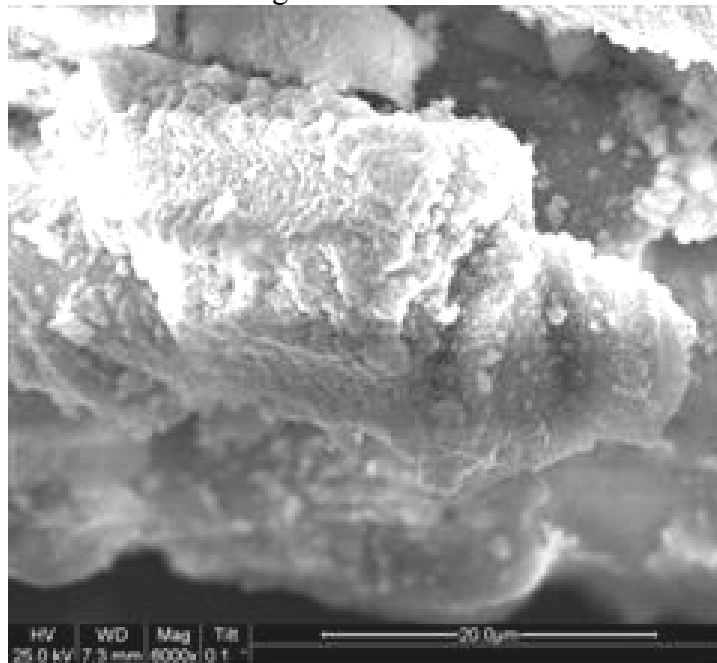


Figure 135. SEM micrograph of the fracture surface of the N720/AM specimen subjected to tensile test to failure following 100 h at 32 MPa at 1200°C in laboratory air.

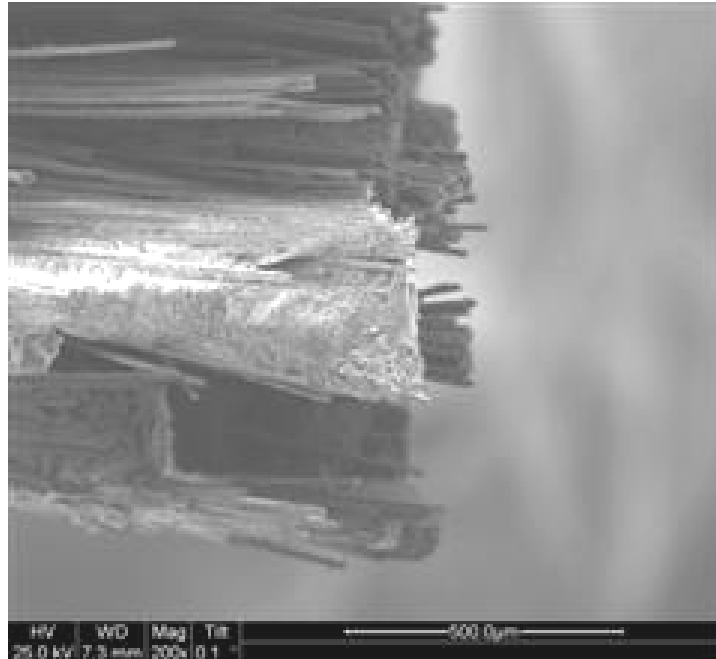


Figure 136. SEM micrograph of the fracture surface of the N720/AM specimen subjected to tensile test to failure following 100 h at 32 MPa at 1200°C in laboratory air.

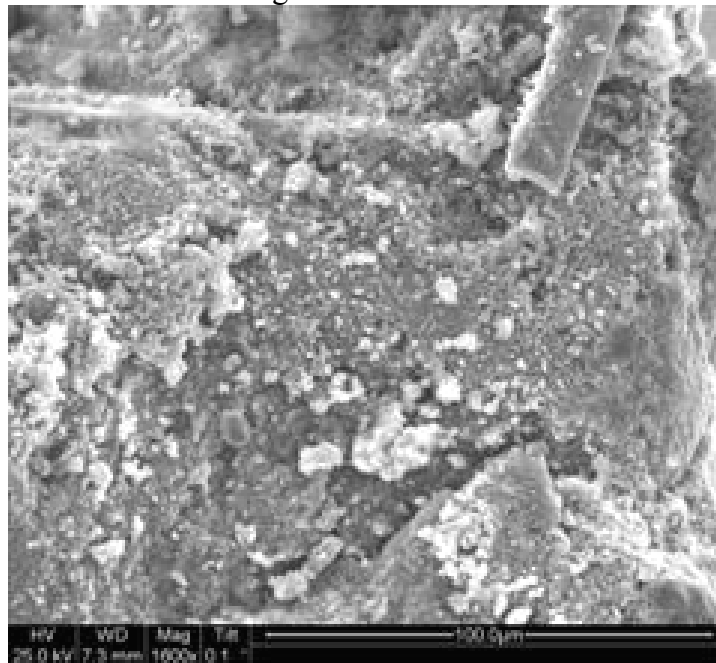


Figure 137. SEM micrograph of the fracture surface of the N720/AM specimen subjected to tensile test to failure following 100 h at 32 MPa at 1200°C in laboratory air.

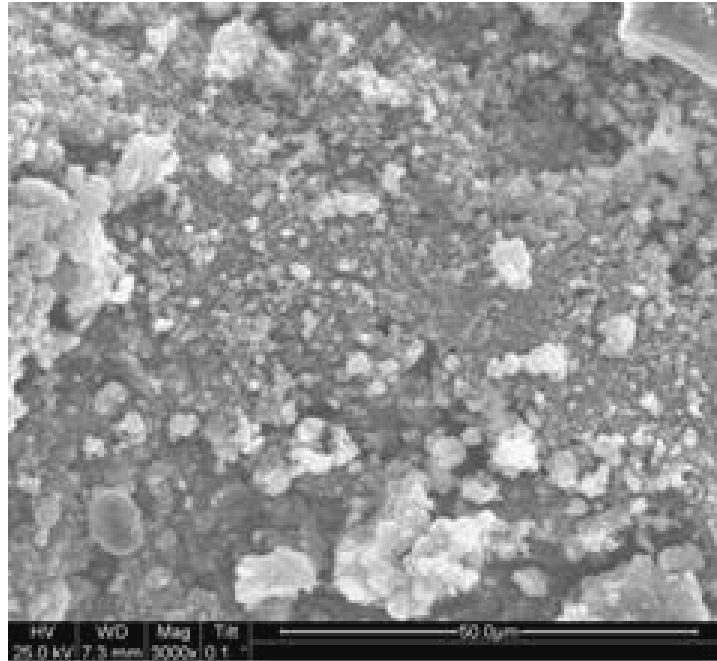


Figure 138. SEM micrograph of the fracture surface of the N720/AM specimen subjected to tensile test to failure following 100 h at 32 MPa at 1200°C in laboratory air.

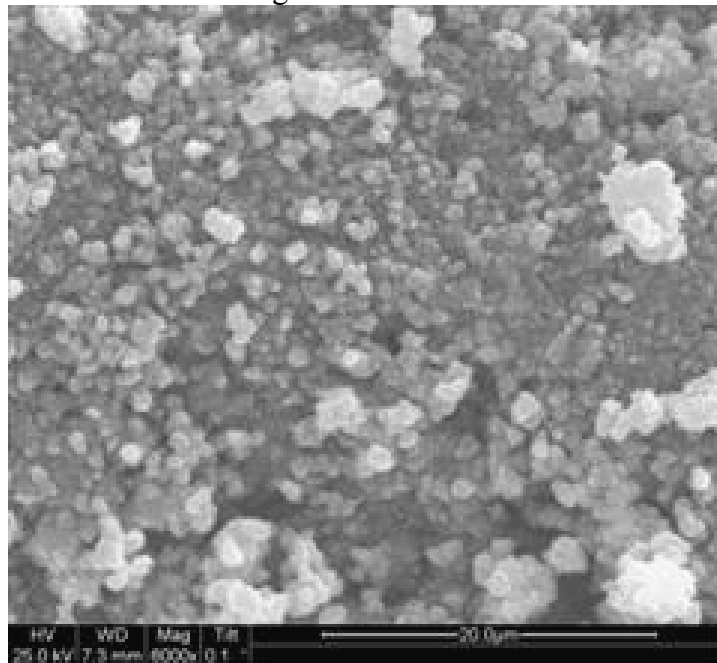


Figure 139. SEM micrograph of the fracture surface of the N720/AM specimen subjected to tensile test to failure following 100 h at 32 MPa at 1200°C in laboratory air.

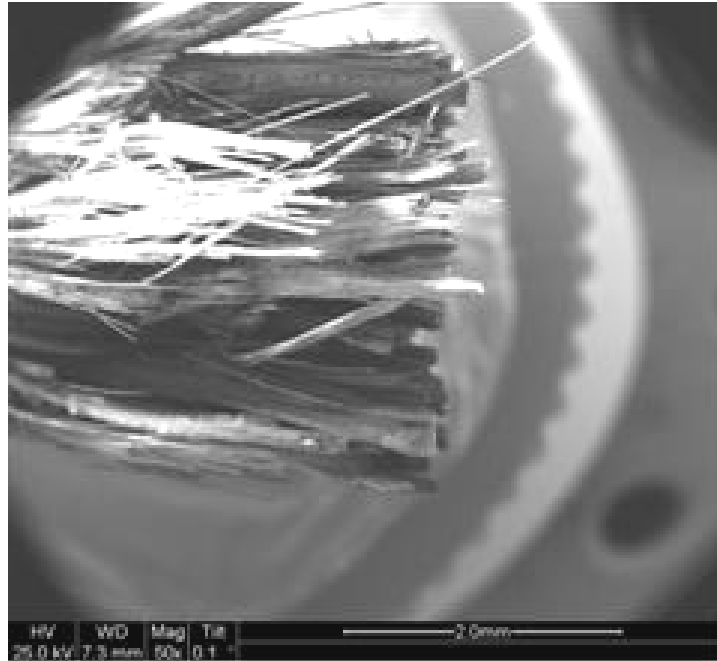


Figure 140. SEM micrograph of the fracture surface of the N720/AM specimen subjected to tensile test to failure following 100 h at 32 MPa at 1200°C in laboratory air.

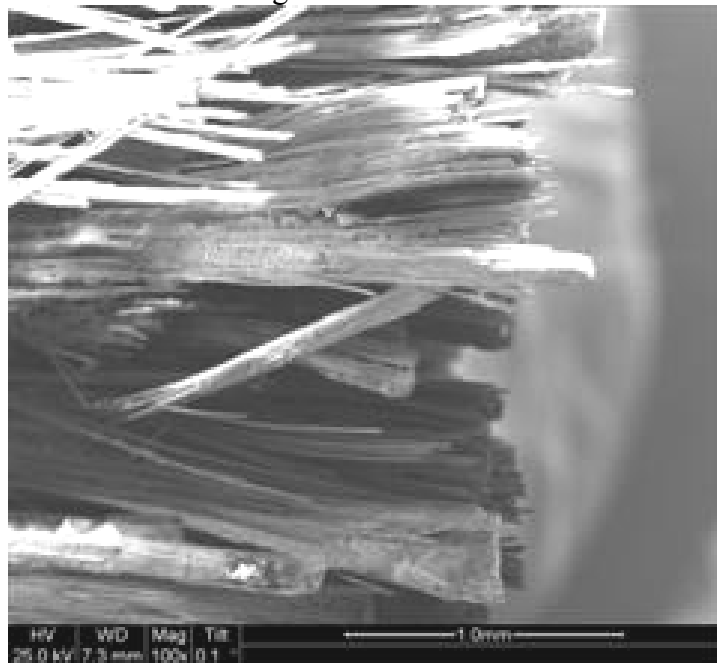


Figure 141. SEM micrograph of the fracture surface of the N720/AM specimen subjected to tensile test to failure following 100 h at 32 MPa at 1200°C in laboratory air.

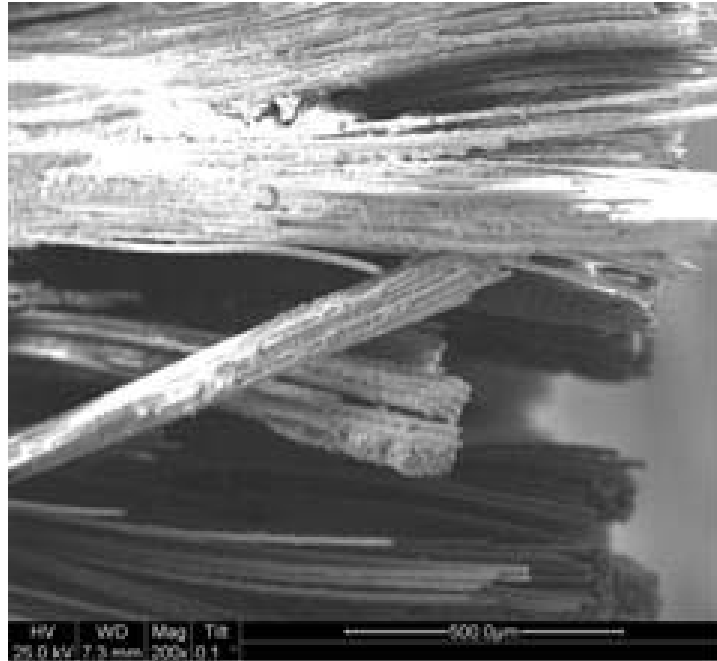


Figure 142. SEM micrograph of the fracture surface of the N720/AM specimen subjected to tensile test to failure following 100 h at 32 MPa at 1200°C in laboratory air.

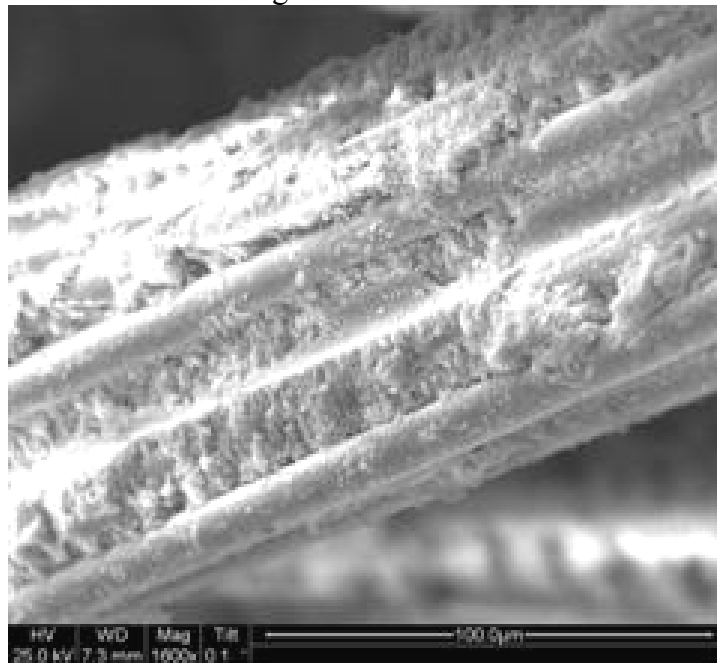


Figure 143. SEM micrograph of the fracture surface of the N720/AM specimen subjected to tensile test to failure following 100 h at 32 MPa at 1200°C in laboratory air.

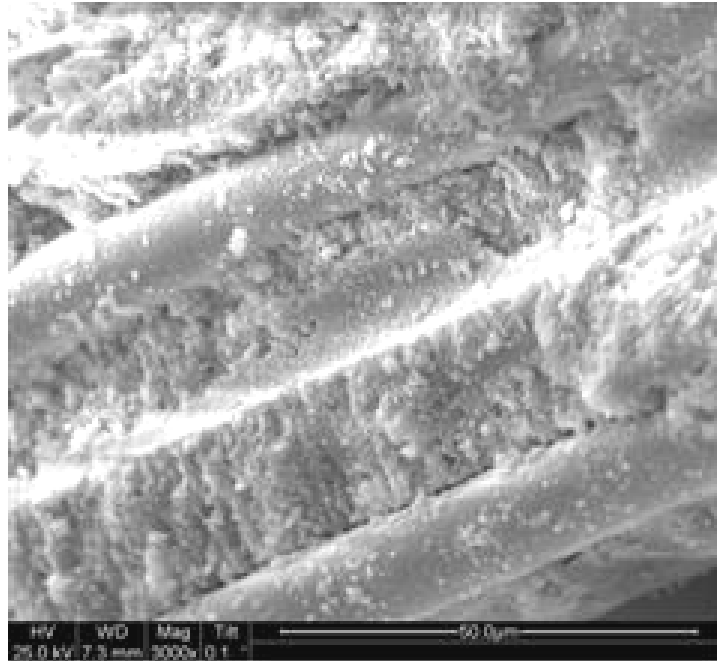


Figure 144. SEM micrograph of the fracture surface of the N720/AM specimen subjected to tensile test to failure following 100 h at 32 MPa at 1200°C in laboratory air.

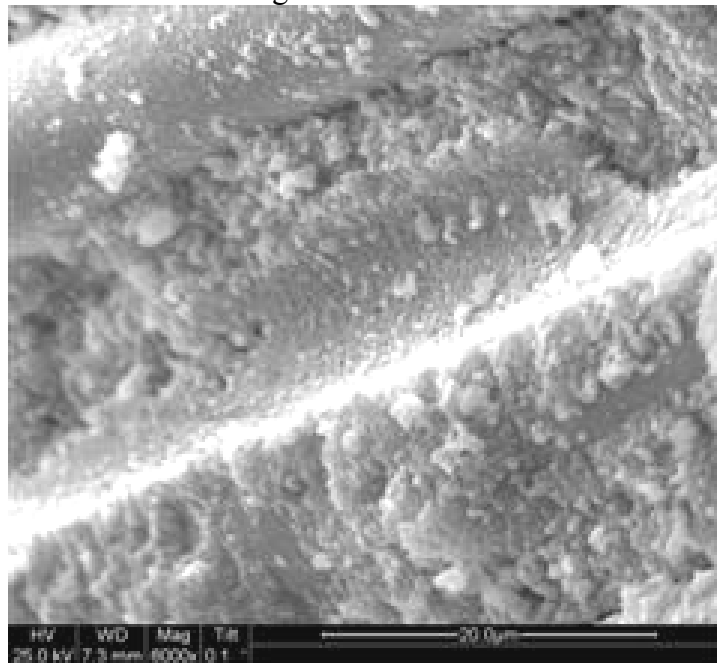


Figure 145. SEM micrograph of the fracture surface of the N720/AM specimen subjected to tensile test to failure following 100 h at 32 MPa at 1200°C in laboratory air.

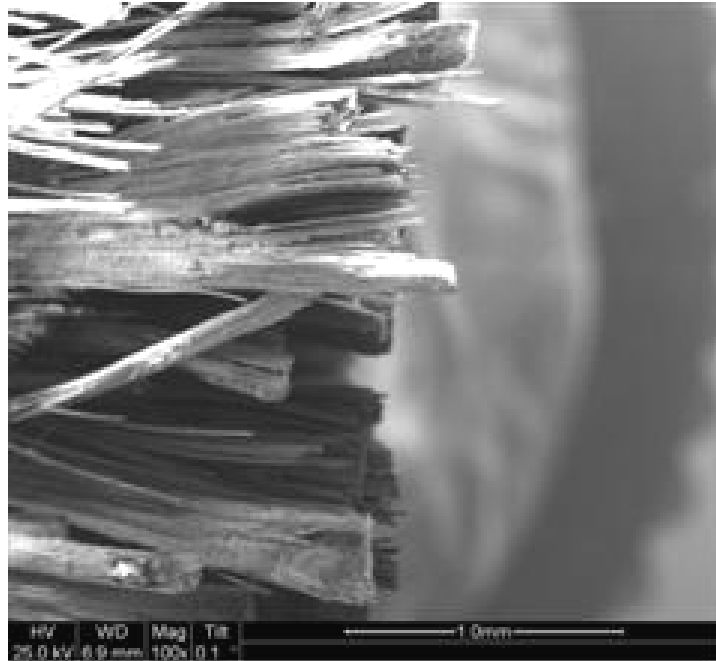


Figure 146. SEM micrograph of the fracture surface of the N720/AM specimen subjected to tensile test to failure following 100 h at 32 MPa at 1200°C in laboratory air.

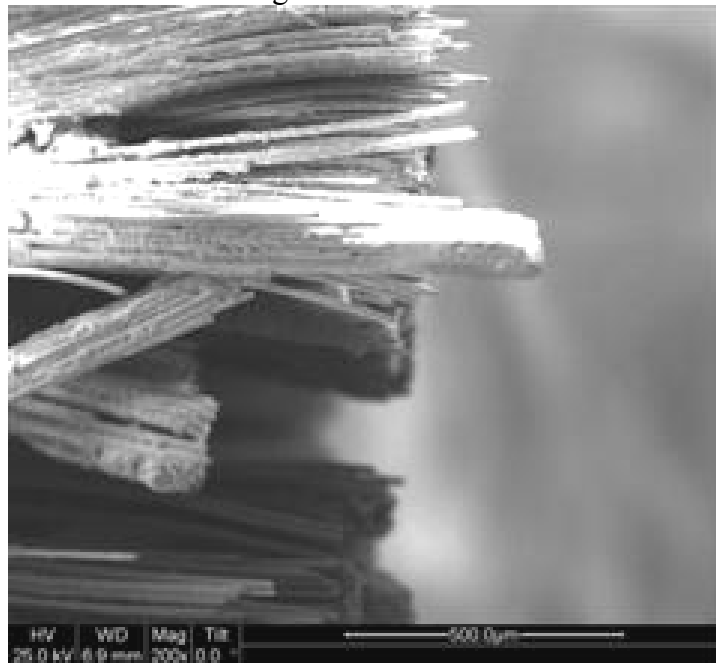


Figure 147. SEM micrograph of the fracture surface of the N720/AM specimen subjected to tensile test to failure following 100 h at 32 MPa at 1200°C in laboratory air.

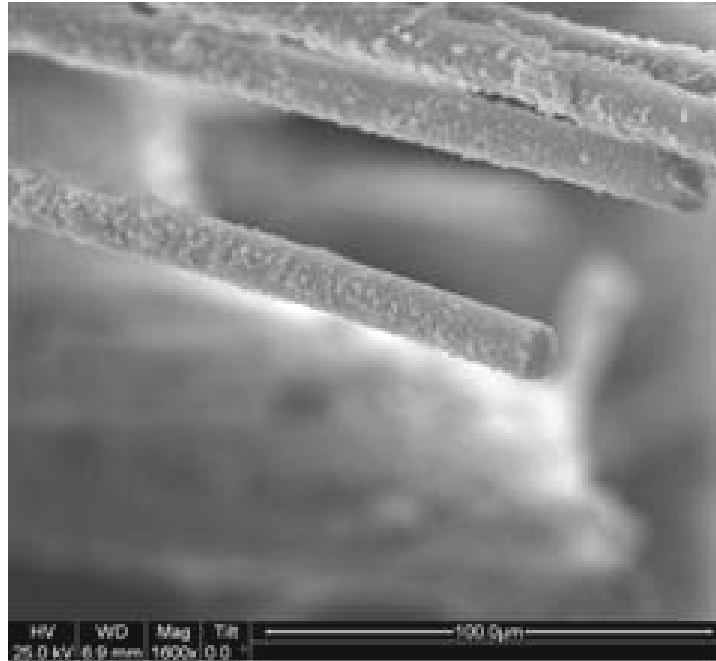


Figure 148. SEM micrograph of the fracture surface of the N720/AM specimen subjected to tensile test to failure following 100 h at 32 MPa at 1200°C in laboratory air.

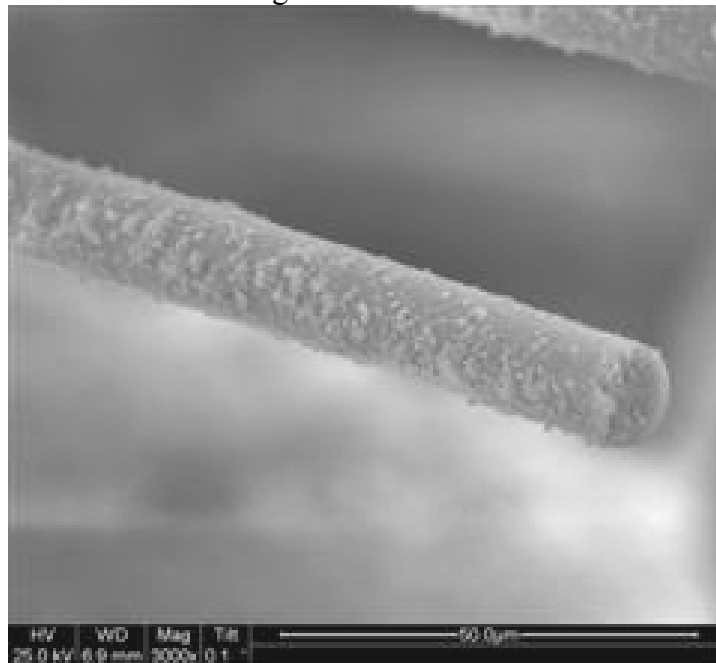


Figure 149. SEM micrograph of the fracture surface of the N720/AM specimen subjected to tensile test to failure following 100 h at 32 MPa at 1200°C in laboratory air.

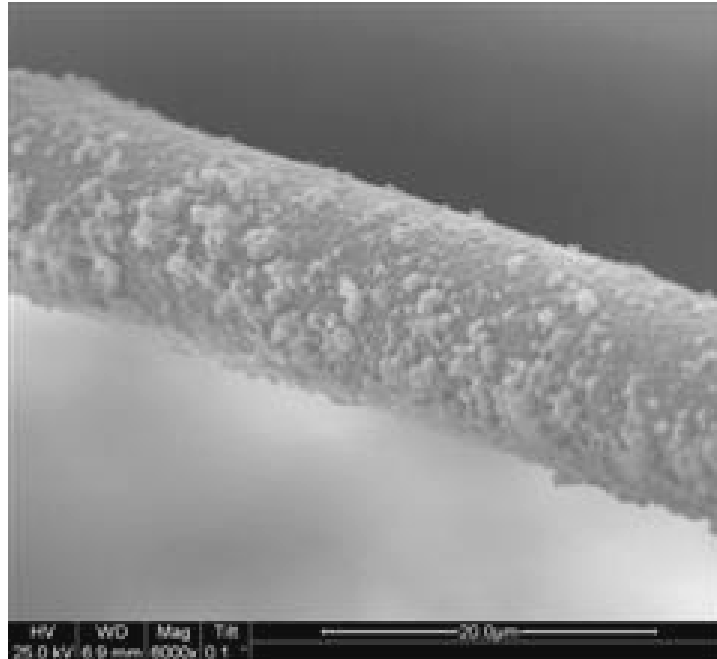


Figure 150. SEM micrograph of the fracture surface of the N720/AM specimen subjected to tensile test to failure following 100 h at 32 MPa at 1200°C in laboratory air.

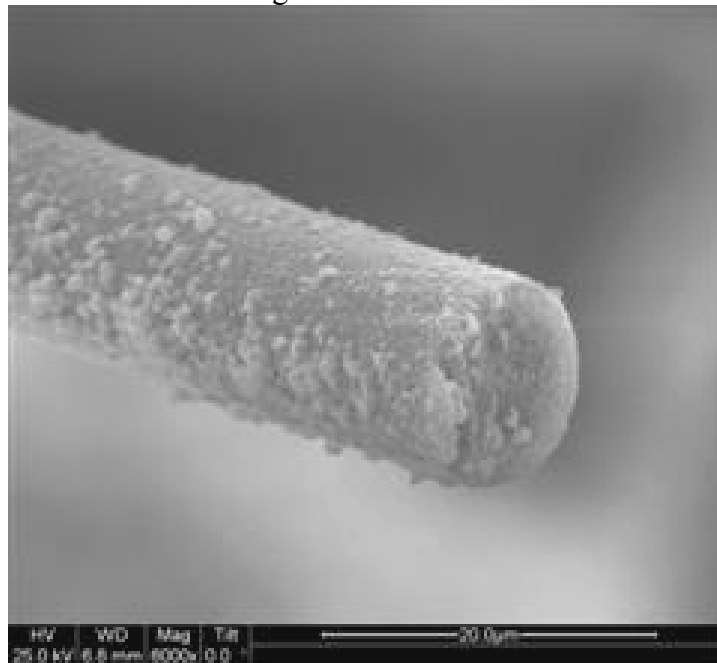


Figure 151. SEM micrograph of the fracture surface of the N720/AM specimen subjected to tensile test to failure following 100 h at 32 MPa at 1200°C in laboratory air.

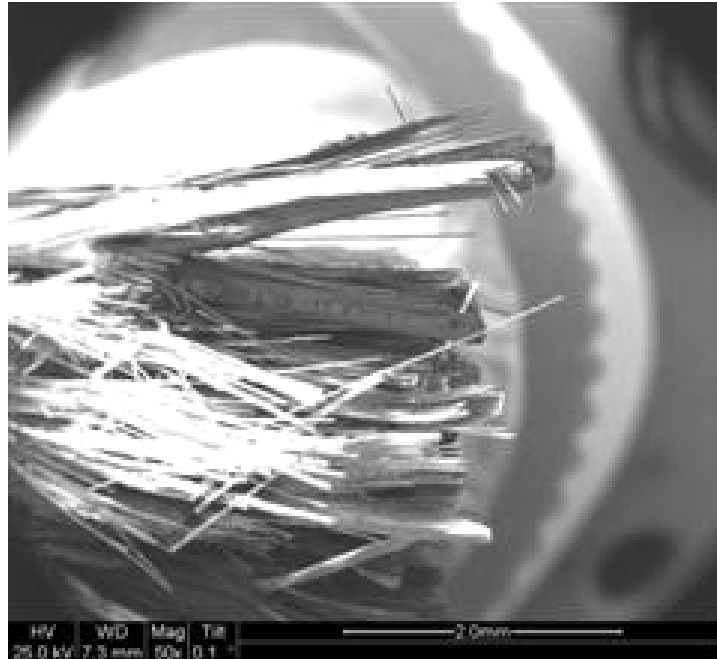


Figure 152. SEM micrograph of the fracture surface of the N720/AM specimen subjected to tensile test to failure following 100 h at 32 MPa at 1200°C in laboratory air.

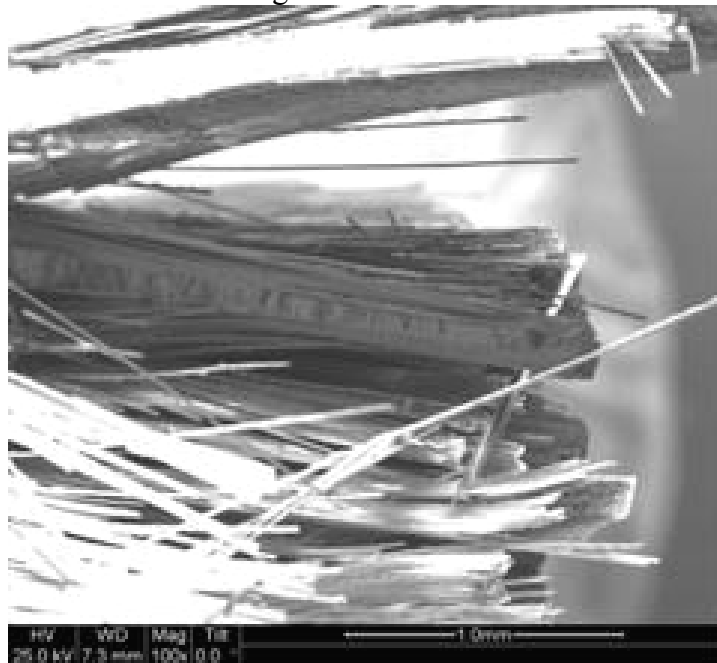


Figure 153. SEM micrograph of the fracture surface of the N720/AM specimen subjected to tensile test to failure following 100 h at 32 MPa at 1200°C in laboratory air.

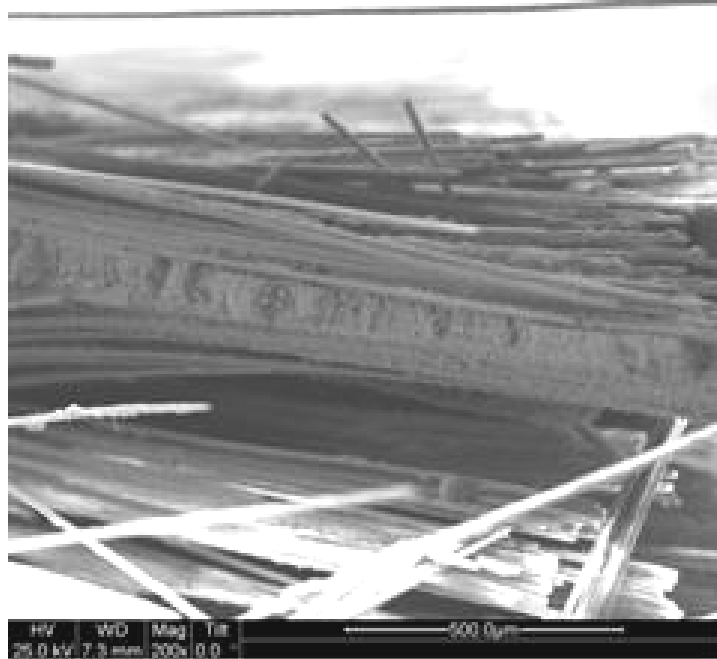


Figure 154. SEM micrograph of the fracture surface of the N720/AM specimen subjected to tensile test to failure following 100 h at 32 MPa at 1200°C in laboratory air.

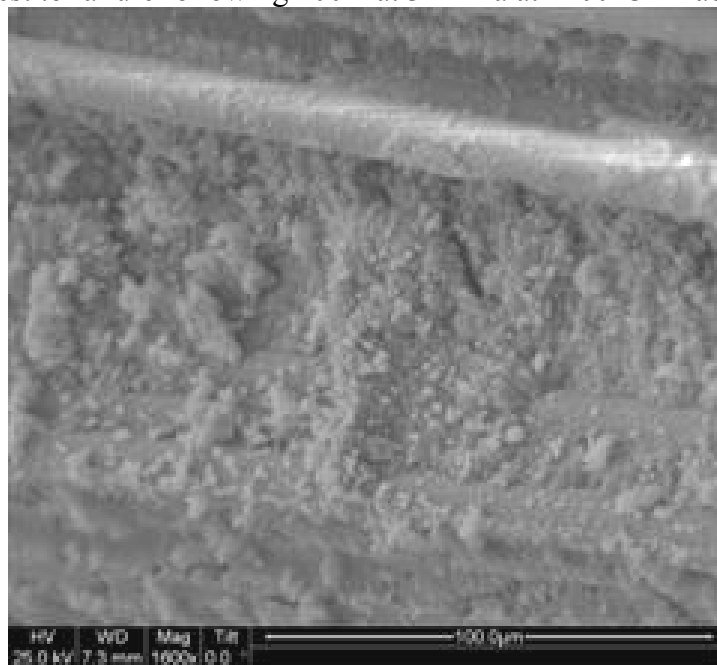


Figure 155. SEM micrograph of the fracture surface of the N720/AM specimen subjected to tensile test to failure following 100 h at 32 MPa at 1200°C in laboratory air.

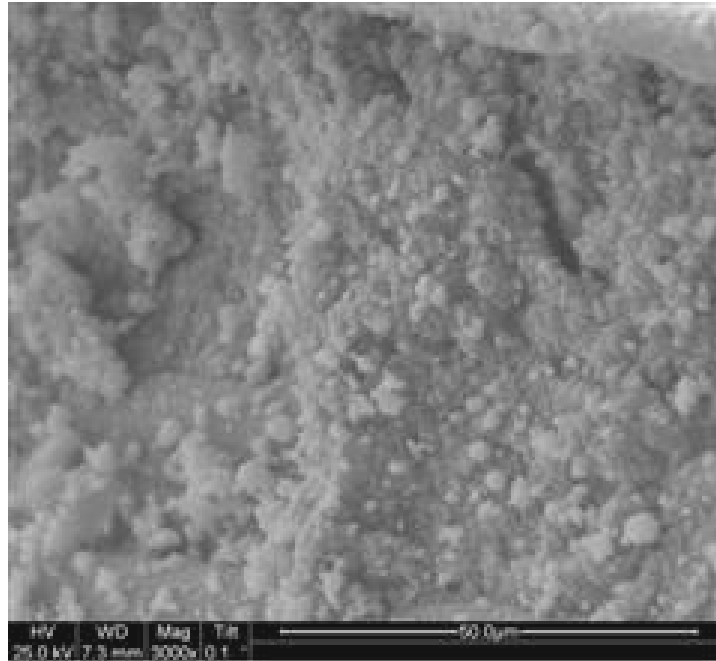


Figure 156. SEM micrograph of the fracture surface of the N720/AM specimen subjected to tensile test to failure following 100 h at 32 MPa at 1200°C in laboratory air.

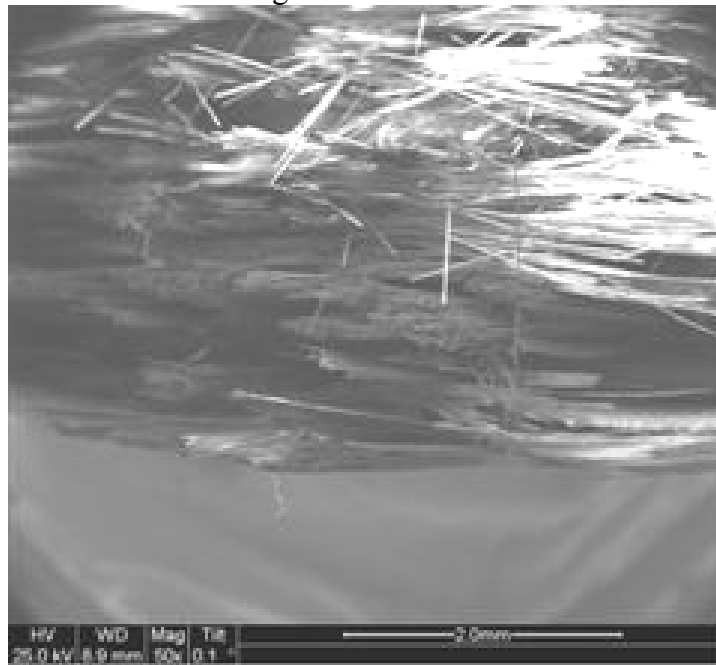


Figure 157. SEM micrograph of the fracture surface of the N720/AM specimen subjected to tensile test to failure following 100 h at 32 MPa at 1200°C in laboratory air.

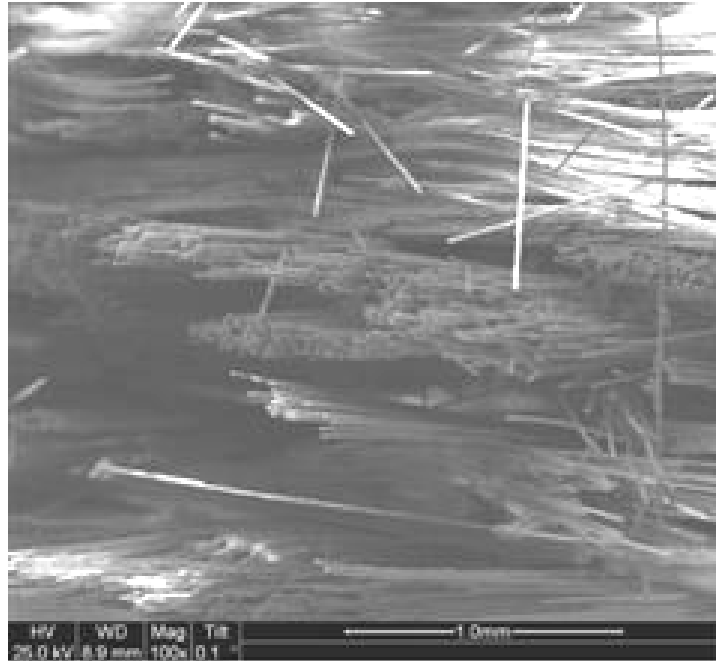


Figure 158. SEM micrograph of the fracture surface of the N720/AM specimen subjected to tensile test to failure following 100 h at 32 MPa at 1200°C in laboratory air.

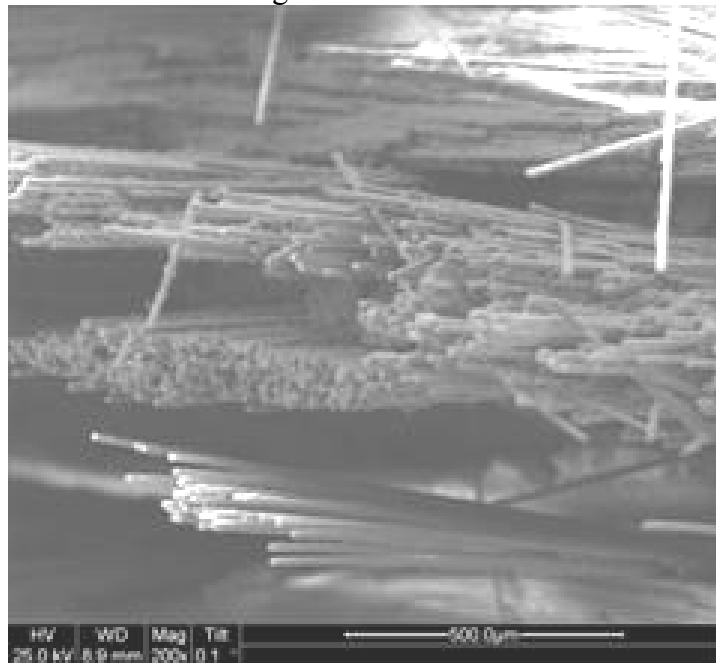


Figure 159. SEM micrograph of the fracture surface of the N720/AM specimen subjected to tensile test to failure following 100 h at 32 MPa at 1200°C in laboratory air.

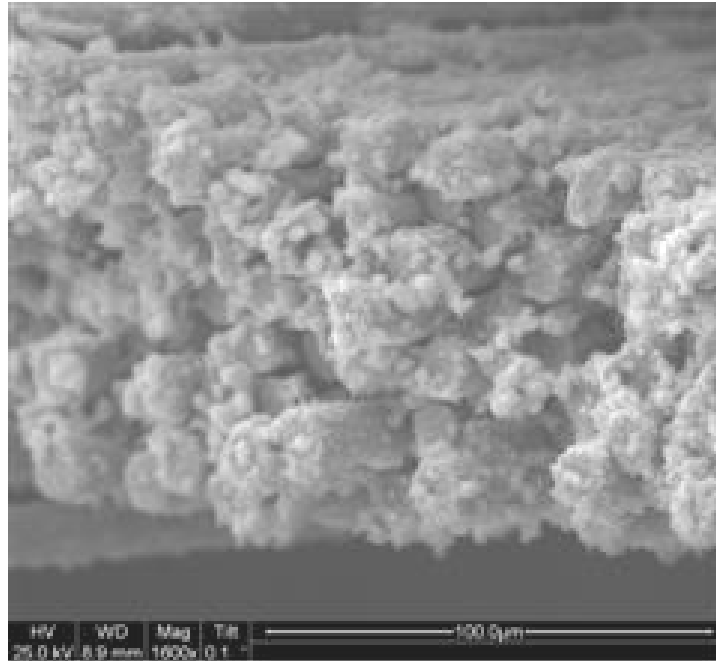


Figure 160. SEM micrograph of the fracture surface of the N720/AM specimen subjected to tensile test to failure following 100 h at 32 MPa at 1200°C in laboratory air.

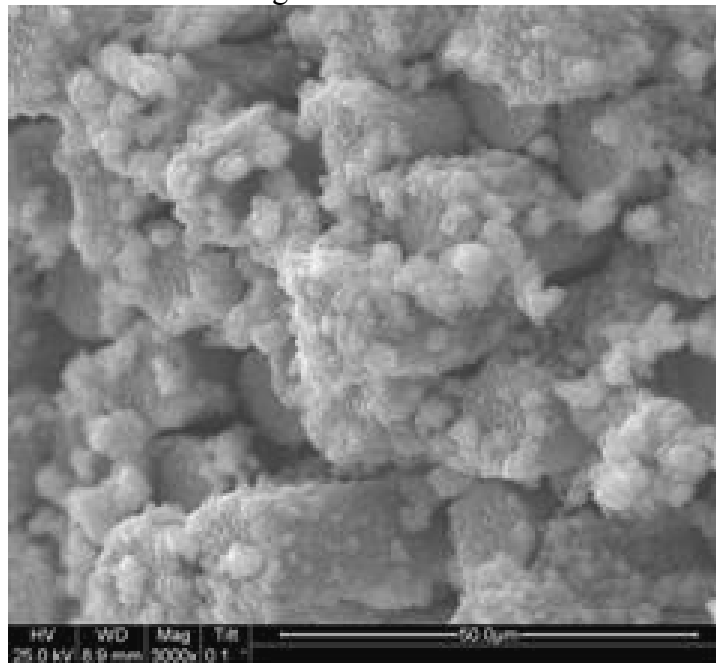


Figure 161. SEM micrograph of the fracture surface of the N720/AM specimen subjected to tensile test to failure following 100 h at 32 MPa at 1200°C in laboratory air.

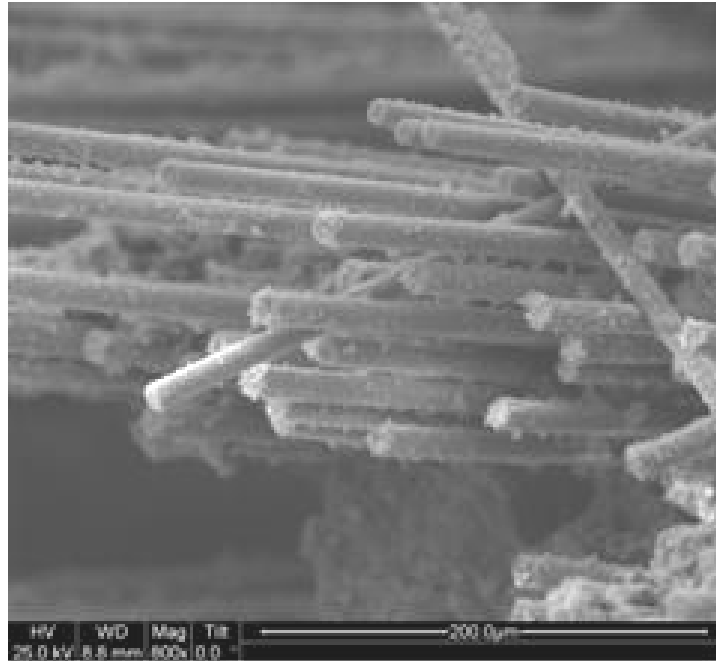


Figure 162. SEM micrograph of the fracture surface of the N720/AM specimen subjected to tensile test to failure following 100 h at 32 MPa at 1200°C in laboratory air.

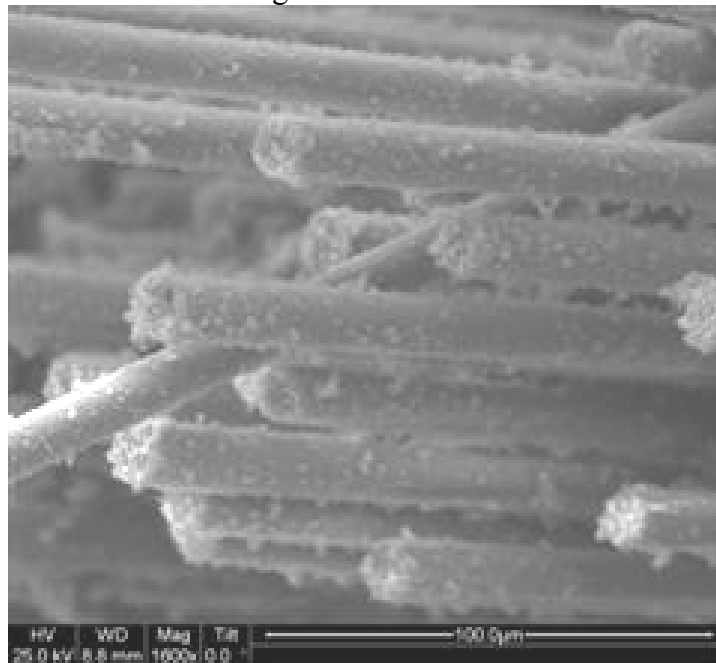


Figure 163. SEM micrograph of the fracture surface of the N720/AM specimen subjected to tensile test to failure following 100 h at 32 MPa at 1200°C in laboratory air.

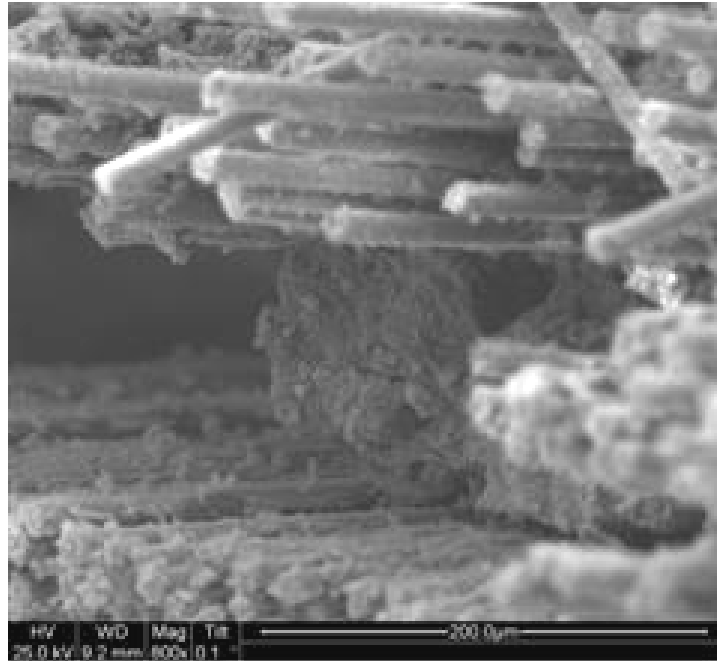


Figure 164. SEM micrograph of the fracture surface of the N720/AM specimen subjected to tensile test to failure following 100 h at 32 MPa at 1200°C in laboratory air.

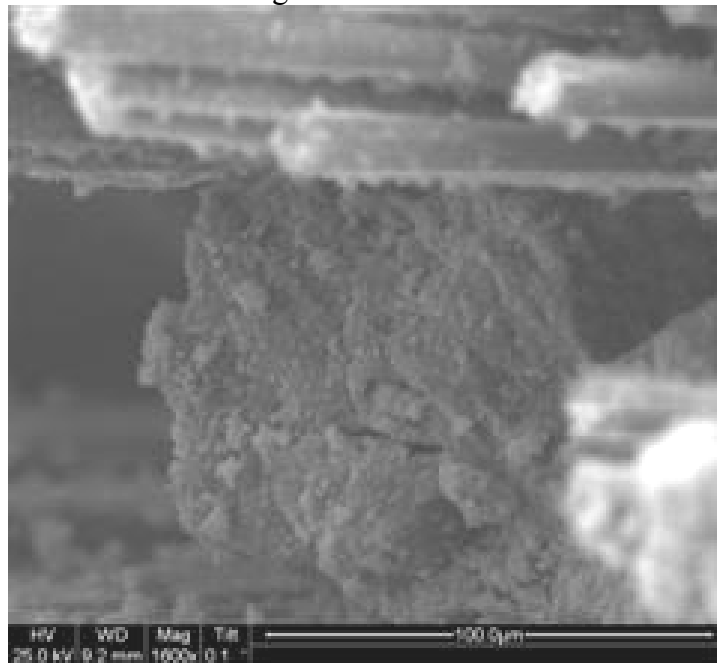


Figure 165. SEM micrograph of the fracture surface of the N720/AM specimen subjected to tensile test to failure following 100 h at 32 MPa at 1200°C in laboratory air.

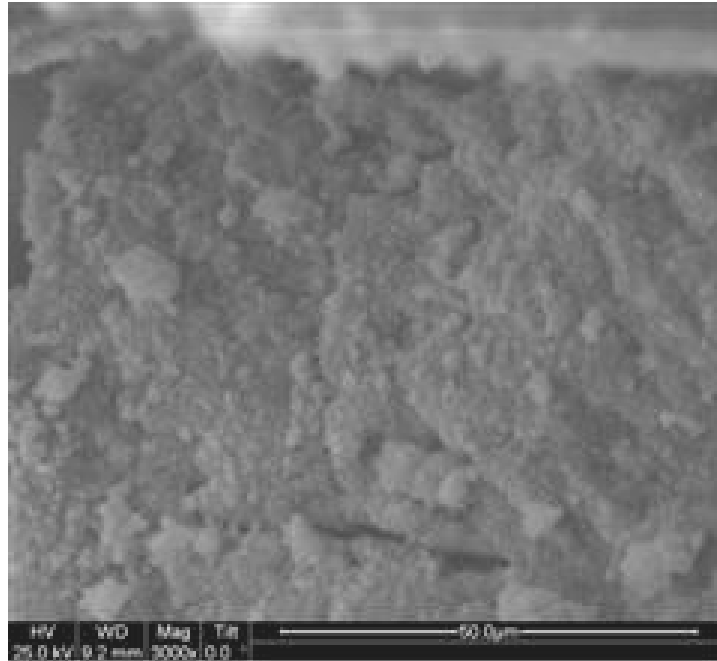


Figure 166. SEM micrograph of the fracture surface of the N720/AM specimen subjected to tensile test to failure following 100 h at 32 MPa at 1200°C in laboratory air.

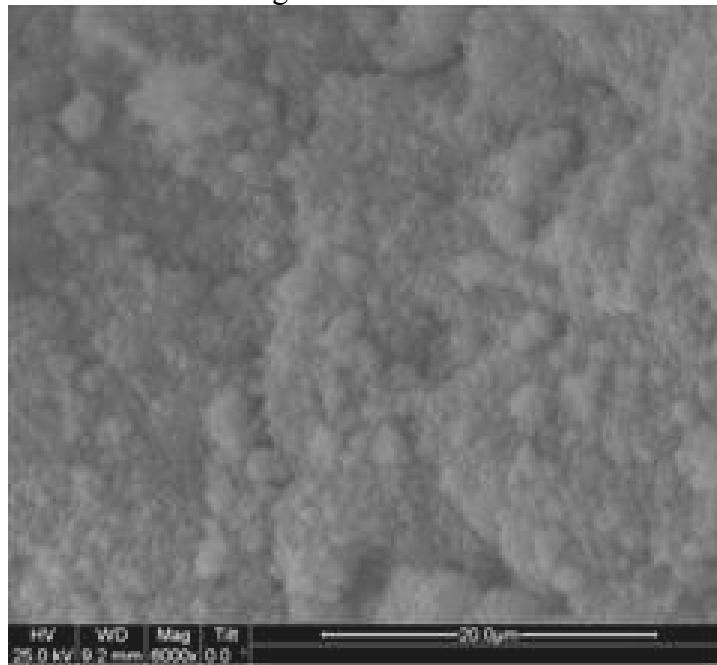


Figure 167. SEM micrograph of the fracture surface of the N720/AM specimen subjected to tensile test to failure following 100 h at 32 MPa at 1200°C in laboratory air.

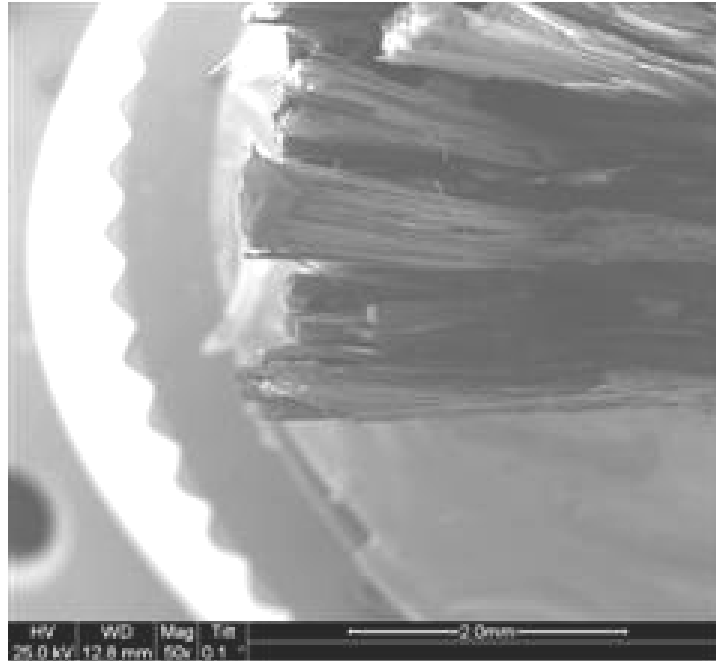


Figure 168. SEM micrograph of the fracture surface of the N720/AM specimen subjected to tensile test to failure following 100 h at 32 MPa at 1200°C in laboratory air.

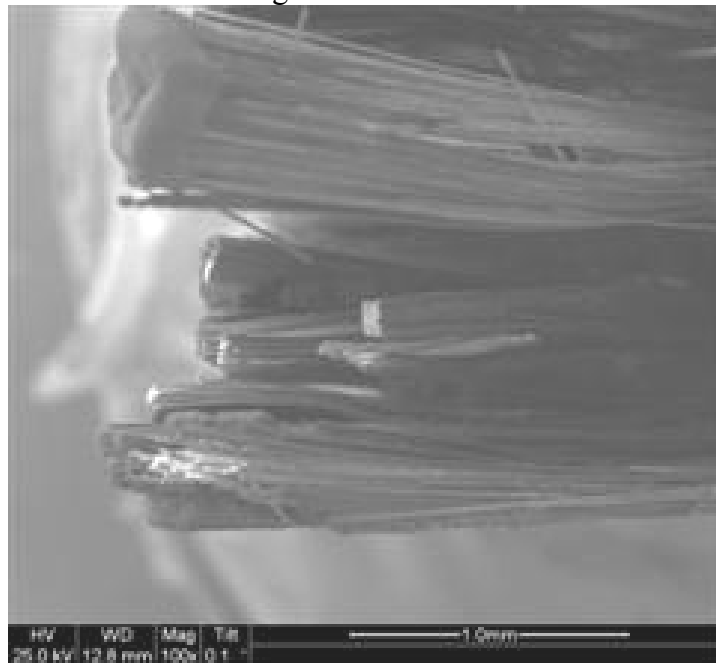


Figure 169. SEM micrograph of the fracture surface of the N720/AM specimen subjected to tensile test to failure following 100 h at 32 MPa at 1200°C in laboratory air.

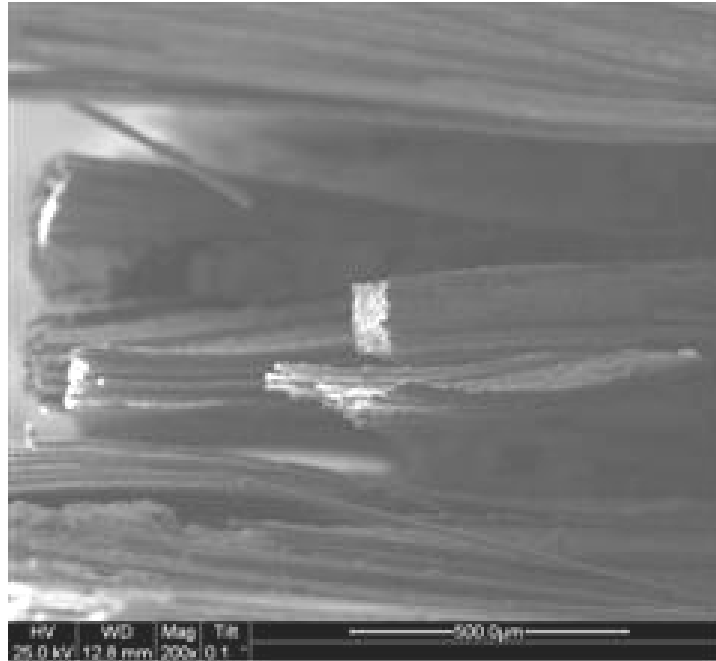


Figure 170. SEM micrograph of the fracture surface of the N720/AM specimen subjected to tensile test to failure following 100 h at 32 MPa at 1200°C in laboratory air.

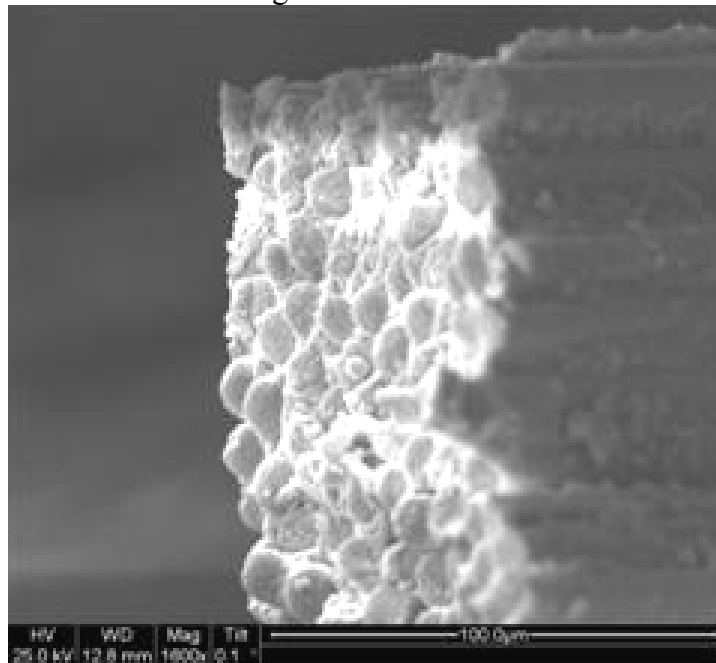


Figure 171. SEM micrograph of the fracture surface of the N720/AM specimen subjected to tensile test to failure following 100 h at 32 MPa at 1200°C in laboratory air.

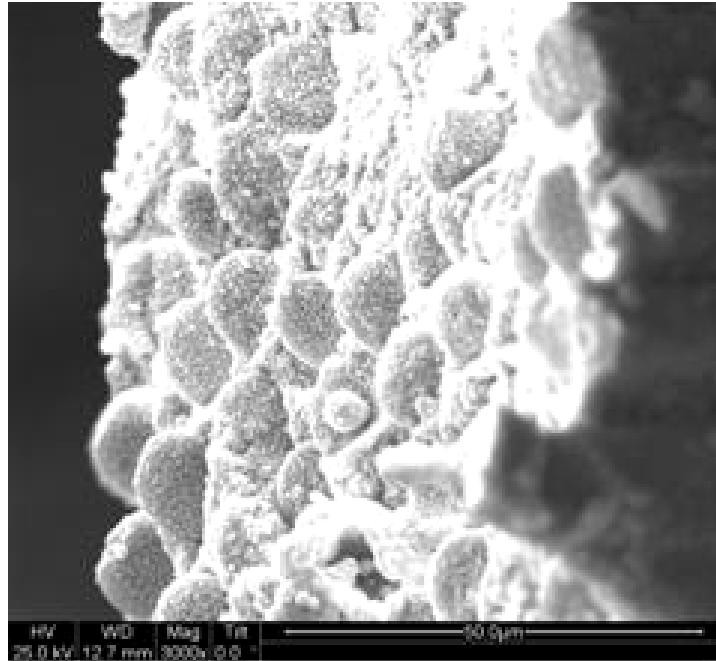


Figure 172. SEM micrograph of the fracture surface of the N720/AM specimen subjected to tensile test to failure following 100 h at 32 MPa at 1200°C in laboratory air.

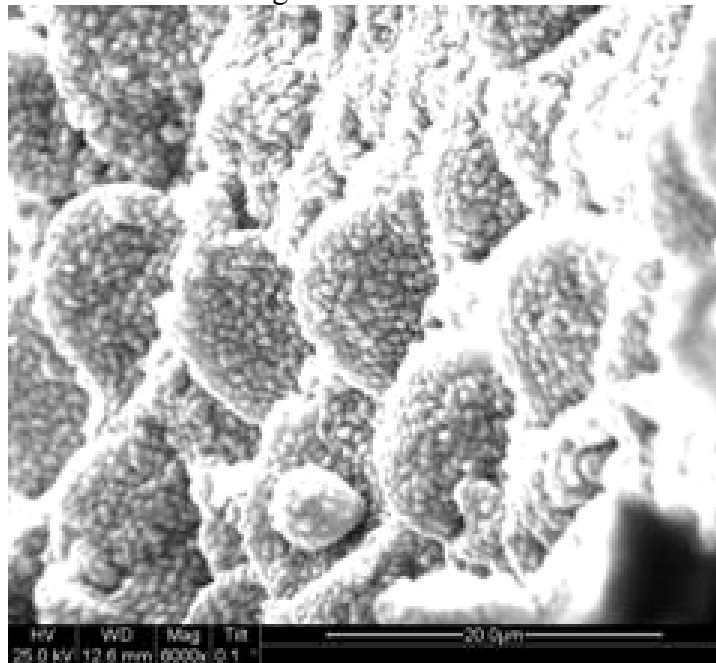


Figure 173. SEM micrograph of the fracture surface of the N720/AM specimen subjected to tensile test to failure following 100 h at 32 MPa at 1200°C in laboratory air.

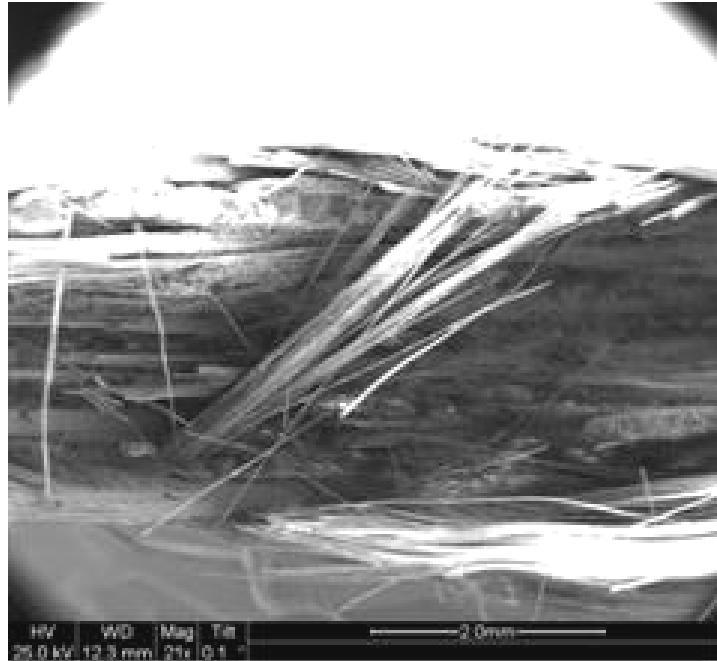


Figure 174. SEM micrograph of the fracture surface of the N720/AM specimen subjected to tensile test to failure following 100 h at 13 MPa at 1200°C in steam.

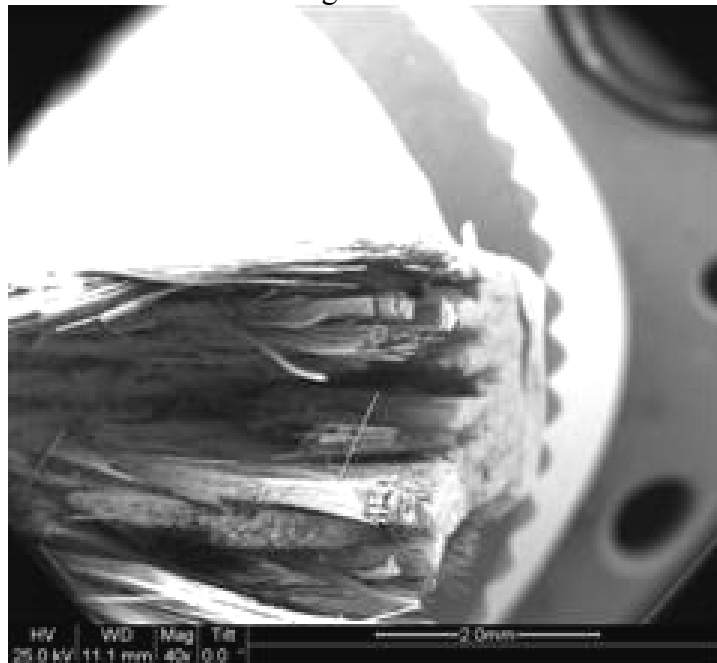


Figure 175. SEM micrograph of the fracture surface of the N720/AM specimen subjected to tensile test to failure following 100 h at 13 MPa at 1200°C in steam.

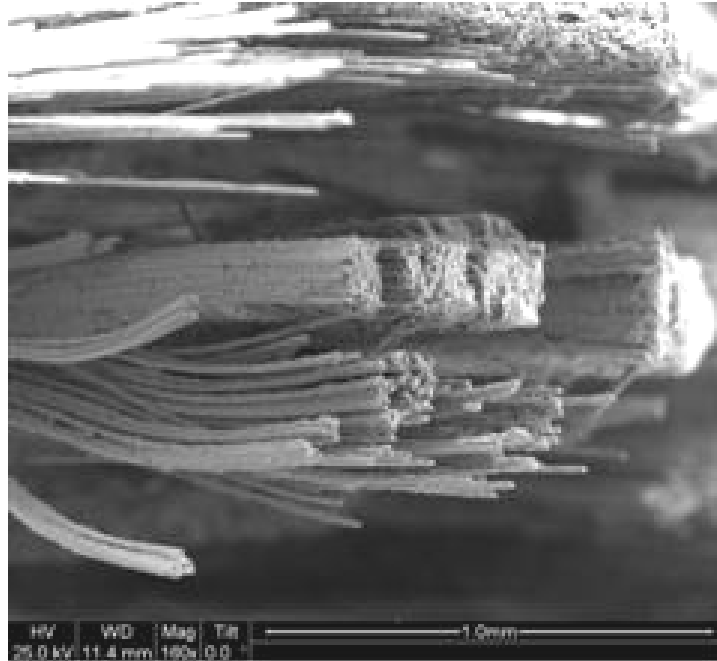


Figure 176. SEM micrograph of the fracture surface of the N720/AM specimen subjected to tensile test to failure following 100 h at 13 MPa at 1200°C in steam.

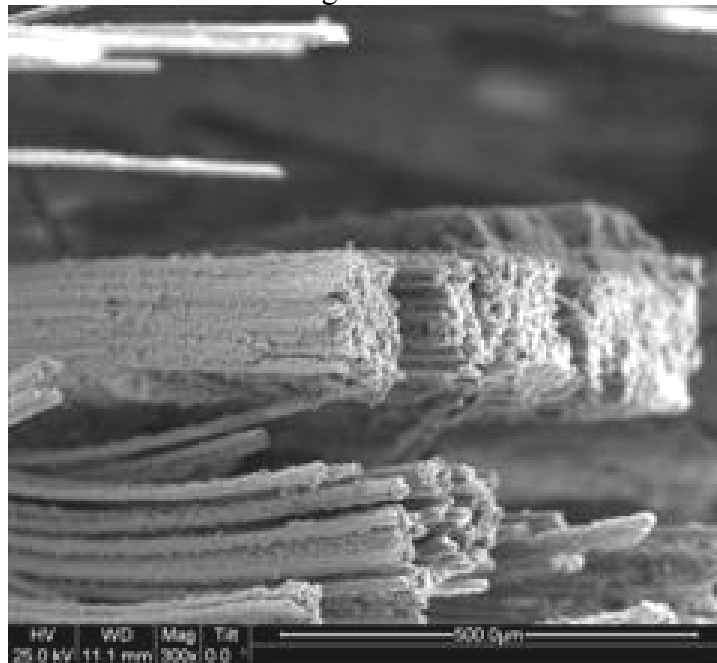


Figure 177. SEM micrograph of the fracture surface of the N720/AM specimen subjected to tensile test to failure following 100 h at 13 MPa at 1200°C in steam.

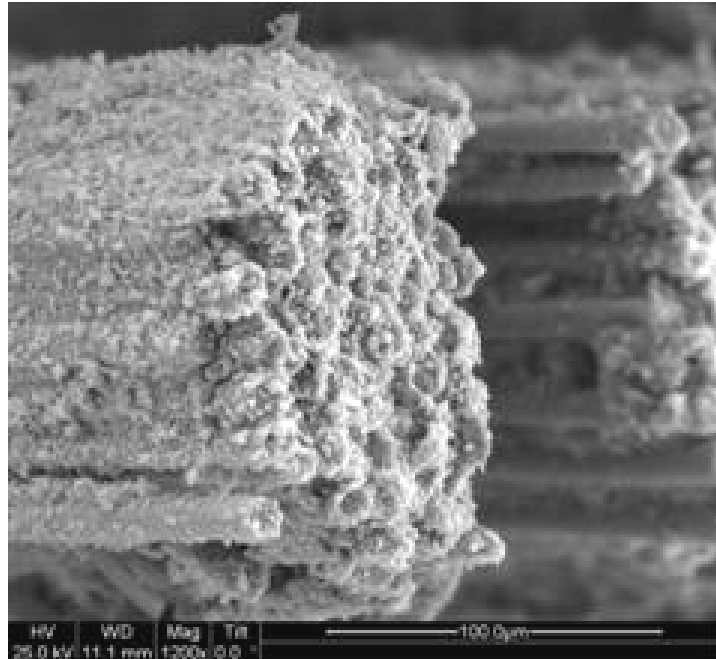


Figure 178. SEM micrograph of the fracture surface of the N720/AM specimen subjected to tensile test to failure following 100 h at 13 MPa at 1200°C in steam.

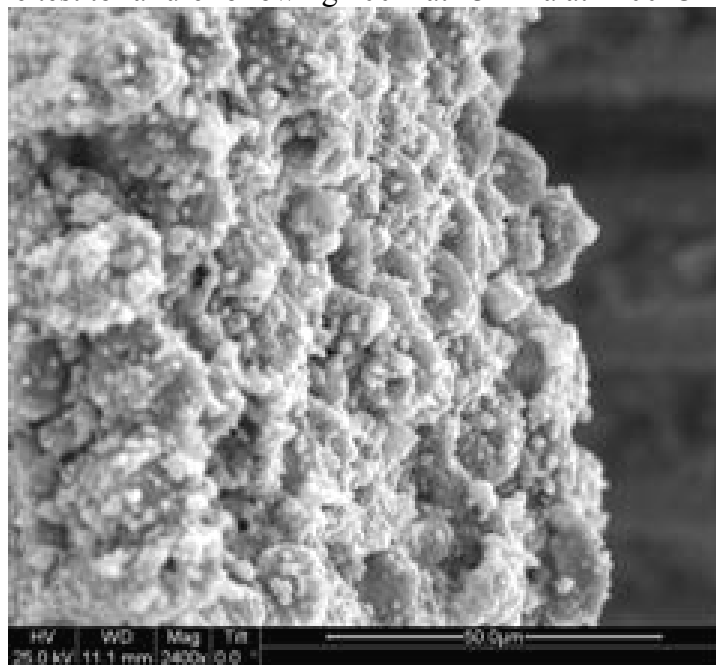


Figure 179. SEM micrograph of the fracture surface of the N720/AM specimen subjected to tensile test to failure following 100 h at 13 MPa at 1200°C in steam.

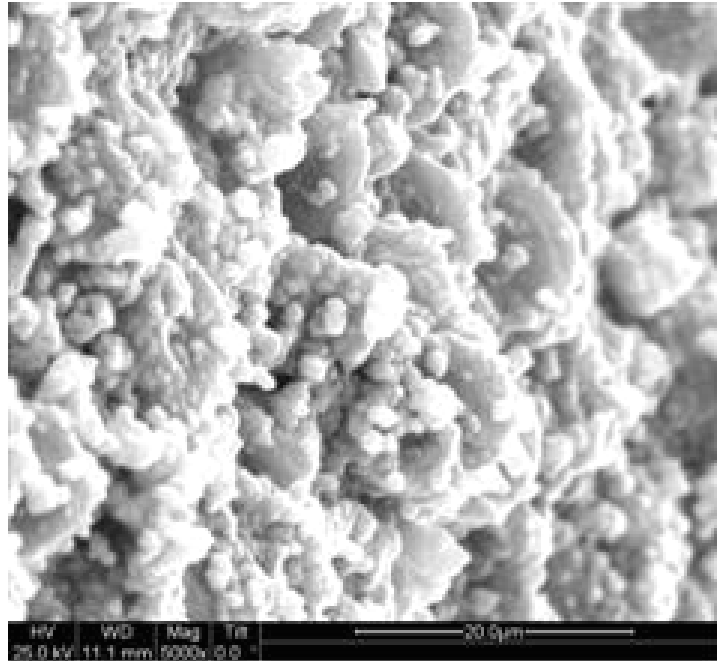


Figure 180. SEM micrograph of the fracture surface of the N720/AM specimen subjected to tensile test to failure following 100 h at 13 MPa at 1200°C in steam.

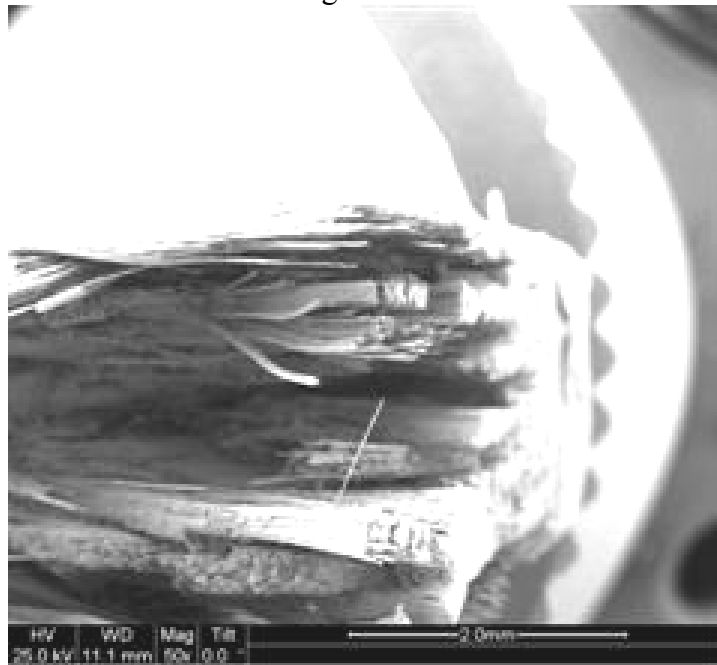


Figure 181. SEM micrograph of the fracture surface of the N720/AM specimen subjected to tensile test to failure following 100 h at 13 MPa at 1200°C in steam.

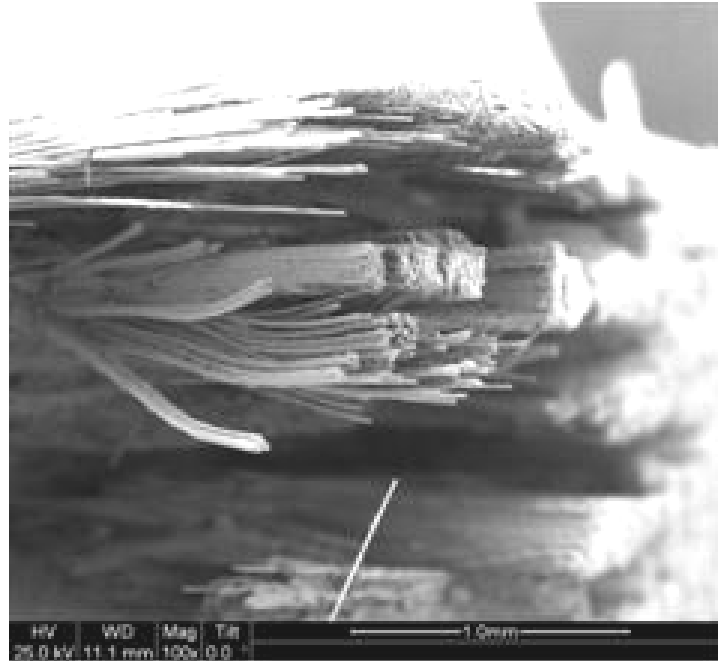


Figure 182. SEM micrograph of the fracture surface of the N720/AM specimen subjected to tensile test to failure following 100 h at 13 MPa at 1200°C in steam.

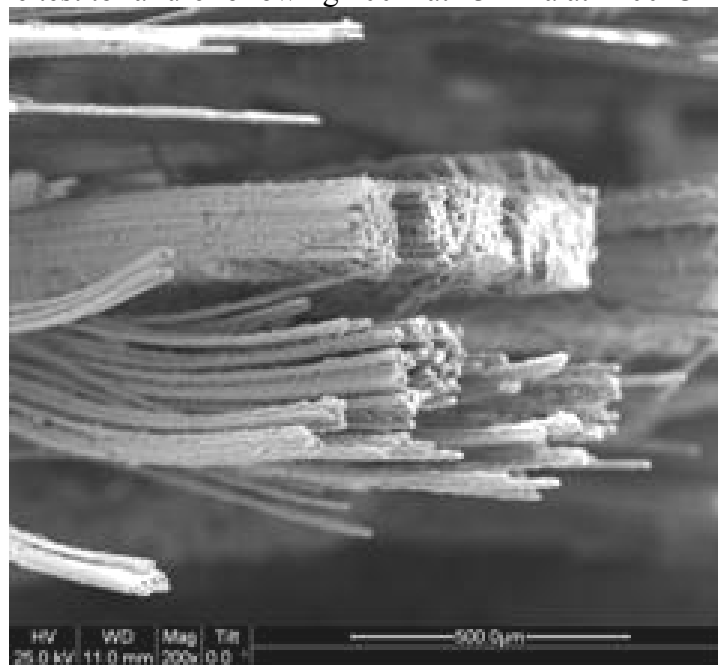


Figure 183. SEM micrograph of the fracture surface of the N720/AM specimen subjected to tensile test to failure following 100 h at 13 MPa at 1200°C in steam.



Figure 184. SEM micrograph of the fracture surface of the N720/AM specimen subjected to tensile test to failure following 100 h at 13 MPa at 1200°C in steam.

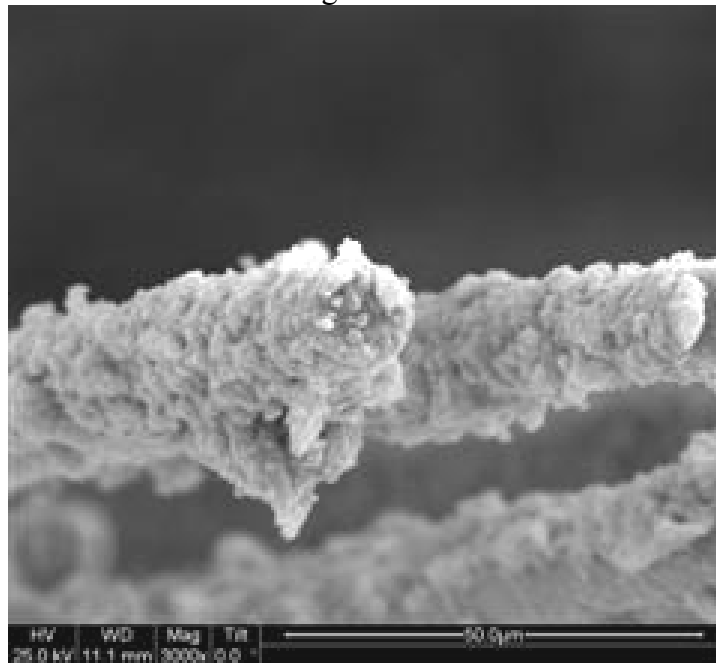


Figure 185. SEM micrograph of the fracture surface of the N720/AM specimen subjected to tensile test to failure following 100 h at 13 MPa at 1200°C in steam.

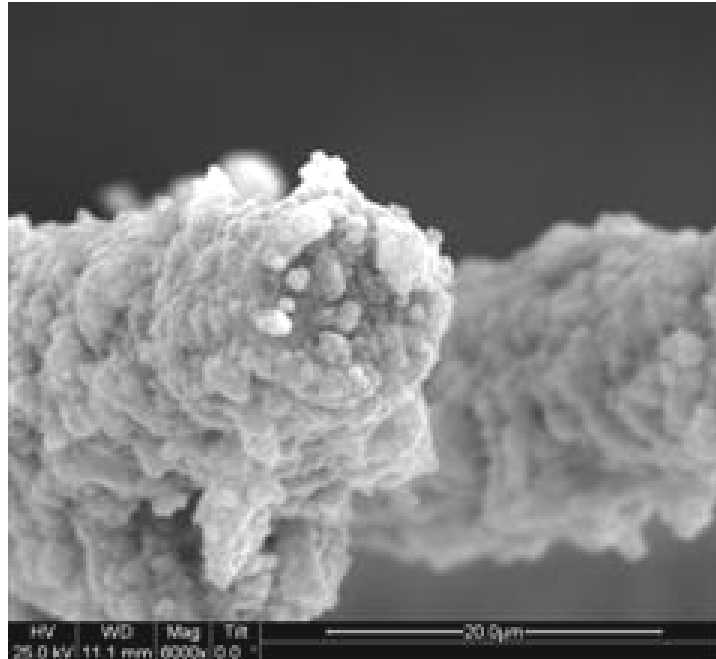


Figure 186. SEM micrograph of the fracture surface of the N720/AM specimen subjected to tensile test to failure following 100 h at 13 MPa at 1200°C in steam.



Figure 187. SEM micrograph of the fracture surface of the N720/AM specimen subjected to tensile test to failure following 100 h at 13 MPa at 1200°C in steam.

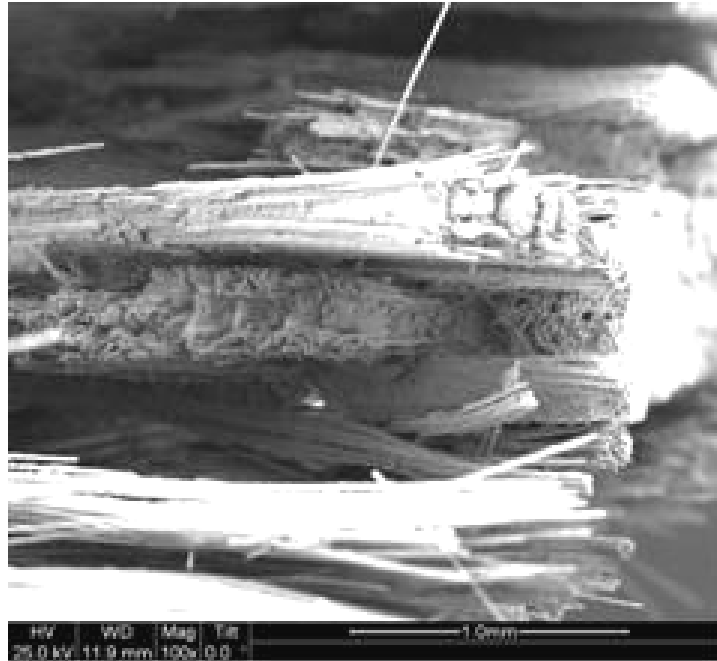


Figure 188. SEM micrograph of the fracture surface of the N720/AM specimen subjected to tensile test to failure following 100 h at 13 MPa at 1200°C in steam.

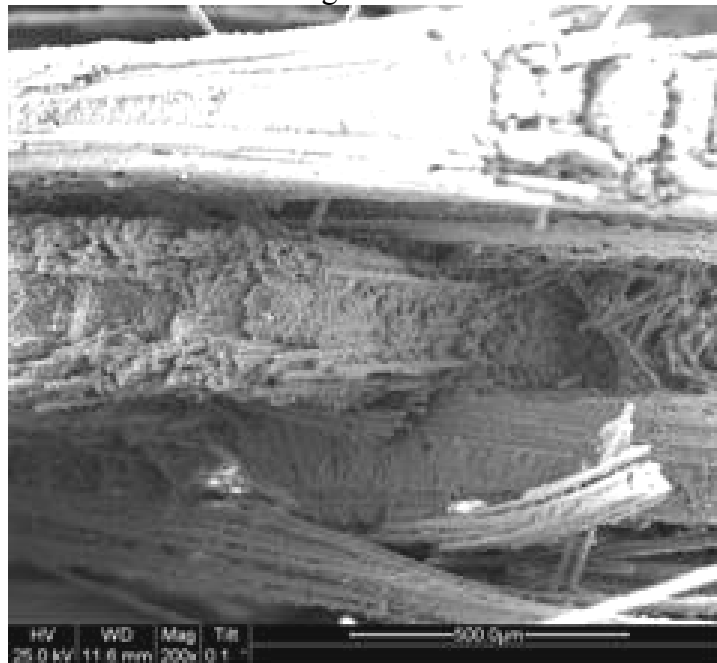


Figure 189. SEM micrograph of the fracture surface of the N720/AM specimen subjected to tensile test to failure following 100 h at 13 MPa at 1200°C in steam.

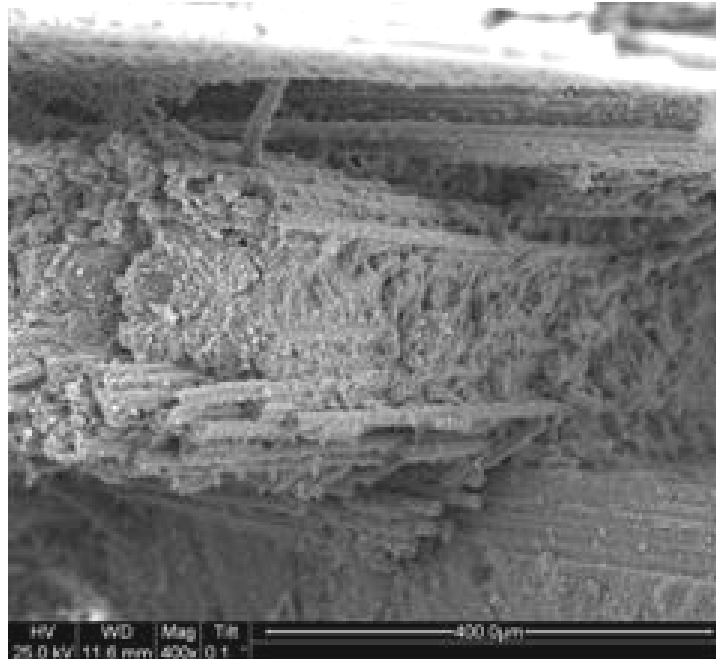


Figure 190. SEM micrograph of the fracture surface of the N720/AM specimen subjected to tensile test to failure following 100 h at 13 MPa at 1200°C in steam.

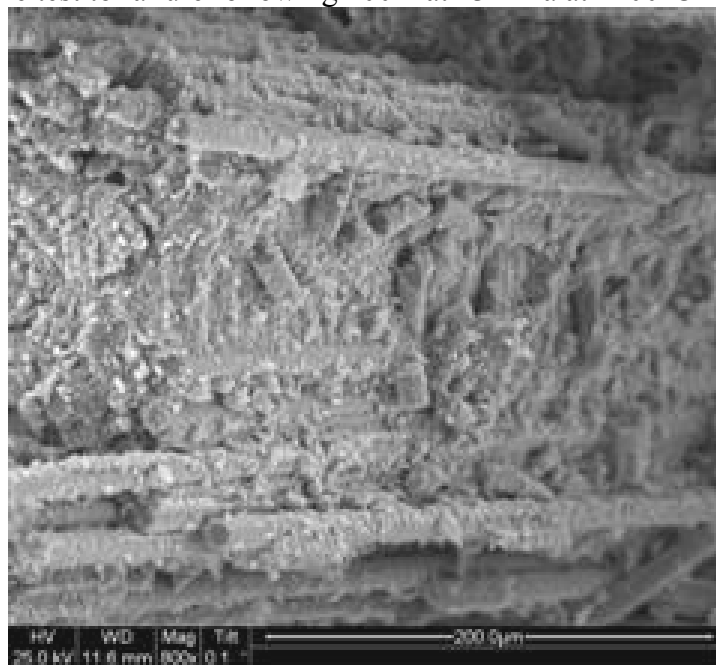


Figure 191. SEM micrograph of the fracture surface of the N720/AM specimen subjected to tensile test to failure following 100 h at 13 MPa at 1200°C in steam.

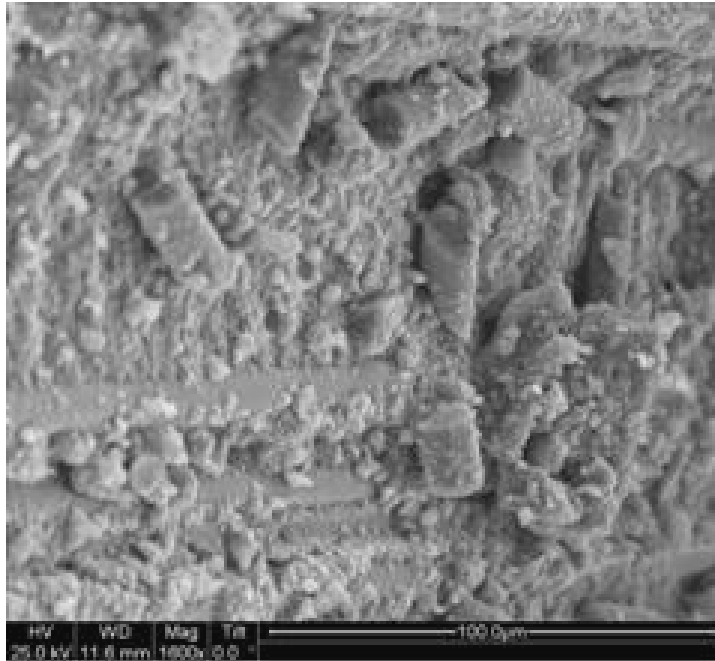


Figure 192. SEM micrograph of the fracture surface of the N720/AM specimen subjected to tensile test to failure following 100 h at 13 MPa at 1200°C in steam.

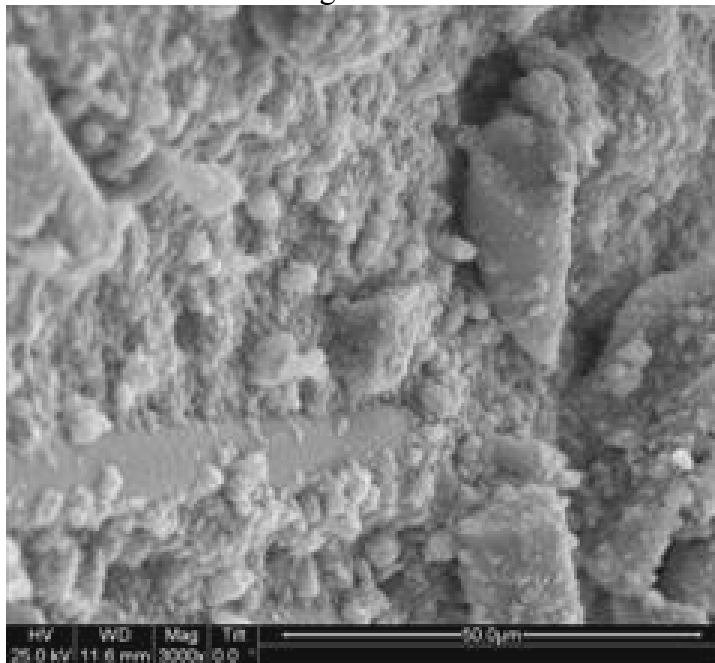


Figure 193. SEM micrograph of the fracture surface of the N720/AM specimen subjected to tensile test to failure following 100 h at 13 MPa at 1200°C in steam.

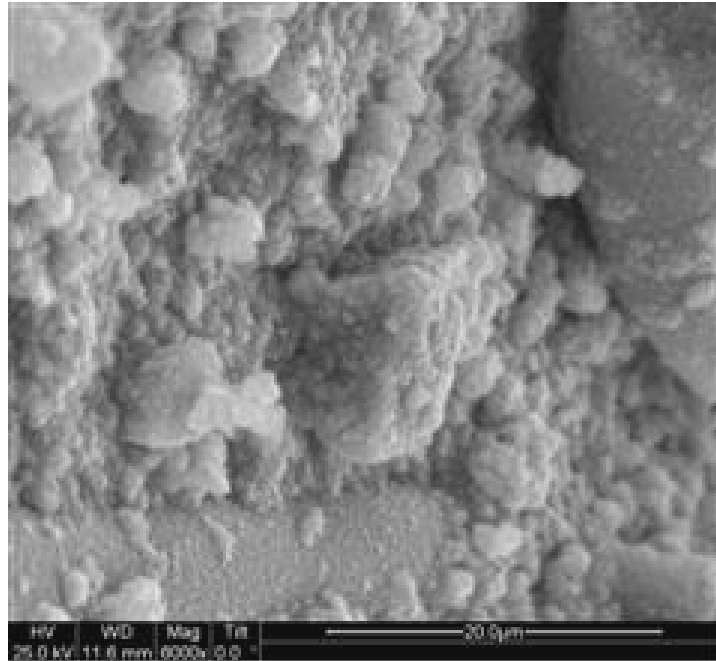


Figure 194. SEM micrograph of the fracture surface of the N720/AM specimen subjected to tensile test to failure following 100 h at 13 MPa at 1200°C in steam.

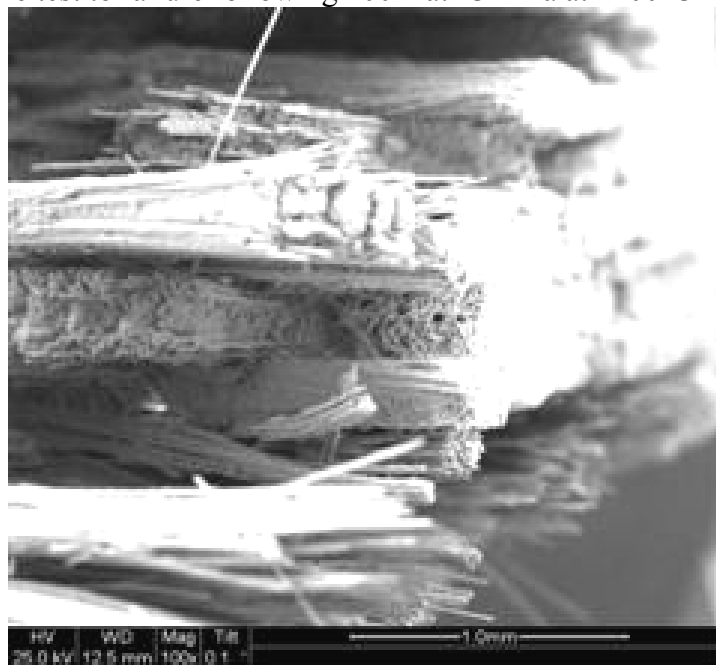


Figure 195. SEM micrograph of the fracture surface of the N720/AM specimen subjected to tensile test to failure following 100 h at 13 MPa at 1200°C in steam.

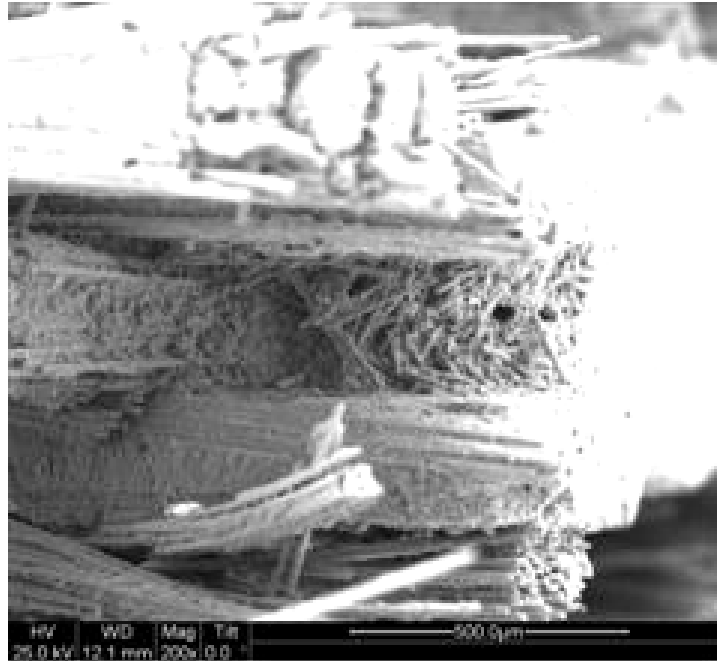


Figure 196. SEM micrograph of the fracture surface of the N720/AM specimen subjected to tensile test to failure following 100 h at 13 MPa at 1200°C in steam.

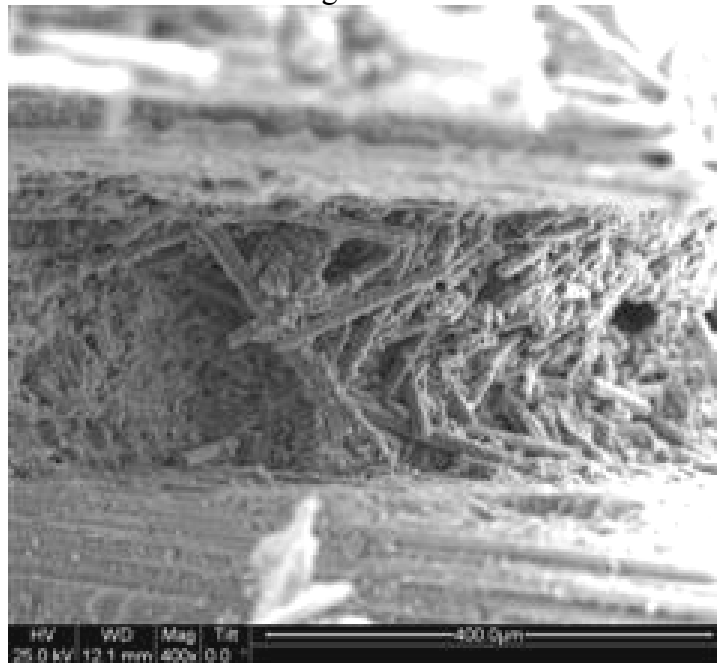


Figure 197. SEM micrograph of the fracture surface of the N720/AM specimen subjected to tensile test to failure following 100 h at 13 MPa at 1200°C in steam.

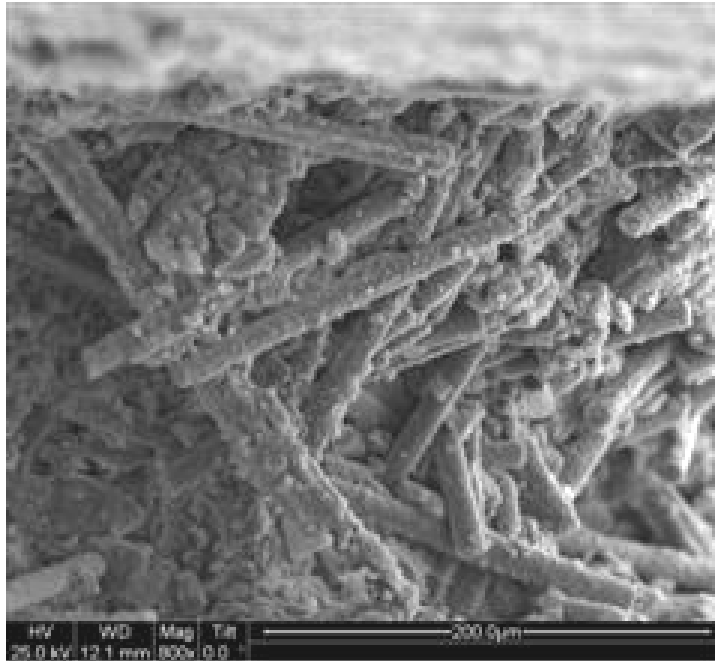


Figure 198. SEM micrograph of the fracture surface of the N720/AM specimen subjected to tensile test to failure following 100 h at 13 MPa at 1200°C in steam.

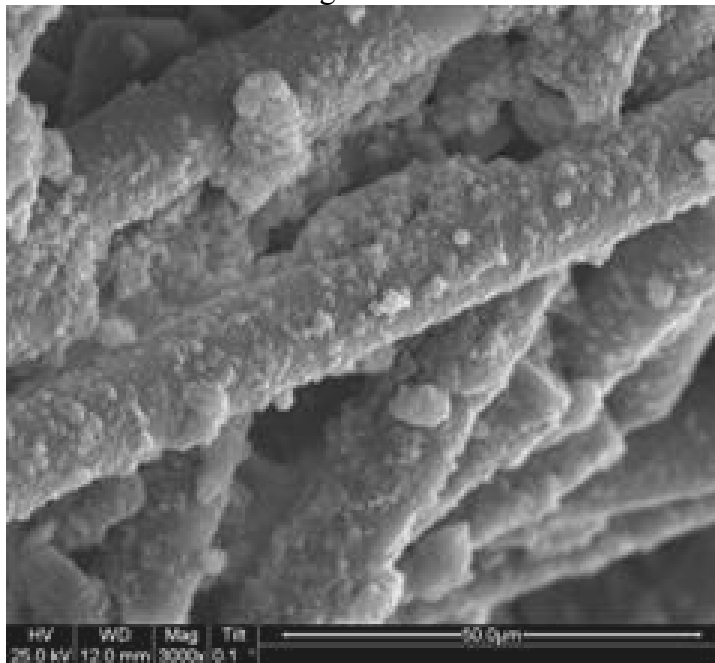


Figure 199. SEM micrograph of the fracture surface of the N720/AM specimen subjected to tensile test to failure following 100 h at 13 MPa at 1200°C in steam.

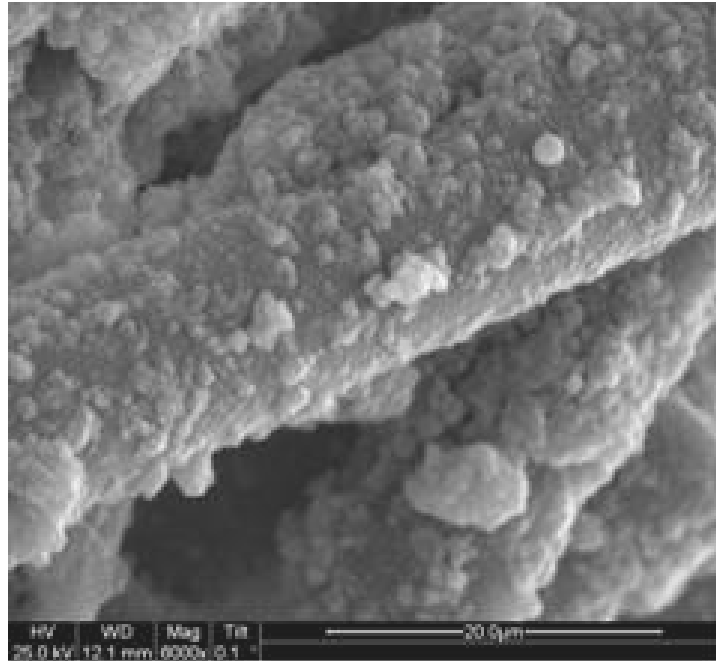


Figure 200. SEM micrograph of the fracture surface of the N720/AM specimen subjected to tensile test to failure following 100 h at 13 MPa at 1200°C in steam.

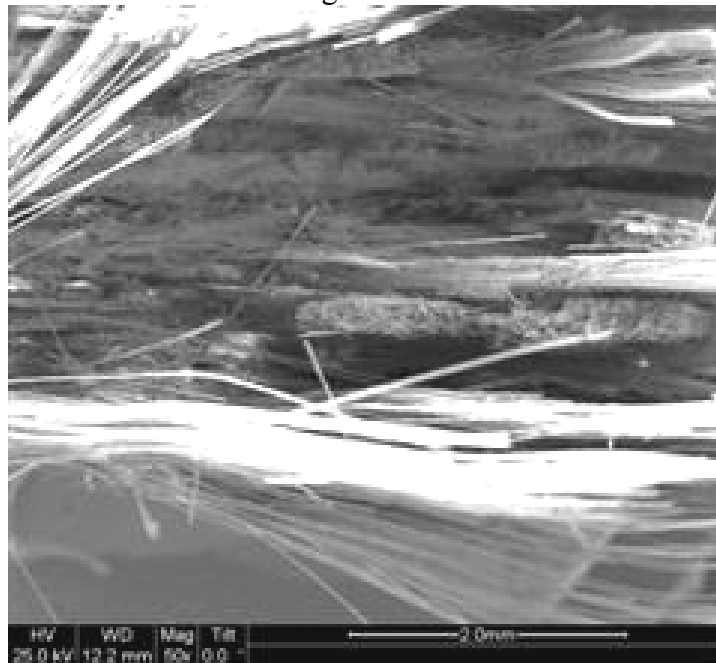


Figure 201. SEM micrograph of the fracture surface of the N720/AM specimen subjected to tensile test to failure following 100 h at 13 MPa at 1200°C in steam.



Figure 202. SEM micrograph of the fracture surface of the N720/AM specimen subjected to tensile test to failure following 100 h at 13 MPa at 1200°C in steam.

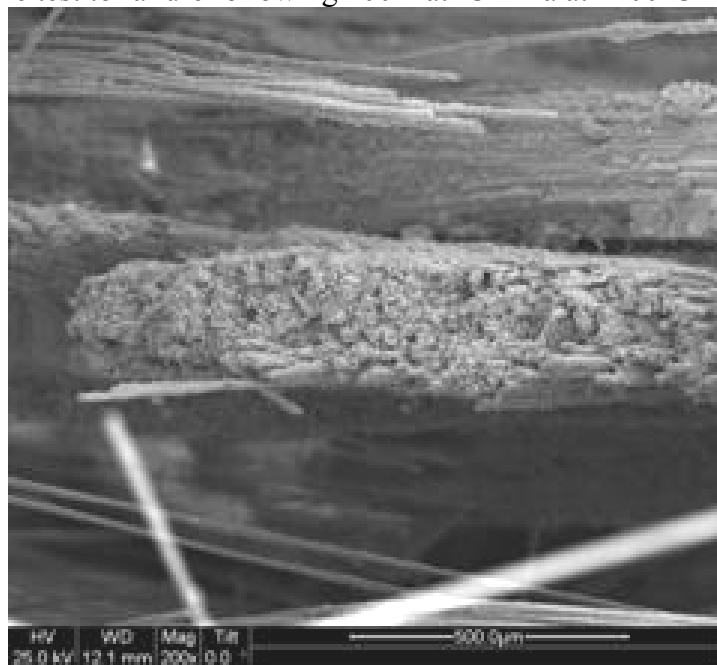


Figure 203. SEM micrograph of the fracture surface of the N720/AM specimen subjected to tensile test to failure following 100 h at 13 MPa at 1200°C in steam.

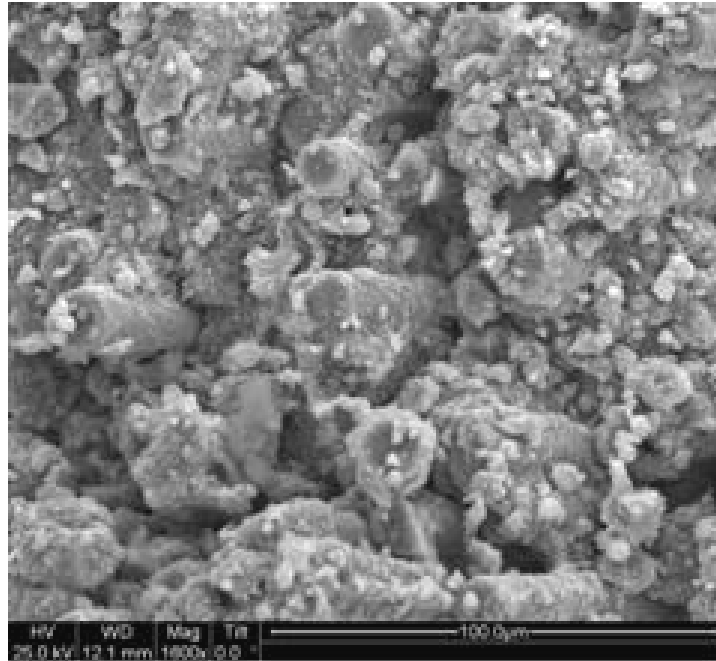


Figure 204. SEM micrograph of the fracture surface of the N720/AM specimen subjected to tensile test to failure following 100 h at 13 MPa at 1200°C in steam.

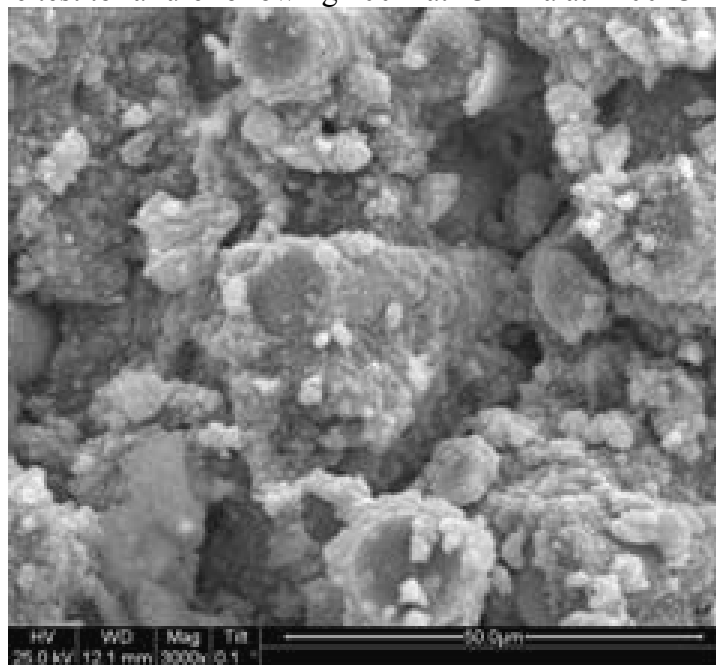


Figure 205. SEM micrograph of the fracture surface of the N720/AM specimen subjected to tensile test to failure following 100 h at 13 MPa at 1200°C in steam.

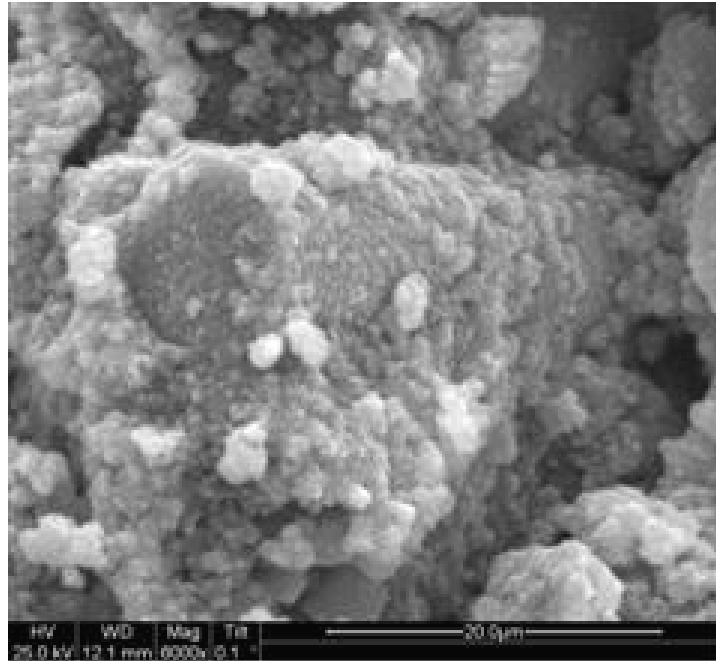


Figure 206. SEM micrograph of the fracture surface of the N720/AM specimen subjected to tensile test to failure following 100 h at 13 MPa at 1200°C in steam.

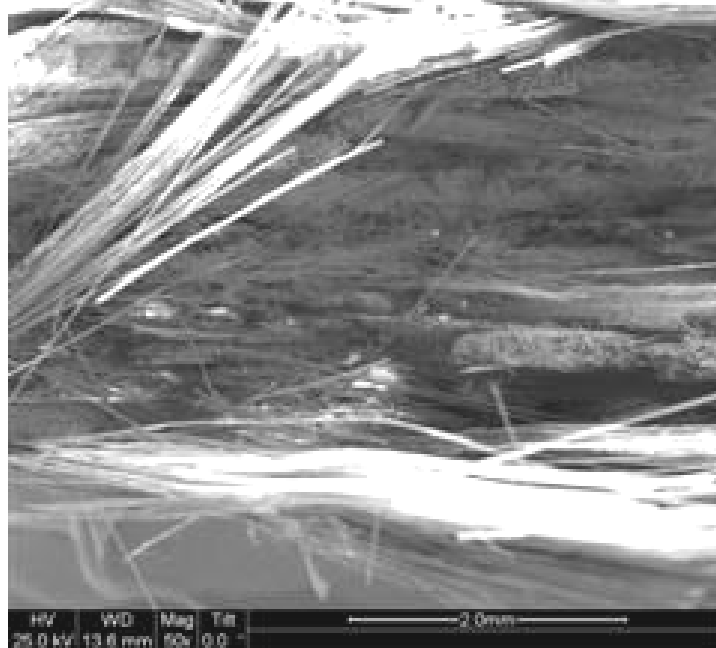


Figure 207. SEM micrograph of the fracture surface of the N720/AM specimen subjected to tensile test to failure following 100 h at 13 MPa at 1200°C in steam.

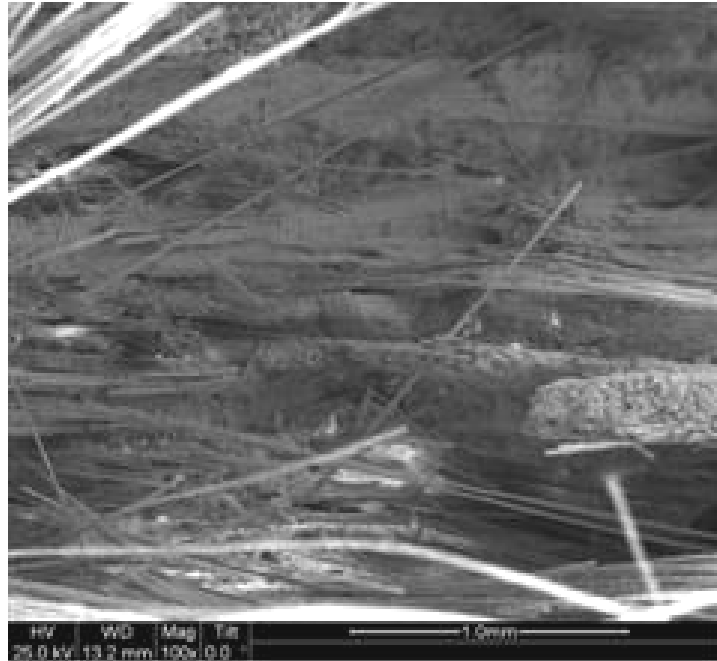


Figure 208. SEM micrograph of the fracture surface of the N720/AM specimen subjected to tensile test to failure following 100 h at 13 MPa at 1200°C in steam.

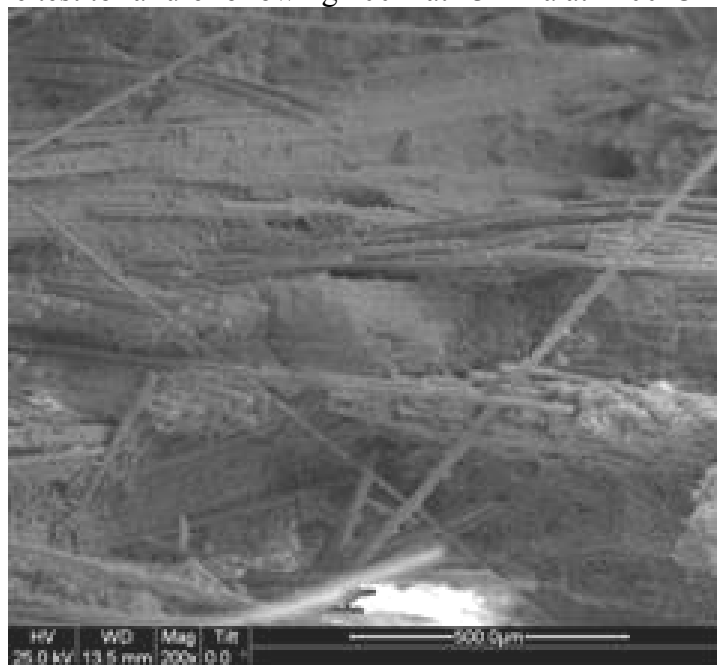


Figure 209. SEM micrograph of the fracture surface of the N720/AM specimen subjected to tensile test to failure following 100 h at 13 MPa at 1200°C in steam.

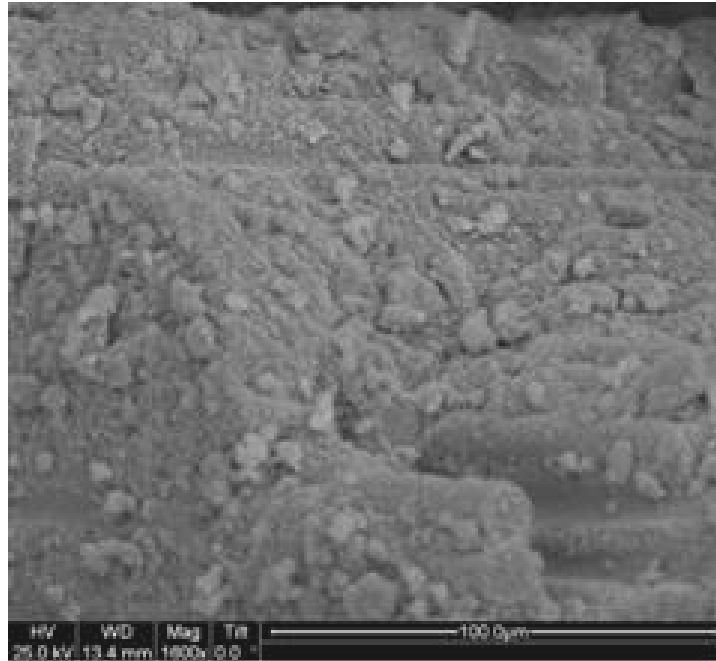


Figure 210. SEM micrograph of the fracture surface of the N720/AM specimen subjected to tensile test to failure following 100 h at 13 MPa at 1200°C in steam.

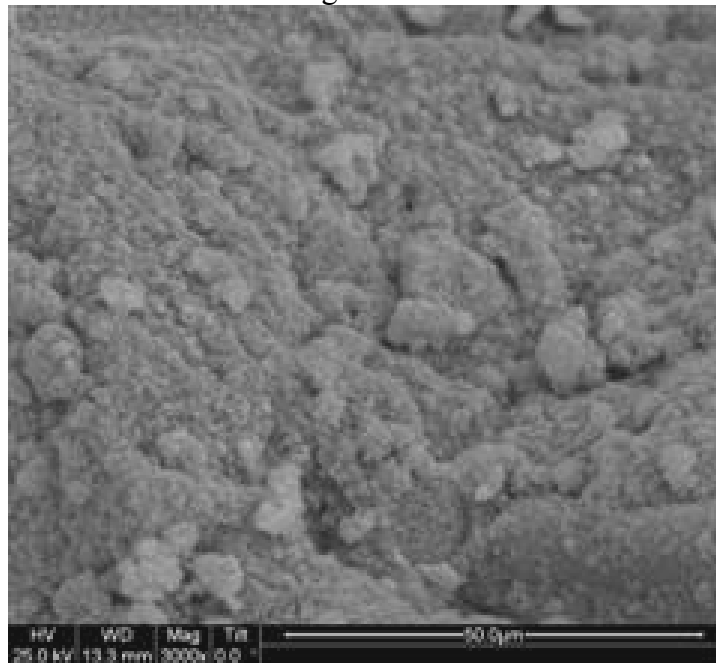


Figure 211. SEM micrograph of the fracture surface of the N720/AM specimen subjected to tensile test to failure following 100 h at 13 MPa at 1200°C in steam.

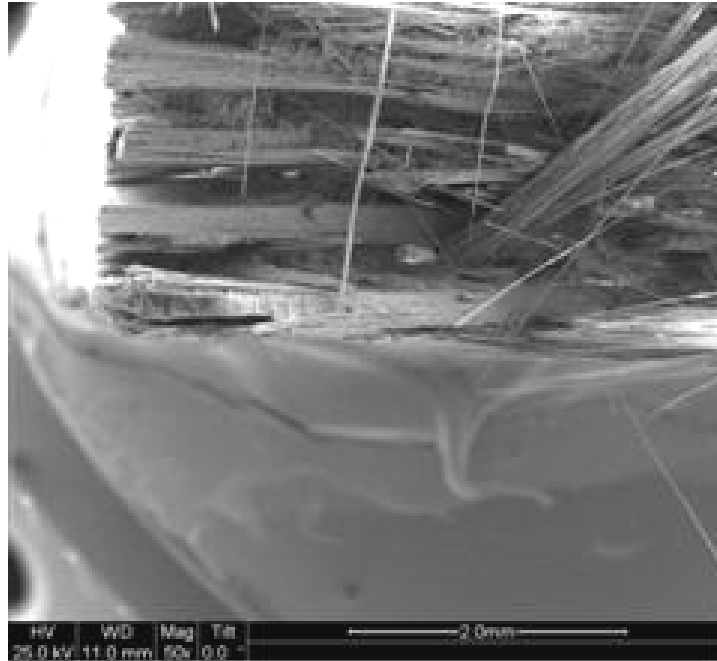


Figure 212. SEM micrograph of the fracture surface of the N720/AM specimen subjected to tensile test to failure following 100 h at 13 MPa at 1200°C in steam.

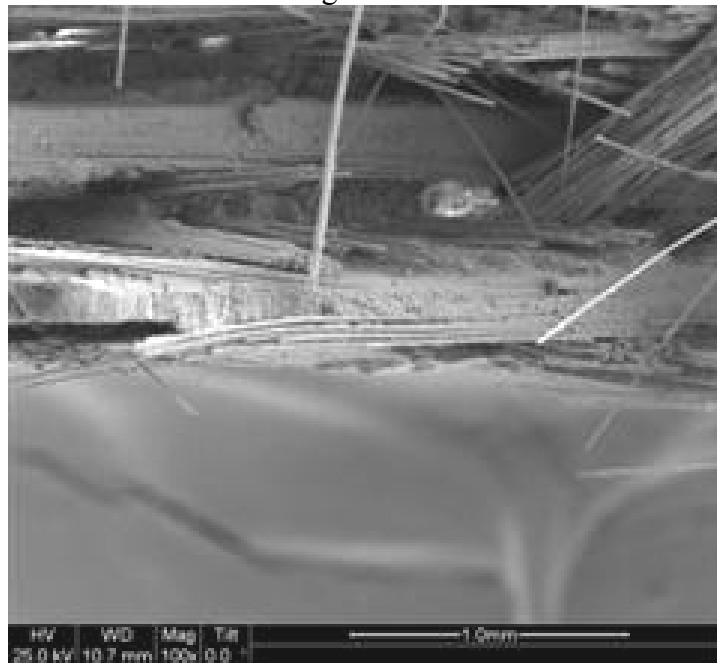


Figure 213. SEM micrograph of the fracture surface of the N720/AM specimen subjected to tensile test to failure following 100 h at 13 MPa at 1200°C in steam.

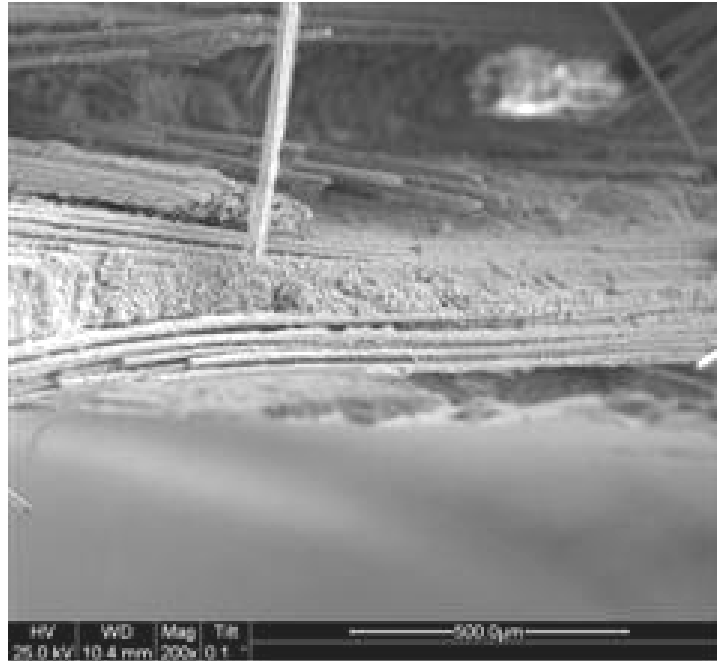


Figure 214. SEM micrograph of the fracture surface of the N720/AM specimen subjected to tensile test to failure following 100 h at 13 MPa at 1200°C in steam.

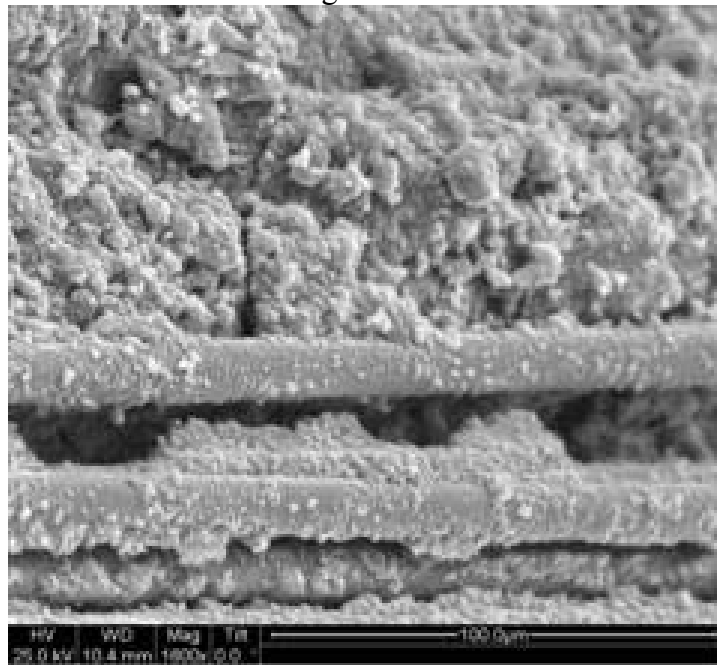


Figure 215. SEM micrograph of the fracture surface of the N720/AM specimen subjected to tensile test to failure following 100 h at 13 MPa at 1200°C in steam.

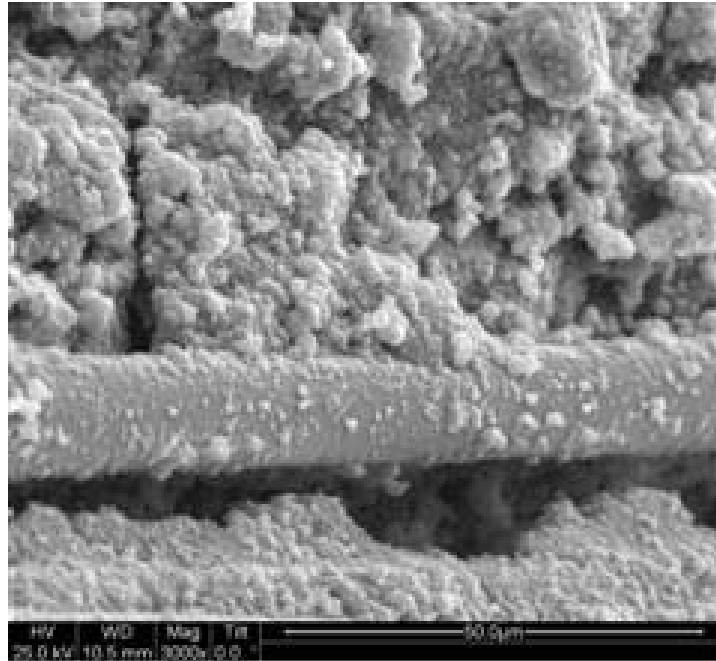


Figure 216. SEM micrograph of the fracture surface of the N720/AM specimen subjected to tensile test to failure following 100 h at 13 MPa at 1200°C in steam.

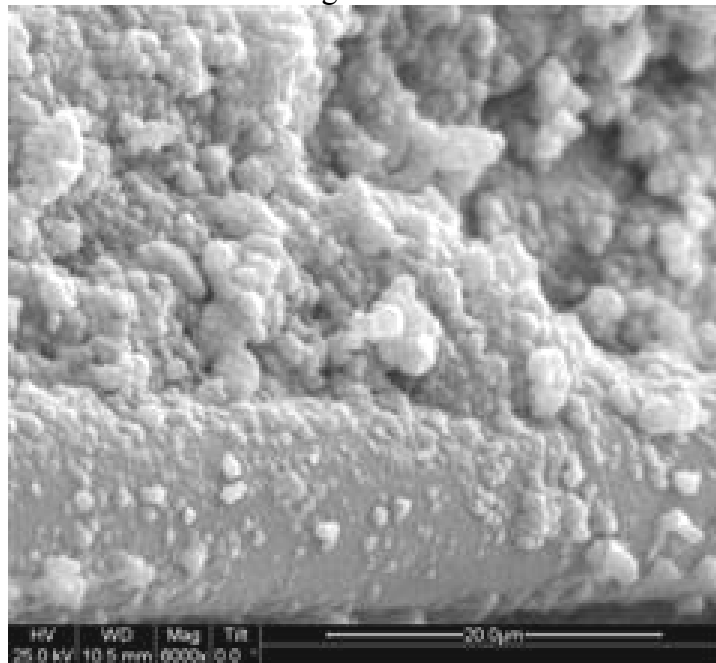


Figure 217. SEM micrograph of the fracture surface of the N720/AM specimen subjected to tensile test to failure following 100 h at 13 MPa at 1200°C in steam.

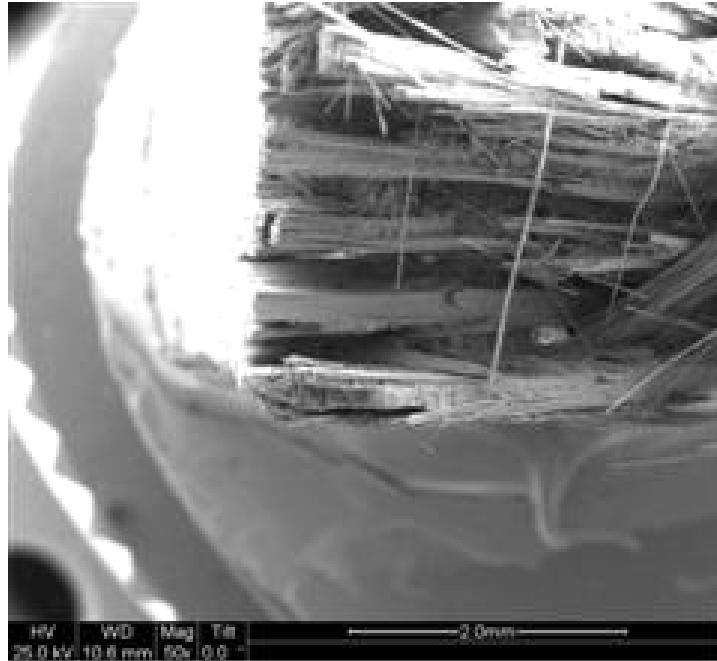


Figure 218. SEM micrograph of the fracture surface of the N720/AM specimen subjected to tensile test to failure following 100 h at 13 MPa at 1200°C in steam.

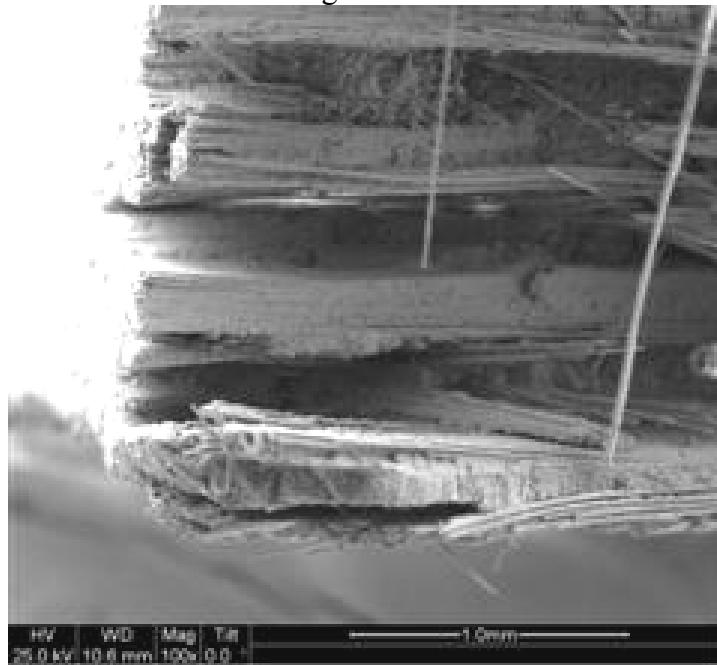


Figure 219. SEM micrograph of the fracture surface of the N720/AM specimen subjected to tensile test to failure following 100 h at 13 MPa at 1200°C in steam.

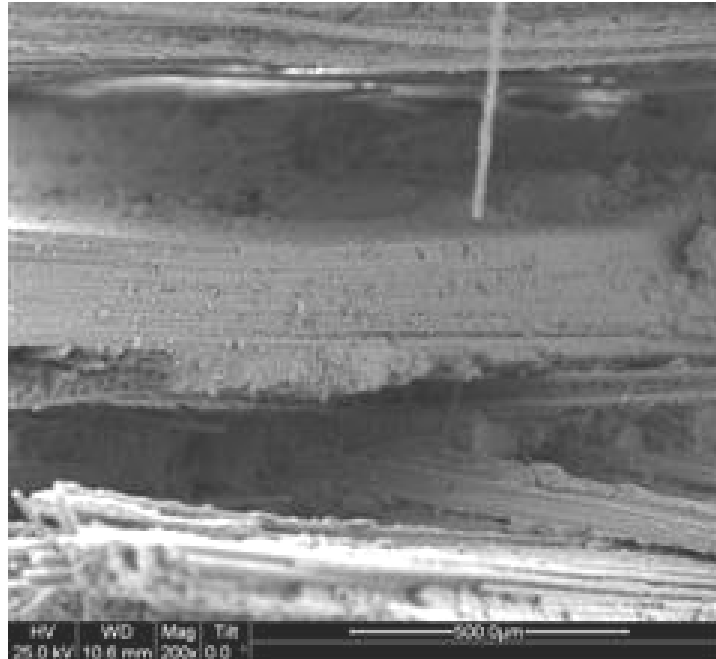


Figure 220. SEM micrograph of the fracture surface of the N720/AM specimen subjected to tensile test to failure following 100 h at 13 MPa at 1200°C in steam.

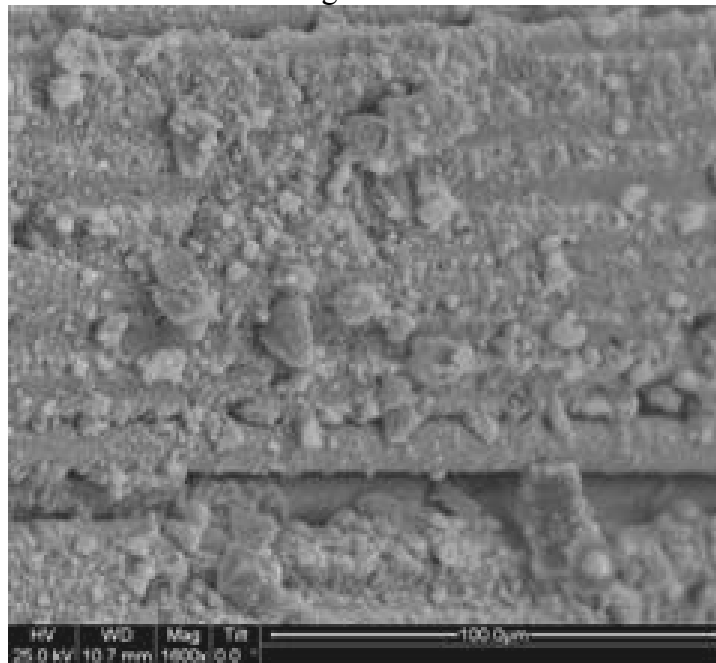


Figure 221. SEM micrograph of the fracture surface of the N720/AM specimen subjected to tensile test to failure following 100 h at 13 MPa at 1200°C in steam.

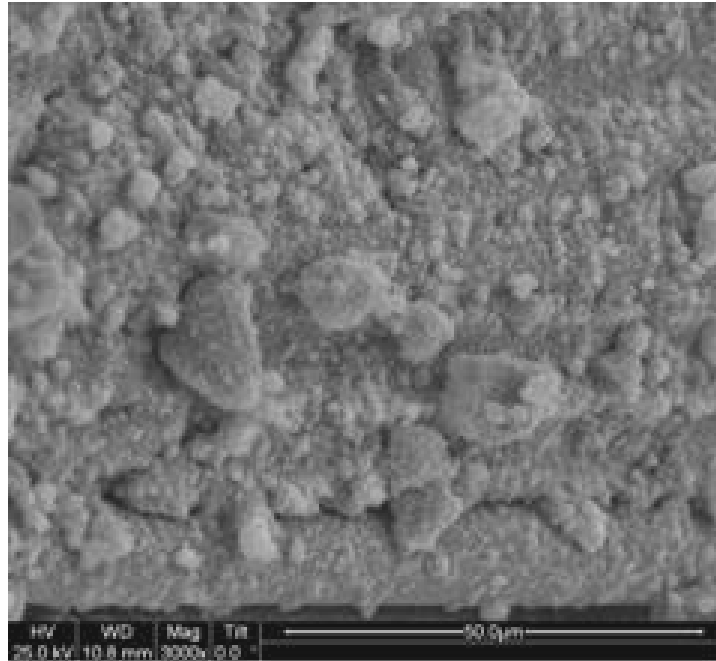


Figure 222. SEM micrograph of the fracture surface of the N720/AM specimen subjected to tensile test to failure following 100 h at 13 MPa at 1200°C in steam.

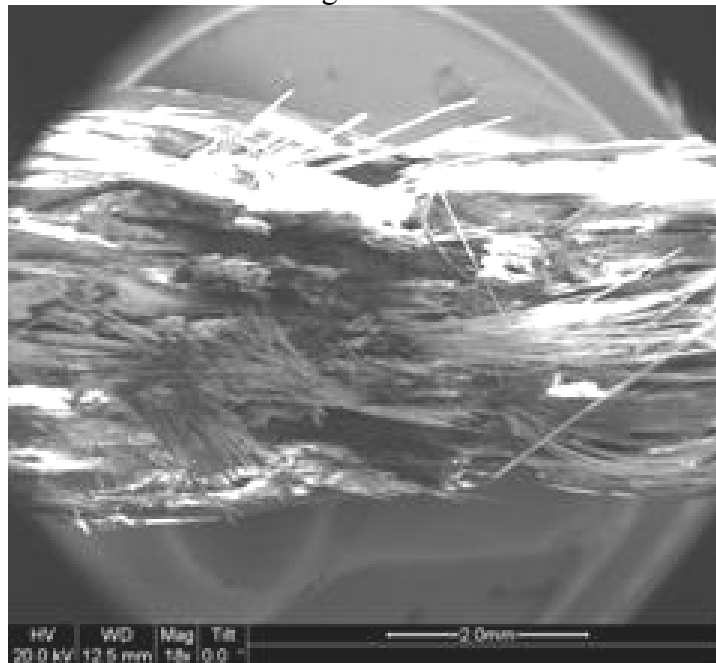


Figure 223. SEM micrograph of the fracture surface of the N720/AM specimen with  $\pm 45^\circ$  fiber orientation obtained in creep test conducted at 30 MPa at 1200°C in steam. Creep lifetime  $t_f = 1.08$  h.

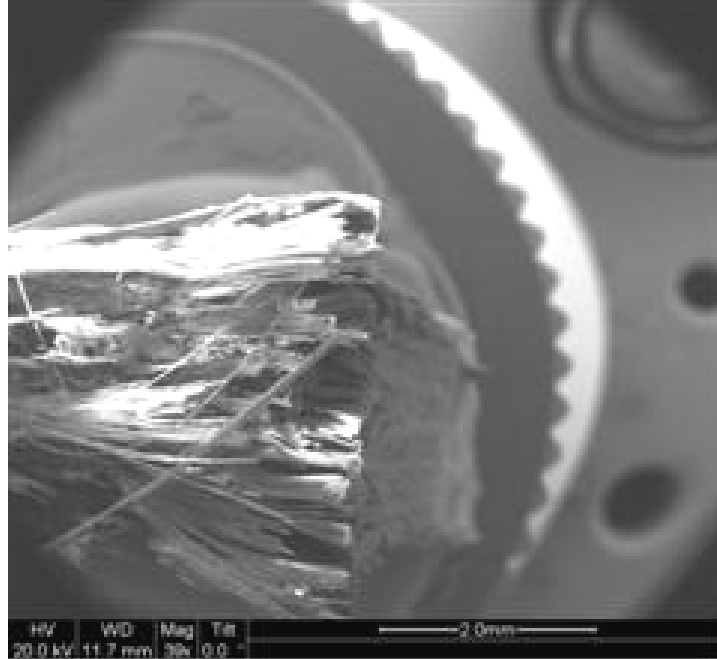


Figure 224. SEM micrograph of the fracture surface of the N720/AM specimen with  $\pm 45^\circ$  fiber orientation obtained in creep test conducted at 30 MPa at 1200°C in steam. Creep lifetime  $t_f = 1.08$  h.

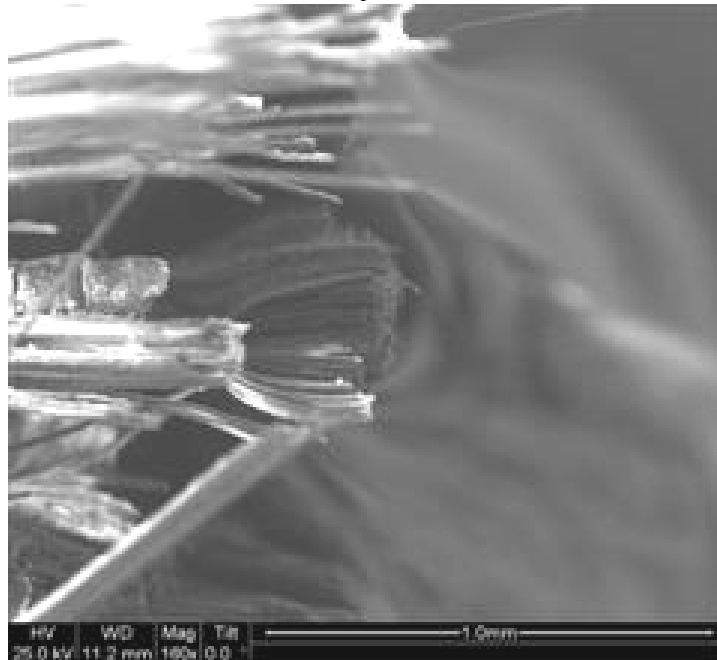


Figure 225. SEM micrograph of the fracture surface of the N720/AM specimen with  $\pm 45^\circ$  fiber orientation obtained in creep test conducted at 30 MPa at 1200°C in steam. Creep lifetime  $t_f = 1.08$  h.

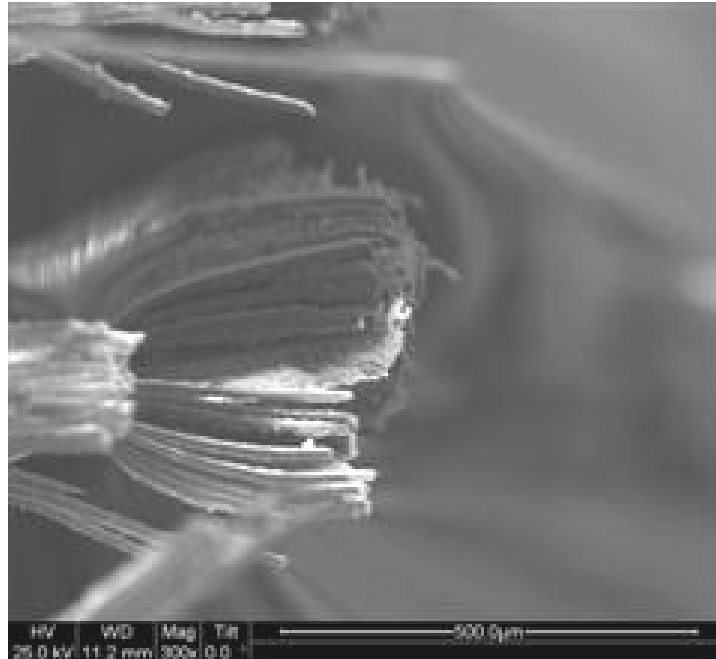


Figure 226. SEM micrograph of the fracture surface of the N720/AM specimen with  $\pm 45^\circ$  fiber orientation obtained in creep test conducted at 30 MPa at 1200°C in steam. Creep lifetime  $t_f = 1.08$  h.

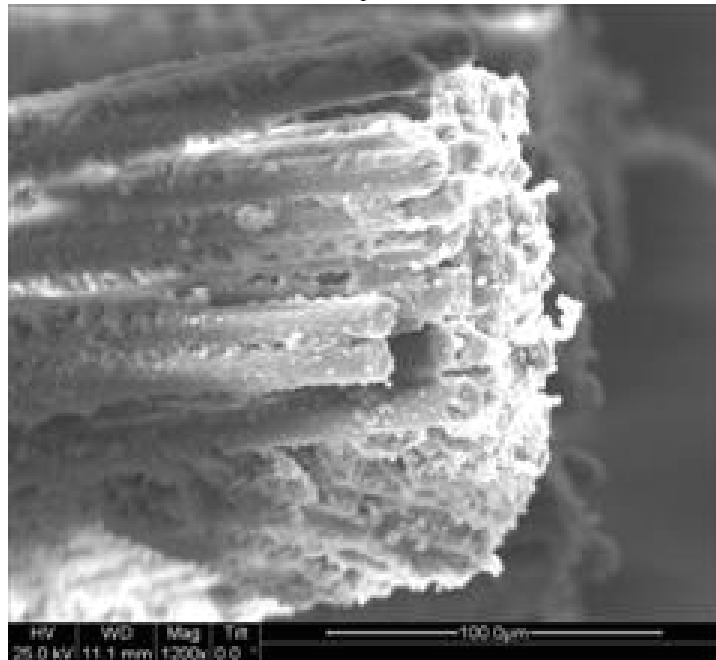


Figure 227. SEM micrograph of the fracture surface of the N720/AM specimen with  $\pm 45^\circ$  fiber orientation obtained in creep test conducted at 30 MPa at 1200°C in steam. Creep lifetime  $t_f = 1.08$  h.

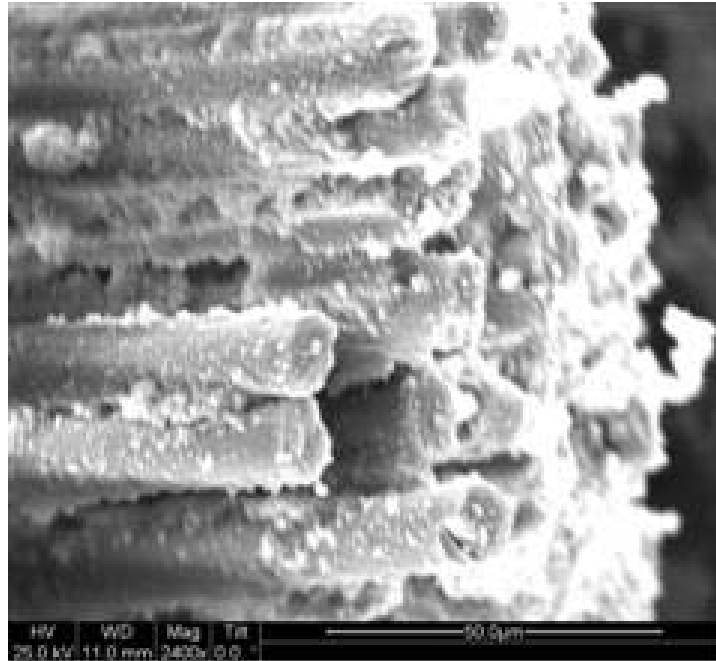


Figure 228. SEM micrograph of the fracture surface of the N720/AM specimen with  $\pm 45^\circ$  fiber orientation obtained in creep test conducted at 30 MPa at 1200°C in steam. Creep lifetime  $t_f = 1.08$  h.

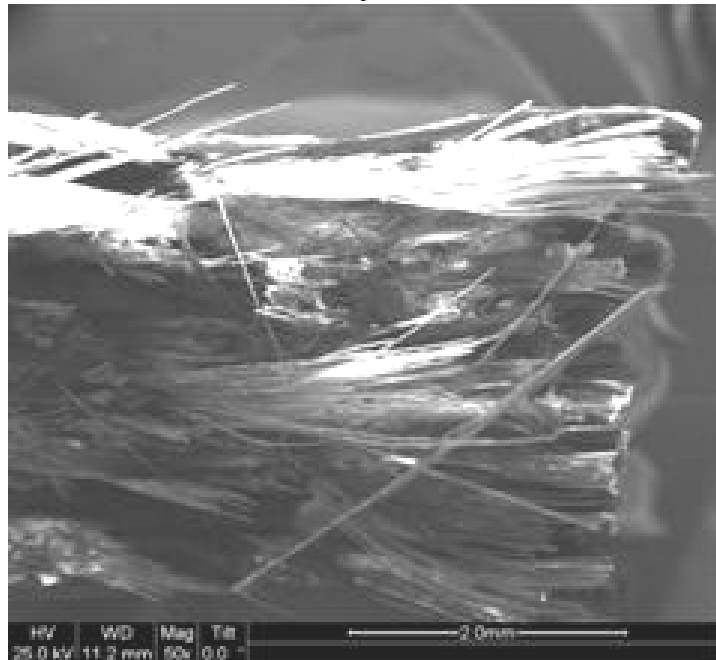


Figure 229. SEM micrograph of the fracture surface of the N720/AM specimen with  $\pm 45^\circ$  fiber orientation obtained in creep test conducted at 30 MPa at 1200°C in steam. Creep lifetime  $t_f = 1.08$  h.

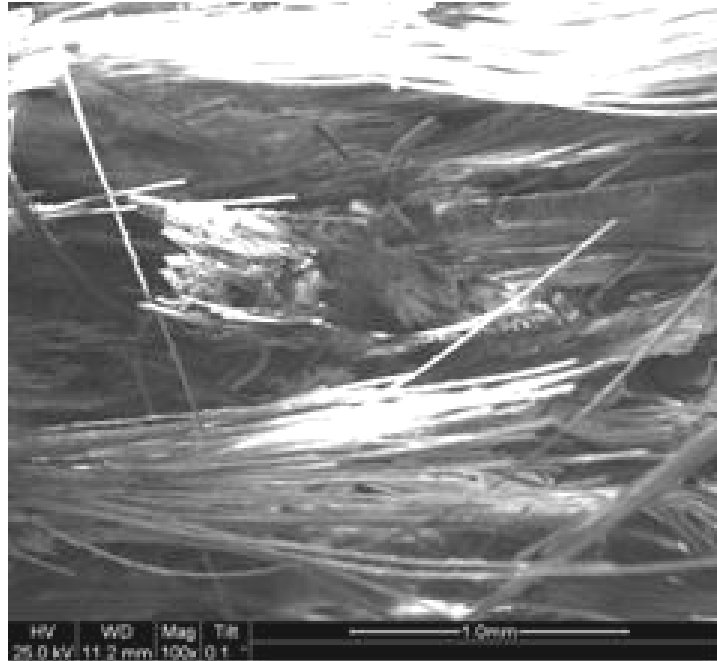


Figure 230. SEM micrograph of the fracture surface of the N720/AM specimen with  $\pm 45^\circ$  fiber orientation obtained in creep test conducted at 30 MPa at 1200°C in steam. Creep lifetime  $t_f = 1.08$  h.

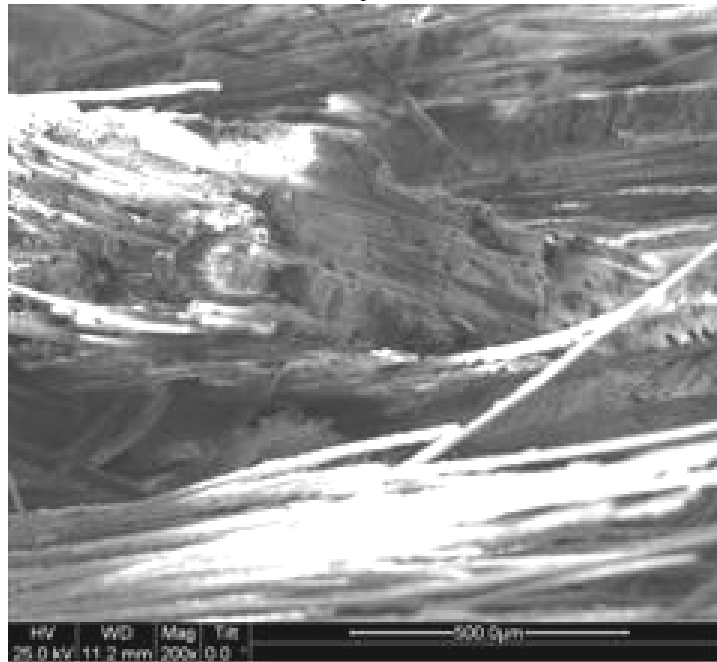


Figure 231. SEM micrograph of the fracture surface of the N720/AM specimen with  $\pm 45^\circ$  fiber orientation obtained in creep test conducted at 30 MPa at 1200°C in steam. Creep lifetime  $t_f = 1.08$  h.

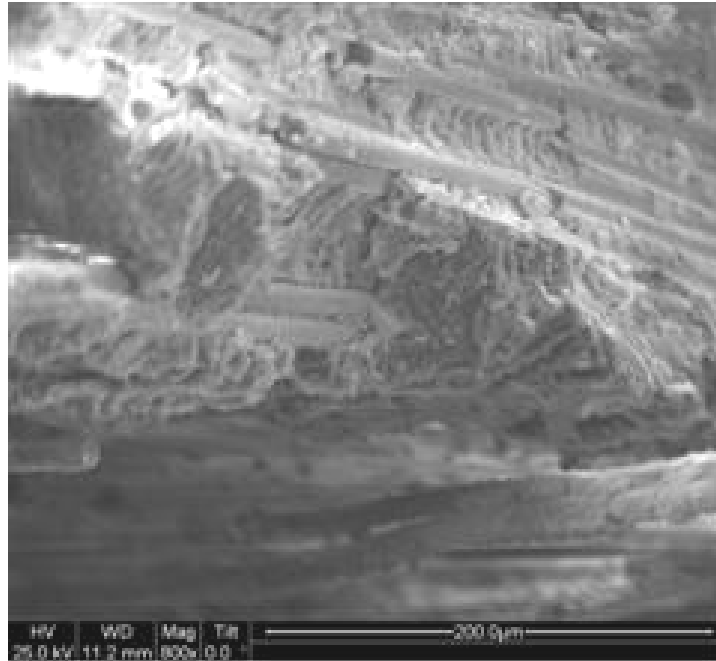


Figure 232. SEM micrograph of the fracture surface of the N720/AM specimen with  $\pm 45^\circ$  fiber orientation obtained in creep test conducted at 30 MPa at 1200°C in steam. Creep lifetime  $t_f = 1.08$  h.

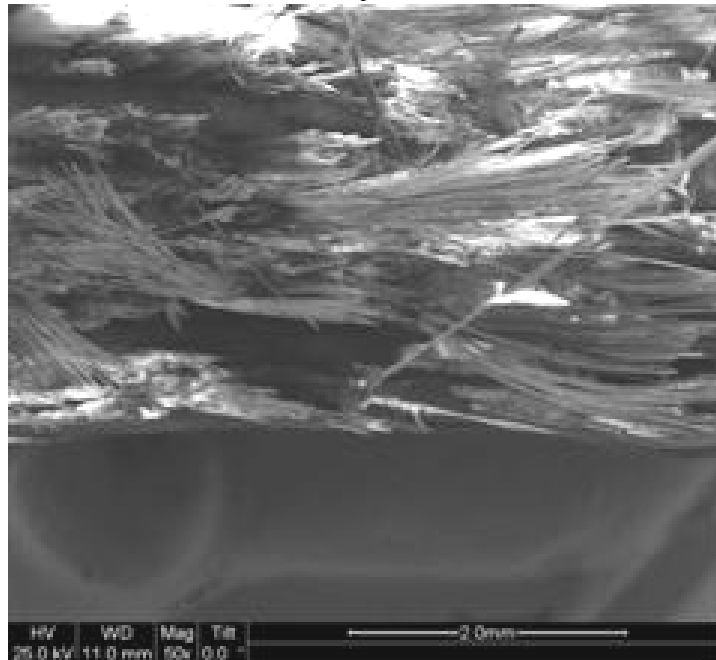


Figure 233. SEM micrograph of the fracture surface of the N720/AM specimen with  $\pm 45^\circ$  fiber orientation obtained in creep test conducted at 30 MPa at 1200°C in steam. Creep lifetime  $t_f = 1.08$  h.

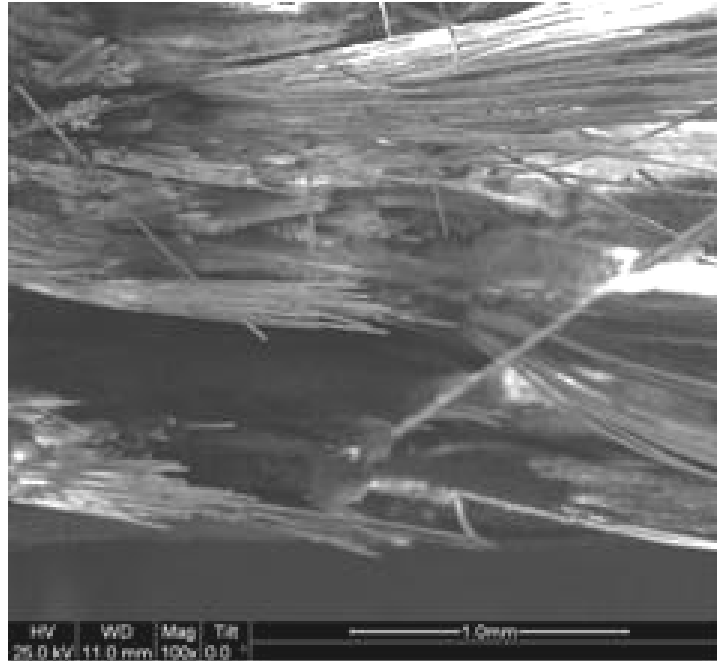


Figure 234. SEM micrograph of the fracture surface of the N720/AM specimen with  $\pm 45^\circ$  fiber orientation obtained in creep test conducted at 30 MPa at 1200°C in steam. Creep lifetime  $t_f = 1.08$  h.

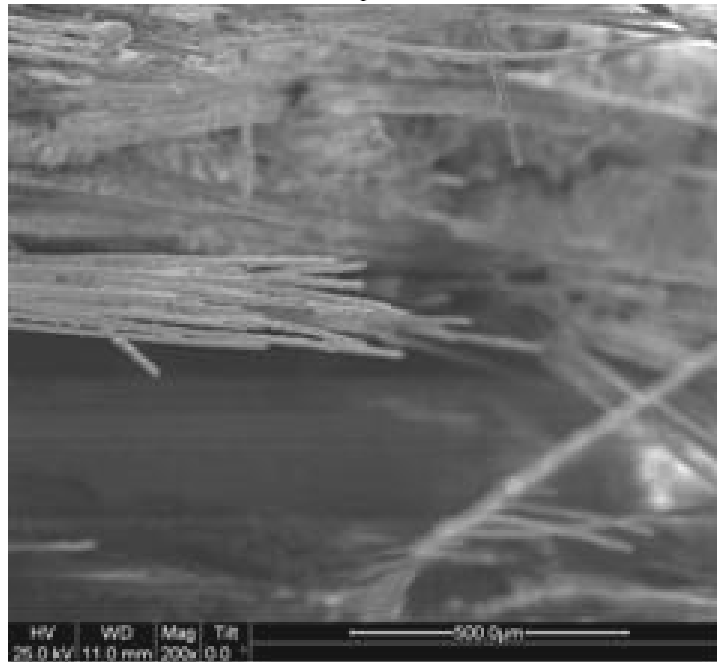


Figure 235. SEM micrograph of the fracture surface of the N720/AM specimen with  $\pm 45^\circ$  fiber orientation obtained in creep test conducted at 30 MPa at 1200°C in steam. Creep lifetime  $t_f = 1.08$  h.



Figure 236. SEM micrograph of the fracture surface of the N720/AM specimen with  $\pm 45^\circ$  fiber orientation obtained in creep test conducted at 30 MPa at 1200°C in steam. Creep lifetime  $t_f = 1.08$  h.

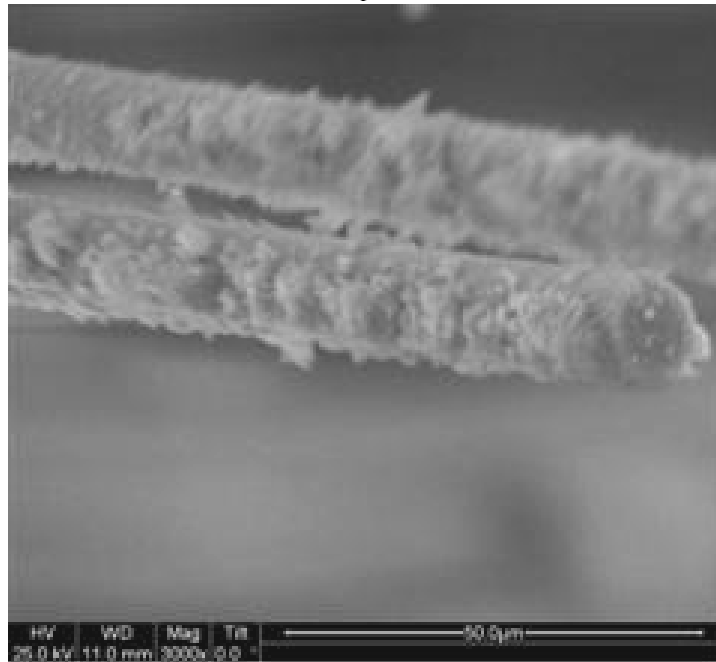


Figure 237. SEM micrograph of the fracture surface of the N720/AM specimen with  $\pm 45^\circ$  fiber orientation obtained in creep test conducted at 30 MPa at 1200°C in steam. Creep lifetime  $t_f = 1.08$  h.

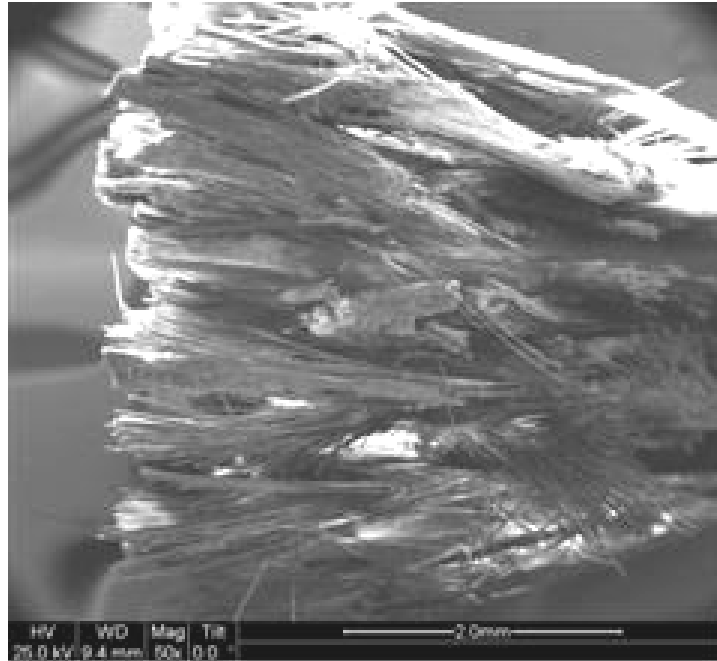


Figure 238. SEM micrograph of the fracture surface of the N720/AM specimen with  $\pm 45^\circ$  fiber orientation obtained in creep test conducted at 30 MPa at 1200°C in steam. Creep lifetime  $t_f = 1.08$  h.

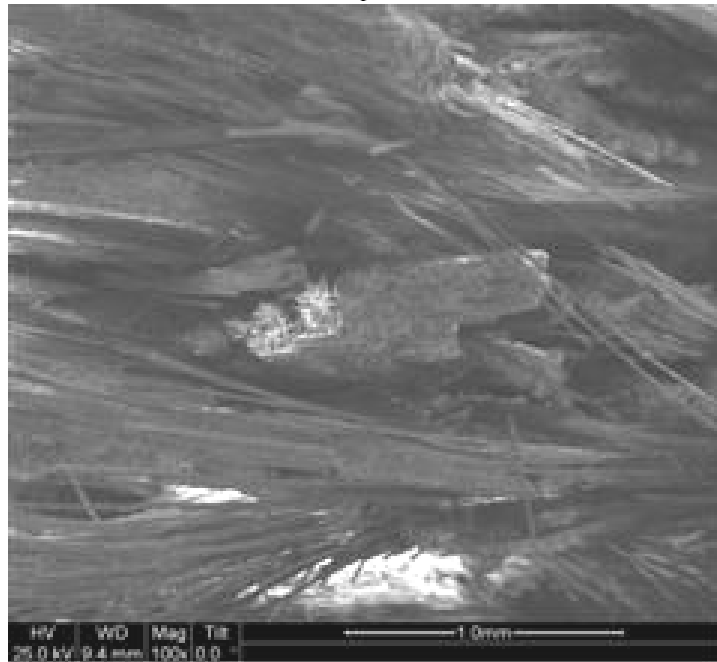


Figure 239. SEM micrograph of the fracture surface of the N720/AM specimen with  $\pm 45^\circ$  fiber orientation obtained in creep test conducted at 30 MPa at 1200°C in steam. Creep lifetime  $t_f = 1.08$  h.

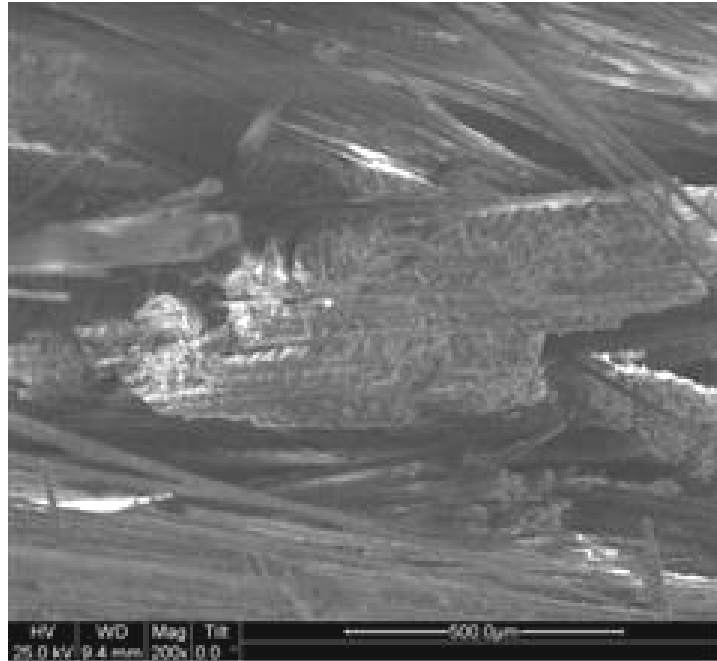


Figure 240. SEM micrograph of the fracture surface of the N720/AM specimen with  $\pm 45^\circ$  fiber orientation obtained in creep test conducted at 30 MPa at  $1200^\circ\text{C}$  in steam. Creep lifetime  $t_f = 1.08$  h.

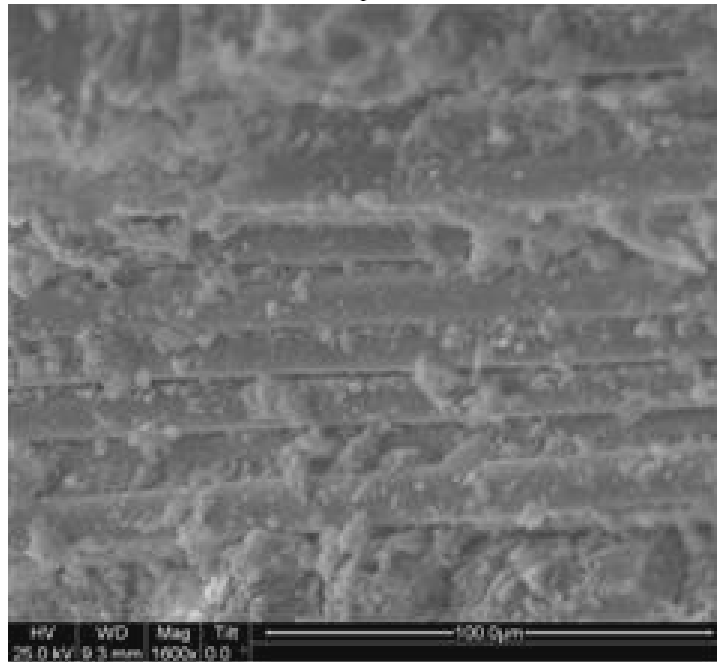


Figure 241. SEM micrograph of the fracture surface of the N720/AM specimen with  $\pm 45^\circ$  fiber orientation obtained in creep test conducted at 30 MPa at  $1200^\circ\text{C}$  in steam. Creep lifetime  $t_f = 1.08$  h.

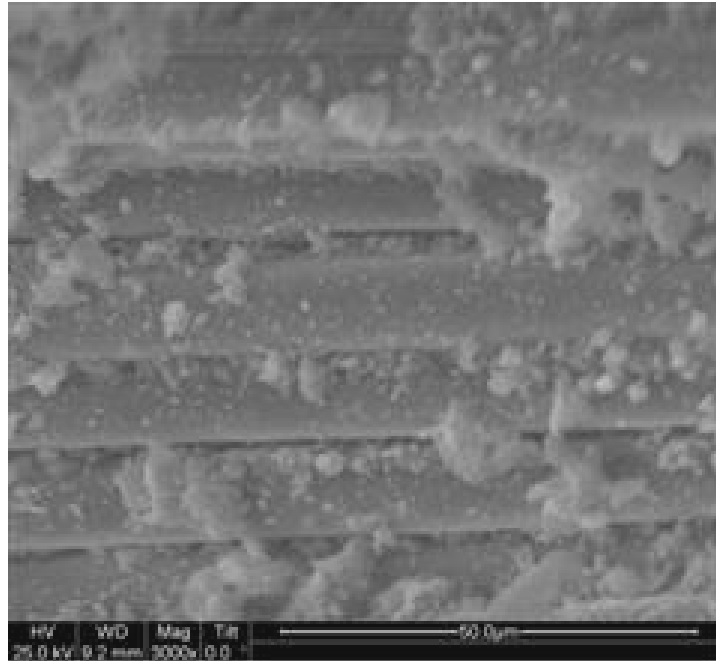


Figure 242. SEM micrograph of the fracture surface of the N720/AM specimen with  $\pm 45^\circ$  fiber orientation obtained in creep test conducted at 30 MPa at 1200°C in steam. Creep lifetime  $t_f = 1.08$  h.

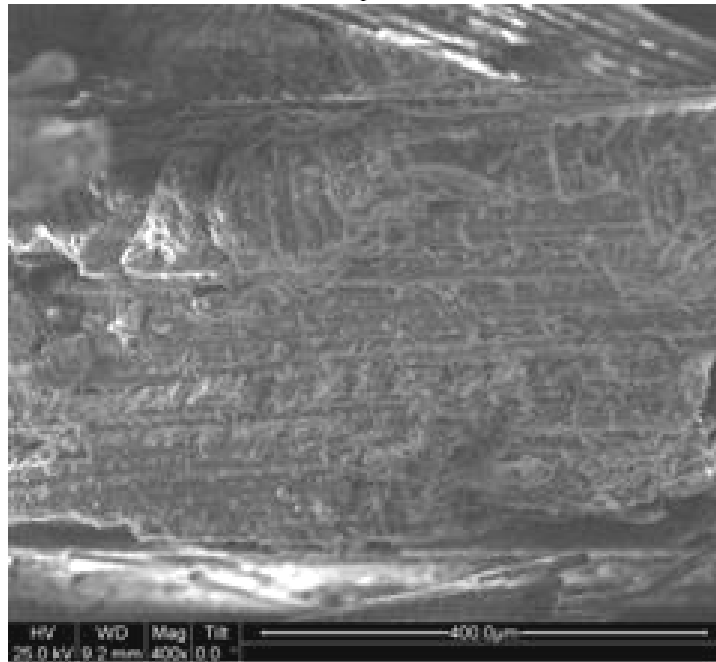


Figure 243. SEM micrograph of the fracture surface of the N720/AM specimen with  $\pm 45^\circ$  fiber orientation obtained in creep test conducted at 30 MPa at 1200°C in steam. Creep lifetime  $t_f = 1.08$  h.

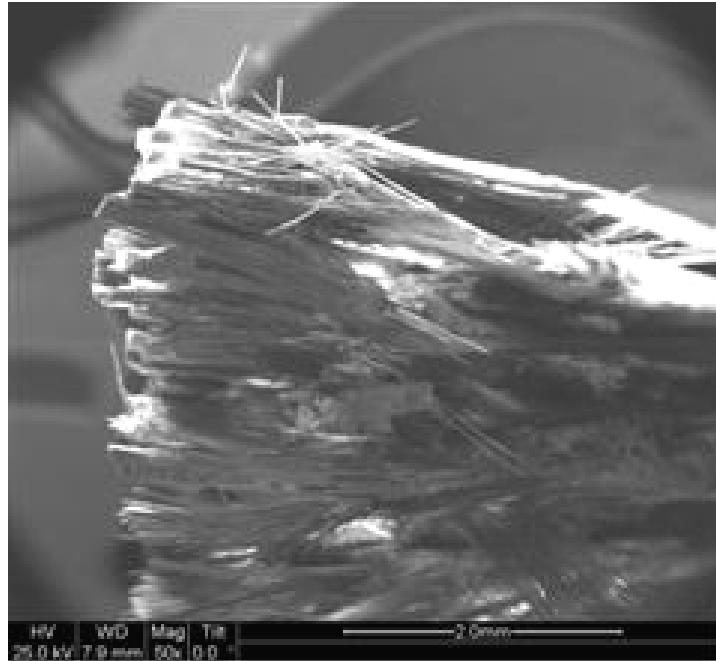


Figure 244. SEM micrograph of the fracture surface of the N720/AM specimen with  $\pm 45^\circ$  fiber orientation obtained in creep test conducted at 30 MPa at  $1200^\circ\text{C}$  in steam. Creep lifetime  $t_f = 1.08$  h.

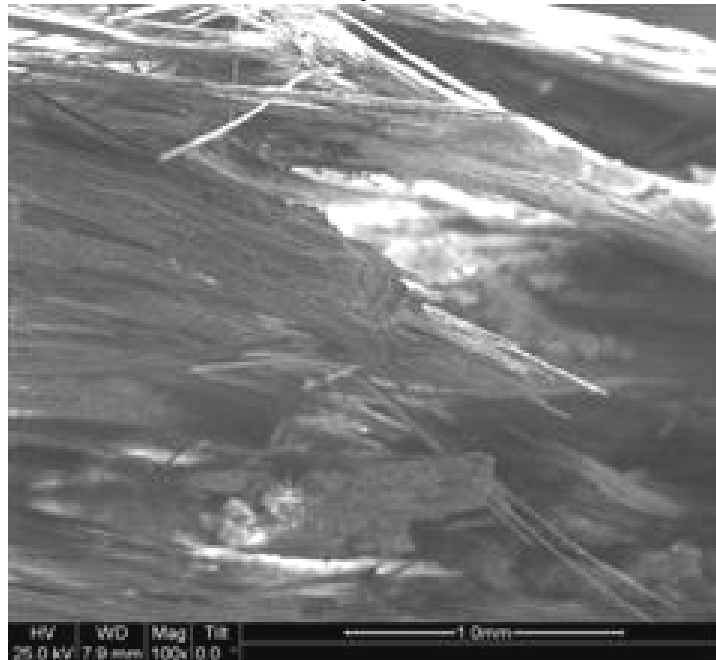


Figure 245. SEM micrograph of the fracture surface of the N720/AM specimen with  $\pm 45^\circ$  fiber orientation obtained in creep test conducted at 30 MPa at  $1200^\circ\text{C}$  in steam. Creep lifetime  $t_f = 1.08$  h.

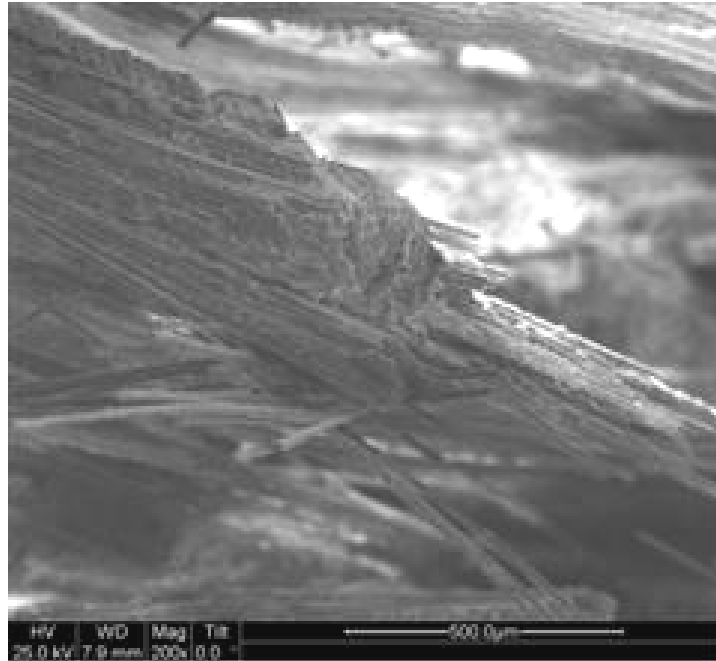


Figure 246. SEM micrograph of the fracture surface of the N720/AM specimen with  $\pm 45^\circ$  fiber orientation obtained in creep test conducted at 30 MPa at 1200°C in steam. Creep lifetime  $t_f = 1.08$  h.

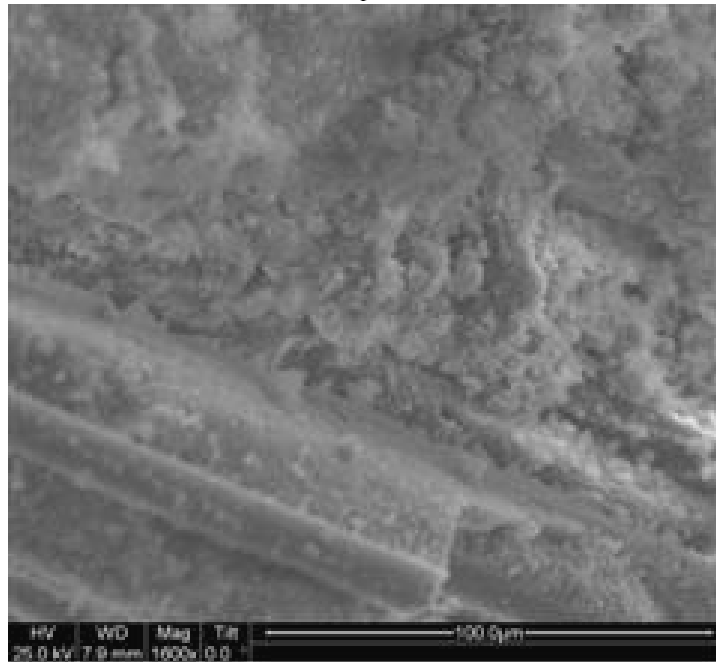


Figure 247. SEM micrograph of the fracture surface of the N720/AM specimen with  $\pm 45^\circ$  fiber orientation obtained in creep test conducted at 30 MPa at 1200°C in steam. Creep lifetime  $t_f = 1.08$  h.

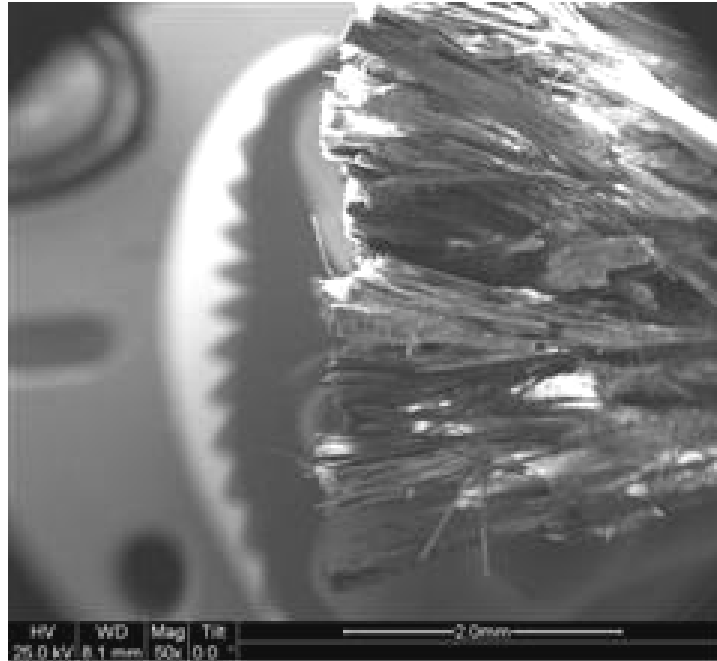


Figure 248. SEM micrograph of the fracture surface of the N720/AM specimen with  $\pm 45^\circ$  fiber orientation obtained in creep test conducted at 30 MPa at 1200°C in steam. Creep lifetime  $t_f = 1.08$  h.

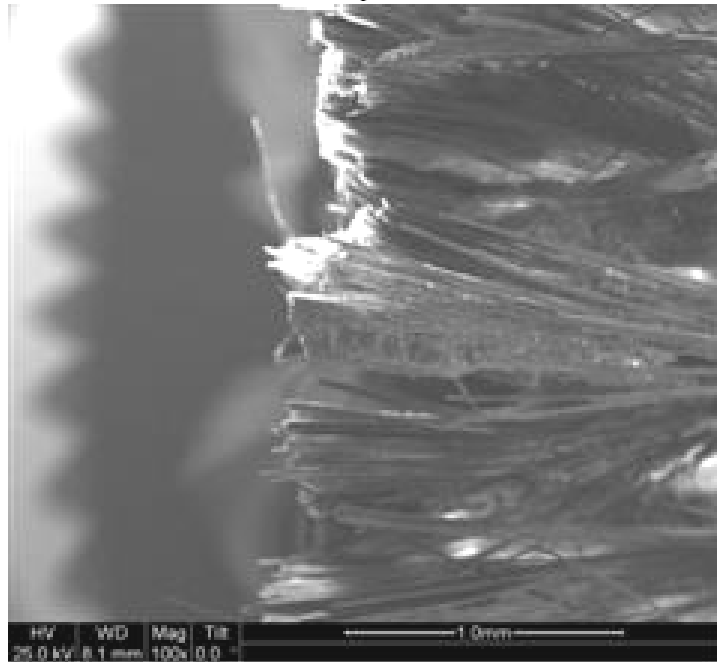


Figure 249. SEM micrograph of the fracture surface of the N720/AM specimen with  $\pm 45^\circ$  fiber orientation obtained in creep test conducted at 30 MPa at 1200°C in steam. Creep lifetime  $t_f = 1.08$  h.

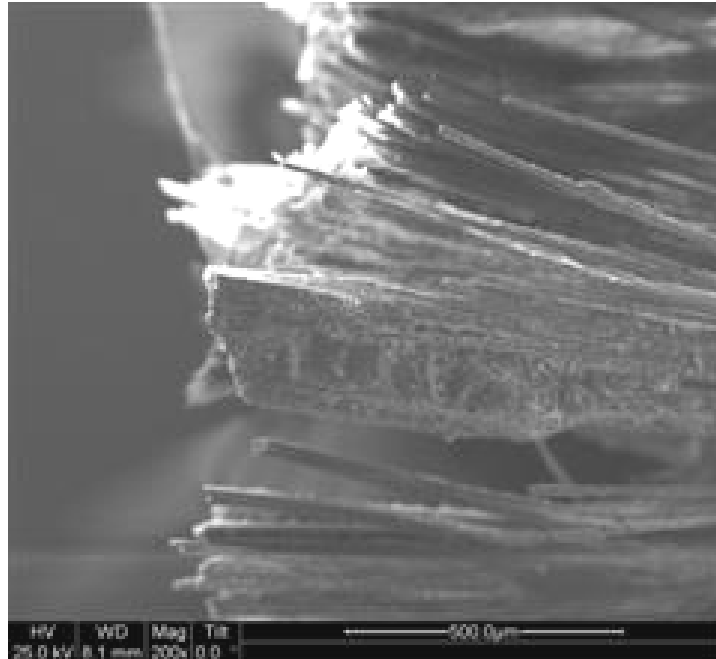


Figure 250. SEM micrograph of the fracture surface of the N720/AM specimen with  $\pm 45^\circ$  fiber orientation obtained in creep test conducted at 30 MPa at  $1200^\circ\text{C}$  in steam. Creep lifetime  $t_f = 1.08$  h.

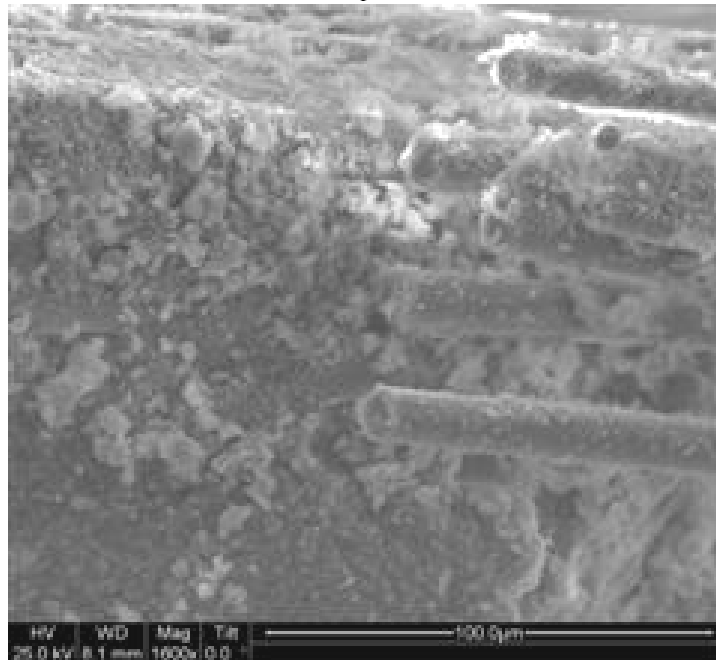


Figure 251. SEM micrograph of the fracture surface of the N720/AM specimen with  $\pm 45^\circ$  fiber orientation obtained in creep test conducted at 30 MPa at  $1200^\circ\text{C}$  in steam. Creep lifetime  $t_f = 1.08$  h.

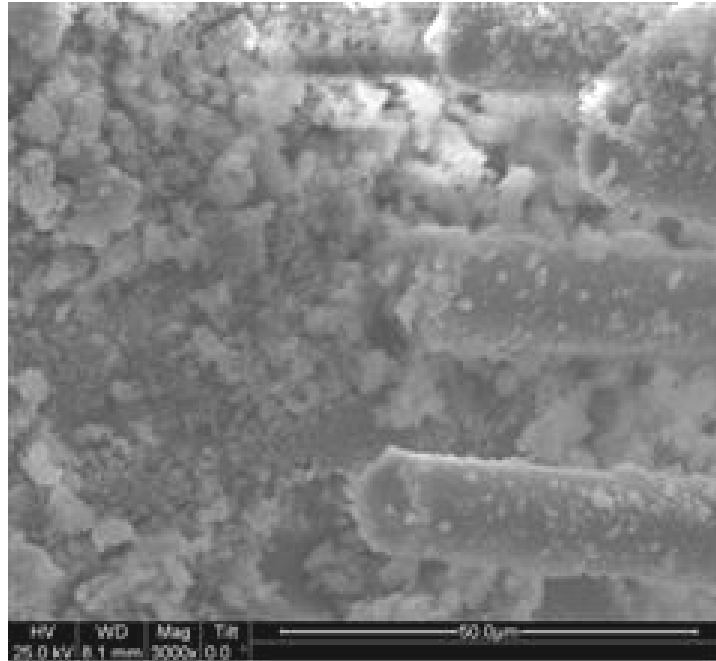


Figure 252. SEM micrograph of the fracture surface of the N720/AM specimen with  $\pm 45^\circ$  fiber orientation obtained in creep test conducted at 30 MPa at 1200°C in steam. Creep lifetime  $t_f = 1.08$  h.

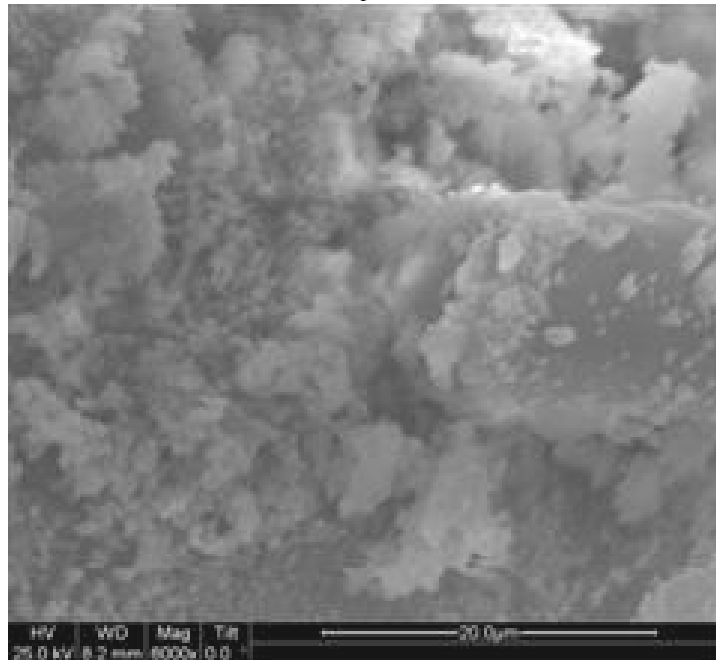


Figure 253. SEM micrograph of the fracture surface of the N720/AM specimen with  $\pm 45^\circ$  fiber orientation obtained in creep test conducted at 30 MPa at 1200°C in steam. Creep lifetime  $t_f = 1.08$  h.

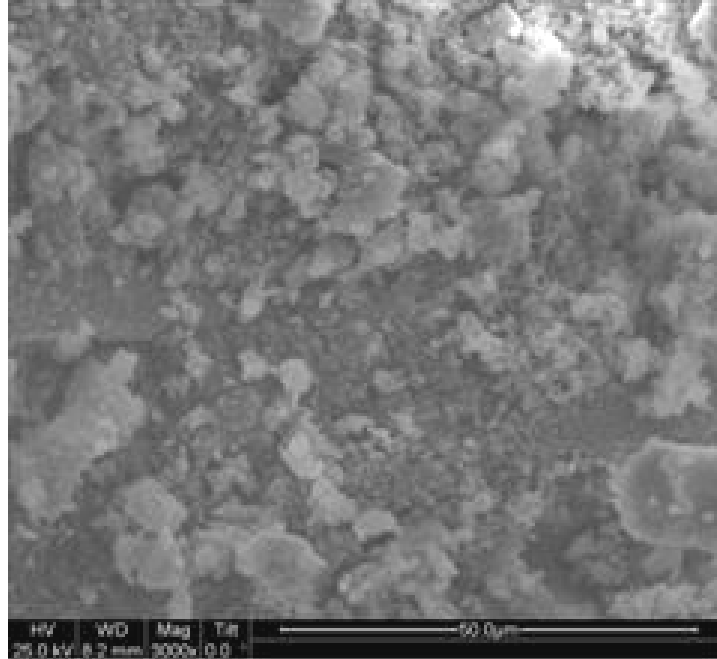


Figure 254. SEM micrograph of the fracture surface of the N720/AM specimen with  $\pm 45^\circ$  fiber orientation obtained in creep test conducted at 30 MPa at 1200°C in steam. Creep lifetime  $t_f = 1.08$  h.

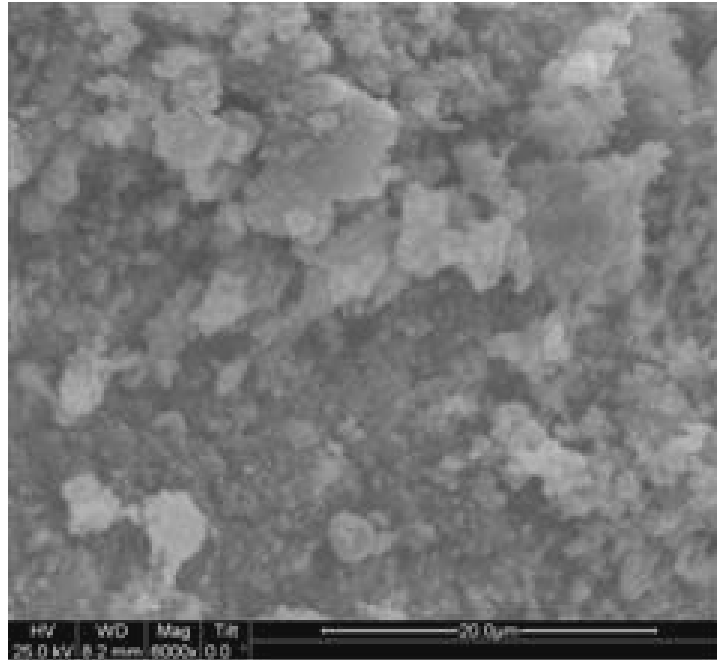


Figure 255. SEM micrograph of the fracture surface of the N720/AM specimen with  $\pm 45^\circ$  fiber orientation obtained in creep test conducted at 30 MPa at 1200°C in steam. Creep lifetime  $t_f = 1.08$  h.

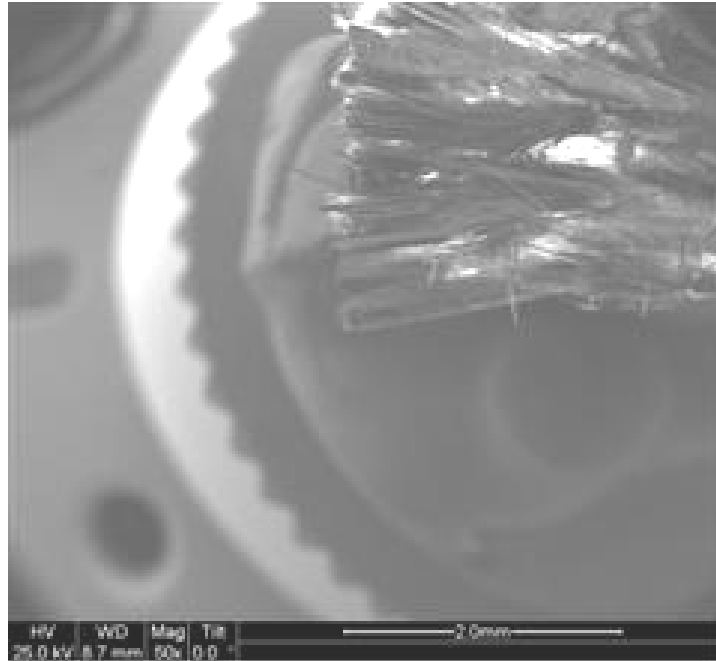


Figure 256. SEM micrograph of the fracture surface of the N720/AM specimen with  $\pm 45^\circ$  fiber orientation obtained in creep test conducted at 30 MPa at 1200°C in steam. Creep lifetime  $t_f = 1.08$  h.



Figure 257. SEM micrograph of the fracture surface of the N720/AM specimen with  $\pm 45^\circ$  fiber orientation obtained in creep test conducted at 30 MPa at 1200°C in steam. Creep lifetime  $t_f = 1.08$  h.

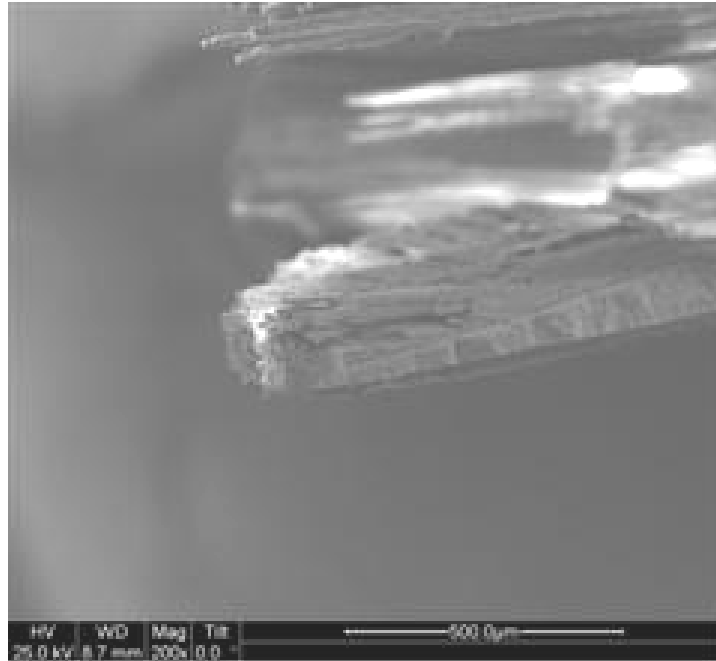


Figure 258. SEM micrograph of the fracture surface of the N720/AM specimen with  $\pm 45^\circ$  fiber orientation obtained in creep test conducted at 30 MPa at 1200°C in steam. Creep lifetime  $t_f = 1.08$  h.

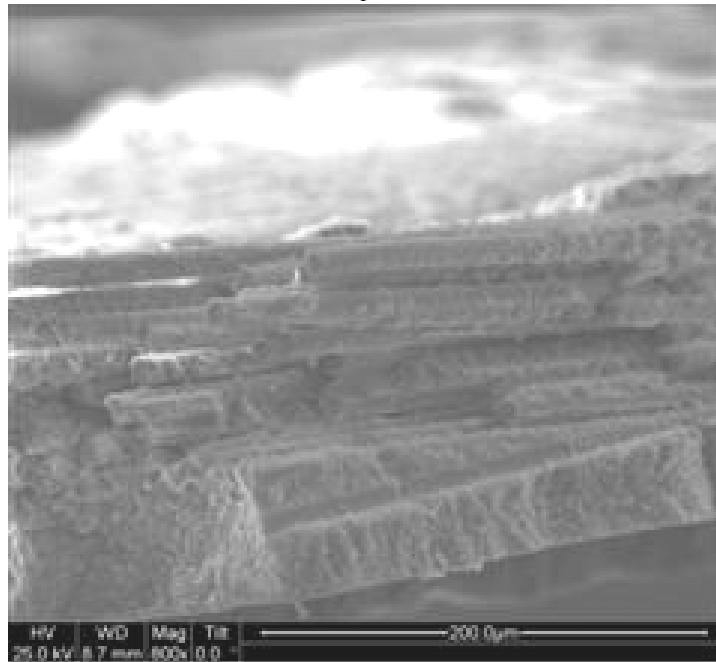


Figure 259. SEM micrograph of the fracture surface of the N720/AM specimen with  $\pm 45^\circ$  fiber orientation obtained in creep test conducted at 30 MPa at 1200°C in steam. Creep lifetime  $t_f = 1.08$  h.

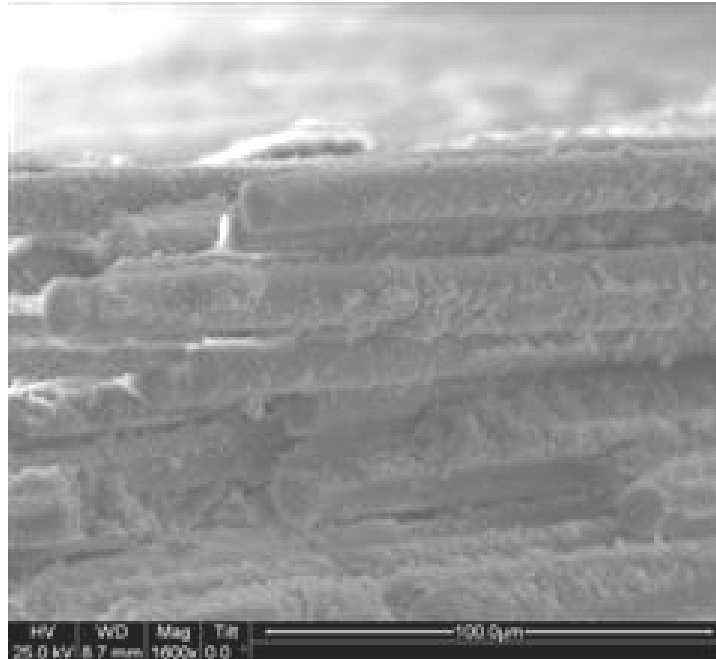


Figure 260. SEM micrograph of the fracture surface of the N720/AM specimen with  $\pm 45^\circ$  fiber orientation obtained in creep test conducted at 30 MPa at 1200°C in steam. Creep lifetime  $t_f = 1.08$  h.

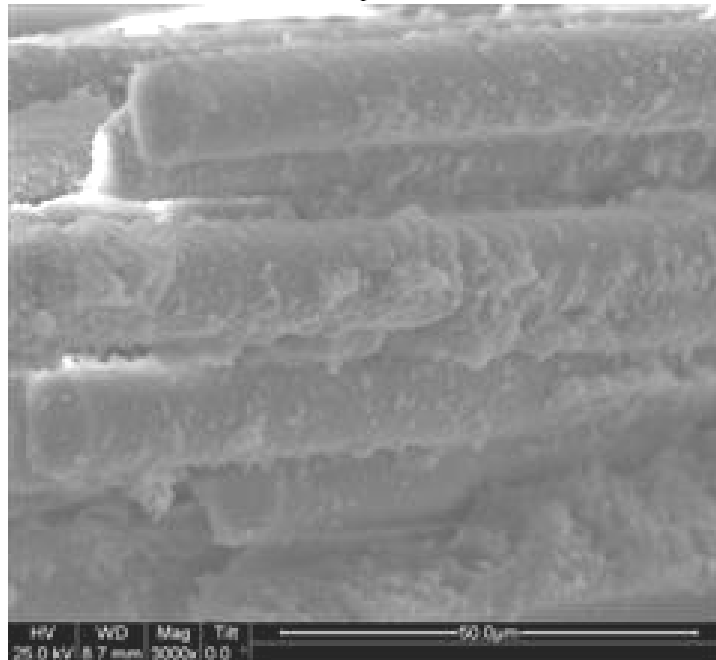


Figure 261. SEM micrograph of the fracture surface of the N720/AM specimen with  $\pm 45^\circ$  fiber orientation obtained in creep test conducted at 30 MPa at 1200°C in steam. Creep lifetime  $t_f = 1.08$  h.

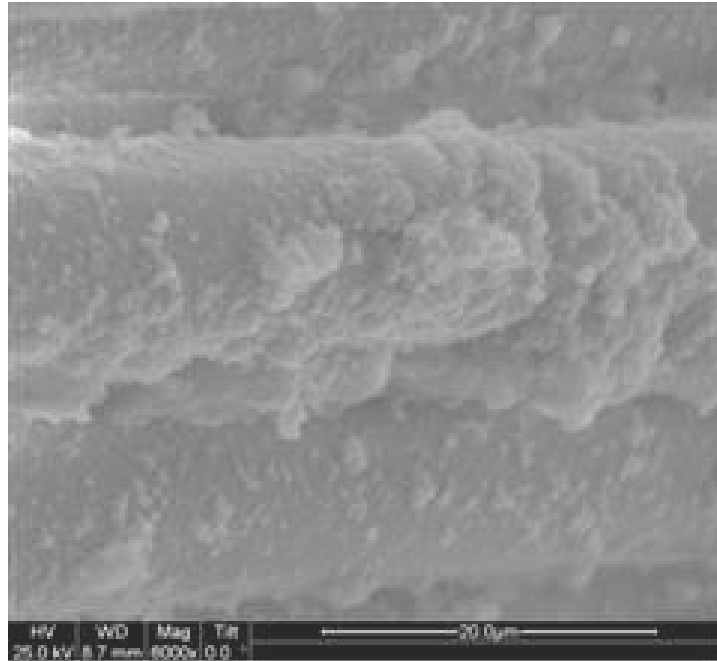


Figure 262. SEM micrograph of the fracture surface of the N720/AM specimen with  $\pm 45^\circ$  fiber orientation obtained in creep test conducted at 30 MPa at 1200°C in steam. Creep lifetime  $t_f = 1.08$  h.

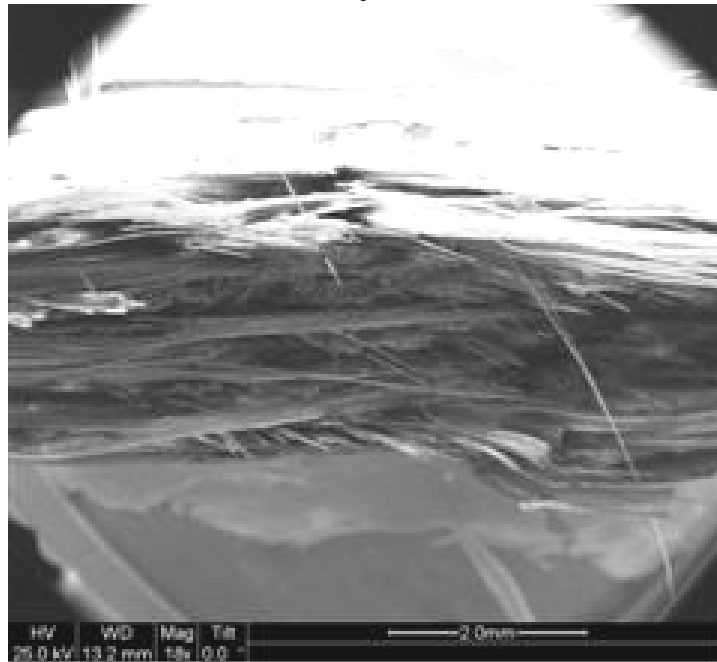


Figure 263. SEM micrograph of the fracture surface of the N720/AM specimen with  $\pm 45^\circ$  fiber orientation obtained in creep test conducted at 32 MPa at 1200°C in steam. Creep lifetime  $t_f = 0.02$  h.

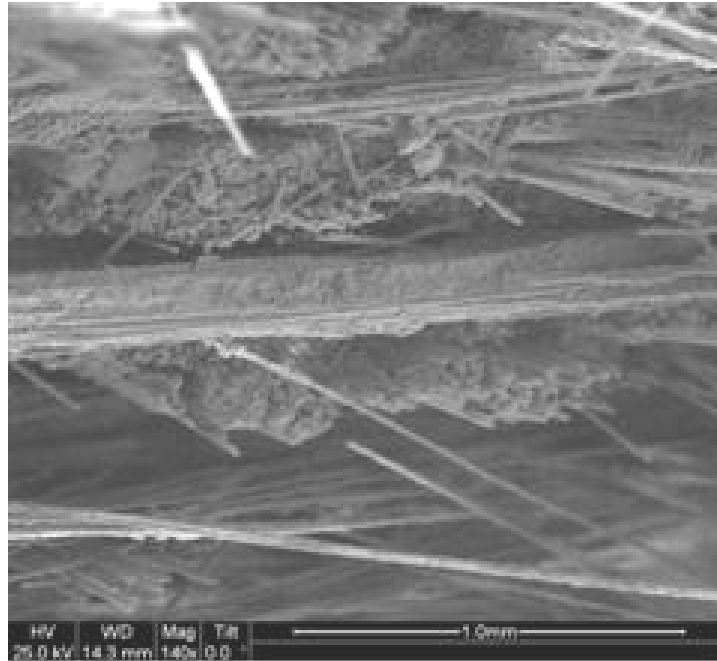


Figure 264. SEM micrograph of the fracture surface of the N720/AM specimen with  $\pm 45^\circ$  fiber orientation obtained in creep test conducted at 32 MPa at 1200°C in steam. Creep lifetime  $t_f = 0.02$  h.

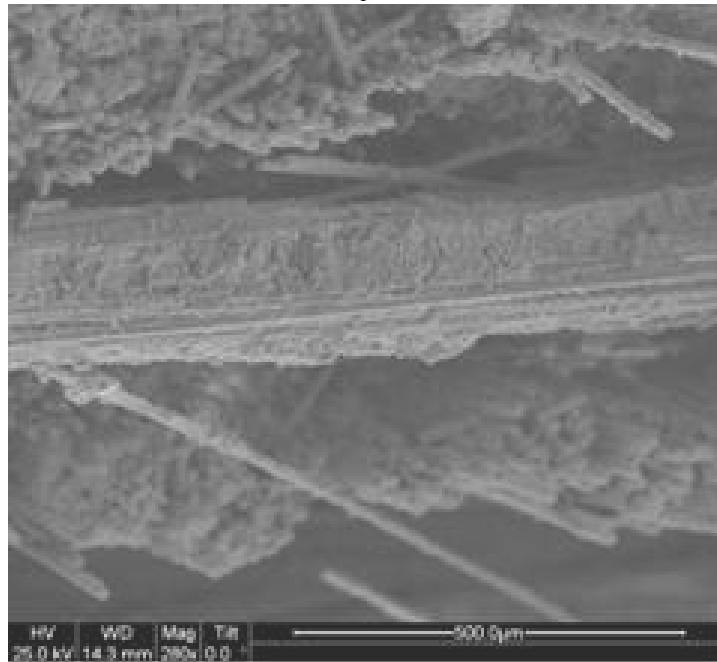


Figure 265. SEM micrograph of the fracture surface of the N720/AM specimen with  $\pm 45^\circ$  fiber orientation obtained in creep test conducted at 32 MPa at 1200°C in steam. Creep lifetime  $t_f = 0.02$  h.

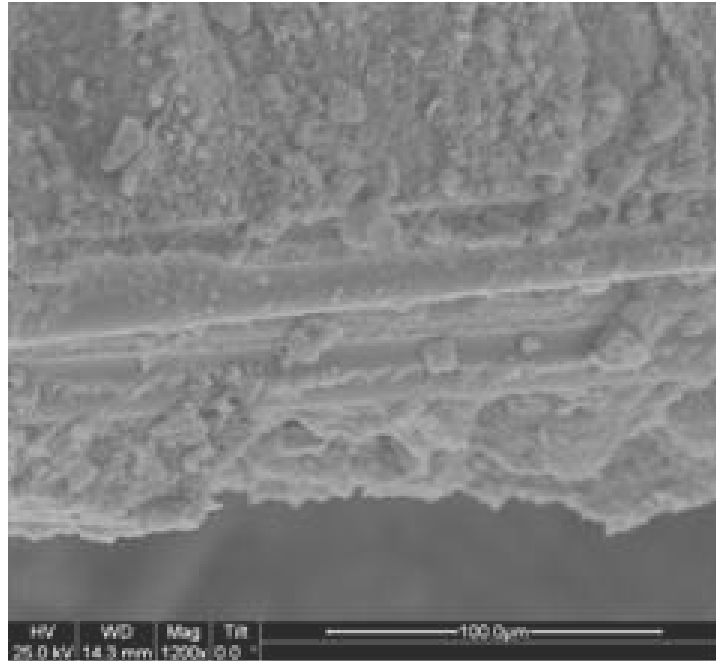


Figure 266. SEM micrograph of the fracture surface of the N720/AM specimen with  $\pm 45^\circ$  fiber orientation obtained in creep test conducted at 32 MPa at 1200°C in steam. Creep lifetime  $t_f = 0.02$  h.

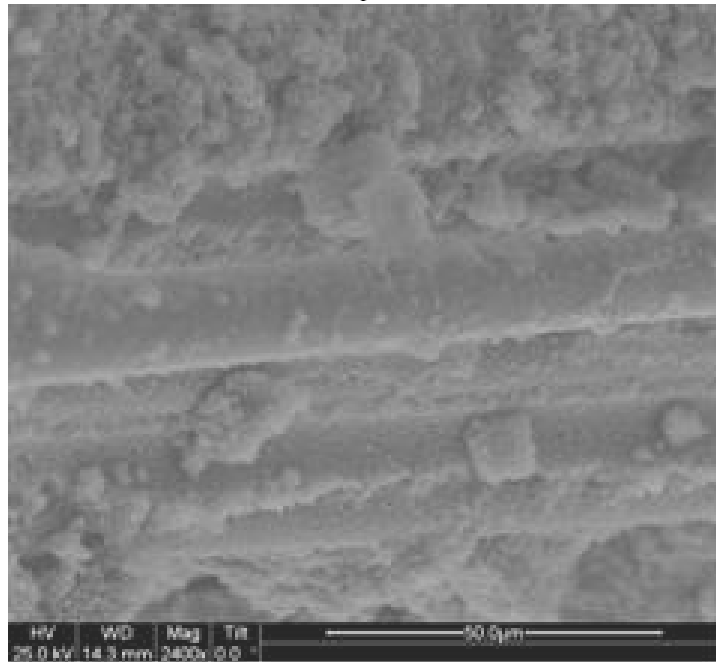


Figure 267. SEM micrograph of the fracture surface of the N720/AM specimen with  $\pm 45^\circ$  fiber orientation obtained in creep test conducted at 32 MPa at 1200°C in steam. Creep lifetime  $t_f = 0.02$  h.

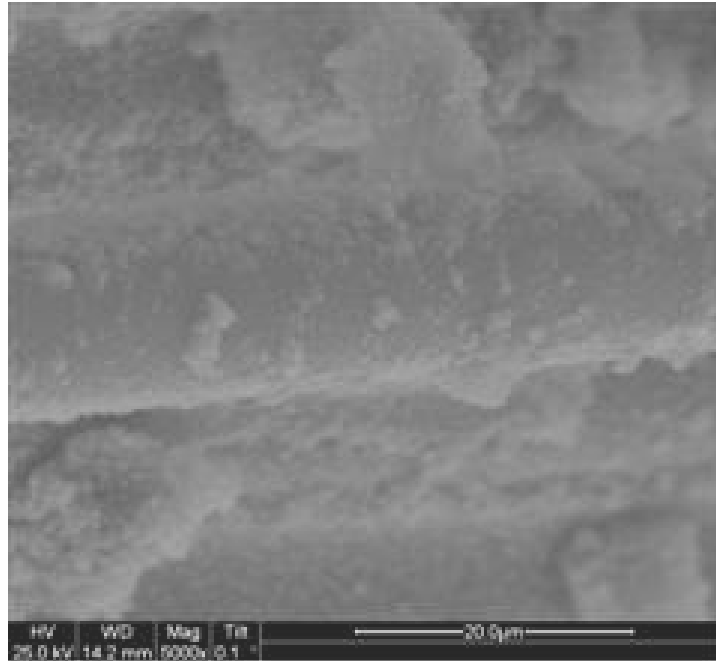


Figure 268. SEM micrograph of the fracture surface of the N720/AM specimen with  $\pm 45^\circ$  fiber orientation obtained in creep test conducted at 32 MPa at 1200°C in steam. Creep lifetime  $t_f = 0.02$  h.

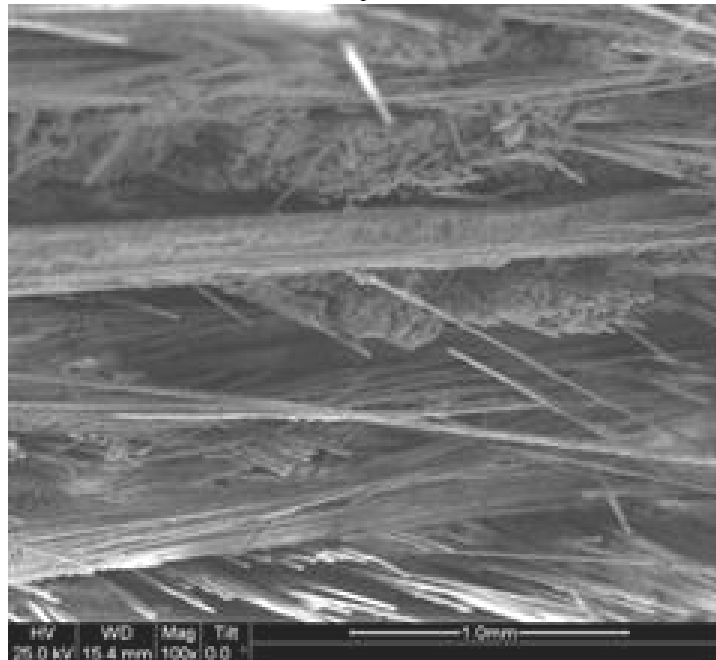


Figure 269. SEM micrograph of the fracture surface of the N720/AM specimen with  $\pm 45^\circ$  fiber orientation obtained in creep test conducted at 32 MPa at 1200°C in steam. Creep lifetime  $t_f = 0.02$  h.

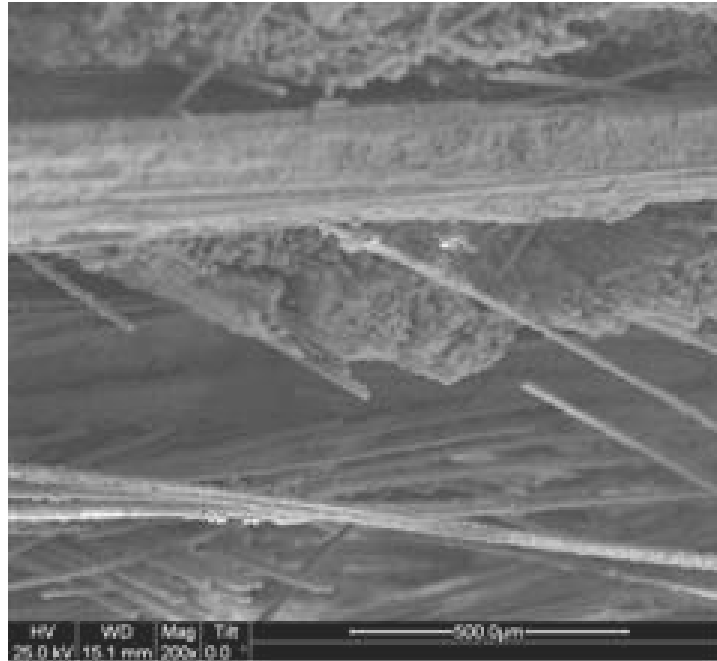


Figure 270. SEM micrograph of the fracture surface of the N720/AM specimen with  $\pm 45^\circ$  fiber orientation obtained in creep test conducted at 32 MPa at 1200°C in steam. Creep lifetime  $t_f = 0.02$  h.

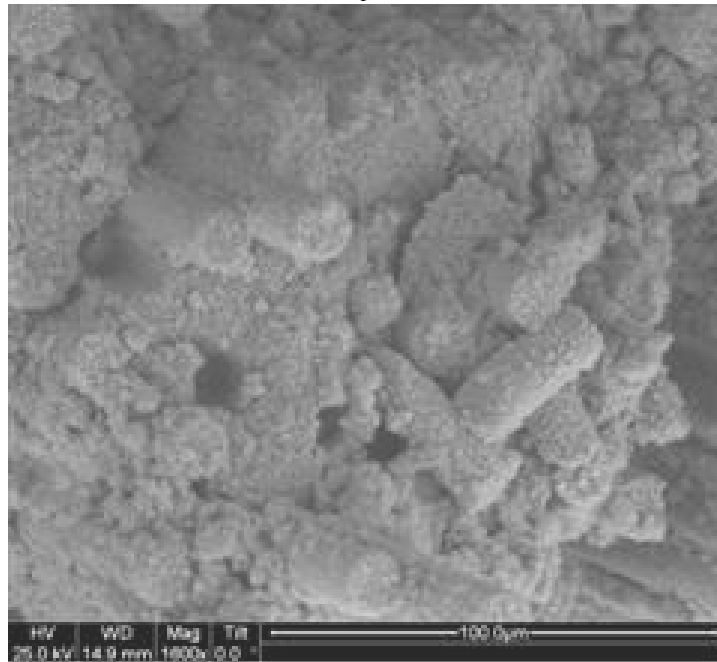


Figure 271. SEM micrograph of the fracture surface of the N720/AM specimen with  $\pm 45^\circ$  fiber orientation obtained in creep test conducted at 32 MPa at 1200°C in steam. Creep lifetime  $t_f = 0.02$  h.

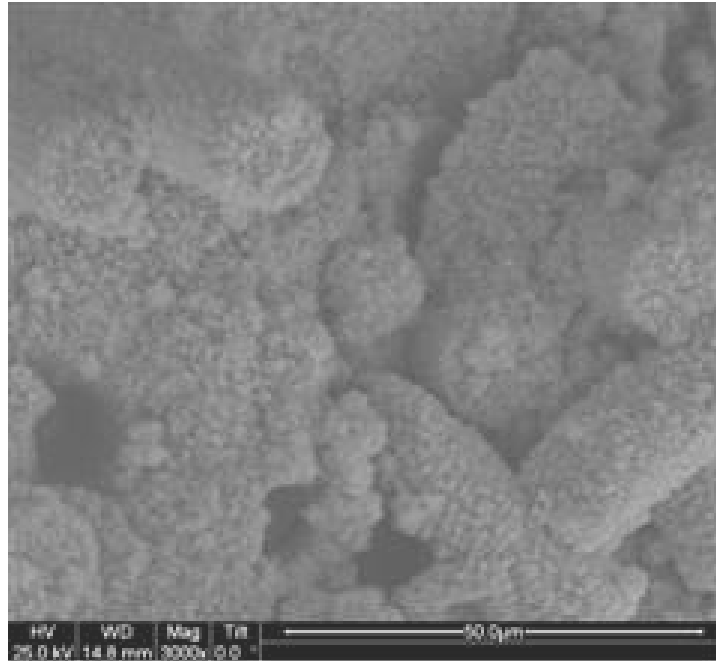


Figure 272. SEM micrograph of the fracture surface of the N720/AM specimen with  $\pm 45^\circ$  fiber orientation obtained in creep test conducted at 32 MPa at 1200°C in steam. Creep lifetime  $t_f = 0.02$  h.

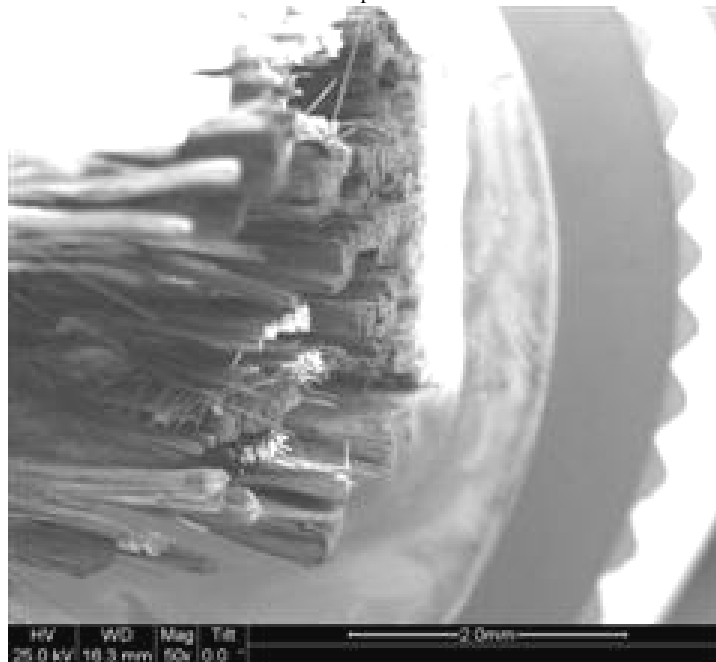


Figure 273. SEM micrograph of the fracture surface of the N720/AM specimen with  $\pm 45^\circ$  fiber orientation obtained in creep test conducted at 32 MPa at 1200°C in steam. Creep lifetime  $t_f = 0.02$  h.

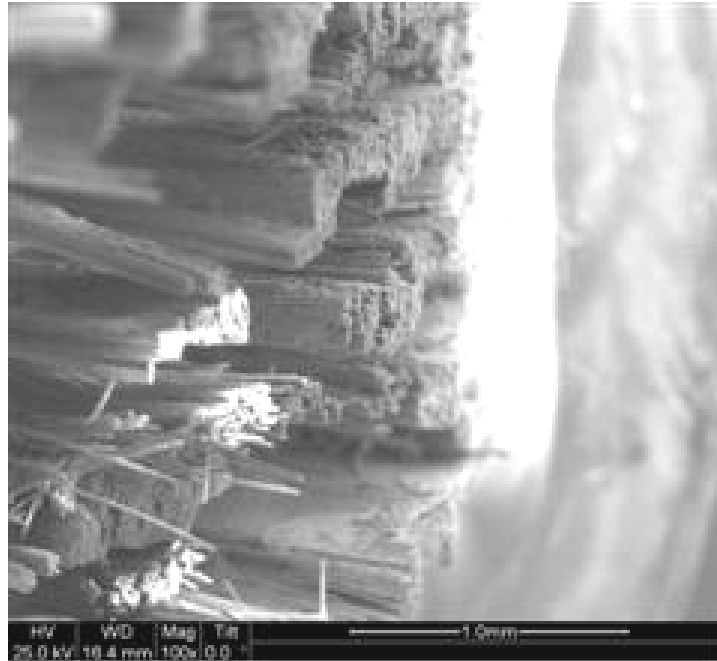


Figure 274. SEM micrograph of the fracture surface of the N720/AM specimen with  $\pm 45^\circ$  fiber orientation obtained in creep test conducted at 32 MPa at 1200°C in steam. Creep lifetime  $t_f = 0.02$  h.

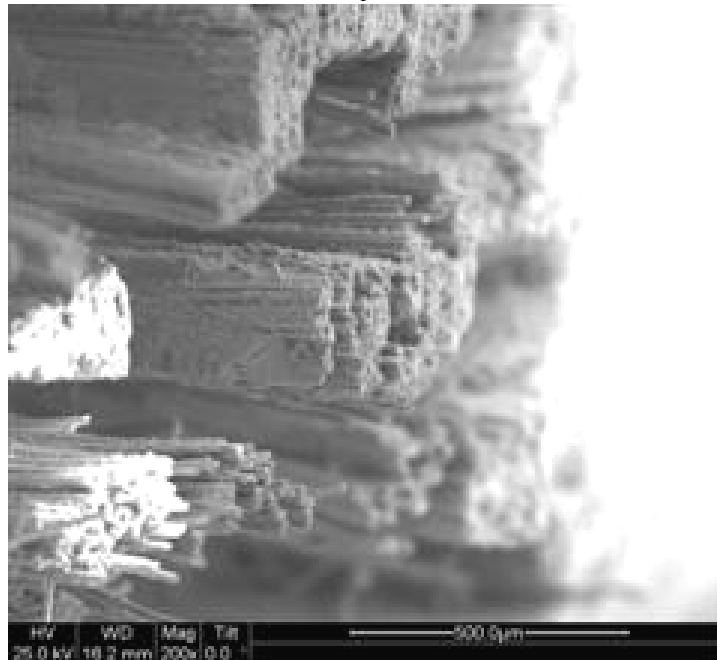


Figure 275. SEM micrograph of the fracture surface of the N720/AM specimen with  $\pm 45^\circ$  fiber orientation obtained in creep test conducted at 32 MPa at 1200°C in steam. Creep lifetime  $t_f = 0.02$  h.

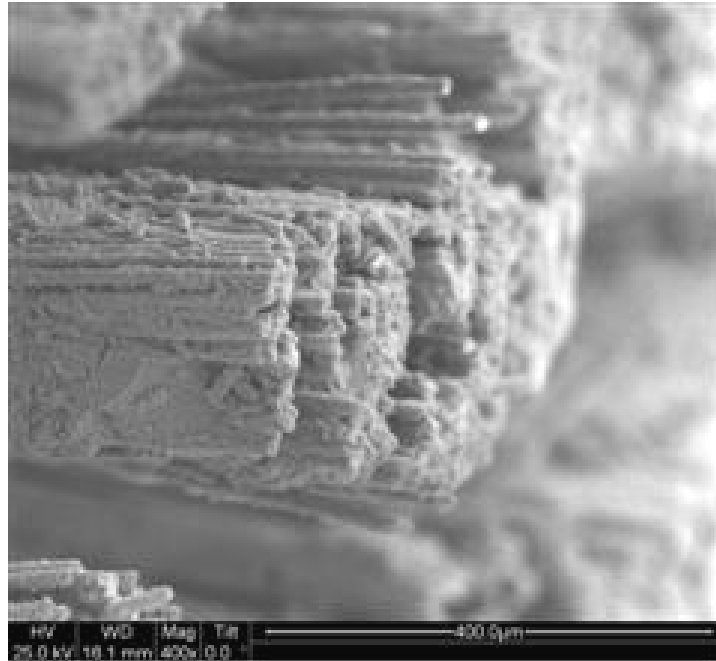


Figure 276. SEM micrograph of the fracture surface of the N720/AM specimen with  $\pm 45^\circ$  fiber orientation obtained in creep test conducted at 32 MPa at 1200°C in steam. Creep lifetime  $t_f = 0.02$  h.

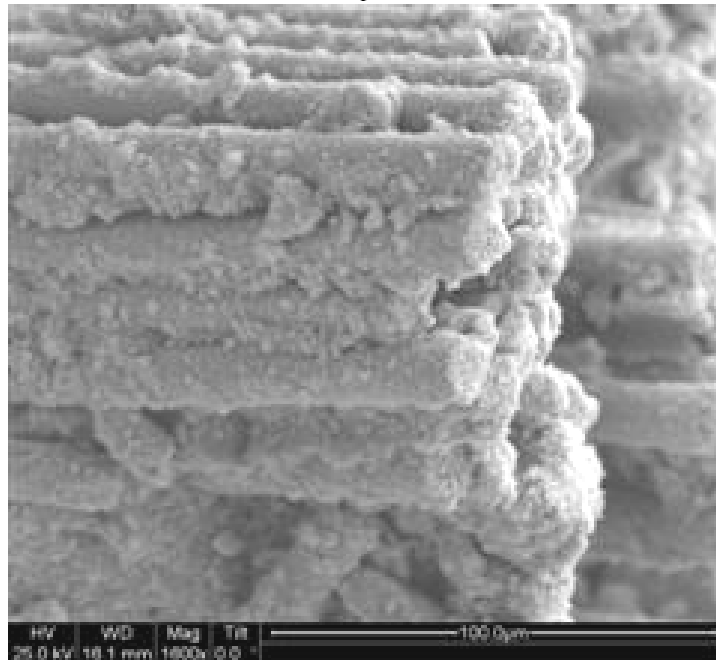


Figure 277. SEM micrograph of the fracture surface of the N720/AM specimen with  $\pm 45^\circ$  fiber orientation obtained in creep test conducted at 32 MPa at 1200°C in steam. Creep lifetime  $t_f = 0.02$  h.

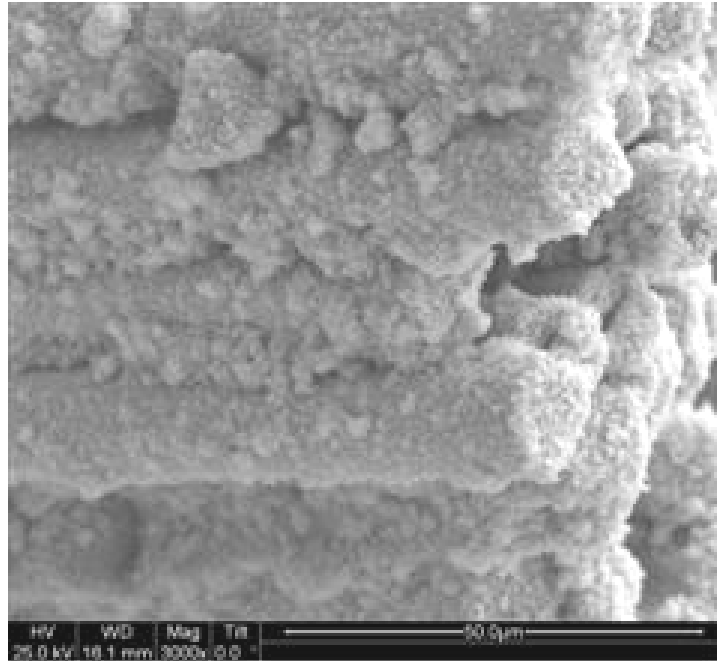


Figure 278. SEM micrograph of the fracture surface of the N720/AM specimen with  $\pm 45^\circ$  fiber orientation obtained in creep test conducted at 32 MPa at 1200°C in steam. Creep lifetime  $t_f = 0.02$  h.

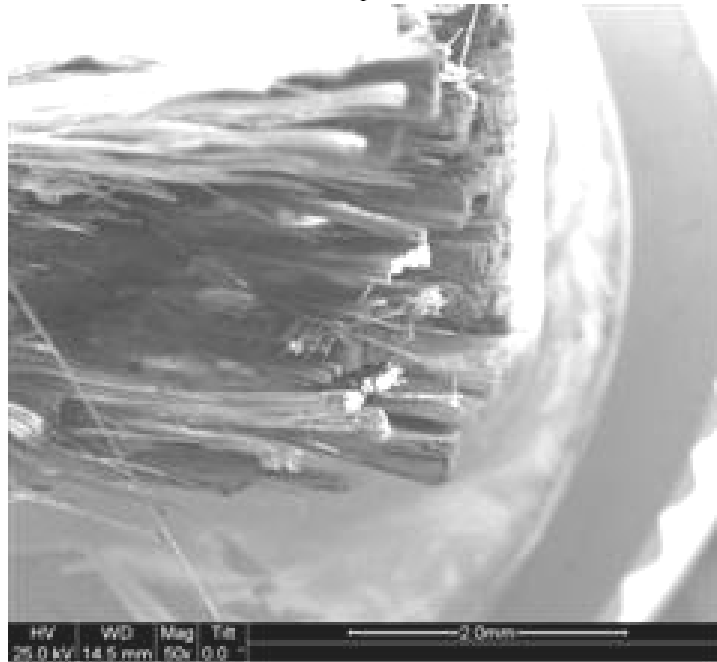


Figure 279. SEM micrograph of the fracture surface of the N720/AM specimen with  $\pm 45^\circ$  fiber orientation obtained in creep test conducted at 32 MPa at 1200°C in steam. Creep lifetime  $t_f = 0.02$  h.

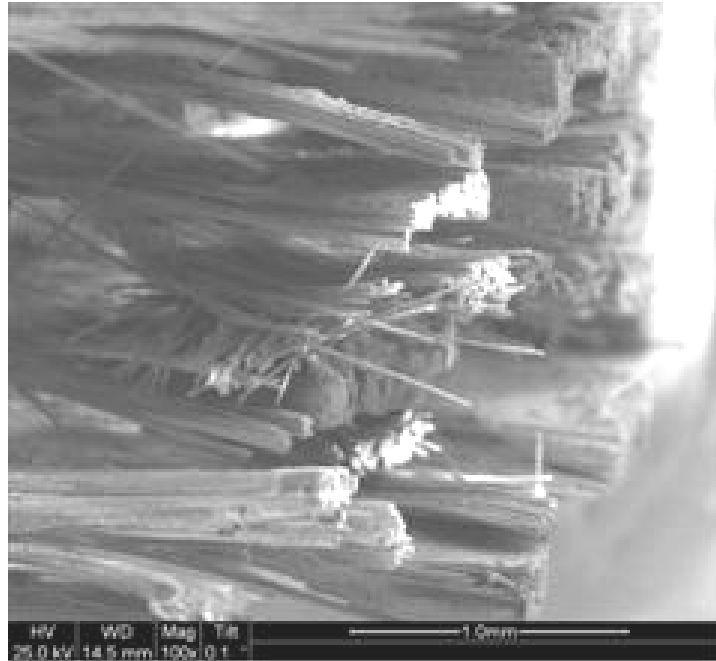


Figure 280. SEM micrograph of the fracture surface of the N720/AM specimen with  $\pm 45^\circ$  fiber orientation obtained in creep test conducted at 32 MPa at 1200°C in steam. Creep lifetime  $t_f = 0.02$  h.



Figure 281. SEM micrograph of the fracture surface of the N720/AM specimen with  $\pm 45^\circ$  fiber orientation obtained in creep test conducted at 32 MPa at 1200°C in steam. Creep lifetime  $t_f = 0.02$  h.

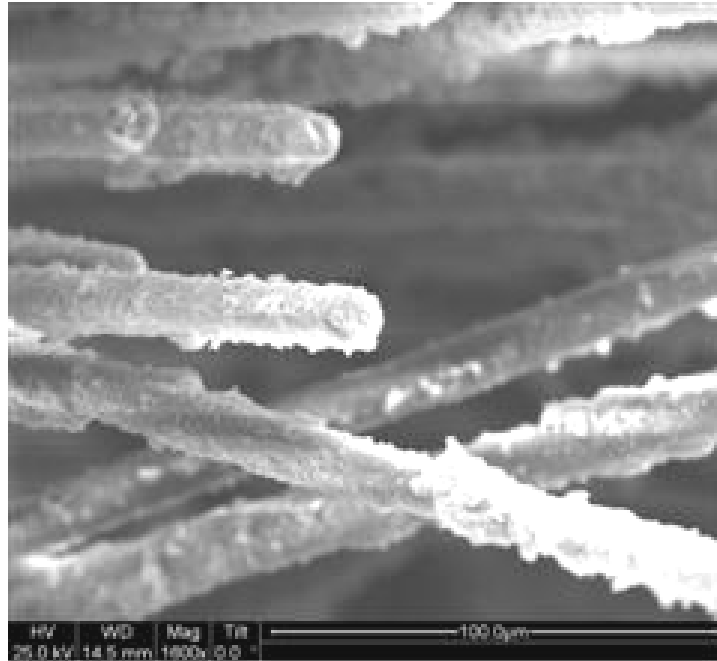


Figure 282. SEM micrograph of the fracture surface of the N720/AM specimen with  $\pm 45^\circ$  fiber orientation obtained in creep test conducted at 32 MPa at 1200°C in steam. Creep lifetime  $t_f = 0.02$  h.

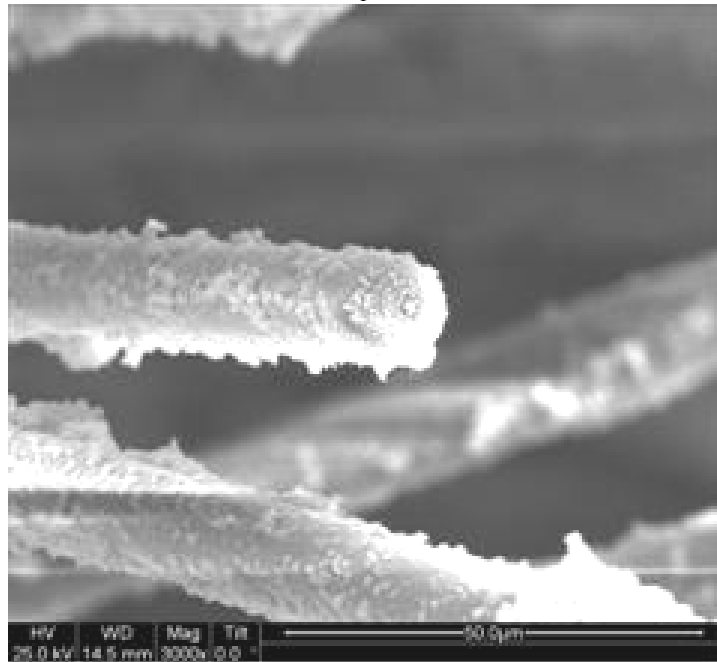


Figure 283. SEM micrograph of the fracture surface of the N720/AM specimen with  $\pm 45^\circ$  fiber orientation obtained in creep test conducted at 32 MPa at 1200°C in steam. Creep lifetime  $t_f = 0.02$  h.

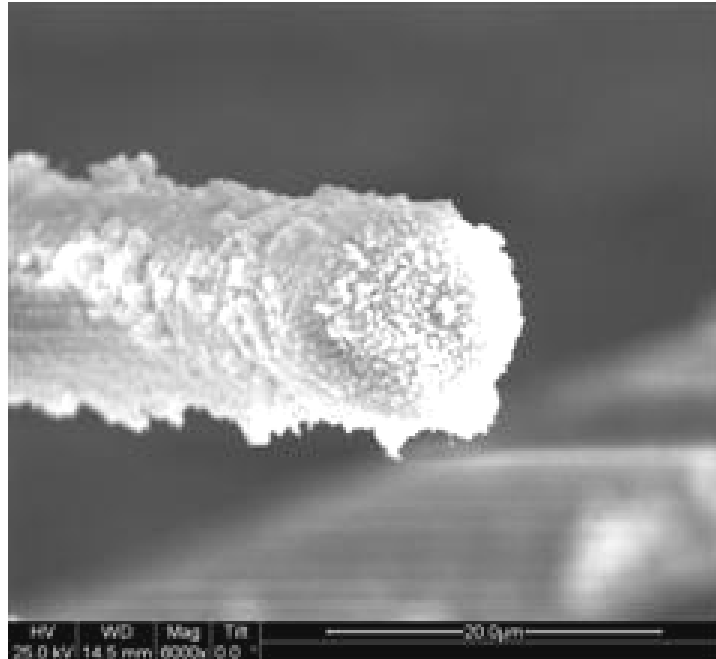


Figure 284. SEM micrograph of the fracture surface of the N720/AM specimen with  $\pm 45^\circ$  fiber orientation obtained in creep test conducted at 32 MPa at 1200°C in steam. Creep lifetime  $t_f = 0.02$  h.

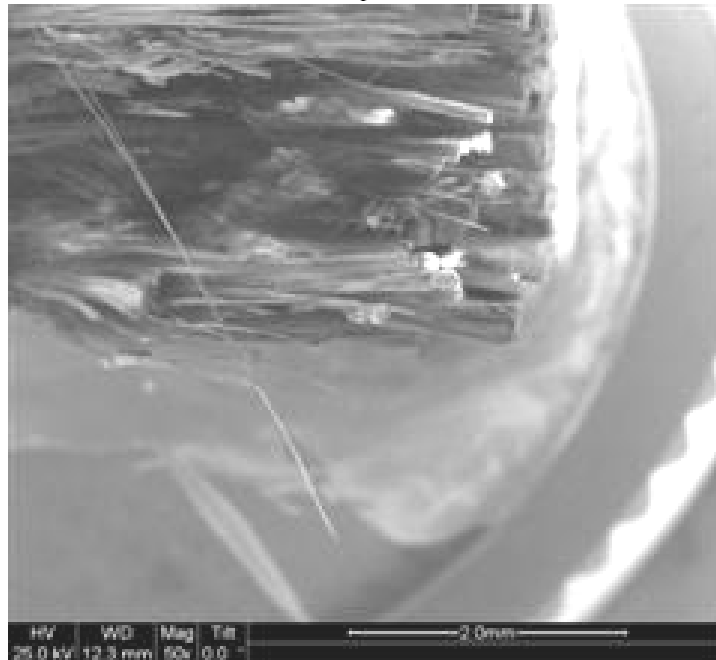


Figure 285. SEM micrograph of the fracture surface of the N720/AM specimen with  $\pm 45^\circ$  fiber orientation obtained in creep test conducted at 32 MPa at 1200°C in steam. Creep lifetime  $t_f = 0.02$  h.

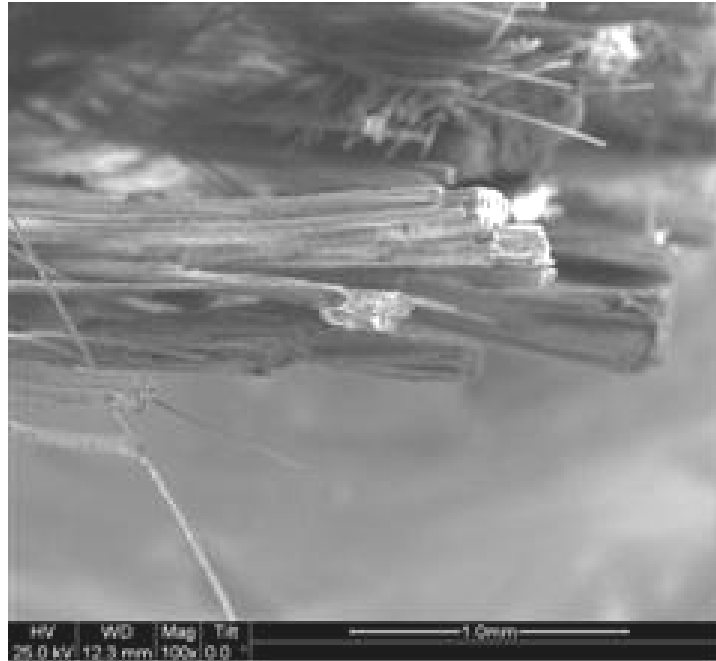


Figure 286. SEM micrograph of the fracture surface of the N720/AM specimen with  $\pm 45^\circ$  fiber orientation obtained in creep test conducted at 32 MPa at 1200°C in steam. Creep lifetime  $t_f = 0.02$  h.

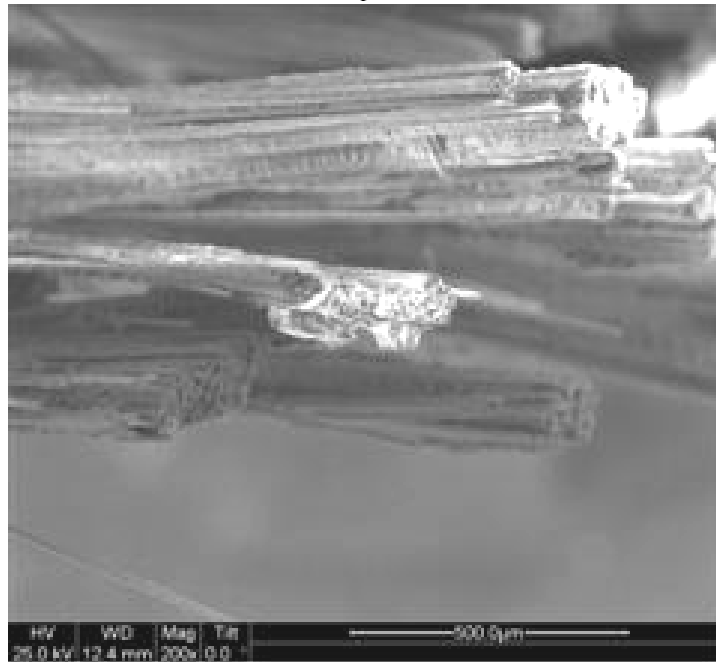


Figure 287. SEM micrograph of the fracture surface of the N720/AM specimen with  $\pm 45^\circ$  fiber orientation obtained in creep test conducted at 32 MPa at 1200°C in steam. Creep lifetime  $t_f = 0.02$  h.

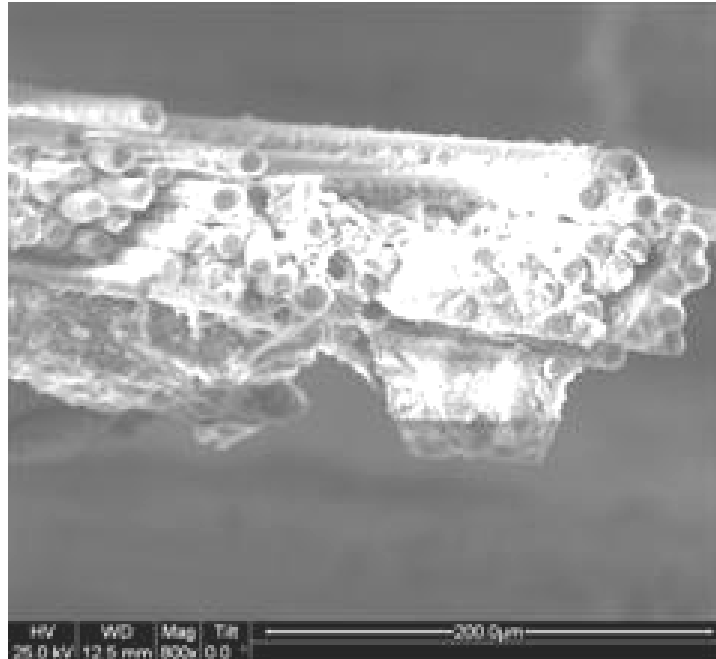


Figure 288. SEM micrograph of the fracture surface of the N720/AM specimen with  $\pm 45^\circ$  fiber orientation obtained in creep test conducted at 32 MPa at 1200°C in steam. Creep lifetime  $t_f = 0.02$  h.

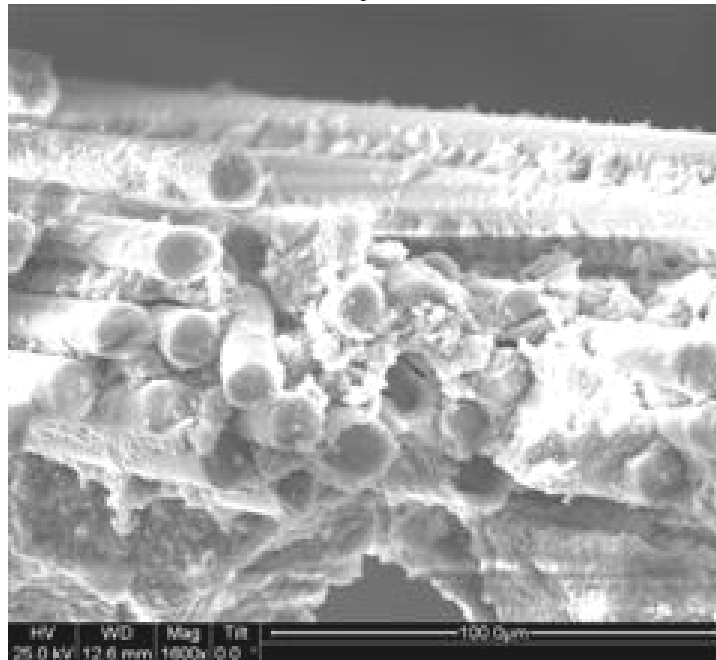


Figure 289. SEM micrograph of the fracture surface of the N720/AM specimen with  $\pm 45^\circ$  fiber orientation obtained in creep test conducted at 32 MPa at 1200°C in steam. Creep lifetime  $t_f = 0.02$  h.

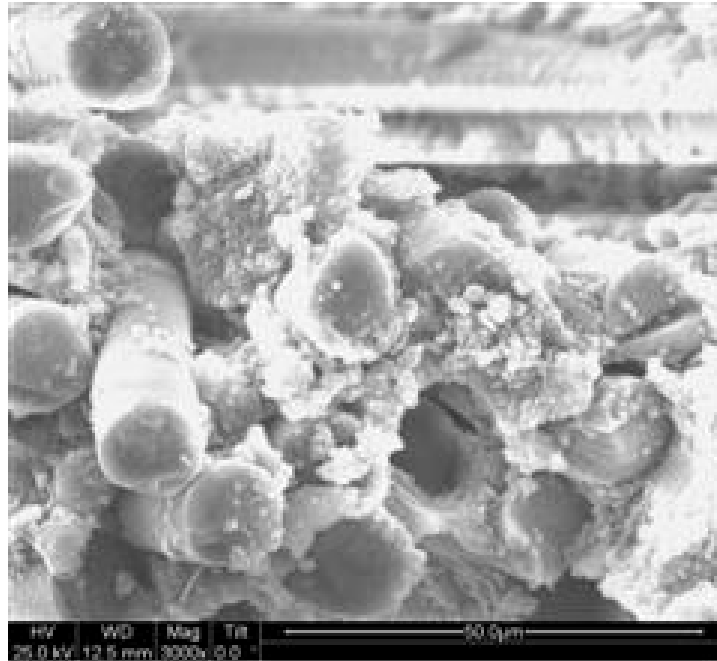


Figure 290. SEM micrograph of the fracture surface of the N720/AM specimen with  $\pm 45^\circ$  fiber orientation obtained in creep test conducted at 32 MPa at 1200°C in steam. Creep lifetime  $t_f = 0.02$  h.

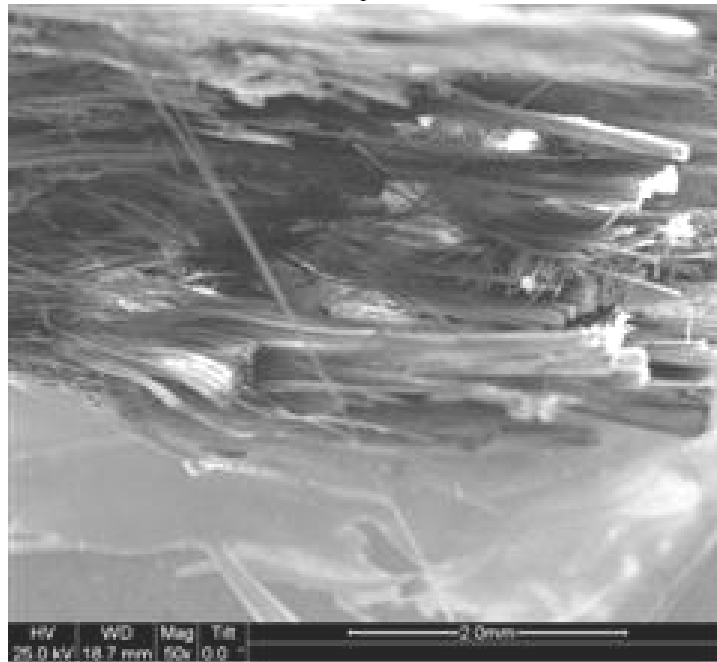


Figure 291. SEM micrograph of the fracture surface of the N720/AM specimen with  $\pm 45^\circ$  fiber orientation obtained in creep test conducted at 32 MPa at 1200°C in steam. Creep lifetime  $t_f = 0.02$  h.

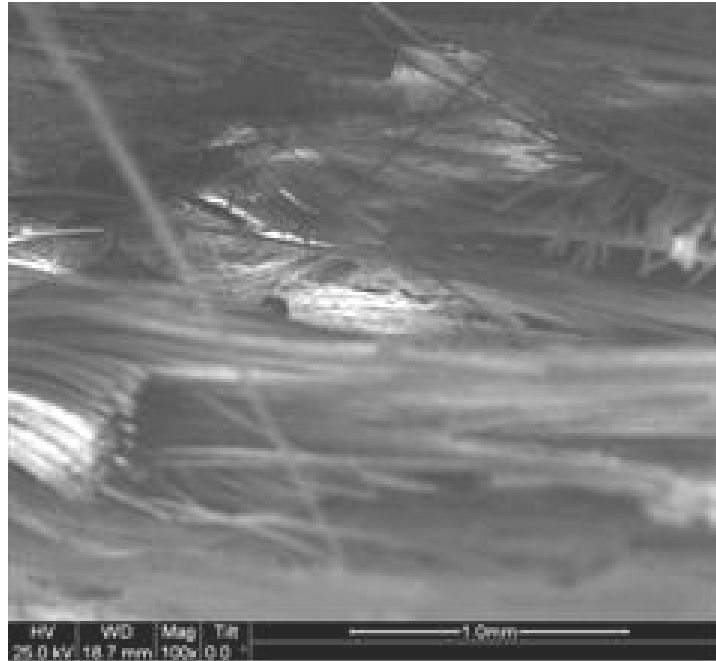


Figure 292. SEM micrograph of the fracture surface of the N720/AM specimen with  $\pm 45^\circ$  fiber orientation obtained in creep test conducted at 32 MPa at 1200°C in steam. Creep lifetime  $t_f = 0.02$  h.

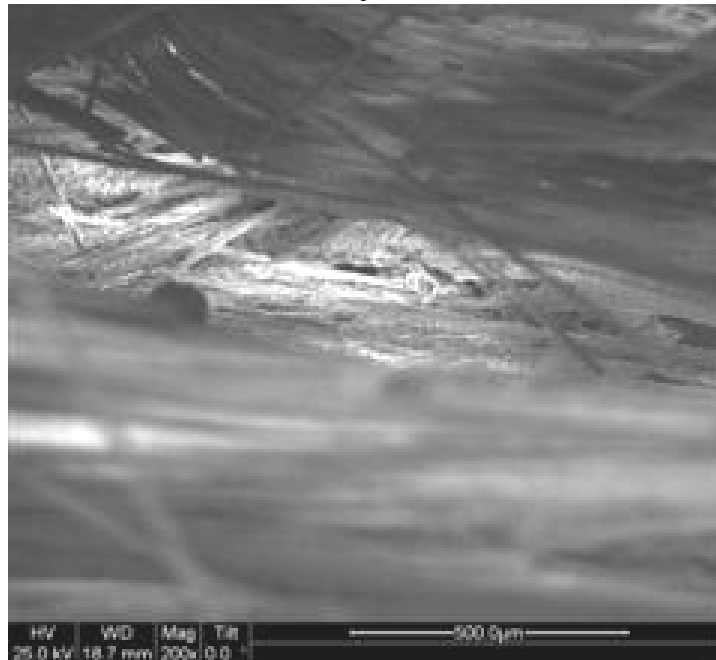


Figure 293. SEM micrograph of the fracture surface of the N720/AM specimen with  $\pm 45^\circ$  fiber orientation obtained in creep test conducted at 32 MPa at 1200°C in steam. Creep lifetime  $t_f = 0.02$  h.

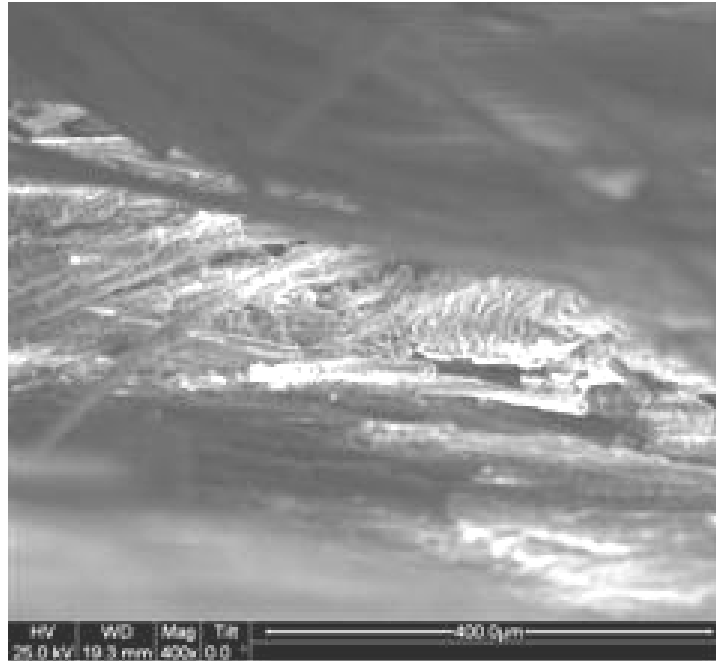


Figure 294. SEM micrograph of the fracture surface of the N720/AM specimen with  $\pm 45^\circ$  fiber orientation obtained in creep test conducted at 32 MPa at 1200°C in steam. Creep lifetime  $t_f = 0.02$  h.

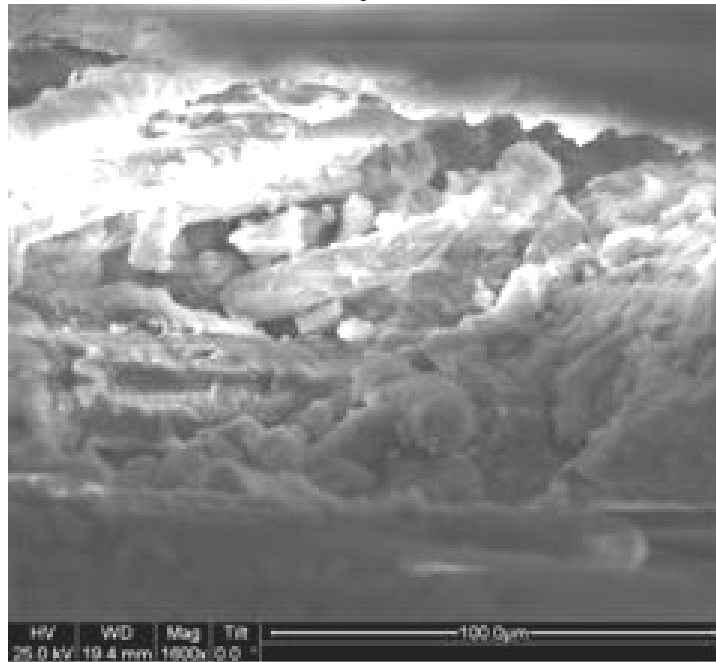


Figure 295. SEM micrograph of the fracture surface of the N720/AM specimen with  $\pm 45^\circ$  fiber orientation obtained in creep test conducted at 32 MPa at 1200°C in steam. Creep lifetime  $t_f = 0.02$  h.

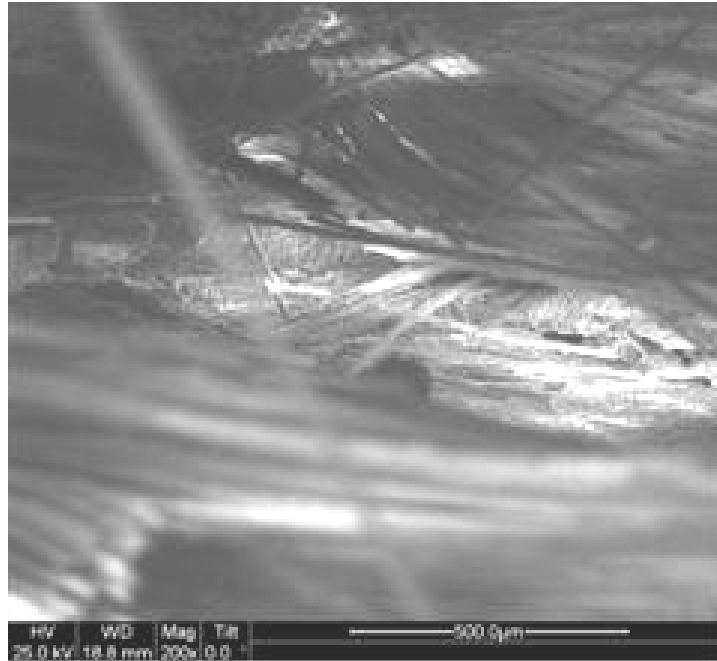


Figure 296. SEM micrograph of the fracture surface of the N720/AM specimen with  $\pm 45^\circ$  fiber orientation obtained in creep test conducted at 32 MPa at 1200°C in steam. Creep lifetime  $t_f = 0.02$  h.

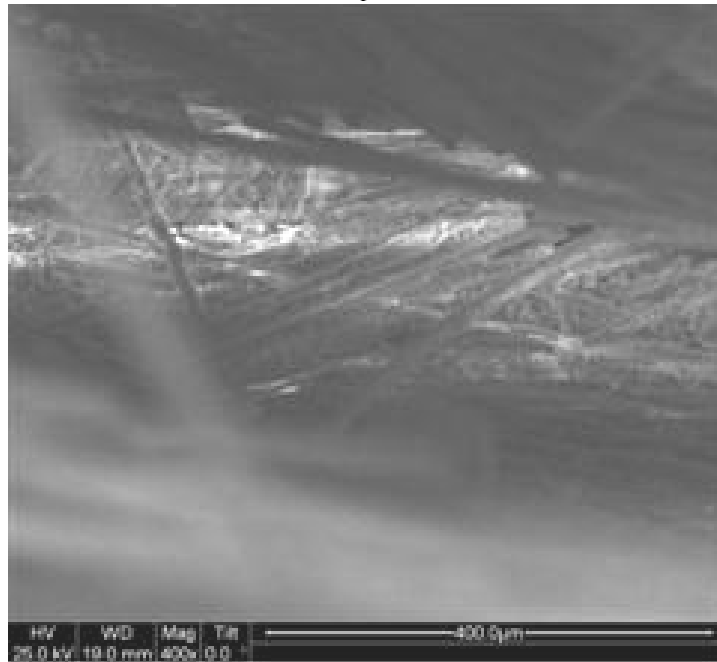


Figure 297. SEM micrograph of the fracture surface of the N720/AM specimen with  $\pm 45^\circ$  fiber orientation obtained in creep test conducted at 32 MPa at 1200°C in steam. Creep lifetime  $t_f = 0.02$  h.

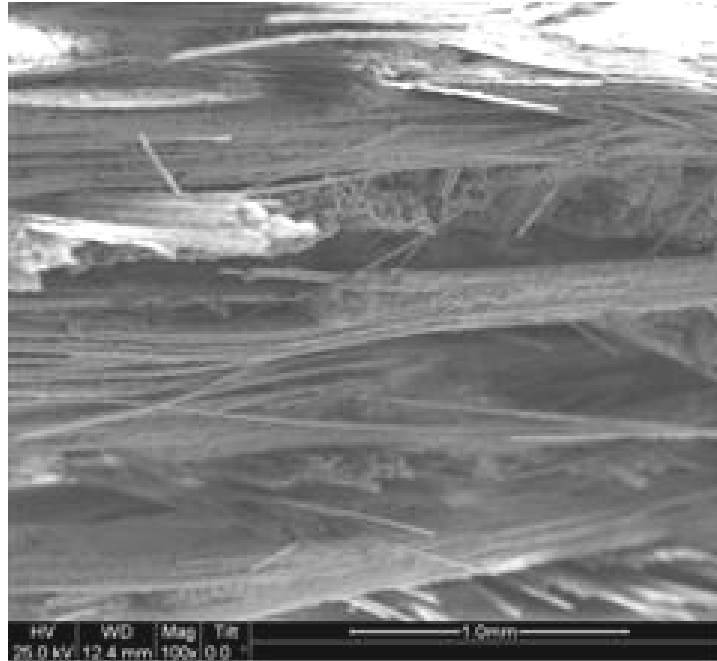


Figure 298. SEM micrograph of the fracture surface of the N720/AM specimen with  $\pm 45^\circ$  fiber orientation obtained in creep test conducted at 32 MPa at 1200°C in steam. Creep lifetime  $t_f = 0.02$  h.

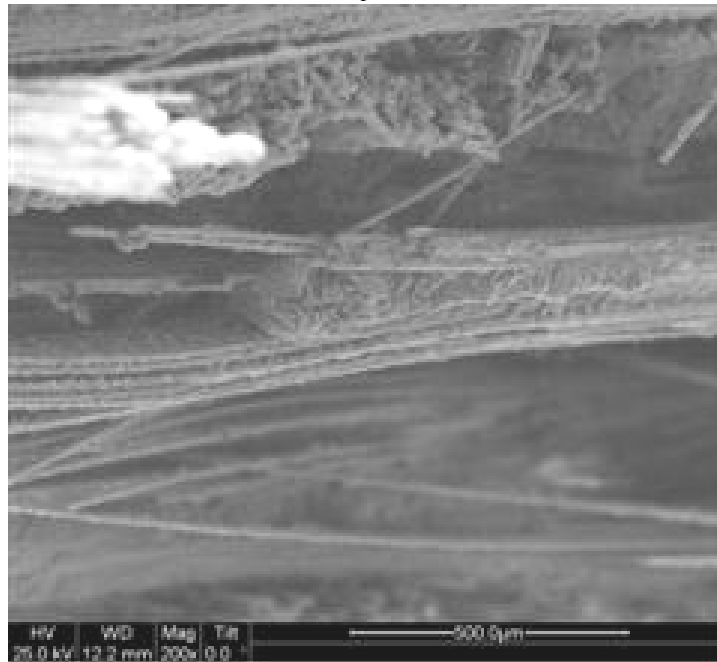


Figure 299. SEM micrograph of the fracture surface of the N720/AM specimen with  $\pm 45^\circ$  fiber orientation obtained in creep test conducted at 32 MPa at 1200°C in steam. Creep lifetime  $t_f = 0.02$  h.

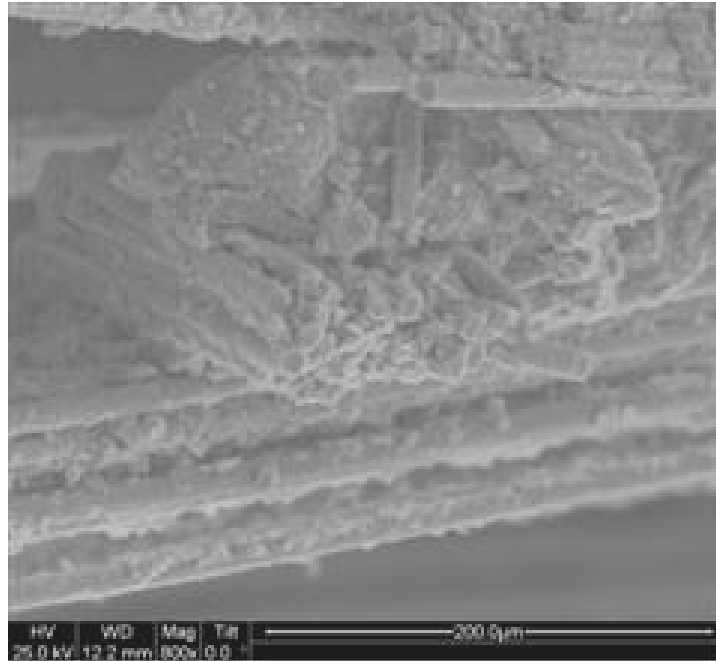


Figure 300. SEM micrograph of the fracture surface of the N720/AM specimen with  $\pm 45^\circ$  fiber orientation obtained in creep test conducted at 32 MPa at 1200°C in steam. Creep lifetime  $t_f = 0.02$  h.

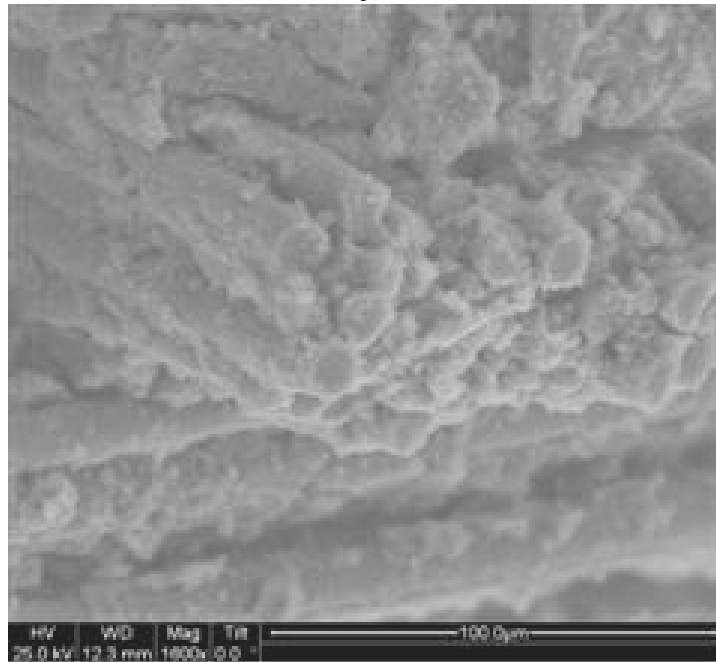


Figure 301. SEM micrograph of the fracture surface of the N720/AM specimen with  $\pm 45^\circ$  fiber orientation obtained in creep test conducted at 32 MPa at 1200°C in steam. Creep lifetime  $t_f = 0.02$  h.

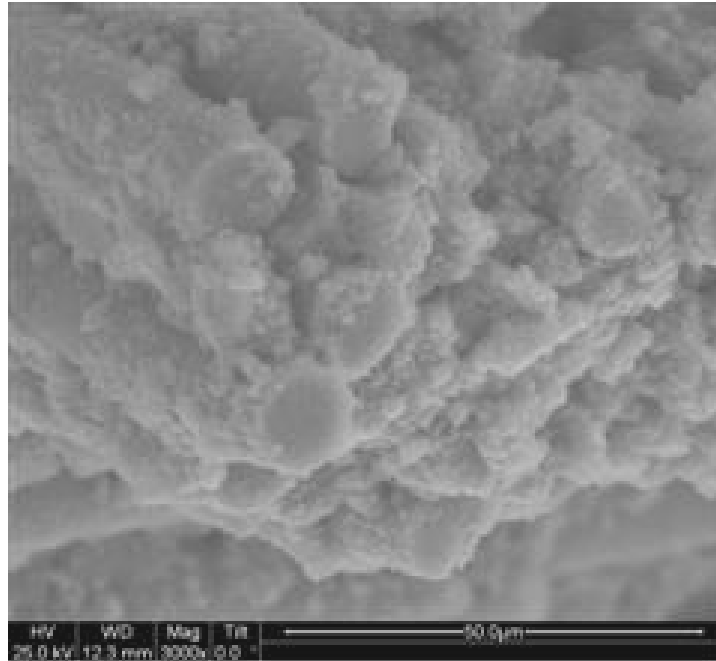


Figure 302. SEM micrograph of the fracture surface of the N720/AM specimen with  $\pm 45^\circ$  fiber orientation obtained in creep test conducted at 32 MPa at 1200°C in steam. Creep lifetime  $t_f = 0.02$  h.

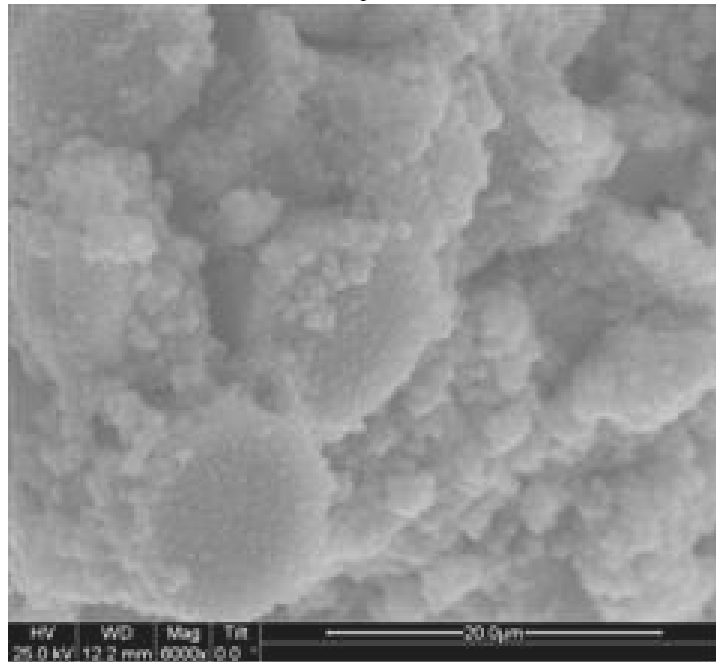


Figure 303. SEM micrograph of the fracture surface of the N720/AM specimen with  $\pm 45^\circ$  fiber orientation obtained in creep test conducted at 32 MPa at 1200°C in steam. Creep lifetime  $t_f = 0.02$  h.

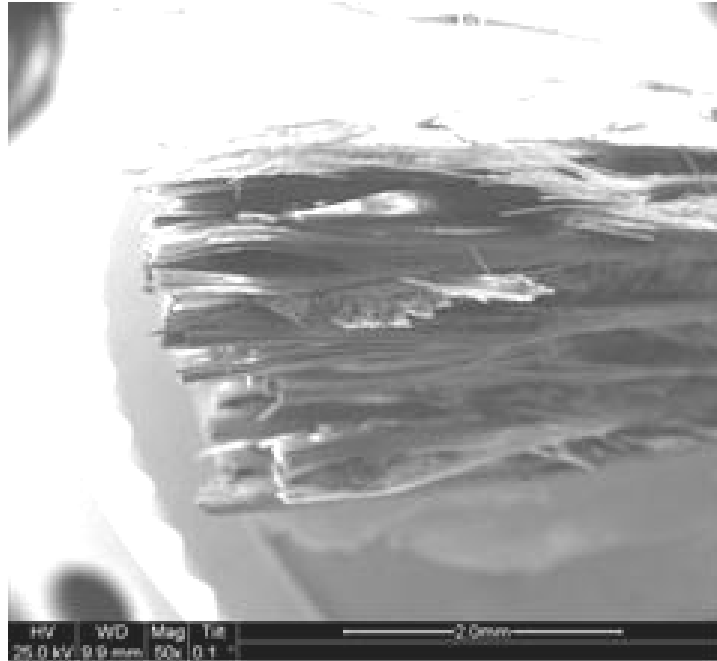


Figure 304. SEM micrograph of the fracture surface of the N720/AM specimen with  $\pm 45^\circ$  fiber orientation obtained in creep test conducted at 32 MPa at 1200°C in steam. Creep lifetime  $t_f = 0.02$  h.

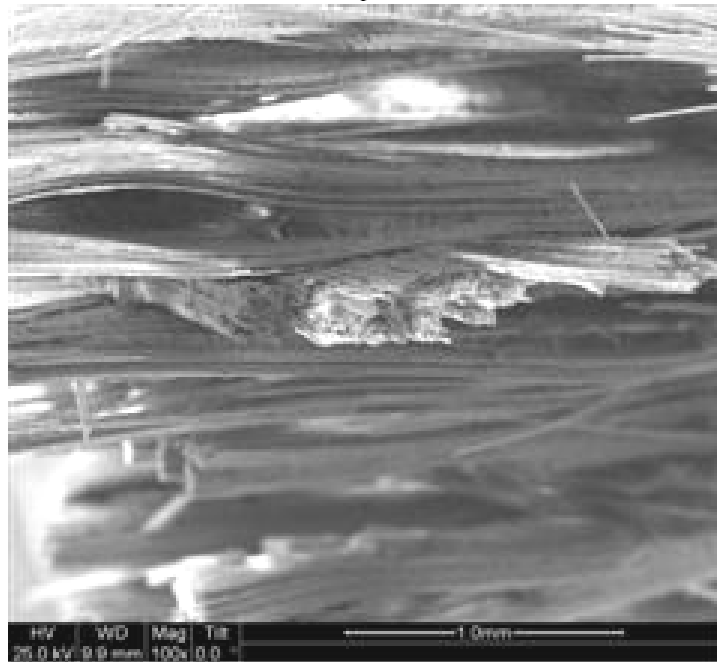


Figure 305. SEM micrograph of the fracture surface of the N720/AM specimen with  $\pm 45^\circ$  fiber orientation obtained in creep test conducted at 32 MPa at 1200°C in steam. Creep lifetime  $t_f = 0.02$  h.

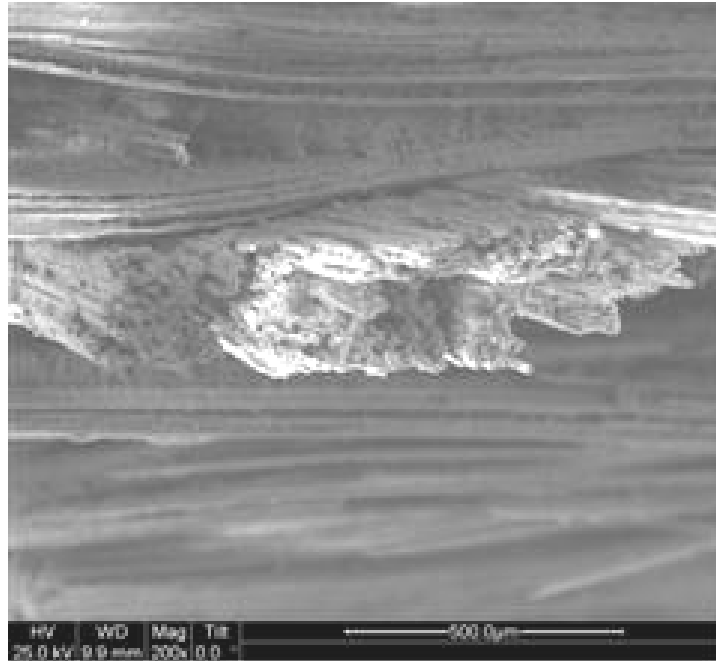


Figure 306. SEM micrograph of the fracture surface of the N720/AM specimen with  $\pm 45^\circ$  fiber orientation obtained in creep test conducted at 32 MPa at 1200°C in steam. Creep lifetime  $t_f = 0.02$  h.

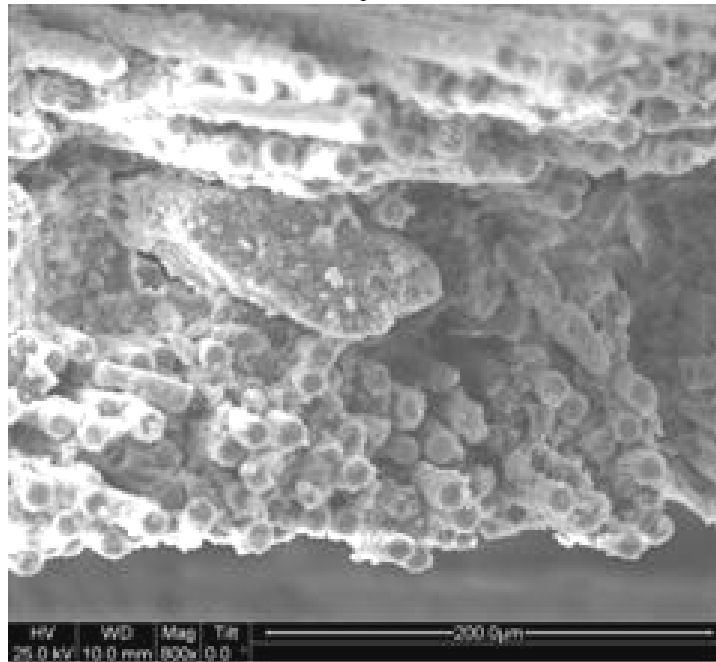


Figure 307. SEM micrograph of the fracture surface of the N720/AM specimen with  $\pm 45^\circ$  fiber orientation obtained in creep test conducted at 32 MPa at 1200°C in steam. Creep lifetime  $t_f = 0.02$  h.

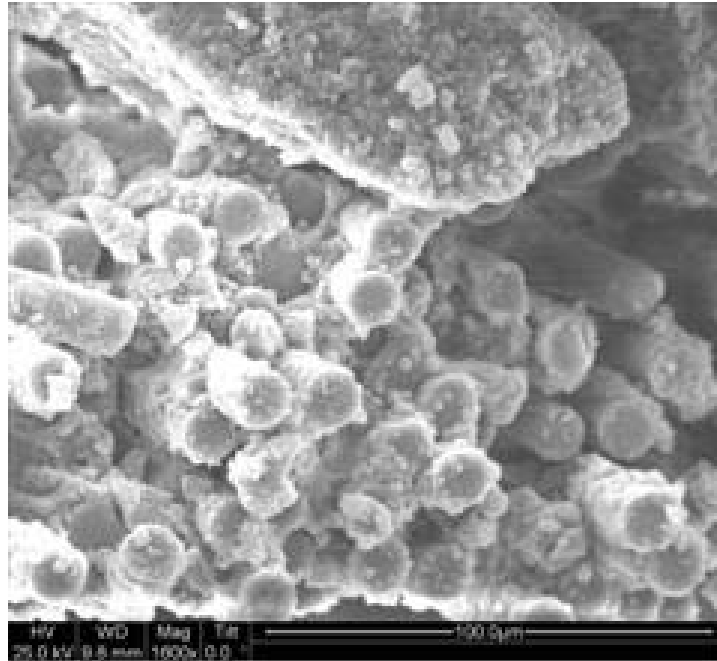


Figure 308. SEM micrograph of the fracture surface of the N720/AM specimen with  $\pm 45^\circ$  fiber orientation obtained in creep test conducted at 32 MPa at 1200°C in steam. Creep lifetime  $t_f = 0.02$  h.

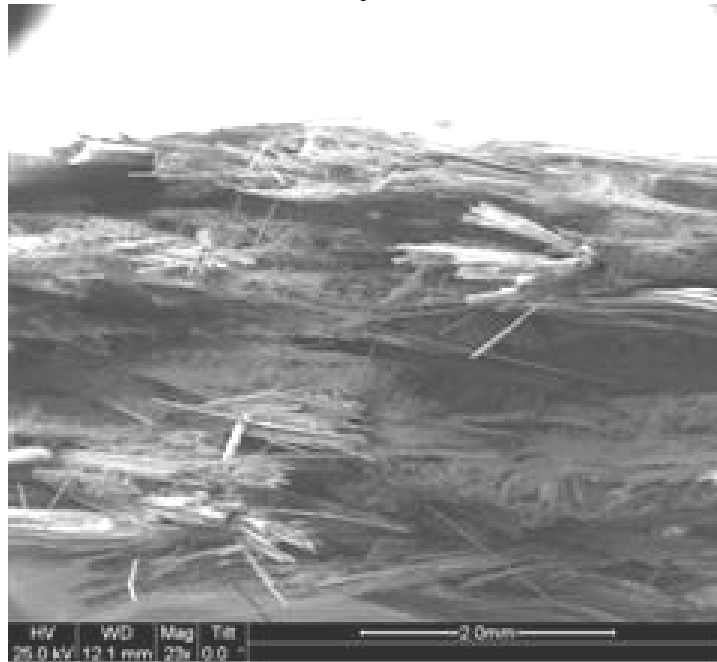


Figure 309. SEM micrograph of the fracture surface of the N720/AM specimen subjected to tensile test to failure following 100 h at 20 MPa at 1200°C in argon.

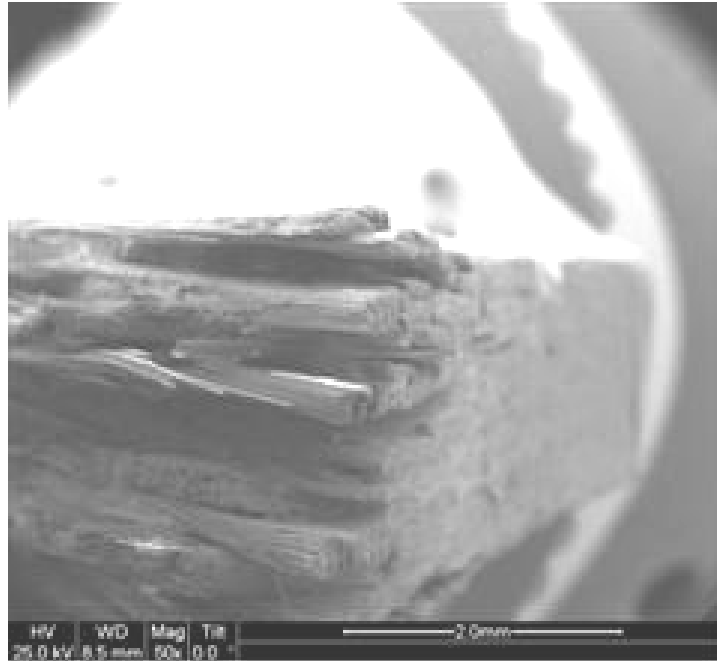


Figure 310. SEM micrograph of the fracture surface of the N720/AM specimen subjected to tensile test to failure following 100 h at 20 MPa at 1200°C in argon.

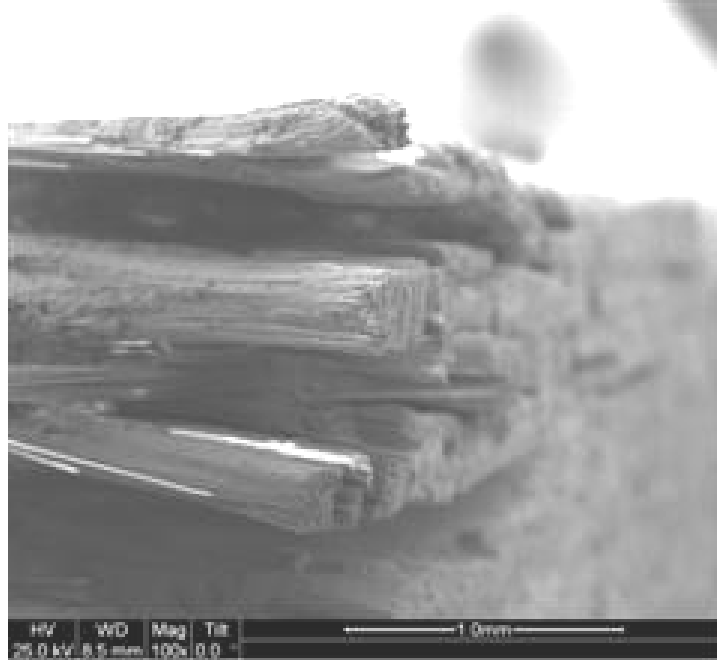


Figure 311. SEM micrograph of the fracture surface of the N720/AM specimen subjected to tensile test to failure following 100 h at 20 MPa at 1200°C in argon.

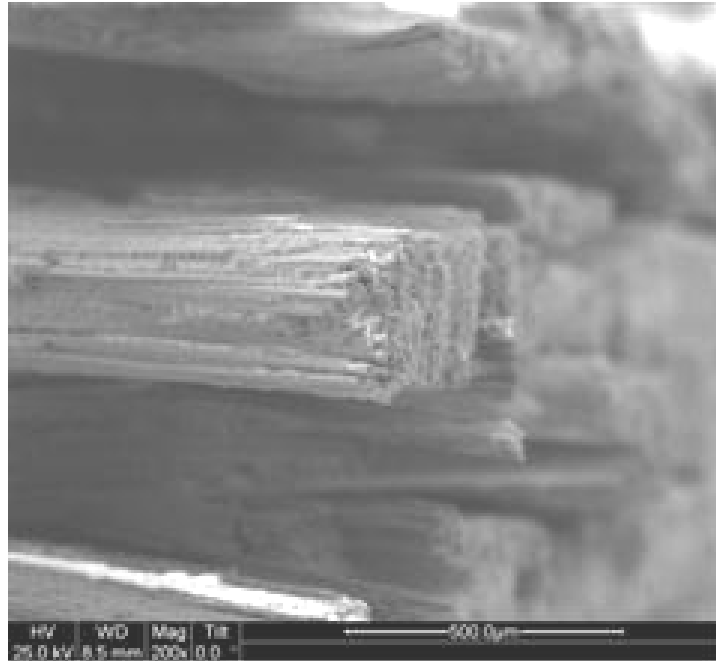


Figure 312. SEM micrograph of the fracture surface of the N720/AM specimen subjected to tensile test to failure following 100 h at 20 MPa at 1200°C in argon.

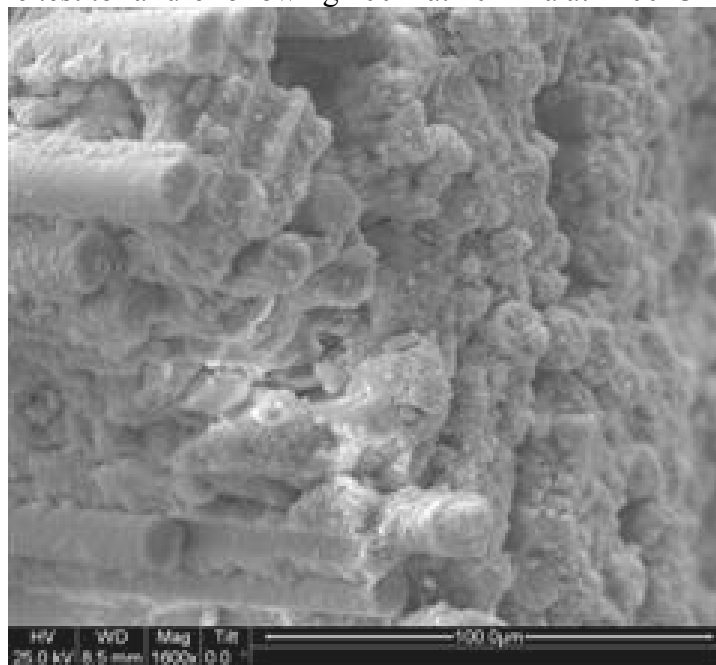


Figure 313. SEM micrograph of the fracture surface of the N720/AM specimen subjected to tensile test to failure following 100 h at 20 MPa at 1200°C in argon.

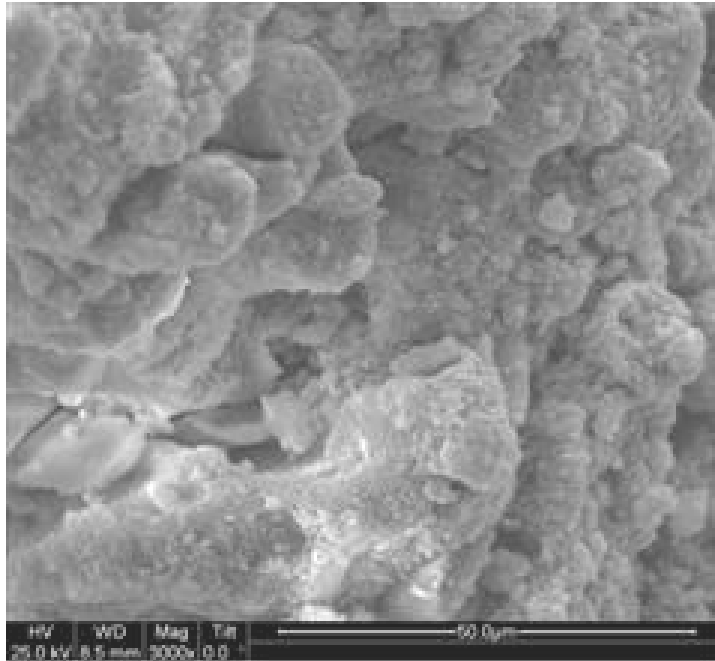


Figure 314. SEM micrograph of the fracture surface of the N720/AM specimen subjected to tensile test to failure following 100 h at 20 MPa at 1200°C in argon.

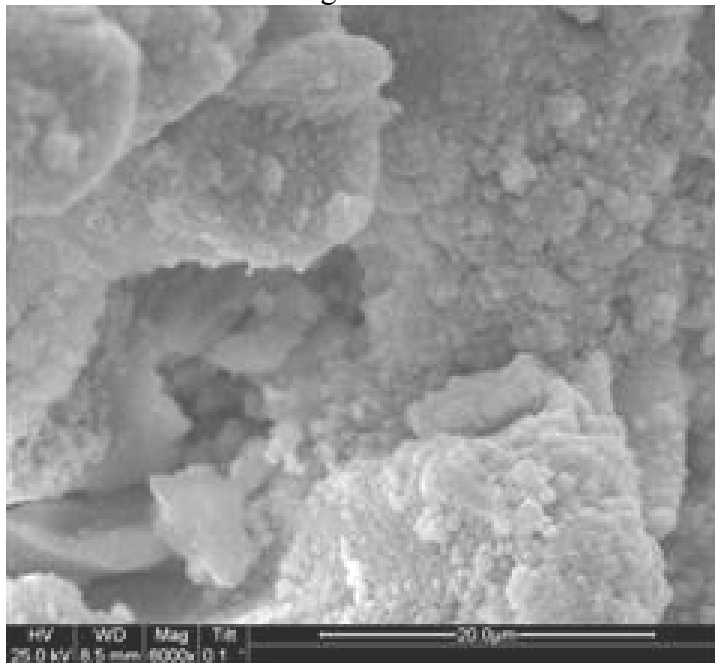


Figure 315. SEM micrograph of the fracture surface of the N720/AM specimen subjected to tensile test to failure following 100 h at 20 MPa at 1200°C in argon.

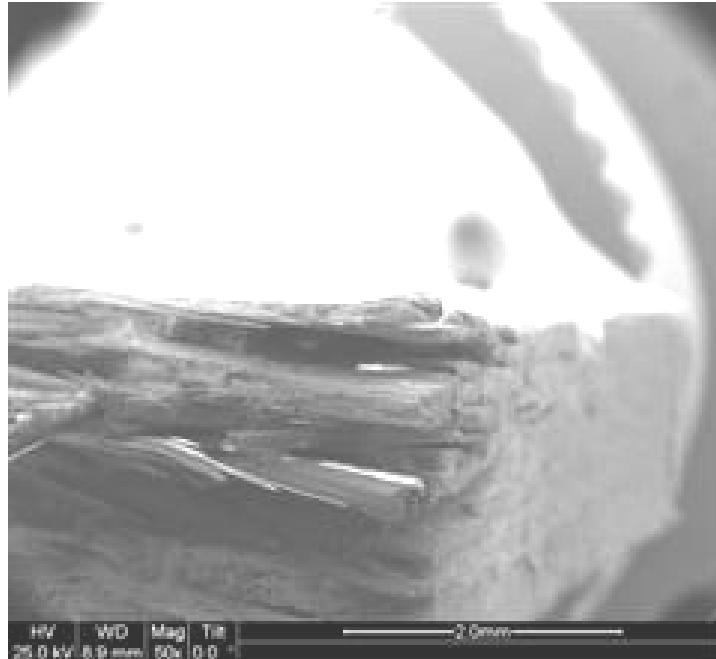


Figure 316. SEM micrograph of the fracture surface of the N720/AM specimen subjected to tensile test to failure following 100 h at 20 MPa at 1200°C in argon.

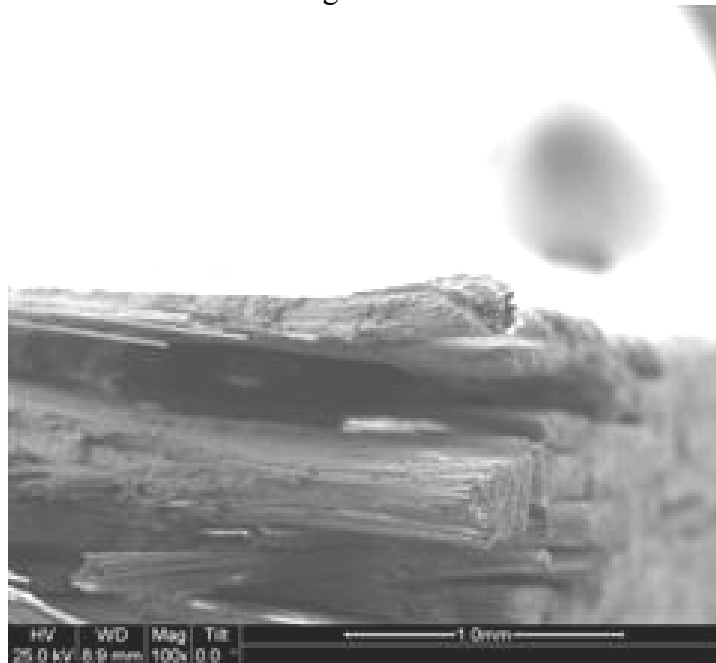


Figure 317. SEM micrograph of the fracture surface of the N720/AM specimen subjected to tensile test to failure following 100 h at 20 MPa at 1200°C in argon.

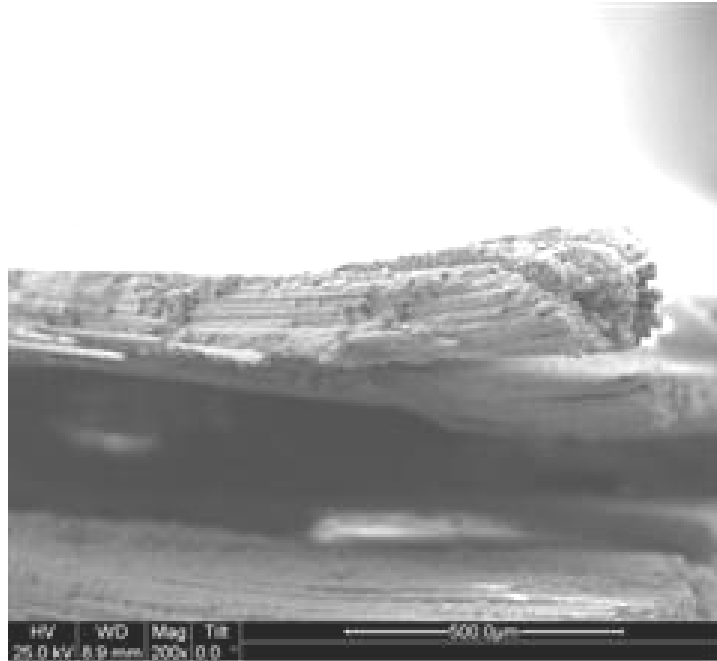


Figure 318. SEM micrograph of the fracture surface of the N720/AM specimen subjected to tensile test to failure following 100 h at 20 MPa at 1200°C in argon.

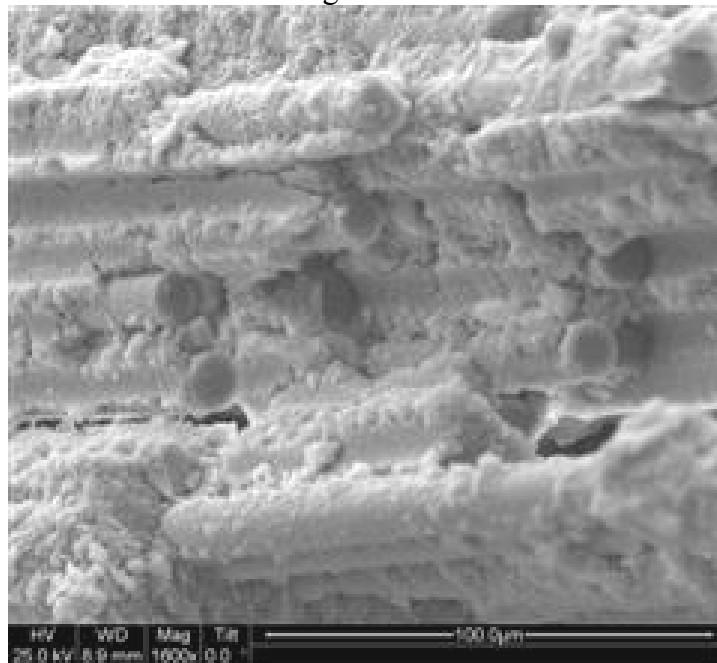


Figure 319. SEM micrograph of the fracture surface of the N720/AM specimen subjected to tensile test to failure following 100 h at 20 MPa at 1200°C in argon.

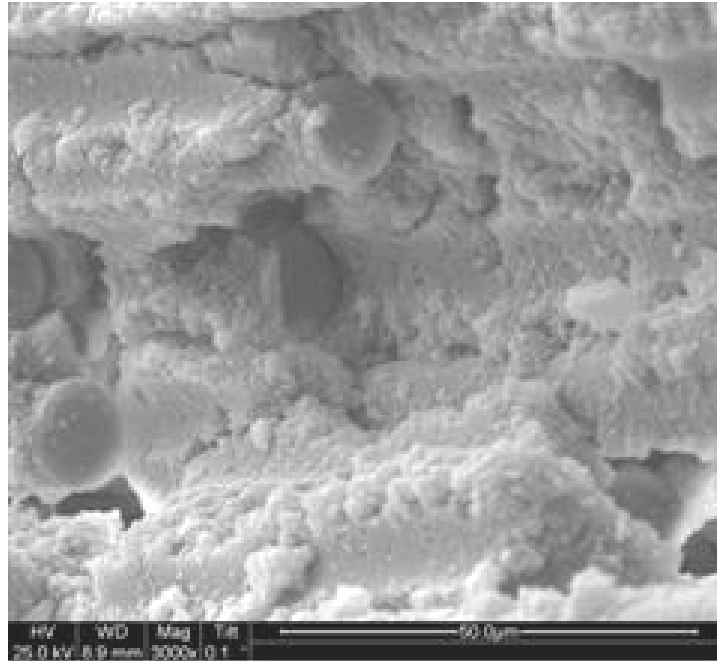


Figure 320. SEM micrograph of the fracture surface of the N720/AM specimen subjected to tensile test to failure following 100 h at 20 MPa at 1200°C in argon.

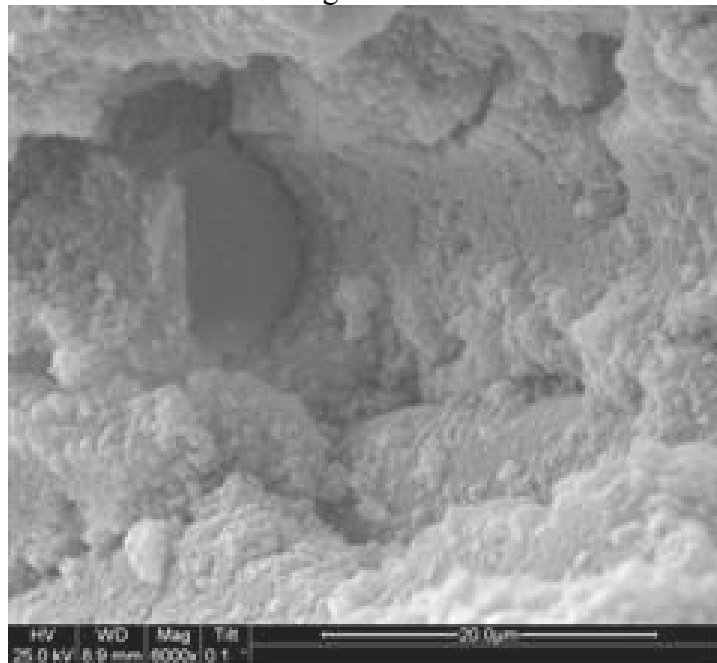


Figure 321. SEM micrograph of the fracture surface of the N720/AM specimen subjected to tensile test to failure following 100 h at 20 MPa at 1200°C in argon.

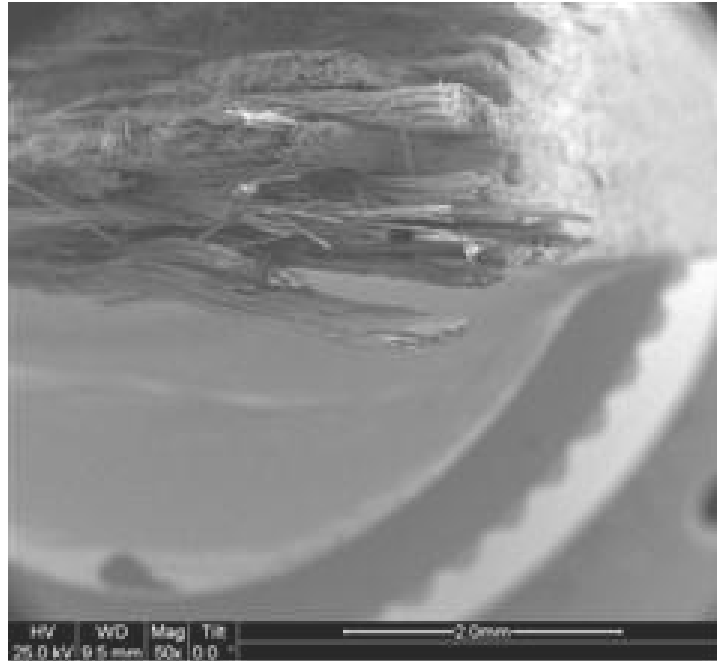


Figure 322. SEM micrograph of the fracture surface of the N720/AM specimen subjected to tensile test to failure following 100 h at 20 MPa at 1200°C in argon.

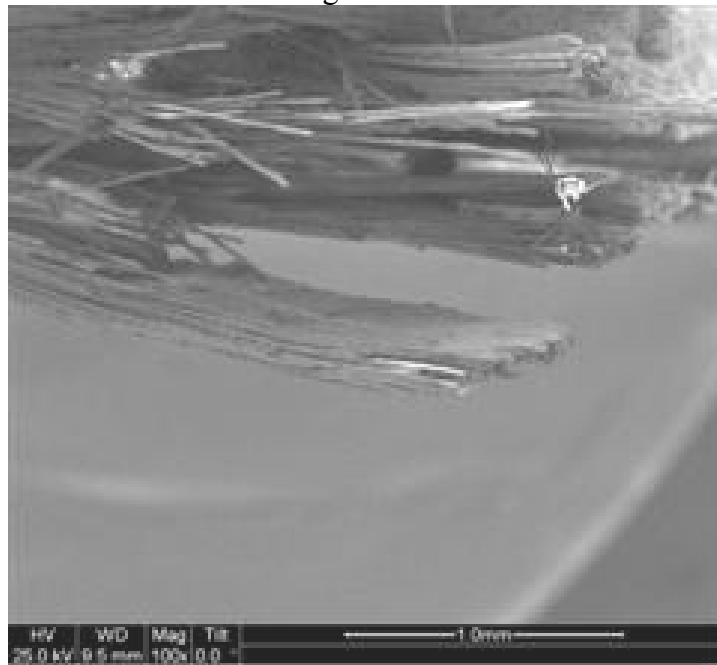


Figure 323. SEM micrograph of the fracture surface of the N720/AM specimen subjected to tensile test to failure following 100 h at 20 MPa at 1200°C in argon.

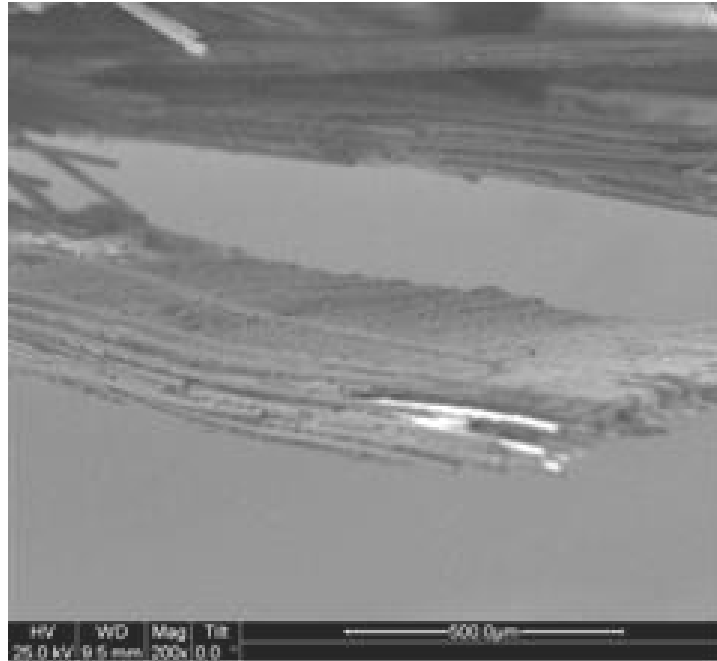


Figure 324. SEM micrograph of the fracture surface of the N720/AM specimen subjected to tensile test to failure following 100 h at 20 MPa at 1200°C in argon.

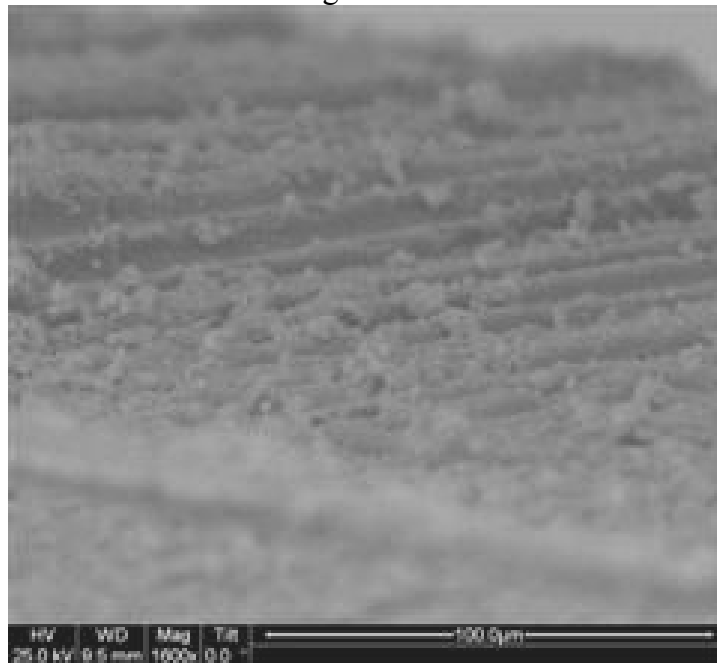


Figure 325. SEM micrograph of the fracture surface of the N720/AM specimen subjected to tensile test to failure following 100 h at 20 MPa at 1200°C in argon.

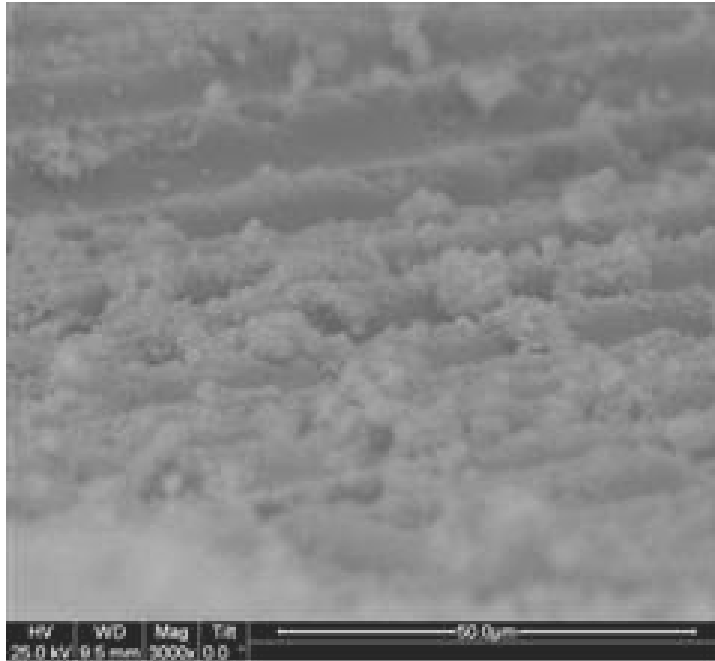


Figure 326. SEM micrograph of the fracture surface of the N720/AM specimen subjected to tensile test to failure following 100 h at 20 MPa at 1200°C in argon.

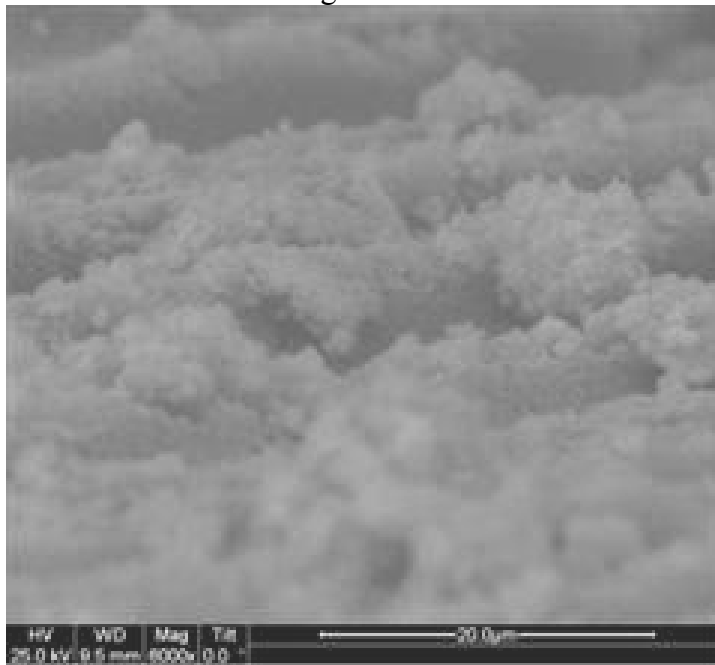


Figure 327. SEM micrograph of the fracture surface of the N720/AM specimen subjected to tensile test to failure following 100 h at 20 MPa at 1200°C in argon.

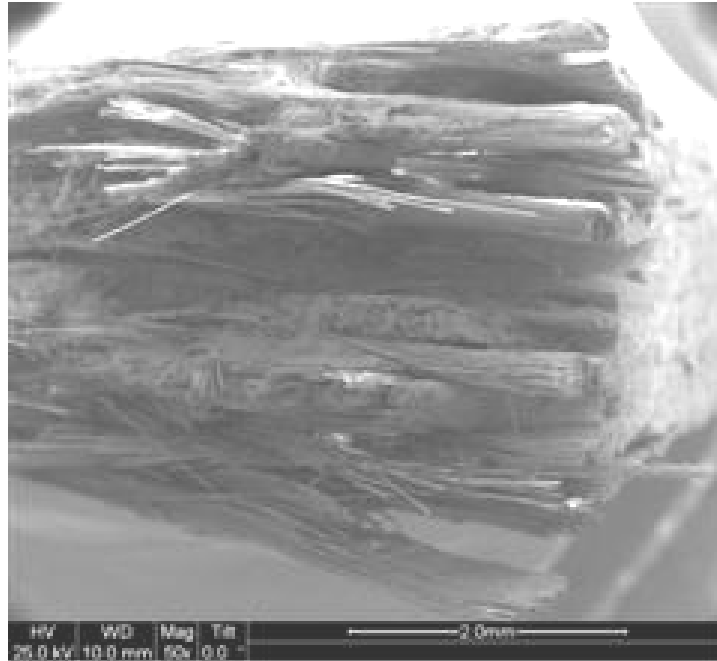


Figure 328. SEM micrograph of the fracture surface of the N720/AM specimen subjected to tensile test to failure following 100 h at 20 MPa at 1200°C in argon.

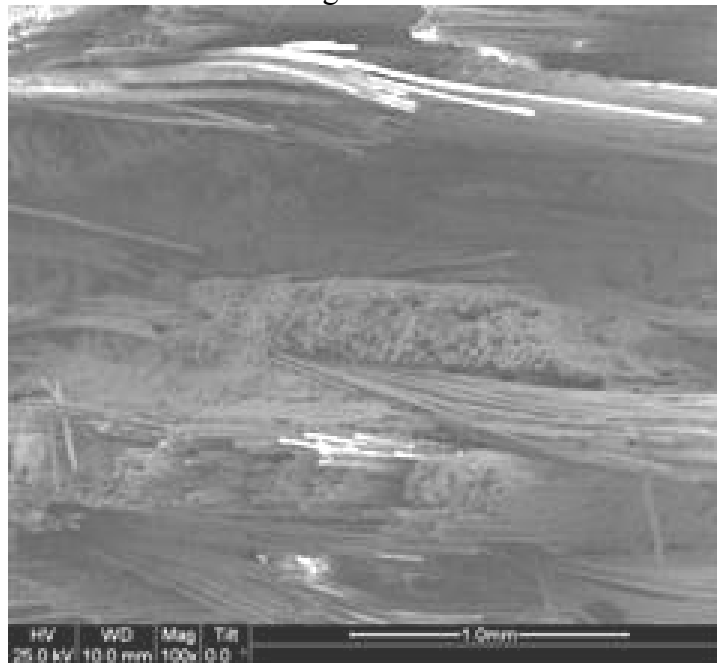


Figure 329. SEM micrograph of the fracture surface of the N720/AM specimen subjected to tensile test to failure following 100 h at 20 MPa at 1200°C in argon.



Figure 330. SEM micrograph of the fracture surface of the N720/AM specimen subjected to tensile test to failure following 100 h at 20 MPa at 1200°C in argon.

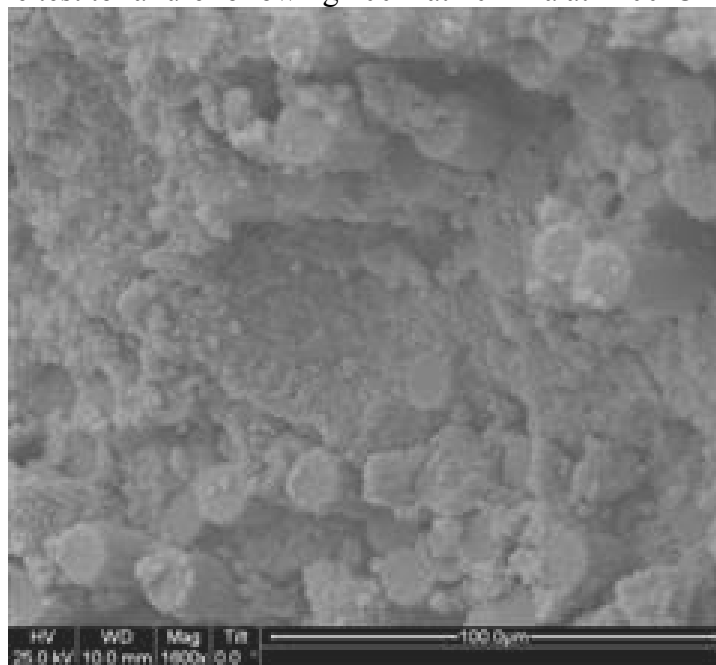


Figure 331. SEM micrograph of the fracture surface of the N720/AM specimen subjected to tensile test to failure following 100 h at 20 MPa at 1200°C in argon.

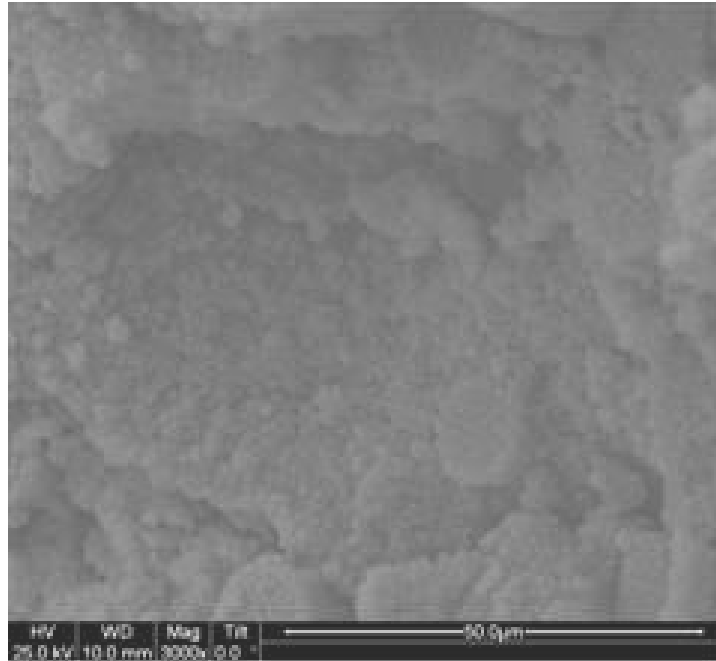


Figure 332. SEM micrograph of the fracture surface of the N720/AM specimen subjected to tensile test to failure following 100 h at 20 MPa at 1200°C in argon.

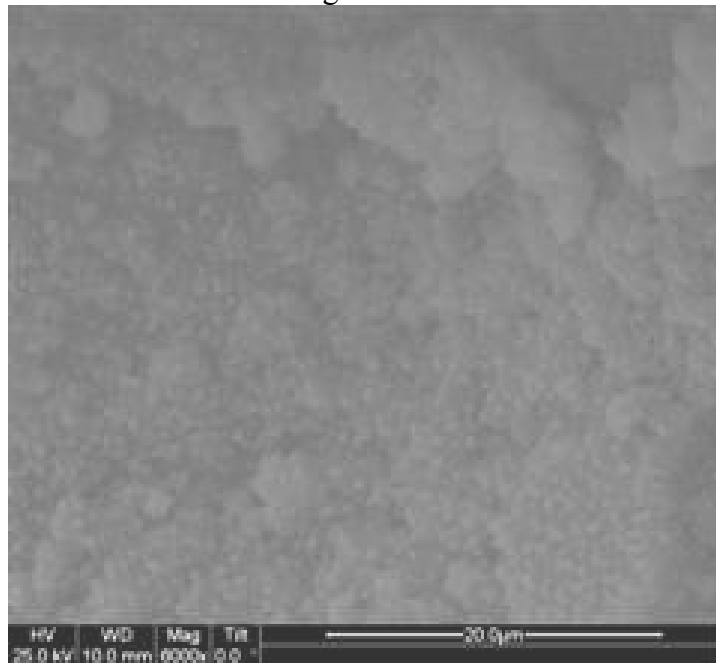


Figure 333. SEM micrograph of the fracture surface of the N720/AM specimen subjected to tensile test to failure following 100 h at 20 MPa at 1200°C in argon.

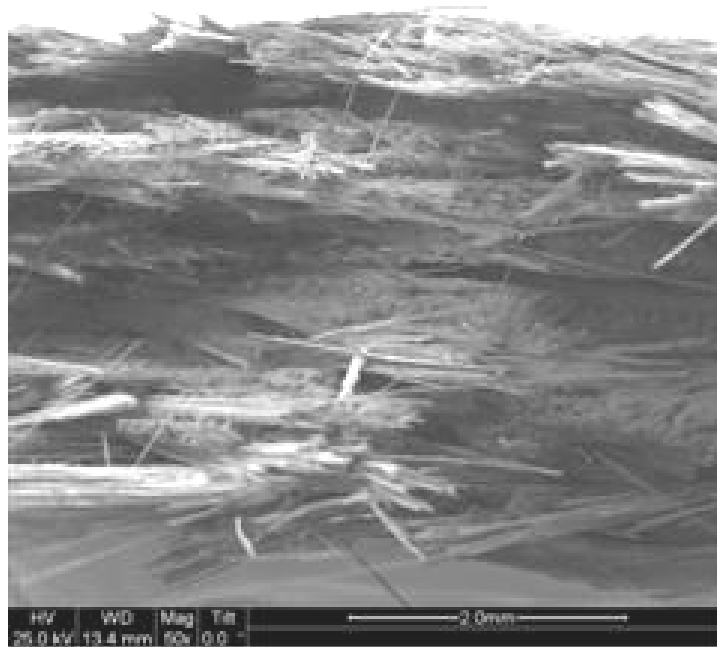


Figure 334. SEM micrograph of the fracture surface of the N720/AM specimen subjected to tensile test to failure following 100 h at 20 MPa at 1200°C in argon.

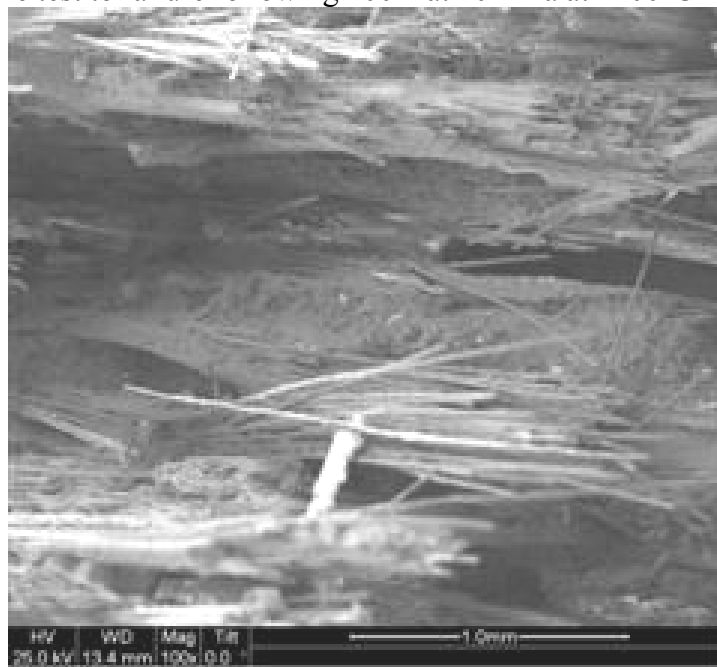


Figure 335. SEM micrograph of the fracture surface of the N720/AM specimen subjected to tensile test to failure following 100 h at 20 MPa at 1200°C in argon.



Figure 336. SEM micrograph of the fracture surface of the N720/AM specimen subjected to tensile test to failure following 100 h at 20 MPa at 1200°C in argon.

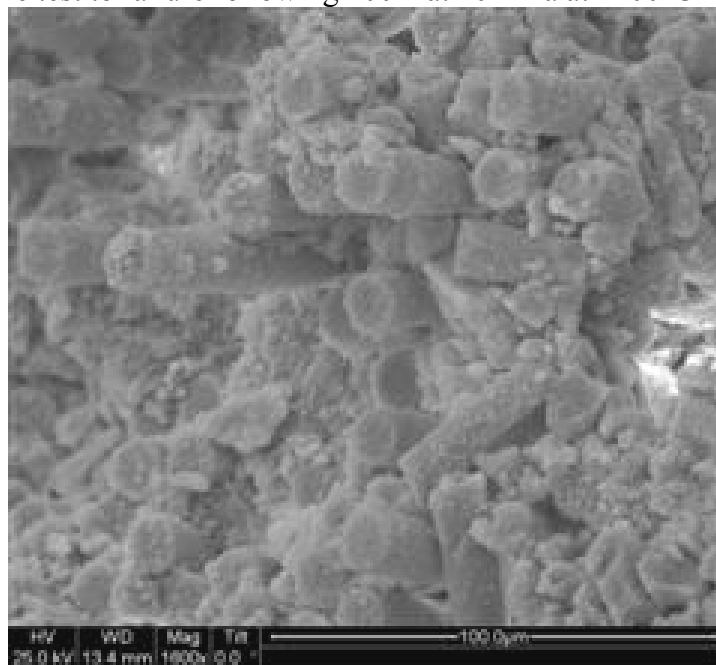


Figure 337. SEM micrograph of the fracture surface of the N720/AM specimen subjected to tensile test to failure following 100 h at 20 MPa at 1200°C in argon.

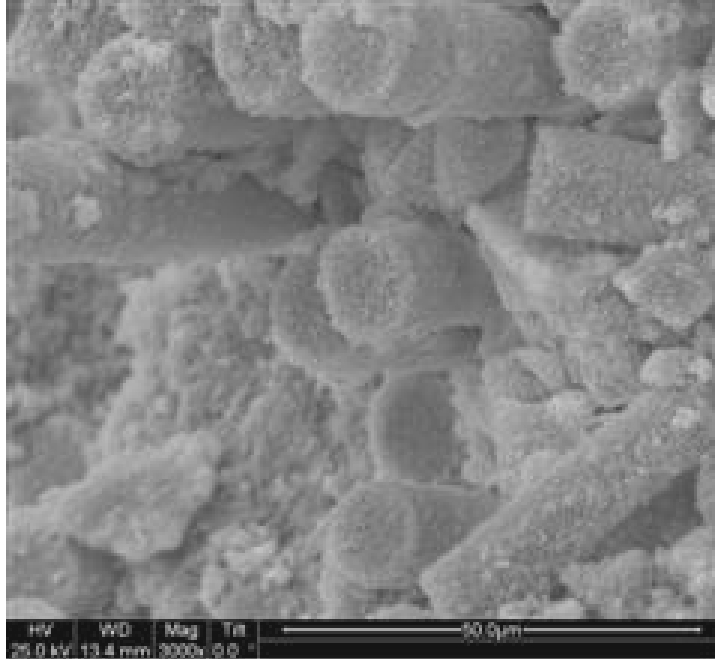


Figure 338. SEM micrograph of the fracture surface of the N720/AM specimen subjected to tensile test to failure following 100 h at 20 MPa at 1200°C in argon.

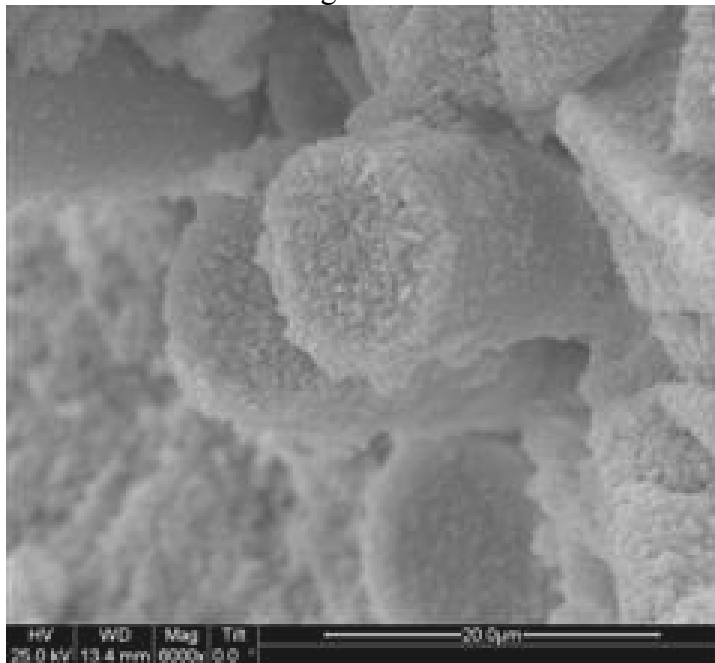


Figure 339. SEM micrograph of the fracture surface of the N720/AM specimen subjected to tensile test to failure following 100 h at 20 MPa at 1200°C in argon.

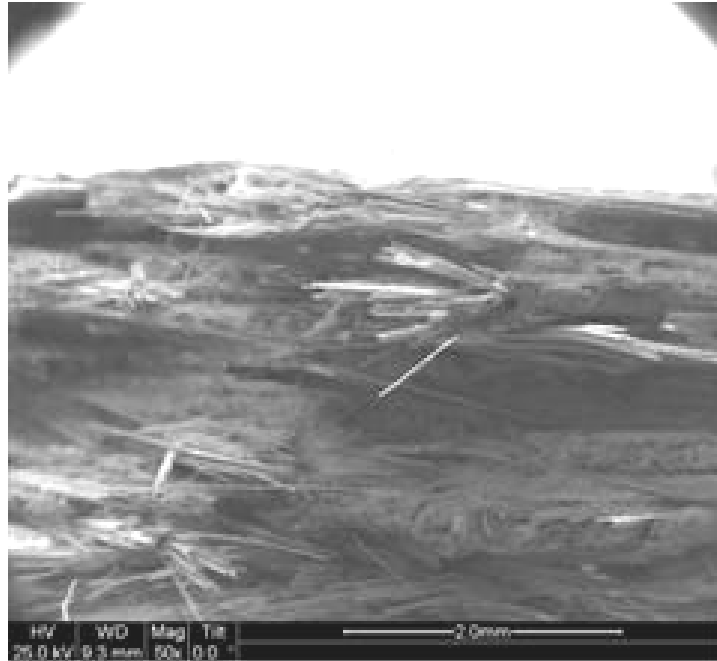


Figure 340. SEM micrograph of the fracture surface of the N720/AM specimen subjected to tensile test to failure following 100 h at 20 MPa at 1200°C in argon.

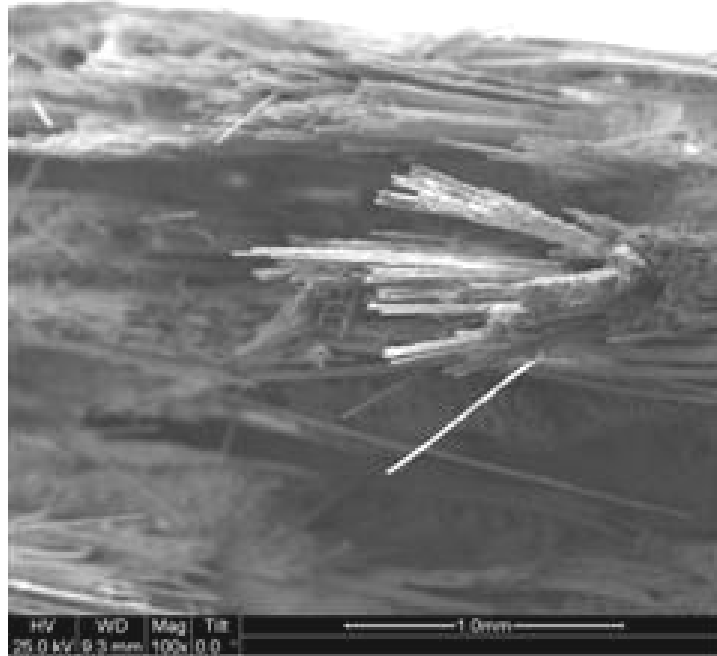


Figure 341. SEM micrograph of the fracture surface of the N720/AM specimen subjected to tensile test to failure following 100 h at 20 MPa at 1200°C in argon.

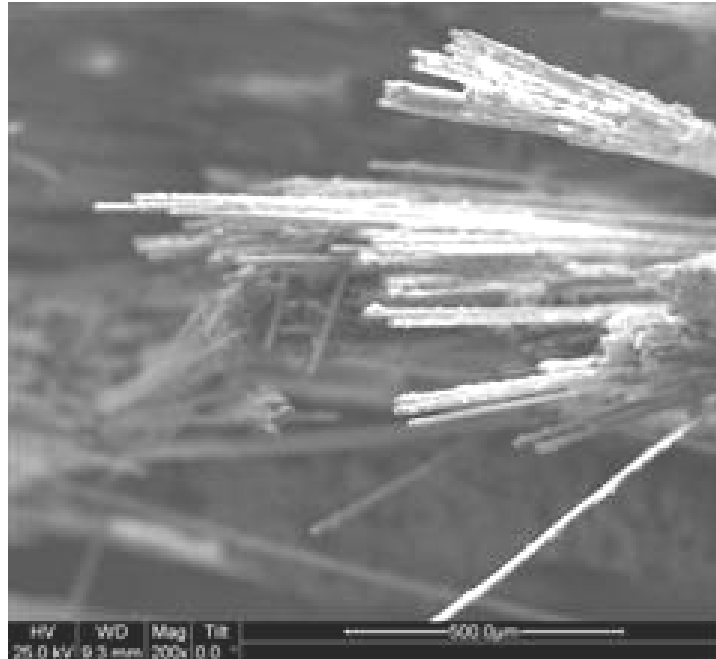


Figure 342. SEM micrograph of the fracture surface of the N720/AM specimen subjected to tensile test to failure following 100 h at 20 MPa at 1200°C in argon.



Figure 343. SEM micrograph of the fracture surface of the N720/AM specimen subjected to tensile test to failure following 100 h at 20 MPa at 1200°C in argon.



Figure 344. SEM micrograph of the fracture surface of the N720/AM specimen subjected to tensile test to failure following 100 h at 20 MPa at 1200°C in argon.

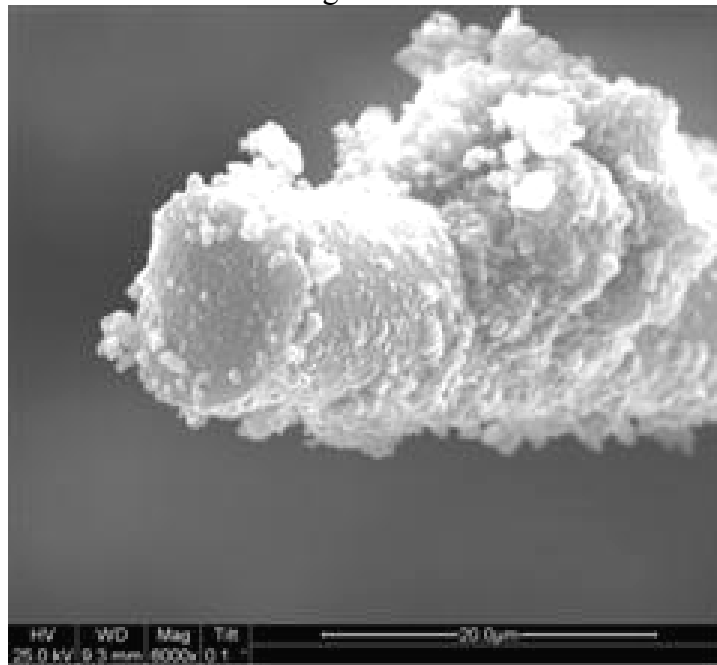


Figure 345. SEM micrograph of the fracture surface of the N720/AM specimen subjected to tensile test to failure following 100 h at 20 MPa at 1200°C in argon.

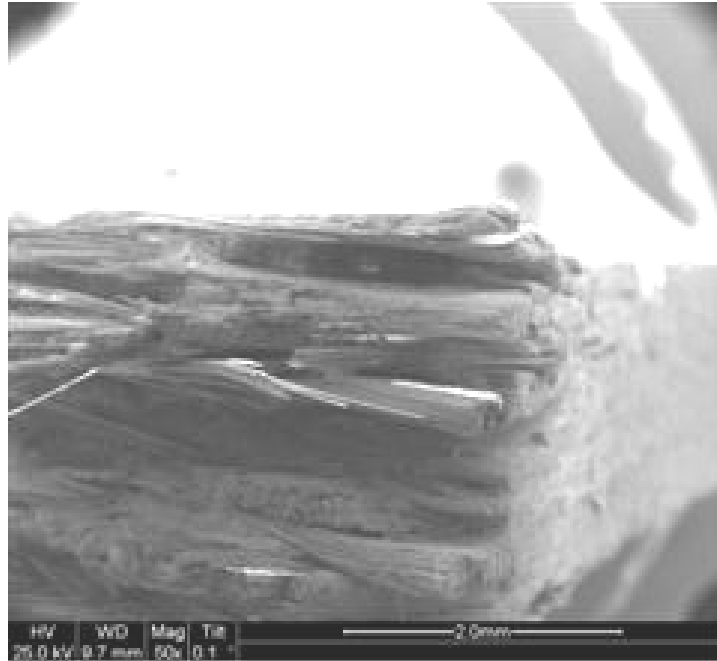


Figure 346. SEM micrograph of the fracture surface of the N720/AM specimen subjected to tensile test to failure following 100 h at 20 MPa at 1200°C in argon.

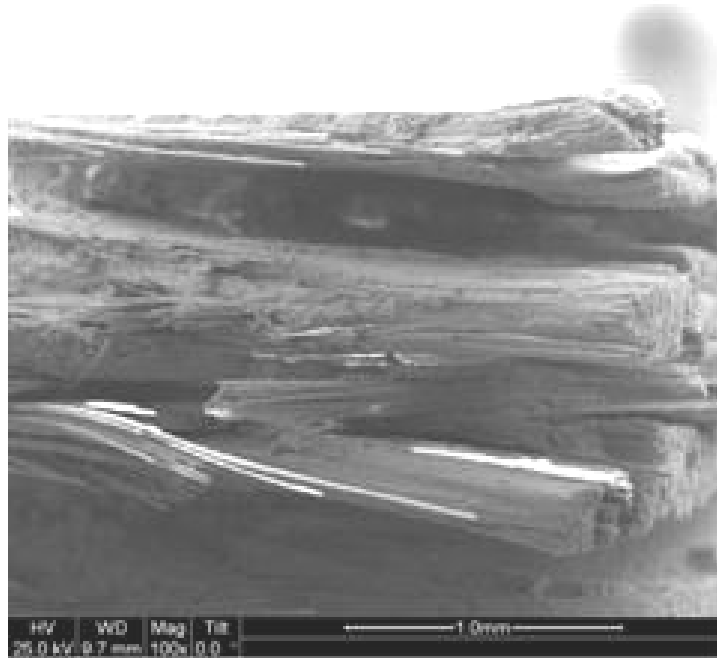


Figure 347. SEM micrograph of the fracture surface of the N720/AM specimen subjected to tensile test to failure following 100 h at 20 MPa at 1200°C in argon.

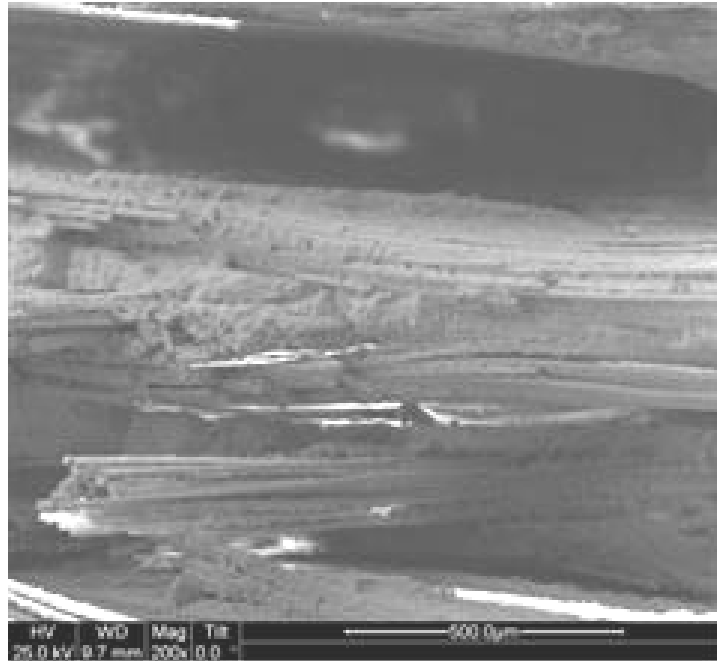


Figure 348. SEM micrograph of the fracture surface of the N720/AM specimen subjected to tensile test to failure following 100 h at 20 MPa at 1200°C in argon.

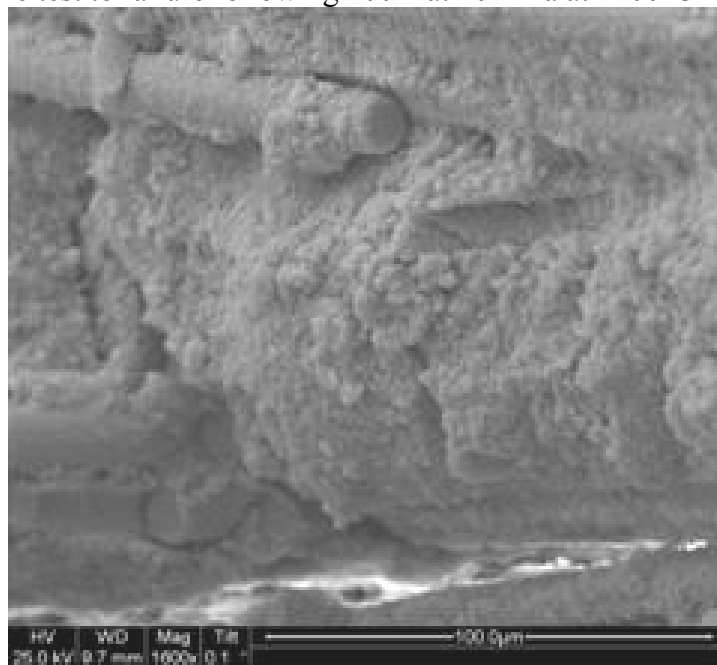


Figure 349. SEM micrograph of the fracture surface of the N720/AM specimen subjected to tensile test to failure following 100 h at 20 MPa at 1200°C in argon.

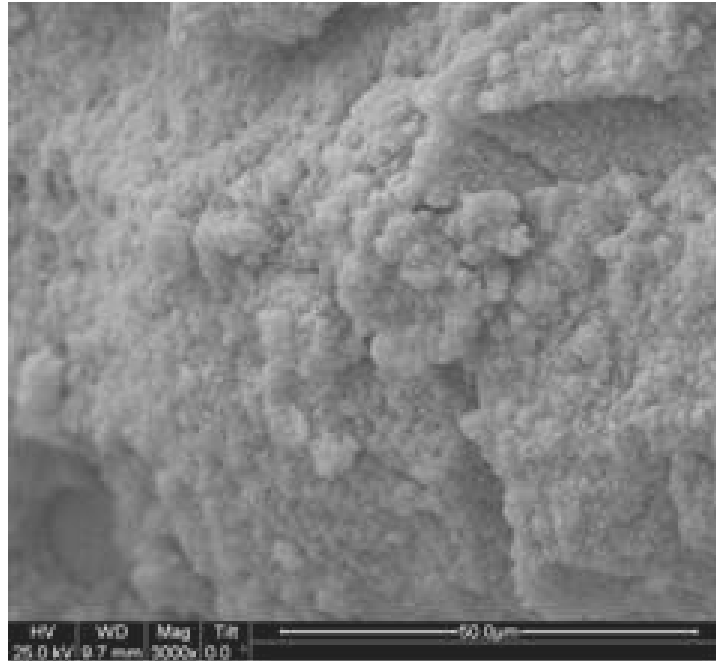


Figure 350. SEM micrograph of the fracture surface of the N720/AM specimen subjected to tensile test to failure following 100 h at 20 MPa at 1200°C in argon.

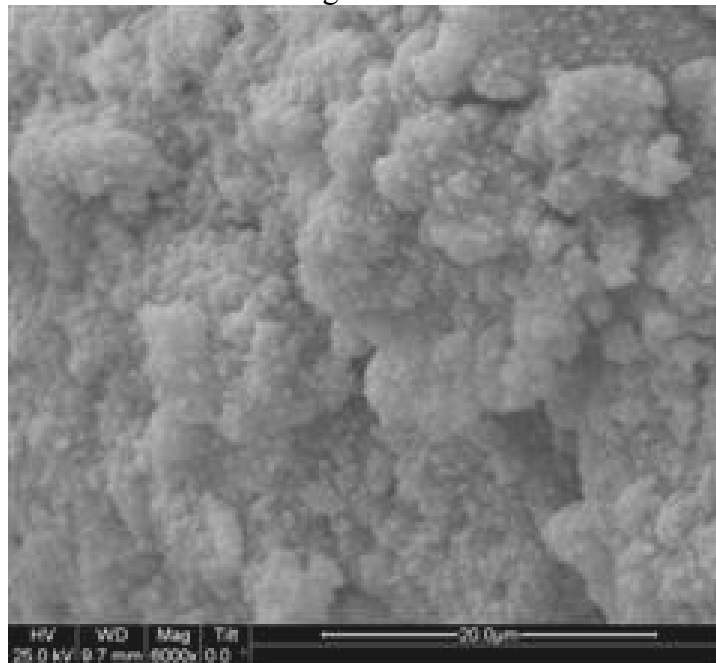


Figure 351. SEM micrograph of the fracture surface of the N720/AM specimen subjected to tensile test to failure following 100 h at 20 MPa at 1200°C in argon.

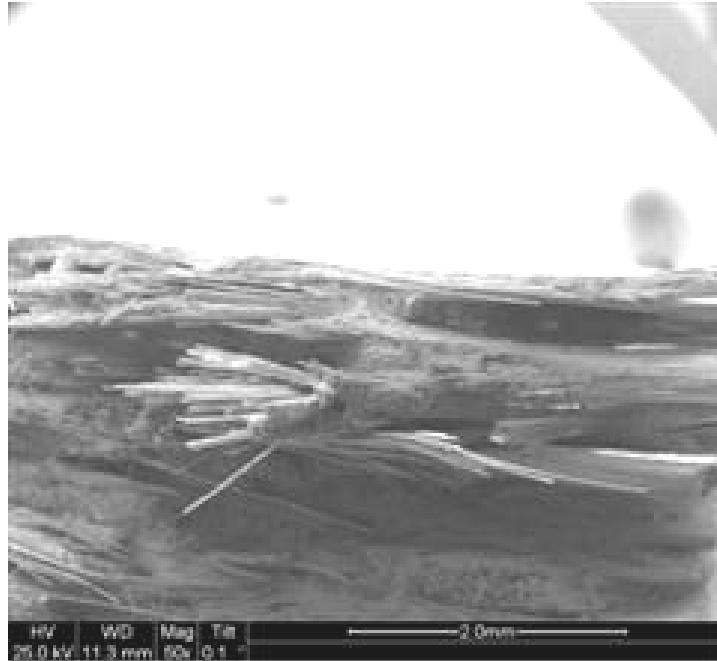


Figure 352. SEM micrograph of the fracture surface of the N720/AM specimen subjected to tensile test to failure following 100 h at 20 MPa at 1200°C in argon.

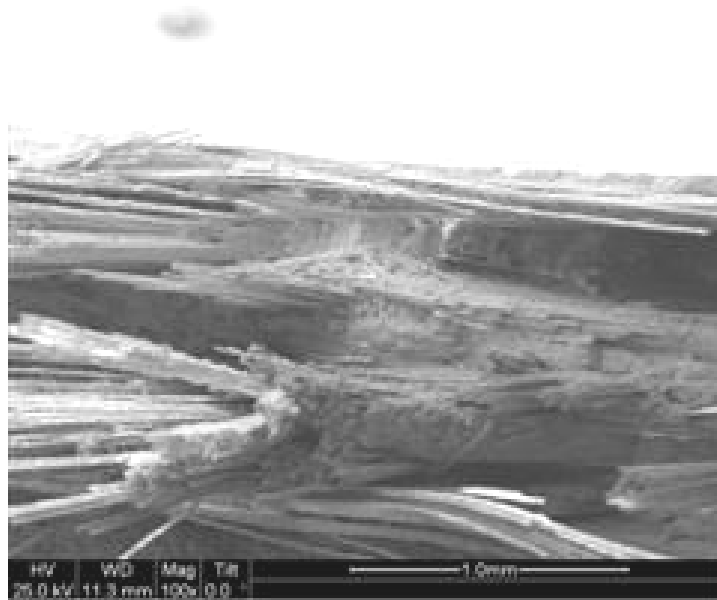


Figure 353. SEM micrograph of the fracture surface of the N720/AM specimen subjected to tensile test to failure following 100 h at 20 MPa at 1200°C in argon.

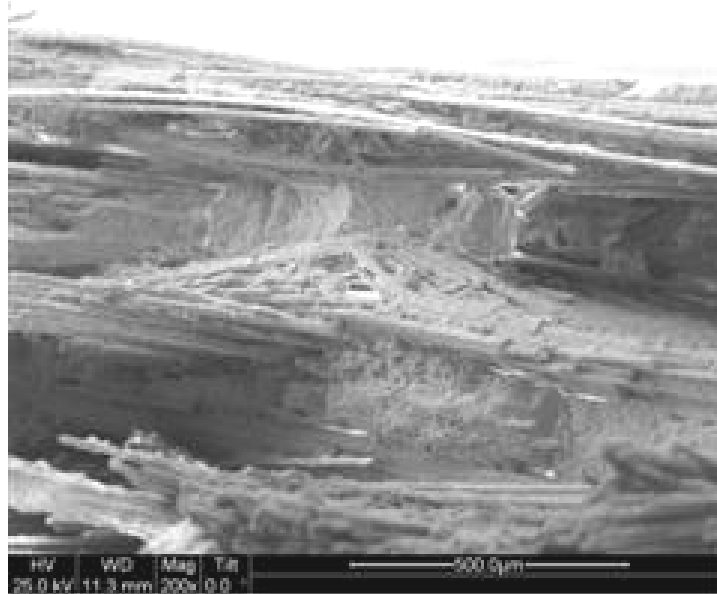


Figure 354. SEM micrograph of the fracture surface of the N720/AM specimen subjected to tensile test to failure following 100 h at 20 MPa at 1200°C in argon.



Figure 355. SEM micrograph of the fracture surface of the N720/AM specimen subjected to tensile test to failure following 100 h at 20 MPa at 1200°C in argon.

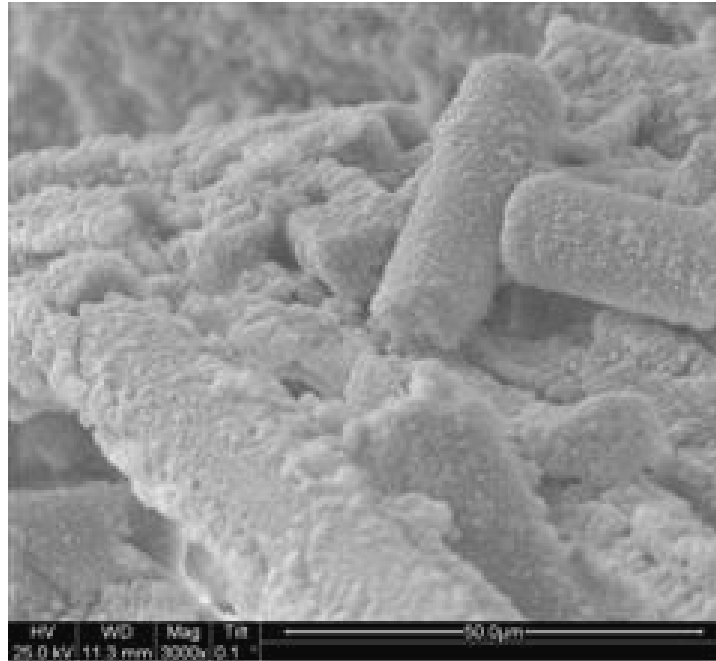


Figure 356. SEM micrograph of the fracture surface of the N720/AM specimen subjected to tensile test to failure following 100 h at 20 MPa at 1200°C in argon.

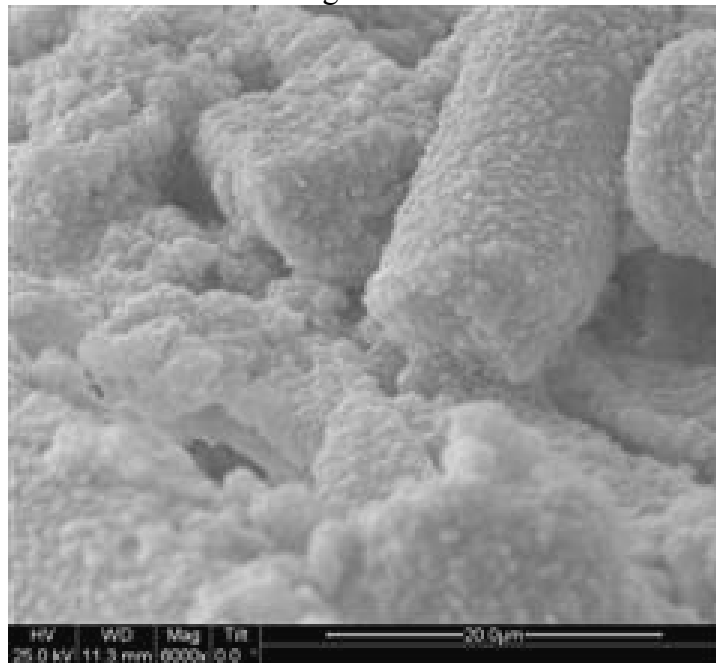


Figure 357. SEM micrograph of the fracture surface of the N720/AM specimen subjected to tensile test to failure following 100 h at 20 MPa at 1200°C in argon.

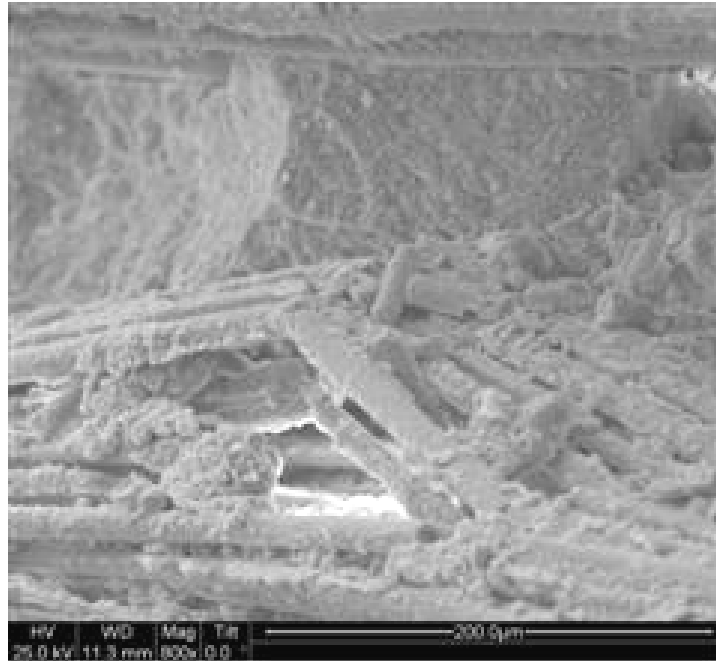


Figure 358. SEM micrograph of the fracture surface of the N720/AM specimen subjected to tensile test to failure following 100 h at 20 MPa at 1200°C in argon.

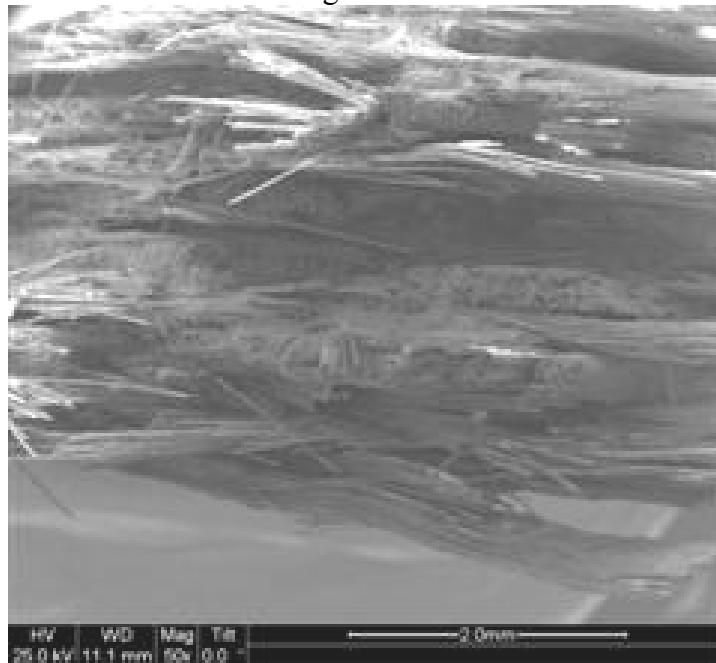


Figure 359. SEM micrograph of the fracture surface of the N720/AM specimen subjected to tensile test to failure following 100 h at 20 MPa at 1200°C in argon.

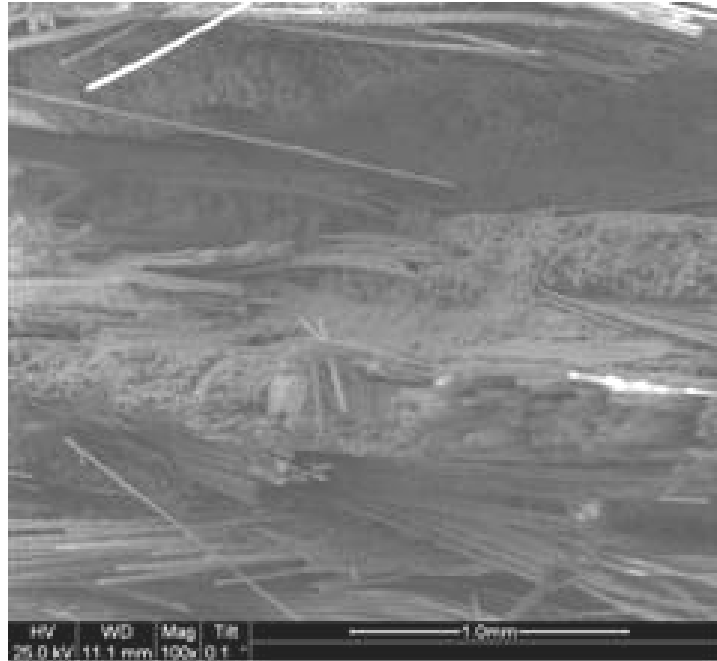


Figure 360. SEM micrograph of the fracture surface of the N720/AM specimen subjected to tensile test to failure following 100 h at 20 MPa at 1200°C in argon.

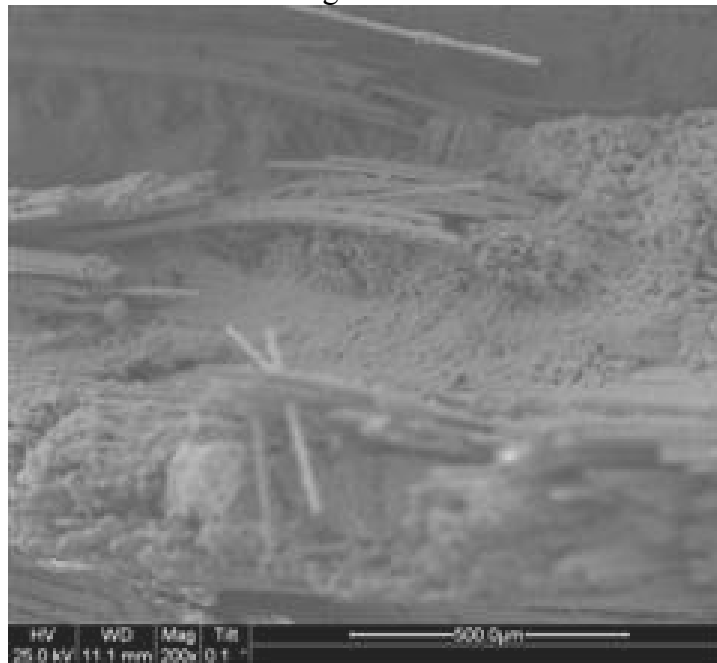


Figure 361. SEM micrograph of the fracture surface of the N720/AM specimen subjected to tensile test to failure following 100 h at 20 MPa at 1200°C in argon.

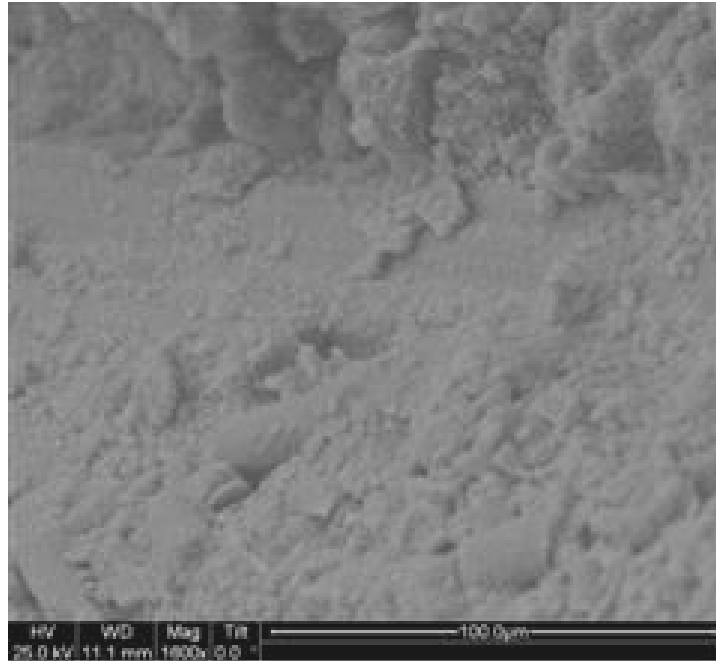


Figure 362. SEM micrograph of the fracture surface of the N720/AM specimen subjected to tensile test to failure following 100 h at 20 MPa at 1200°C in argon.

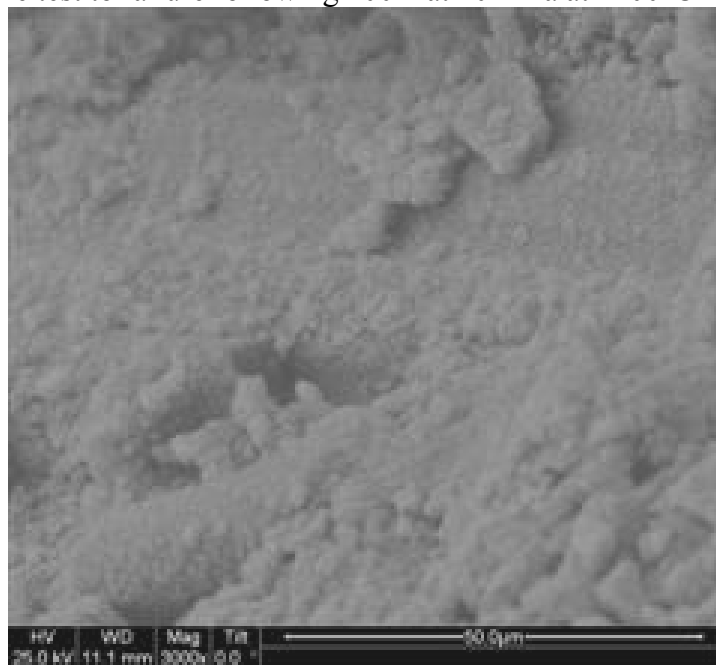


Figure 363. SEM micrograph of the fracture surface of the N720/AM specimen subjected to tensile test to failure following 100 h at 20 MPa at 1200°C in argon.

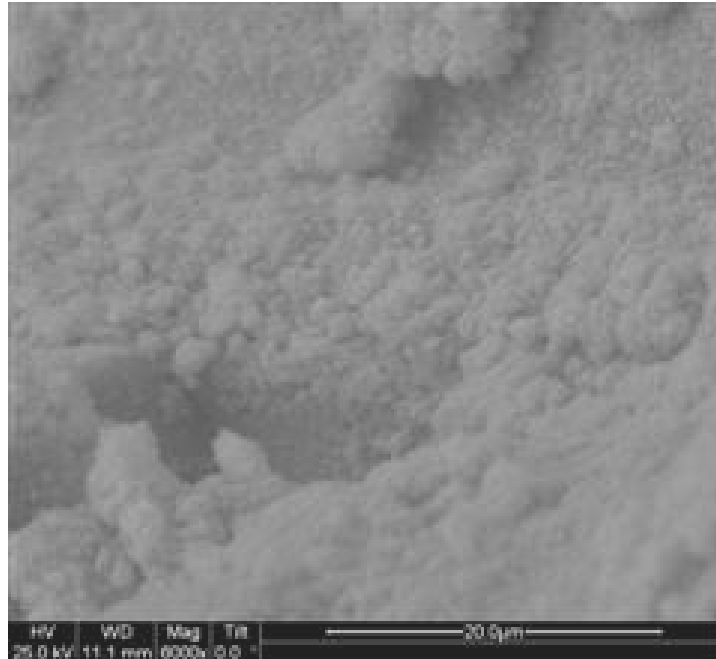


Figure 364. SEM micrograph of the fracture surface of the N720/AM specimen subjected to tensile test to failure following 100 h at 20 MPa at 1200°C in argon.

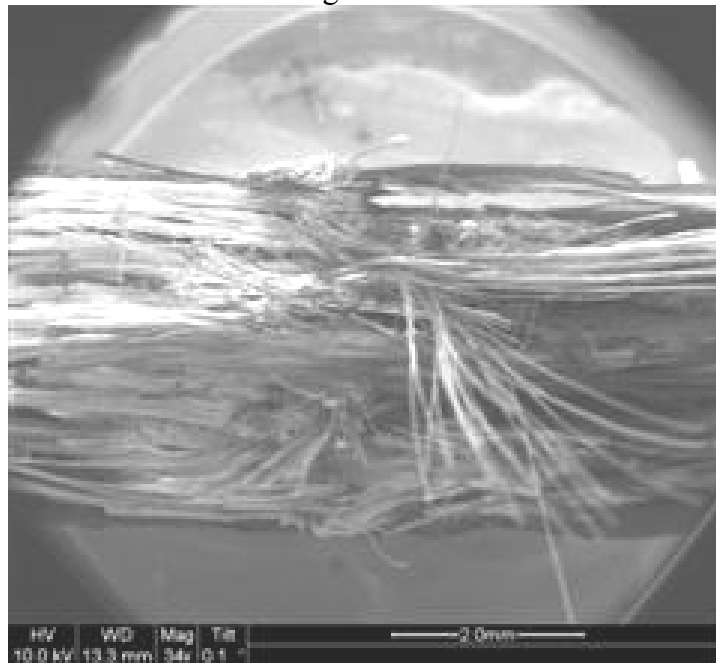


Figure 365. SEM micrograph of the fracture surface of the N720/AM specimen with  $\pm 45^\circ$  fiber orientation obtained in creep test conducted at 30 MPa at 1200°C in argon. Creep lifetime  $t_f = 3.42$  h.

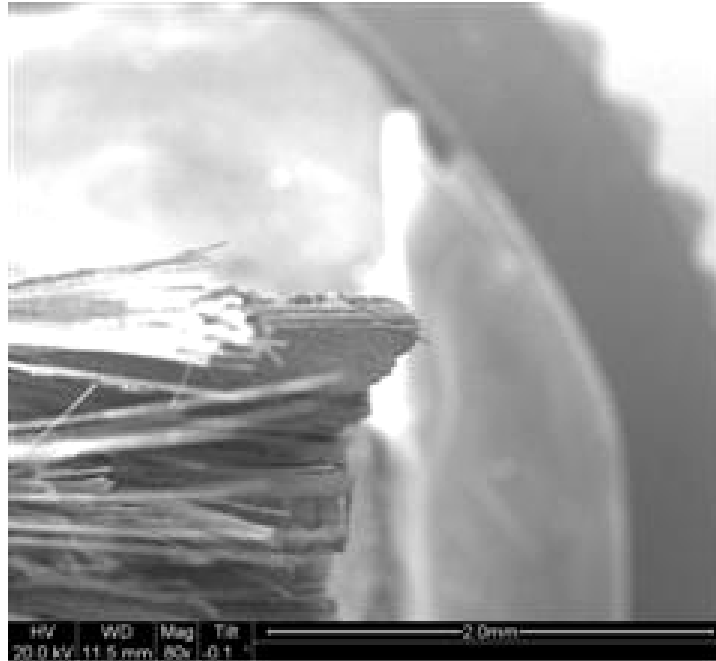


Figure 366. SEM micrograph of the fracture surface of the N720/AM specimen with  $\pm 45^\circ$  fiber orientation obtained in creep test conducted at 30 MPa at 1200°C in argon. Creep lifetime  $t_f = 3.42$  h.

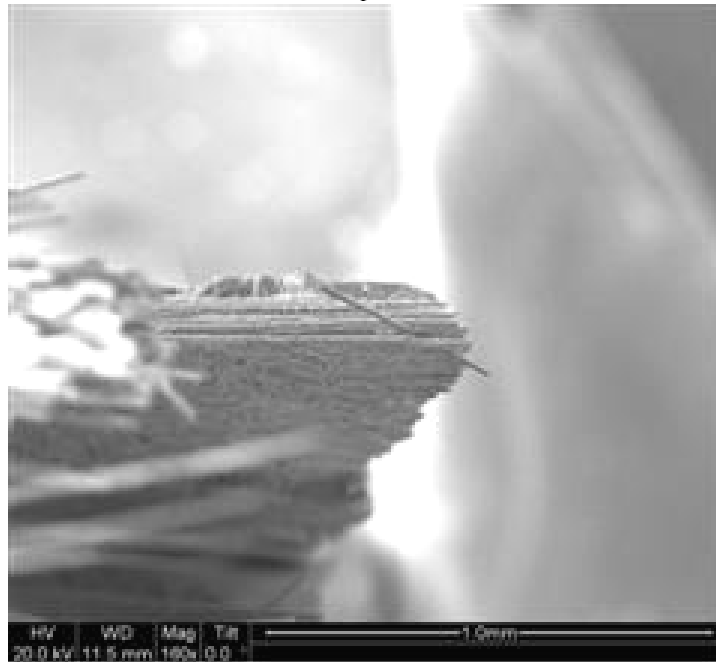


Figure 367. SEM micrograph of the fracture surface of the N720/AM specimen with  $\pm 45^\circ$  fiber orientation obtained in creep test conducted at 30 MPa at 1200°C in argon. Creep lifetime  $t_f = 3.42$  h.

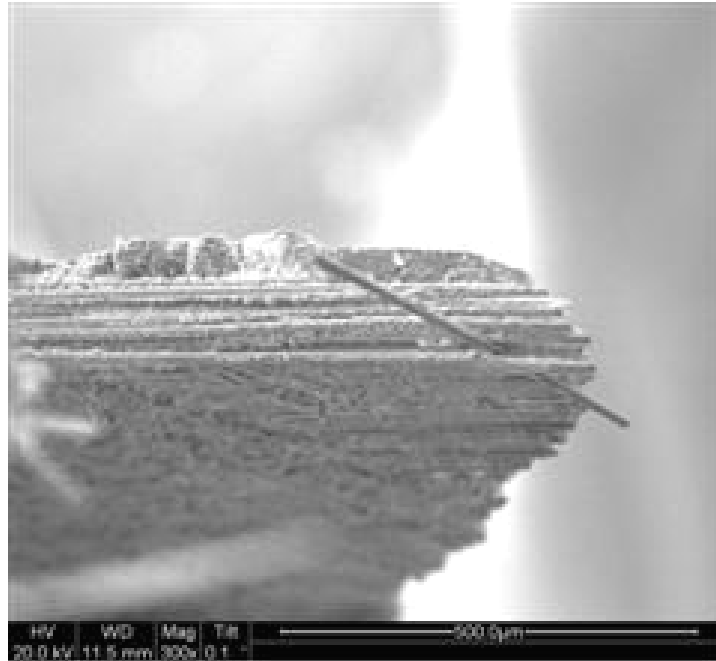


Figure 368. SEM micrograph of the fracture surface of the N720/AM specimen with  $\pm 45^\circ$  fiber orientation obtained in creep test conducted at 30 MPa at 1200°C in argon. Creep lifetime  $t_f = 3.42$  h.

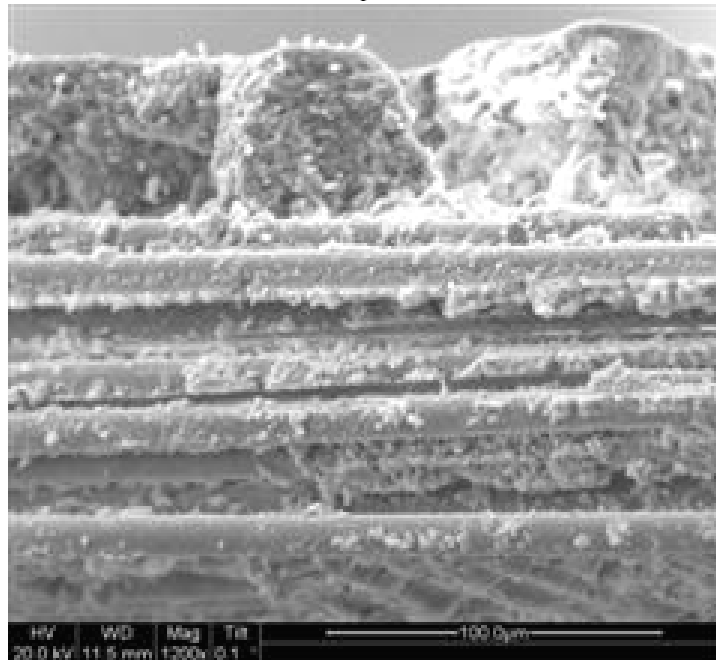


Figure 369. SEM micrograph of the fracture surface of the N720/AM specimen with  $\pm 45^\circ$  fiber orientation obtained in creep test conducted at 30 MPa at 1200°C in argon. Creep lifetime  $t_f = 3.42$  h.

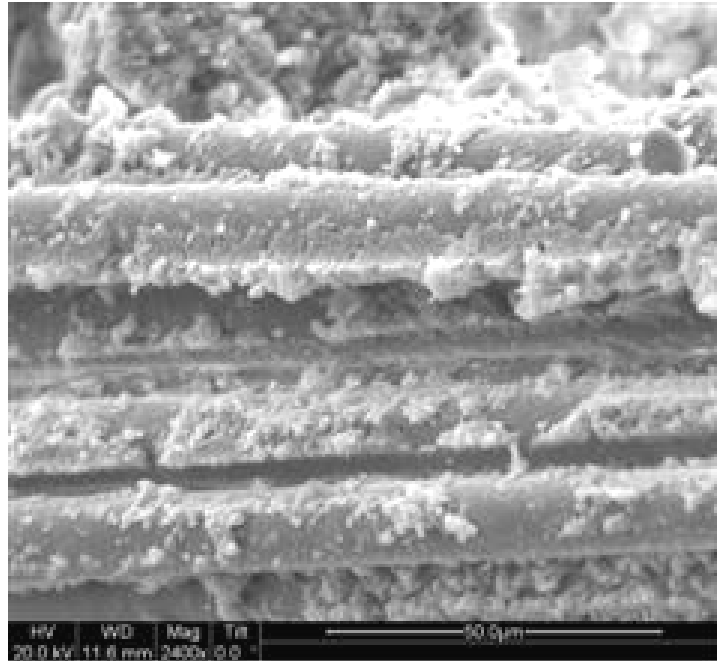


Figure 370. SEM micrograph of the fracture surface of the N720/AM specimen with  $\pm 45^\circ$  fiber orientation obtained in creep test conducted at 30 MPa at 1200°C in argon. Creep lifetime  $t_f = 3.42$  h.

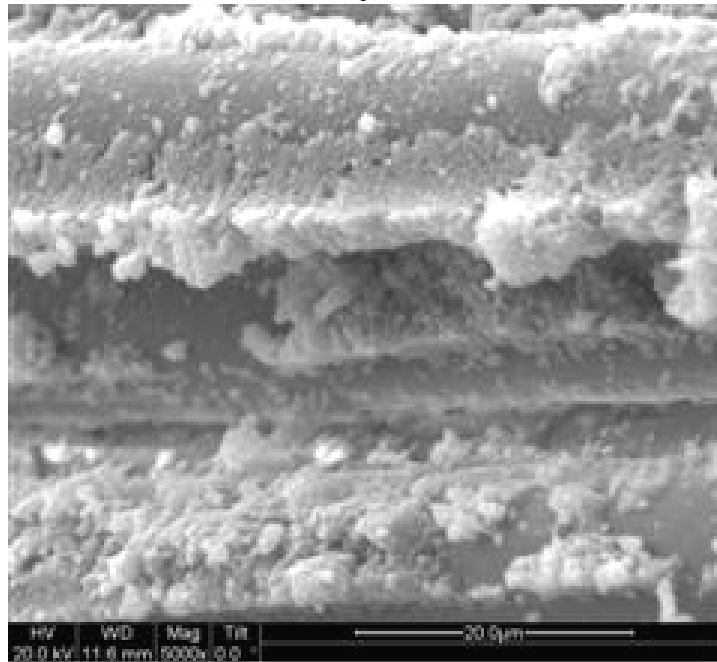


Figure 371. SEM micrograph of the fracture surface of the N720/AM specimen with  $\pm 45^\circ$  fiber orientation obtained in creep test conducted at 30 MPa at 1200°C in argon. Creep lifetime  $t_f = 3.42$  h.

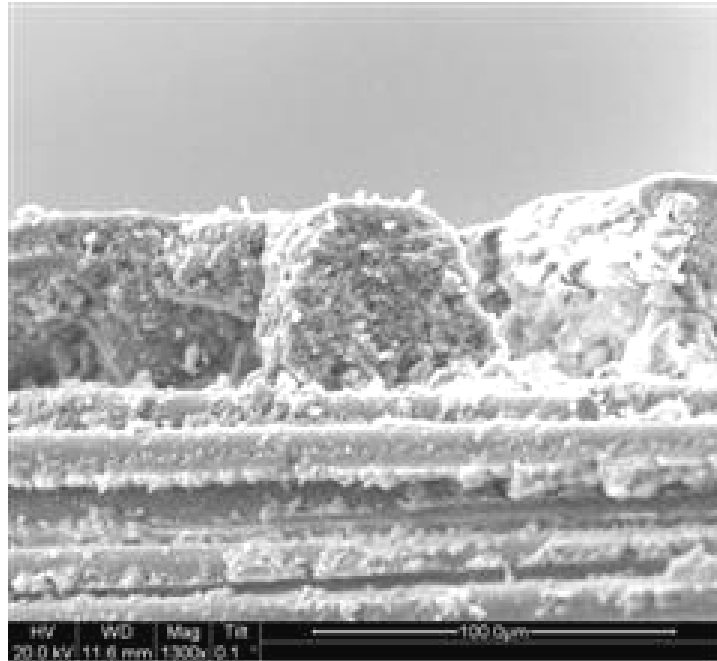


Figure 372. SEM micrograph of the fracture surface of the N720/AM specimen with  $\pm 45^\circ$  fiber orientation obtained in creep test conducted at 30 MPa at 1200°C in argon. Creep lifetime  $t_f = 3.42$  h.

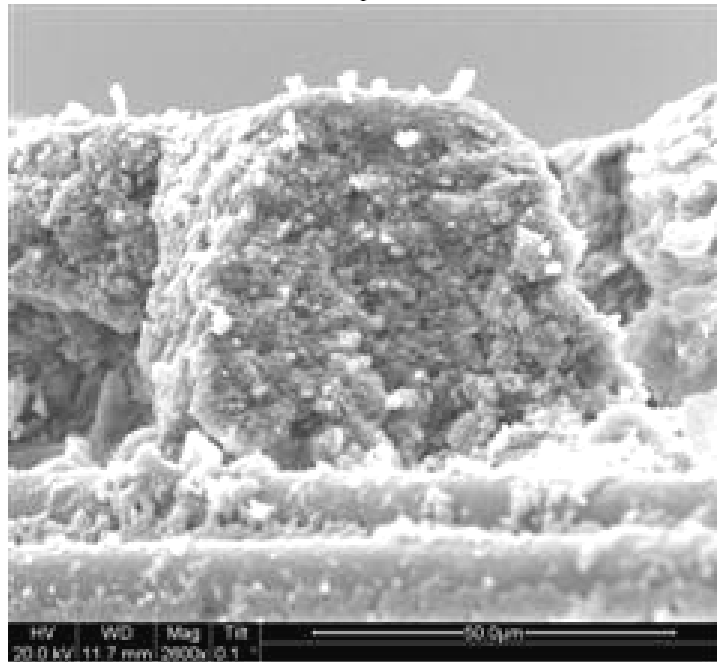


Figure 373. SEM micrograph of the fracture surface of the N720/AM specimen with  $\pm 45^\circ$  fiber orientation obtained in creep test conducted at 30 MPa at 1200°C in argon. Creep lifetime  $t_f = 3.42$  h.

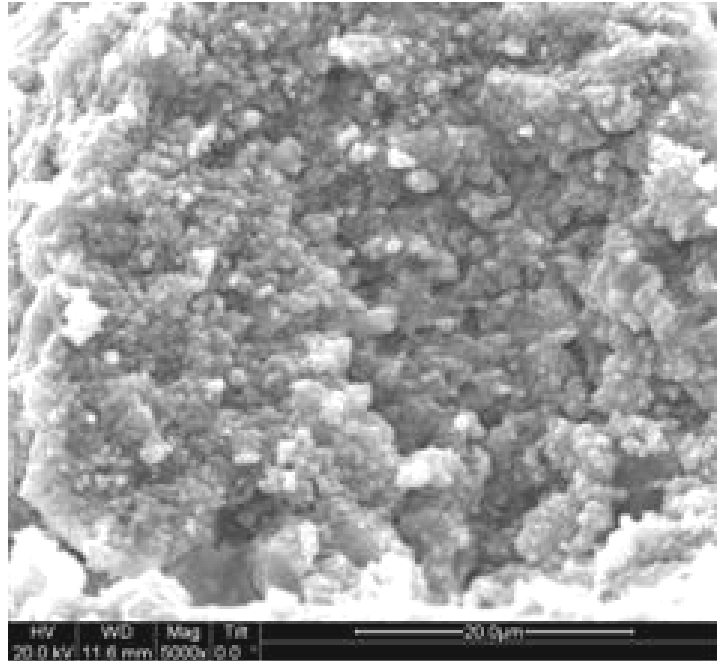


Figure 374. SEM micrograph of the fracture surface of the N720/AM specimen with  $\pm 45^\circ$  fiber orientation obtained in creep test conducted at 30 MPa at 1200°C in argon. Creep lifetime  $t_f = 3.42$  h.

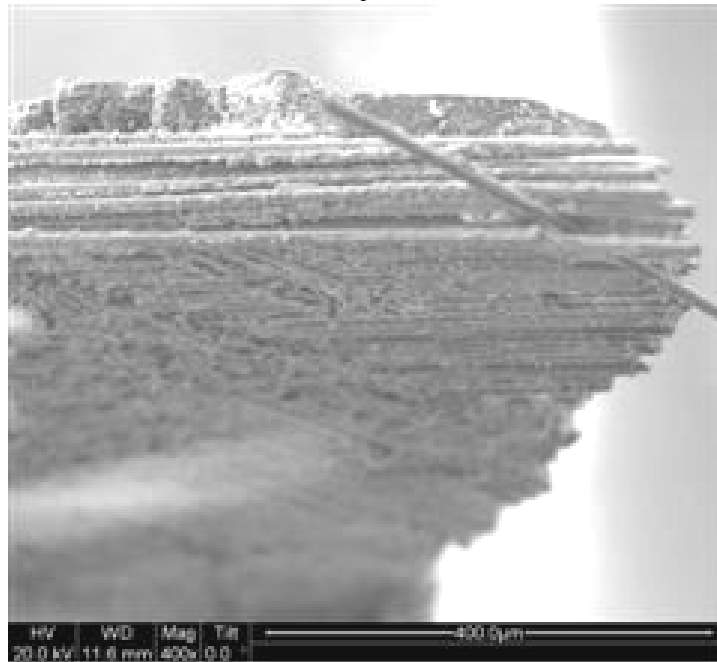


Figure 375. SEM micrograph of the fracture surface of the N720/AM specimen with  $\pm 45^\circ$  fiber orientation obtained in creep test conducted at 30 MPa at 1200°C in argon. Creep lifetime  $t_f = 3.42$  h.

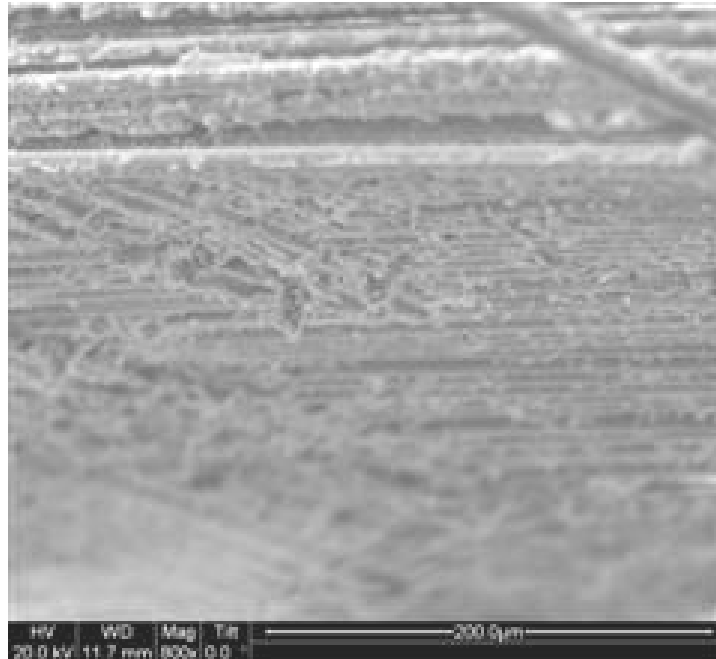


Figure 376. SEM micrograph of the fracture surface of the N720/AM specimen with  $\pm 45^\circ$  fiber orientation obtained in creep test conducted at 30 MPa at 1200°C in argon. Creep lifetime  $t_f = 3.42$  h.

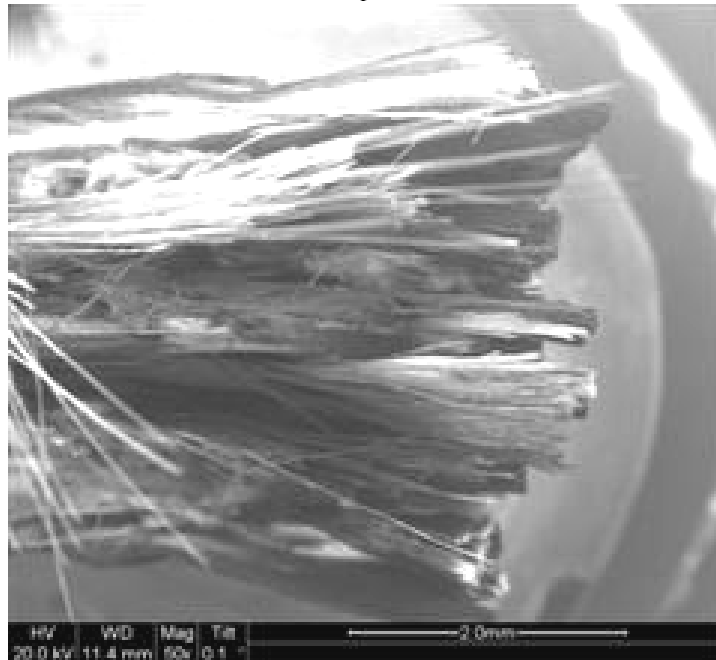


Figure 377. SEM micrograph of the fracture surface of the N720/AM specimen with  $\pm 45^\circ$  fiber orientation obtained in creep test conducted at 30 MPa at 1200°C in argon. Creep lifetime  $t_f = 3.42$  h.

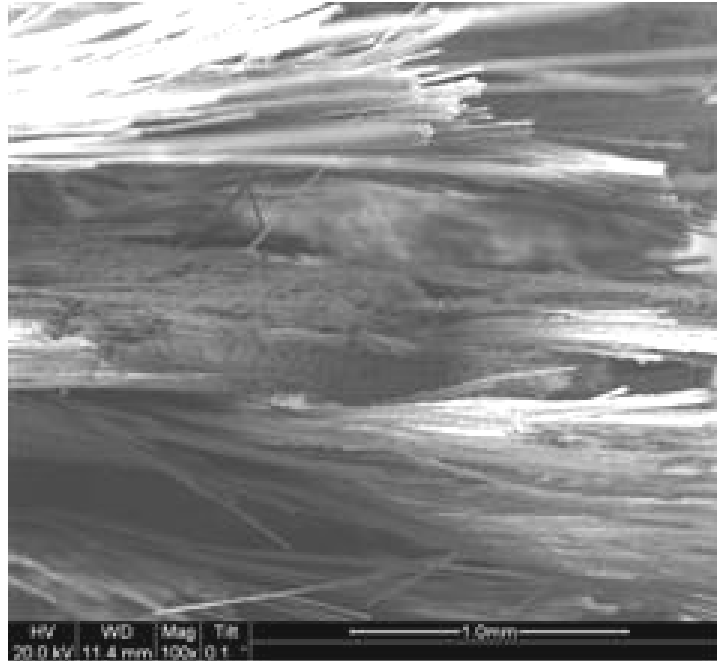


Figure 378. SEM micrograph of the fracture surface of the N720/AM specimen with  $\pm 45^\circ$  fiber orientation obtained in creep test conducted at 30 MPa at 1200°C in argon. Creep lifetime  $t_f = 3.42$  h.

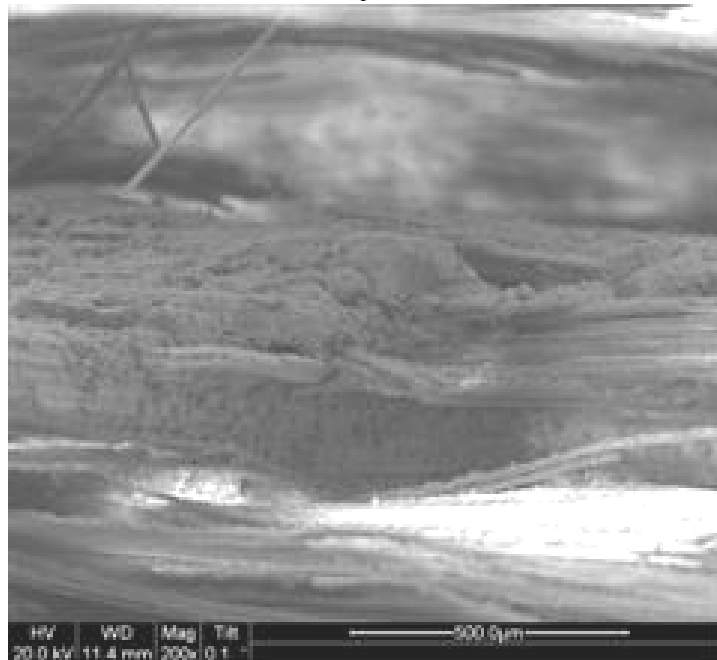


Figure 379. SEM micrograph of the fracture surface of the N720/AM specimen with  $\pm 45^\circ$  fiber orientation obtained in creep test conducted at 30 MPa at 1200°C in argon. Creep lifetime  $t_f = 3.42$  h.

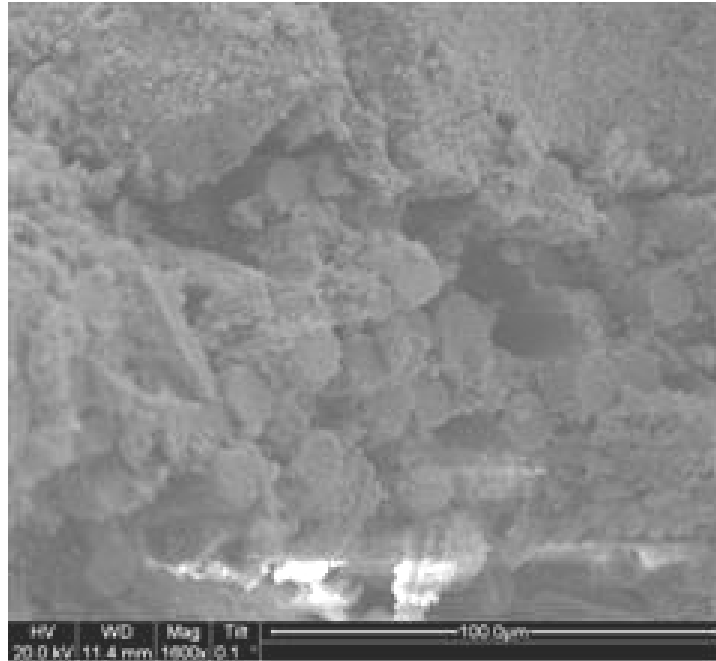


Figure 380. SEM micrograph of the fracture surface of the N720/AM specimen with  $\pm 45^\circ$  fiber orientation obtained in creep test conducted at 30 MPa at 1200°C in argon. Creep lifetime  $t_f = 3.42$  h.

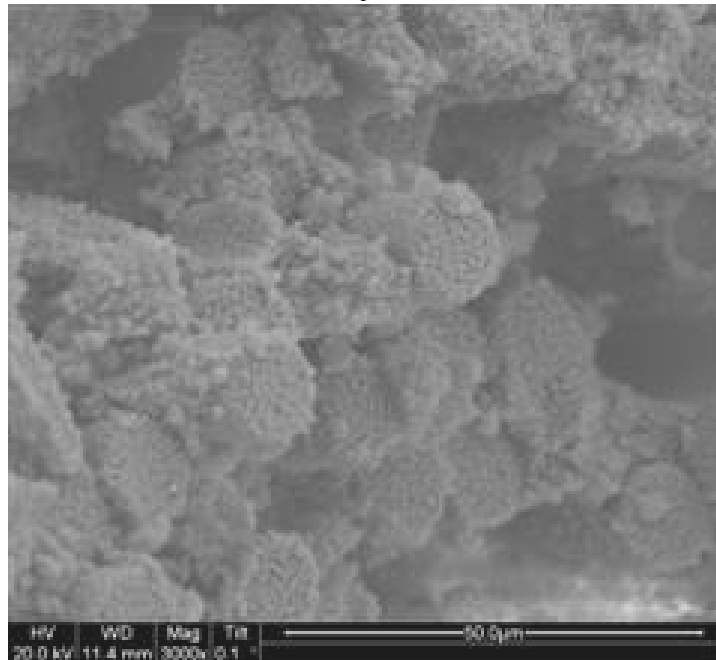


Figure 381. SEM micrograph of the fracture surface of the N720/AM specimen with  $\pm 45^\circ$  fiber orientation obtained in creep test conducted at 30 MPa at 1200°C in argon. Creep lifetime  $t_f = 3.42$  h.

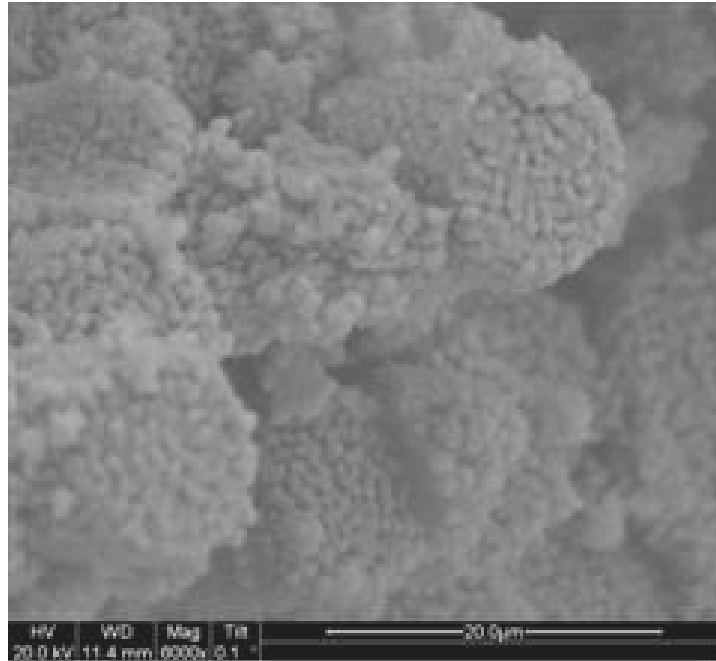


Figure 382. SEM micrograph of the fracture surface of the N720/AM specimen with  $\pm 45^\circ$  fiber orientation obtained in creep test conducted at 30 MPa at 1200°C in argon. Creep lifetime  $t_f = 3.42$  h.

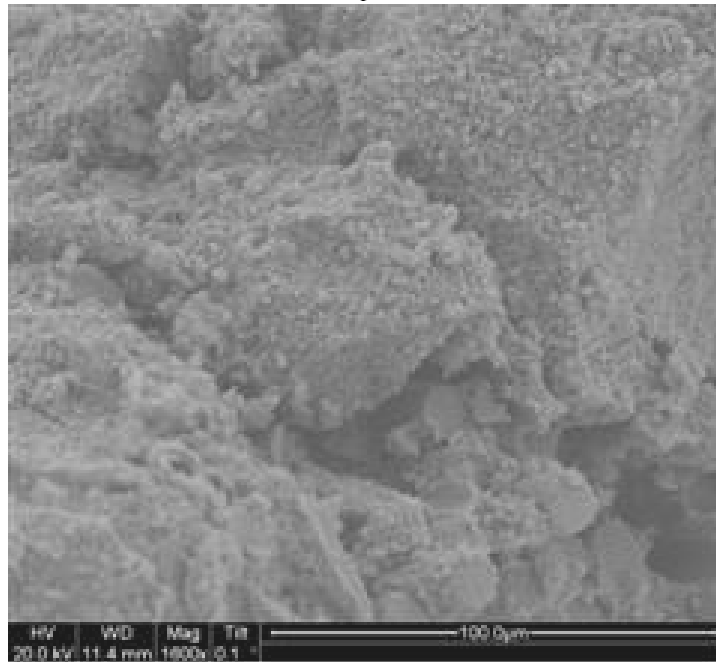


Figure 383. SEM micrograph of the fracture surface of the N720/AM specimen with  $\pm 45^\circ$  fiber orientation obtained in creep test conducted at 30 MPa at 1200°C in argon. Creep lifetime  $t_f = 3.42$  h.

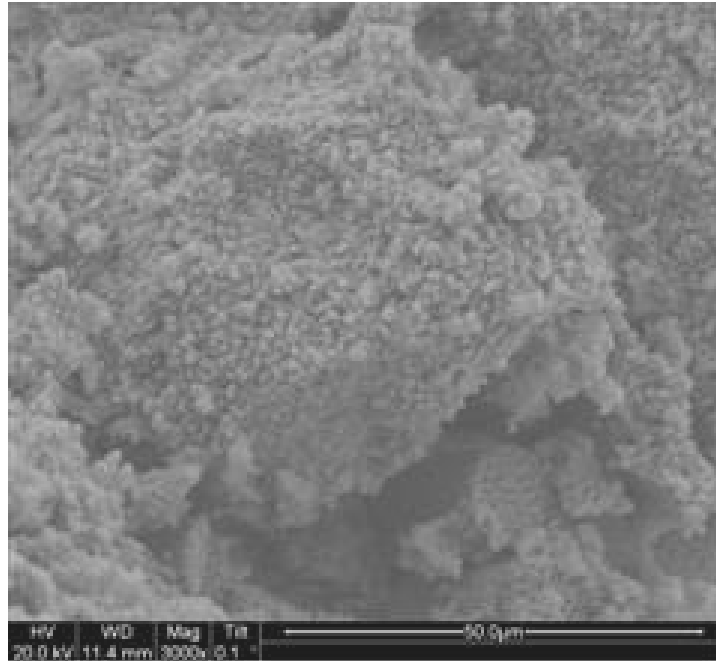


Figure 384. SEM micrograph of the fracture surface of the N720/AM specimen with  $\pm 45^\circ$  fiber orientation obtained in creep test conducted at 30 MPa at 1200°C in argon. Creep lifetime  $t_f = 3.42$  h.

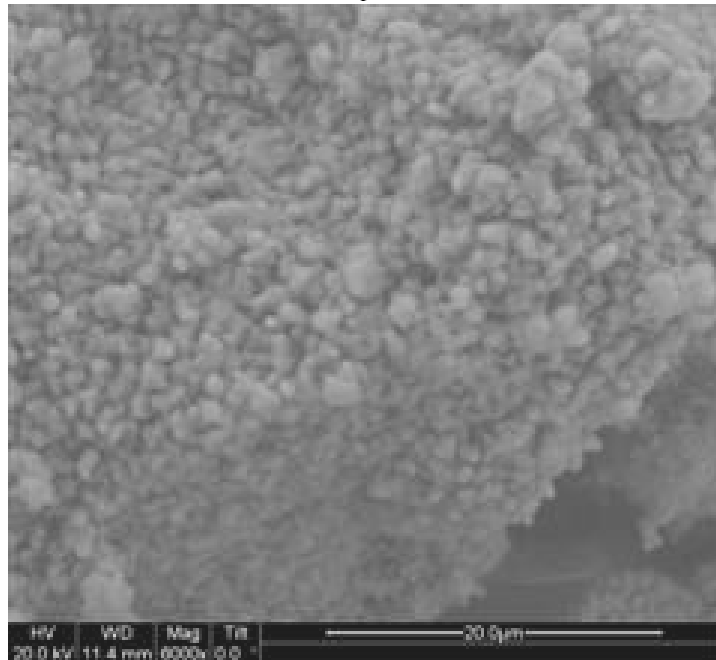


Figure 385. SEM micrograph of the fracture surface of the N720/AM specimen with  $\pm 45^\circ$  fiber orientation obtained in creep test conducted at 30 MPa at 1200°C in argon. Creep lifetime  $t_f = 3.42$  h.

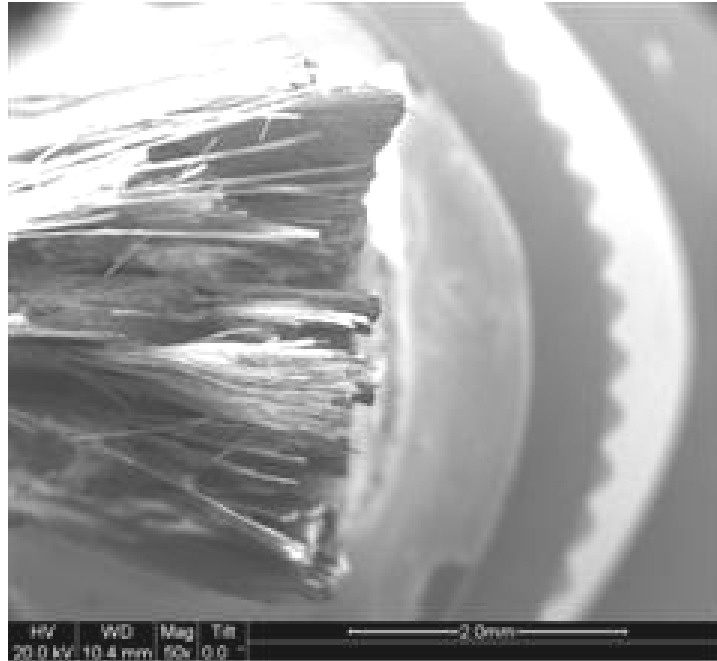


Figure 386. SEM micrograph of the fracture surface of the N720/AM specimen with  $\pm 45^\circ$  fiber orientation obtained in creep test conducted at 30 MPa at 1200°C in argon. Creep lifetime  $t_f = 3.42$  h.

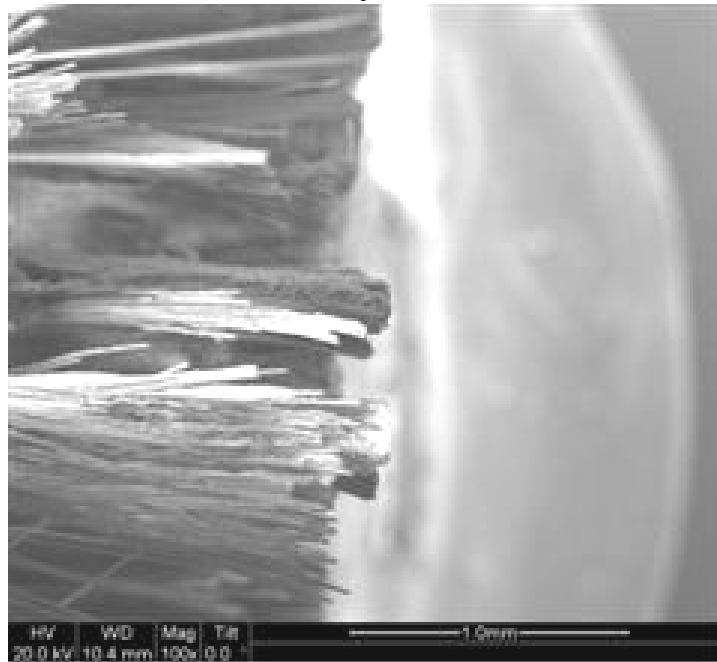


Figure 387. SEM micrograph of the fracture surface of the N720/AM specimen with  $\pm 45^\circ$  fiber orientation obtained in creep test conducted at 30 MPa at 1200°C in argon. Creep lifetime  $t_f = 3.42$  h.

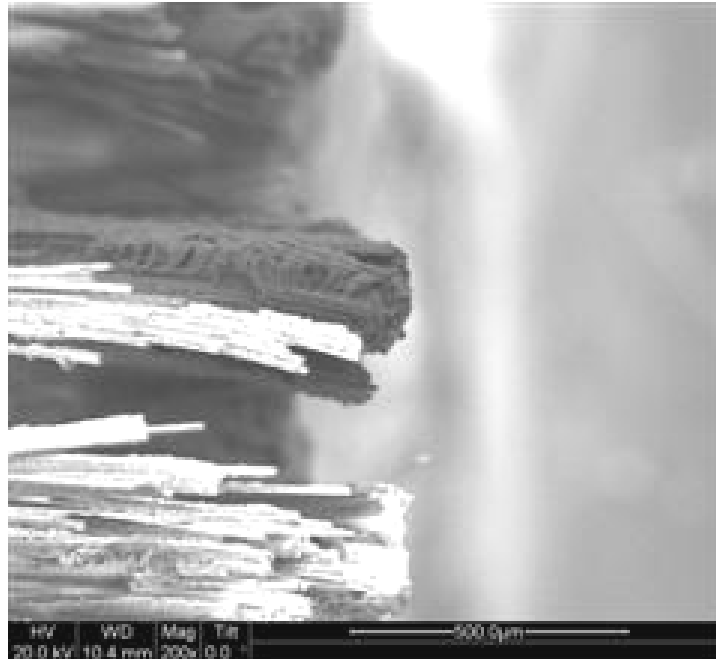


Figure 388. SEM micrograph of the fracture surface of the N720/AM specimen with  $\pm 45^\circ$  fiber orientation obtained in creep test conducted at 30 MPa at 1200°C in argon. Creep lifetime  $t_f = 3.42$  h.

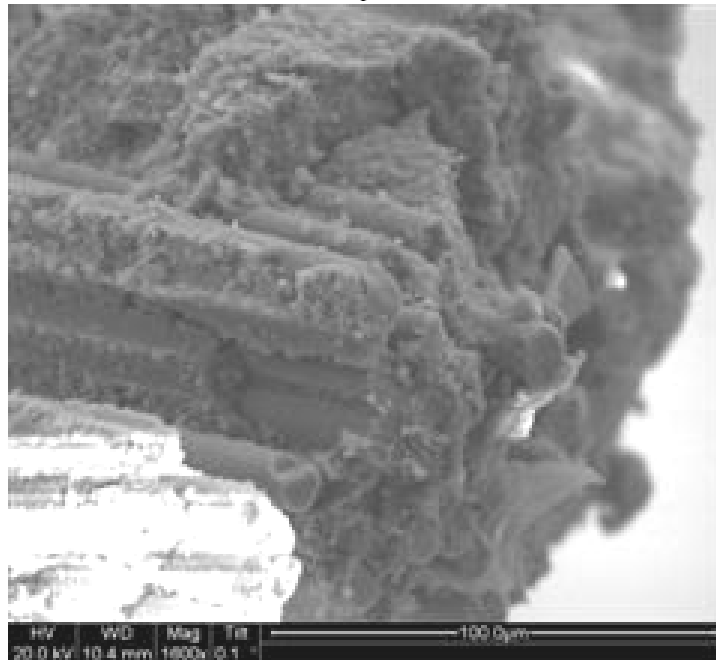


Figure 389. SEM micrograph of the fracture surface of the N720/AM specimen with  $\pm 45^\circ$  fiber orientation obtained in creep test conducted at 30 MPa at 1200°C in argon. Creep lifetime  $t_f = 3.42$  h.

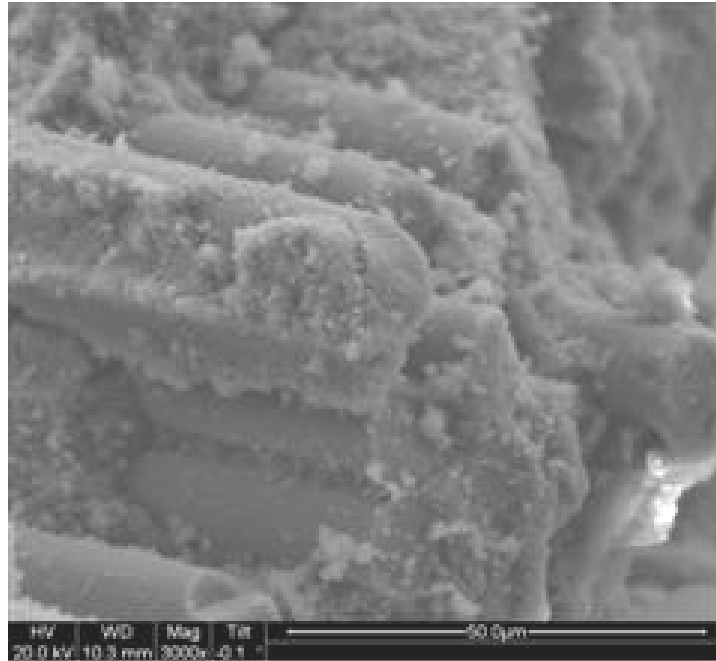


Figure 390. SEM micrograph of the fracture surface of the N720/AM specimen with  $\pm 45^\circ$  fiber orientation obtained in creep test conducted at 30 MPa at 1200°C in argon. Creep lifetime  $t_f = 3.42$  h.

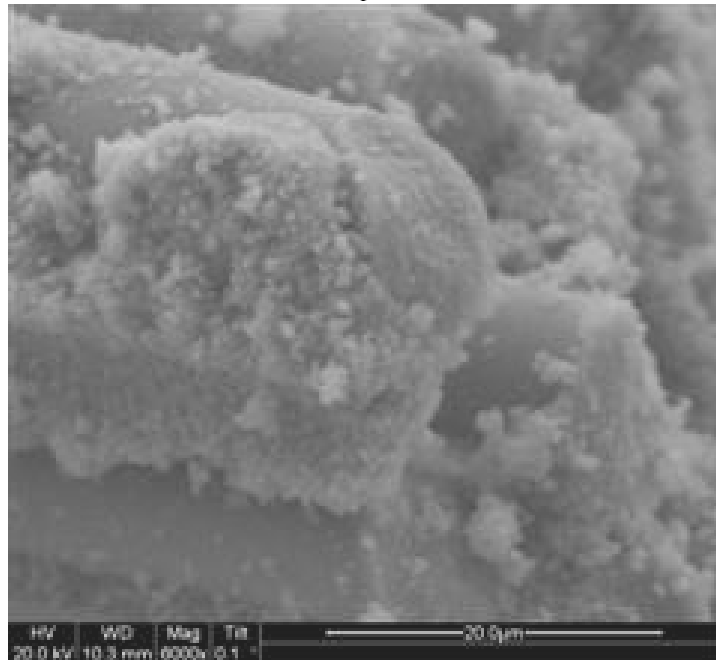


Figure 391. SEM micrograph of the fracture surface of the N720/AM specimen with  $\pm 45^\circ$  fiber orientation obtained in creep test conducted at 30 MPa at 1200°C in argon. Creep lifetime  $t_f = 3.42$  h.

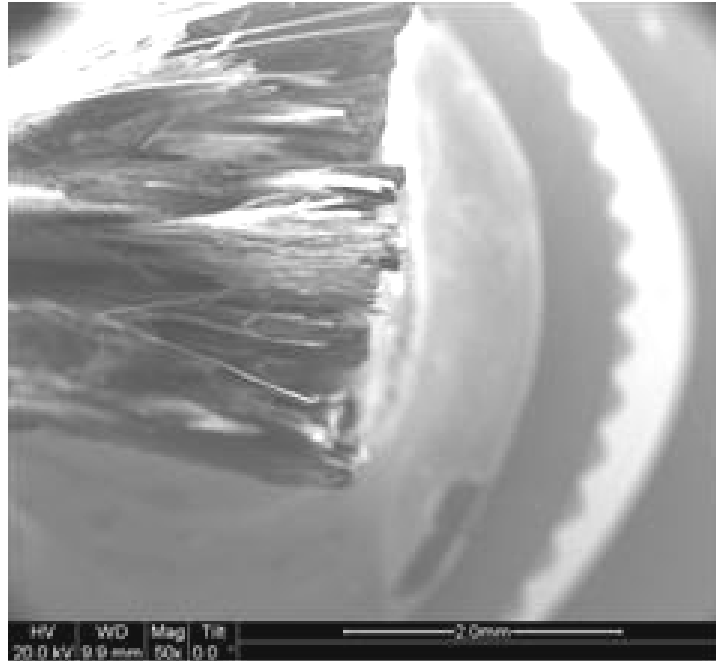


Figure 392. SEM micrograph of the fracture surface of the N720/AM specimen with  $\pm 45^\circ$  fiber orientation obtained in creep test conducted at 30 MPa at 1200°C in argon. Creep lifetime  $t_f = 3.42$  h.

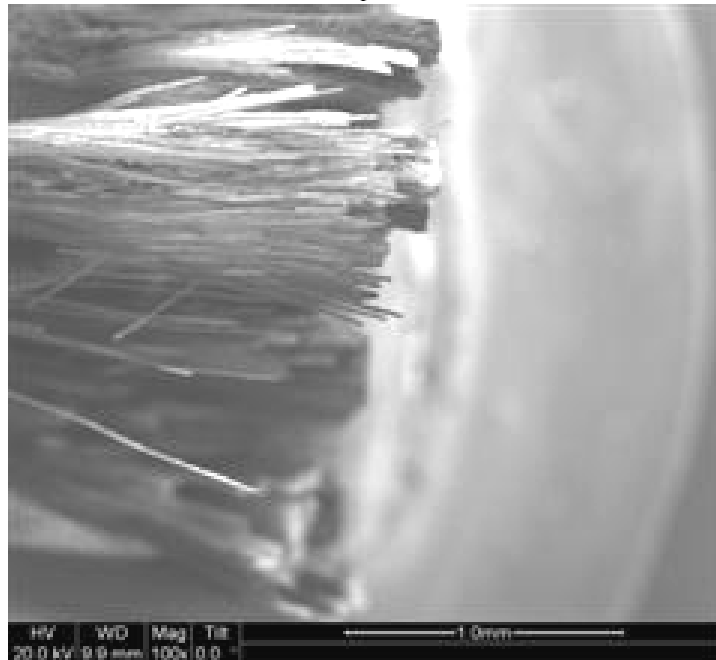


Figure 393. SEM micrograph of the fracture surface of the N720/AM specimen with  $\pm 45^\circ$  fiber orientation obtained in creep test conducted at 30 MPa at 1200°C in argon. Creep lifetime  $t_f = 3.42$  h.

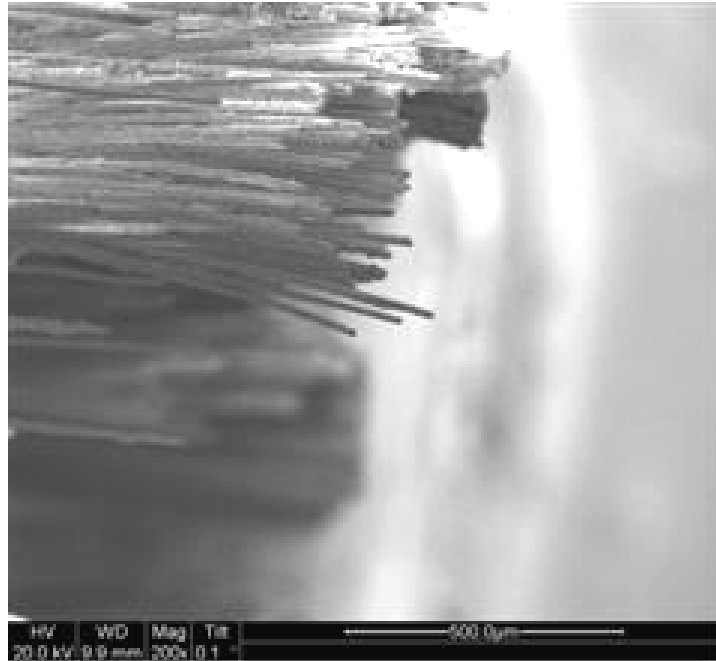


Figure 394. SEM micrograph of the fracture surface of the N720/AM specimen with  $\pm 45^\circ$  fiber orientation obtained in creep test conducted at 30 MPa at 1200°C in argon. Creep lifetime  $t_f = 3.42$  h.

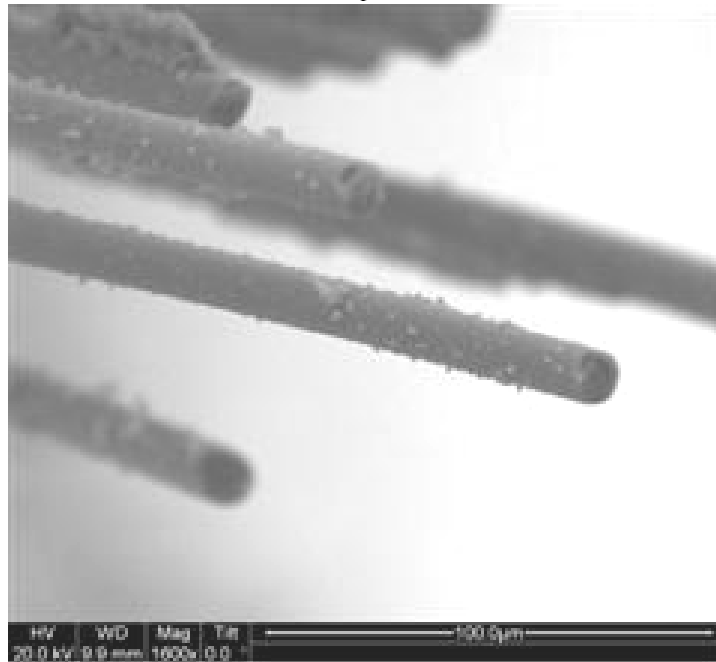


Figure 395. SEM micrograph of the fracture surface of the N720/AM specimen with  $\pm 45^\circ$  fiber orientation obtained in creep test conducted at 30 MPa at 1200°C in argon. Creep lifetime  $t_f = 3.42$  h.

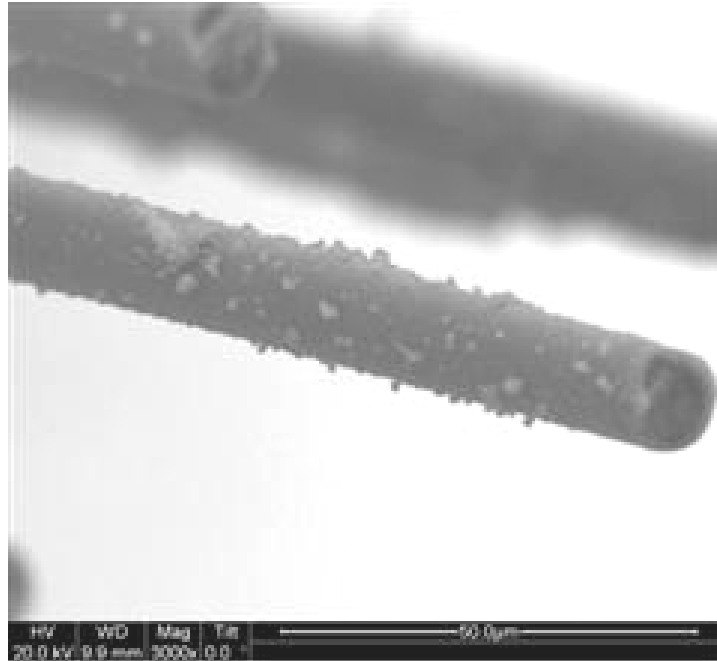


Figure 396. SEM micrograph of the fracture surface of the N720/AM specimen with  $\pm 45^\circ$  fiber orientation obtained in creep test conducted at 30 MPa at 1200°C in argon. Creep lifetime  $t_f = 3.42$  h.

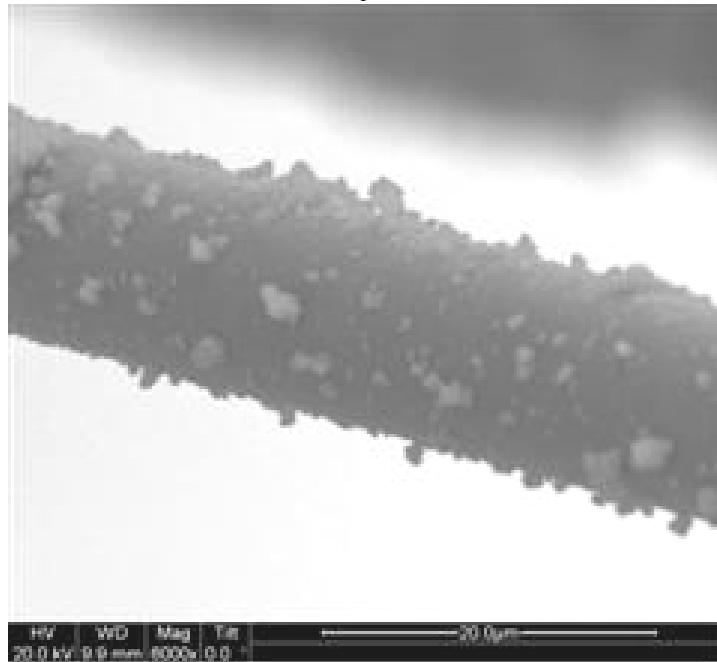


Figure 397. SEM micrograph of the fracture surface of the N720/AM specimen with  $\pm 45^\circ$  fiber orientation obtained in creep test conducted at 30 MPa at 1200°C in argon. Creep lifetime  $t_f = 3.42$  h.

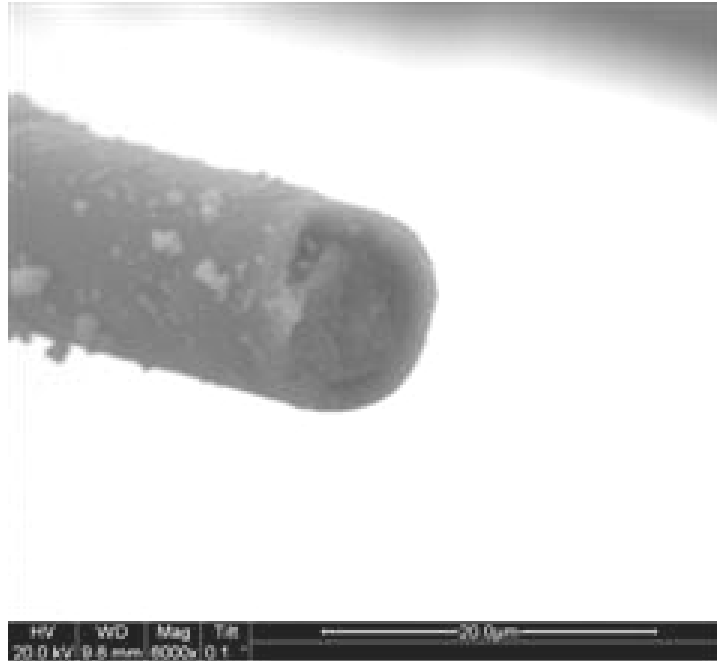


Figure 398. SEM micrograph of the fracture surface of the N720/AM specimen with  $\pm 45^\circ$  fiber orientation obtained in creep test conducted at 30 MPa at 1200°C in argon. Creep lifetime  $t_f = 3.42$  h.

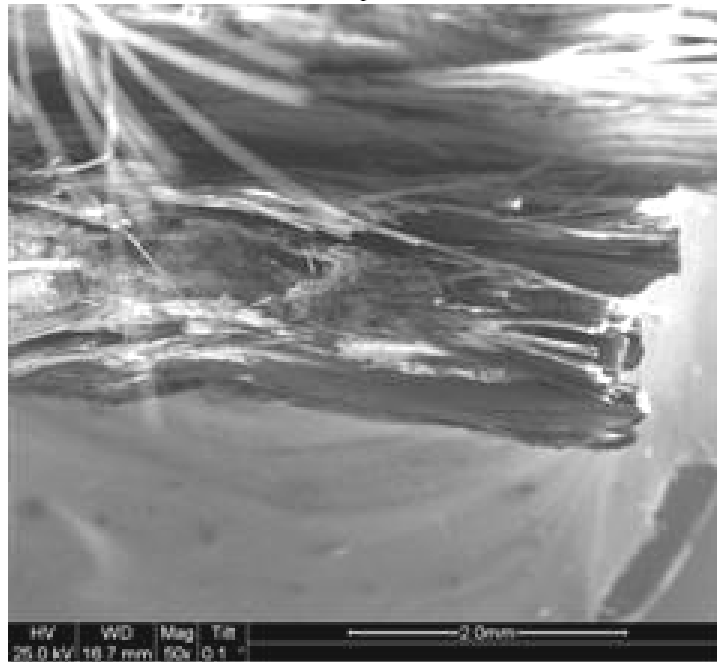


Figure 399. SEM micrograph of the fracture surface of the N720/AM specimen with  $\pm 45^\circ$  fiber orientation obtained in creep test conducted at 30 MPa at 1200°C in argon. Creep lifetime  $t_f = 3.42$  h.

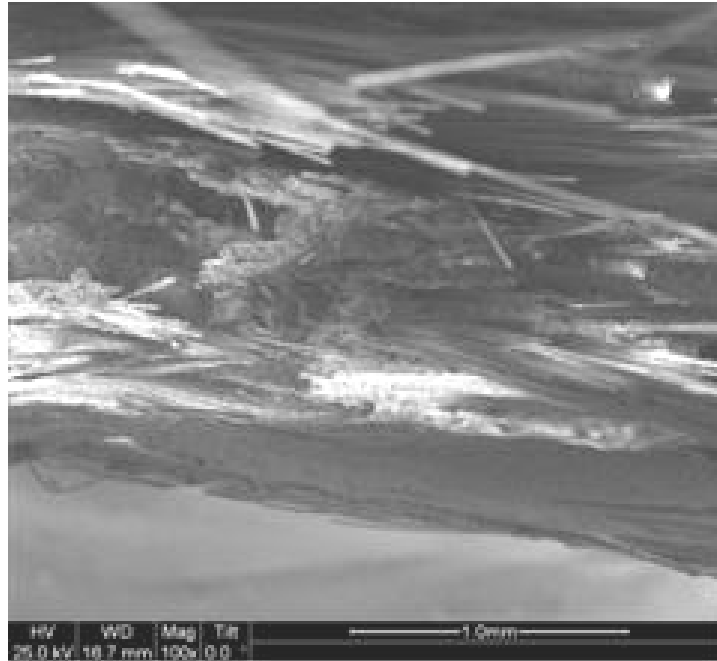


Figure 400. SEM micrograph of the fracture surface of the N720/AM specimen with  $\pm 45^\circ$  fiber orientation obtained in creep test conducted at 30 MPa at 1200°C in argon. Creep lifetime  $t_f = 3.42$  h.

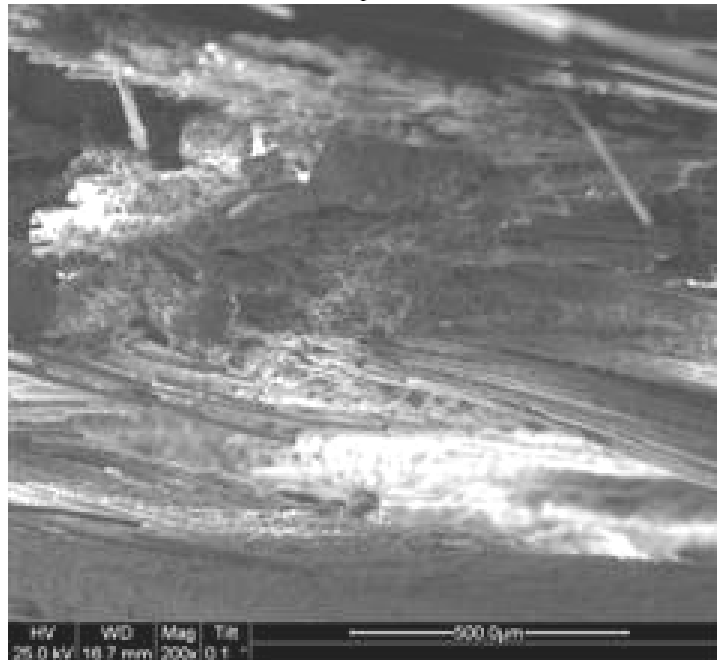


Figure 401. SEM micrograph of the fracture surface of the N720/AM specimen with  $\pm 45^\circ$  fiber orientation obtained in creep test conducted at 30 MPa at 1200°C in argon. Creep lifetime  $t_f = 3.42$  h.

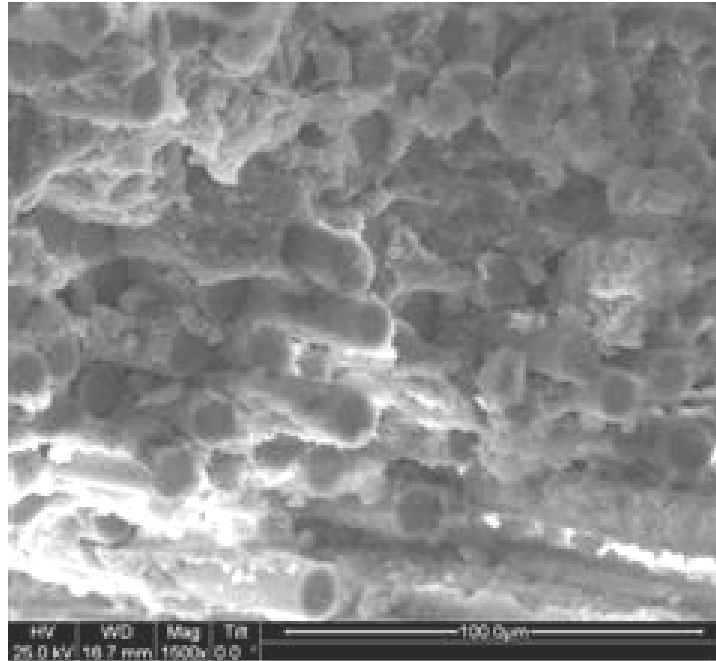


Figure 402. SEM micrograph of the fracture surface of the N720/AM specimen with  $\pm 45^\circ$  fiber orientation obtained in creep test conducted at 30 MPa at 1200°C in argon. Creep lifetime  $t_f = 3.42$  h.

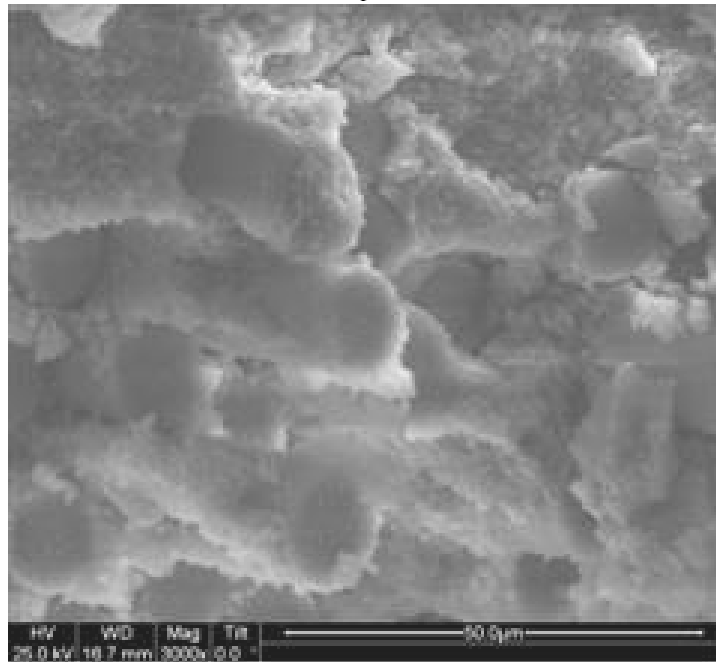


Figure 403. SEM micrograph of the fracture surface of the N720/AM specimen with  $\pm 45^\circ$  fiber orientation obtained in creep test conducted at 30 MPa at 1200°C in argon. Creep lifetime  $t_f = 3.42$  h.

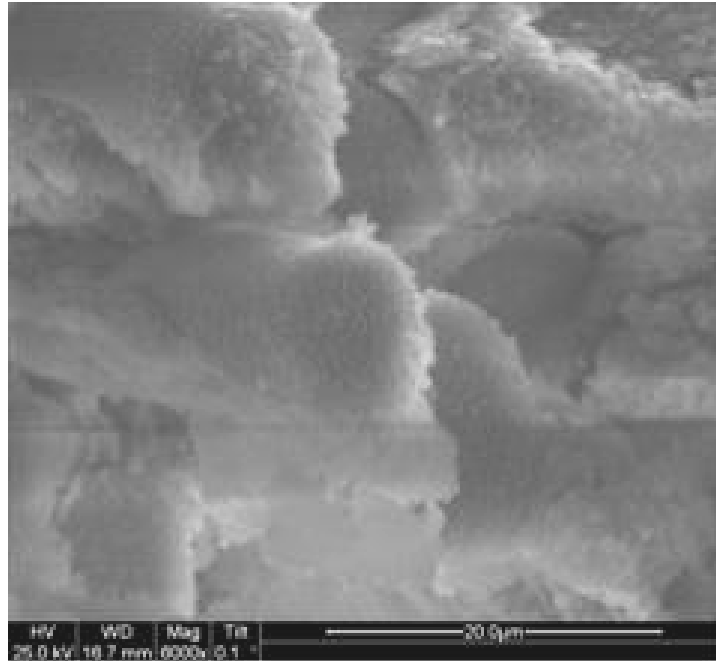


Figure 404. SEM micrograph of the fracture surface of the N720/AM specimen with  $\pm 45^\circ$  fiber orientation obtained in creep test conducted at 30 MPa at 1200°C in argon. Creep lifetime  $t_f = 3.42$  h.

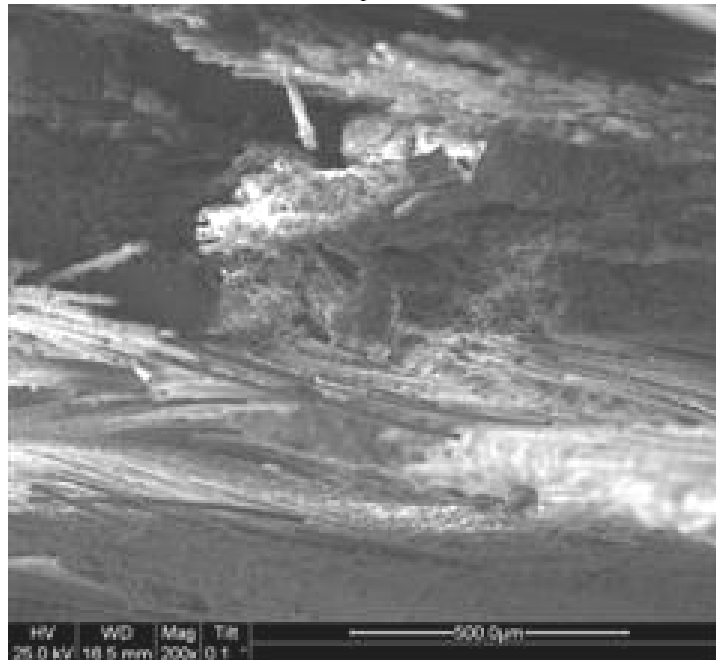


Figure 405. SEM micrograph of the fracture surface of the N720/AM specimen with  $\pm 45^\circ$  fiber orientation obtained in creep test conducted at 30 MPa at 1200°C in argon. Creep lifetime  $t_f = 3.42$  h.

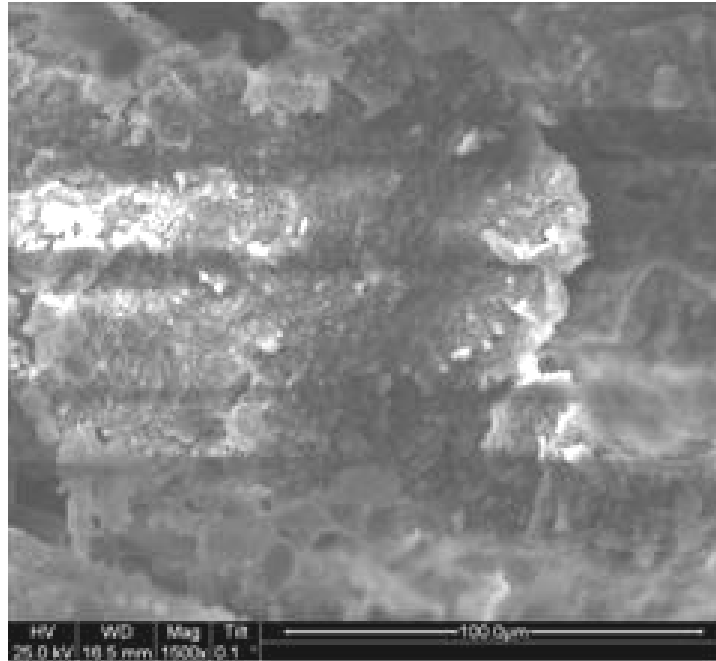


Figure 406. SEM micrograph of the fracture surface of the N720/AM specimen with  $\pm 45^\circ$  fiber orientation obtained in creep test conducted at 30 MPa at 1200°C in argon. Creep lifetime  $t_f = 3.42$  h.

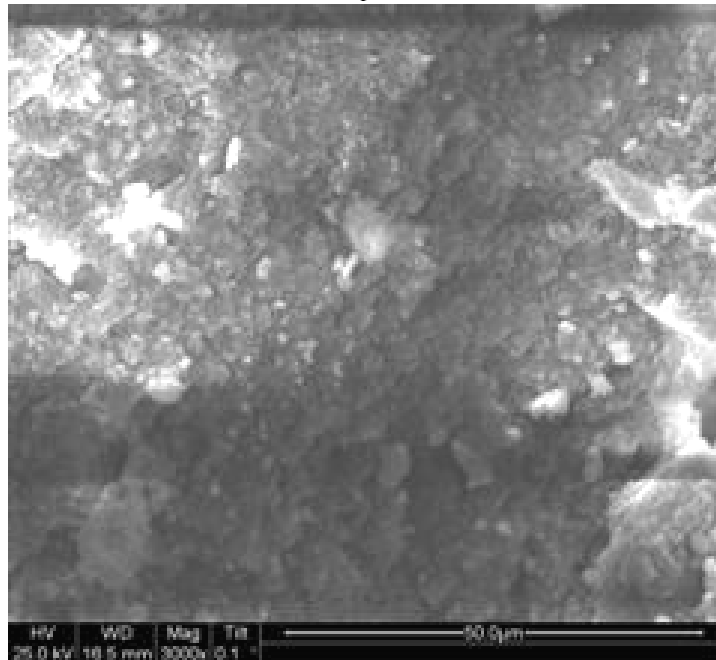


Figure 407. SEM micrograph of the fracture surface of the N720/AM specimen with  $\pm 45^\circ$  fiber orientation obtained in creep test conducted at 30 MPa at 1200°C in argon. Creep lifetime  $t_f = 3.42$  h.

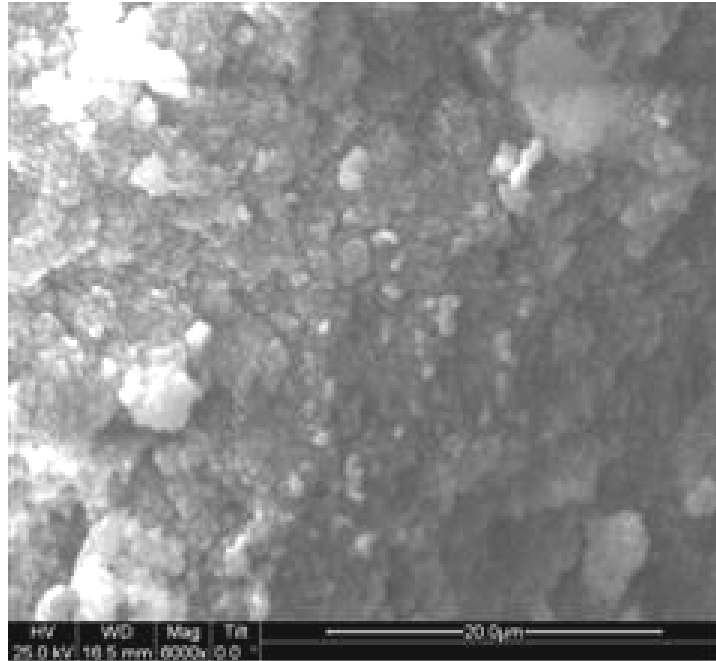


Figure 408. SEM micrograph of the fracture surface of the N720/AM specimen with  $\pm 45^\circ$  fiber orientation obtained in creep test conducted at 30 MPa at 1200°C in argon. Creep lifetime  $t_f = 3.42$  h.

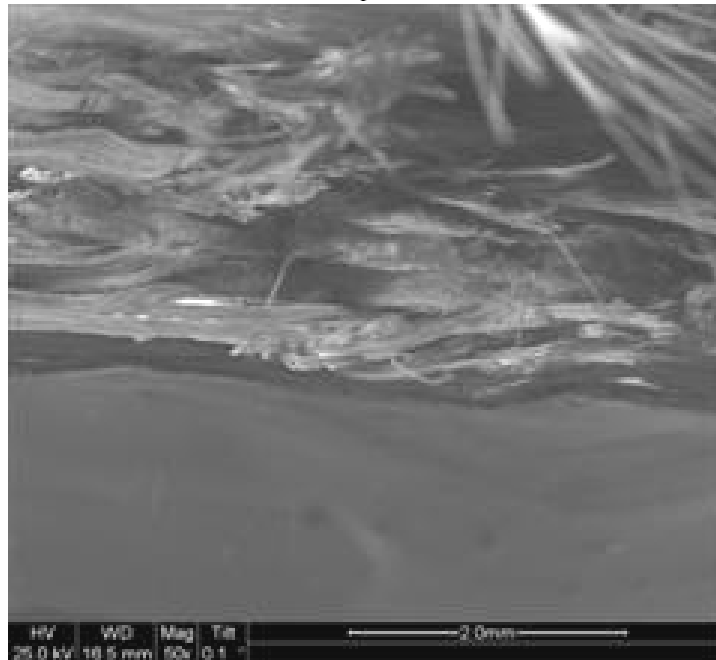


Figure 409. SEM micrograph of the fracture surface of the N720/AM specimen with  $\pm 45^\circ$  fiber orientation obtained in creep test conducted at 30 MPa at 1200°C in argon. Creep lifetime  $t_f = 3.42$  h.

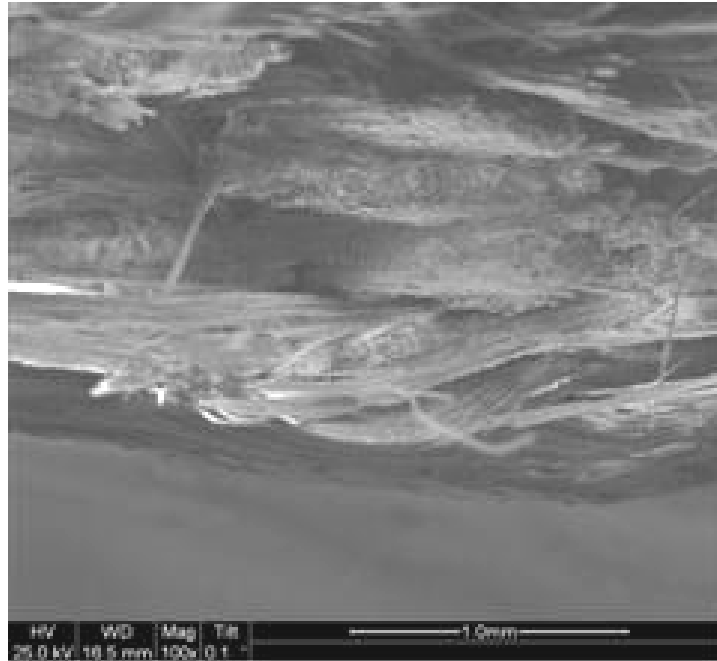


Figure 410. SEM micrograph of the fracture surface of the N720/AM specimen with  $\pm 45^\circ$  fiber orientation obtained in creep test conducted at 30 MPa at 1200°C in argon. Creep lifetime  $t_f = 3.42$  h.

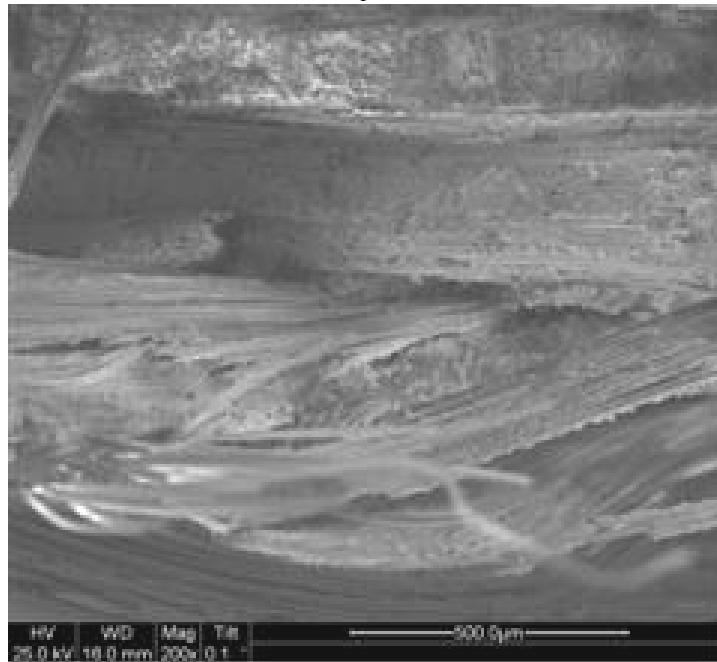


Figure 411. SEM micrograph of the fracture surface of the N720/AM specimen with  $\pm 45^\circ$  fiber orientation obtained in creep test conducted at 30 MPa at 1200°C in argon. Creep lifetime  $t_f = 3.42$  h.

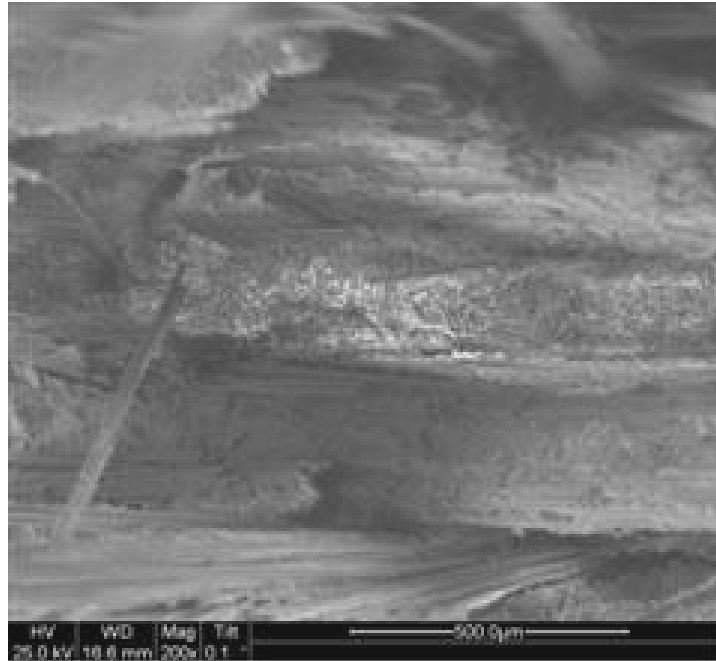


Figure 412. SEM micrograph of the fracture surface of the N720/AM specimen with  $\pm 45^\circ$  fiber orientation obtained in creep test conducted at 30 MPa at 1200°C in argon. Creep lifetime  $t_f = 3.42$  h.

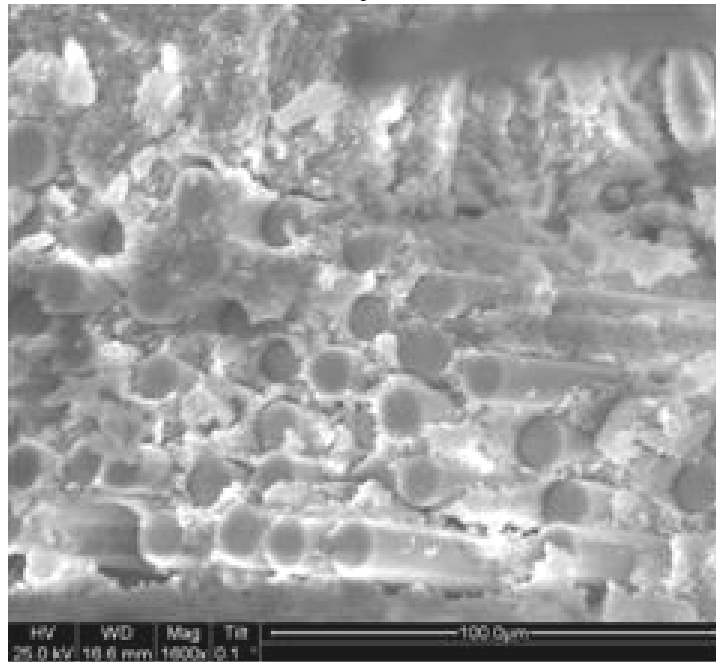


Figure 413. SEM micrograph of the fracture surface of the N720/AM specimen with  $\pm 45^\circ$  fiber orientation obtained in creep test conducted at 30 MPa at 1200°C in argon. Creep lifetime  $t_f = 3.42$  h.

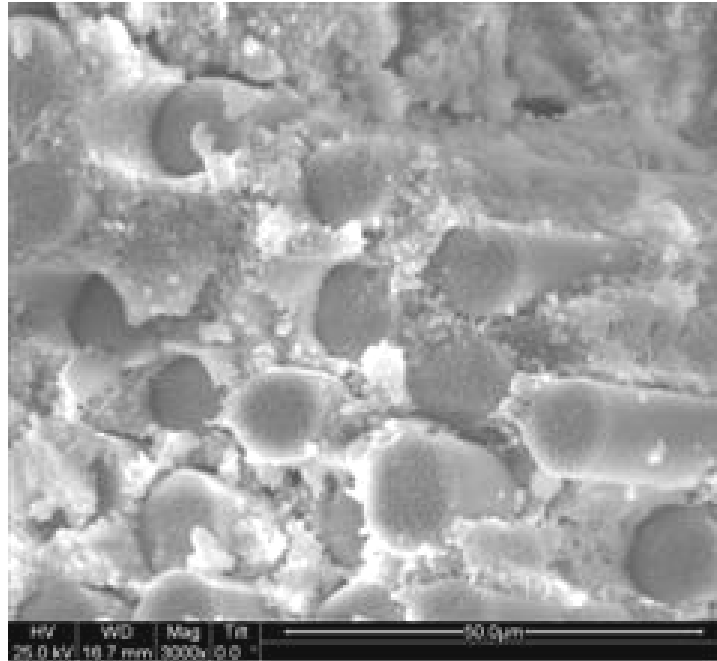


Figure 414. SEM micrograph of the fracture surface of the N720/AM specimen with  $\pm 45^\circ$  fiber orientation obtained in creep test conducted at 30 MPa at 1200°C in argon. Creep lifetime  $t_f = 3.42$  h.

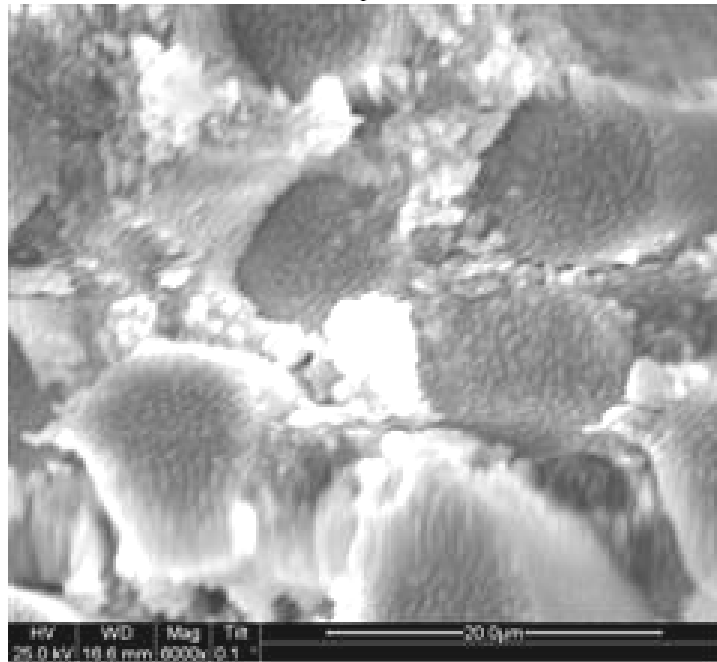


Figure 415. SEM micrograph of the fracture surface of the N720/AM specimen with  $\pm 45^\circ$  fiber orientation obtained in creep test conducted at 30 MPa at 1200°C in argon. Creep lifetime  $t_f = 3.42$  h.

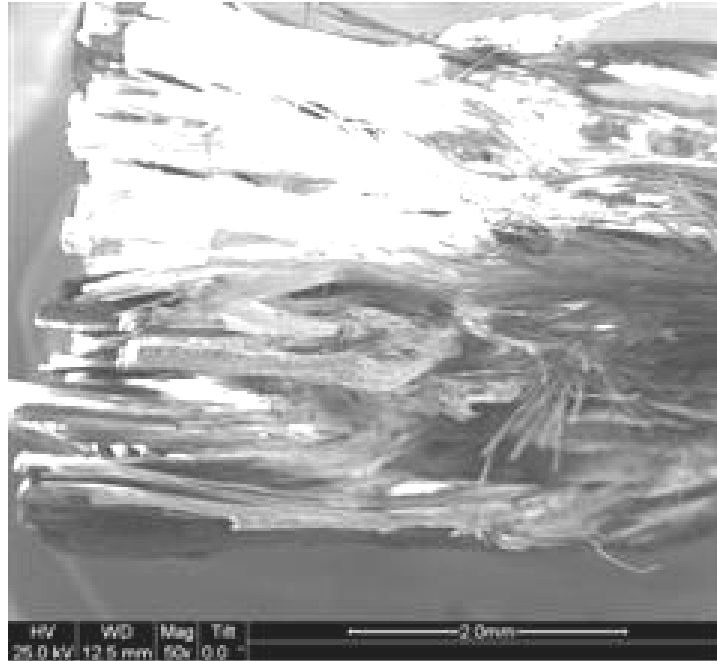


Figure 416. SEM micrograph of the fracture surface of the N720/AM specimen with  $\pm 45^\circ$  fiber orientation obtained in creep test conducted at 30 MPa at 1200°C in argon. Creep lifetime  $t_f = 3.42$  h.

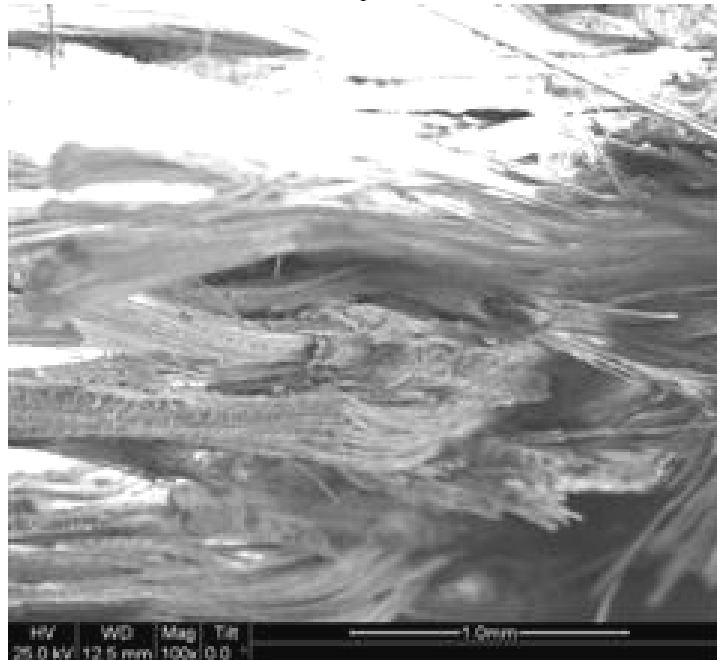


Figure 417. SEM micrograph of the fracture surface of the N720/AM specimen with  $\pm 45^\circ$  fiber orientation obtained in creep test conducted at 30 MPa at 1200°C in argon. Creep lifetime  $t_f = 3.42$  h.

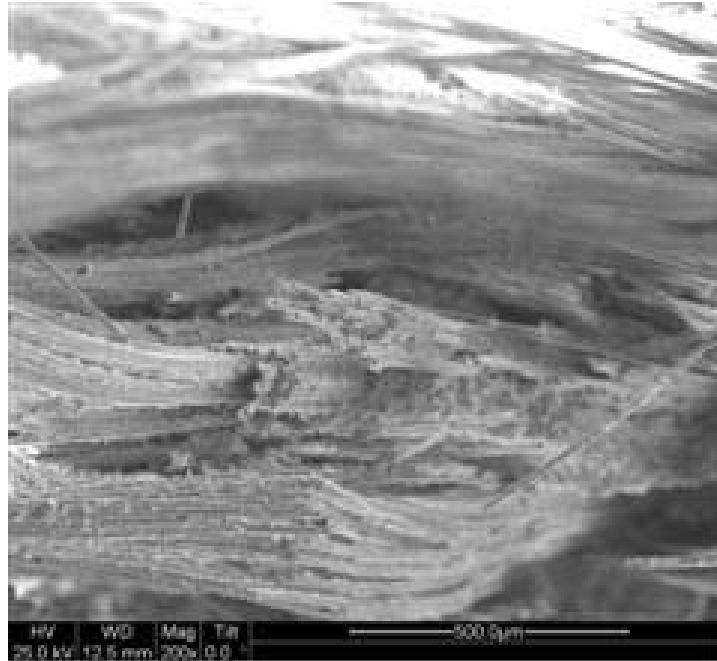


Figure 418. SEM micrograph of the fracture surface of the N720/AM specimen with  $\pm 45^\circ$  fiber orientation obtained in creep test conducted at 30 MPa at 1200°C in argon. Creep lifetime  $t_f = 3.42$  h.

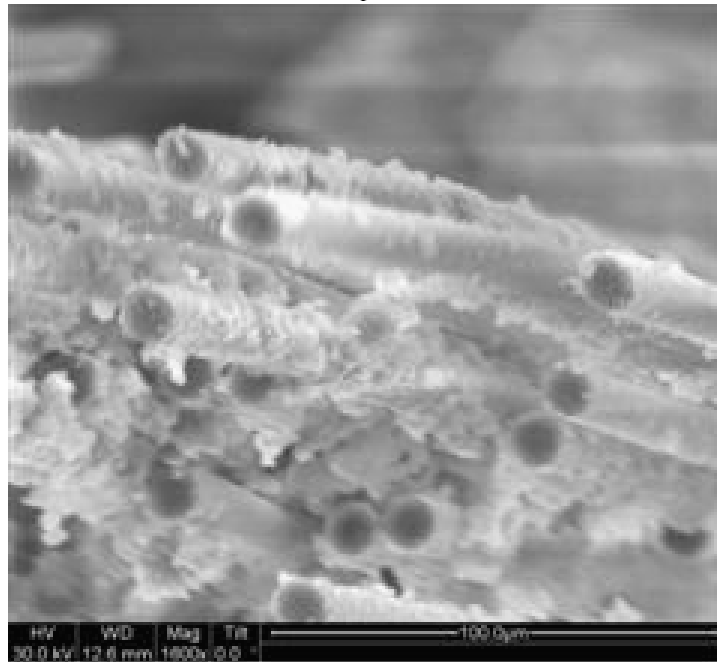


Figure 419. SEM micrograph of the fracture surface of the N720/AM specimen with  $\pm 45^\circ$  fiber orientation obtained in creep test conducted at 30 MPa at 1200°C in argon. Creep lifetime  $t_f = 3.42$  h.

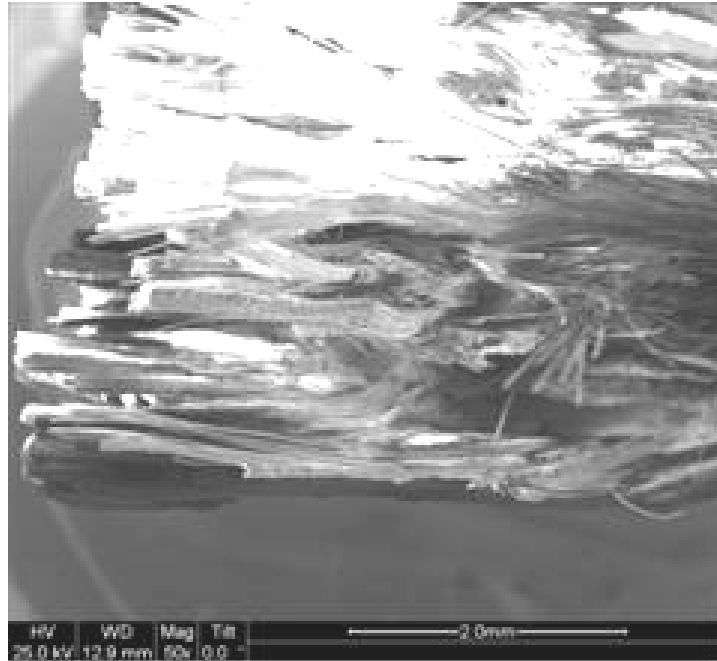


Figure 420. SEM micrograph of the fracture surface of the N720/AM specimen with  $\pm 45^\circ$  fiber orientation obtained in creep test conducted at 30 MPa at 1200°C in argon. Creep lifetime  $t_f = 3.42$  h.

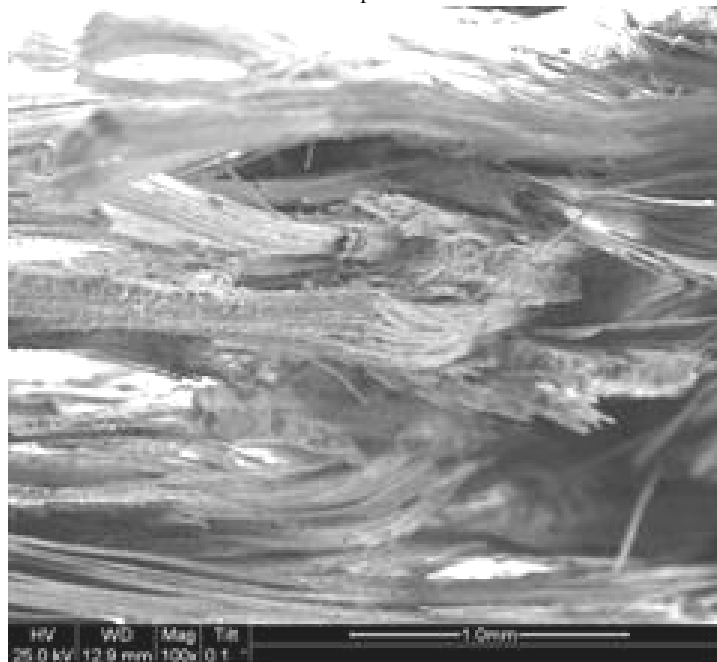


Figure 421. SEM micrograph of the fracture surface of the N720/AM specimen with  $\pm 45^\circ$  fiber orientation obtained in creep test conducted at 30 MPa at 1200°C in argon. Creep lifetime  $t_f = 3.42$  h.

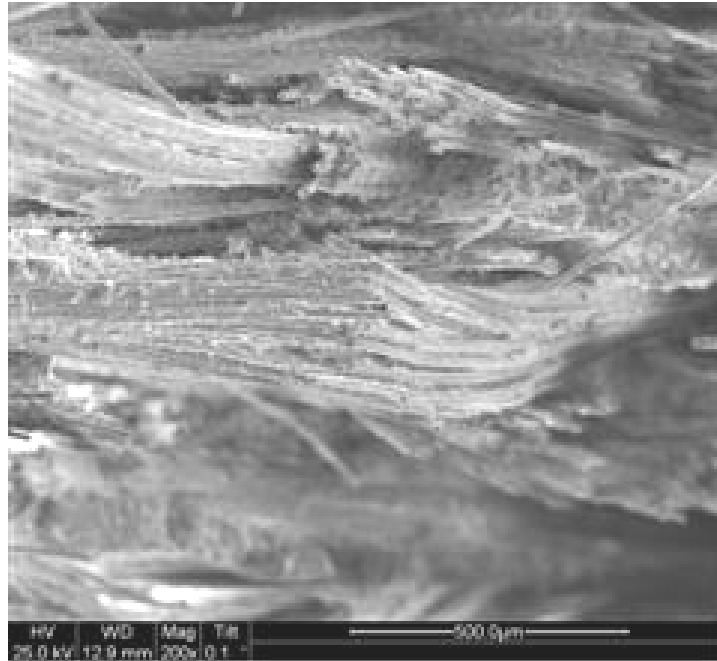


Figure 422. SEM micrograph of the fracture surface of the N720/AM specimen with  $\pm 45^\circ$  fiber orientation obtained in creep test conducted at 30 MPa at 1200°C in argon. Creep lifetime  $t_f = 3.42$  h.

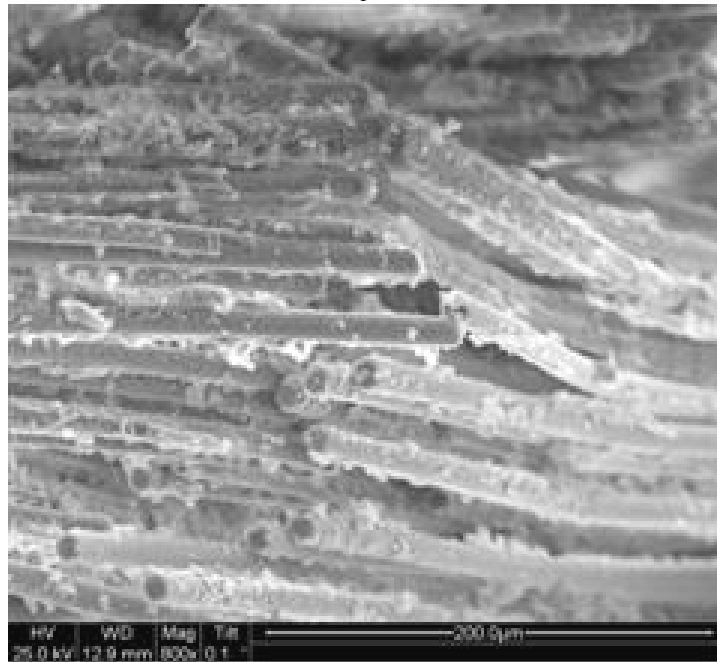


Figure 423. SEM micrograph of the fracture surface of the N720/AM specimen with  $\pm 45^\circ$  fiber orientation obtained in creep test conducted at 30 MPa at 1200°C in argon. Creep lifetime  $t_f = 3.42$  h.

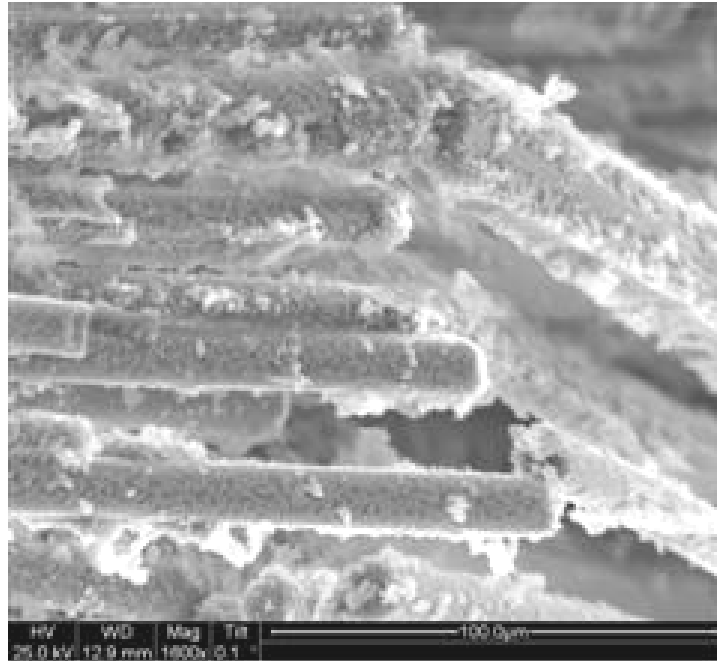


Figure 424. SEM micrograph of the fracture surface of the N720/AM specimen with  $\pm 45^\circ$  fiber orientation obtained in creep test conducted at 30 MPa at 1200°C in argon. Creep lifetime  $t_f = 3.42$  h.

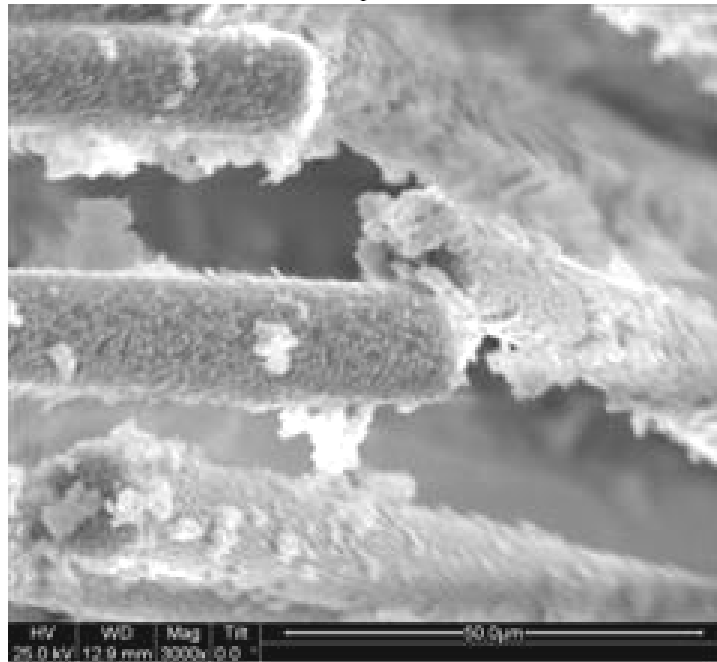


Figure 425. SEM micrograph of the fracture surface of the N720/AM specimen with  $\pm 45^\circ$  fiber orientation obtained in creep test conducted at 30 MPa at 1200°C in argon. Creep lifetime  $t_f = 3.42$  h.

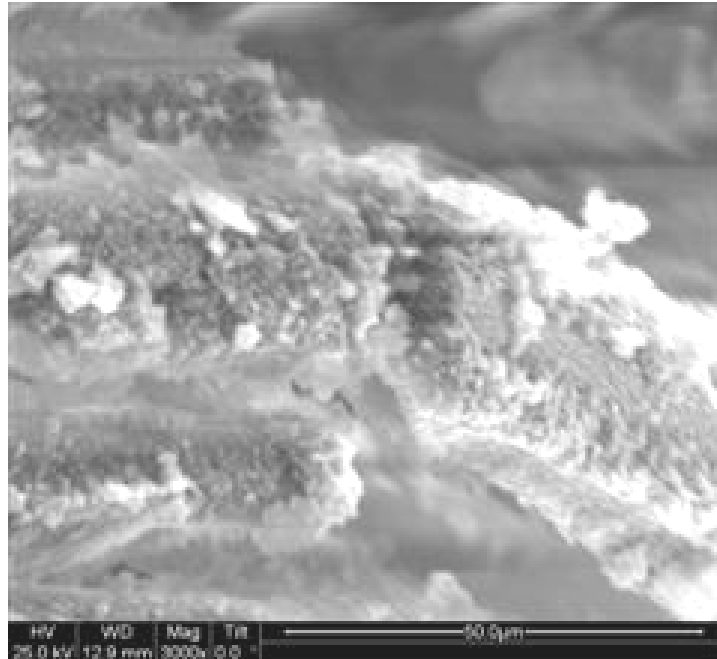


Figure 426. SEM micrograph of the fracture surface of the N720/AM specimen with  $\pm 45^\circ$  fiber orientation obtained in creep test conducted at 30 MPa at 1200°C in argon. Creep lifetime  $t_f = 3.42$  h.

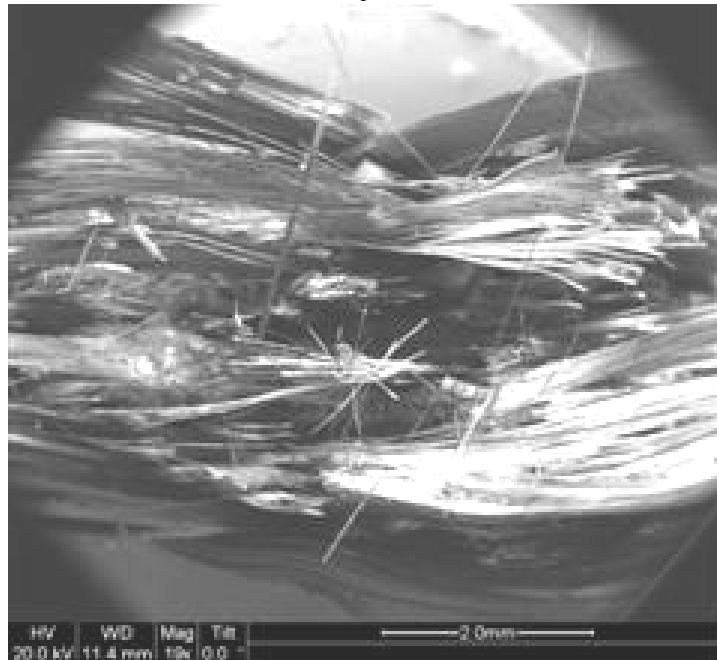


Figure 427. SEM micrograph of the fracture surface of the N720/AM specimen with  $\pm 45^\circ$  fiber orientation obtained in creep test conducted at 32 MPa at 1200°C in argon. Creep lifetime  $t_f = 0.08$  h.

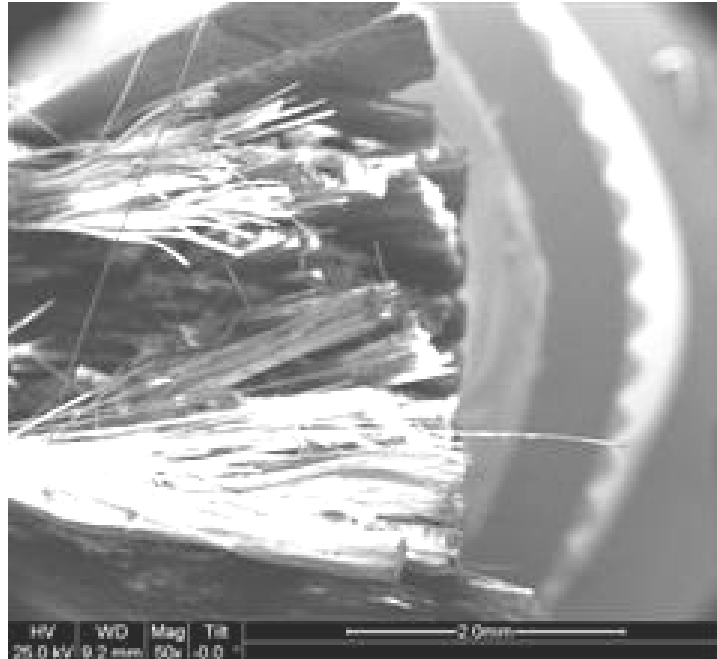


Figure 428. SEM micrograph of the fracture surface of the N720/AM specimen with  $\pm 45^\circ$  fiber orientation obtained in creep test conducted at 32 MPa at 1200°C in argon. Creep lifetime  $t_f = 0.08$  h.

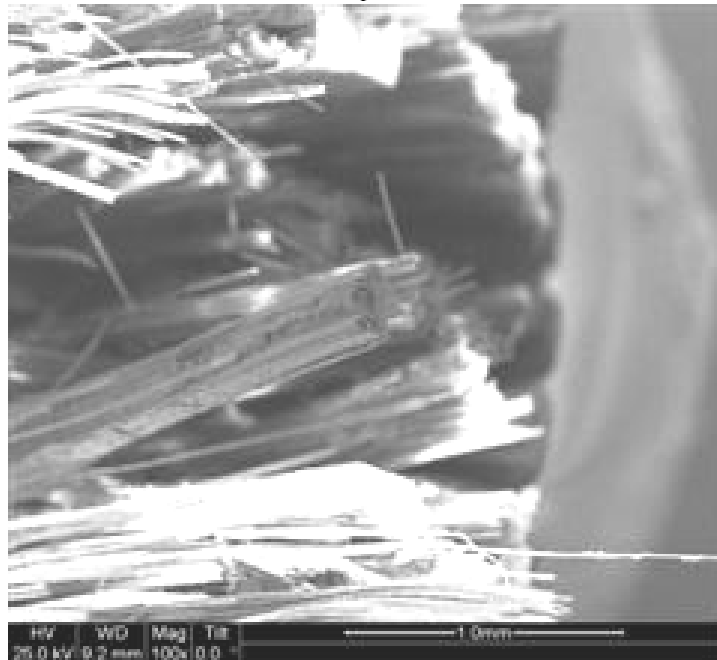


Figure 429. SEM micrograph of the fracture surface of the N720/AM specimen with  $\pm 45^\circ$  fiber orientation obtained in creep test conducted at 32 MPa at 1200°C in argon. Creep lifetime  $t_f = 0.08$  h.



Figure 430. SEM micrograph of the fracture surface of the N720/AM specimen with  $\pm 45^\circ$  fiber orientation obtained in creep test conducted at 32 MPa at 1200°C in argon. Creep lifetime  $t_f = 0.08$  h.

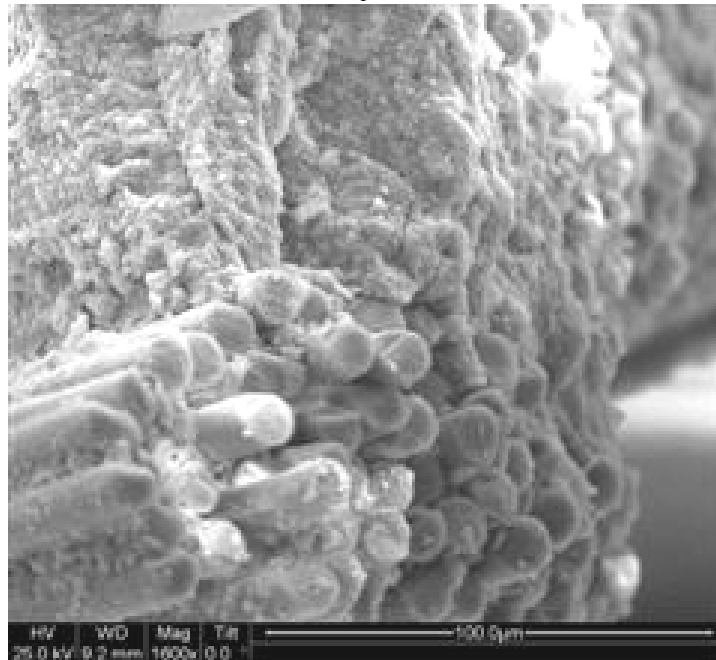


Figure 431. SEM micrograph of the fracture surface of the N720/AM specimen with  $\pm 45^\circ$  fiber orientation obtained in creep test conducted at 32 MPa at 1200°C in argon. Creep lifetime  $t_f = 0.08$  h.

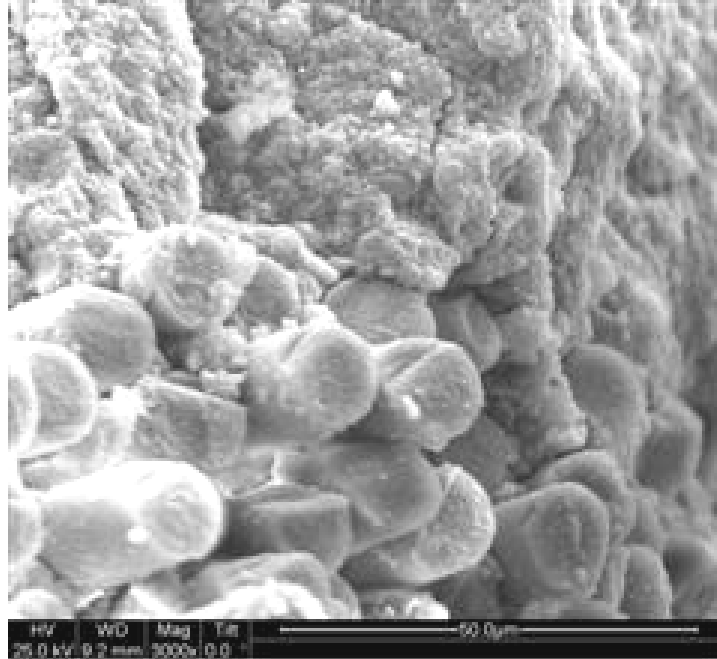


Figure 432. SEM micrograph of the fracture surface of the N720/AM specimen with  $\pm 45^\circ$  fiber orientation obtained in creep test conducted at 32 MPa at 1200°C in argon. Creep lifetime  $t_f = 0.08$  h.

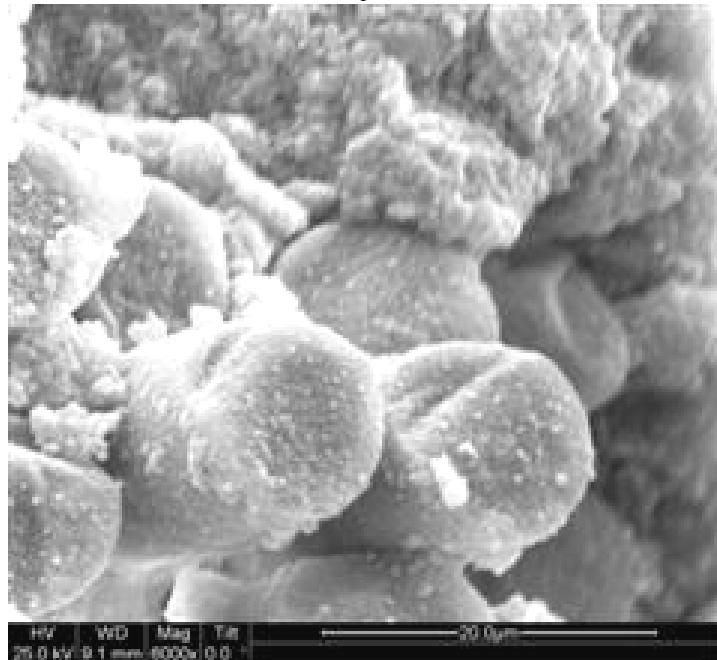


Figure 433. SEM micrograph of the fracture surface of the N720/AM specimen with  $\pm 45^\circ$  fiber orientation obtained in creep test conducted at 32 MPa at 1200°C in argon. Creep lifetime  $t_f = 0.08$  h.



Figure 434. SEM micrograph of the fracture surface of the N720/AM specimen with  $\pm 45^\circ$  fiber orientation obtained in creep test conducted at 32 MPa at 1200°C in argon. Creep lifetime  $t_f = 0.08$  h.

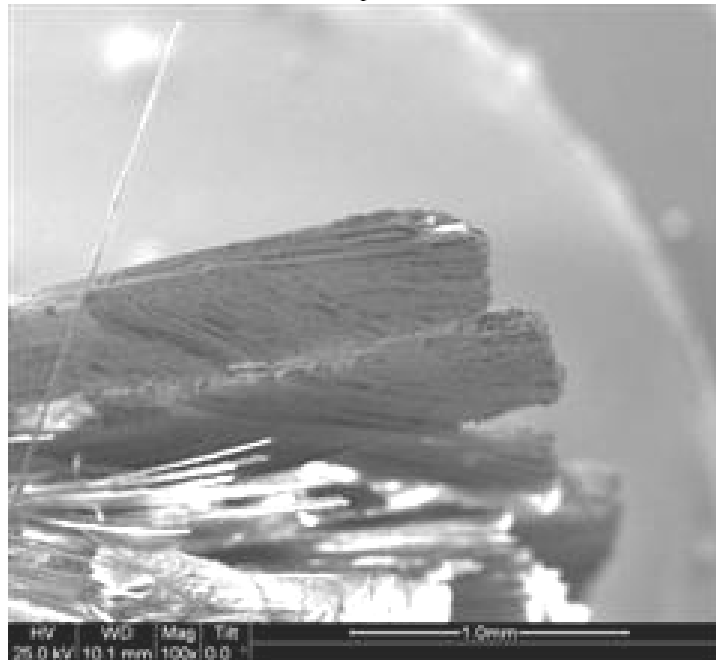


Figure 435. SEM micrograph of the fracture surface of the N720/AM specimen with  $\pm 45^\circ$  fiber orientation obtained in creep test conducted at 32 MPa at 1200°C in argon. Creep lifetime  $t_f = 0.08$  h.

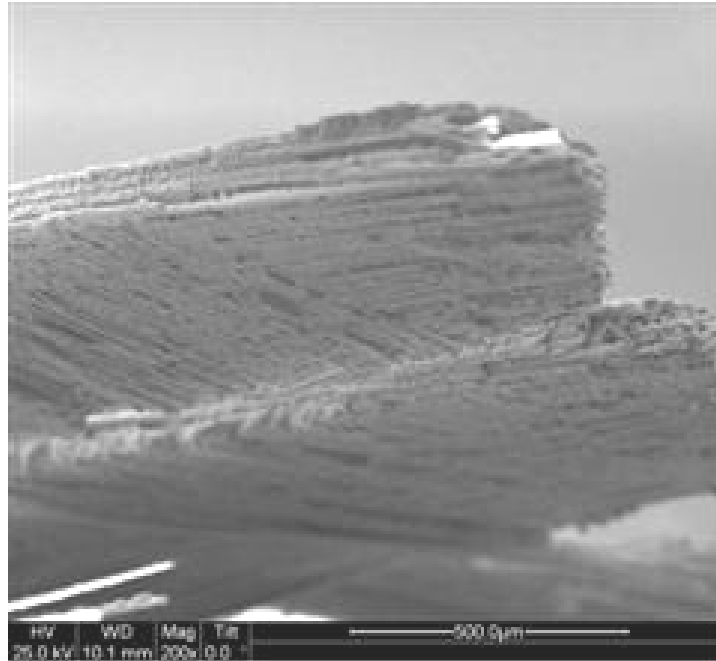


Figure 436. SEM micrograph of the fracture surface of the N720/AM specimen with  $\pm 45^\circ$  fiber orientation obtained in creep test conducted at 32 MPa at 1200°C in argon. Creep lifetime  $t_f = 0.08$  h.

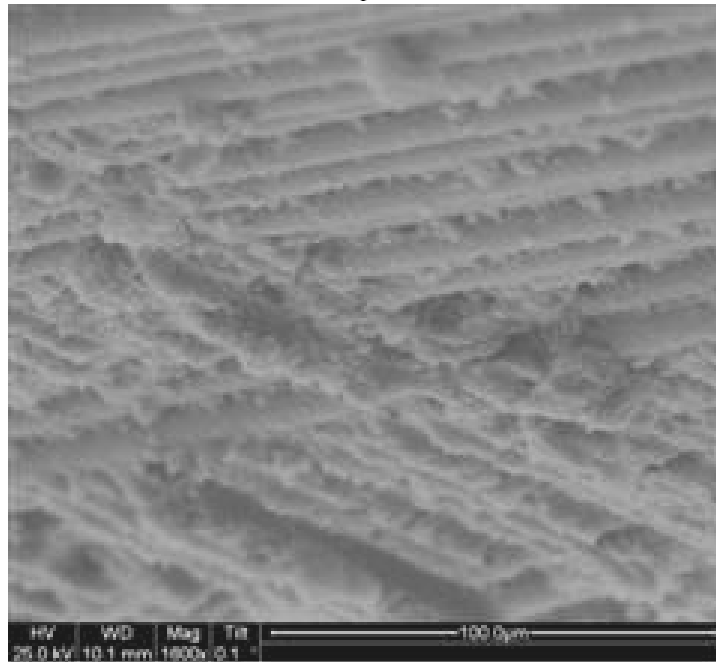


Figure 437. SEM micrograph of the fracture surface of the N720/AM specimen with  $\pm 45^\circ$  fiber orientation obtained in creep test conducted at 32 MPa at 1200°C in argon. Creep lifetime  $t_f = 0.08$  h.

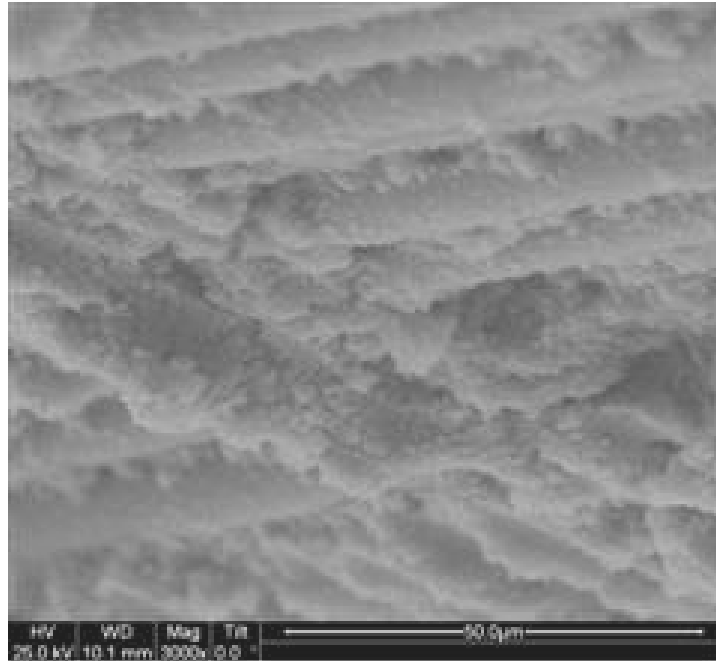


Figure 438. SEM micrograph of the fracture surface of the N720/AM specimen with  $\pm 45^\circ$  fiber orientation obtained in creep test conducted at 32 MPa at 1200°C in argon. Creep lifetime  $t_f = 0.08$  h.

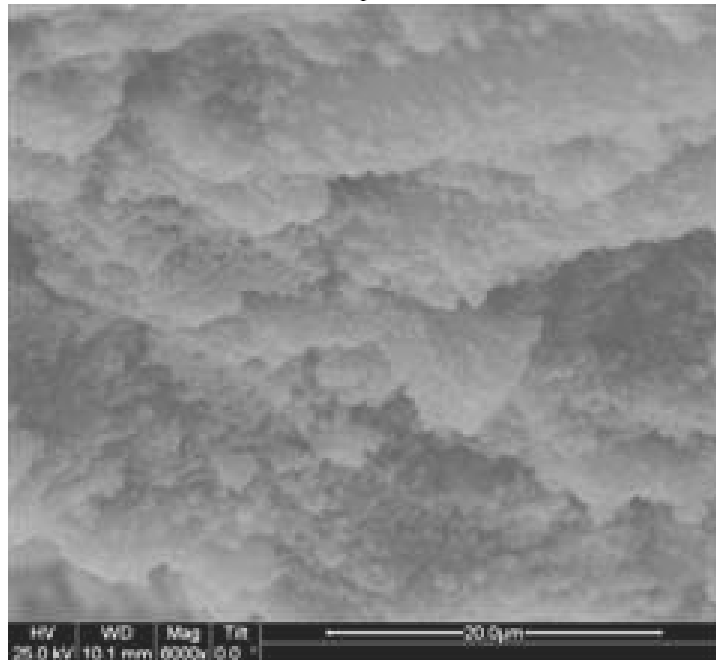


Figure 439. SEM micrograph of the fracture surface of the N720/AM specimen with  $\pm 45^\circ$  fiber orientation obtained in creep test conducted at 32 MPa at 1200°C in argon. Creep lifetime  $t_f = 0.08$  h.

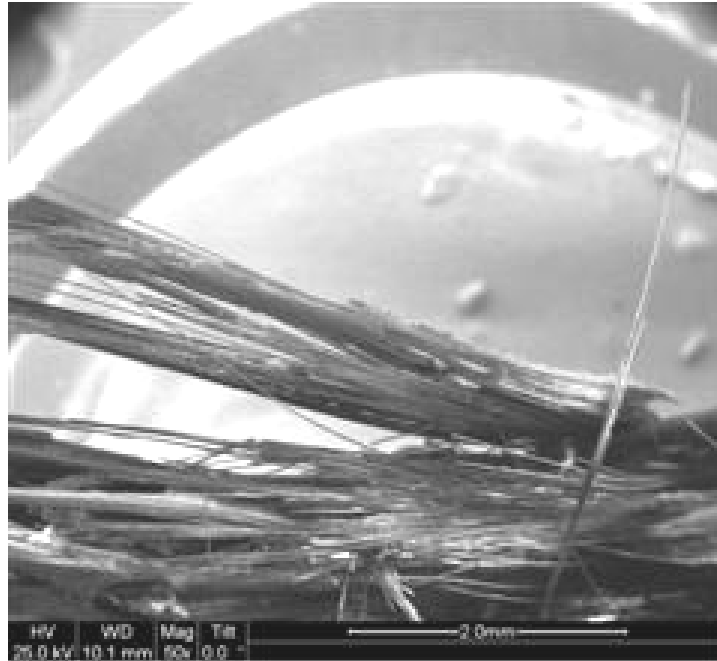


Figure 440. SEM micrograph of the fracture surface of the N720/AM specimen with  $\pm 45^\circ$  fiber orientation obtained in creep test conducted at 32 MPa at 1200°C in argon. Creep lifetime  $t_f = 0.08$  h.

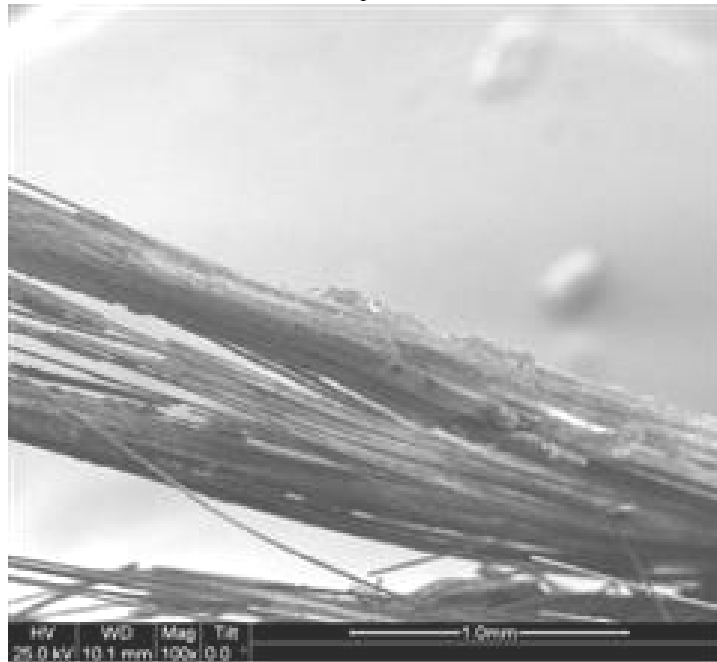


Figure 441. SEM micrograph of the fracture surface of the N720/AM specimen with  $\pm 45^\circ$  fiber orientation obtained in creep test conducted at 32 MPa at 1200°C in argon. Creep lifetime  $t_f = 0.08$  h.

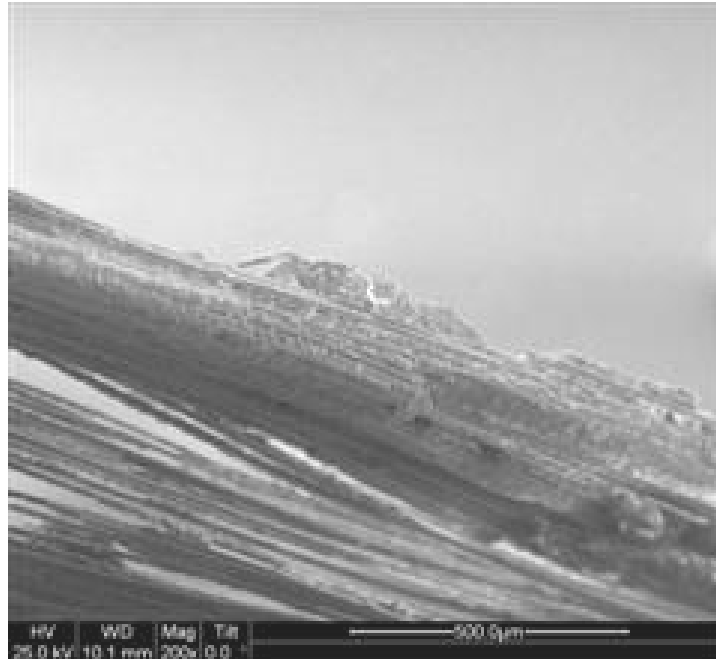


Figure 442. SEM micrograph of the fracture surface of the N720/AM specimen with  $\pm 45^\circ$  fiber orientation obtained in creep test conducted at 32 MPa at 1200°C in argon. Creep lifetime  $t_f = 0.08$  h.

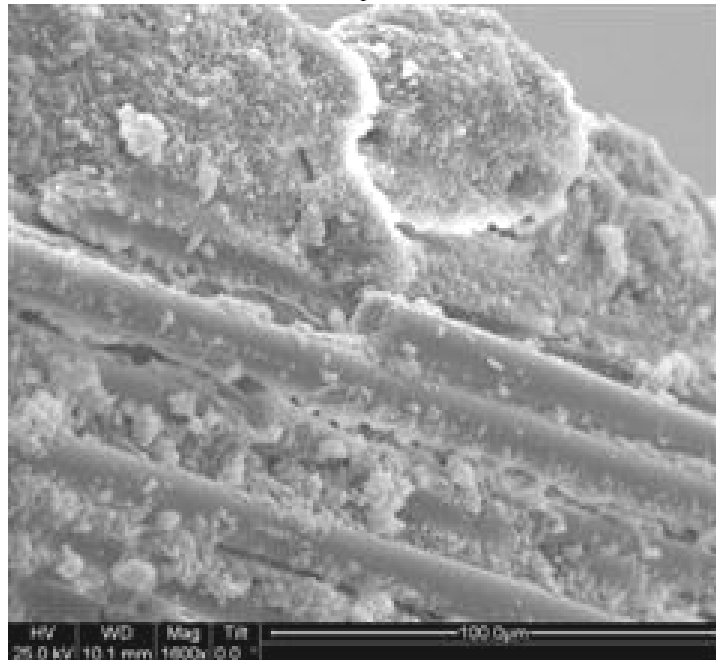


Figure 443. SEM micrograph of the fracture surface of the N720/AM specimen with  $\pm 45^\circ$  fiber orientation obtained in creep test conducted at 32 MPa at 1200°C in argon. Creep lifetime  $t_f = 0.08$  h.

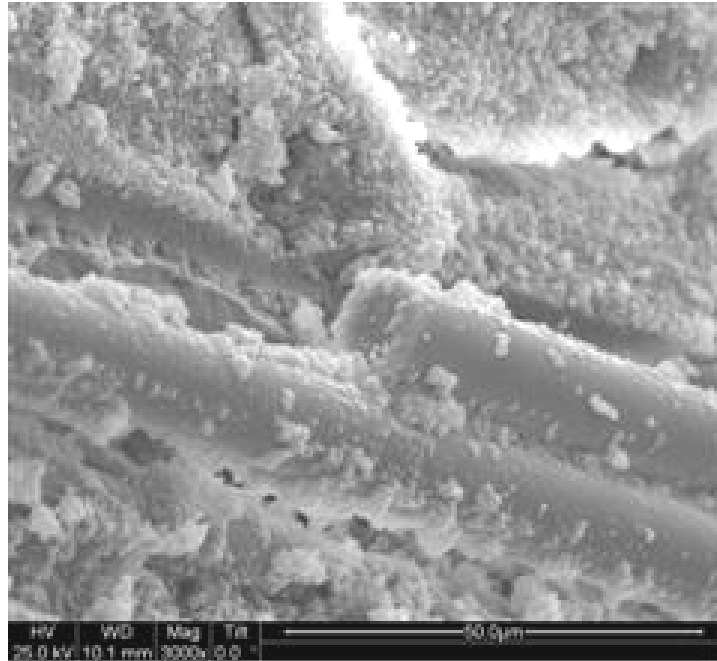


Figure 444. SEM micrograph of the fracture surface of the N720/AM specimen with  $\pm 45^\circ$  fiber orientation obtained in creep test conducted at 32 MPa at 1200°C in argon. Creep lifetime  $t_f = 0.08$  h.

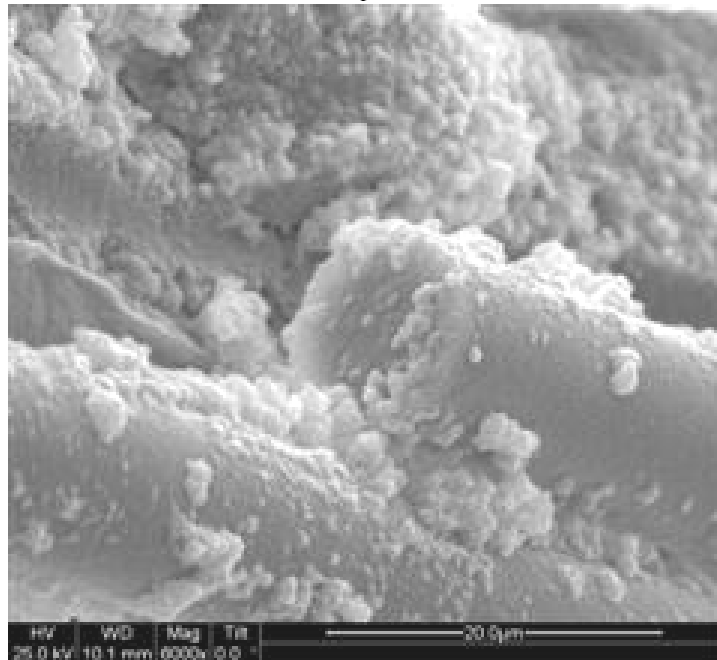


Figure 445. SEM micrograph of the fracture surface of the N720/AM specimen with  $\pm 45^\circ$  fiber orientation obtained in creep test conducted at 32 MPa at 1200°C in argon. Creep lifetime  $t_f = 0.08$  h.

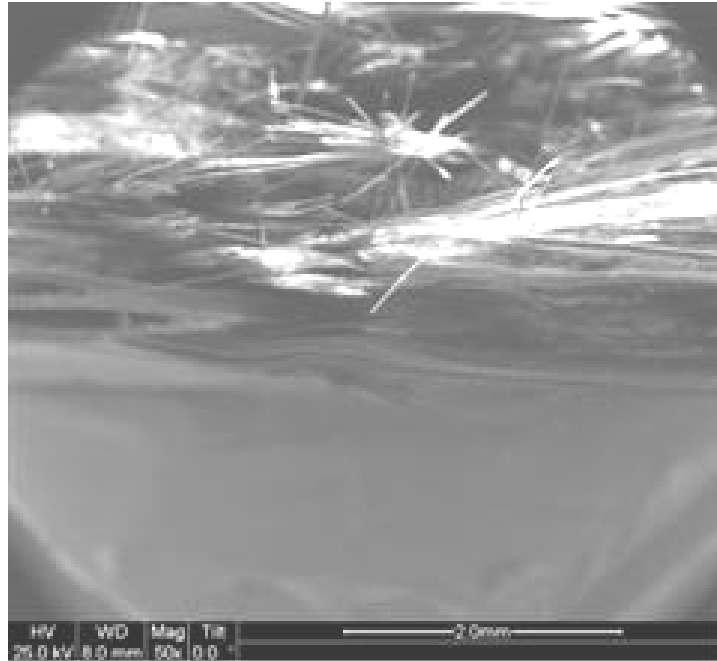


Figure 446. SEM micrograph of the fracture surface of the N720/AM specimen with  $\pm 45^\circ$  fiber orientation obtained in creep test conducted at 32 MPa at 1200°C in argon. Creep lifetime  $t_f = 0.08$  h.

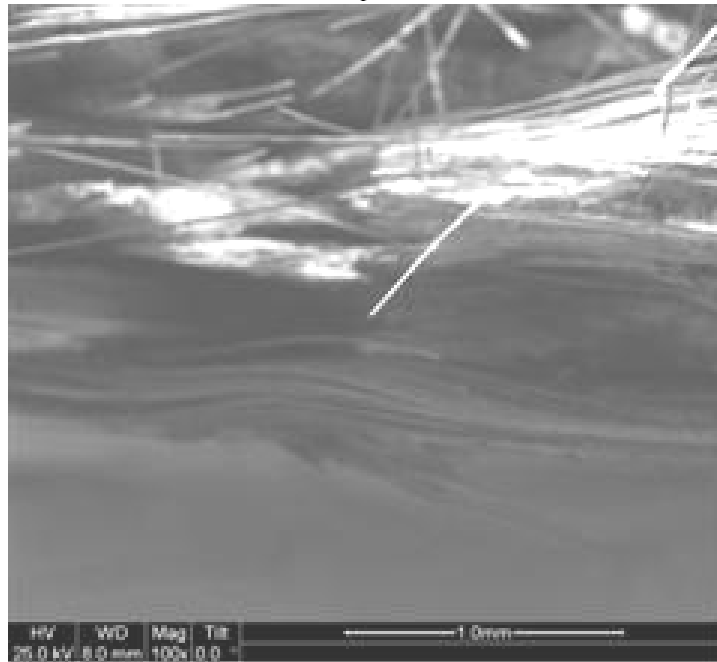


Figure 447. SEM micrograph of the fracture surface of the N720/AM specimen with  $\pm 45^\circ$  fiber orientation obtained in creep test conducted at 32 MPa at 1200°C in argon. Creep lifetime  $t_f = 0.08$  h.

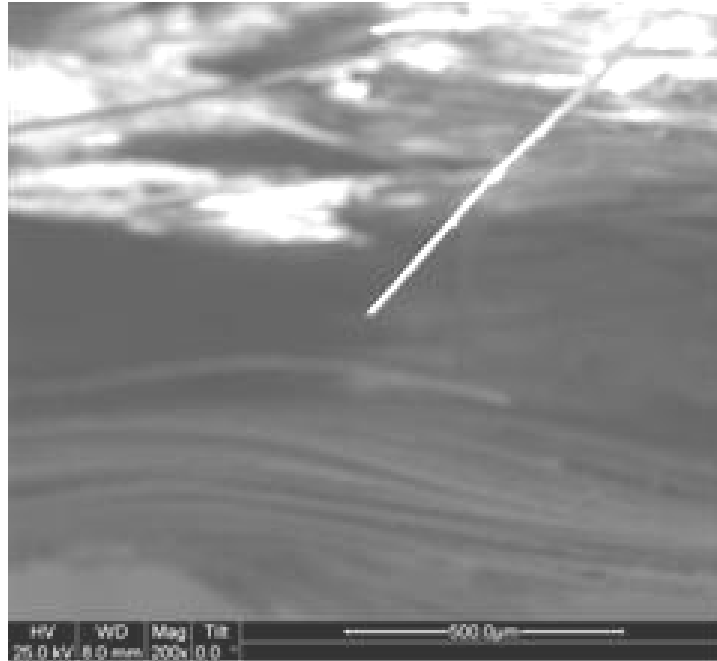


Figure 448. SEM micrograph of the fracture surface of the N720/AM specimen with  $\pm 45^\circ$  fiber orientation obtained in creep test conducted at 32 MPa at 1200°C in argon. Creep lifetime  $t_f = 0.08$  h.



Figure 449. SEM micrograph of the fracture surface of the N720/AM specimen with  $\pm 45^\circ$  fiber orientation obtained in creep test conducted at 32 MPa at 1200°C in argon. Creep lifetime  $t_f = 0.08$  h.

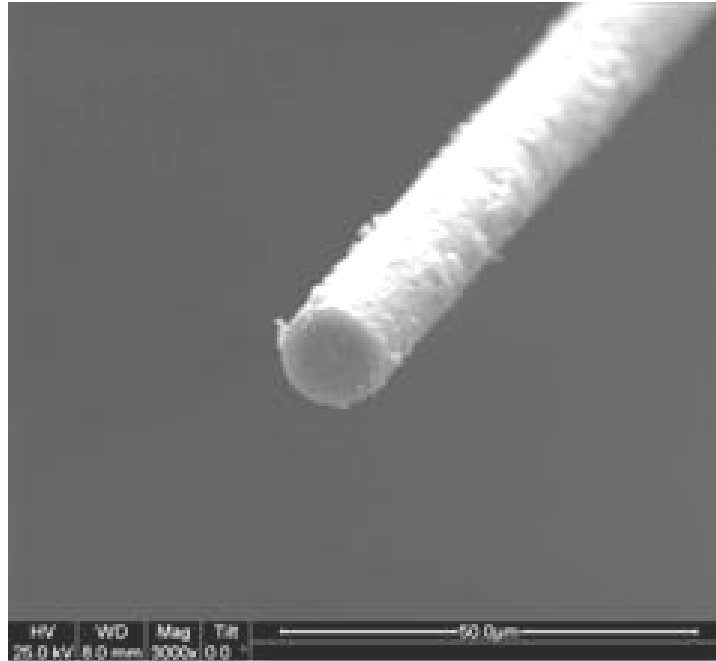


Figure 450. SEM micrograph of the fracture surface of the N720/AM specimen with  $\pm 45^\circ$  fiber orientation obtained in creep test conducted at 32 MPa at 1200°C in argon. Creep lifetime  $t_f = 0.08$  h.

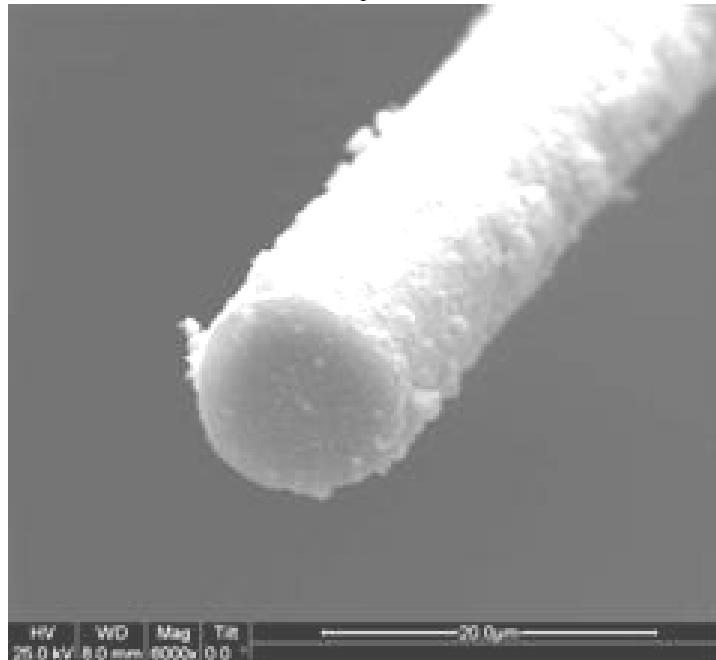


Figure 451. SEM micrograph of the fracture surface of the N720/AM specimen with  $\pm 45^\circ$  fiber orientation obtained in creep test conducted at 32 MPa at 1200°C in argon. Creep lifetime  $t_f = 0.08$  h.

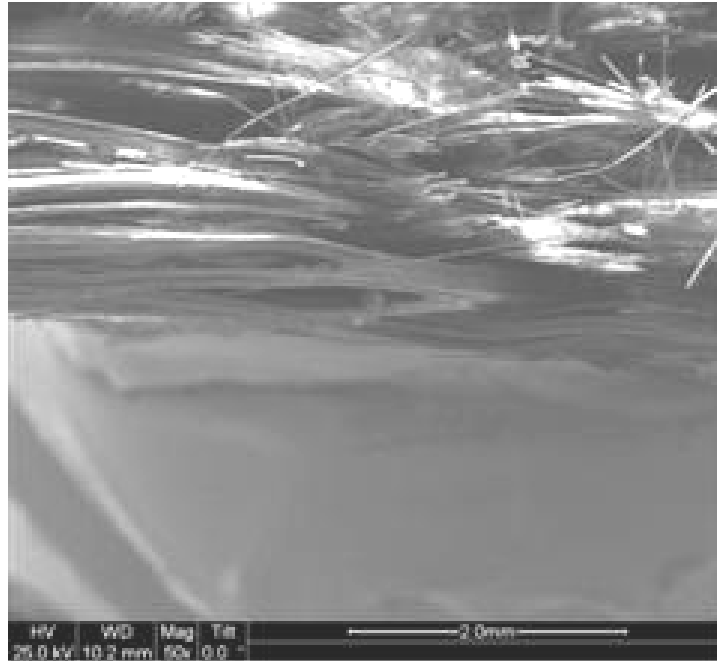


Figure 452. SEM micrograph of the fracture surface of the N720/AM specimen with  $\pm 45^\circ$  fiber orientation obtained in creep test conducted at 32 MPa at 1200°C in argon. Creep lifetime  $t_f = 0.08$  h.

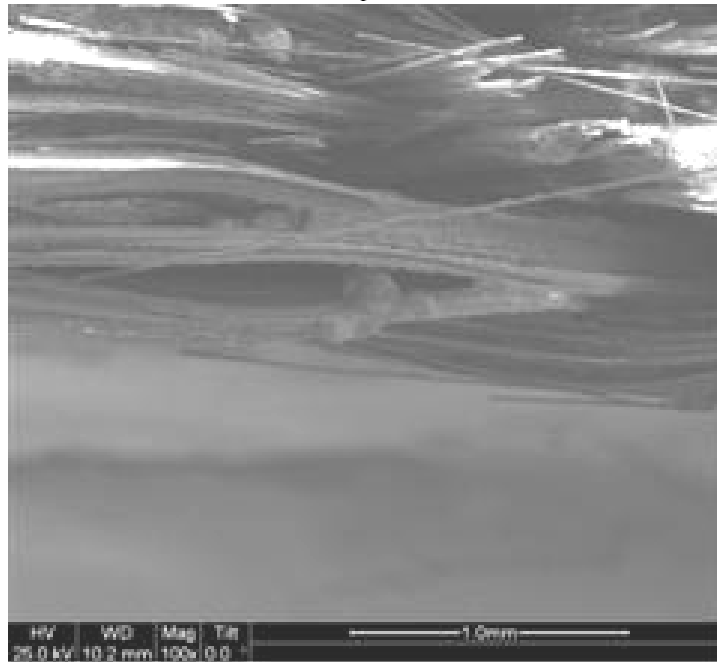


Figure 453. SEM micrograph of the fracture surface of the N720/AM specimen with  $\pm 45^\circ$  fiber orientation obtained in creep test conducted at 32 MPa at 1200°C in argon. Creep lifetime  $t_f = 0.08$  h.

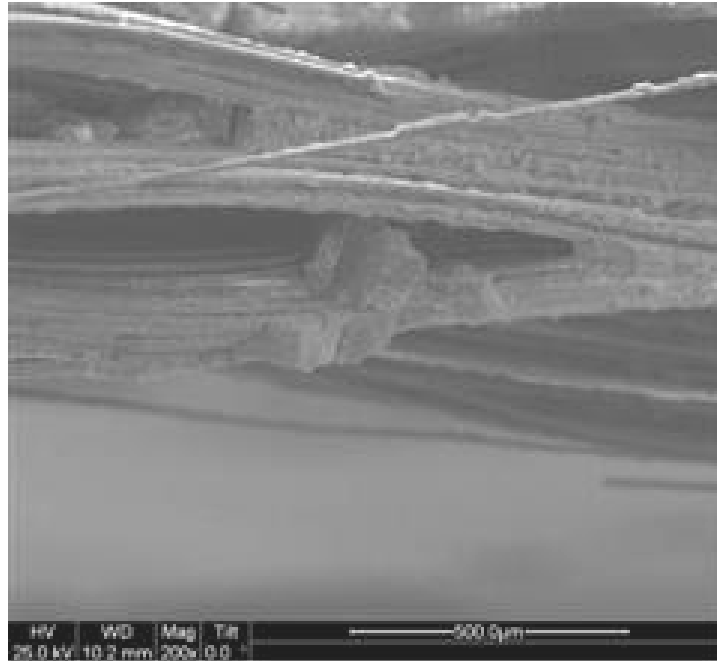


Figure 454. SEM micrograph of the fracture surface of the N720/AM specimen with  $\pm 45^\circ$  fiber orientation obtained in creep test conducted at 32 MPa at 1200°C in argon. Creep lifetime  $t_f = 0.08$  h.

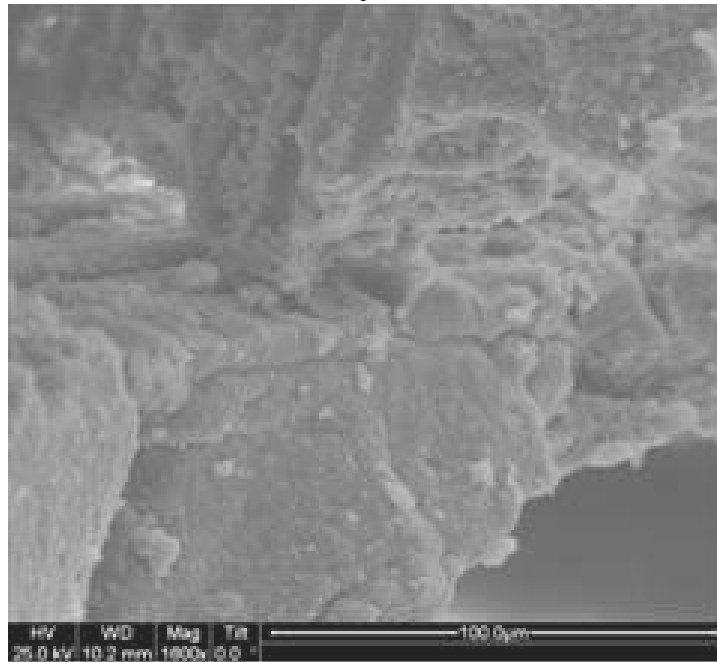


Figure 455. SEM micrograph of the fracture surface of the N720/AM specimen with  $\pm 45^\circ$  fiber orientation obtained in creep test conducted at 32 MPa at 1200°C in argon. Creep lifetime  $t_f = 0.08$  h.

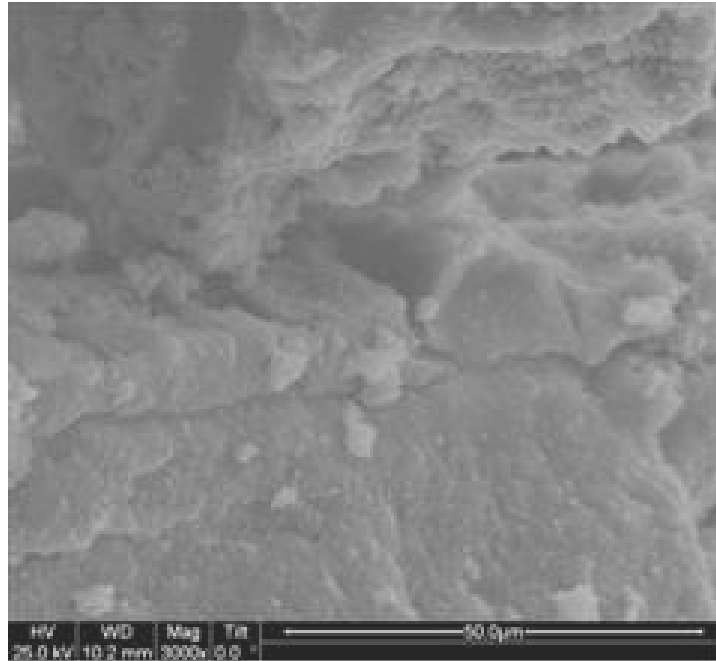


Figure 456. SEM micrograph of the fracture surface of the N720/AM specimen with  $\pm 45^\circ$  fiber orientation obtained in creep test conducted at 32 MPa at 1200°C in argon. Creep lifetime  $t_f = 0.08$  h.

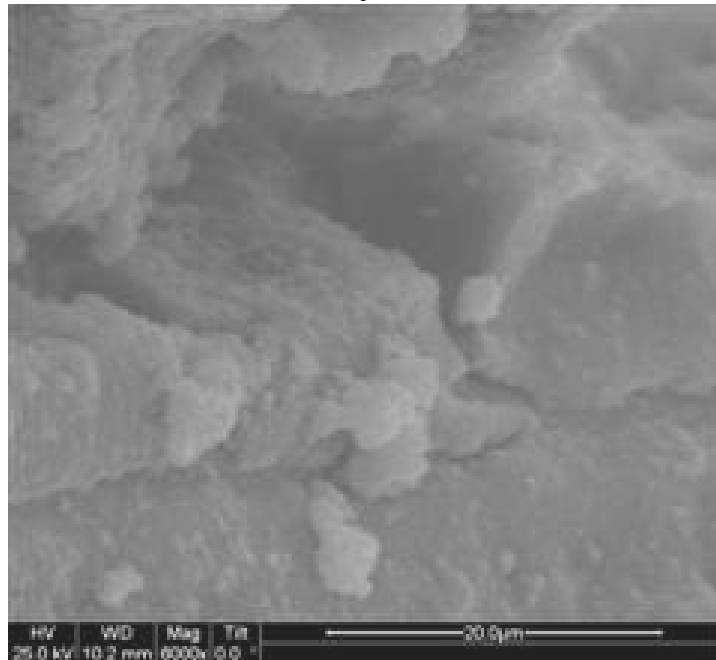


Figure 457. SEM micrograph of the fracture surface of the N720/AM specimen with  $\pm 45^\circ$  fiber orientation obtained in creep test conducted at 32 MPa at 1200°C in argon. Creep lifetime  $t_f = 0.08$  h.

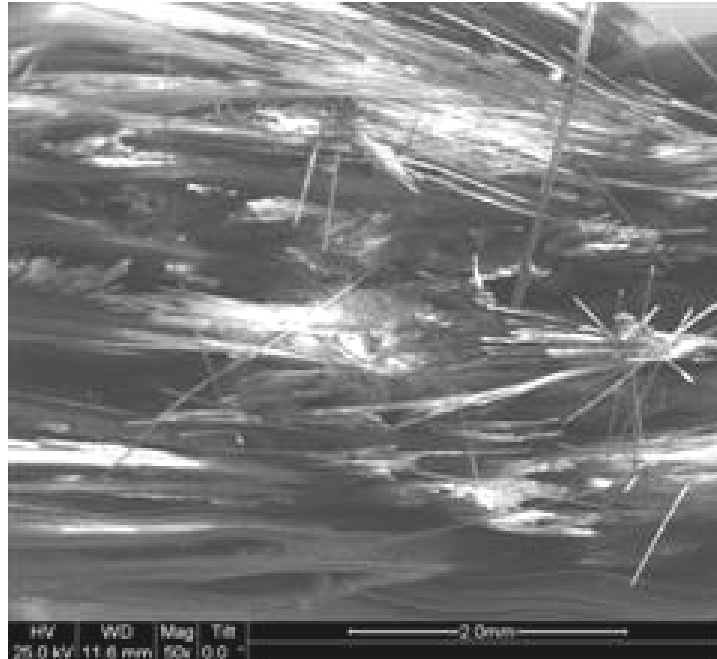


Figure 458. SEM micrograph of the fracture surface of the N720/AM specimen with  $\pm 45^\circ$  fiber orientation obtained in creep test conducted at 32 MPa at 1200°C in argon. Creep lifetime  $t_f = 0.08$  h.

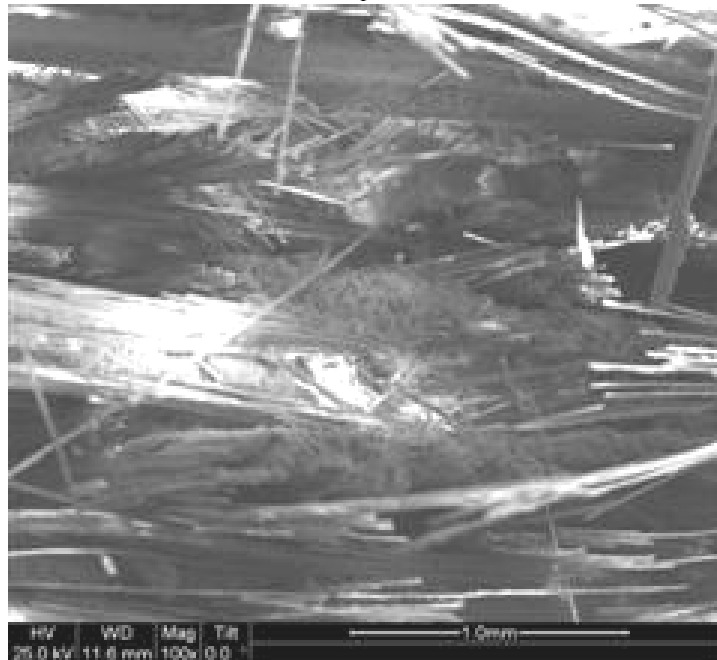


Figure 459. SEM micrograph of the fracture surface of the N720/AM specimen with  $\pm 45^\circ$  fiber orientation obtained in creep test conducted at 32 MPa at 1200°C in argon. Creep lifetime  $t_f = 0.08$  h.

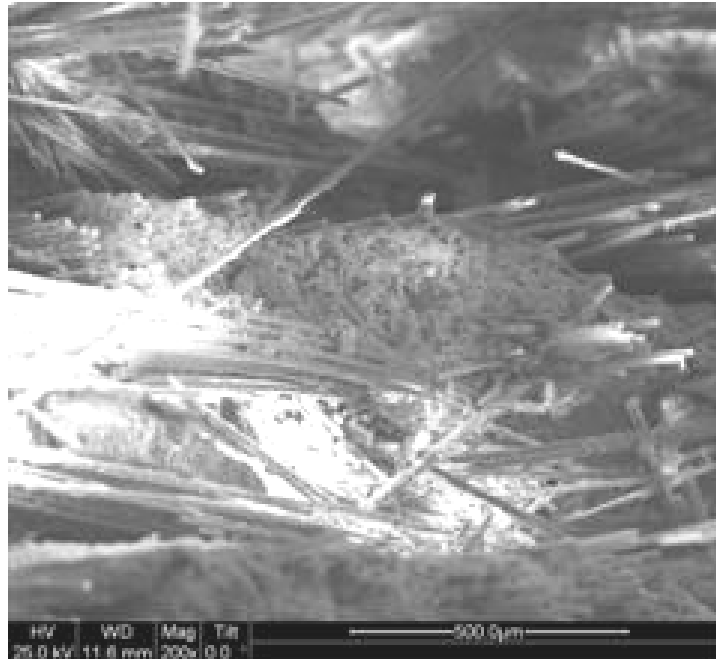


Figure 460. SEM micrograph of the fracture surface of the N720/AM specimen with  $\pm 45^\circ$  fiber orientation obtained in creep test conducted at 32 MPa at 1200°C in argon. Creep lifetime  $t_f = 0.08$  h.

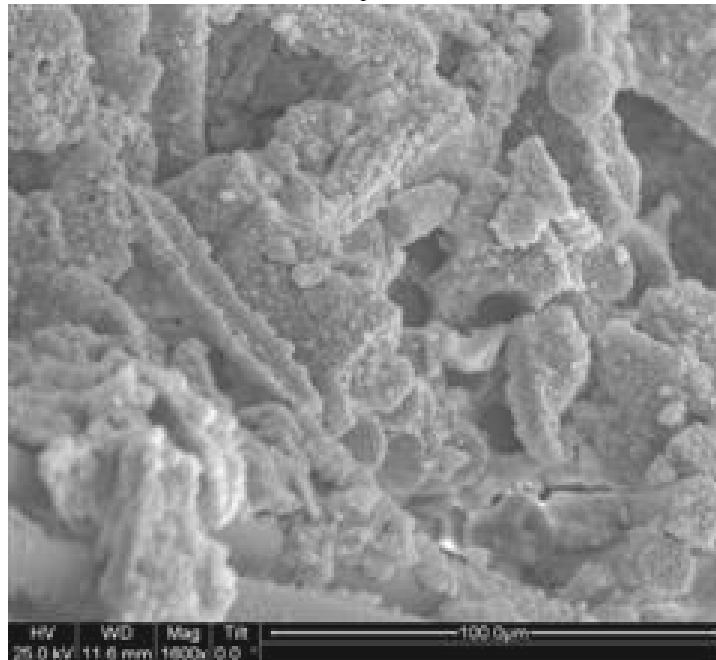


Figure 461. SEM micrograph of the fracture surface of the N720/AM specimen with  $\pm 45^\circ$  fiber orientation obtained in creep test conducted at 32 MPa at 1200°C in argon. Creep lifetime  $t_f = 0.08$  h.

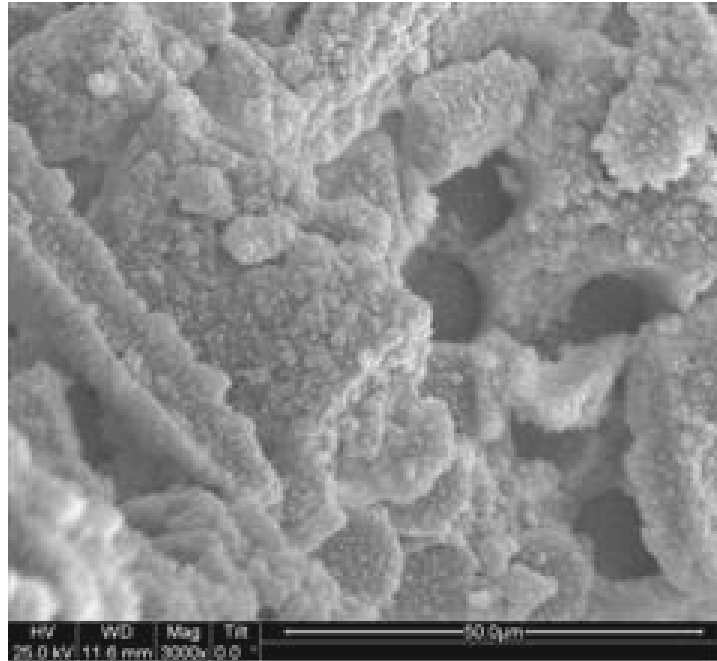


Figure 462. SEM micrograph of the fracture surface of the N720/AM specimen with  $\pm 45^\circ$  fiber orientation obtained in creep test conducted at 32 MPa at 1200°C in argon. Creep lifetime  $t_f = 0.08$  h.

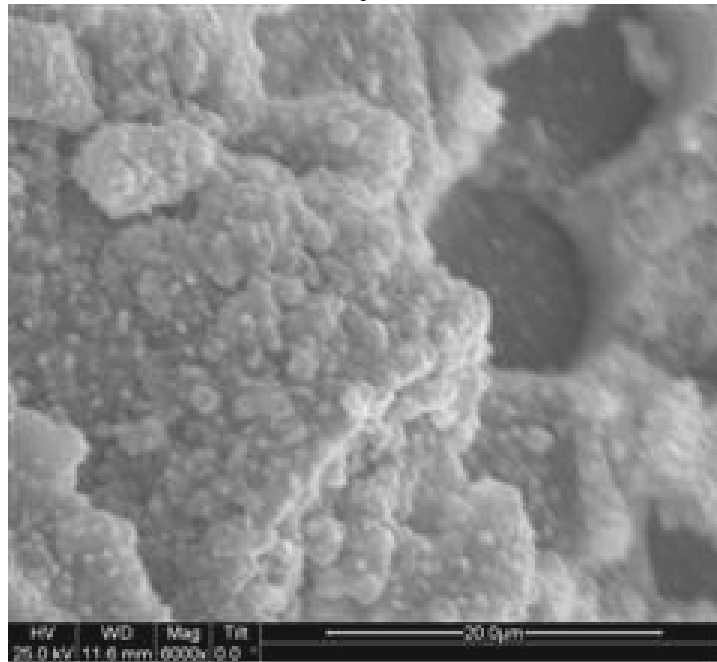


Figure 463. SEM micrograph of the fracture surface of the N720/AM specimen with  $\pm 45^\circ$  fiber orientation obtained in creep test conducted at 32 MPa at 1200°C in argon. Creep lifetime  $t_f = 0.08$  h.

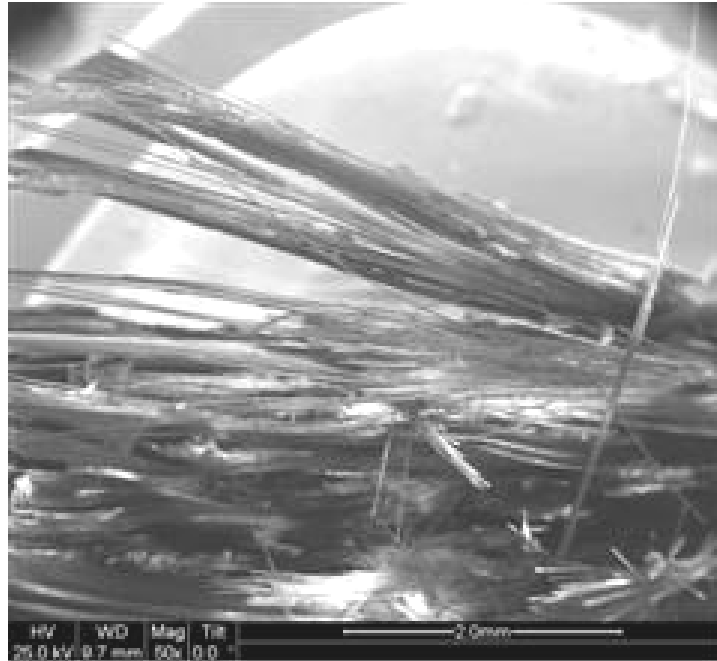


Figure 464. SEM micrograph of the fracture surface of the N720/AM specimen with  $\pm 45^\circ$  fiber orientation obtained in creep test conducted at 32 MPa at 1200°C in argon. Creep lifetime  $t_f = 0.08$  h.

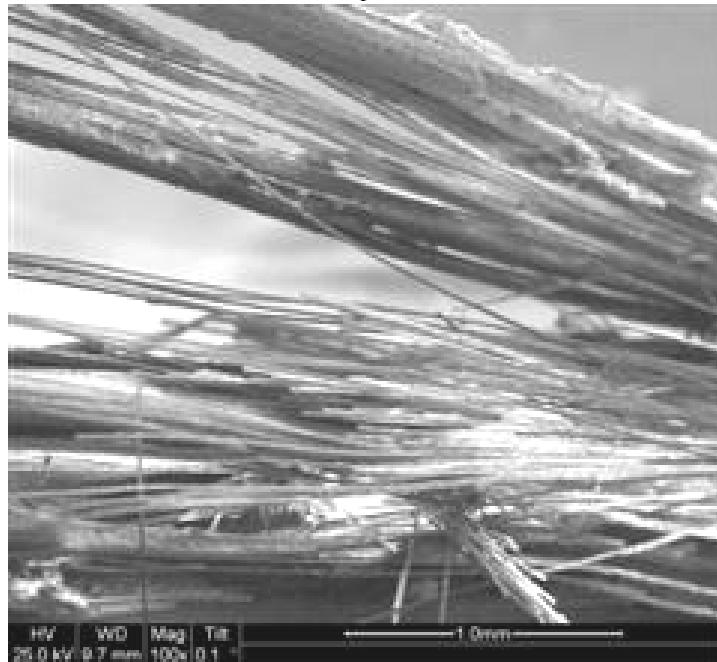


Figure 465. SEM micrograph of the fracture surface of the N720/AM specimen with  $\pm 45^\circ$  fiber orientation obtained in creep test conducted at 32 MPa at 1200°C in argon. Creep lifetime  $t_f = 0.08$  h.

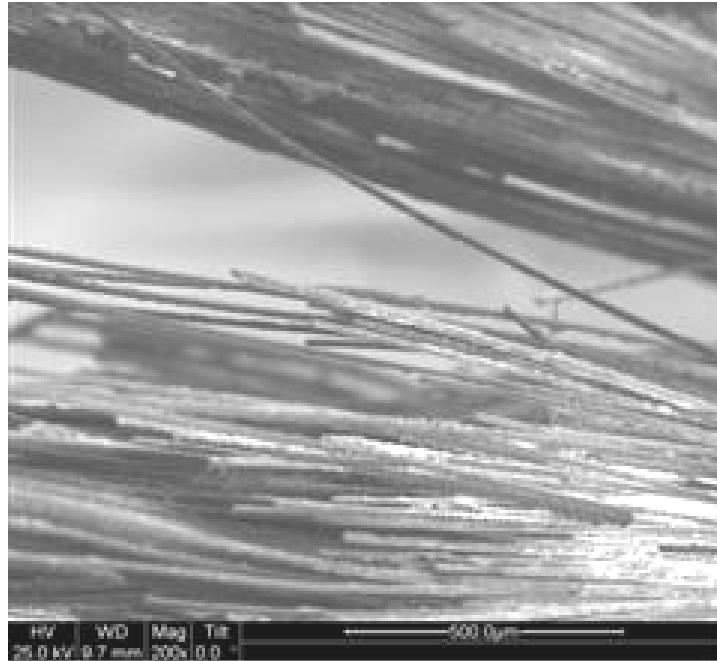


Figure 466. SEM micrograph of the fracture surface of the N720/AM specimen with  $\pm 45^\circ$  fiber orientation obtained in creep test conducted at 32 MPa at 1200°C in argon. Creep lifetime  $t_f = 0.08$  h.

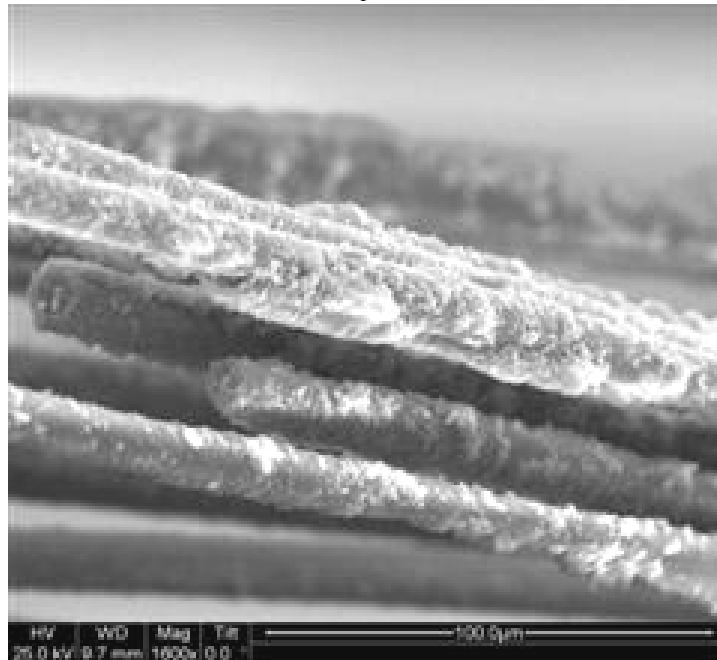


Figure 467. SEM micrograph of the fracture surface of the N720/AM specimen with  $\pm 45^\circ$  fiber orientation obtained in creep test conducted at 32 MPa at 1200°C in argon. Creep lifetime  $t_f = 0.08$  h.

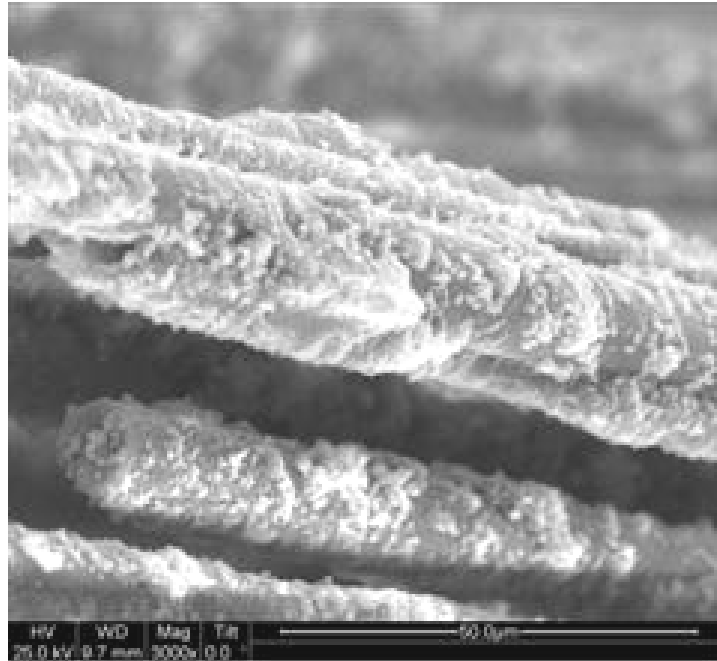


Figure 468. SEM micrograph of the fracture surface of the N720/AM specimen with  $\pm 45^\circ$  fiber orientation obtained in creep test conducted at 32 MPa at 1200°C in argon. Creep lifetime  $t_f = 0.08$  h.

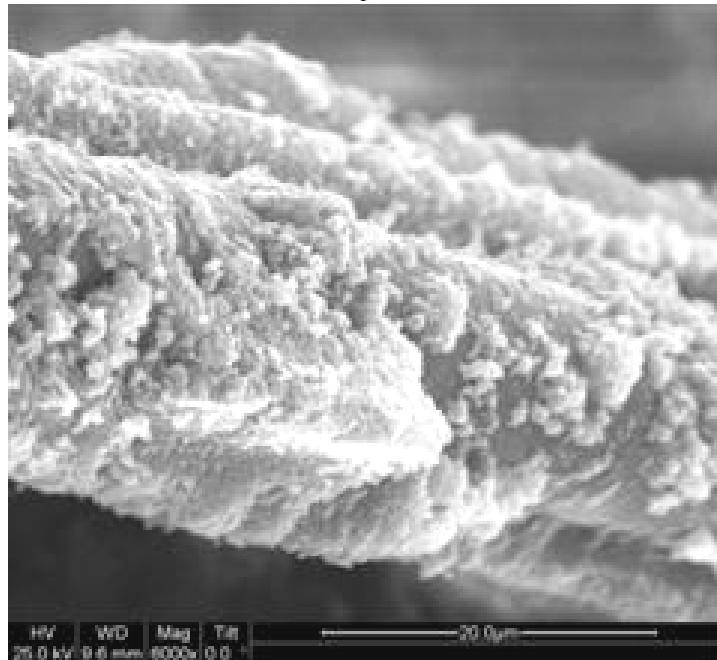


Figure 469. SEM micrograph of the fracture surface of the N720/AM specimen with  $\pm 45^\circ$  fiber orientation obtained in creep test conducted at 32 MPa at 1200°C in argon. Creep lifetime  $t_f = 0.08$  h.

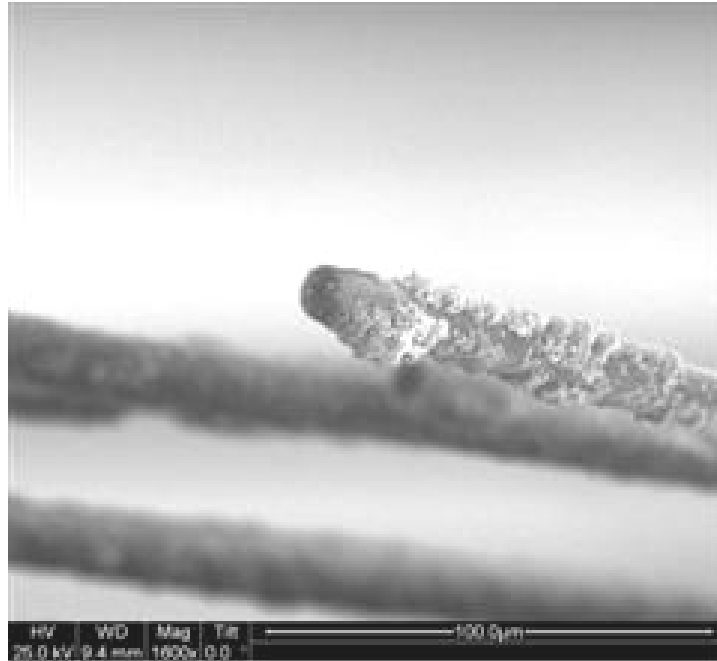


Figure 470. SEM micrograph of the fracture surface of the N720/AM specimen with  $\pm 45^\circ$  fiber orientation obtained in creep test conducted at 32 MPa at 1200°C in argon. Creep lifetime  $t_f = 0.08$  h.

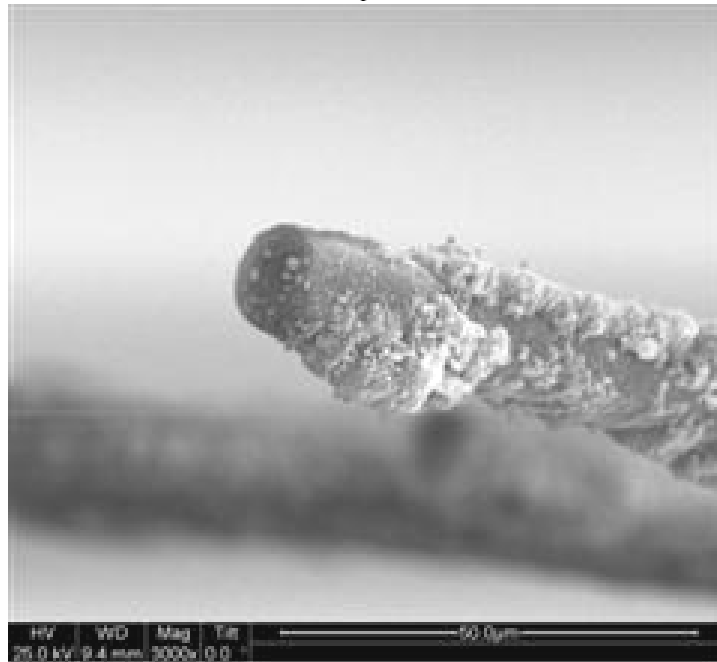


Figure 471. SEM micrograph of the fracture surface of the N720/AM specimen with  $\pm 45^\circ$  fiber orientation obtained in creep test conducted at 32 MPa at 1200°C in argon. Creep lifetime  $t_f = 0.08$  h.

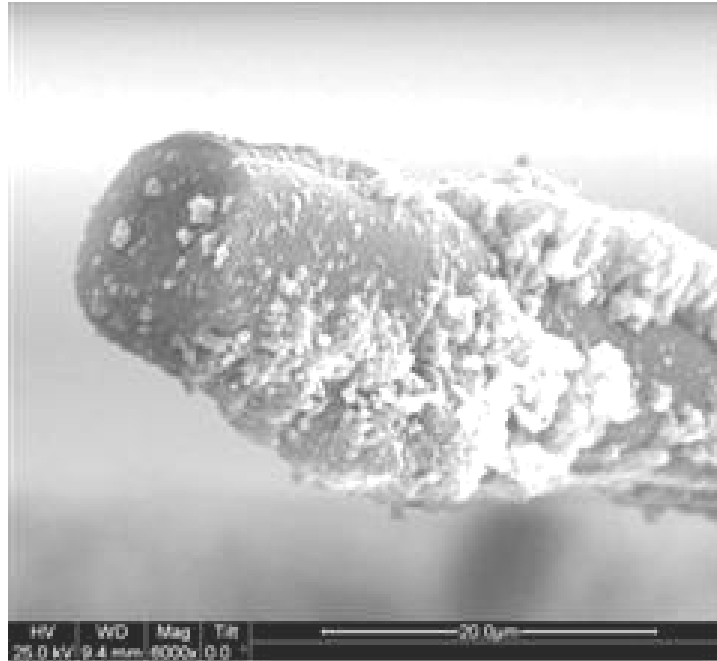


Figure 472. SEM micrograph of the fracture surface of the N720/AM specimen with  $\pm 45^\circ$  fiber orientation obtained in creep test conducted at 32 MPa at 1200°C in argon. Creep lifetime  $t_f = 0.08$  h.

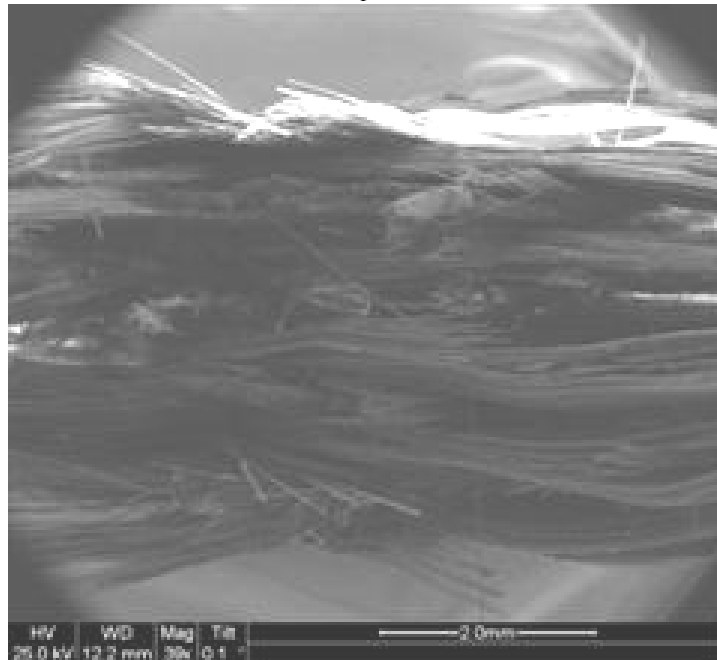


Figure 473. SEM micrograph of the fracture surface of the N720/AM specimen subjected to tensile test to failure with a constant stress rate of 0.0025 MPa/s at 1200°C in laboratory air.

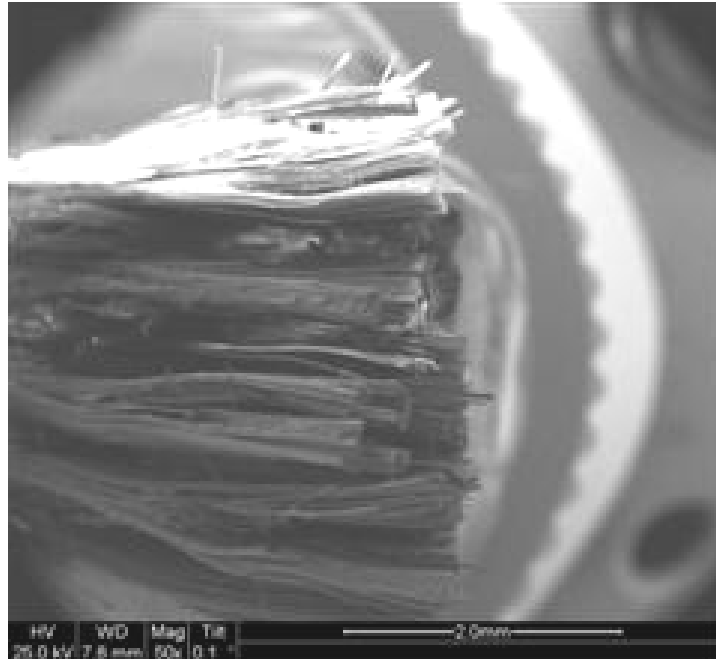


Figure 474. SEM micrograph of the fracture surface of the N720/AM specimen subjected to tensile test to failure with a constant stress rate of 0.0025 MPa/s at 1200°C in laboratory air.

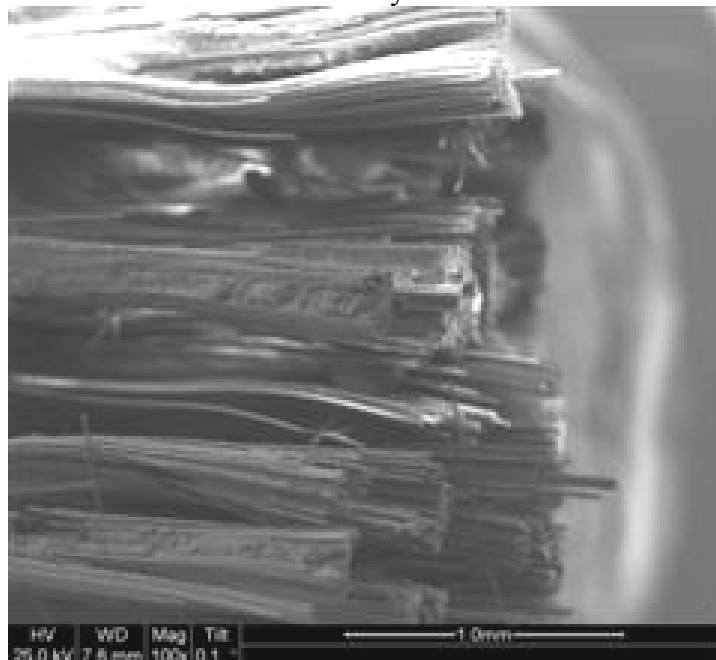


Figure 475. SEM micrograph of the fracture surface of the N720/AM specimen subjected to tensile test to failure with a constant stress rate of 0.0025 MPa/s at 1200°C in laboratory air.

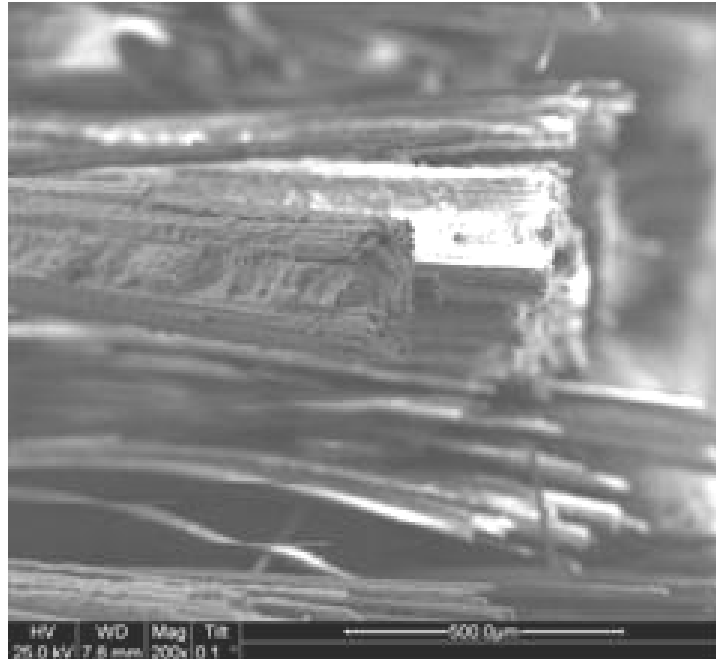


Figure 476. SEM micrograph of the fracture surface of the N720/AM specimen subjected to tensile test to failure with a constant stress rate of 0.0025 MPa/s at 1200°C in laboratory air.



Figure 477. SEM micrograph of the fracture surface of the N720/AM specimen subjected to tensile test to failure with a constant stress rate of 0.0025 MPa/s at 1200°C in laboratory air.

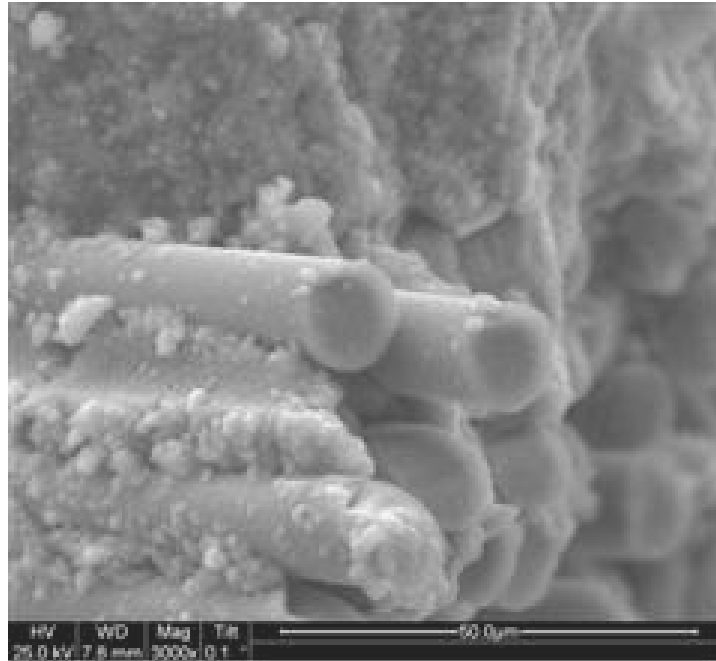


Figure 478. SEM micrograph of the fracture surface of the N720/AM specimen subjected to tensile test to failure with a constant stress rate of 0.0025 MPa/s at 1200°C in laboratory air.

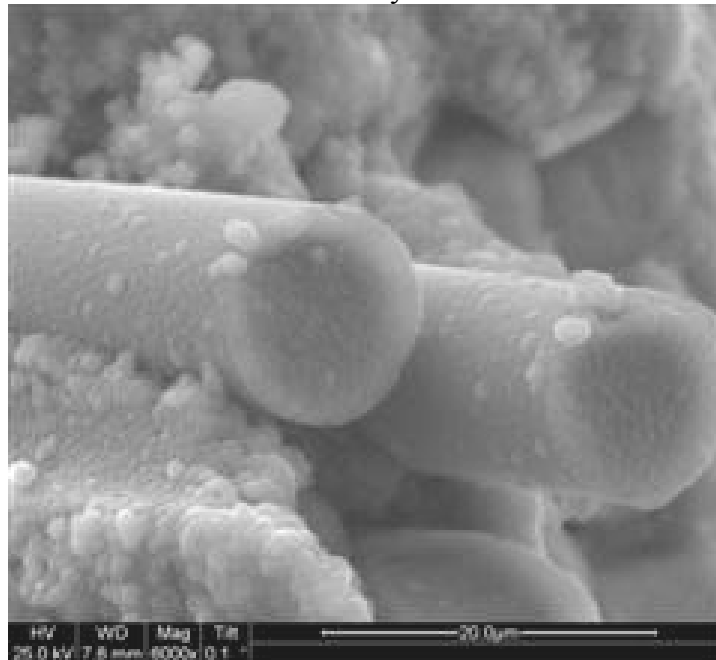


Figure 479. SEM micrograph of the fracture surface of the N720/AM specimen subjected to tensile test to failure with a constant stress rate of 0.0025 MPa/s at 1200°C in laboratory air.

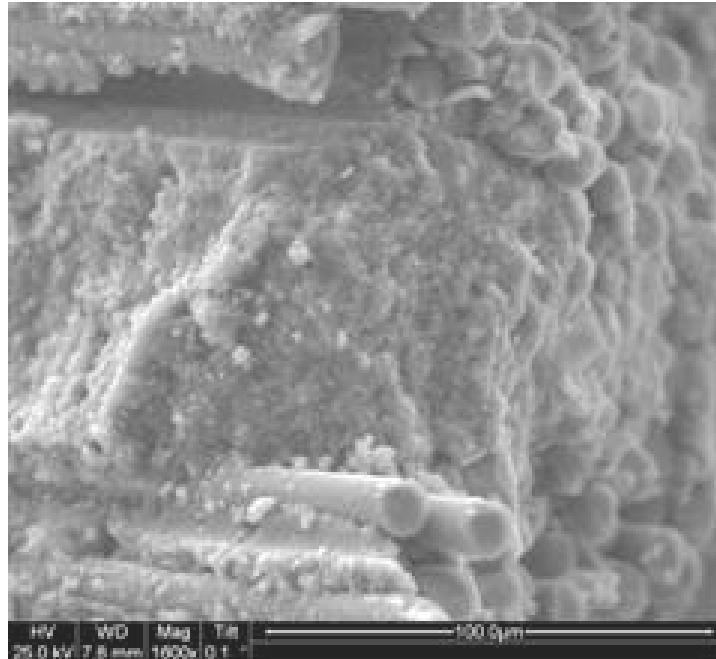


Figure 480. SEM micrograph of the fracture surface of the N720/AM specimen subjected to tensile test to failure with a constant stress rate of 0.0025 MPa/s at 1200°C in laboratory air.

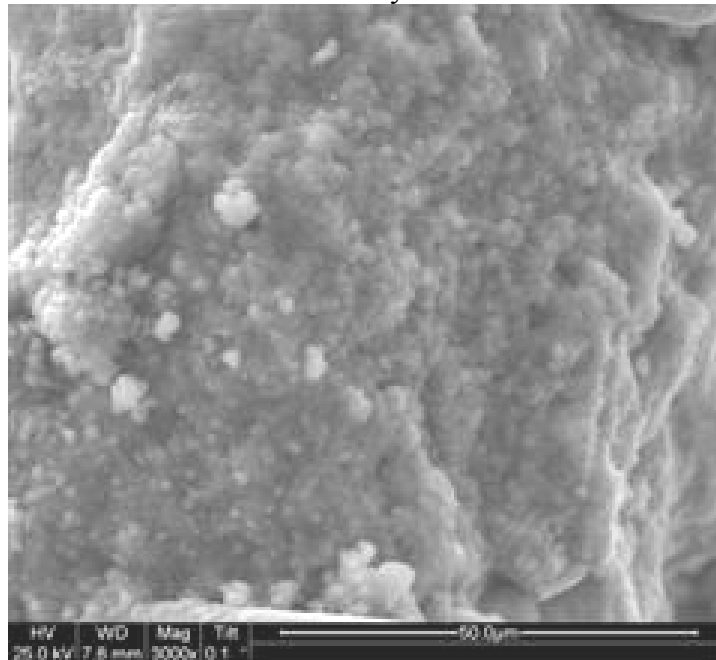


Figure 481. SEM micrograph of the fracture surface of the N720/AM specimen subjected to tensile test to failure with a constant stress rate of 0.0025 MPa/s at 1200°C in laboratory air.

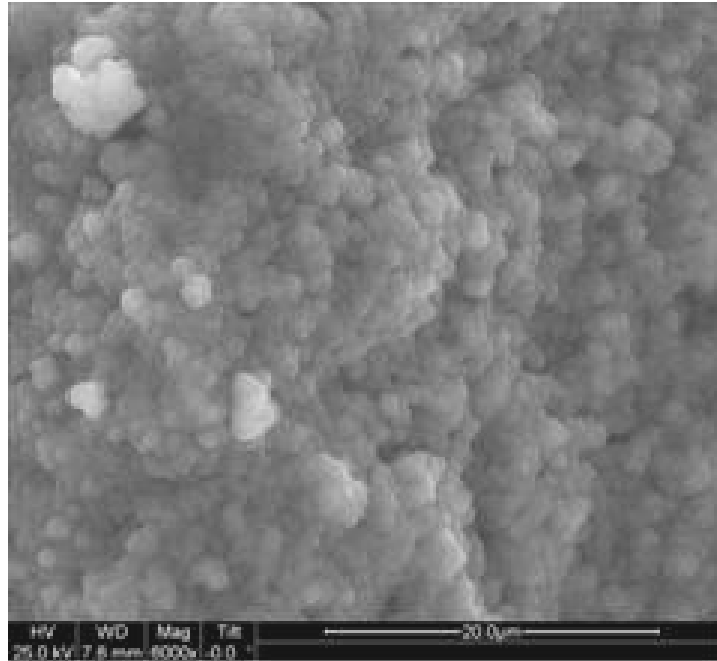


Figure 482. SEM micrograph of the fracture surface of the N720/AM specimen subjected to tensile test to failure with a constant stress rate of 0.0025 MPa/s at 1200°C in laboratory air.

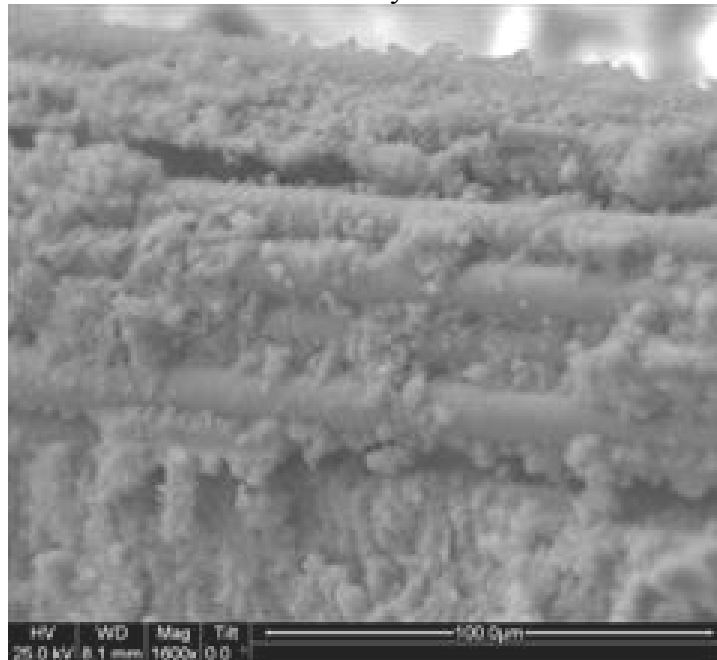


Figure 483. SEM micrograph of the fracture surface of the N720/AM specimen subjected to tensile test to failure with a constant stress rate of 0.0025 MPa/s at 1200°C in laboratory air.

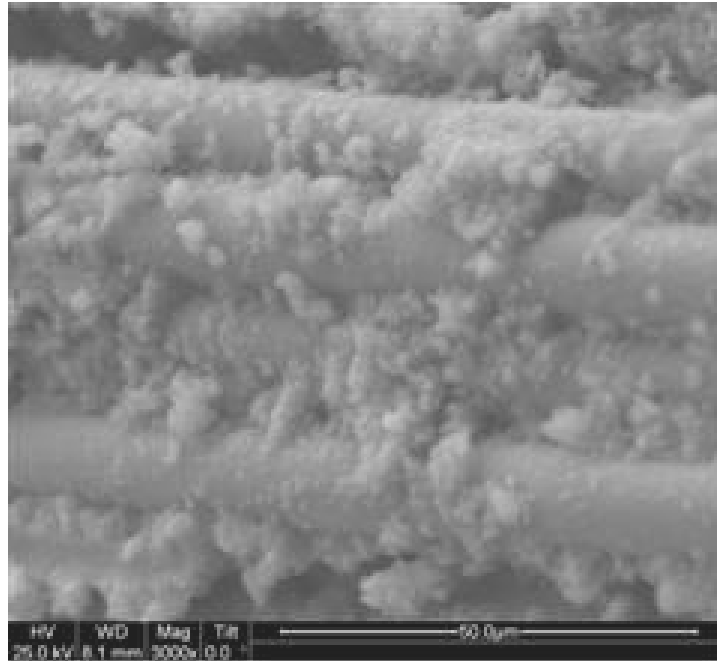


Figure 484. SEM micrograph of the fracture surface of the N720/AM specimen subjected to tensile test to failure with a constant stress rate of 0.0025 MPa/s at 1200°C in laboratory air.

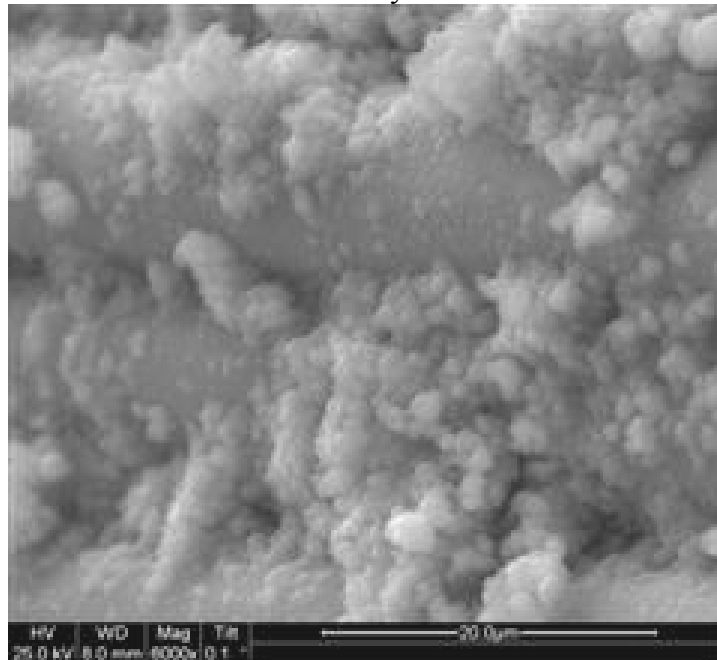


Figure 485. SEM micrograph of the fracture surface of the N720/AM specimen subjected to tensile test to failure with a constant stress rate of 0.0025 MPa/s at 1200°C in laboratory air.

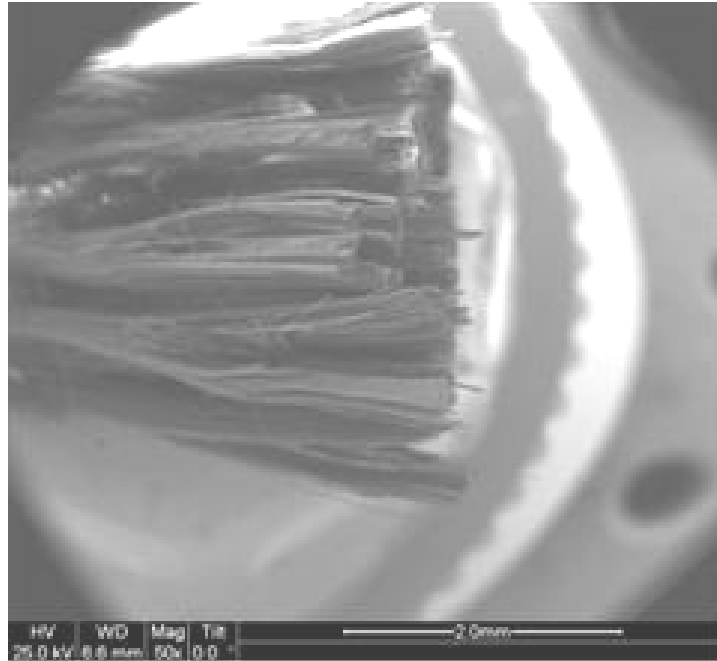


Figure 486. SEM micrograph of the fracture surface of the N720/AM specimen subjected to tensile test to failure with a constant stress rate of 0.0025 MPa/s at 1200°C in laboratory air.

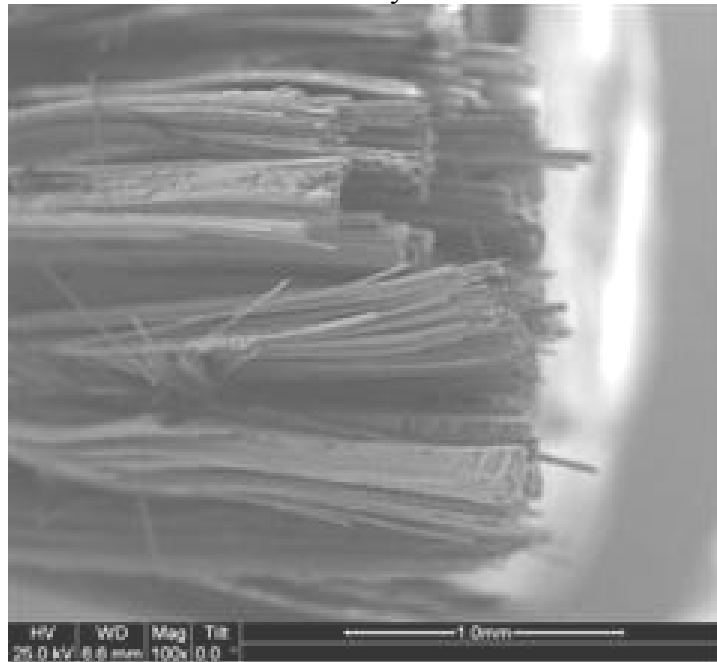


Figure 487. SEM micrograph of the fracture surface of the N720/AM specimen subjected to tensile test to failure with a constant stress rate of 0.0025 MPa/s at 1200°C in laboratory air.

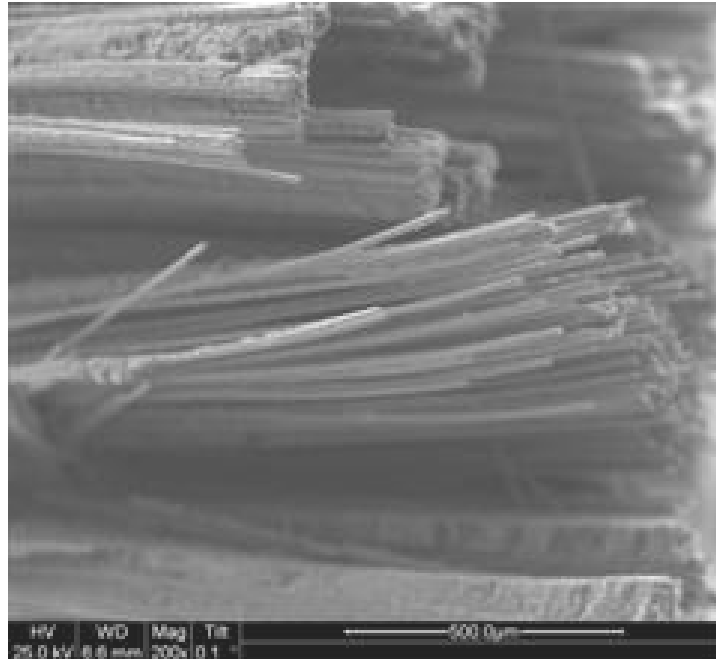


Figure 488. SEM micrograph of the fracture surface of the N720/AM specimen subjected to tensile test to failure with a constant stress rate of 0.0025 MPa/s at 1200°C in laboratory air.

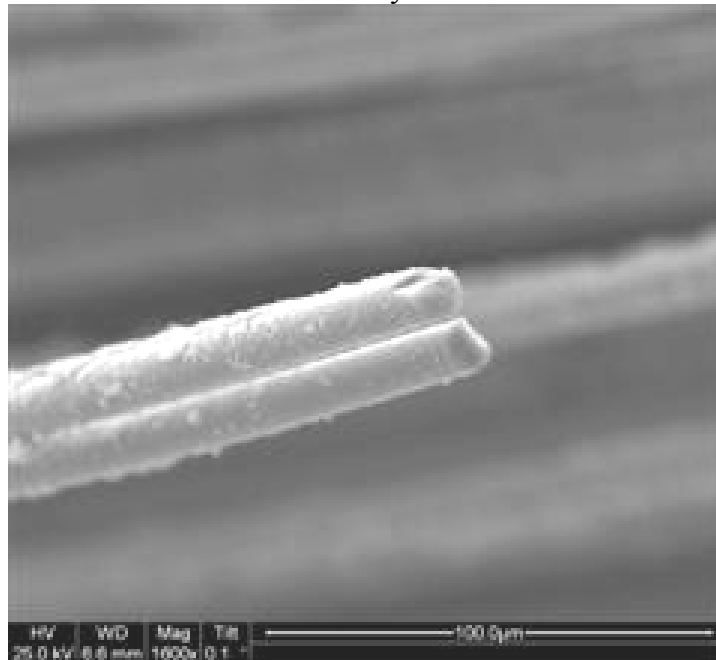


Figure 489. SEM micrograph of the fracture surface of the N720/AM specimen subjected to tensile test to failure with a constant stress rate of 0.0025 MPa/s at 1200°C in laboratory air.

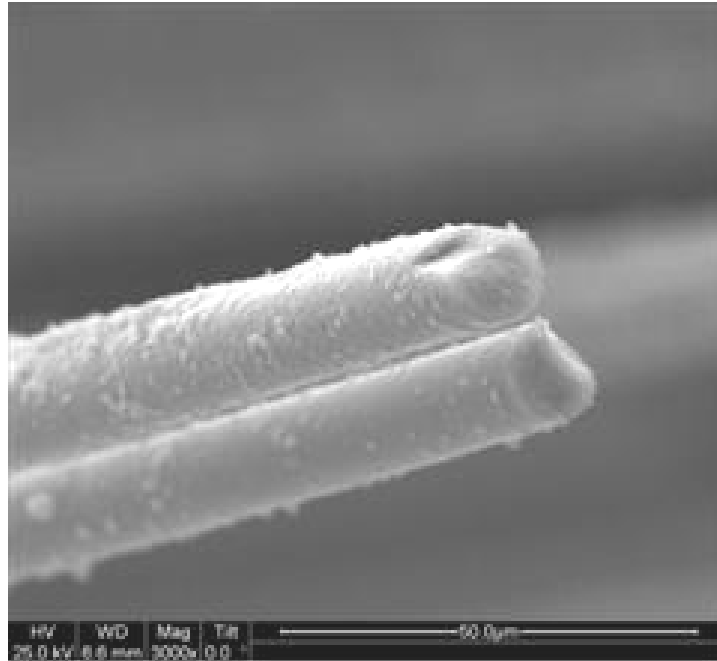


Figure 490. SEM micrograph of the fracture surface of the N720/AM specimen subjected to tensile test to failure with a constant stress rate of 0.0025 MPa/s at 1200°C in laboratory air.

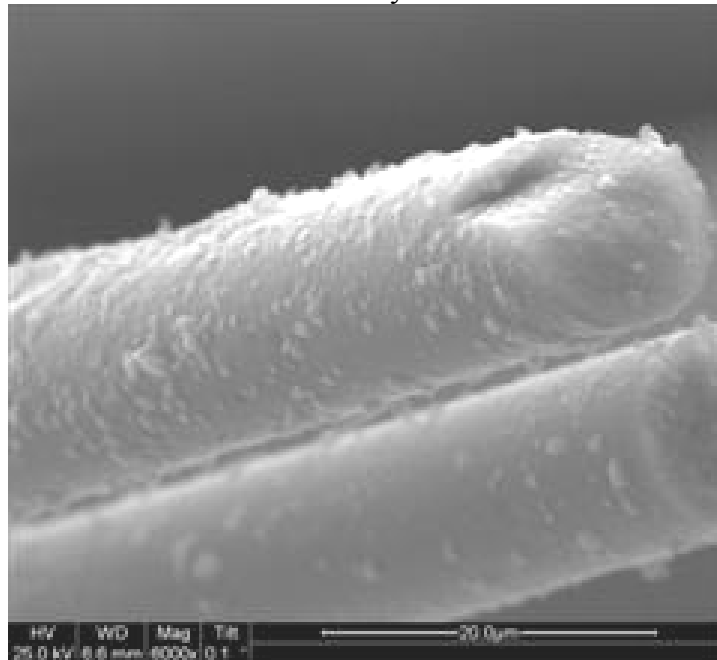


Figure 491. SEM micrograph of the fracture surface of the N720/AM specimen subjected to tensile test to failure with a constant stress rate of 0.0025 MPa/s at 1200°C in laboratory air.

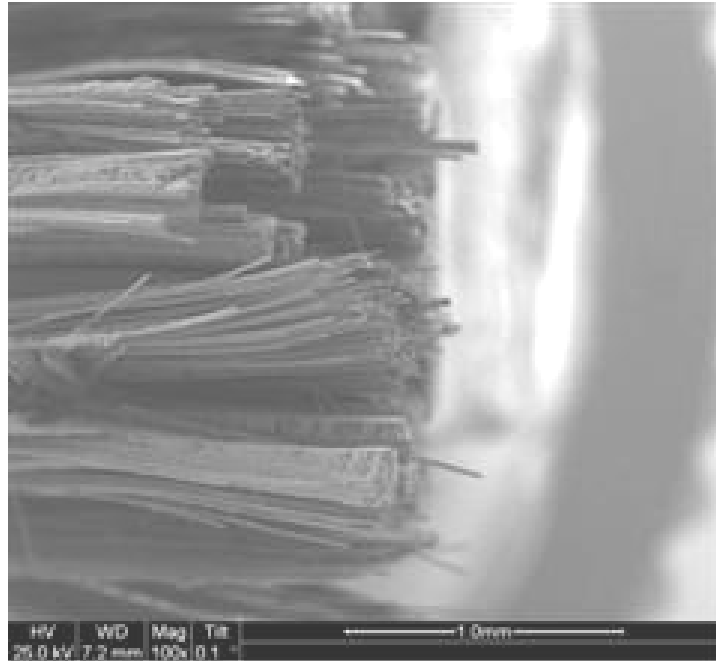


Figure 492. SEM micrograph of the fracture surface of the N720/AM specimen subjected to tensile test to failure with a constant stress rate of 0.0025 MPa/s at 1200°C in laboratory air.

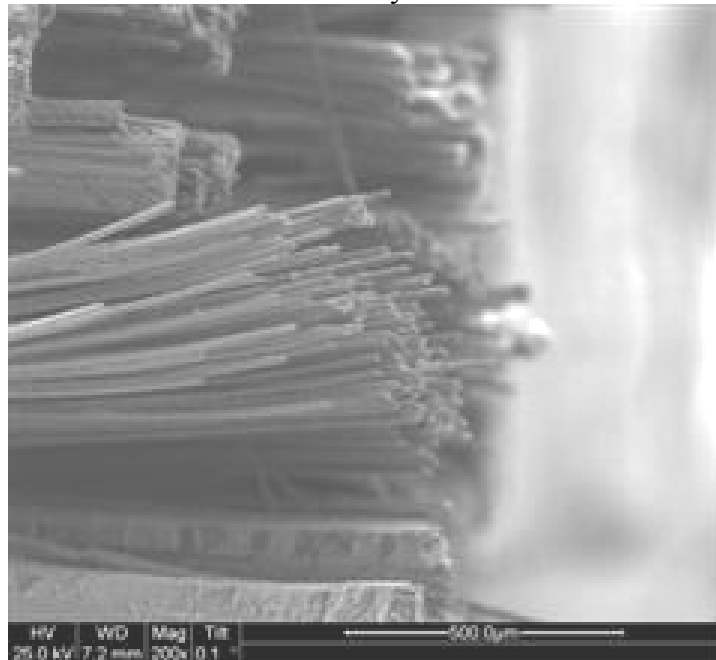


Figure 493. SEM micrograph of the fracture surface of the N720/AM specimen subjected to tensile test to failure with a constant stress rate of 0.0025 MPa/s at 1200°C in laboratory air.

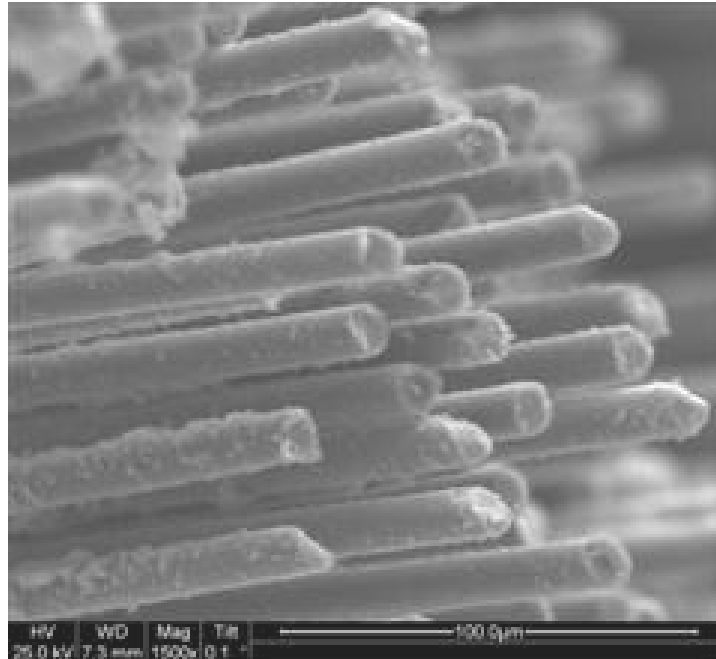


Figure 494. SEM micrograph of the fracture surface of the N720/AM specimen subjected to tensile test to failure with a constant stress rate of 0.0025 MPa/s at 1200°C in laboratory air.

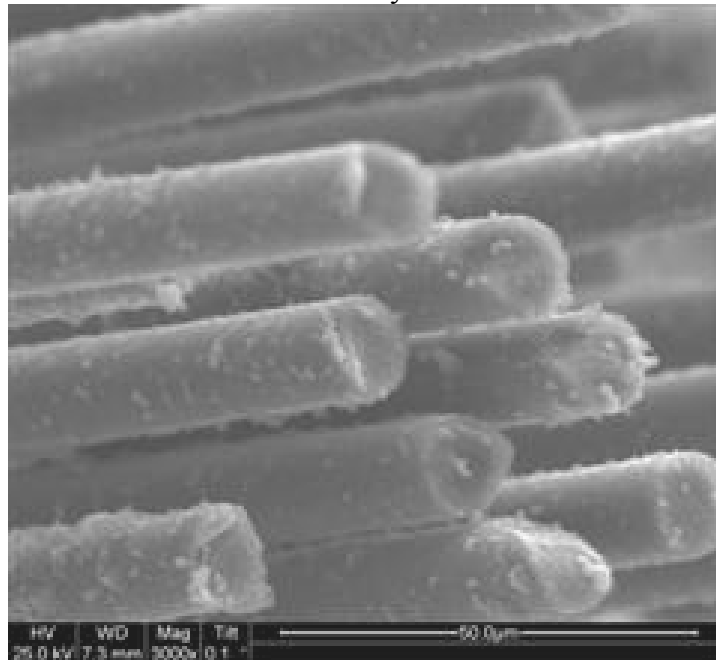


Figure 495. SEM micrograph of the fracture surface of the N720/AM specimen subjected to tensile test to failure with a constant stress rate of 0.0025 MPa/s at 1200°C in laboratory air.

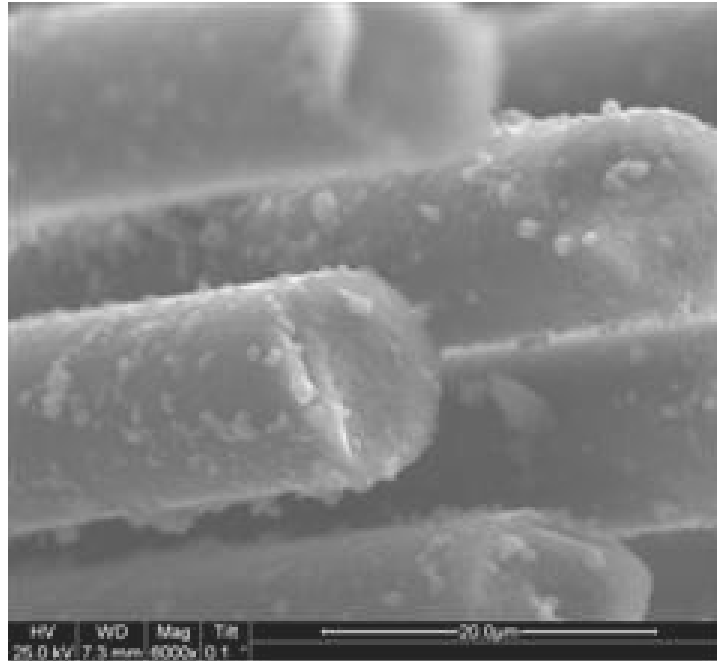


Figure 496. SEM micrograph of the fracture surface of the N720/AM specimen subjected to tensile test to failure with a constant stress rate of 0.0025 MPa/s at 1200°C in laboratory air.

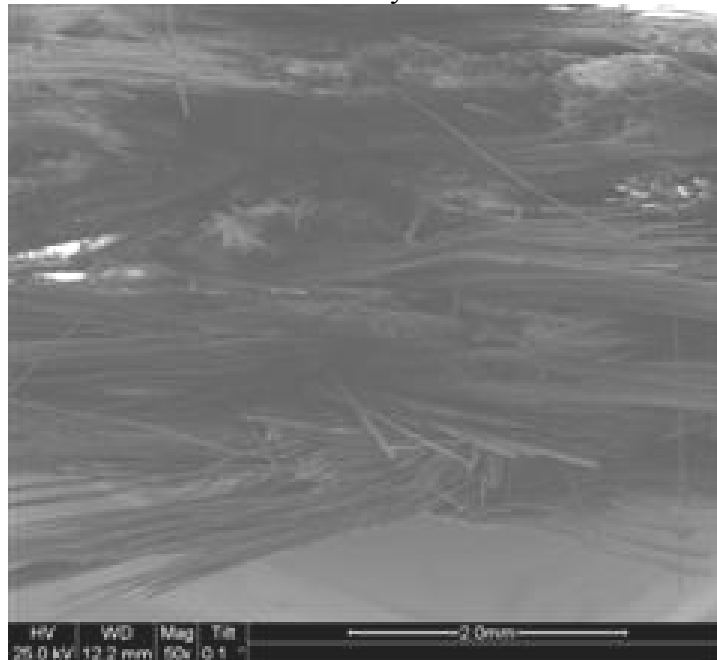


Figure 497. SEM micrograph of the fracture surface of the N720/AM specimen subjected to tensile test to failure with a constant stress rate of 0.0025 MPa/s at 1200°C in laboratory air.

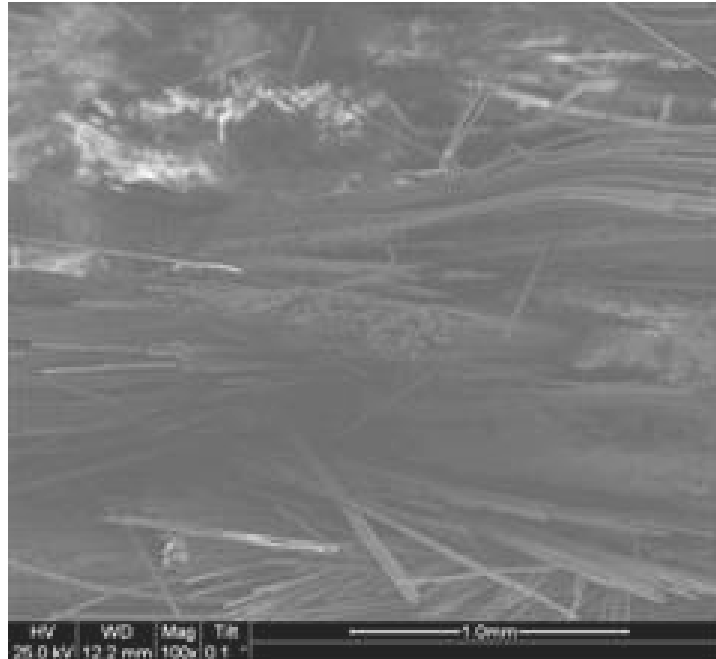


Figure 498. SEM micrograph of the fracture surface of the N720/AM specimen subjected to tensile test to failure with a constant stress rate of 0.0025 MPa/s at 1200°C in laboratory air.

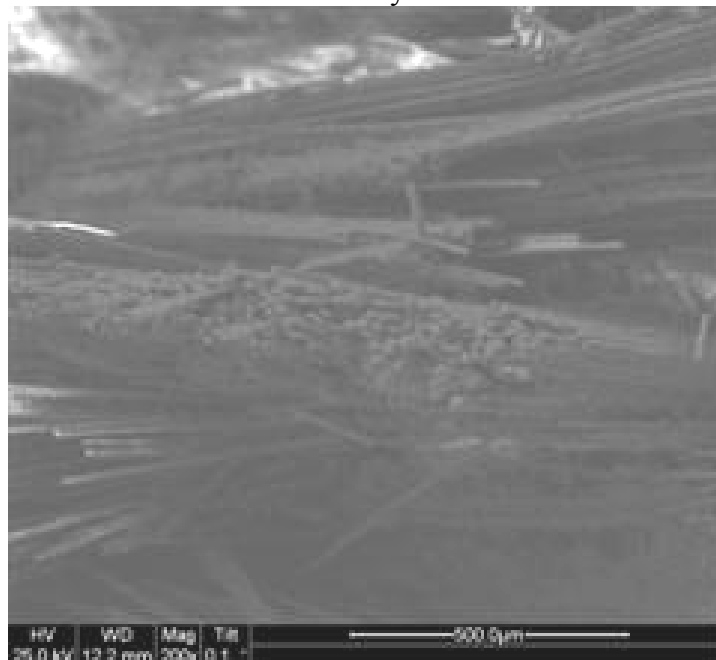


Figure 499. SEM micrograph of the fracture surface of the N720/AM specimen subjected to tensile test to failure with a constant stress rate of 0.0025 MPa/s at 1200°C in laboratory air.

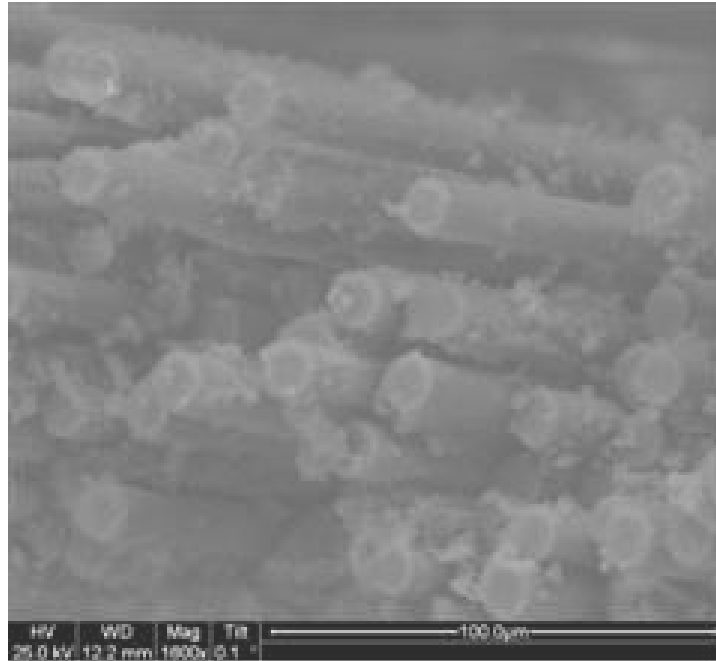


Figure 500. SEM micrograph of the fracture surface of the N720/AM specimen subjected to tensile test to failure with a constant stress rate of 0.0025 MPa/s at 1200°C in laboratory air.

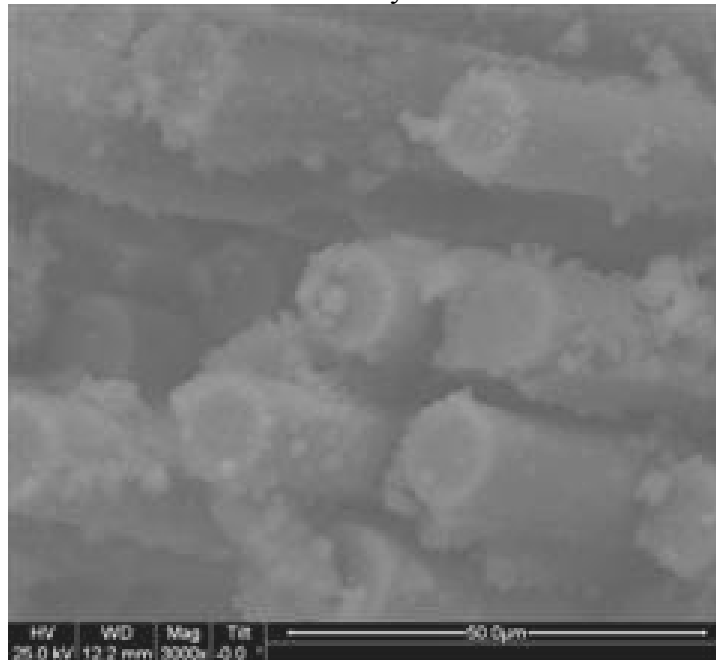


Figure 501. SEM micrograph of the fracture surface of the N720/AM specimen subjected to tensile test to failure with a constant stress rate of 0.0025 MPa/s at 1200°C in laboratory air.

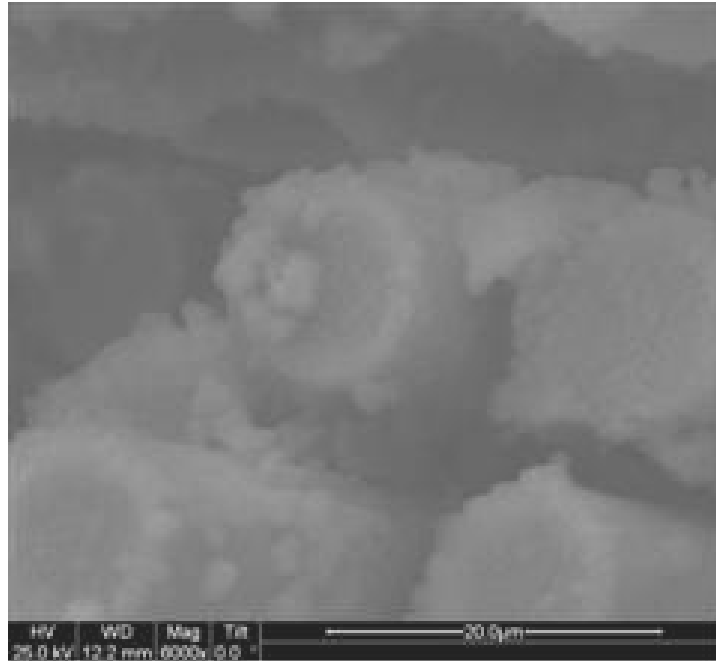


Figure 502. SEM micrograph of the fracture surface of the N720/AM specimen subjected to tensile test to failure with a constant stress rate of 0.0025 MPa/s at 1200°C in laboratory air.

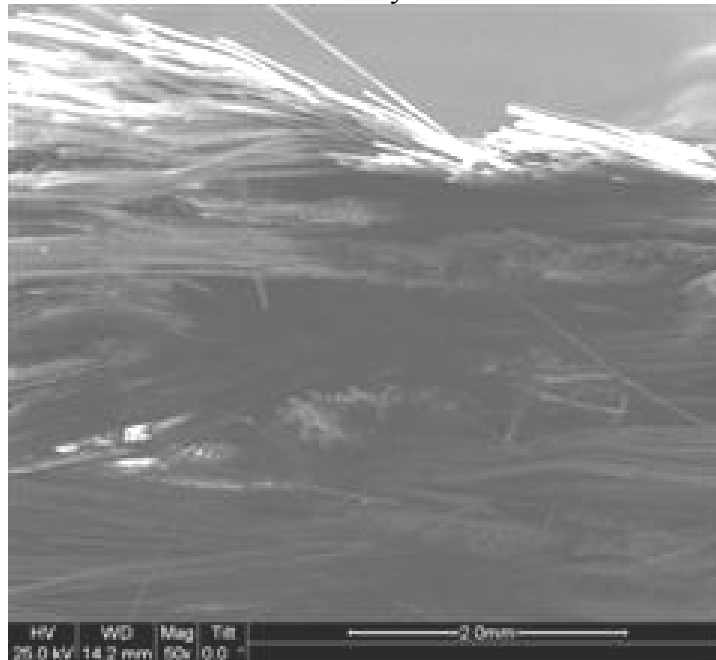


Figure 503. SEM micrograph of the fracture surface of the N720/AM specimen subjected to tensile test to failure with a constant stress rate of 0.0025 MPa/s at 1200°C in laboratory air.

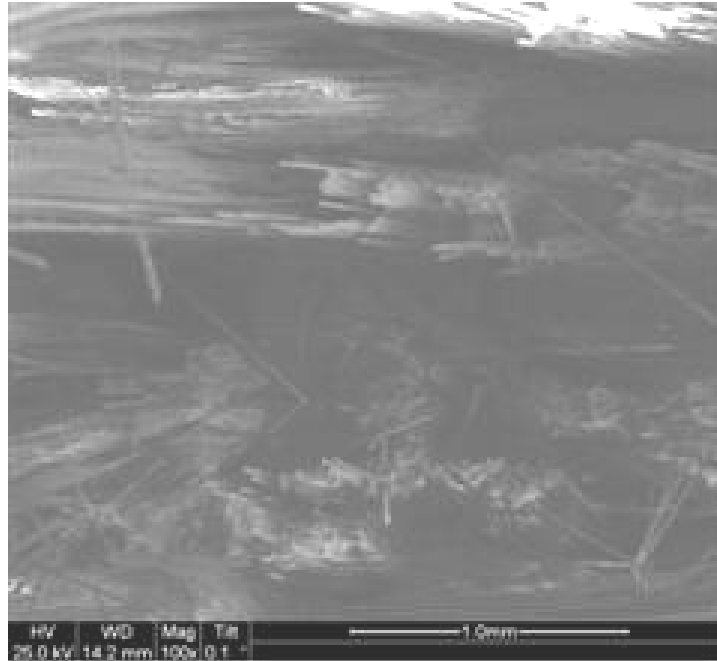


Figure 504. SEM micrograph of the fracture surface of the N720/AM specimen subjected to tensile test to failure with a constant stress rate of 0.0025 MPa/s at 1200°C in laboratory air.

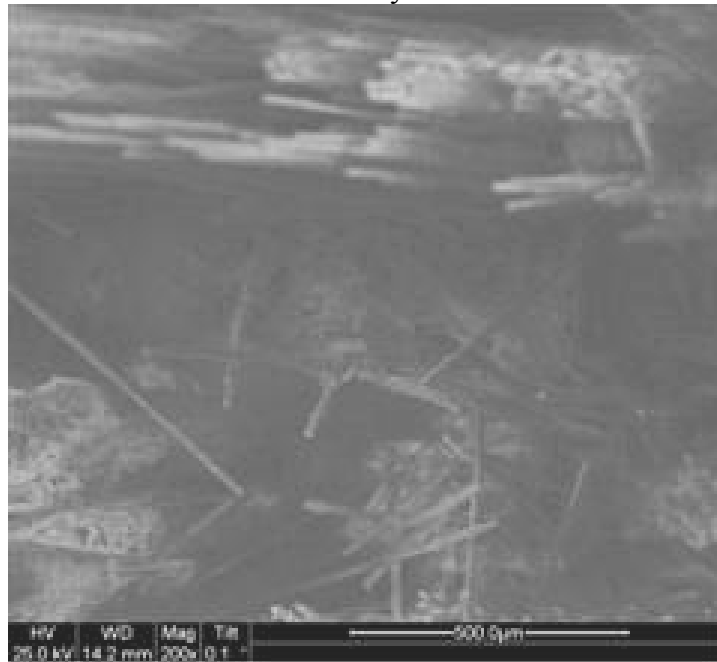


Figure 505. SEM micrograph of the fracture surface of the N720/AM specimen subjected to tensile test to failure with a constant stress rate of 0.0025 MPa/s at 1200°C in laboratory air.



Figure 506. SEM micrograph of the fracture surface of the N720/AM specimen subjected to tensile test to failure with a constant stress rate of 0.0025 MPa/s at 1200°C in laboratory air.

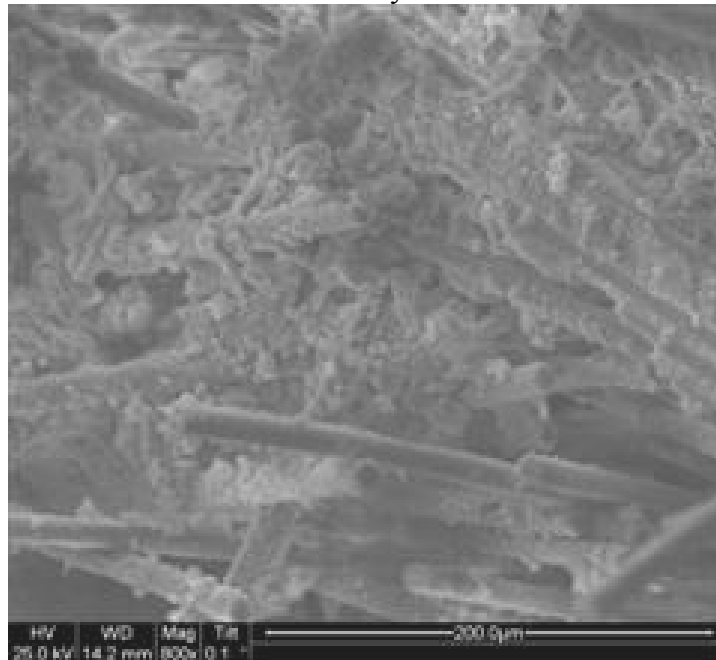


Figure 507. SEM micrograph of the fracture surface of the N720/AM specimen subjected to tensile test to failure with a constant stress rate of 0.0025 MPa/s at 1200°C in laboratory air.

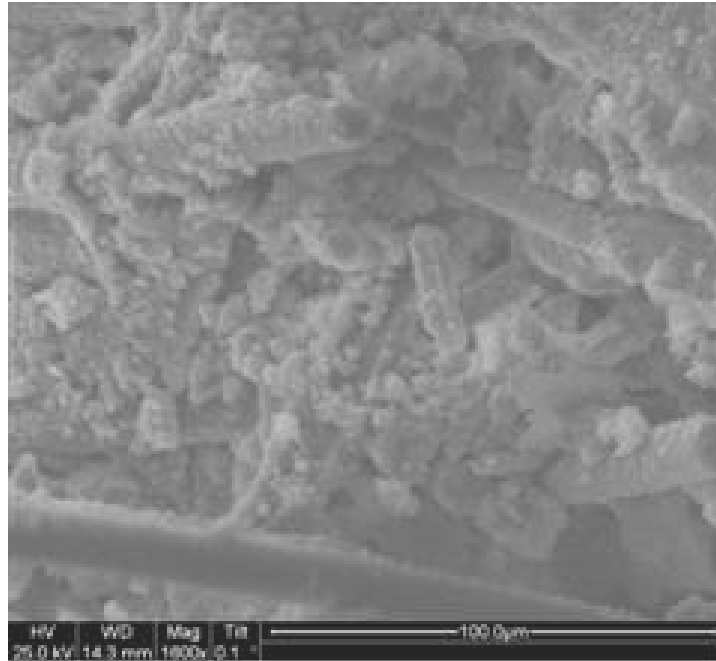


Figure 508. SEM micrograph of the fracture surface of the N720/AM specimen subjected to tensile test to failure with a constant stress rate of 0.0025 MPa/s at 1200°C in laboratory air.

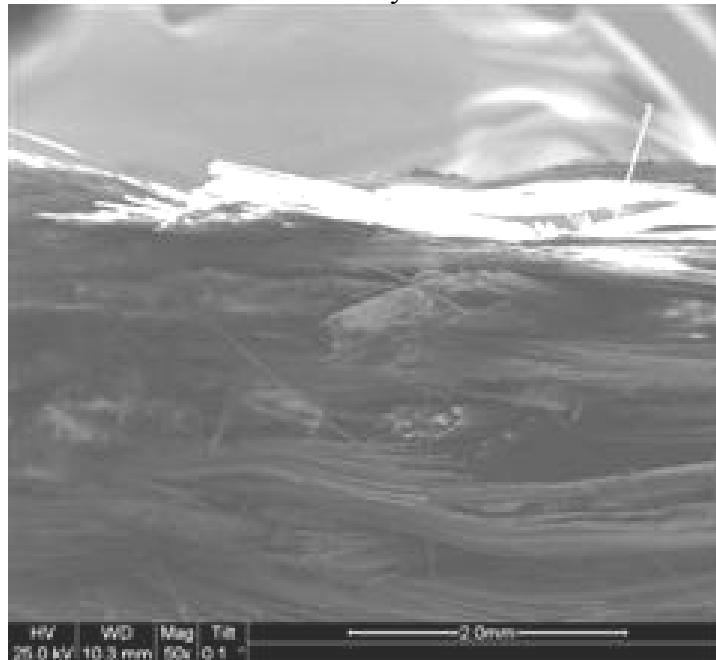


Figure 509. SEM micrograph of the fracture surface of the N720/AM specimen subjected to tensile test to failure with a constant stress rate of 0.0025 MPa/s at 1200°C in laboratory air.

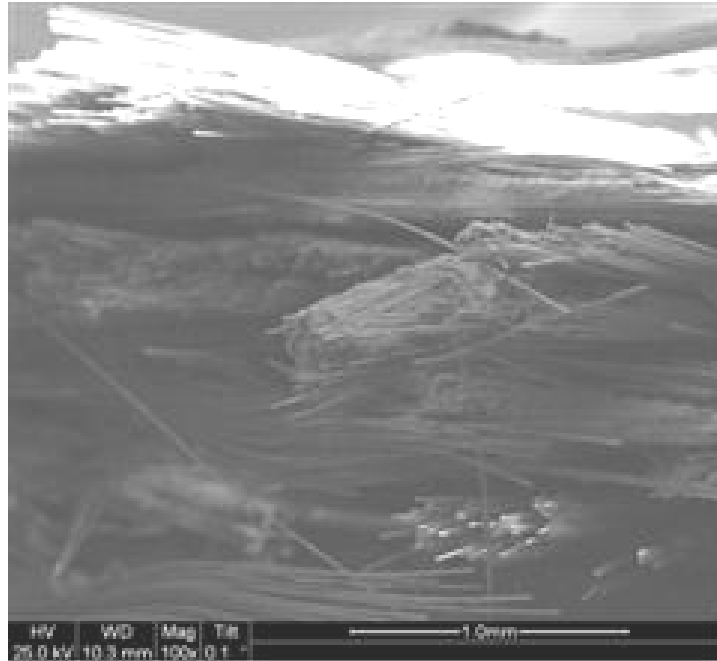


Figure 510. SEM micrograph of the fracture surface of the N720/AM specimen subjected to tensile test to failure with a constant stress rate of 0.0025 MPa/s at 1200°C in laboratory air.

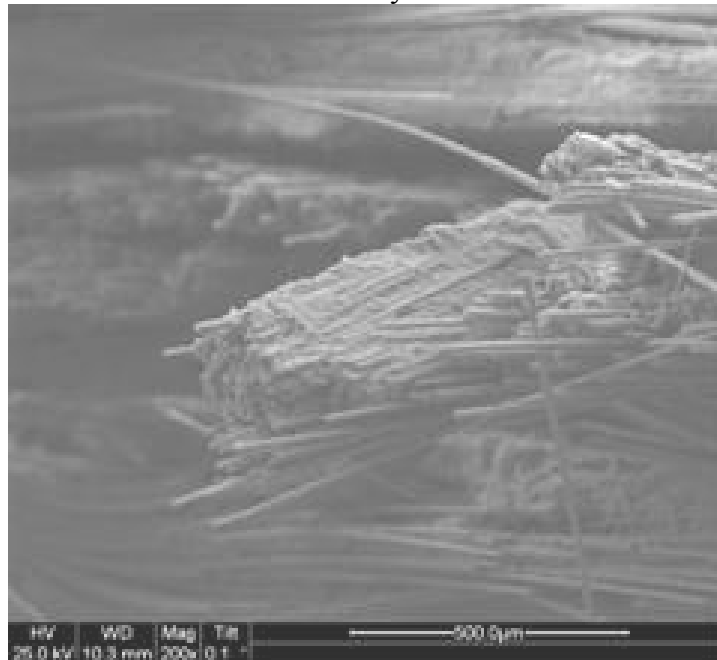


Figure 511. SEM micrograph of the fracture surface of the N720/AM specimen subjected to tensile test to failure with a constant stress rate of 0.0025 MPa/s at 1200°C in laboratory air.

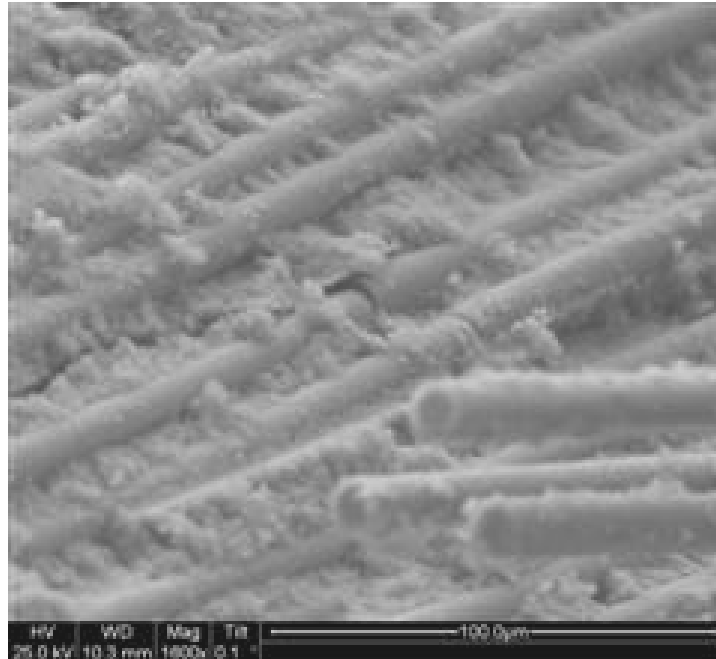


Figure 512. SEM micrograph of the fracture surface of the N720/AM specimen subjected to tensile test to failure with a constant stress rate of 0.0025 MPa/s at 1200°C in laboratory air.

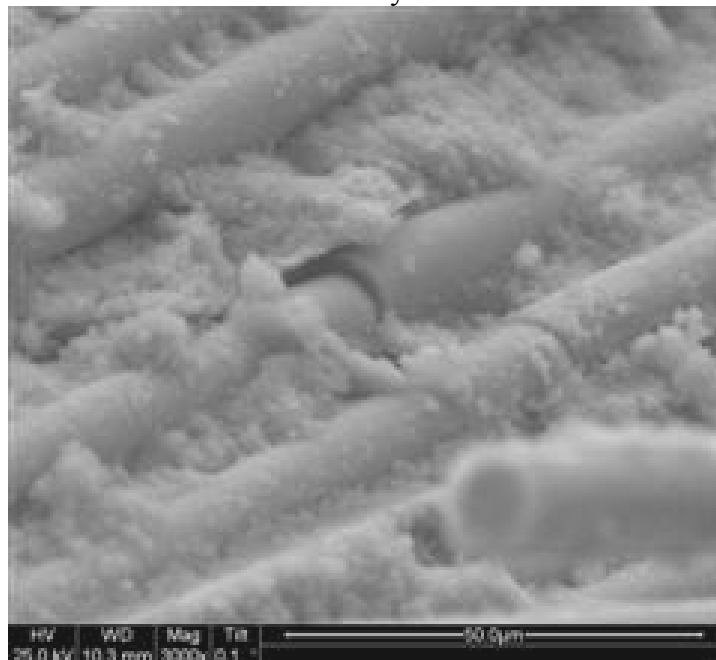


Figure 513. SEM micrograph of the fracture surface of the N720/AM specimen subjected to tensile test to failure with a constant stress rate of 0.0025 MPa/s at 1200°C in laboratory air.

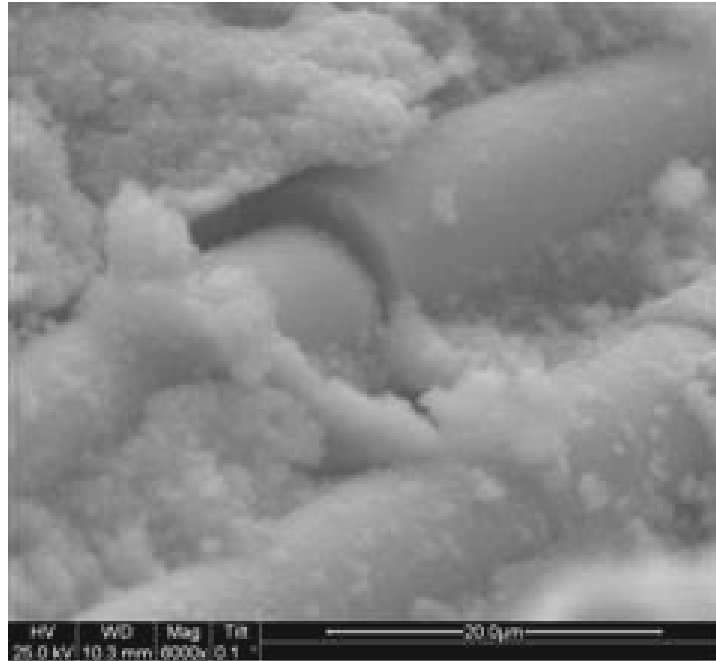


Figure 514. SEM micrograph of the fracture surface of the N720/AM specimen subjected to tensile test to failure with a constant stress rate of 0.0025 MPa/s at 1200°C in laboratory air.

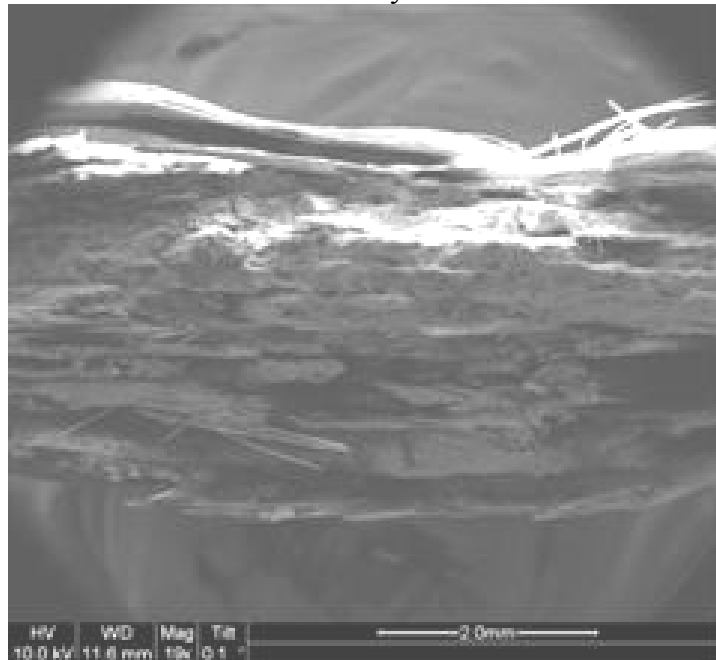


Figure 515. SEM micrograph of the fracture surface of the N720/AM specimen subjected to tensile test to failure with a constant stress rate of 0.0025 MPa/s at 1200°C in steam.

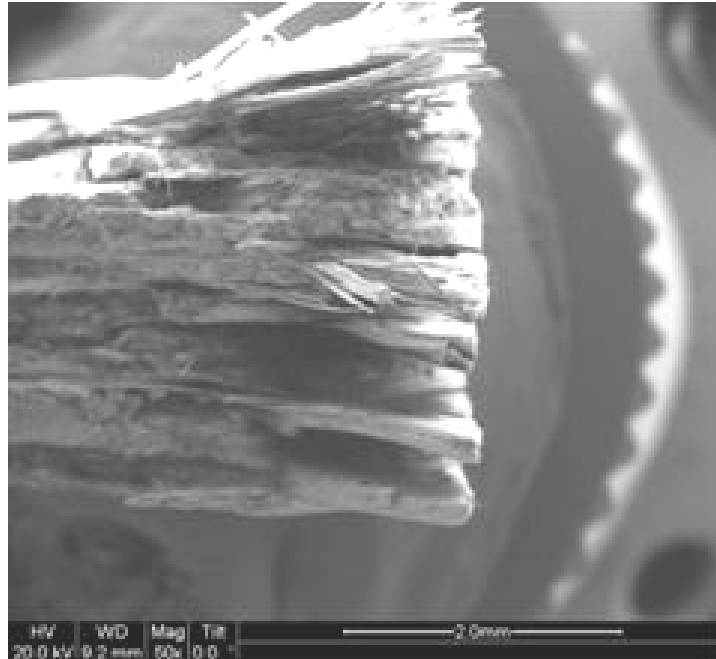


Figure 516. SEM micrograph of the fracture surface of the N720/AM specimen subjected to tensile test to failure with a constant stress rate of 0.0025 MPa/s at 1200°C in steam.

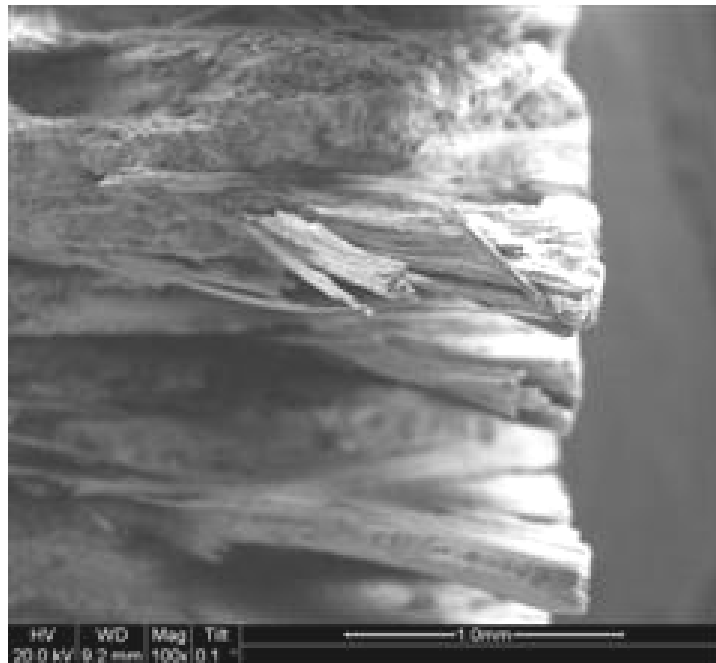


Figure 517. SEM micrograph of the fracture surface of the N720/AM specimen subjected to tensile test to failure with a constant stress rate of 0.0025 MPa/s at 1200°C in steam.

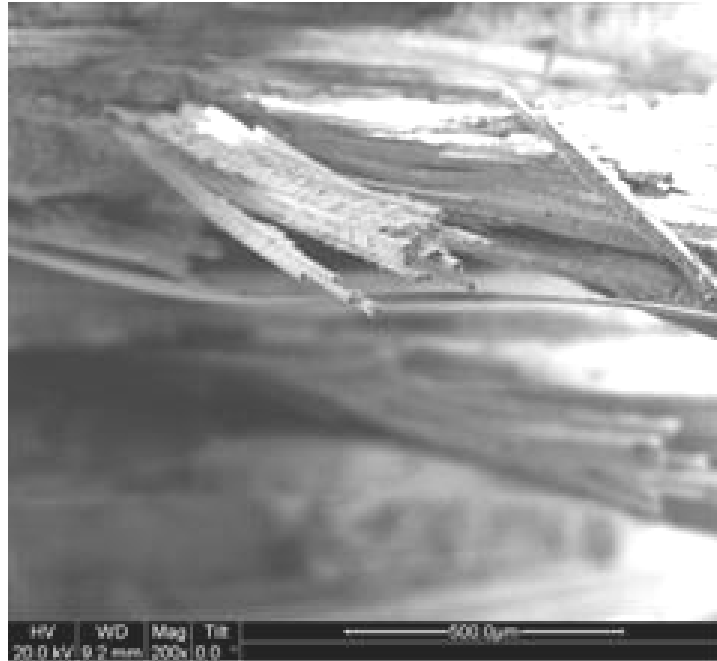


Figure 518. SEM micrograph of the fracture surface of the N720/AM specimen subjected to tensile test to failure with a constant stress rate of 0.0025 MPa/s at 1200°C in steam.



Figure 519. SEM micrograph of the fracture surface of the N720/AM specimen subjected to tensile test to failure with a constant stress rate of 0.0025 MPa/s at 1200°C in steam.



Figure 520. SEM micrograph of the fracture surface of the N720/AM specimen subjected to tensile test to failure with a constant stress rate of 0.0025 MPa/s at 1200°C in steam.

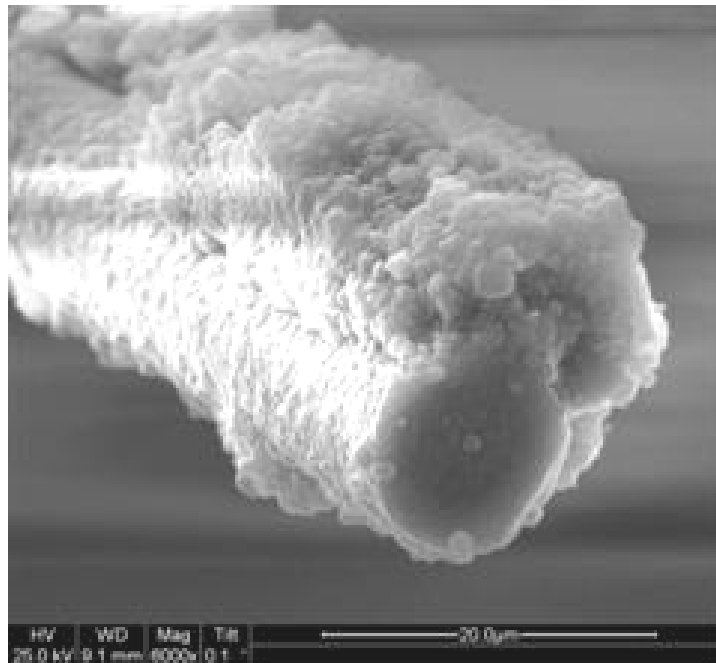


Figure 521. SEM micrograph of the fracture surface of the N720/AM specimen subjected to tensile test to failure with a constant stress rate of 0.0025 MPa/s at 1200°C in steam.

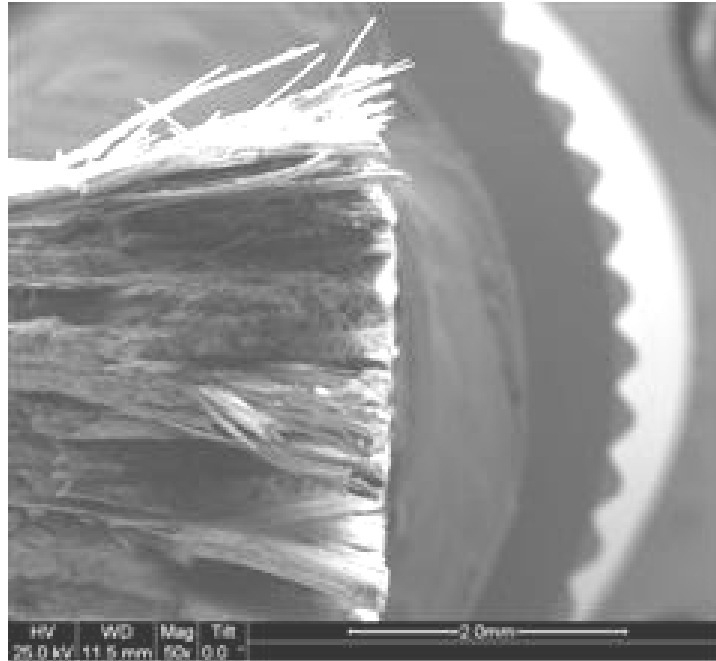


Figure 522. SEM micrograph of the fracture surface of the N720/AM specimen subjected to tensile test to failure with a constant stress rate of 0.0025 MPa/s at 1200°C in steam.

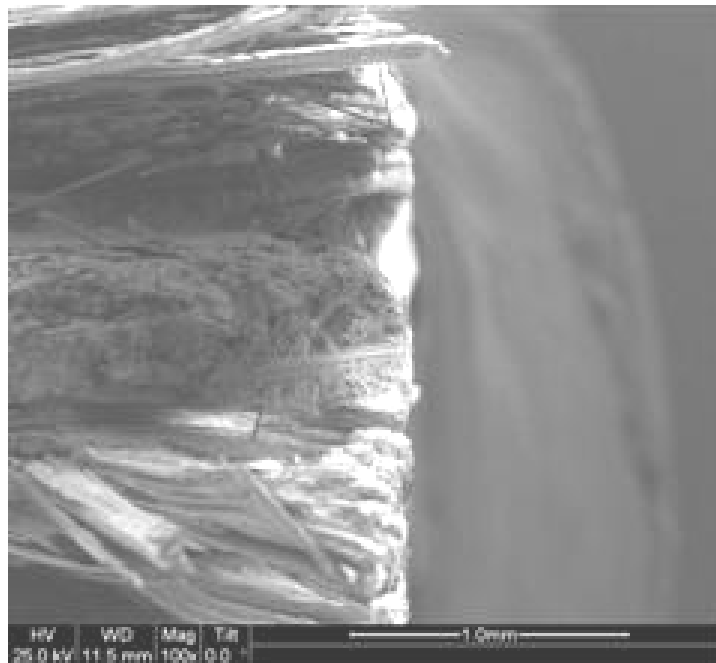


Figure 523. SEM micrograph of the fracture surface of the N720/AM specimen subjected to tensile test to failure with a constant stress rate of 0.0025 MPa/s at 1200°C in steam.



Figure 524. SEM micrograph of the fracture surface of the N720/AM specimen subjected to tensile test to failure with a constant stress rate of 0.0025 MPa/s at 1200°C in steam.

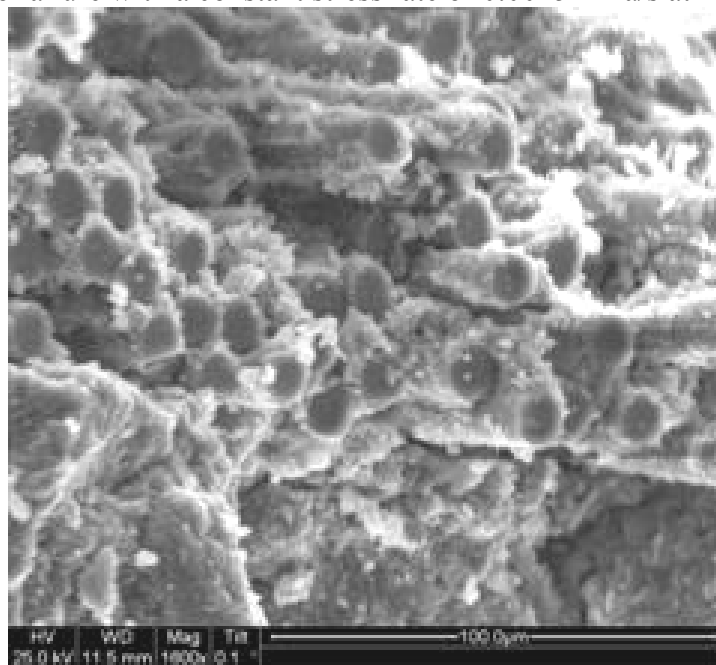


Figure 525. SEM micrograph of the fracture surface of the N720/AM specimen subjected to tensile test to failure with a constant stress rate of 0.0025 MPa/s at 1200°C in steam.

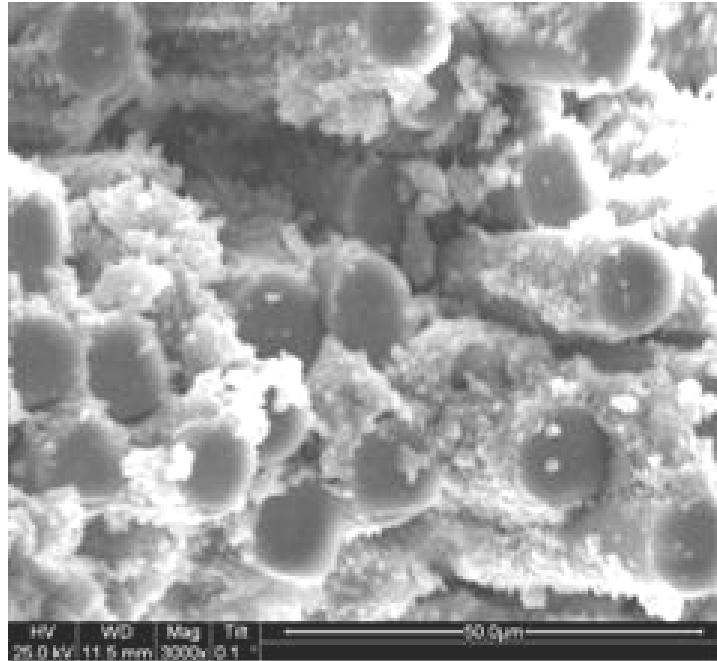


Figure 526. SEM micrograph of the fracture surface of the N720/AM specimen subjected to tensile test to failure with a constant stress rate of 0.0025 MPa/s at 1200°C in steam.

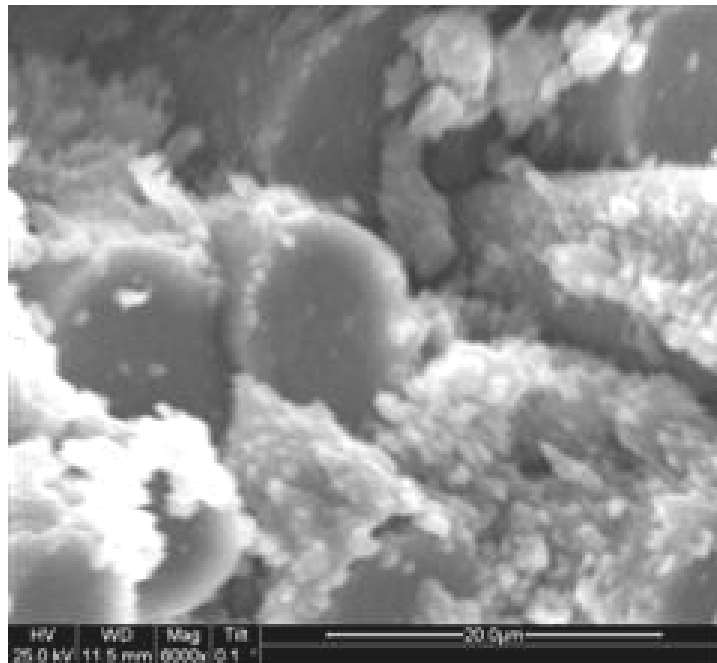


Figure 527. SEM micrograph of the fracture surface of the N720/AM specimen subjected to tensile test to failure with a constant stress rate of 0.0025 MPa/s at 1200°C in steam.

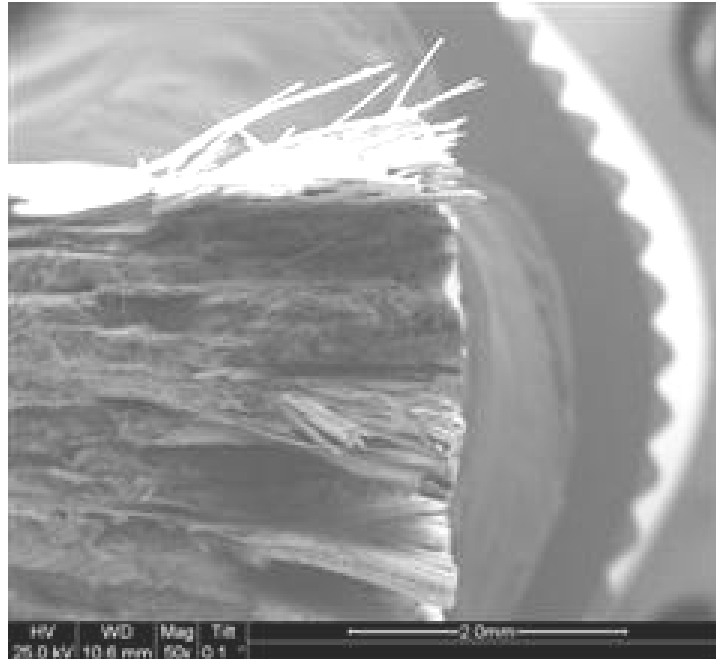


Figure 528. SEM micrograph of the fracture surface of the N720/AM specimen subjected to tensile test to failure with a constant stress rate of 0.0025 MPa/s at 1200°C in steam.

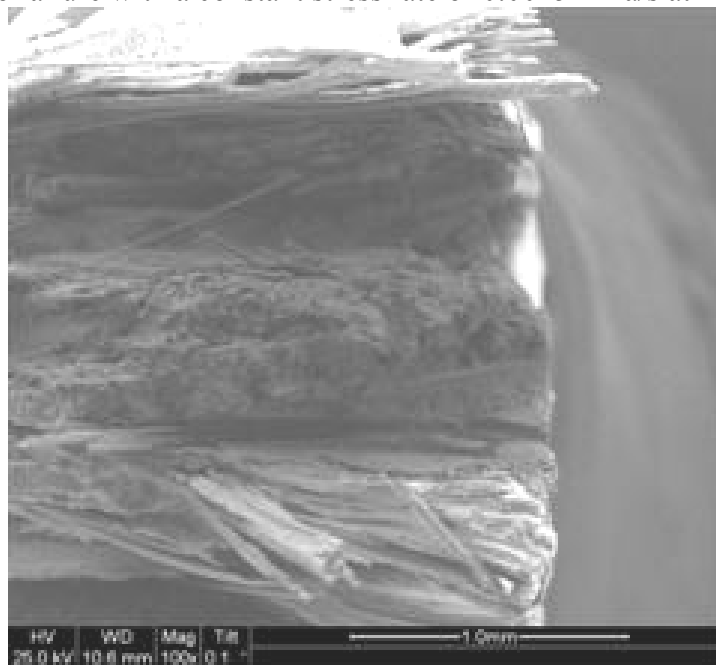


Figure 529. SEM micrograph of the fracture surface of the N720/AM specimen subjected to tensile test to failure with a constant stress rate of 0.0025 MPa/s at 1200°C in steam.



Figure 530. SEM micrograph of the fracture surface of the N720/AM specimen subjected to tensile test to failure with a constant stress rate of 0.0025 MPa/s at 1200°C in steam.

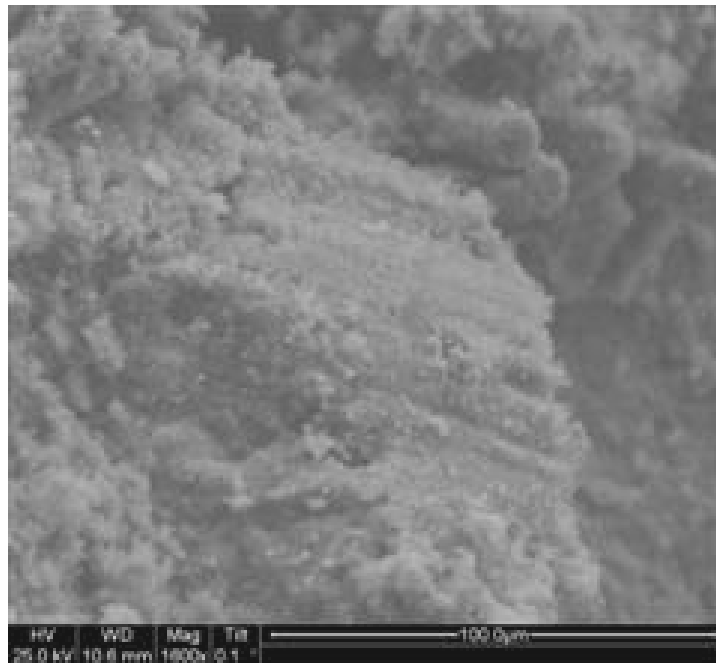


Figure 531. SEM micrograph of the fracture surface of the N720/AM specimen subjected to tensile test to failure with a constant stress rate of 0.0025 MPa/s at 1200°C in steam.

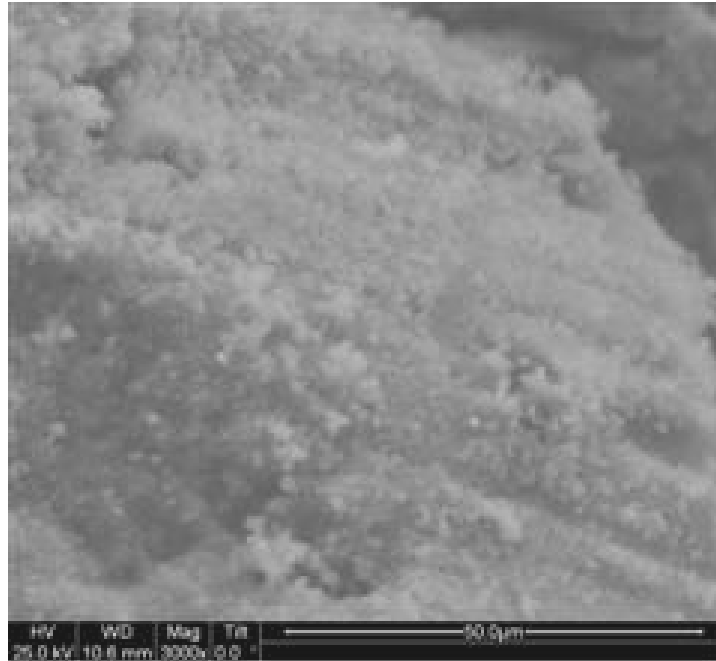


Figure 532. SEM micrograph of the fracture surface of the N720/AM specimen subjected to tensile test to failure with a constant stress rate of 0.0025 MPa/s at 1200°C in steam.

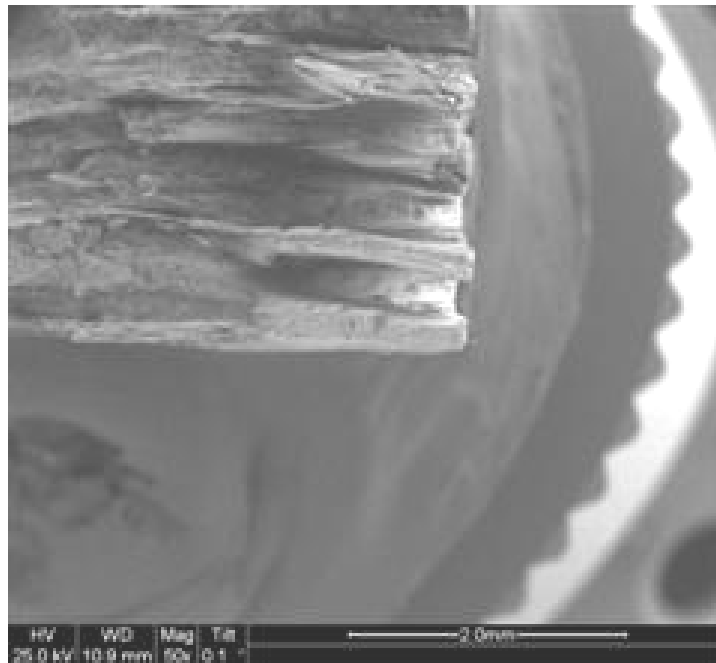


Figure 533. SEM micrograph of the fracture surface of the N720/AM specimen subjected to tensile test to failure with a constant stress rate of 0.0025 MPa/s at 1200°C in steam.

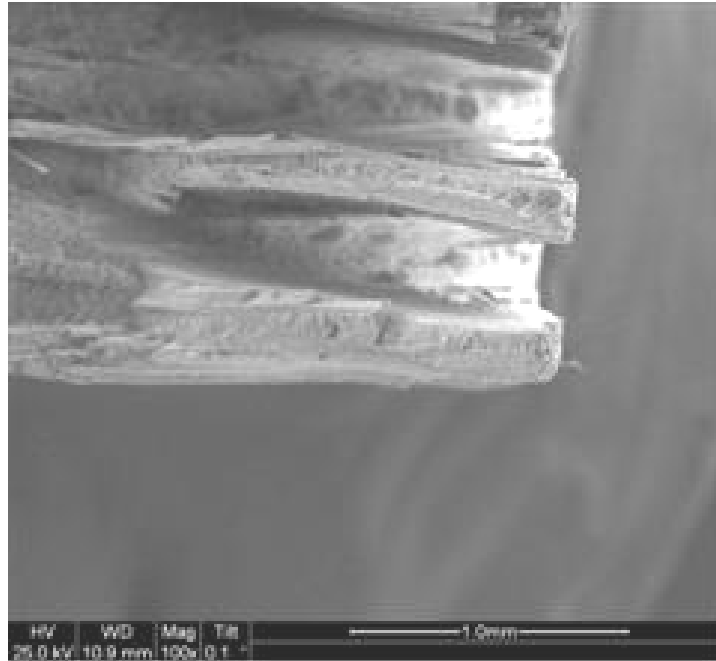


Figure 534. SEM micrograph of the fracture surface of the N720/AM specimen subjected to tensile test to failure with a constant stress rate of 0.0025 MPa/s at 1200°C in steam.

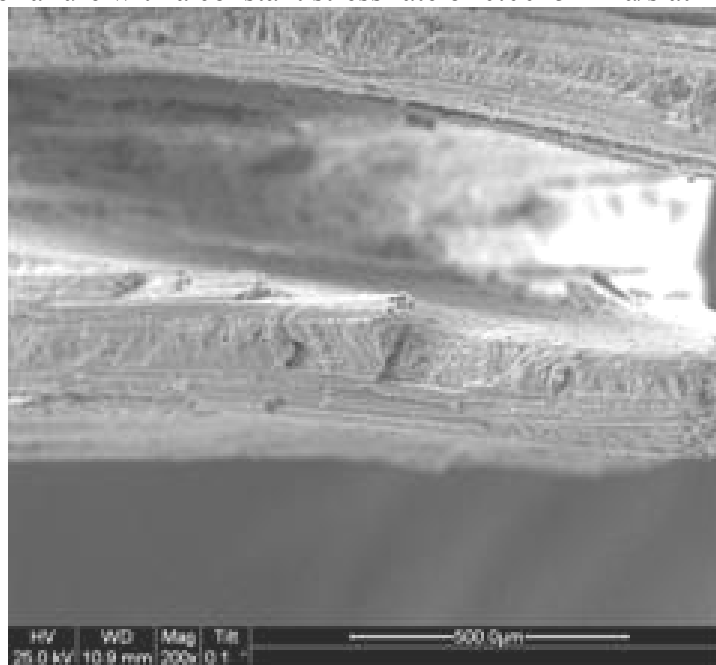


Figure 535. SEM micrograph of the fracture surface of the N720/AM specimen subjected to tensile test to failure with a constant stress rate of 0.0025 MPa/s at 1200°C in steam.

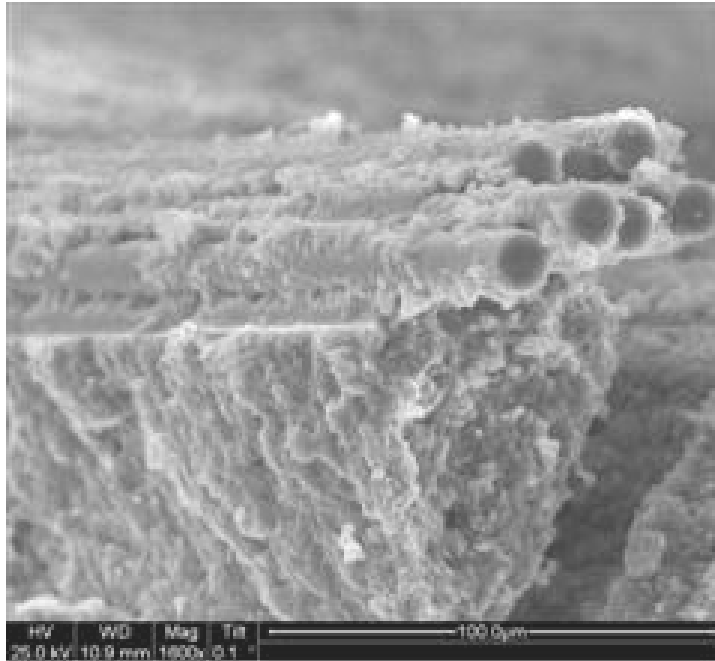


Figure 536. SEM micrograph of the fracture surface of the N720/AM specimen subjected to tensile test to failure with a constant stress rate of 0.0025 MPa/s at 1200°C in steam.

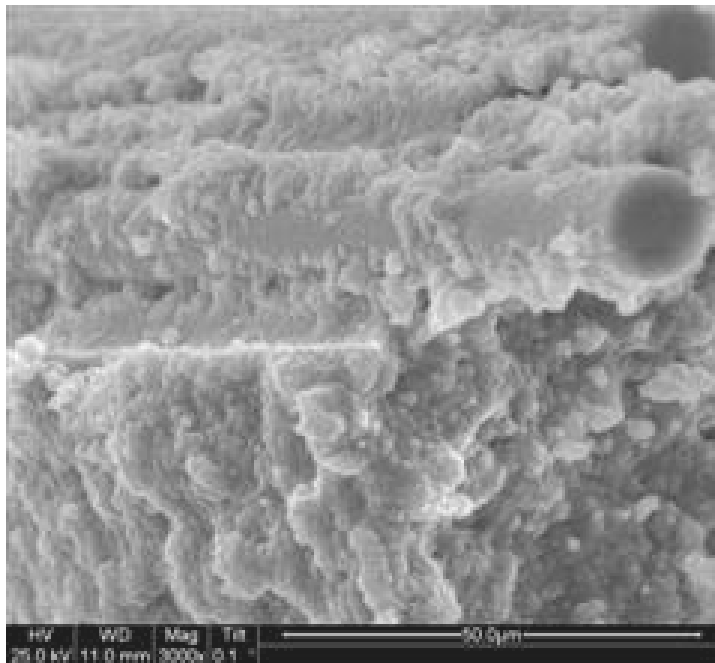


Figure 537. SEM micrograph of the fracture surface of the N720/AM specimen subjected to tensile test to failure with a constant stress rate of 0.0025 MPa/s at 1200°C in steam.

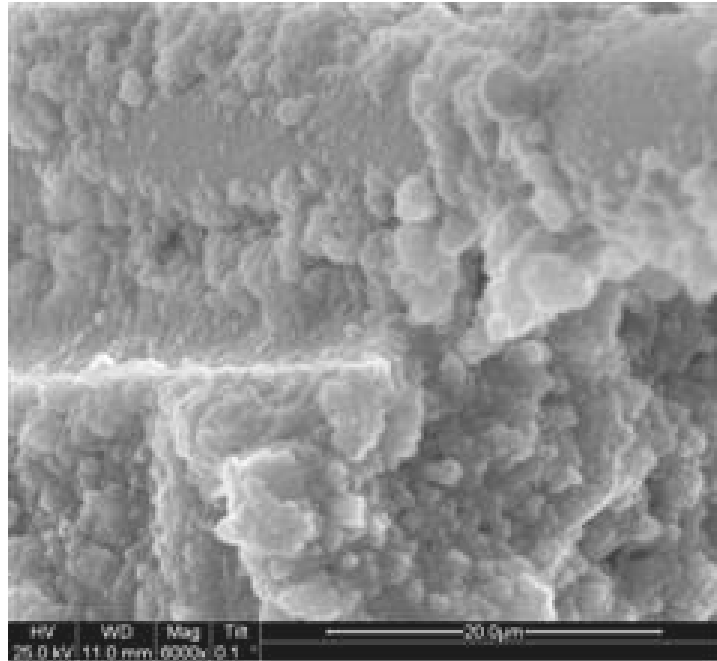


Figure 538. SEM micrograph of the fracture surface of the N720/AM specimen subjected to tensile test to failure with a constant stress rate of 0.0025 MPa/s at 1200°C in steam.

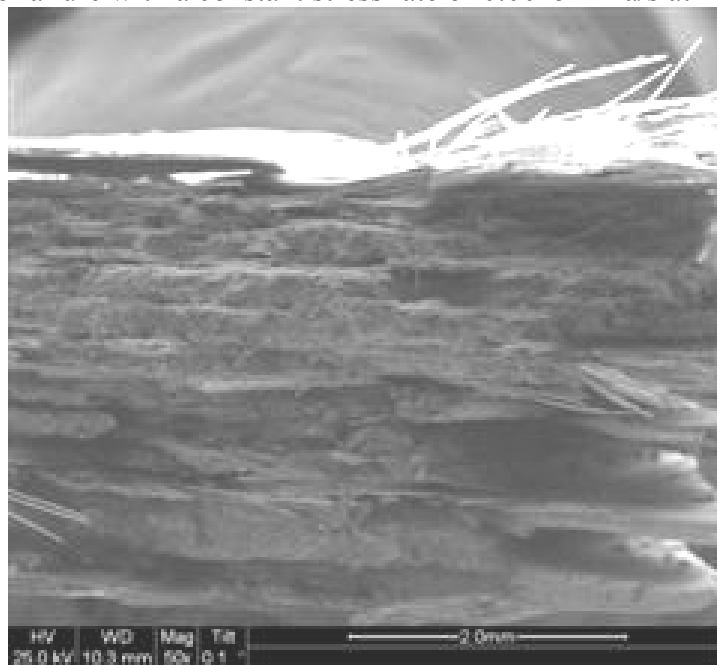


Figure 539. SEM micrograph of the fracture surface of the N720/AM specimen subjected to tensile test to failure with a constant stress rate of 0.0025 MPa/s at 1200°C in steam.

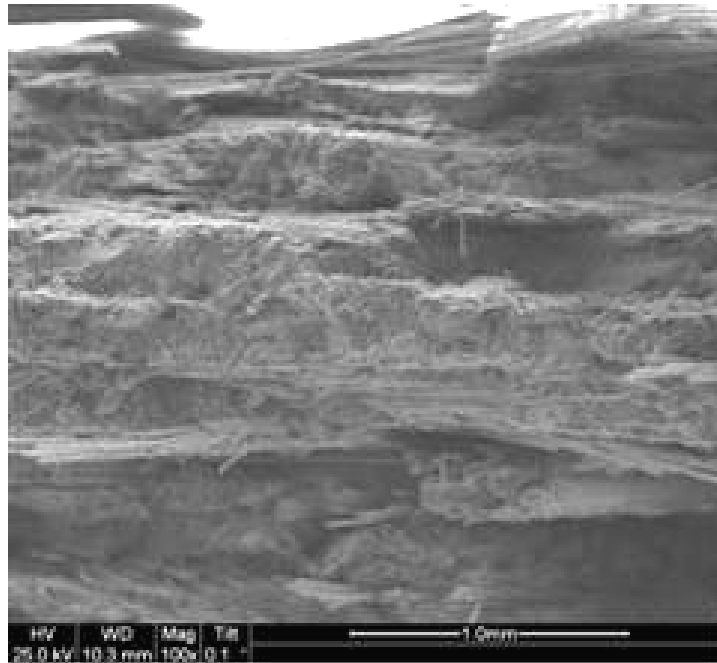


Figure 540. SEM micrograph of the fracture surface of the N720/AM specimen subjected to tensile test to failure with a constant stress rate of 0.0025 MPa/s at 1200°C in steam.

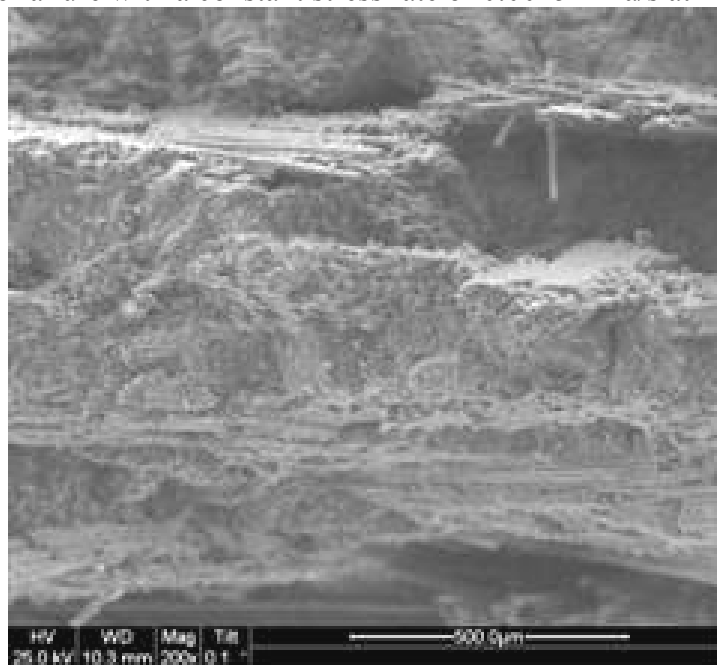


Figure 541. SEM micrograph of the fracture surface of the N720/AM specimen subjected to tensile test to failure with a constant stress rate of 0.0025 MPa/s at 1200°C in steam.

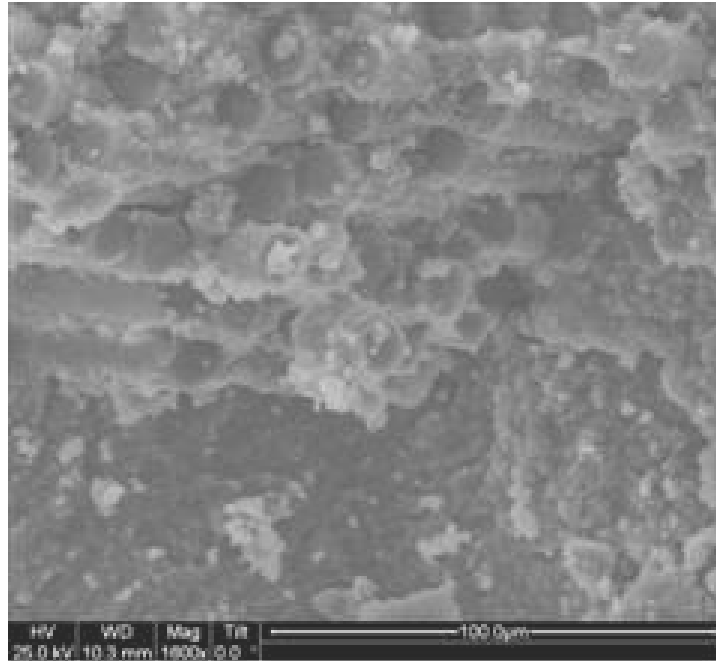


Figure 542. SEM micrograph of the fracture surface of the N720/AM specimen subjected to tensile test to failure with a constant stress rate of 0.0025 MPa/s at 1200°C in steam.

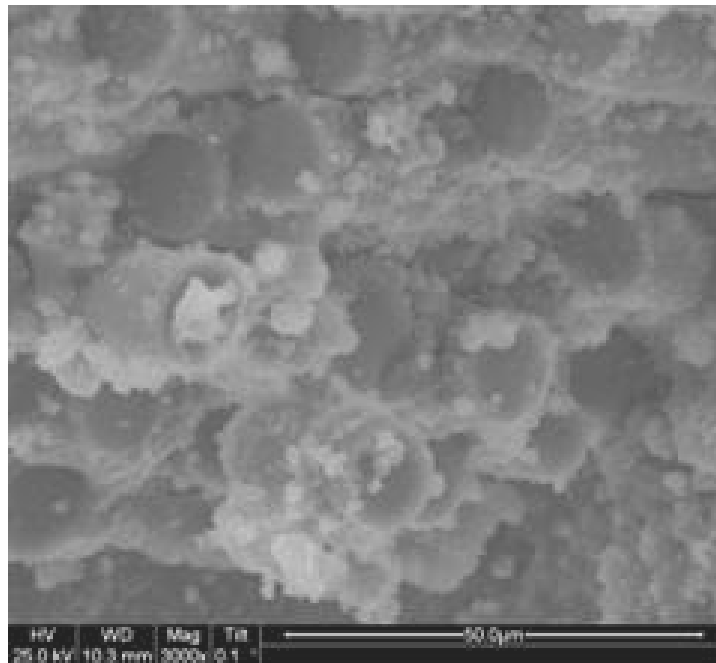


Figure 543. SEM micrograph of the fracture surface of the N720/AM specimen subjected to tensile test to failure with a constant stress rate of 0.0025 MPa/s at 1200°C in steam.

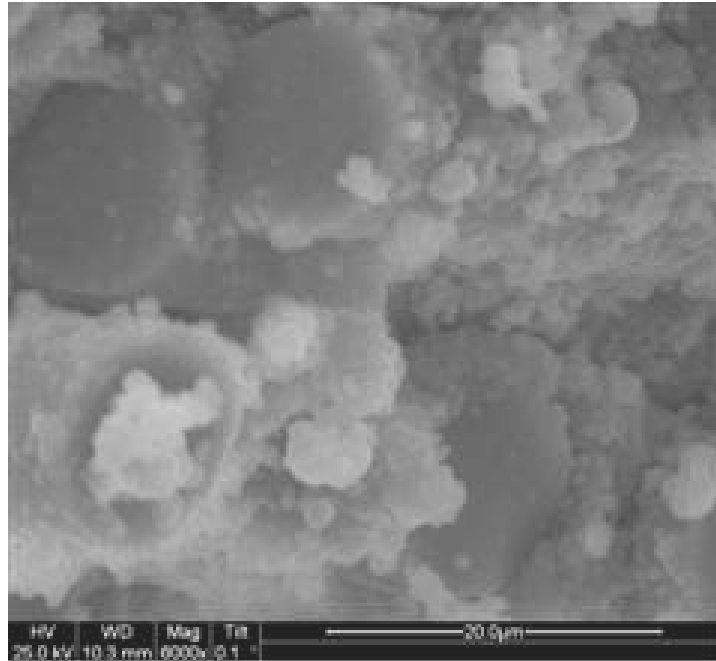


Figure 544. SEM micrograph of the fracture surface of the N720/AM specimen subjected to tensile test to failure with a constant stress rate of 0.0025 MPa/s at 1200°C in steam.

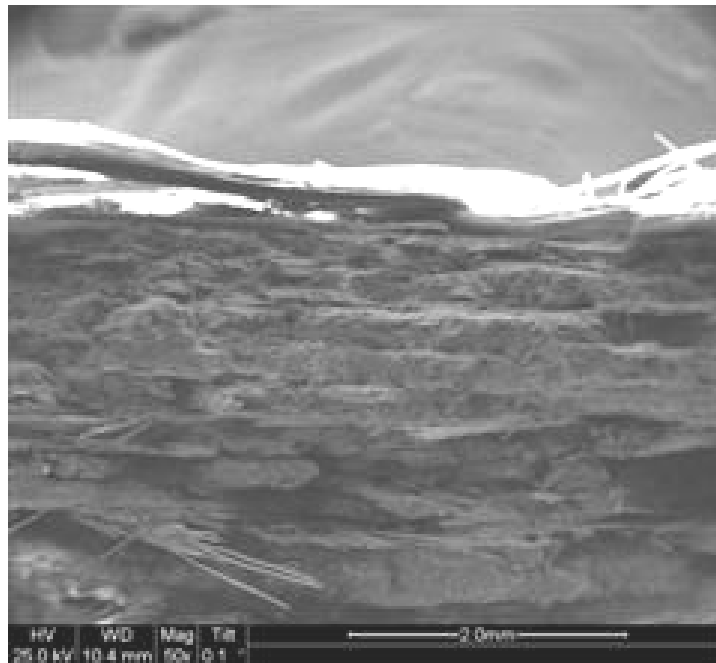


Figure 545. SEM micrograph of the fracture surface of the N720/AM specimen subjected to tensile test to failure with a constant stress rate of 0.0025 MPa/s at 1200°C in steam.

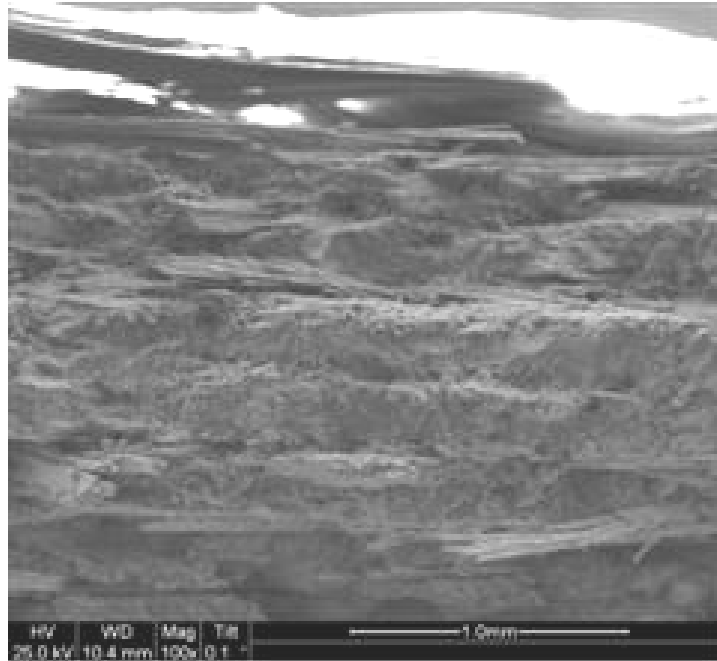


Figure 546. SEM micrograph of the fracture surface of the N720/AM specimen subjected to tensile test to failure with a constant stress rate of 0.0025 MPa/s at 1200°C in steam.

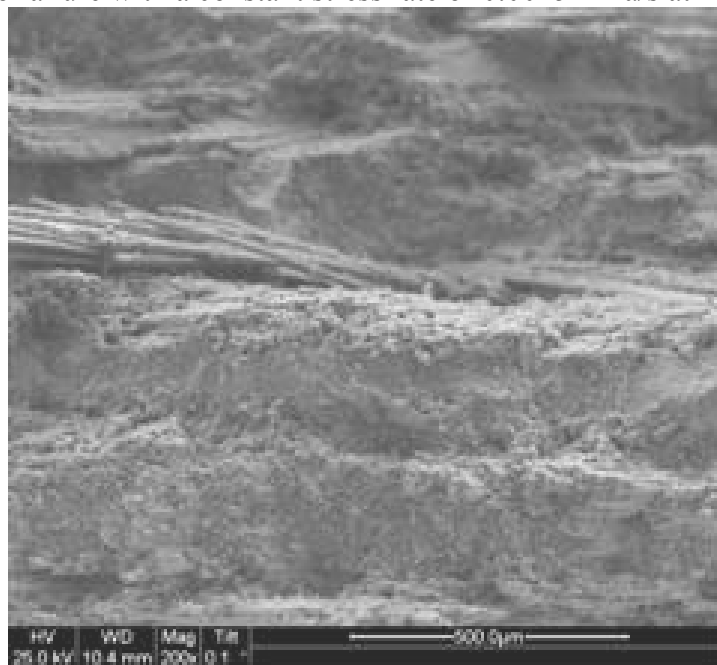


Figure 547. SEM micrograph of the fracture surface of the N720/AM specimen subjected to tensile test to failure with a constant stress rate of 0.0025 MPa/s at 1200°C in steam.

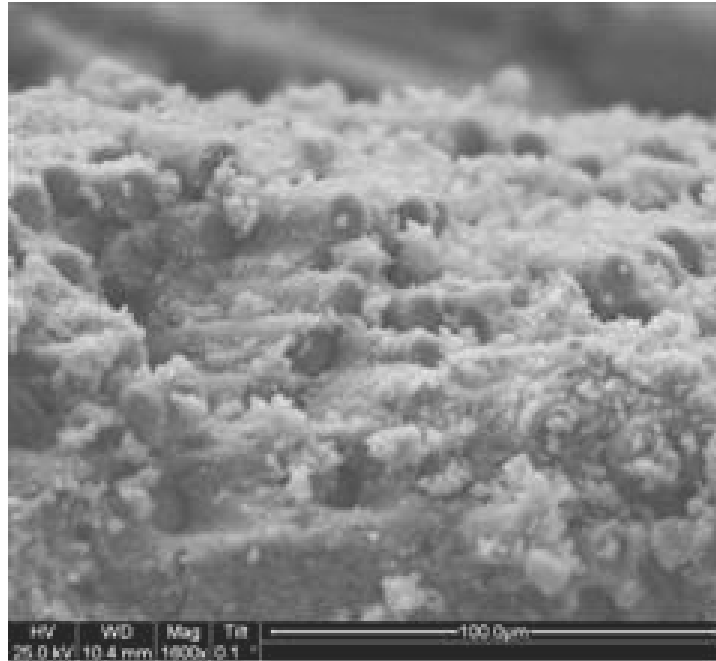


Figure 548. SEM micrograph of the fracture surface of the N720/AM specimen subjected to tensile test to failure with a constant stress rate of 0.0025 MPa/s at 1200°C in steam.

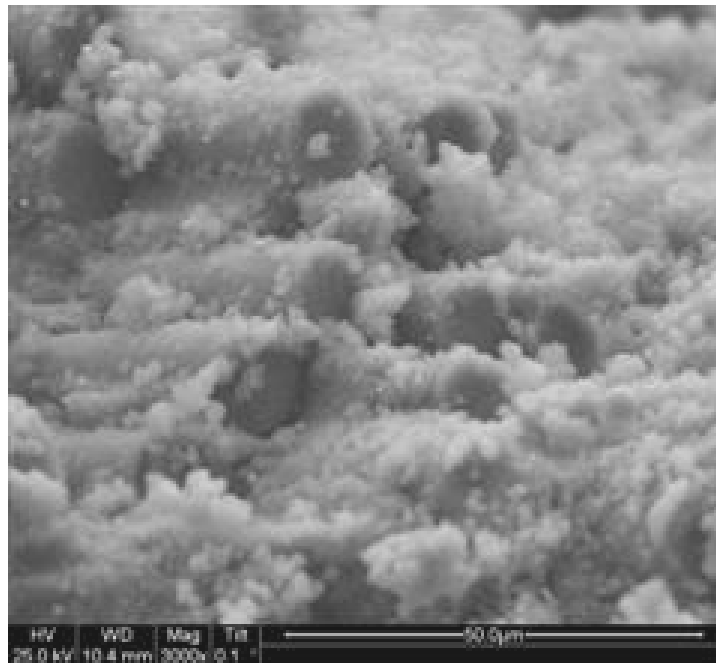


Figure 549. SEM micrograph of the fracture surface of the N720/AM specimen subjected to tensile test to failure with a constant stress rate of 0.0025 MPa/s at 1200°C in steam.

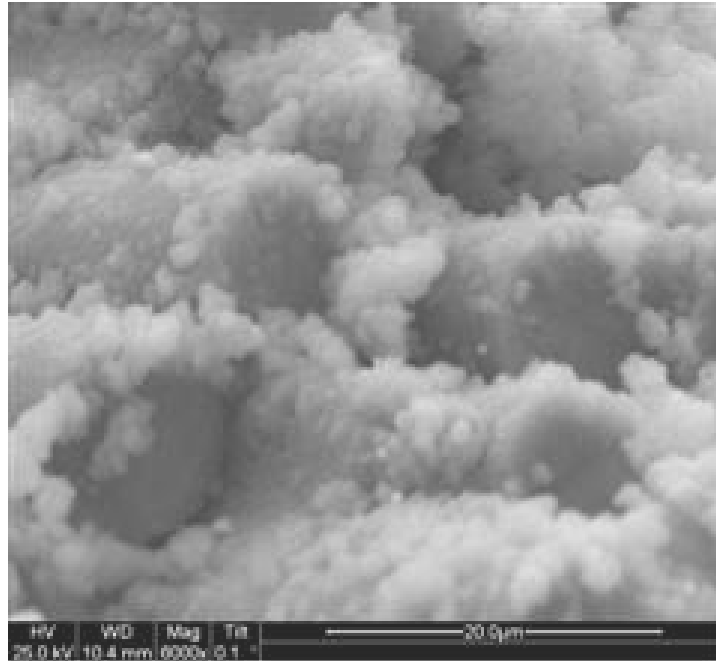


Figure 550. SEM micrograph of the fracture surface of the N720/AM specimen subjected to tensile test to failure with a constant stress rate of 0.0025 MPa/s at 1200°C in steam.

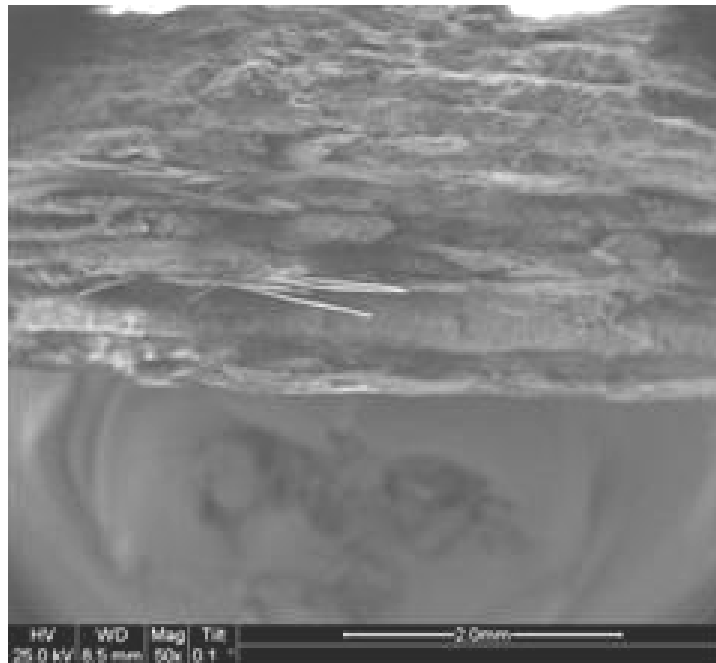


Figure 551. SEM micrograph of the fracture surface of the N720/AM specimen subjected to tensile test to failure with a constant stress rate of 0.0025 MPa/s at 1200°C in steam.

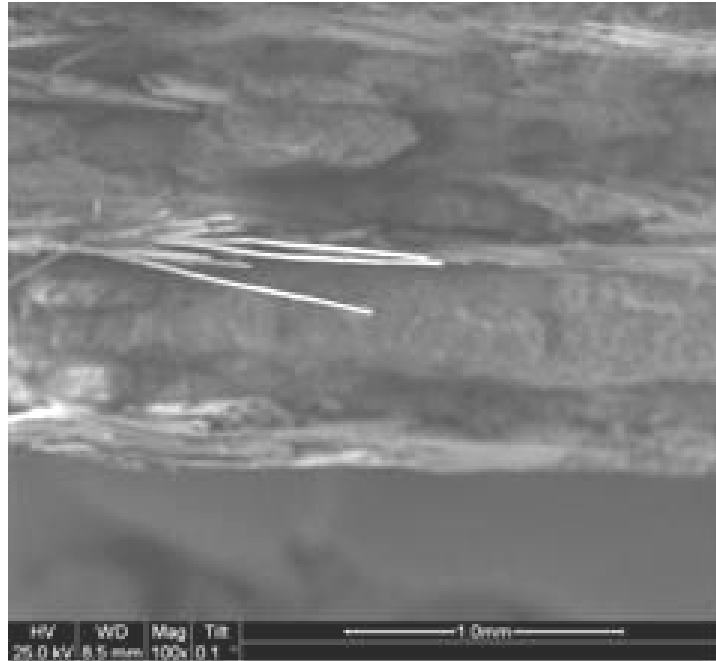


Figure 552. SEM micrograph of the fracture surface of the N720/AM specimen subjected to tensile test to failure with a constant stress rate of 0.0025 MPa/s at 1200°C in steam.



Figure 553. SEM micrograph of the fracture surface of the N720/AM specimen subjected to tensile test to failure with a constant stress rate of 0.0025 MPa/s at 1200°C in steam.

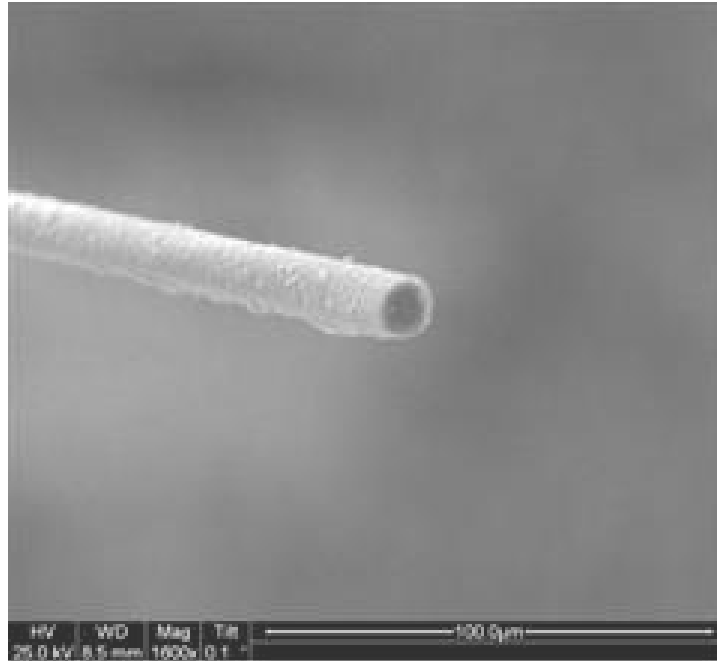


Figure 554. SEM micrograph of the fracture surface of the N720/AM specimen subjected to tensile test to failure with a constant stress rate of 0.0025 MPa/s at 1200°C in steam.

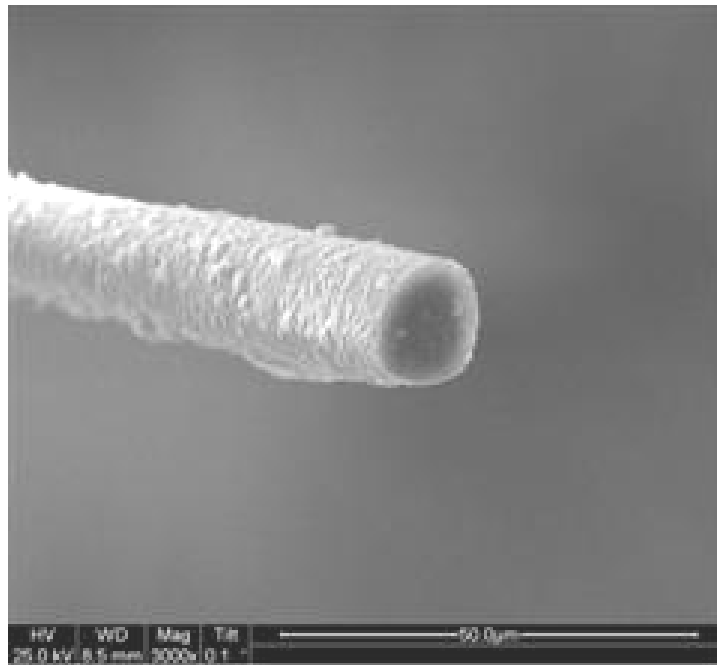


Figure 555. SEM micrograph of the fracture surface of the N720/AM specimen subjected to tensile test to failure with a constant stress rate of 0.0025 MPa/s at 1200°C in steam.

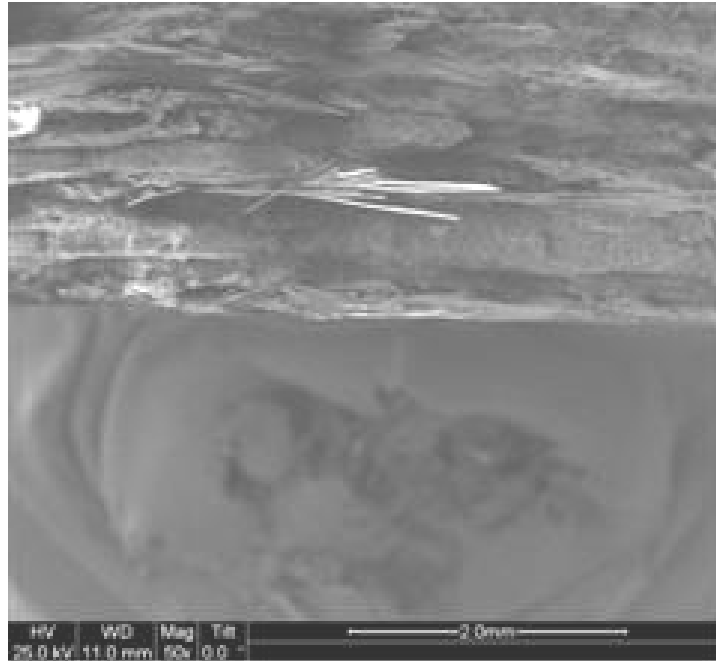


Figure 556. SEM micrograph of the fracture surface of the N720/AM specimen subjected to tensile test to failure with a constant stress rate of 0.0025 MPa/s at 1200°C in steam.

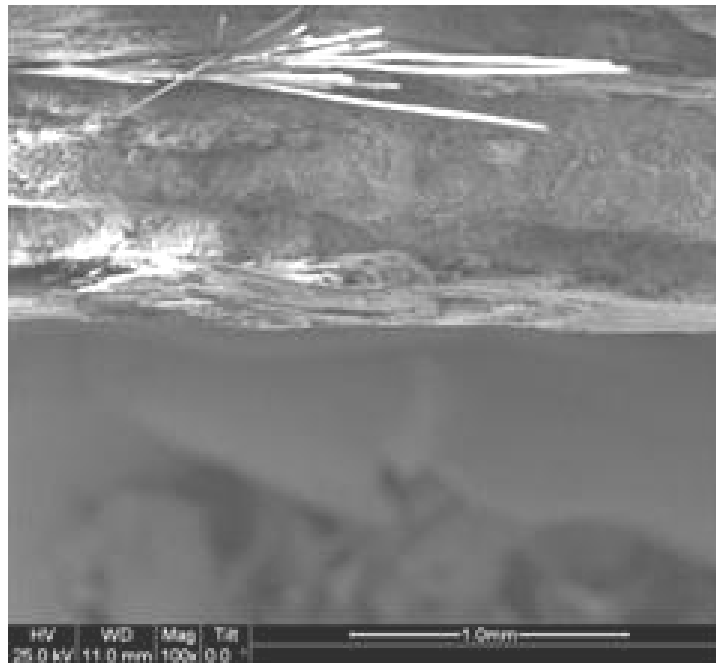


Figure 557. SEM micrograph of the fracture surface of the N720/AM specimen subjected to tensile test to failure with a constant stress rate of 0.0025 MPa/s at 1200°C in steam.

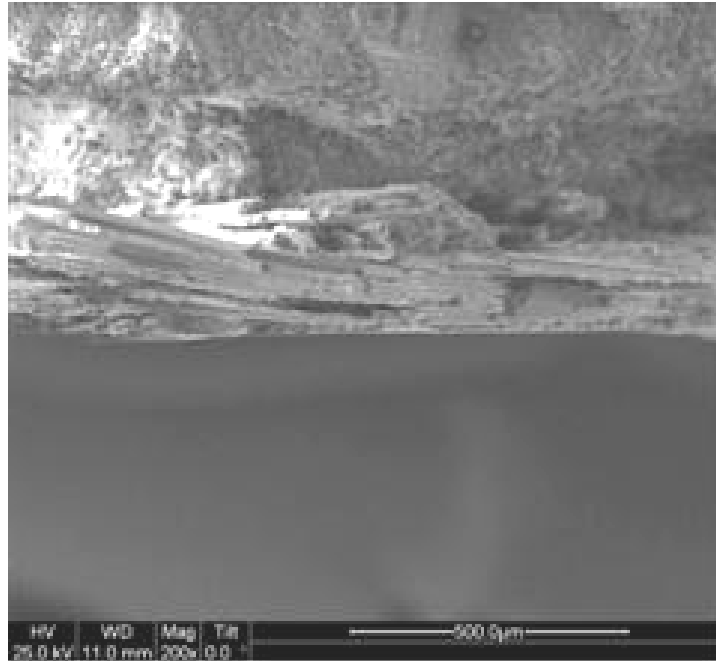


Figure 558. SEM micrograph of the fracture surface of the N720/AM specimen subjected to tensile test to failure with a constant stress rate of 0.0025 MPa/s at 1200°C in steam.

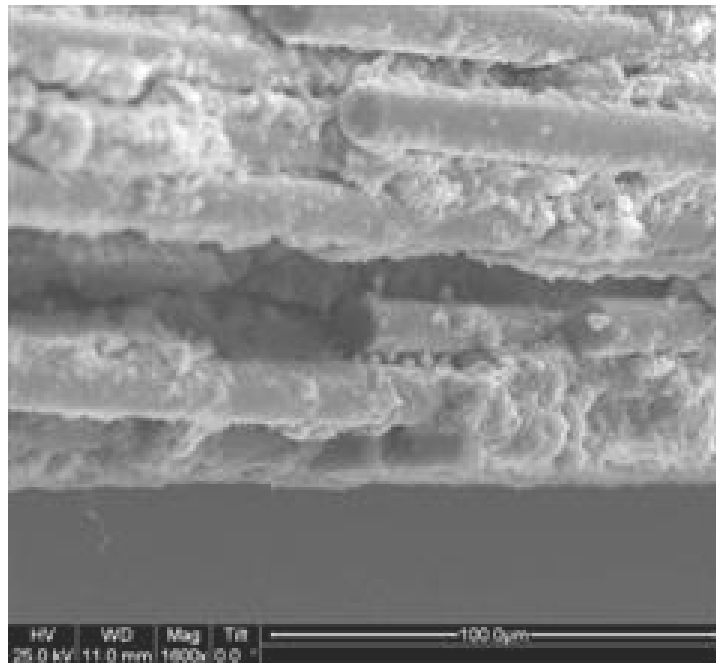


Figure 559. SEM micrograph of the fracture surface of the N720/AM specimen subjected to tensile test to failure with a constant stress rate of 0.0025 MPa/s at 1200°C in steam.

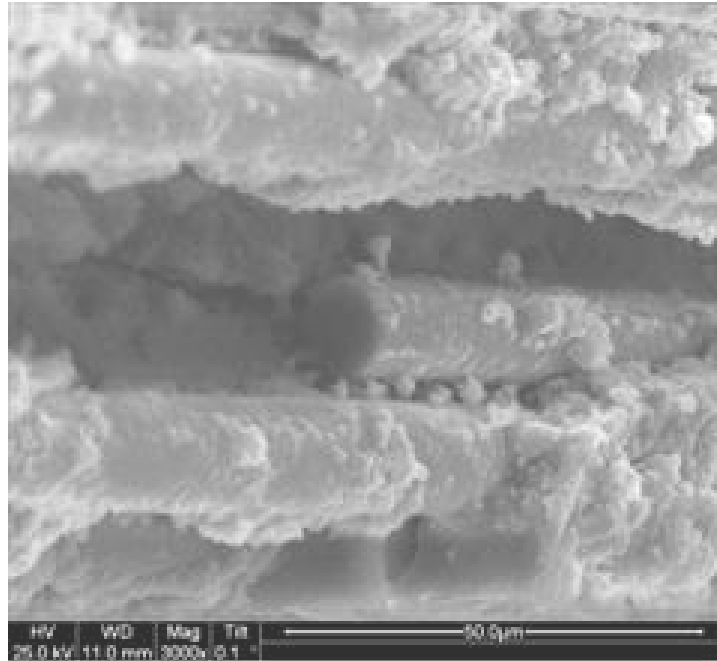


Figure 560. SEM micrograph of the fracture surface of the N720/AM specimen subjected to tensile test to failure with a constant stress rate of 0.0025 MPa/s at 1200°C in steam.

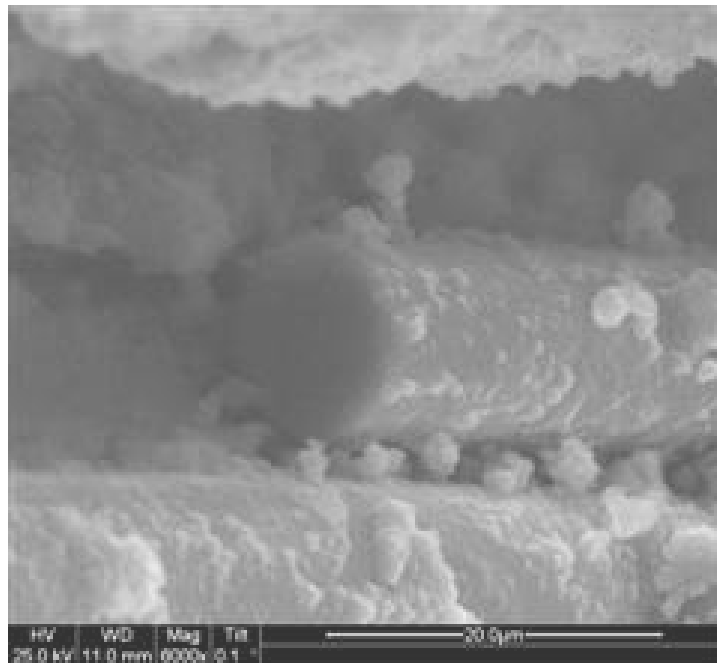


Figure 561. SEM micrograph of the fracture surface of the N720/AM specimen subjected to tensile test to failure with a constant stress rate of 0.0025 MPa/s at 1200°C in steam.

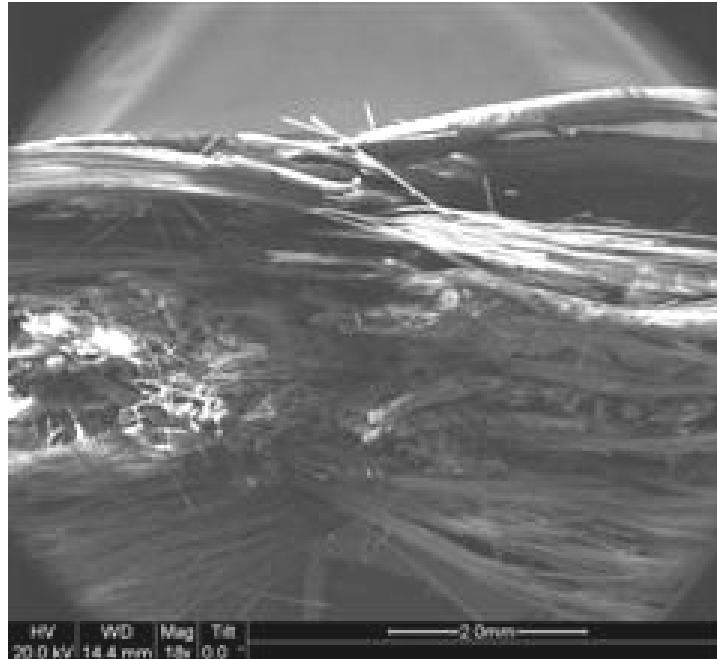


Figure 562. SEM micrograph of the fracture surface of the N720/AM specimen subjected to tensile test to failure with a constant stress rate of 25 MPa/s at 1200°C in laboratory air.

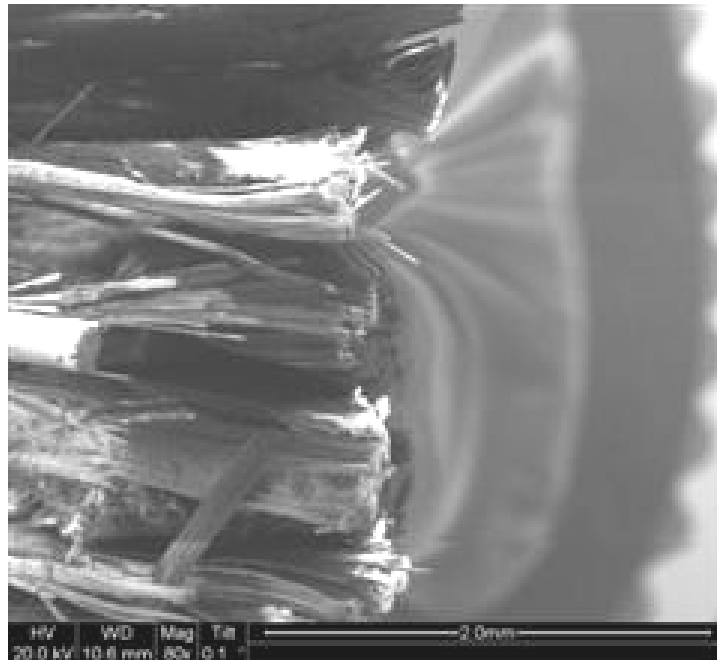


Figure 563. SEM micrograph of the fracture surface of the N720/AM specimen subjected to tensile test to failure with a constant stress rate of 25 MPa/s at 1200°C in laboratory air.

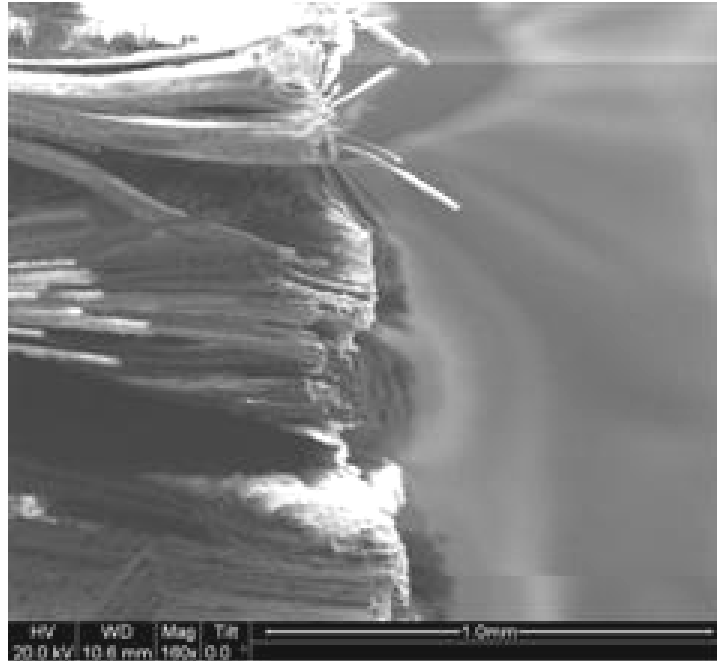


Figure 564. SEM micrograph of the fracture surface of the N720/AM specimen subjected to tensile test to failure with a constant stress rate of 25 MPa/s at 1200°C in laboratory air.

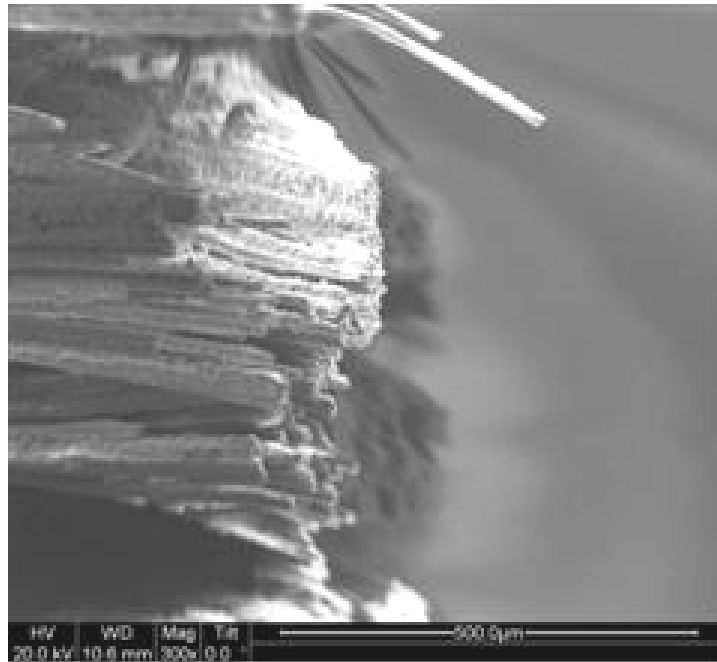


Figure 565. SEM micrograph of the fracture surface of the N720/AM specimen subjected to tensile test to failure with a constant stress rate of 25 MPa/s at 1200°C in laboratory air.

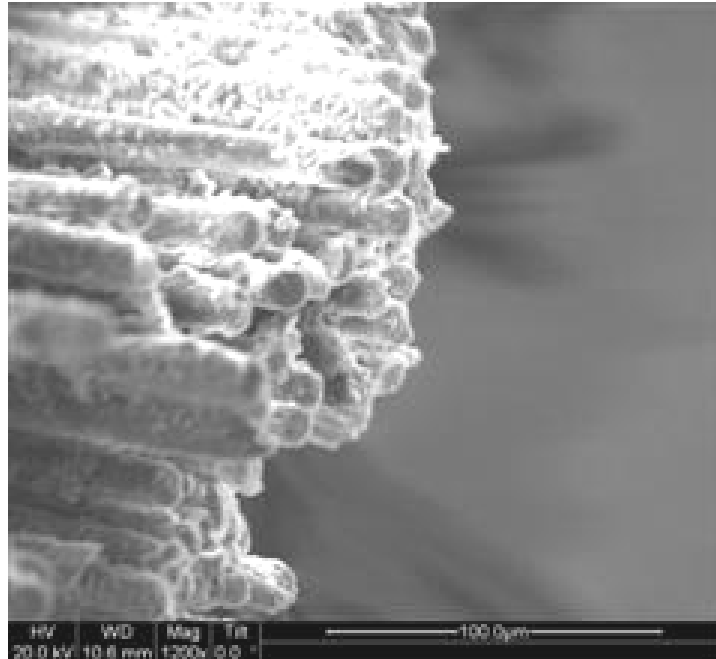


Figure 566. SEM micrograph of the fracture surface of the N720/AM specimen subjected to tensile test to failure with a constant stress rate of 25 MPa/s at 1200°C in laboratory air.

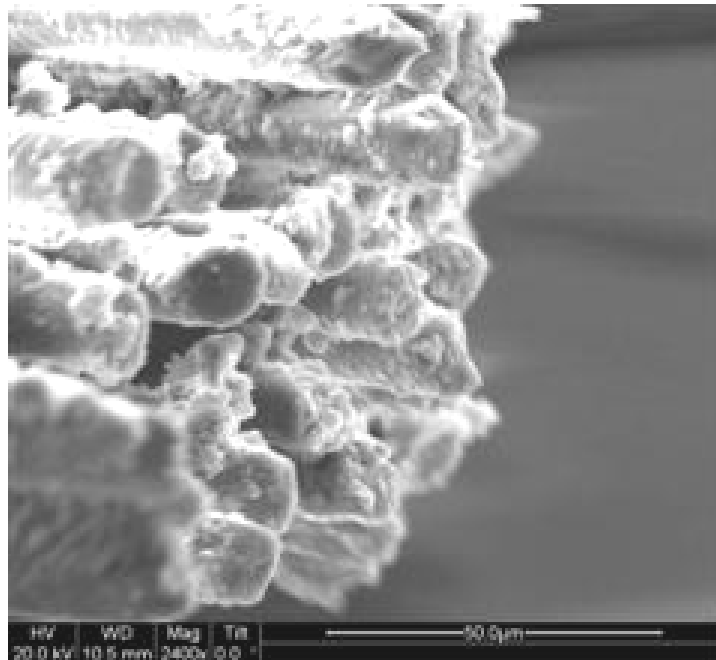


Figure 567. SEM micrograph of the fracture surface of the N720/AM specimen subjected to tensile test to failure with a constant stress rate of 25 MPa/s at 1200°C in laboratory air.

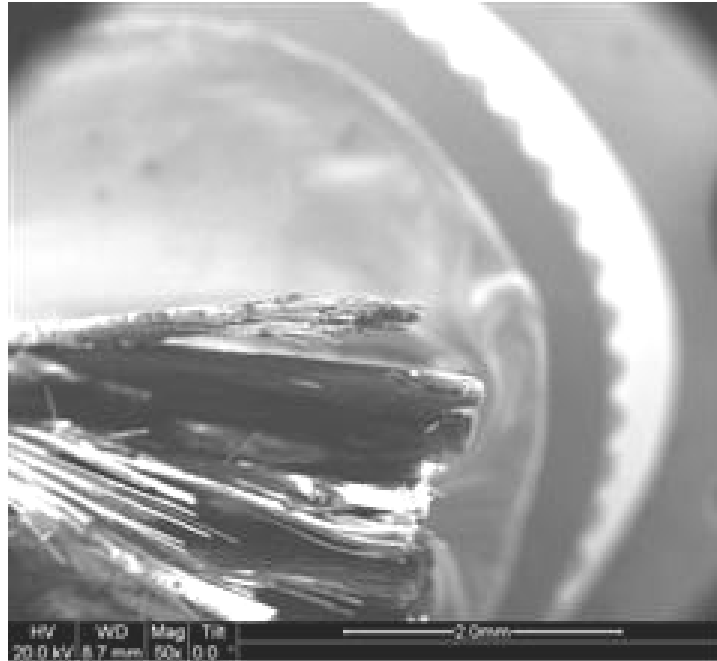


Figure 568. SEM micrograph of the fracture surface of the N720/AM specimen subjected to tensile test to failure with a constant stress rate of 25 MPa/s at 1200°C in laboratory air.

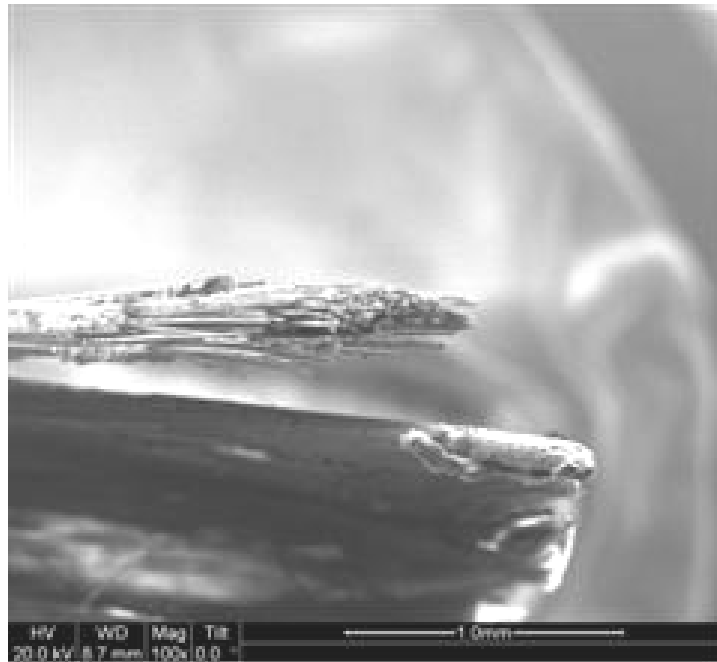


Figure 569. SEM micrograph of the fracture surface of the N720/AM specimen subjected to tensile test to failure with a constant stress rate of 25 MPa/s at 1200°C in laboratory air.

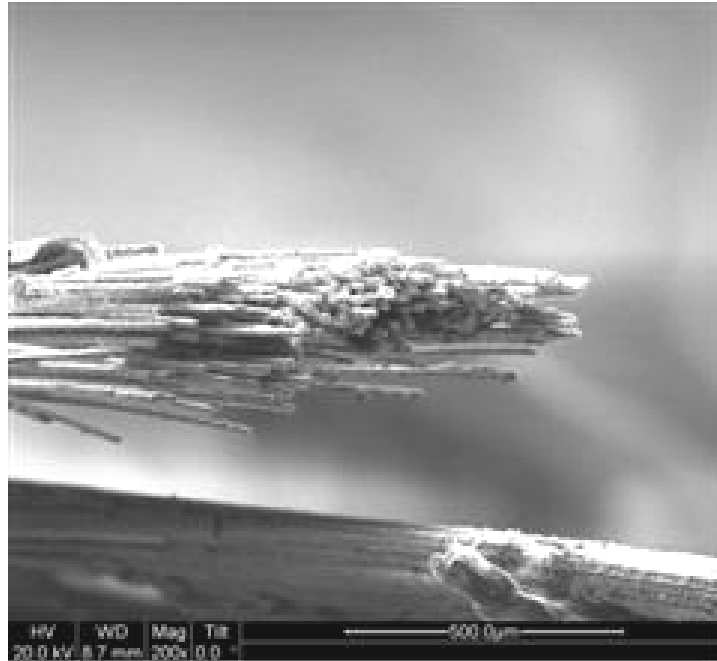


Figure 570. SEM micrograph of the fracture surface of the N720/AM specimen subjected to tensile test to failure with a constant stress rate of 25 MPa/s at 1200°C in laboratory air.

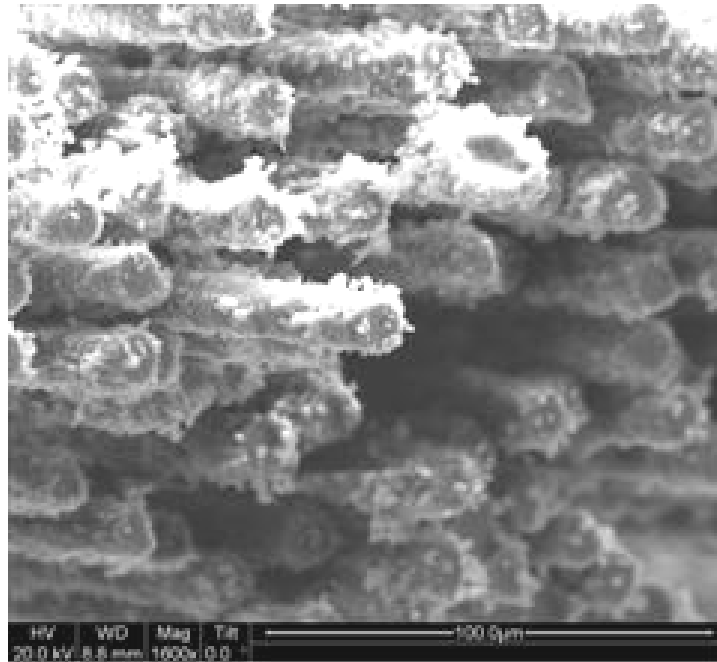


Figure 571. SEM micrograph of the fracture surface of the N720/AM specimen subjected to tensile test to failure with a constant stress rate of 25 MPa/s at 1200°C in laboratory air.

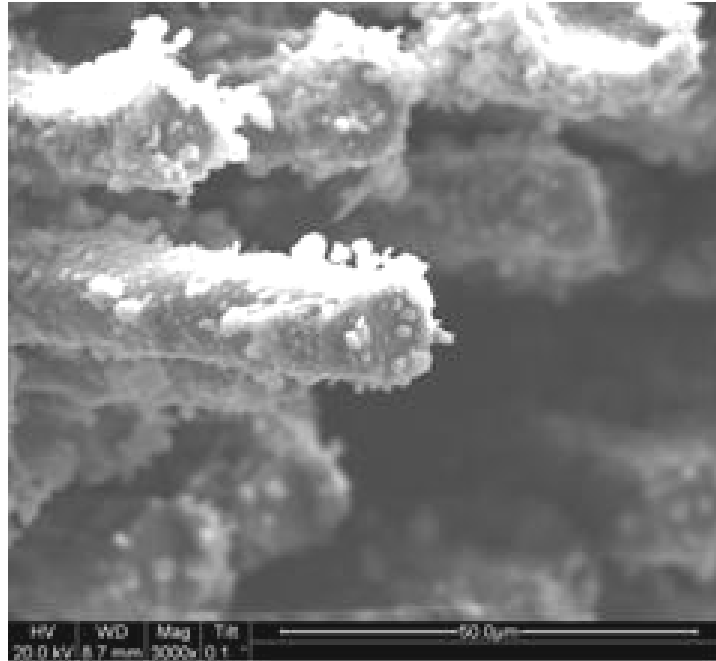


Figure 572. SEM micrograph of the fracture surface of the N720/AM specimen subjected to tensile test to failure with a constant stress rate of 25 MPa/s at 1200°C in laboratory air.



Figure 573. SEM micrograph of the fracture surface of the N720/AM specimen subjected to tensile test to failure with a constant stress rate of 25 MPa/s at 1200°C in laboratory air.

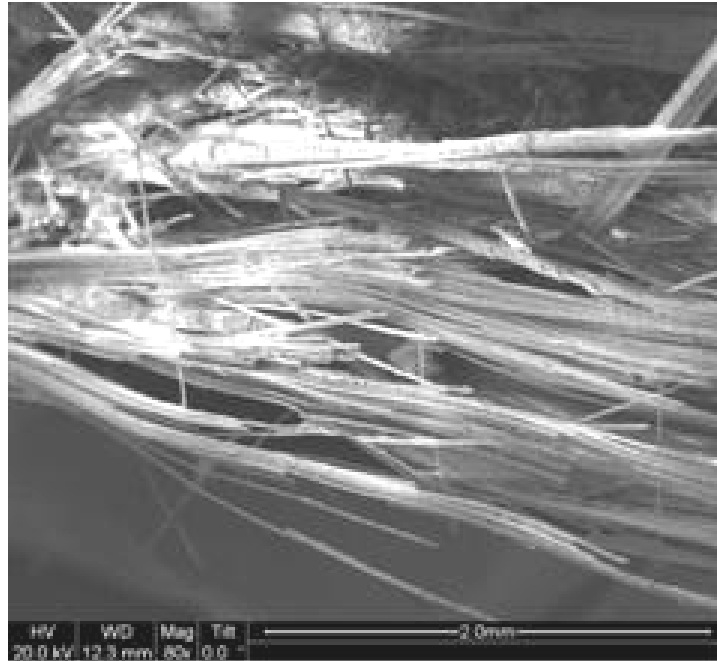


Figure 574. SEM micrograph of the fracture surface of the N720/AM specimen subjected to tensile test to failure with a constant stress rate of 25 MPa/s at 1200°C in laboratory air.

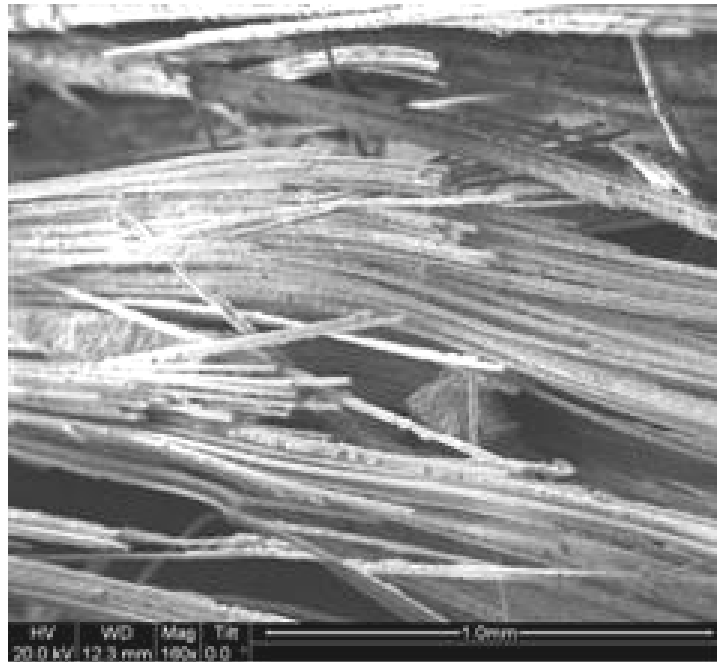


Figure 575. SEM micrograph of the fracture surface of the N720/AM specimen subjected to tensile test to failure with a constant stress rate of 25 MPa/s at 1200°C in laboratory air.



Figure 576. SEM micrograph of the fracture surface of the N720/AM specimen subjected to tensile test to failure with a constant stress rate of 25 MPa/s at 1200°C in laboratory air.

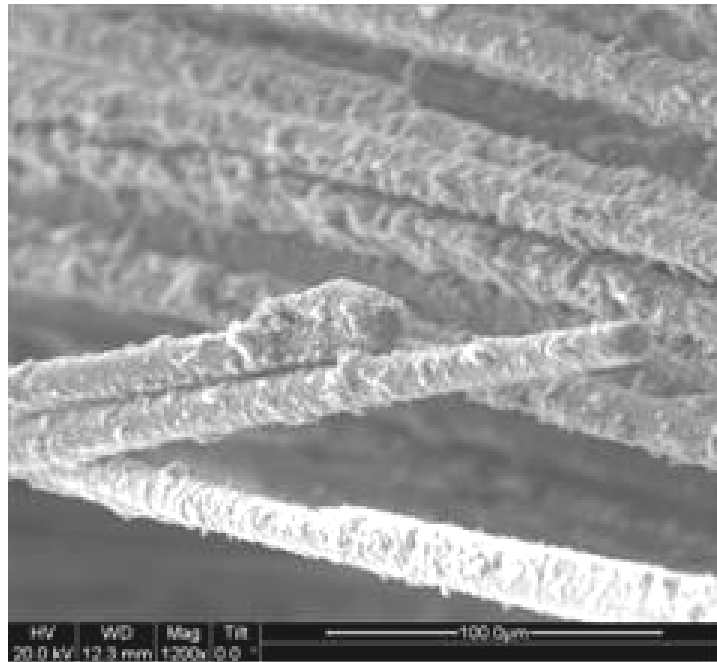


Figure 577. SEM micrograph of the fracture surface of the N720/AM specimen subjected to tensile test to failure with a constant stress rate of 25 MPa/s at 1200°C in laboratory air.

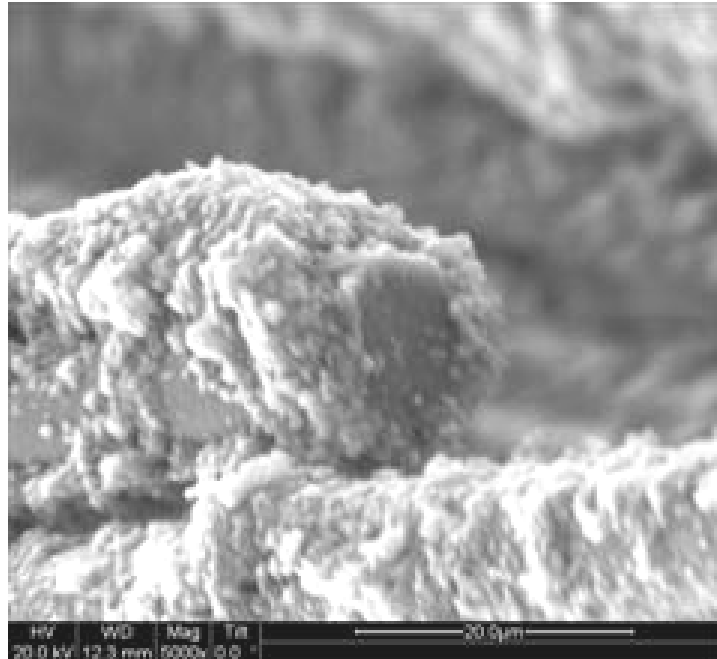


Figure 578. SEM micrograph of the fracture surface of the N720/AM specimen subjected to tensile test to failure with a constant stress rate of 25 MPa/s at 1200°C in laboratory air.

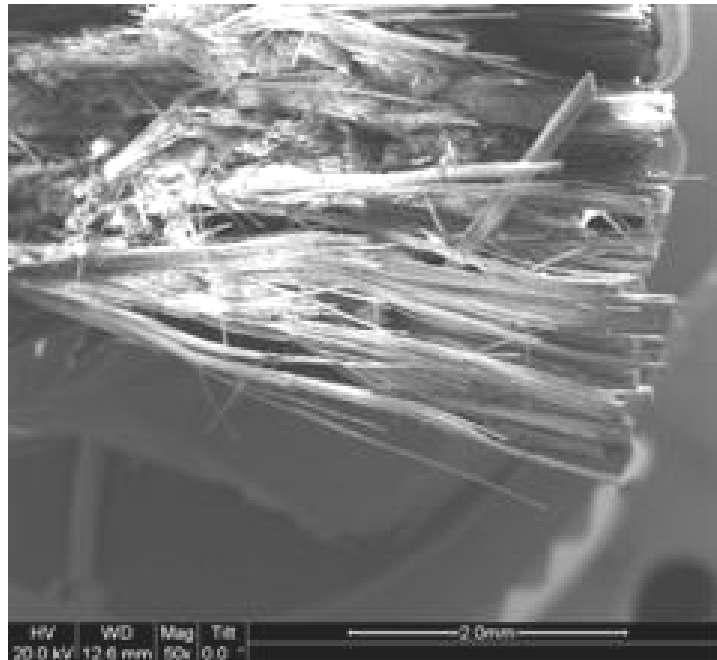


Figure 579. SEM micrograph of the fracture surface of the N720/AM specimen subjected to tensile test to failure with a constant stress rate of 25 MPa/s at 1200°C in laboratory air.

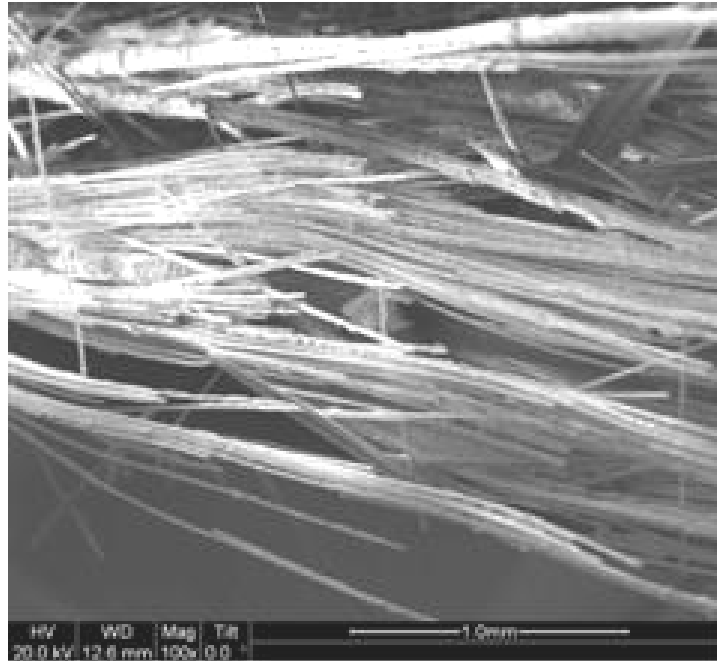


Figure 580. SEM micrograph of the fracture surface of the N720/AM specimen subjected to tensile test to failure with a constant stress rate of 25 MPa/s at 1200°C in laboratory air.



Figure 581. SEM micrograph of the fracture surface of the N720/AM specimen subjected to tensile test to failure with a constant stress rate of 25 MPa/s at 1200°C in laboratory air.

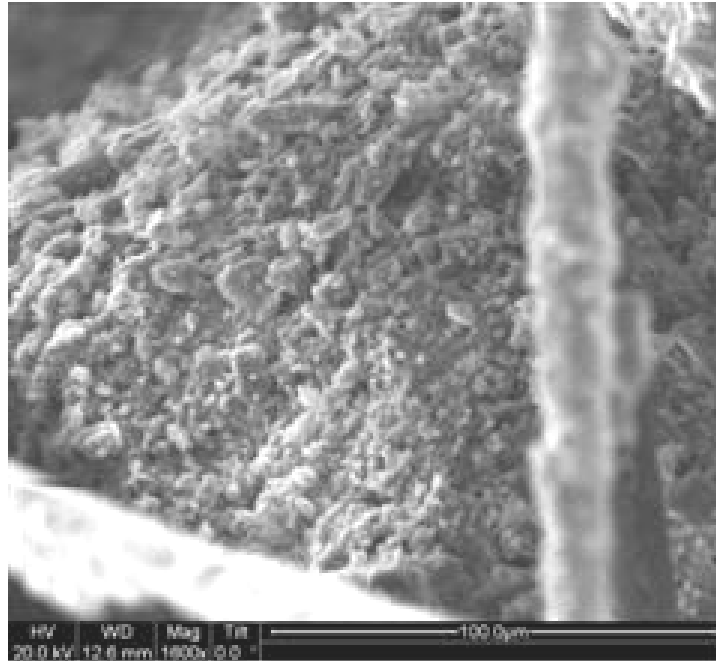


Figure 582. SEM micrograph of the fracture surface of the N720/AM specimen subjected to tensile test to failure with a constant stress rate of 25 MPa/s at 1200°C in laboratory air.

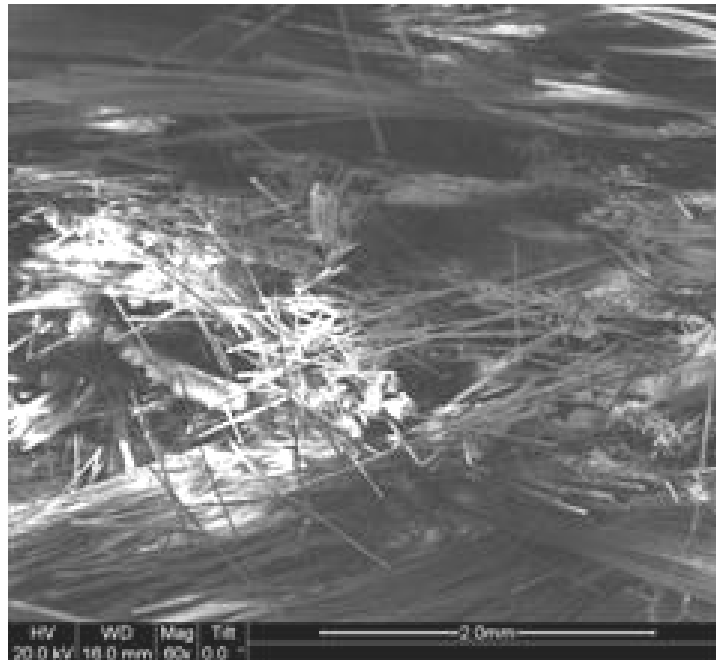


Figure 583. SEM micrograph of the fracture surface of the N720/AM specimen subjected to tensile test to failure with a constant stress rate of 25 MPa/s at 1200°C in laboratory air.

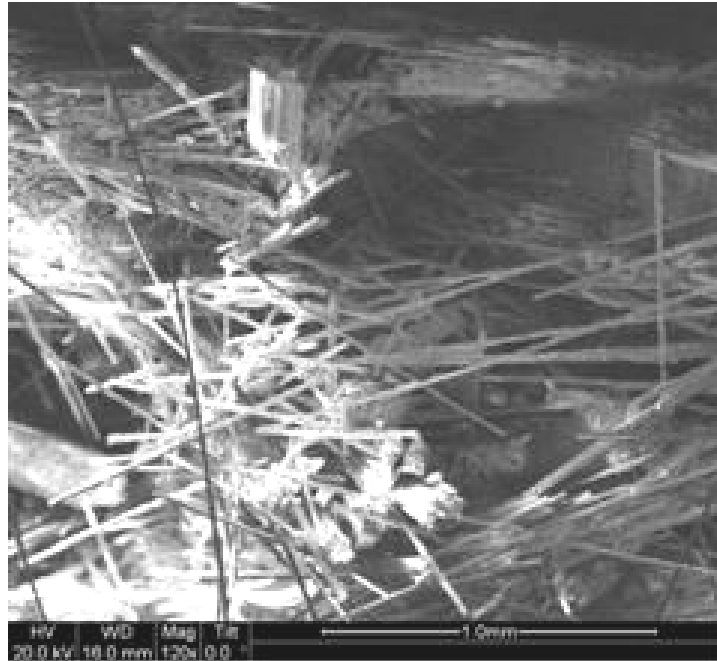


Figure 584. SEM micrograph of the fracture surface of the N720/AM specimen subjected to tensile test to failure with a constant stress rate of 25 MPa/s at 1200°C in laboratory air.

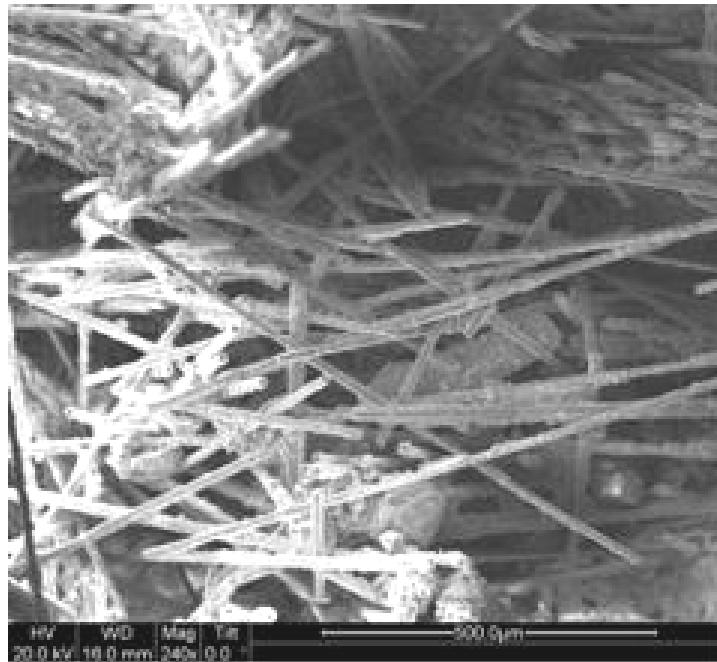


Figure 585. SEM micrograph of the fracture surface of the N720/AM specimen subjected to tensile test to failure with a constant stress rate of 25 MPa/s at 1200°C in laboratory air.

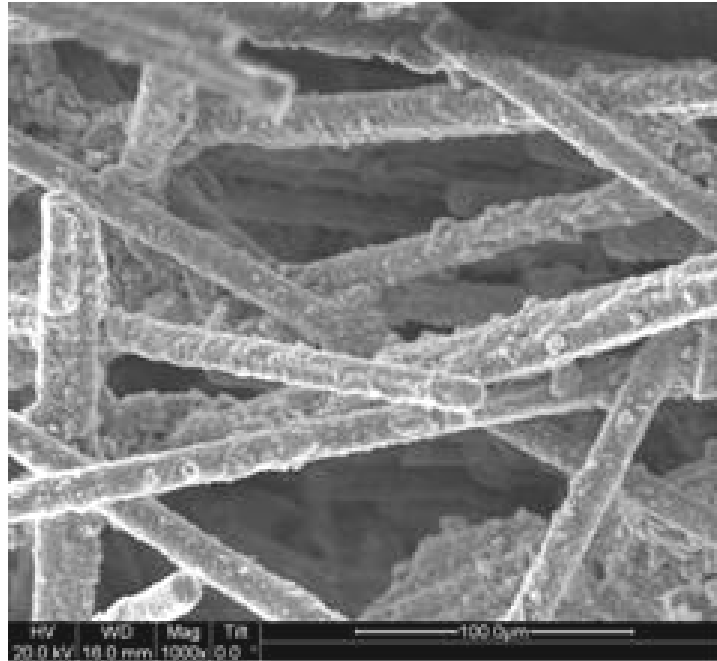


Figure 586. SEM micrograph of the fracture surface of the N720/AM specimen subjected to tensile test to failure with a constant stress rate of 25 MPa/s at 1200°C in laboratory air.

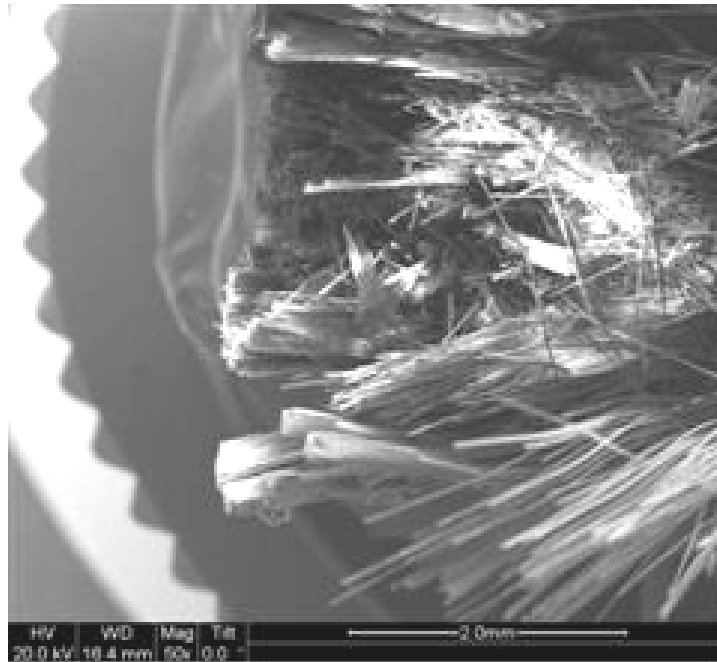


Figure 587. SEM micrograph of the fracture surface of the N720/AM specimen subjected to tensile test to failure with a constant stress rate of 25 MPa/s at 1200°C in laboratory air.

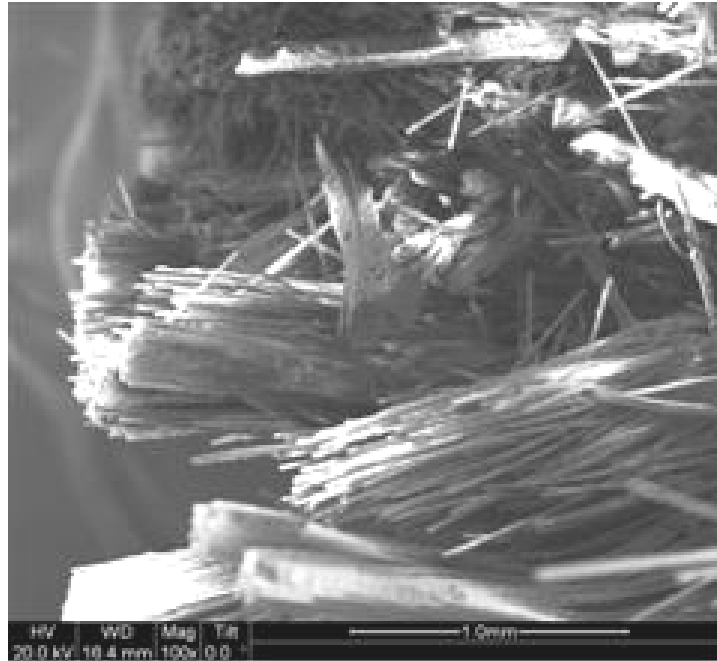


Figure 588. SEM micrograph of the fracture surface of the N720/AM specimen subjected to tensile test to failure with a constant stress rate of 25 MPa/s at 1200°C in laboratory air.

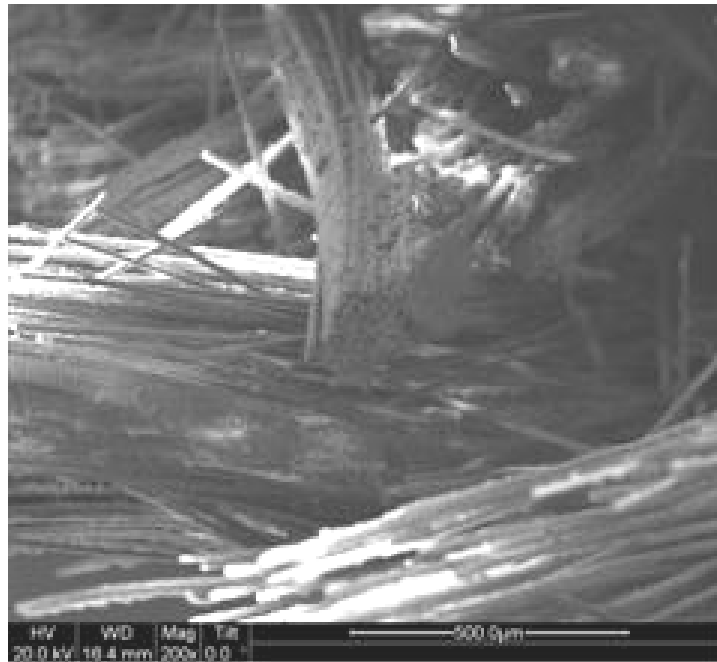


Figure 589. SEM micrograph of the fracture surface of the N720/AM specimen subjected to tensile test to failure with a constant stress rate of 25 MPa/s at 1200°C in laboratory air.

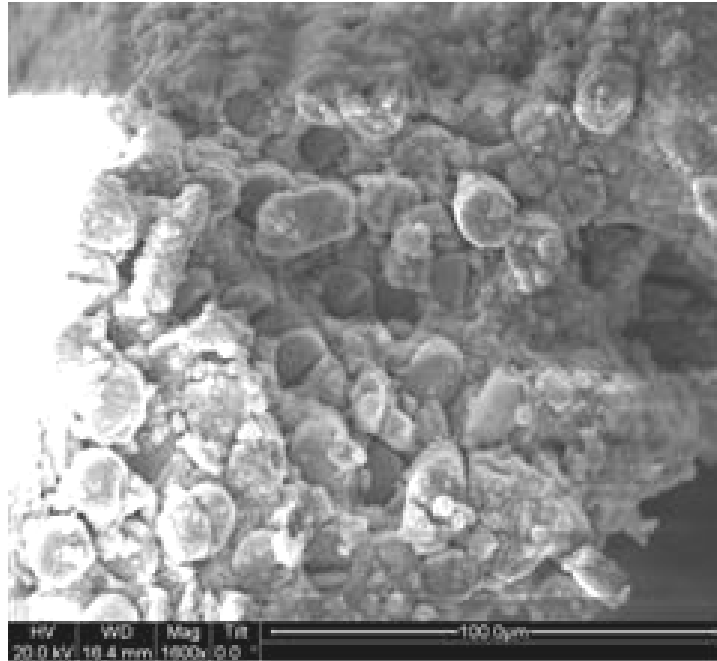


Figure 590. SEM micrograph of the fracture surface of the N720/AM specimen subjected to tensile test to failure with a constant stress rate of 25 MPa/s at 1200°C in laboratory air.

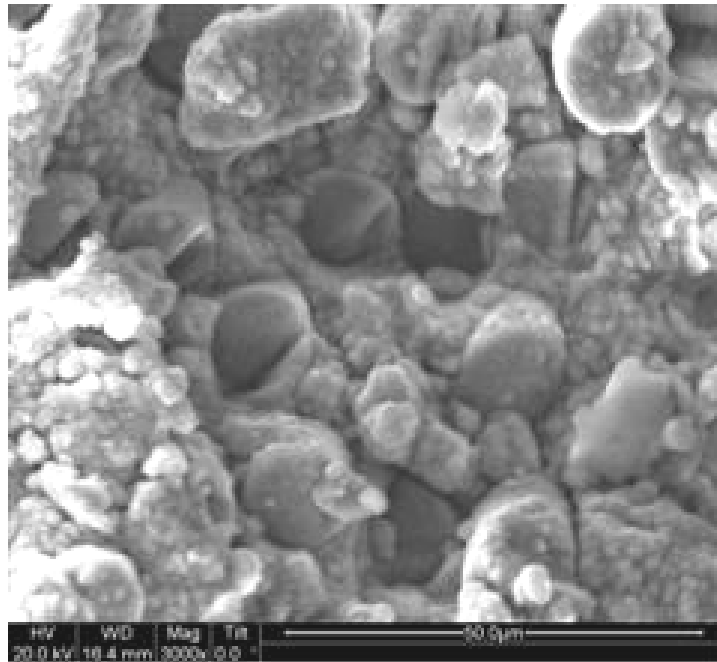


Figure 591. SEM micrograph of the fracture surface of the N720/AM specimen subjected to tensile test to failure with a constant stress rate of 25 MPa/s at 1200°C in laboratory air.

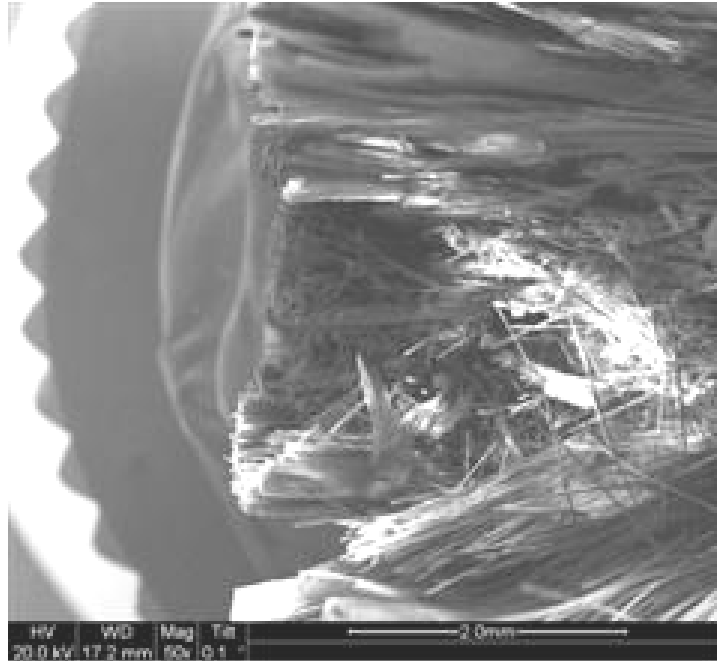


Figure 592. SEM micrograph of the fracture surface of the N720/AM specimen subjected to tensile test to failure with a constant stress rate of 25 MPa/s at 1200°C in laboratory air.

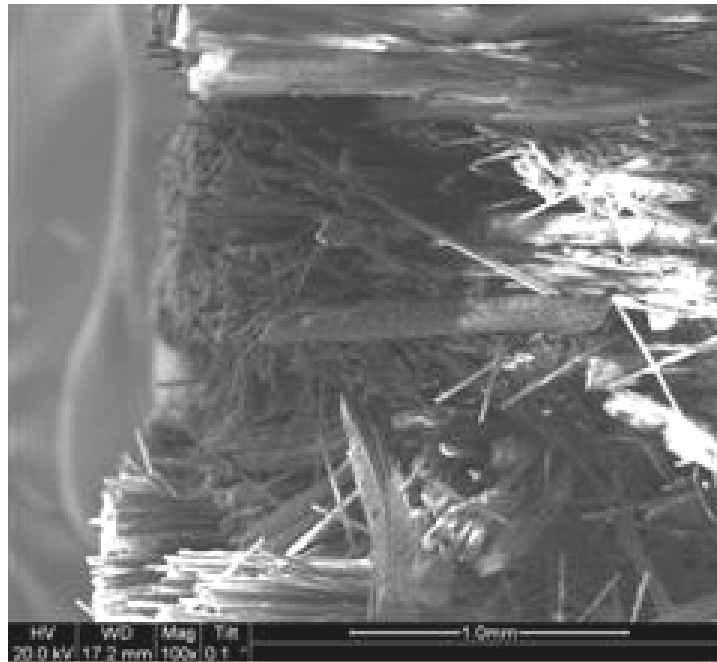


Figure 593. SEM micrograph of the fracture surface of the N720/AM specimen subjected to tensile test to failure with a constant stress rate of 25 MPa/s at 1200°C in laboratory air.



Figure 594. SEM micrograph of the fracture surface of the N720/AM specimen subjected to tensile test to failure with a constant stress rate of 25 MPa/s at 1200°C in laboratory air.

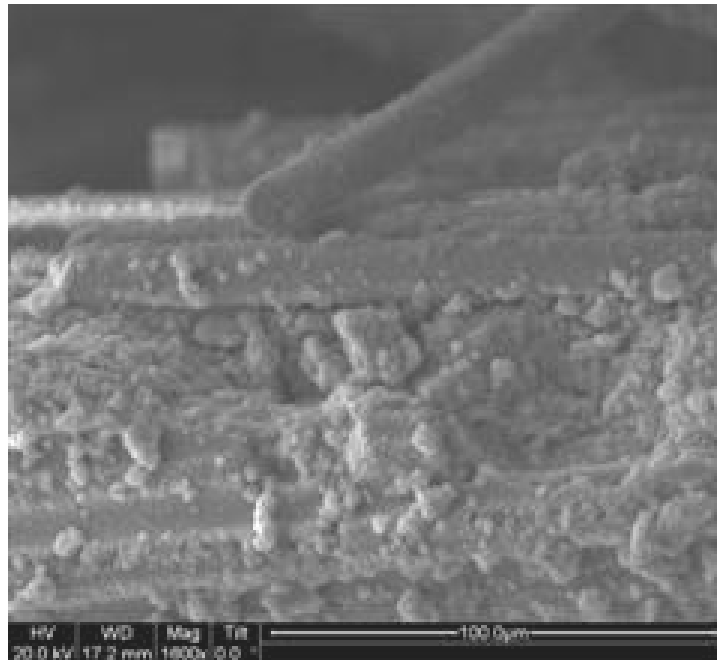


Figure 595. SEM micrograph of the fracture surface of the N720/AM specimen subjected to tensile test to failure with a constant stress rate of 25 MPa/s at 1200°C in laboratory air.

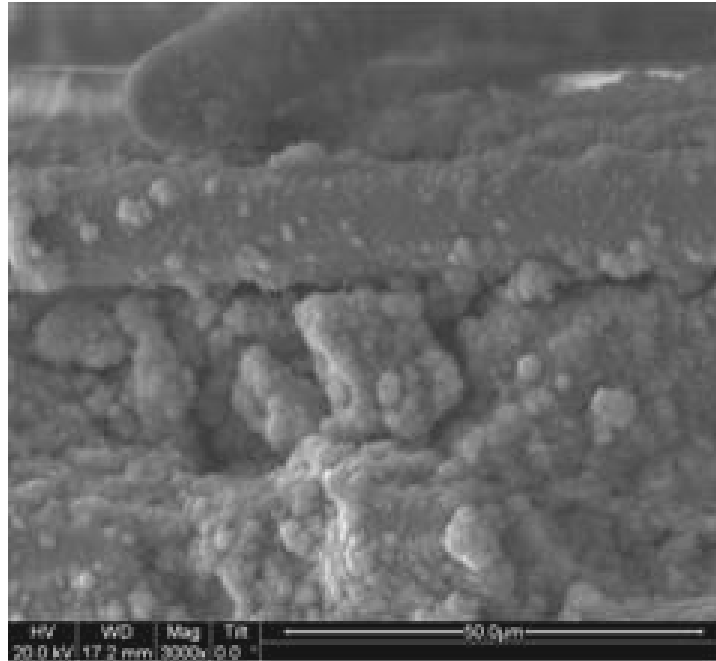


Figure 596. SEM micrograph of the fracture surface of the N720/AM specimen subjected to tensile test to failure with a constant stress rate of 25 MPa/s at 1200°C in laboratory air.

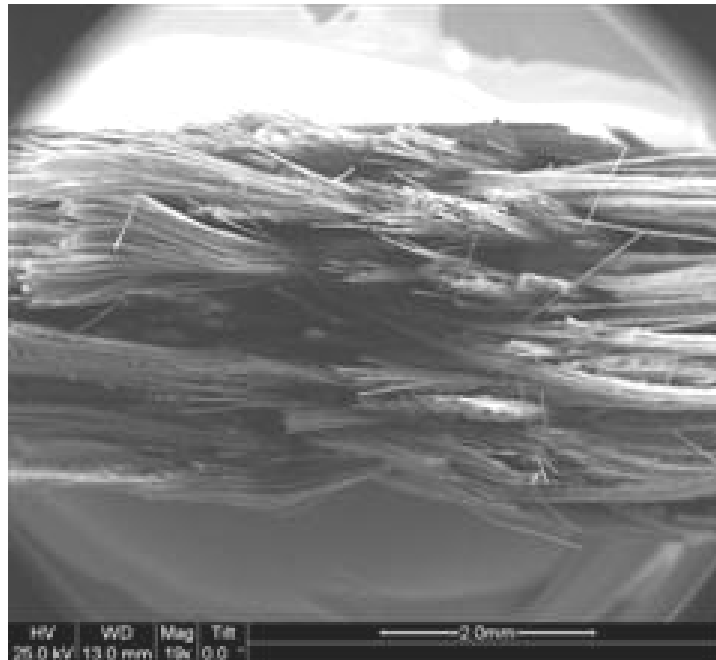


Figure 597. SEM micrograph of the fracture surface of the N720/AM specimen subjected to tensile test to failure with a constant stress rate of 25 MPa/s at 1200°C in steam.

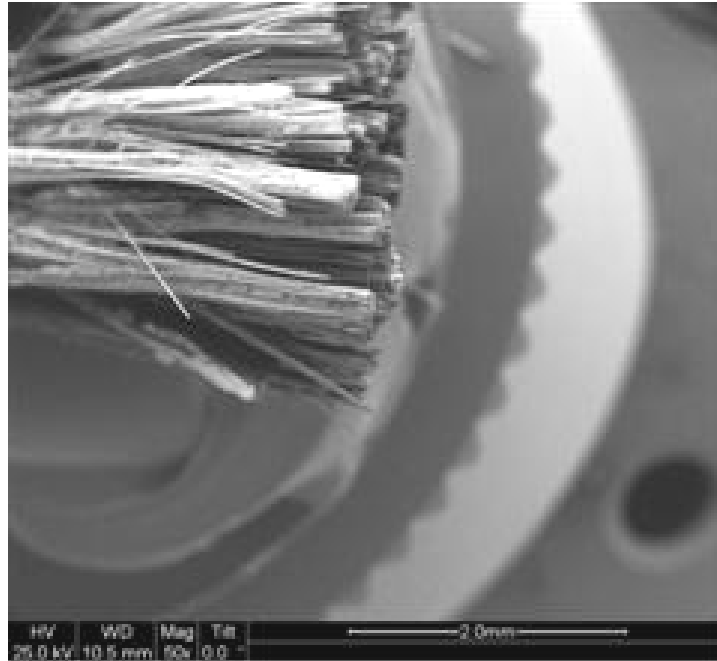


Figure 598. SEM micrograph of the fracture surface of the N720/AM specimen subjected to tensile test to failure with a constant stress rate of 25 MPa/s at 1200°C in steam.

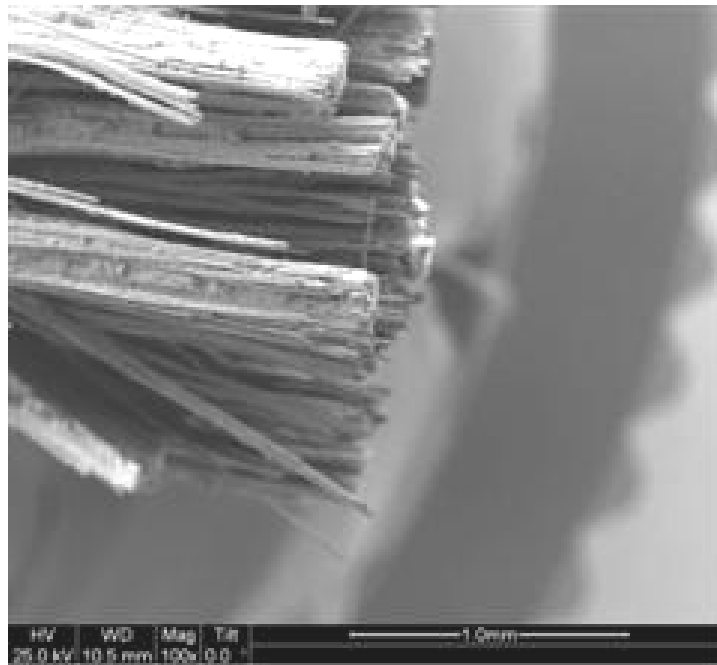


Figure 599. SEM micrograph of the fracture surface of the N720/AM specimen subjected to tensile test to failure with a constant stress rate of 25 MPa/s at 1200°C in steam.

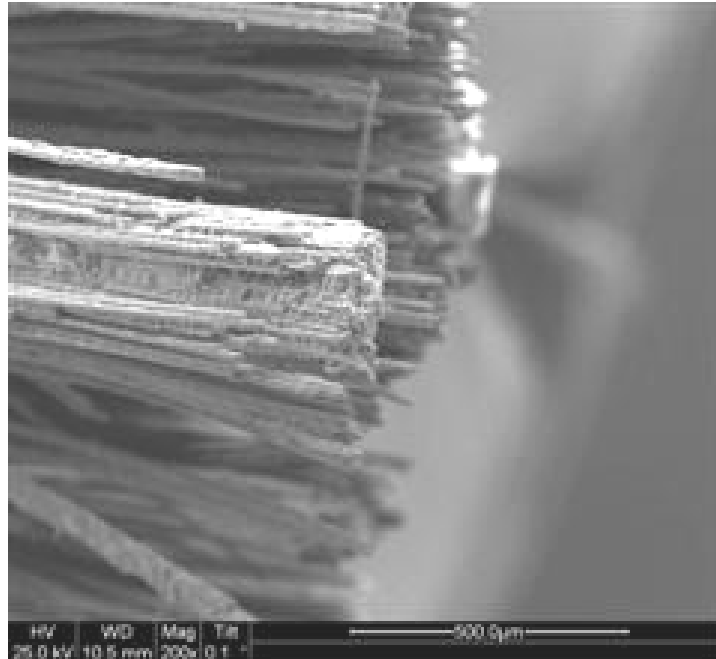


Figure 600. SEM micrograph of the fracture surface of the N720/AM specimen subjected to tensile test to failure with a constant stress rate of 25 MPa/s at 1200°C in steam.

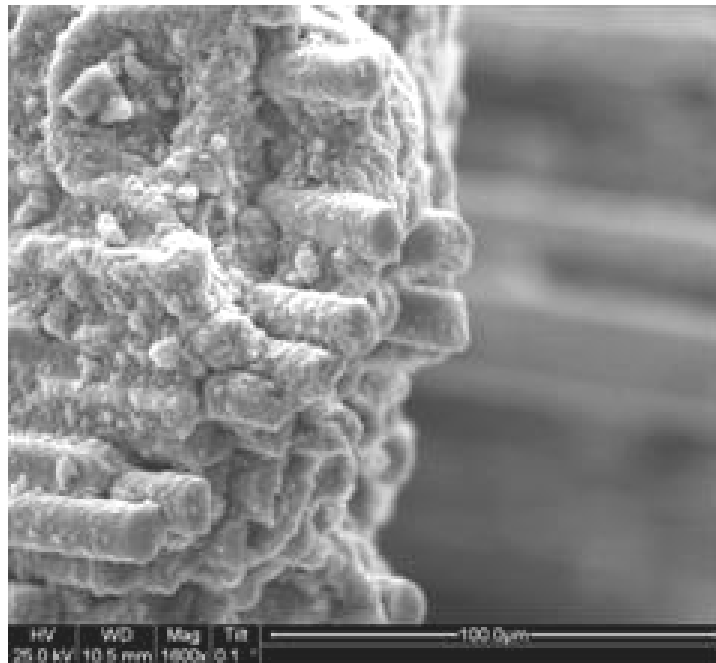


Figure 601. SEM micrograph of the fracture surface of the N720/AM specimen subjected to tensile test to failure with a constant stress rate of 25 MPa/s at 1200°C in steam.

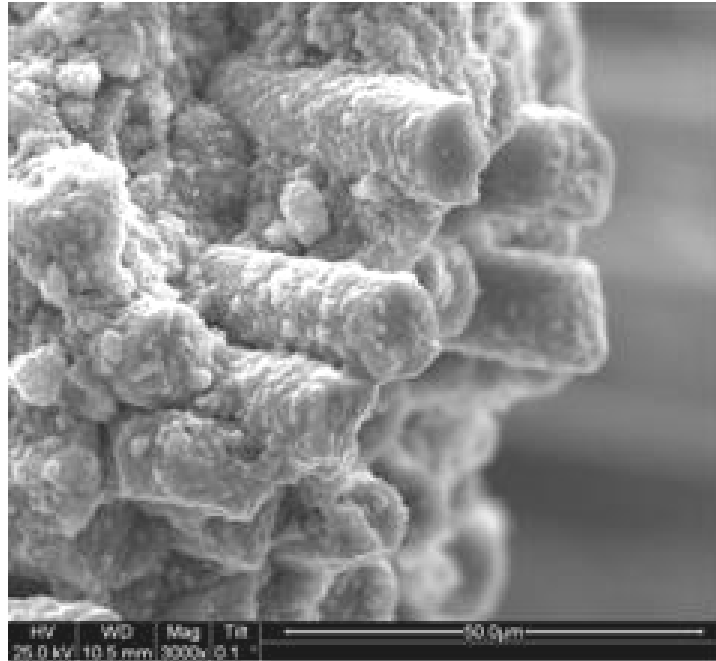


Figure 602. SEM micrograph of the fracture surface of the N720/AM specimen subjected to tensile test to failure with a constant stress rate of 25 MPa/s at 1200°C in steam.

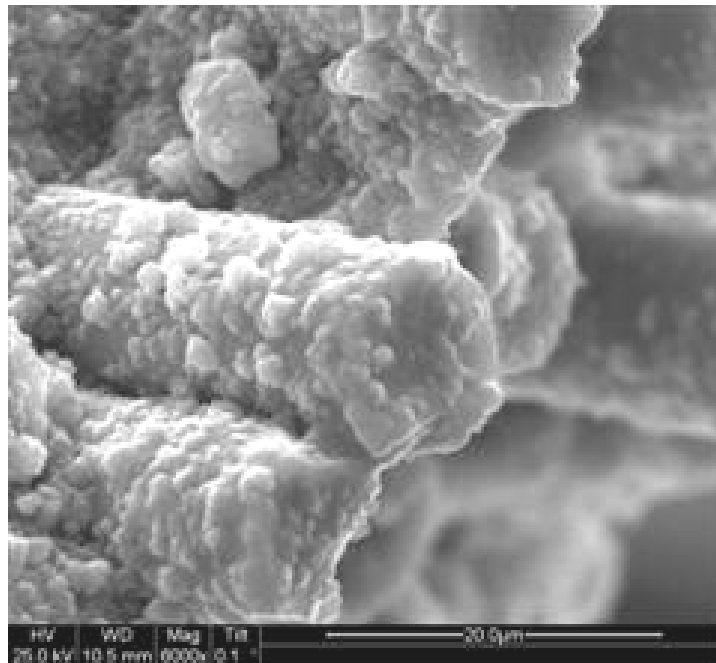


Figure 603. SEM micrograph of the fracture surface of the N720/AM specimen subjected to tensile test to failure with a constant stress rate of 25 MPa/s at 1200°C in steam.

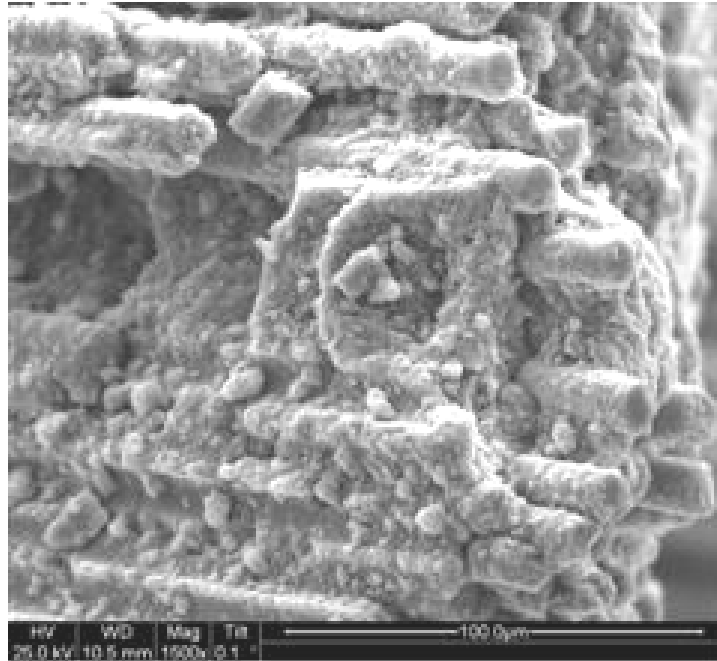


Figure 604. SEM micrograph of the fracture surface of the N720/AM specimen subjected to tensile test to failure with a constant stress rate of 25 MPa/s at 1200°C in steam.

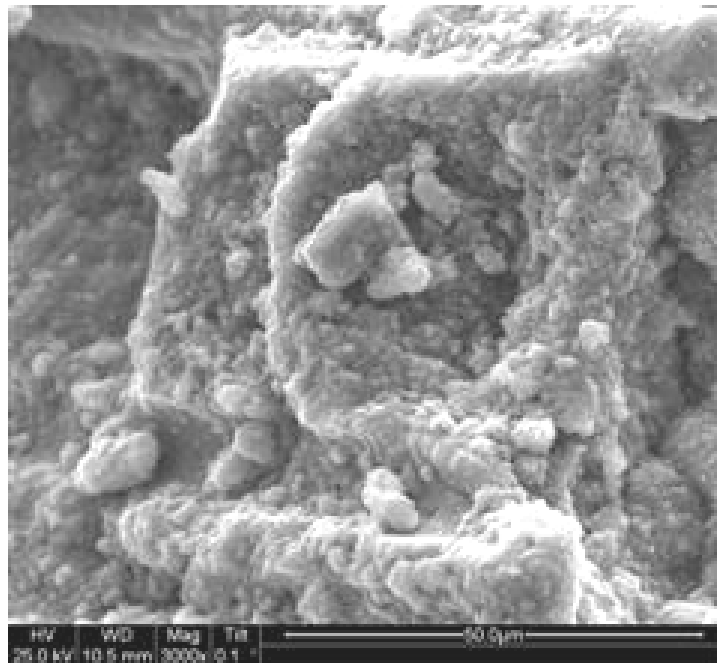


Figure 605. SEM micrograph of the fracture surface of the N720/AM specimen subjected to tensile test to failure with a constant stress rate of 25 MPa/s at 1200°C in steam.

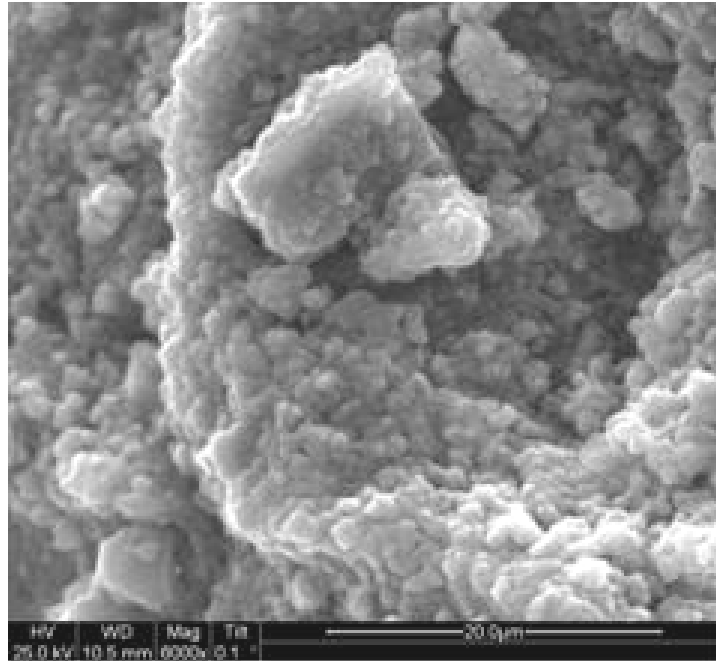


Figure 606. SEM micrograph of the fracture surface of the N720/AM specimen subjected to tensile test to failure with a constant stress rate of 25 MPa/s at 1200°C in steam.

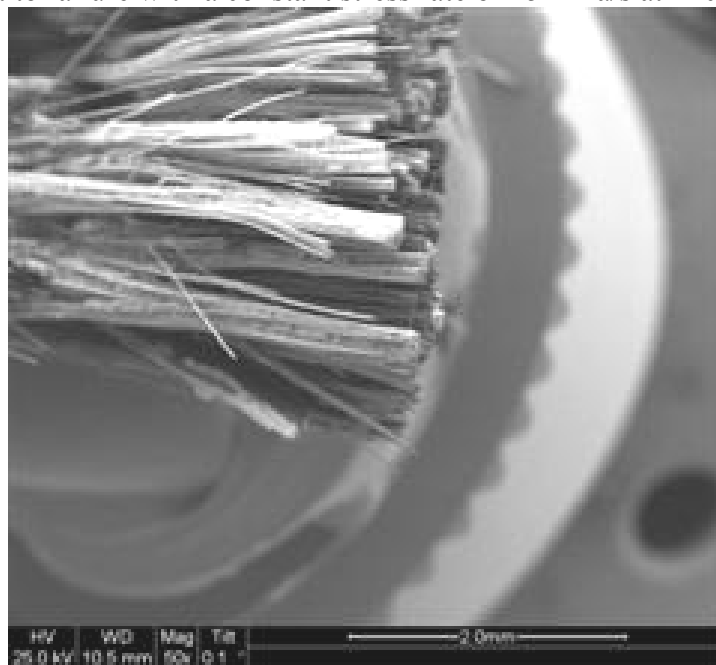


Figure 607. SEM micrograph of the fracture surface of the N720/AM specimen subjected to tensile test to failure with a constant stress rate of 25 MPa/s at 1200°C in steam.

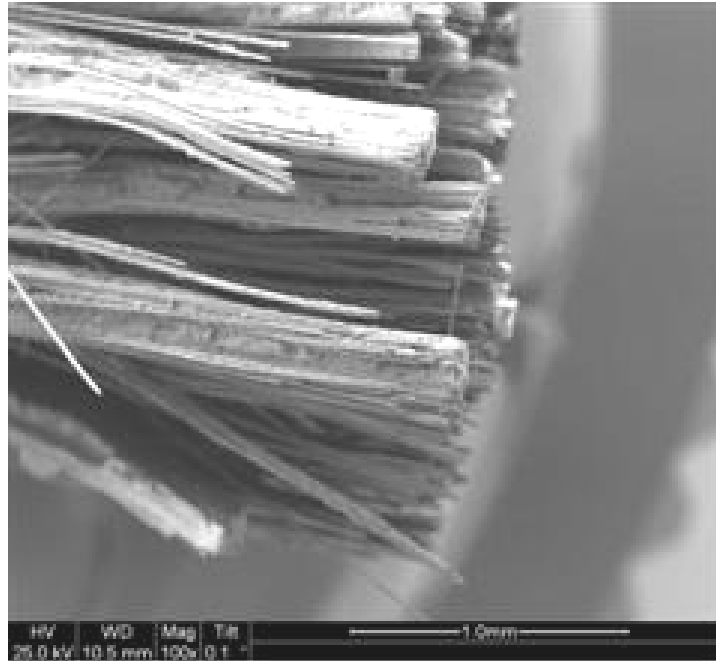


Figure 608. SEM micrograph of the fracture surface of the N720/AM specimen subjected to tensile test to failure with a constant stress rate of 25 MPa/s at 1200°C in steam.

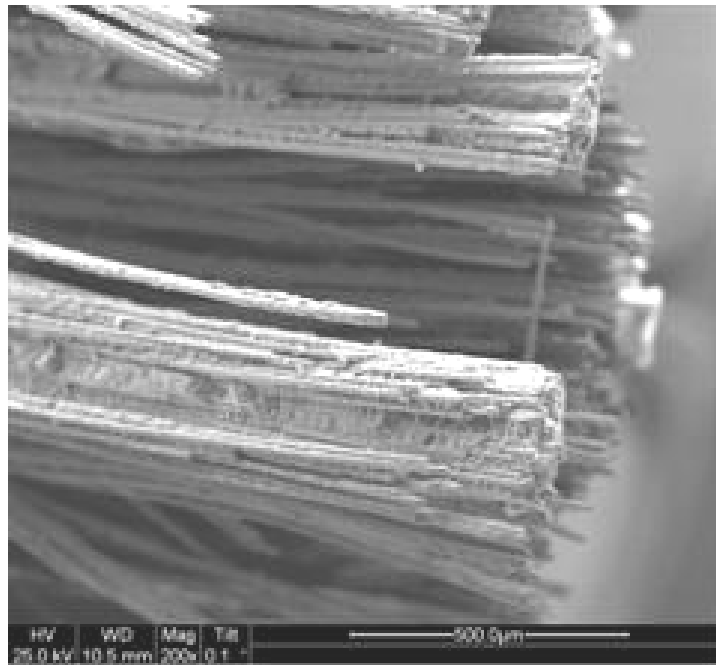


Figure 609. SEM micrograph of the fracture surface of the N720/AM specimen subjected to tensile test to failure with a constant stress rate of 25 MPa/s at 1200°C in steam.



Figure 610. SEM micrograph of the fracture surface of the N720/AM specimen subjected to tensile test to failure with a constant stress rate of 25 MPa/s at 1200°C in steam.



Figure 611. SEM micrograph of the fracture surface of the N720/AM specimen subjected to tensile test to failure with a constant stress rate of 25 MPa/s at 1200°C in steam.

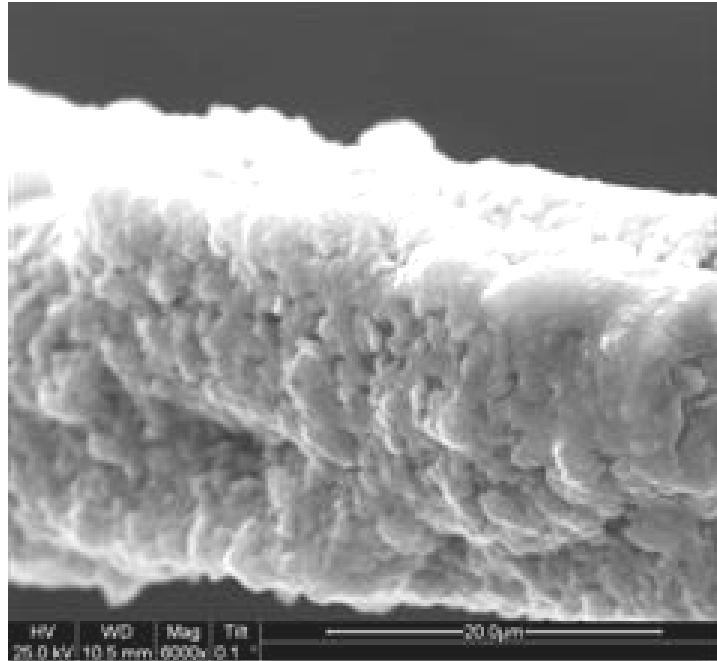


Figure 612. SEM micrograph of the fracture surface of the N720/AM specimen subjected to tensile test to failure with a constant stress rate of 25 MPa/s at 1200°C in steam.

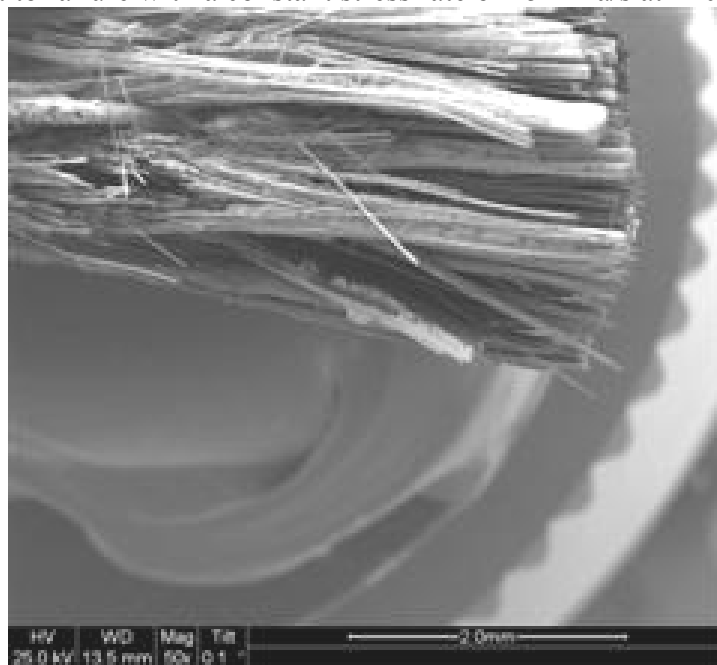


Figure 613. SEM micrograph of the fracture surface of the N720/AM specimen subjected to tensile test to failure with a constant stress rate of 25 MPa/s at 1200°C in steam.

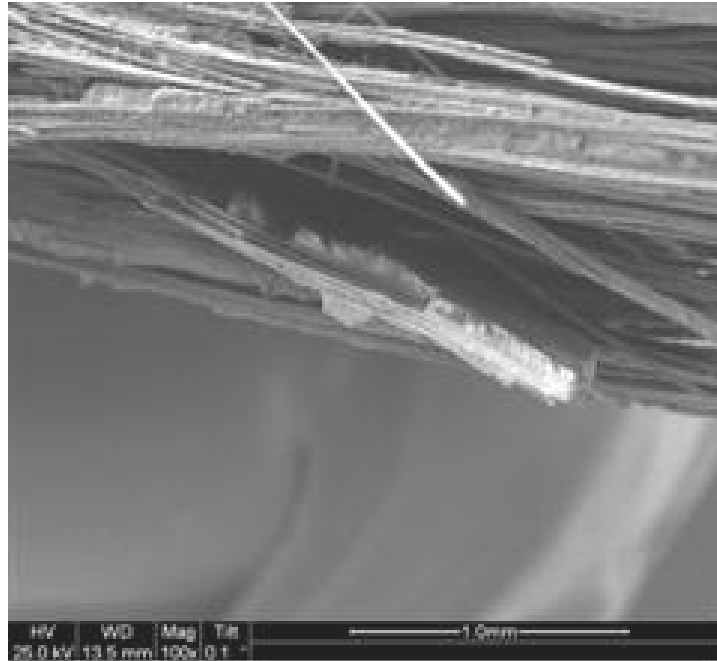


Figure 614. SEM micrograph of the fracture surface of the N720/AM specimen subjected to tensile test to failure with a constant stress rate of 25 MPa/s at 1200°C in steam.

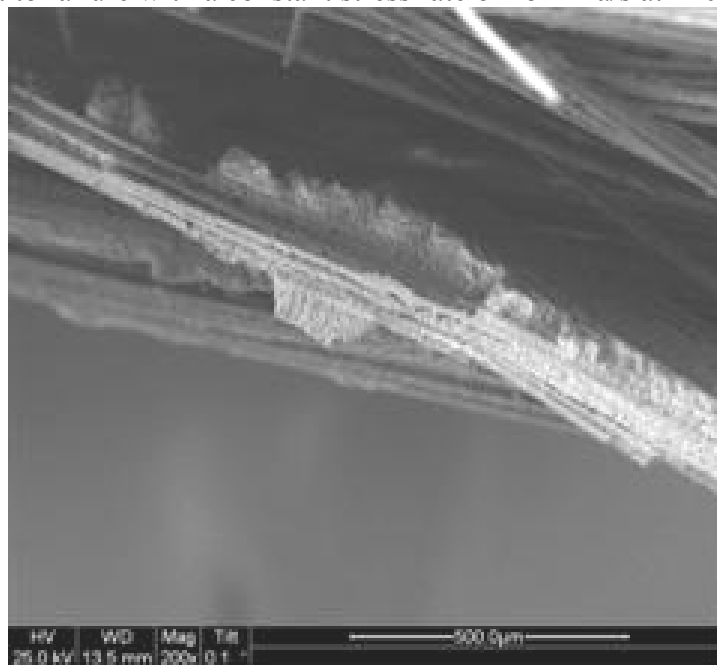


Figure 615. SEM micrograph of the fracture surface of the N720/AM specimen subjected to tensile test to failure with a constant stress rate of 25 MPa/s at 1200°C in steam.

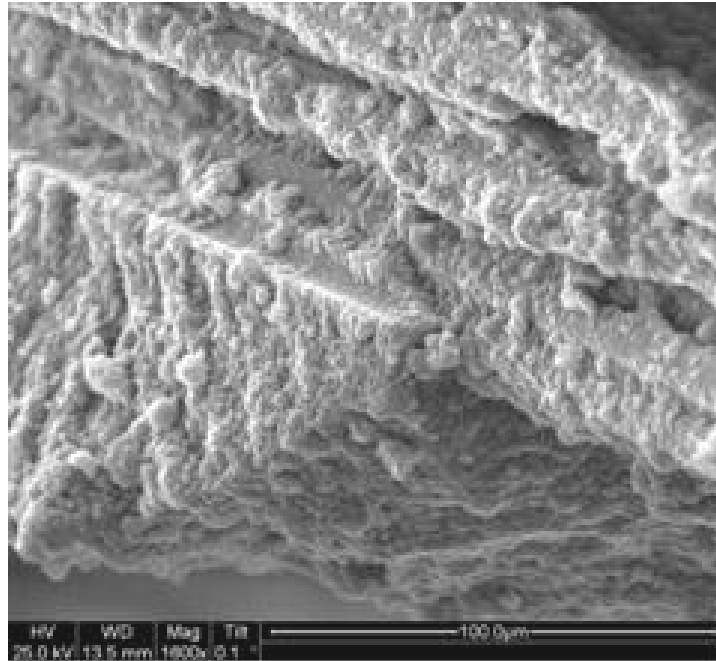


Figure 616. SEM micrograph of the fracture surface of the N720/AM specimen subjected to tensile test to failure with a constant stress rate of 25 MPa/s at 1200°C in steam.

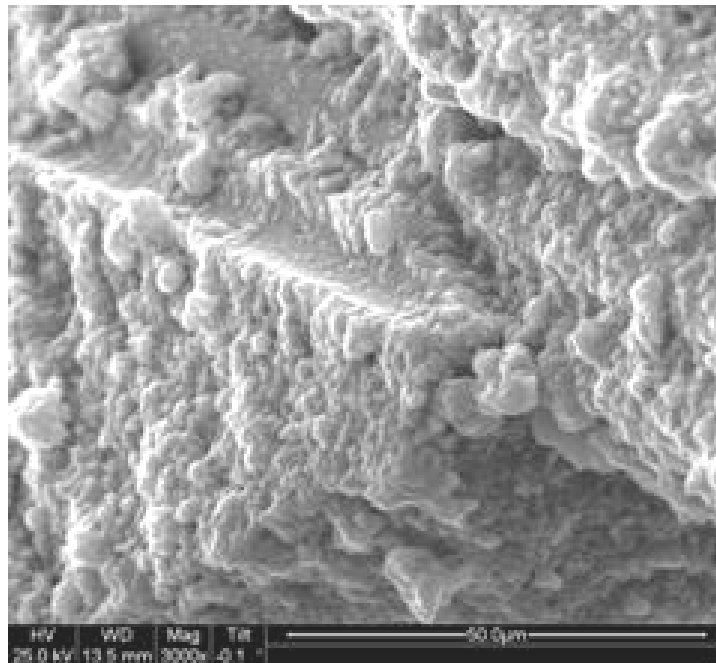


Figure 617. SEM micrograph of the fracture surface of the N720/AM specimen subjected to tensile test to failure with a constant stress rate of 25 MPa/s at 1200°C in steam.

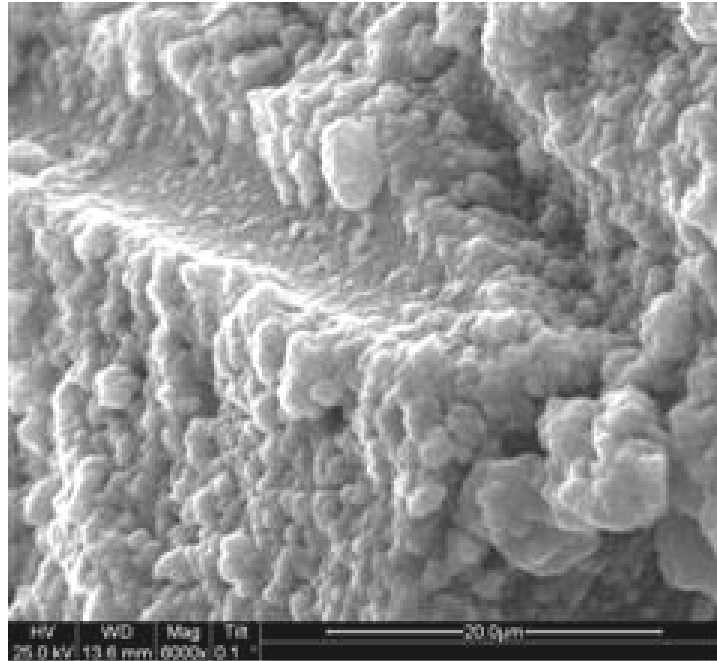


Figure 618. SEM micrograph of the fracture surface of the N720/AM specimen subjected to tensile test to failure with a constant stress rate of 25 MPa/s at 1200°C in steam.

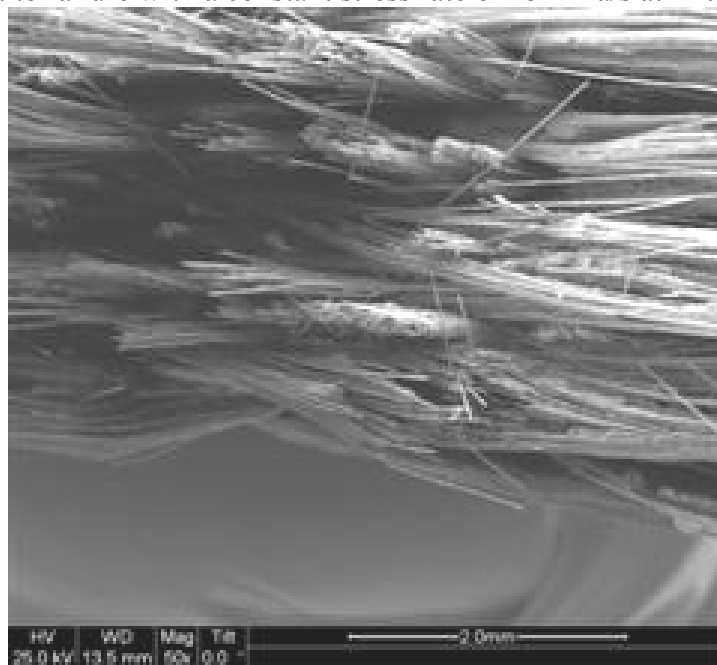


Figure 619. SEM micrograph of the fracture surface of the N720/AM specimen subjected to tensile test to failure with a constant stress rate of 25 MPa/s at 1200°C in steam.

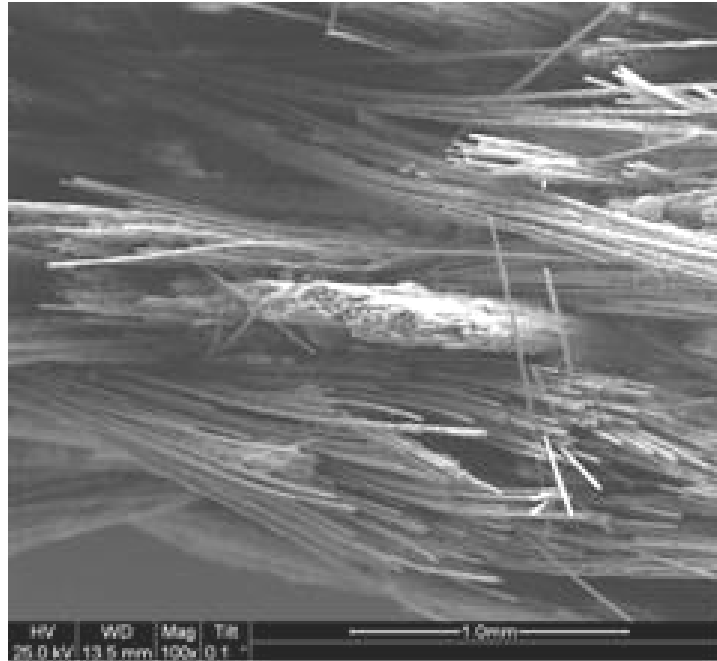


Figure 620. SEM micrograph of the fracture surface of the N720/AM specimen subjected to tensile test to failure with a constant stress rate of 25 MPa/s at 1200°C in steam.

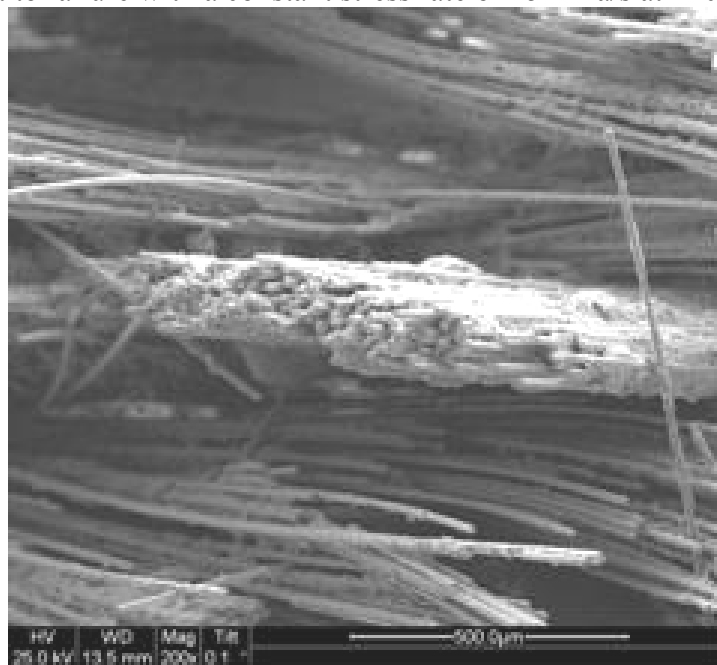


Figure 621. SEM micrograph of the fracture surface of the N720/AM specimen subjected to tensile test to failure with a constant stress rate of 25 MPa/s at 1200°C in steam.

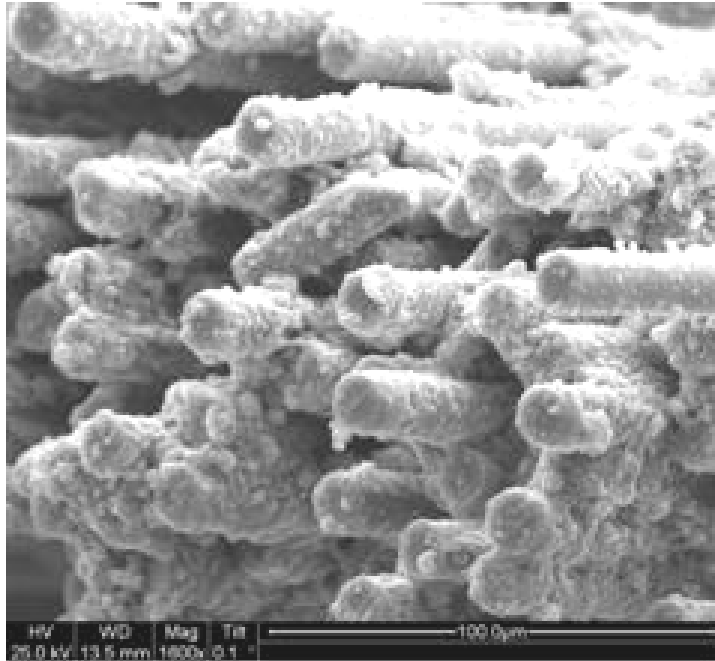


Figure 622. SEM micrograph of the fracture surface of the N720/AM specimen subjected to tensile test to failure with a constant stress rate of 25 MPa/s at 1200°C in steam.

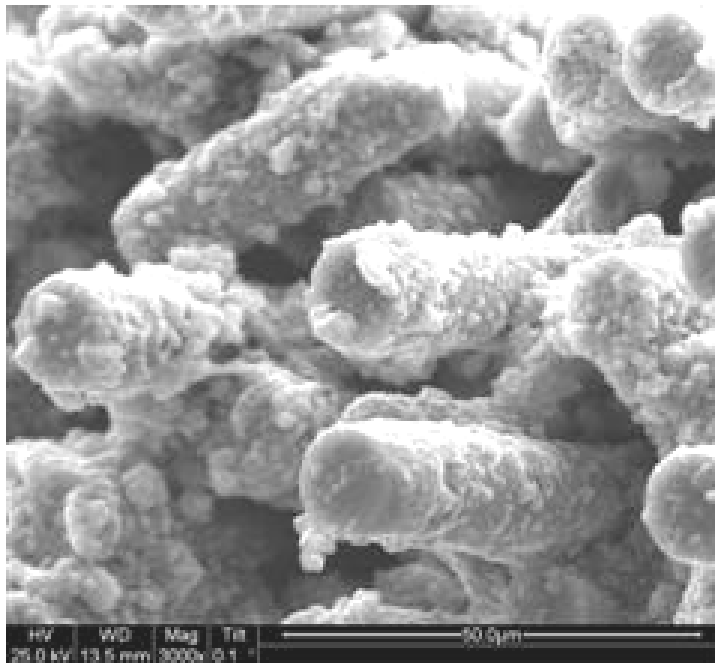


Figure 623. SEM micrograph of the fracture surface of the N720/AM specimen subjected to tensile test to failure with a constant stress rate of 25 MPa/s at 1200°C in steam.

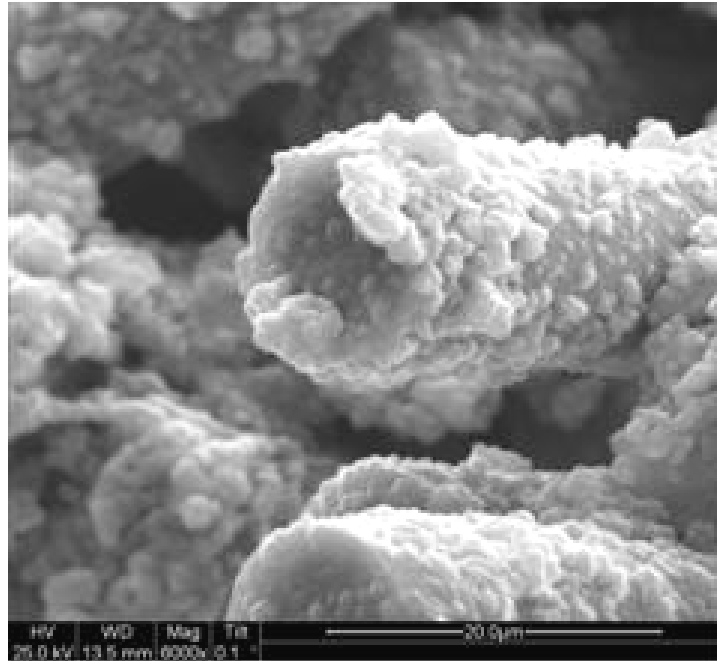


Figure 624. SEM micrograph of the fracture surface of the N720/AM specimen subjected to tensile test to failure with a constant stress rate of 25 MPa/s at 1200°C in steam.

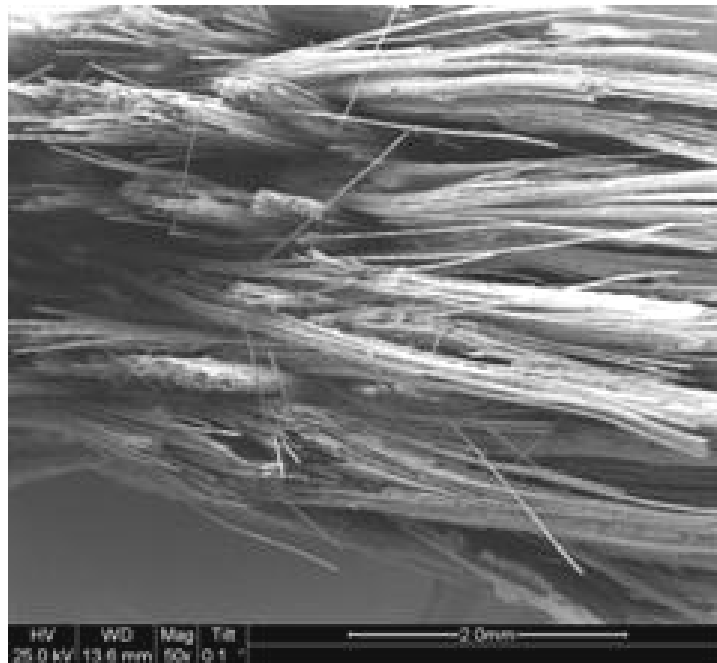


Figure 625. SEM micrograph of the fracture surface of the N720/AM specimen subjected to tensile test to failure with a constant stress rate of 25 MPa/s at 1200°C in steam.

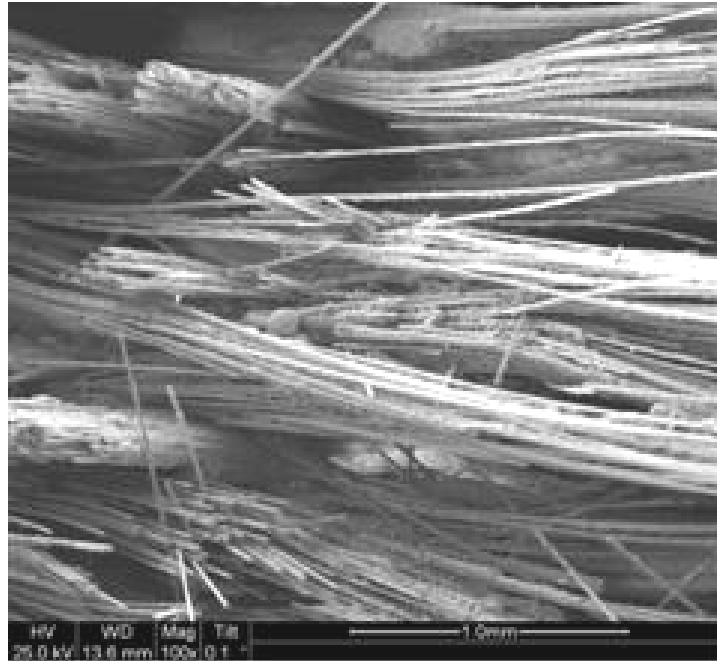


Figure 626. SEM micrograph of the fracture surface of the N720/AM specimen subjected to tensile test to failure with a constant stress rate of 25 MPa/s at 1200°C in steam.



Figure 627. SEM micrograph of the fracture surface of the N720/AM specimen subjected to tensile test to failure with a constant stress rate of 25 MPa/s at 1200°C in steam.

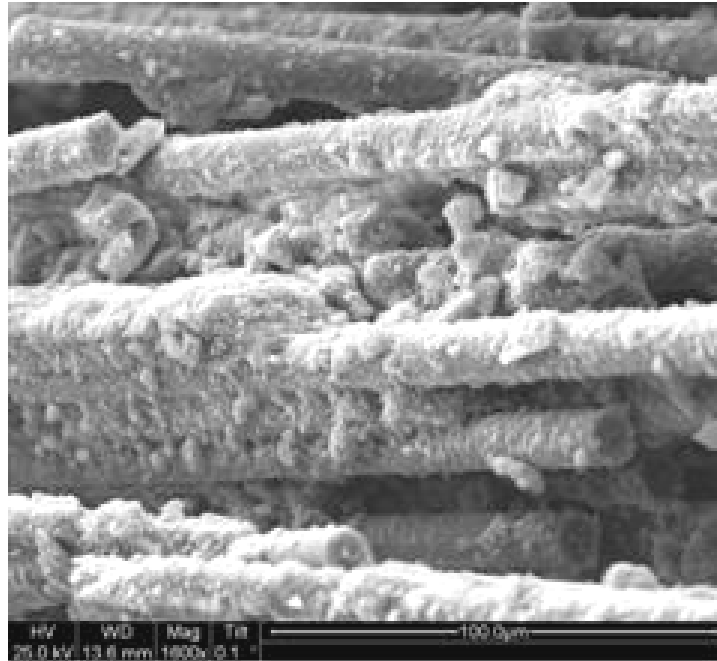


Figure 628. SEM micrograph of the fracture surface of the N720/AM specimen subjected to tensile test to failure with a constant stress rate of 25 MPa/s at 1200°C in steam.

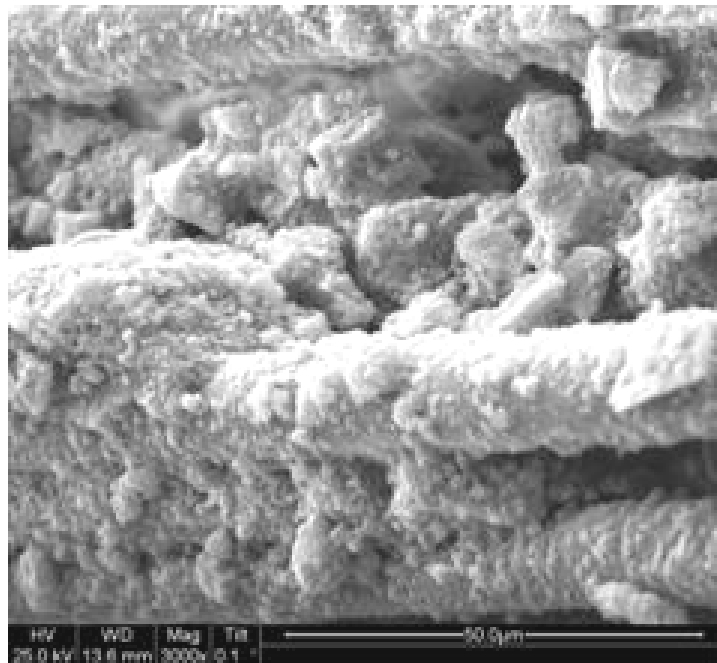


Figure 629. SEM micrograph of the fracture surface of the N720/AM specimen subjected to tensile test to failure with a constant stress rate of 25 MPa/s at 1200°C in steam.

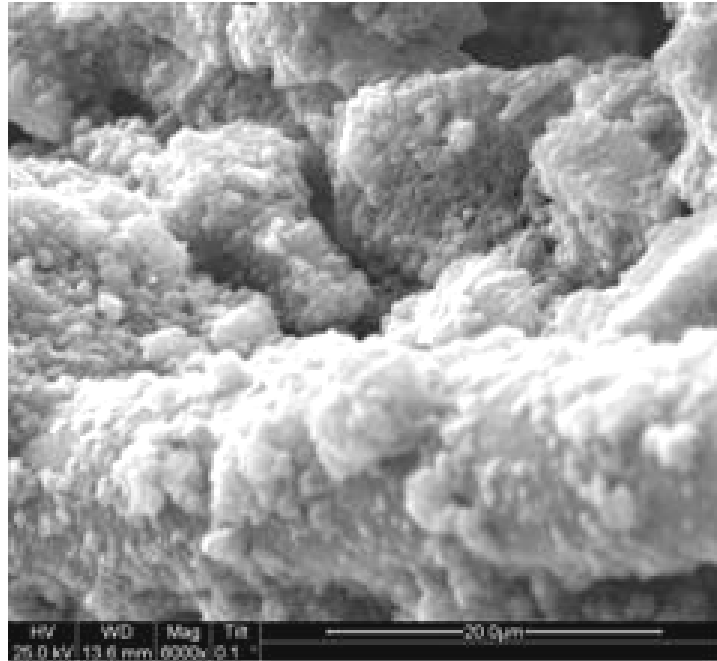


Figure 630. SEM micrograph of the fracture surface of the N720/AM specimen subjected to tensile test to failure with a constant stress rate of 25 MPa/s at 1200°C in steam.

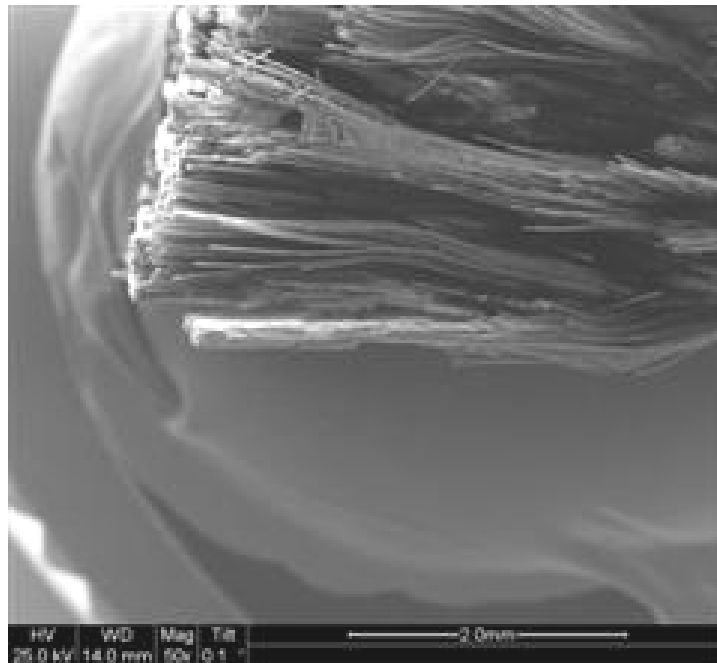


Figure 631. SEM micrograph of the fracture surface of the N720/AM specimen subjected to tensile test to failure with a constant stress rate of 25 MPa/s at 1200°C in steam.

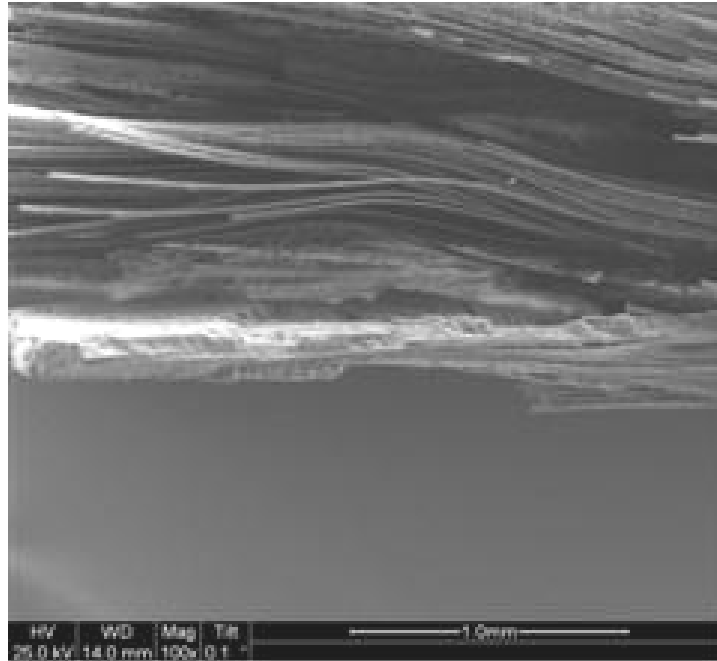


Figure 632. SEM micrograph of the fracture surface of the N720/AM specimen subjected to tensile test to failure with a constant stress rate of 25 MPa/s at 1200°C in steam.

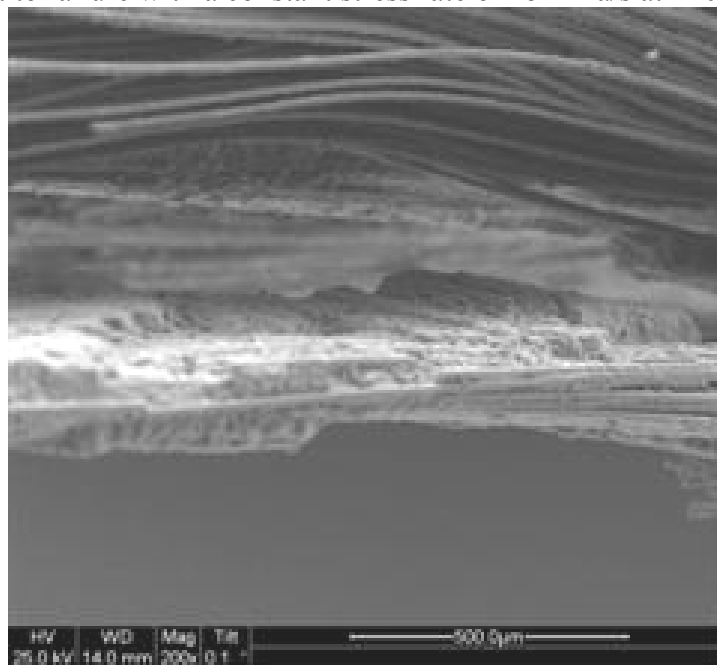


Figure 633. SEM micrograph of the fracture surface of the N720/AM specimen subjected to tensile test to failure with a constant stress rate of 25 MPa/s at 1200°C in steam.

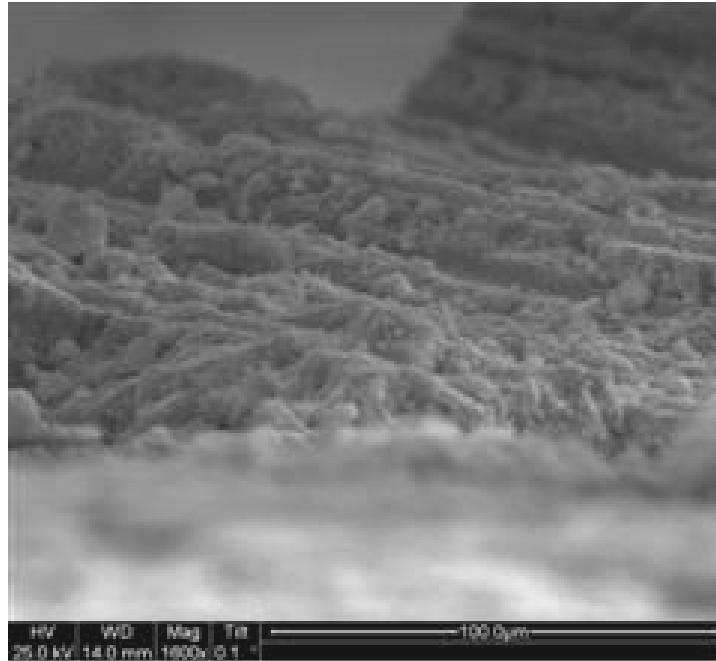


Figure 634. SEM micrograph of the fracture surface of the N720/AM specimen subjected to tensile test to failure with a constant stress rate of 25 MPa/s at 1200°C in steam.

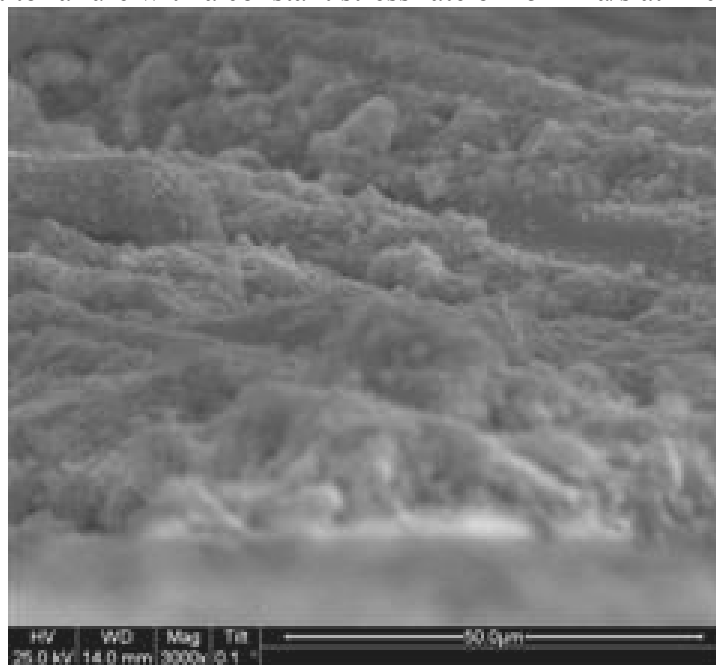


Figure 635. SEM micrograph of the fracture surface of the N720/AM specimen subjected to tensile test to failure with a constant stress rate of 25 MPa/s at 1200°C in steam.

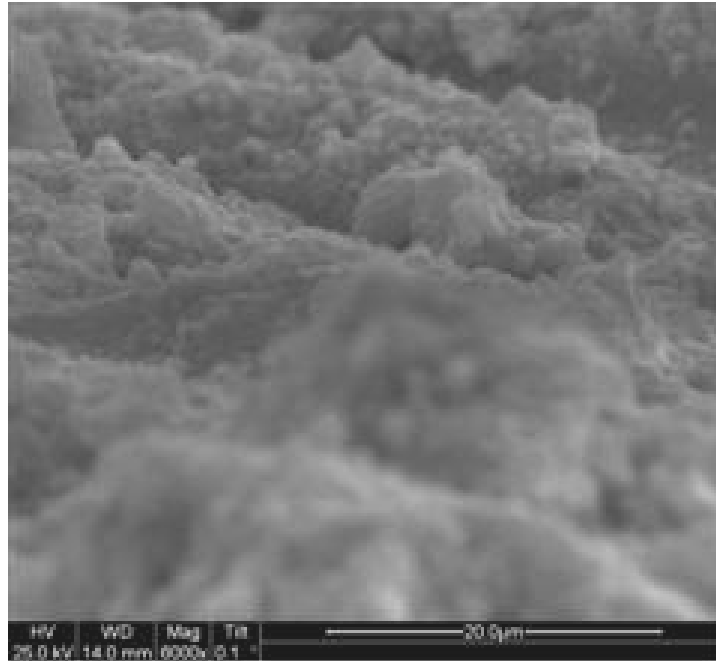


Figure 636. SEM micrograph of the fracture surface of the N720/AM specimen subjected to tensile test to failure with a constant stress rate of 25 MPa/s at 1200°C in steam.

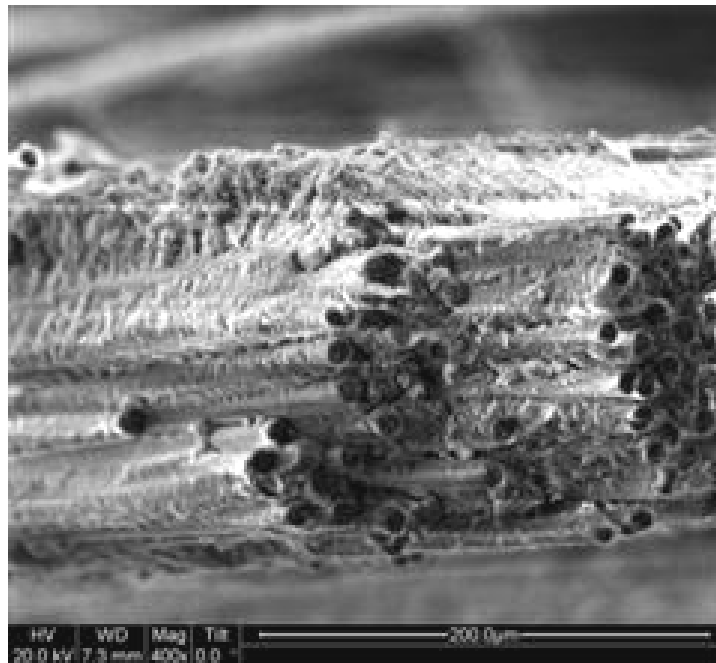


Figure 637. SEM micrograph of the fracture surface of the N720/AM specimen subjected to monotonic tensile test to failure at 1200°C in laboratory air.

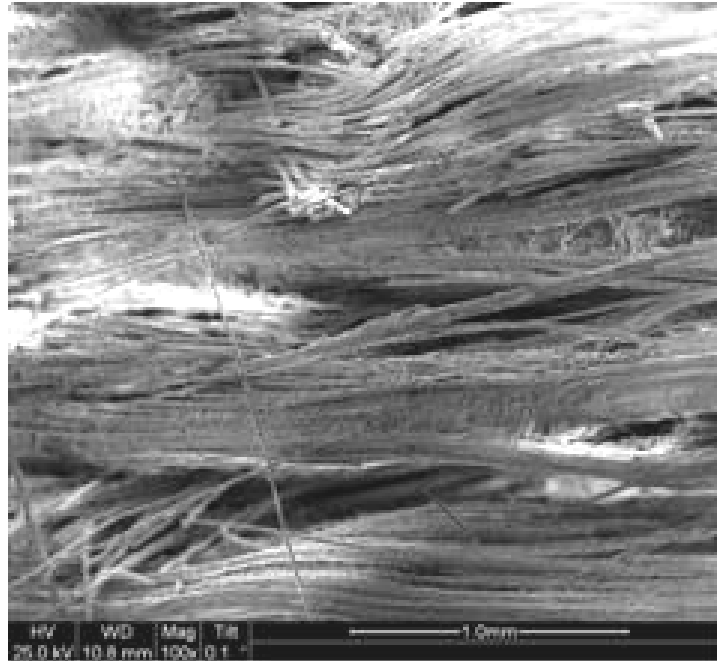


Figure 638. SEM micrograph of the fracture surface of the N720/AM specimen subjected to monotonic tensile test to failure at 1200°C in laboratory air.

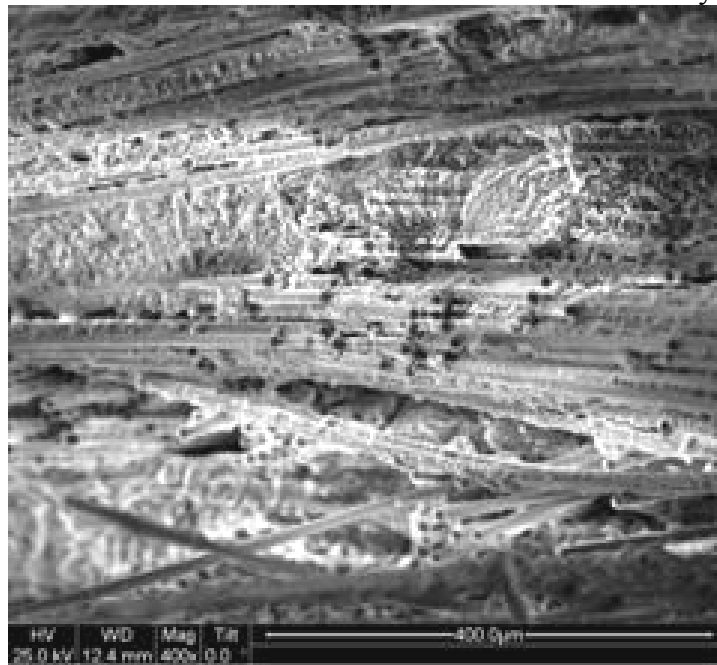


Figure 639. SEM micrograph of the fracture surface of the N720/AM specimen subjected to monotonic tensile test to failure at 1200°C in laboratory air.

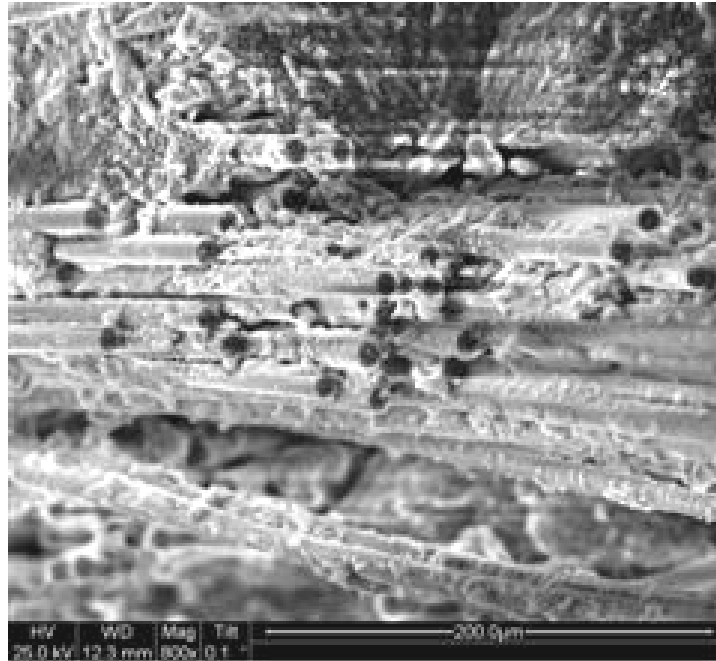


Figure 640. SEM micrograph of the fracture surface of the N720/AM specimen subjected to monotonic tensile test to failure at 1200°C in laboratory air.

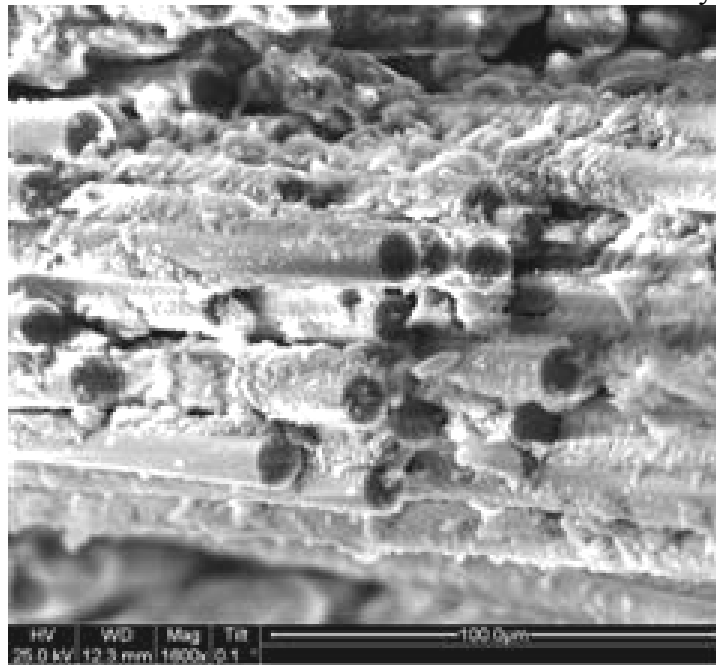


Figure 641. SEM micrograph of the fracture surface of the N720/AM specimen subjected to monotonic tensile test to failure at 1200°C in laboratory air.

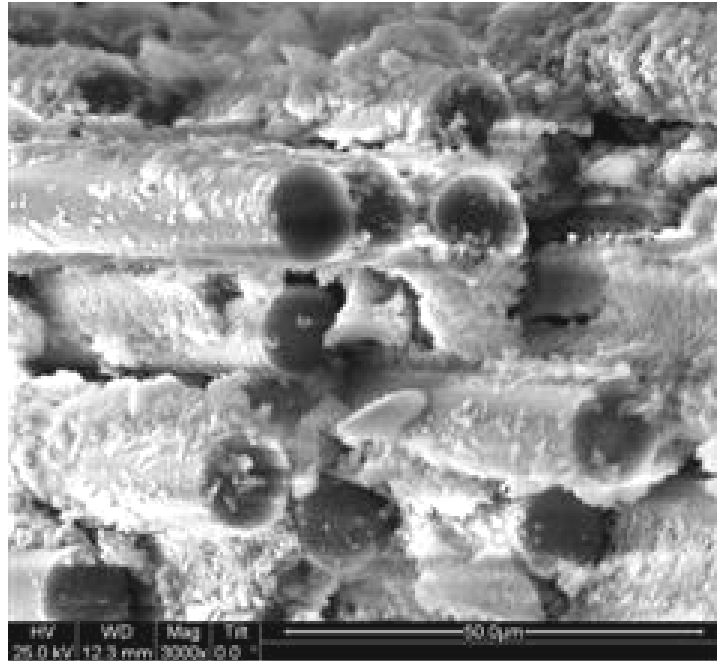


Figure 642. SEM micrograph of the fracture surface of the N720/AM specimen subjected to monotonic tensile test to failure at 1200°C in laboratory air.

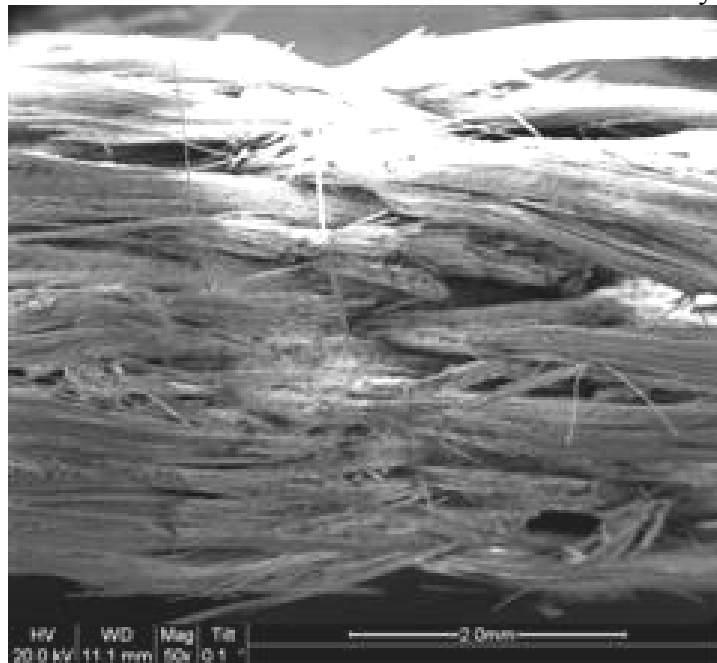


Figure 643. SEM micrograph of the fracture surface of the N720/AM specimen subjected to monotonic tensile test to failure at 1200°C in laboratory air.

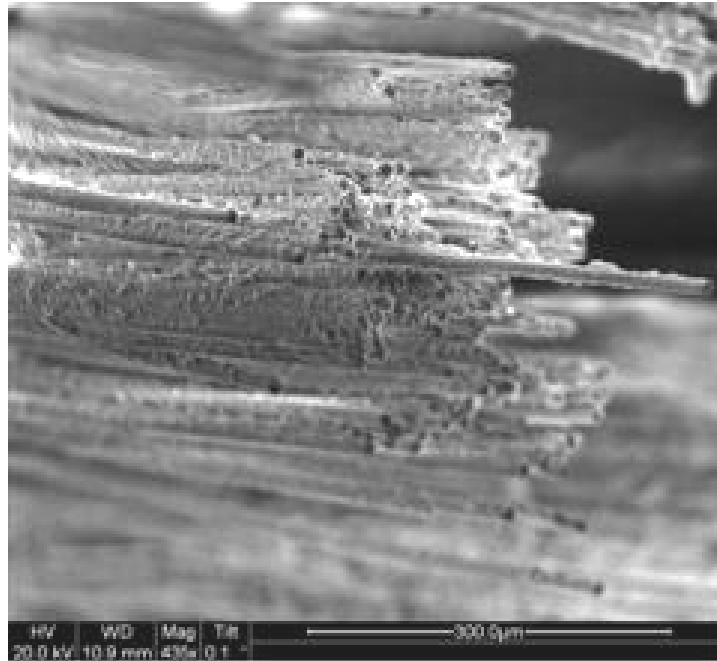


Figure 644. SEM micrograph of the fracture surface of the N720/AM specimen subjected to monotonic tensile test to failure at 1200°C in laboratory air.

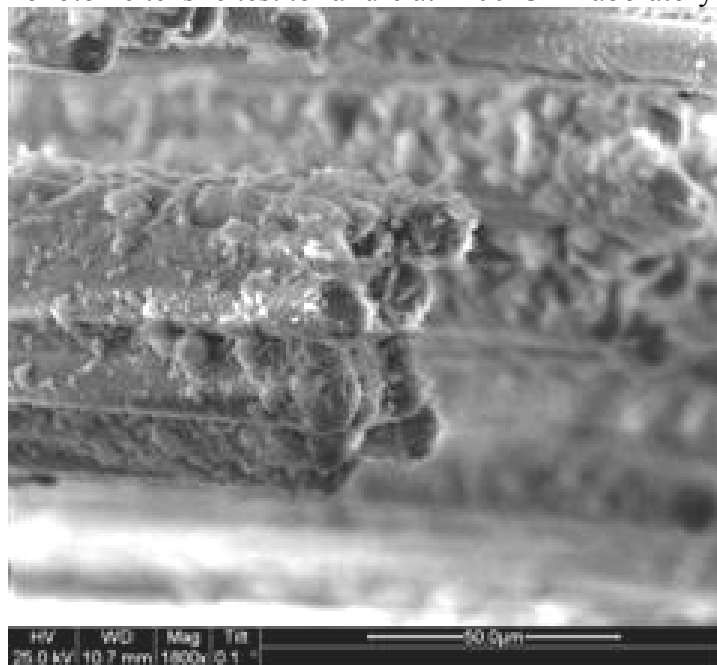


Figure 645. SEM micrograph of the fracture surface of the N720/AM specimen subjected to monotonic tensile test to failure at 1200°C in laboratory air.

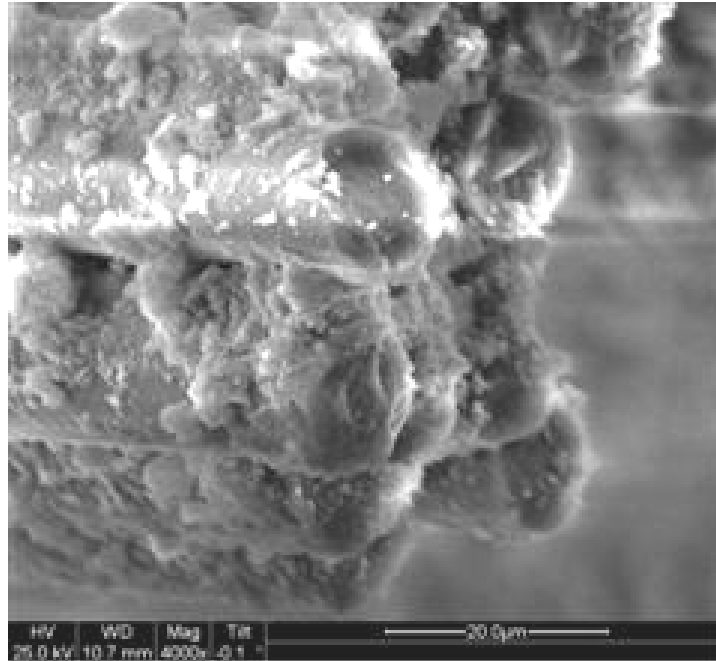


Figure 646. SEM micrograph of the fracture surface of the N720/AM specimen subjected to monotonic tensile test to failure at 1200°C in laboratory air.

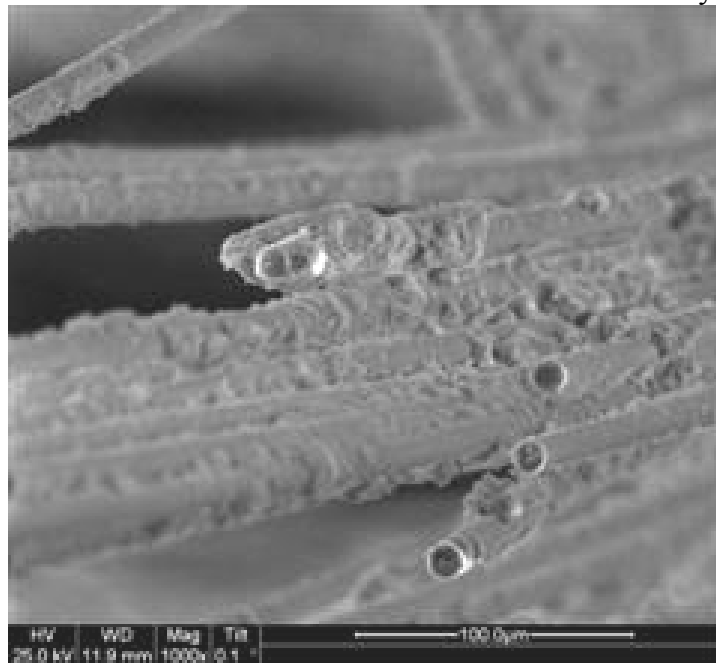


Figure 647. SEM micrograph of the fracture surface of the N720/AM specimen subjected to monotonic tensile test to failure at 1200°C in laboratory air.

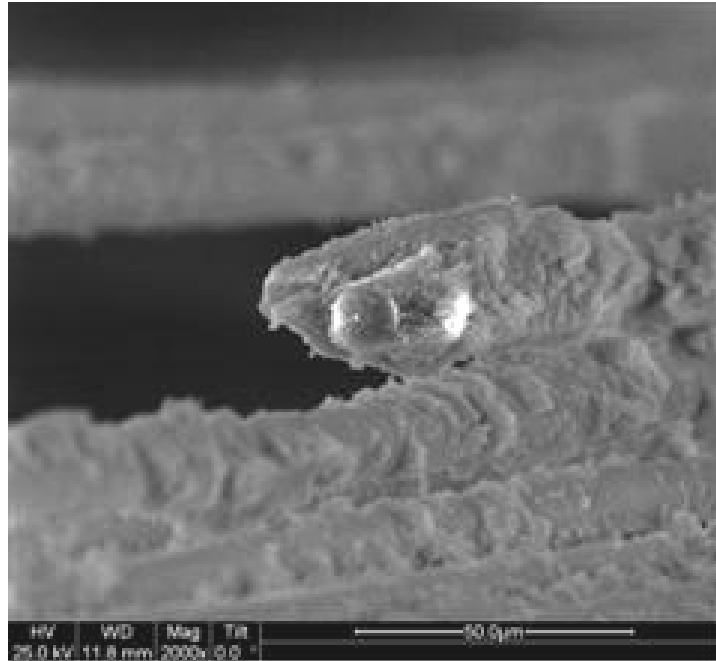


Figure 648. SEM micrograph of the fracture surface of the N720/AM specimen subjected to monotonic tensile test to failure at 1200°C in laboratory air.



Figure 649. SEM micrograph of the fracture surface of the N720/AM specimen subjected to monotonic tensile test to failure at 1200°C in laboratory air.

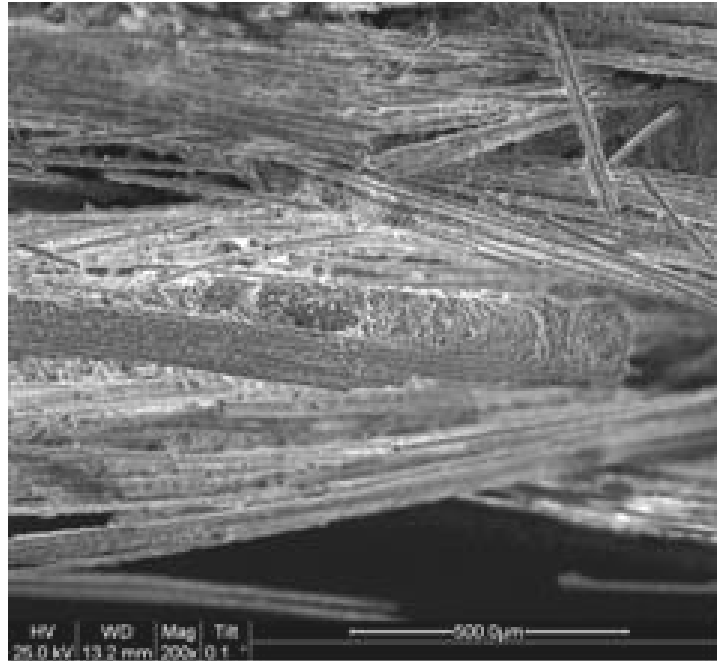


Figure 650. SEM micrograph of the fracture surface of the N720/AM specimen subjected to monotonic tensile test to failure at 1200°C in laboratory air.

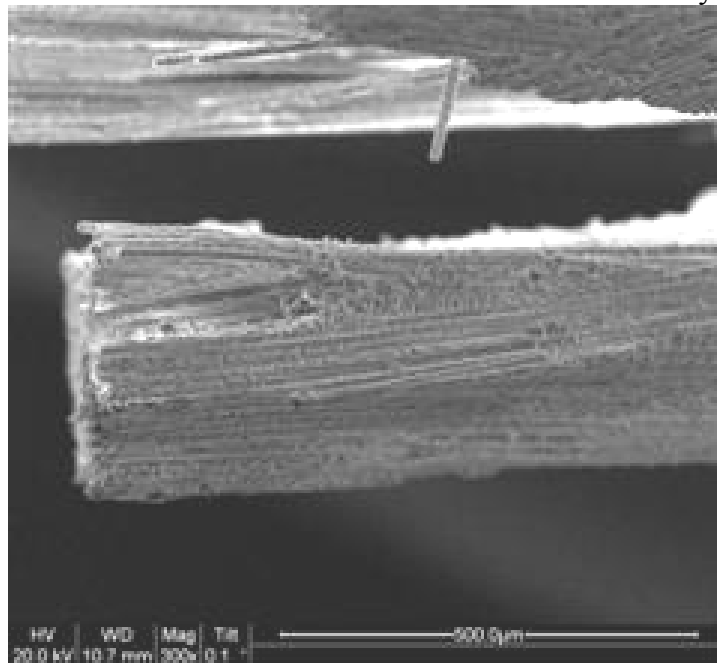


Figure 651. SEM micrograph of the fracture surface of the N720/AM specimen subjected to monotonic tensile test to failure at 1200°C in laboratory air.

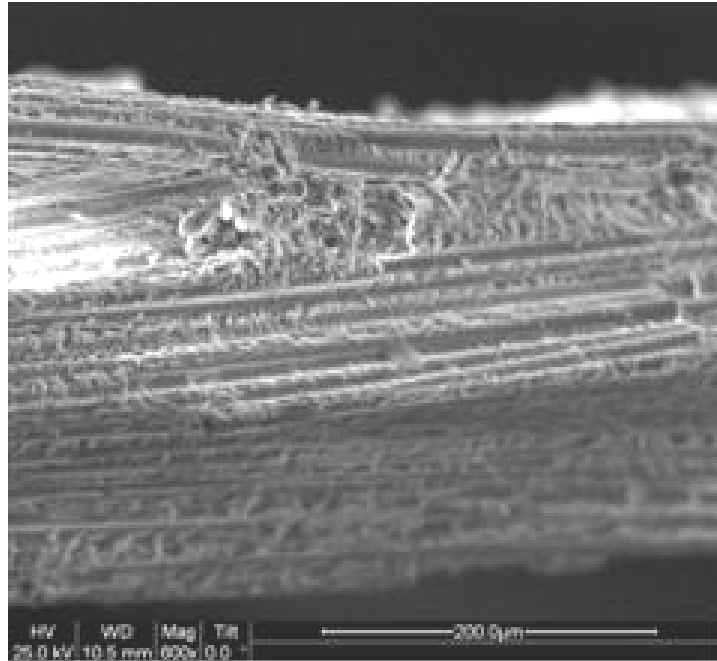


Figure 652. SEM micrograph of the fracture surface of the N720/AM specimen subjected to monotonic tensile test to failure at 1200°C in laboratory air.

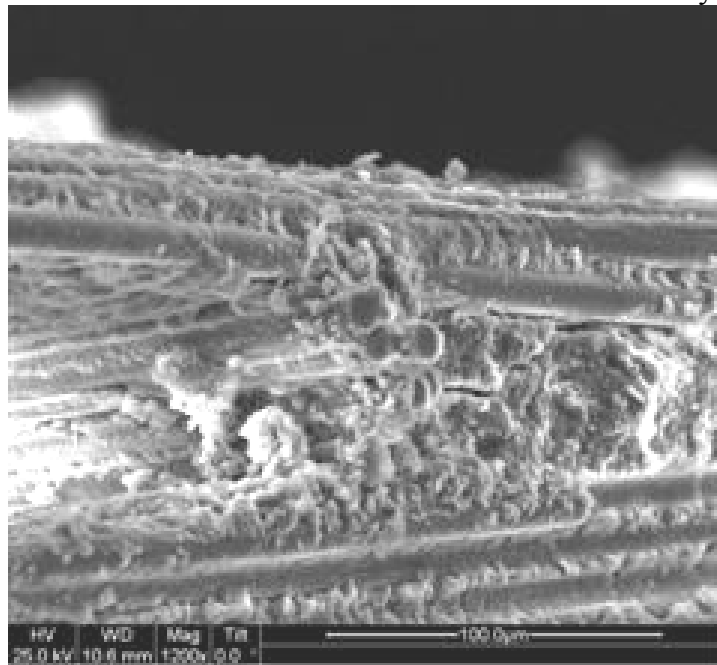


Figure 653. SEM micrograph of the fracture surface of the N720/AM specimen subjected to monotonic tensile test to failure at 1200°C in laboratory air.

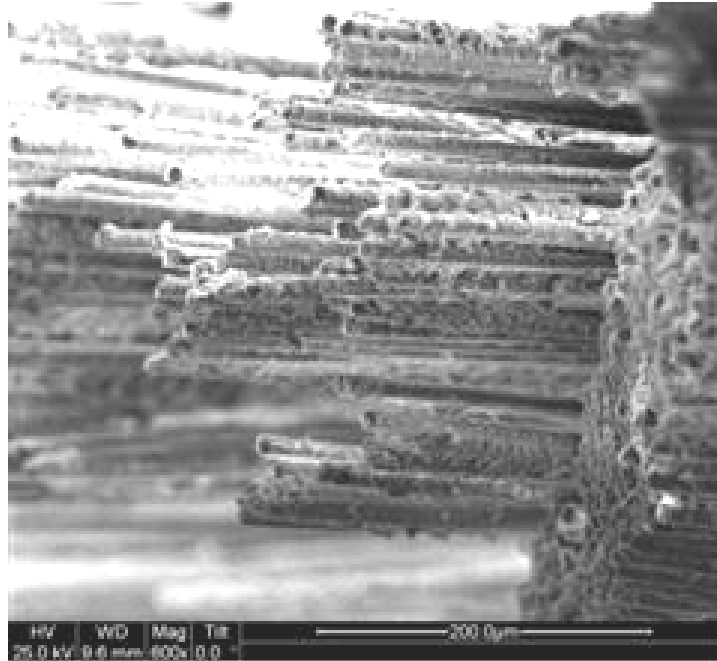


Figure 654. SEM micrograph of the fracture surface of the N720/AM specimen subjected to monotonic tensile test to failure at 1200°C in laboratory air.

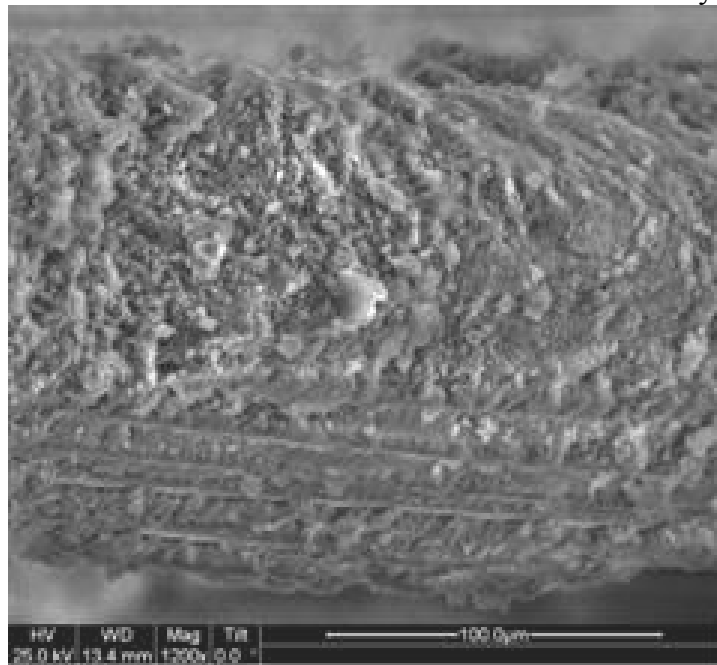


Figure 655. SEM micrograph of the fracture surface of the N720/AM specimen subjected to monotonic tensile test to failure at 1200°C in laboratory air.

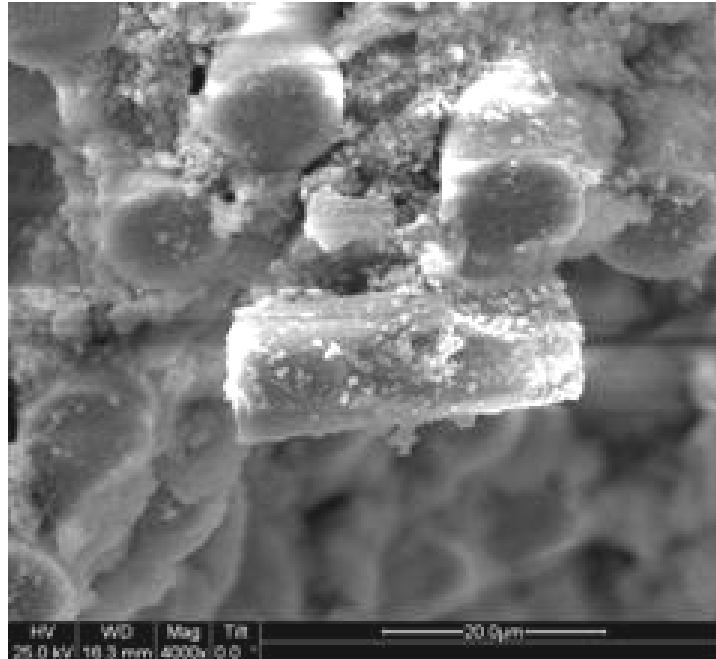


Figure 656. SEM micrograph of the fracture surface of the N720/AM specimen subjected to monotonic tensile test to failure at 1200°C in laboratory air.

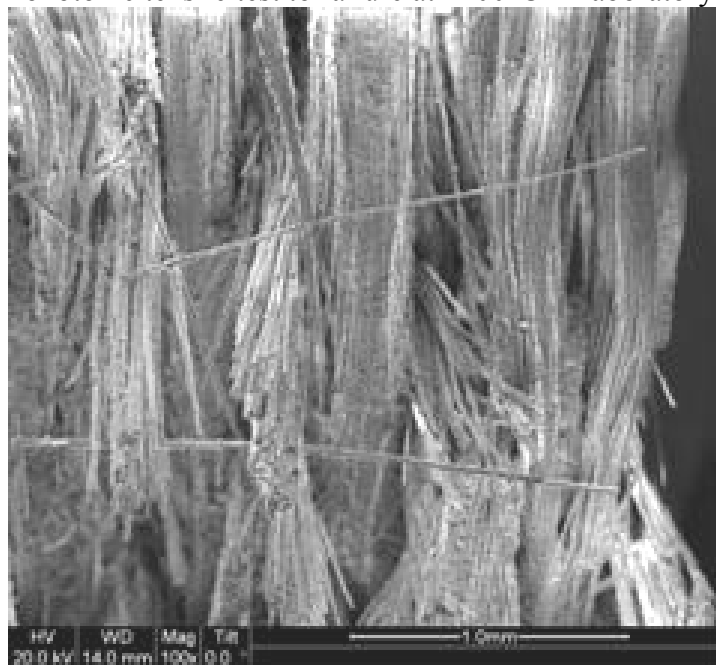


Figure 657. SEM micrograph of the fracture surface of the N720/AM specimen subjected to monotonic tensile test to failure at 1200°C in laboratory air.

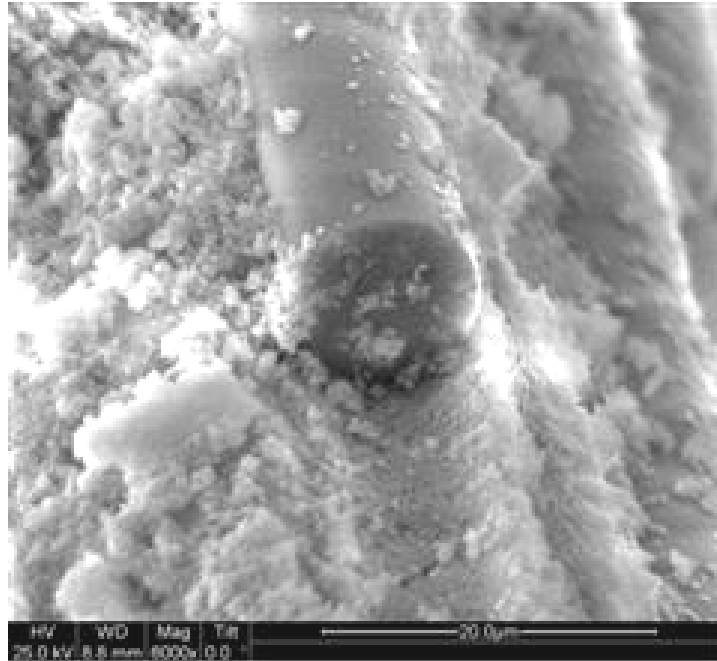


Figure 658. SEM micrograph of the fracture surface of the N720/AM specimen subjected to monotonic tensile test to failure at 1200°C in laboratory air.



Figure 659. SEM micrograph of the fracture surface of the N720/AM specimen subjected to monotonic tensile test to failure at 1200°C in laboratory air.



Figure 660. SEM micrograph of the fracture surface of the N720/AM specimen subjected to monotonic tensile test to failure at 1200°C in laboratory air.

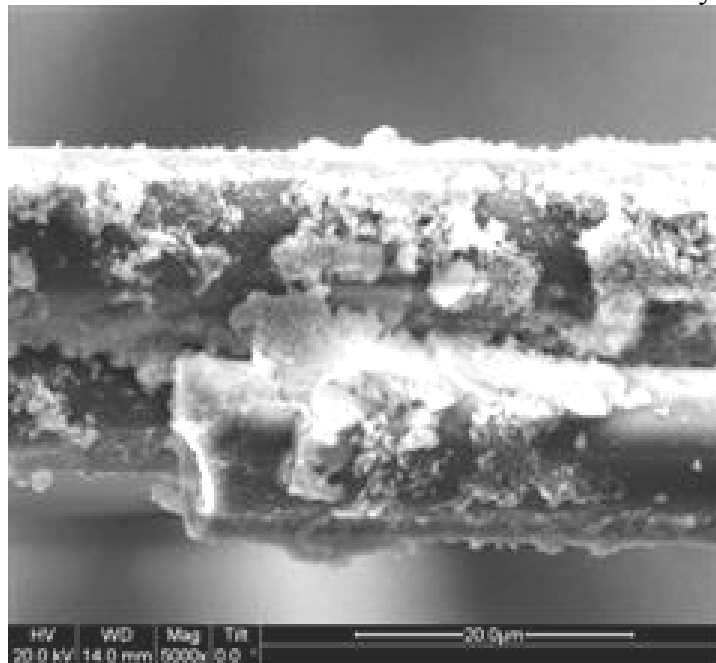


Figure 661. SEM micrograph of the fracture surface of the N720/AM specimen subjected to monotonic tensile test to failure at 1200°C in laboratory air.

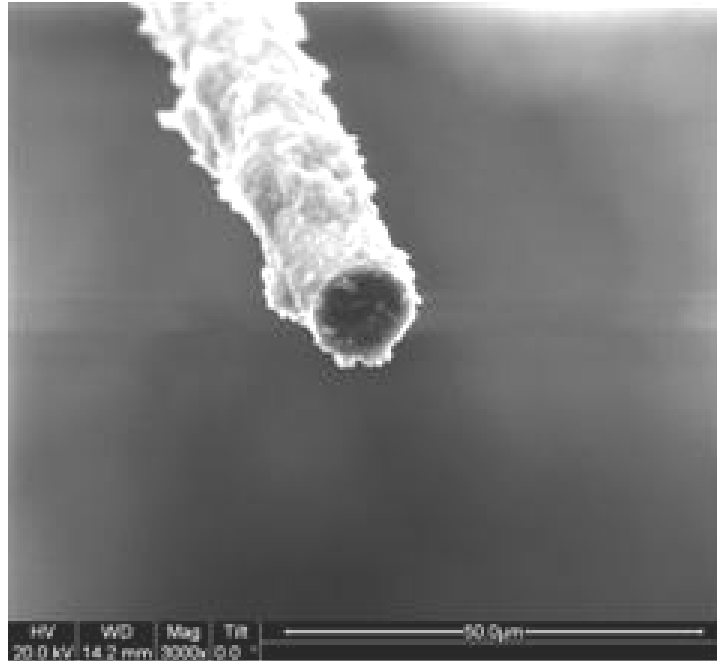


Figure 662. SEM micrograph of the fracture surface of the N720/AM specimen subjected to monotonic tensile test to failure at 1200°C in laboratory air.

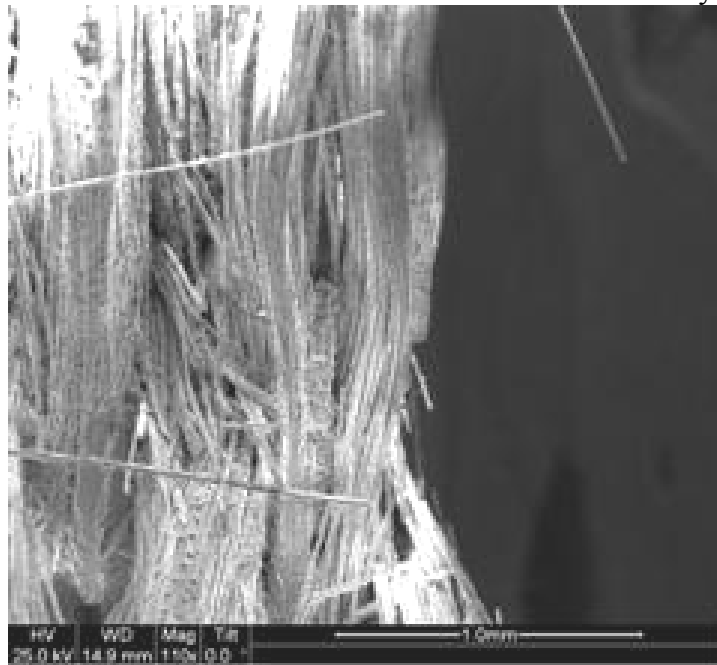


Figure 663. SEM micrograph of the fracture surface of the N720/AM specimen subjected to monotonic tensile test to failure at 1200°C in laboratory air.

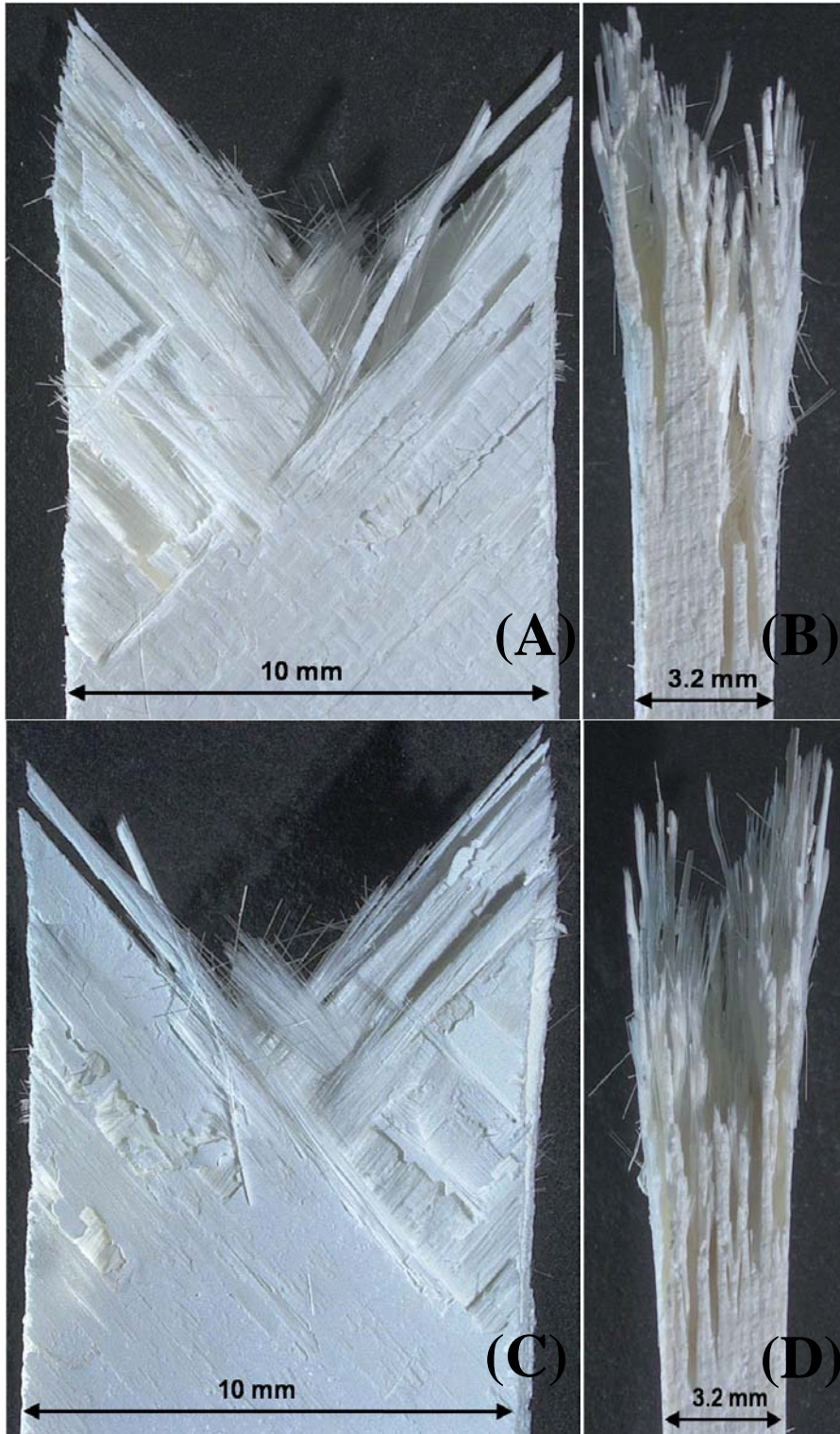


Figure 664. Fracture surface of the N720/AM specimen subjected to tensile test to failure following 100 h at 13 MPa at 1200°C in laboratory air.(a)-(c):front view,(b)-(d):side view

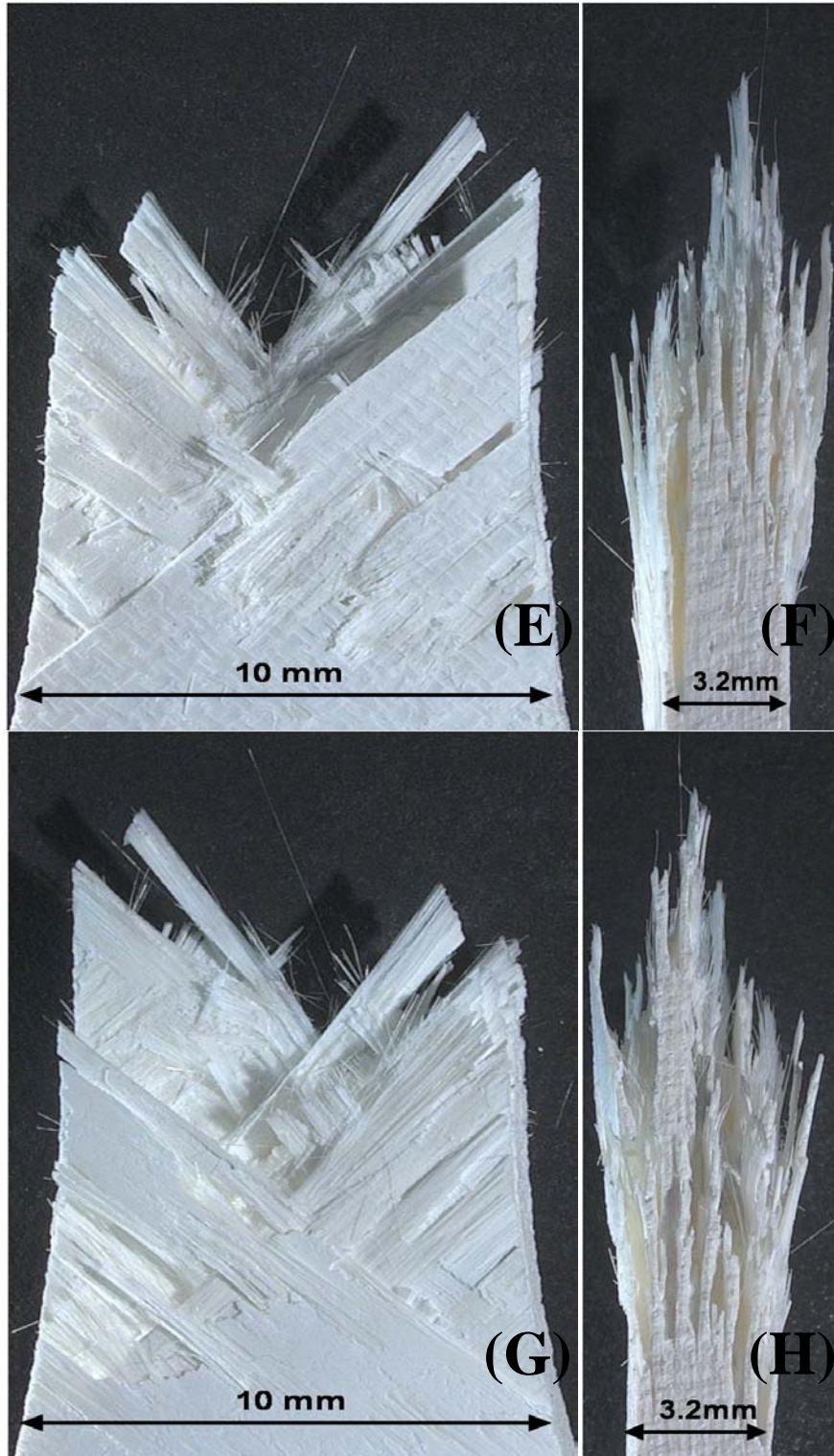


Figure 665. Fracture surface of the N720/AM specimen subjected to tensile test to failure following 100 h at 13 MPa at 1200°C in laboratory air.(e)-(g):front view,(f)-(h):side view

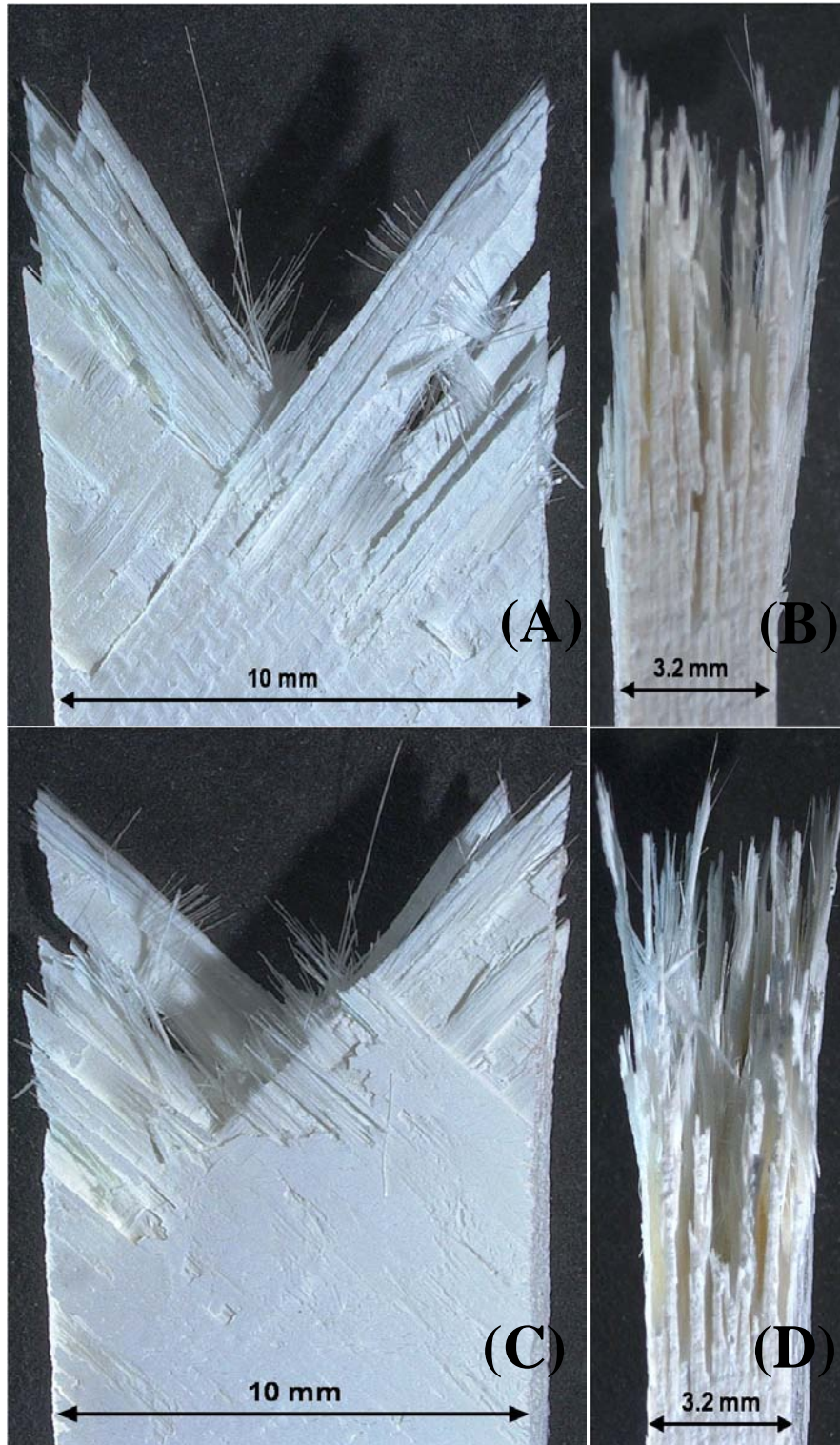


Figure 666. Fracture surface of the N720/AM specimen subjected to tensile test to failure following 100 h at 30 MPa at 1200°C in laboratory air.(a)-(c):front view,(b)-(d):side view

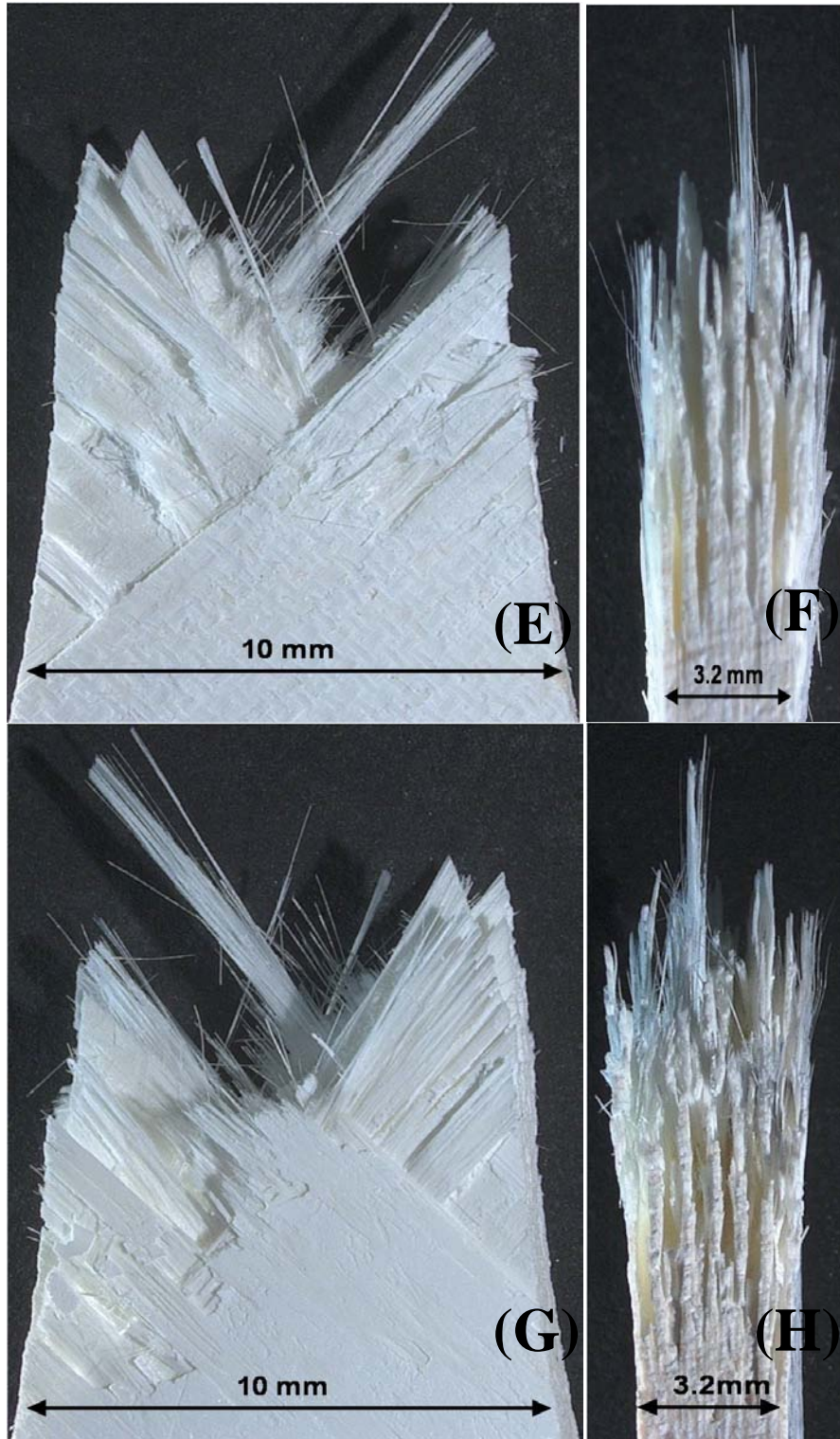


Figure 667. Fracture surface of the N720/AM specimen subjected to tensile test to failure following 100 h at 30 MPa at 1200°C in laboratory air.(e)-(g):front view,(f)-(h):side view

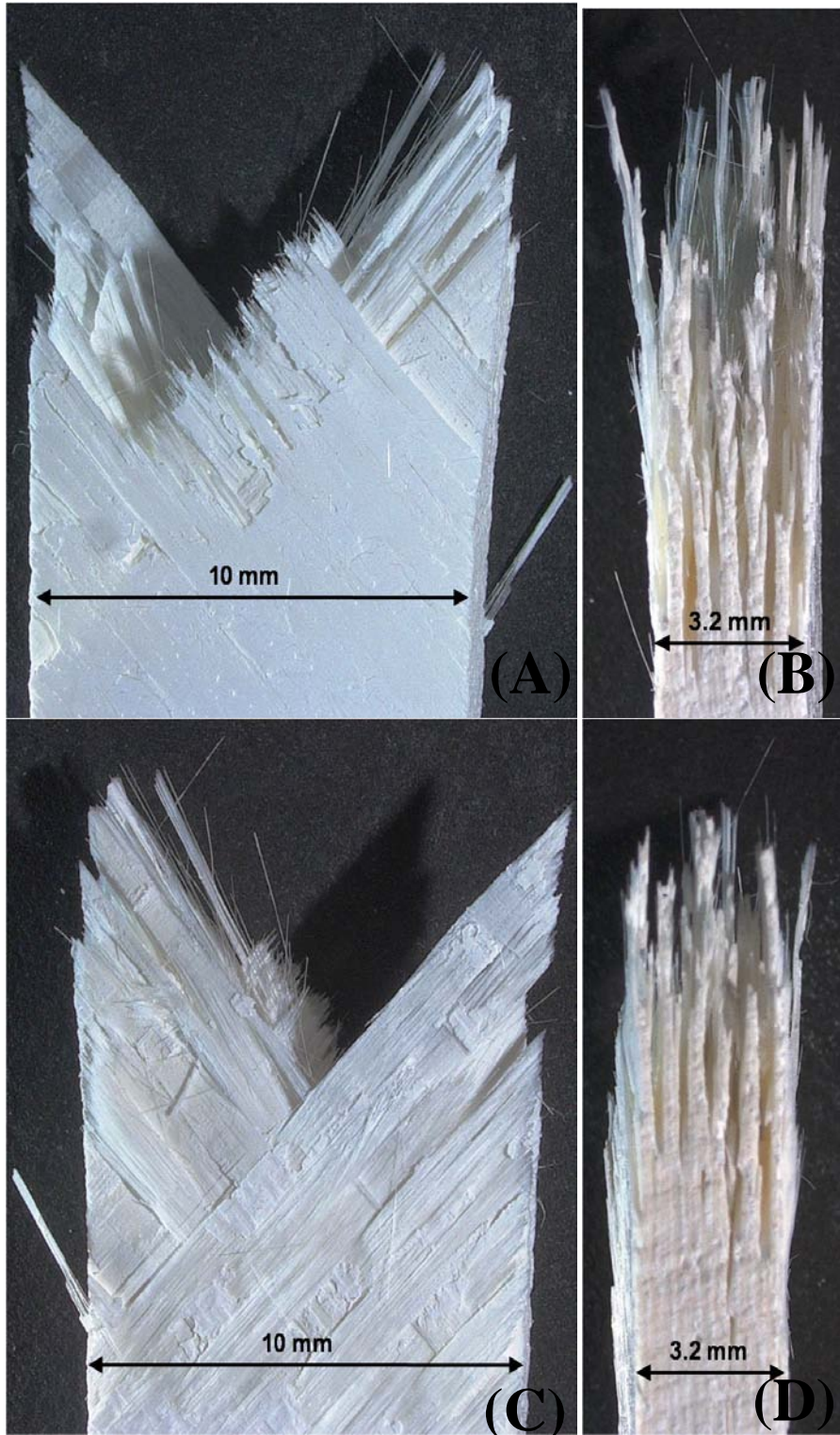


Figure 668. Fracture surface of the N720/AM specimen subjected to tensile test to failure following 100 h at 32 MPa at 1200°C in laboratory air.(a)-(c):front view,(b)-(d):side view

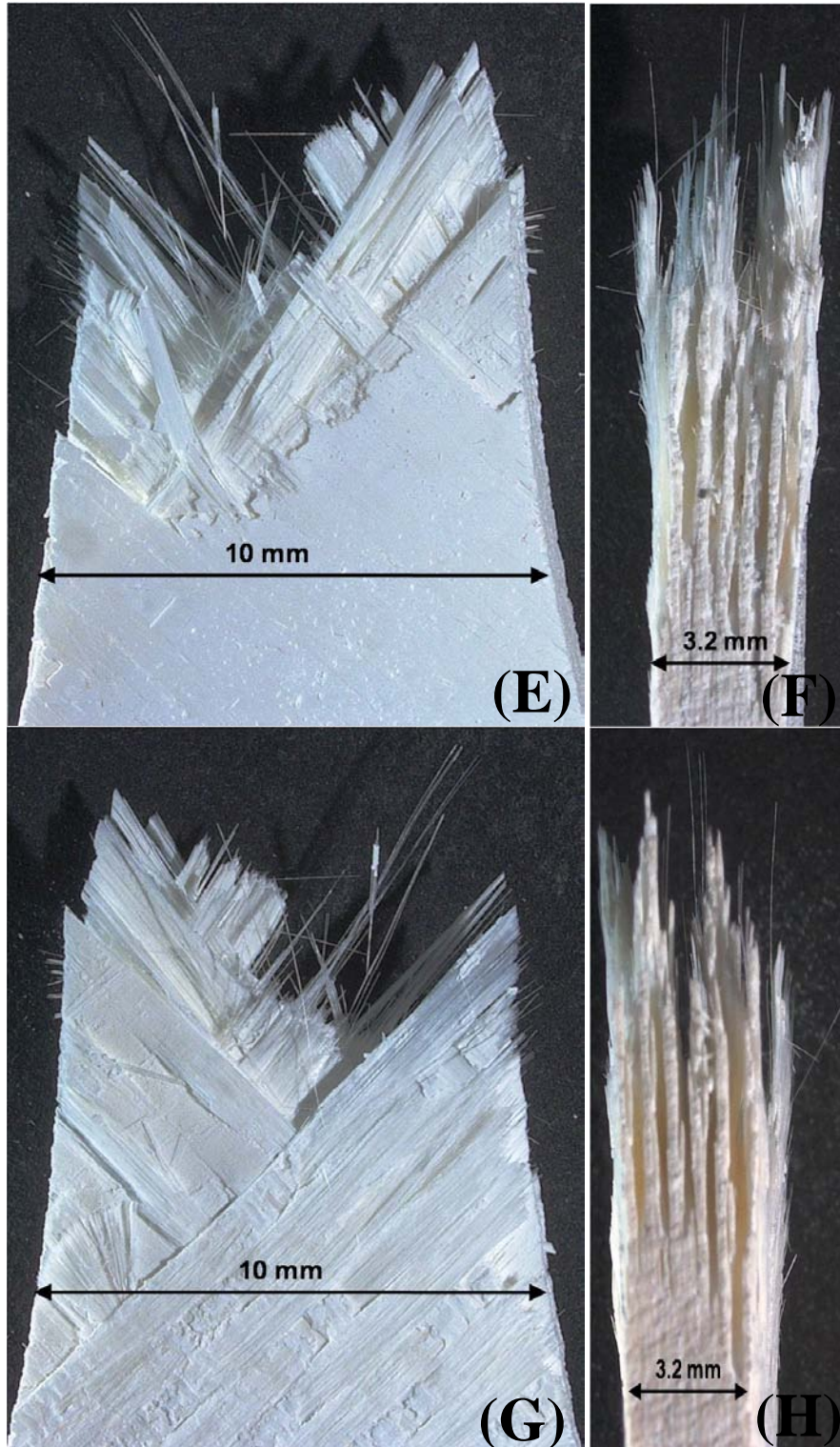


Figure 669. Fracture surface of the N720/AM specimen subjected to tensile test to failure following 100 h at 32 MPa at 1200°C in laboratory air.(e)-(g):front view,(f)-(h):side view

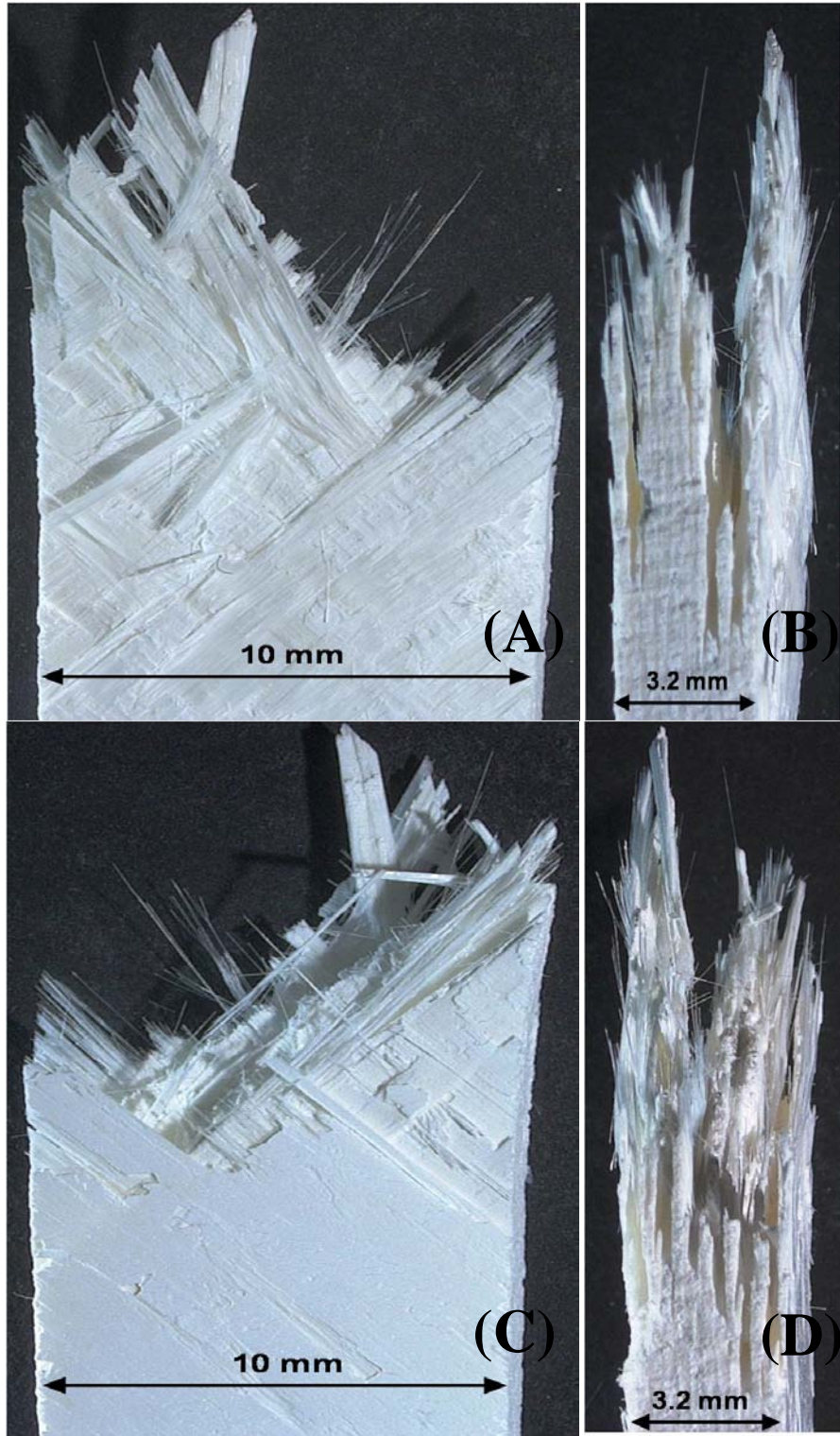


Figure 670. Fracture surface of the N720/AM specimen subjected to tensile test to failure following 100 h at 13 MPa at 1200°C in steam. (a)-(c): front view, (b)-(d): side view

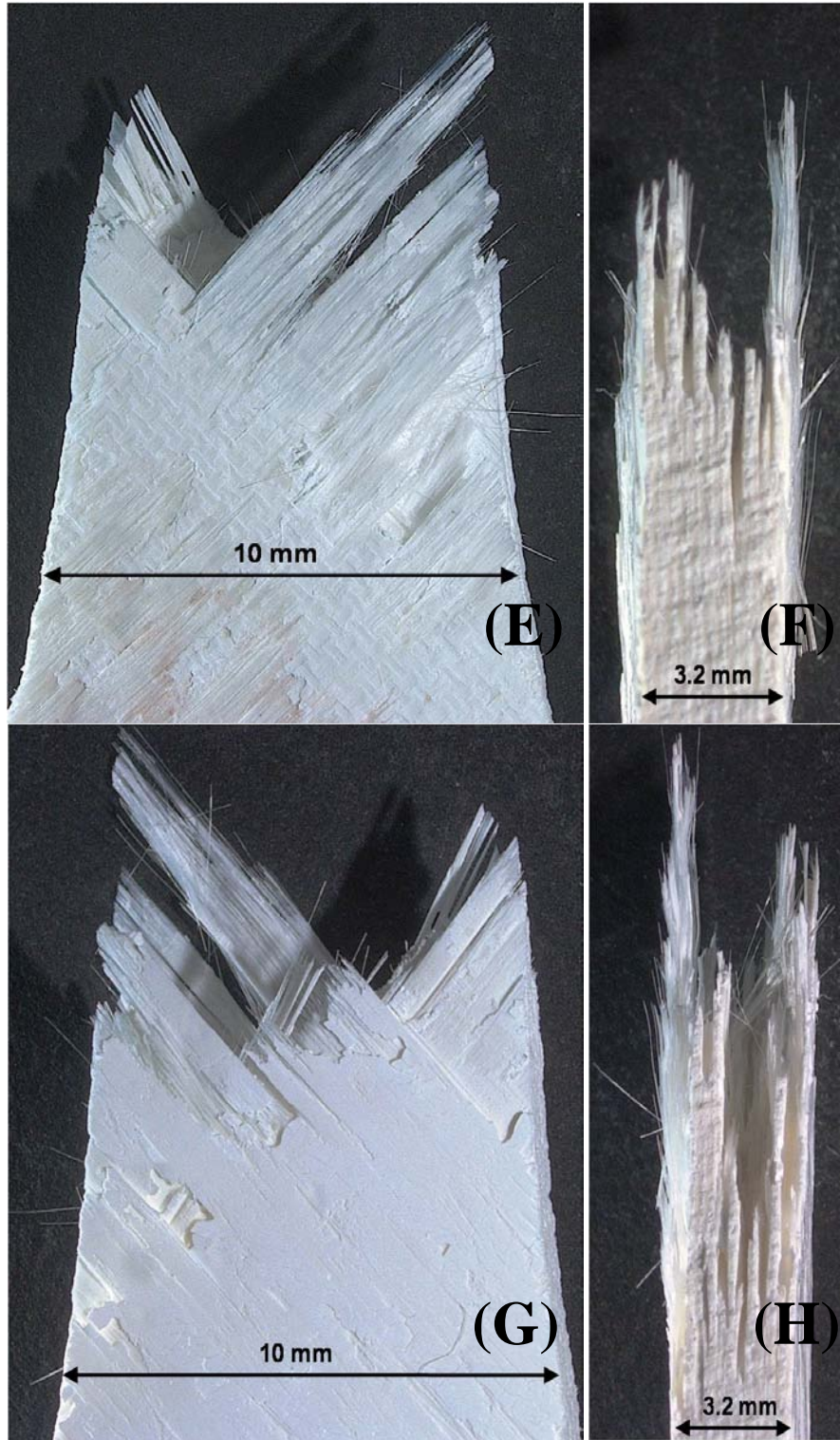


Figure 671. Fracture surface of the N720/AM specimen subjected to tensile test to failure following 100 h at 13 MPa at 1200°C in steam. (e)-(g): front view, (f)-(h): side view

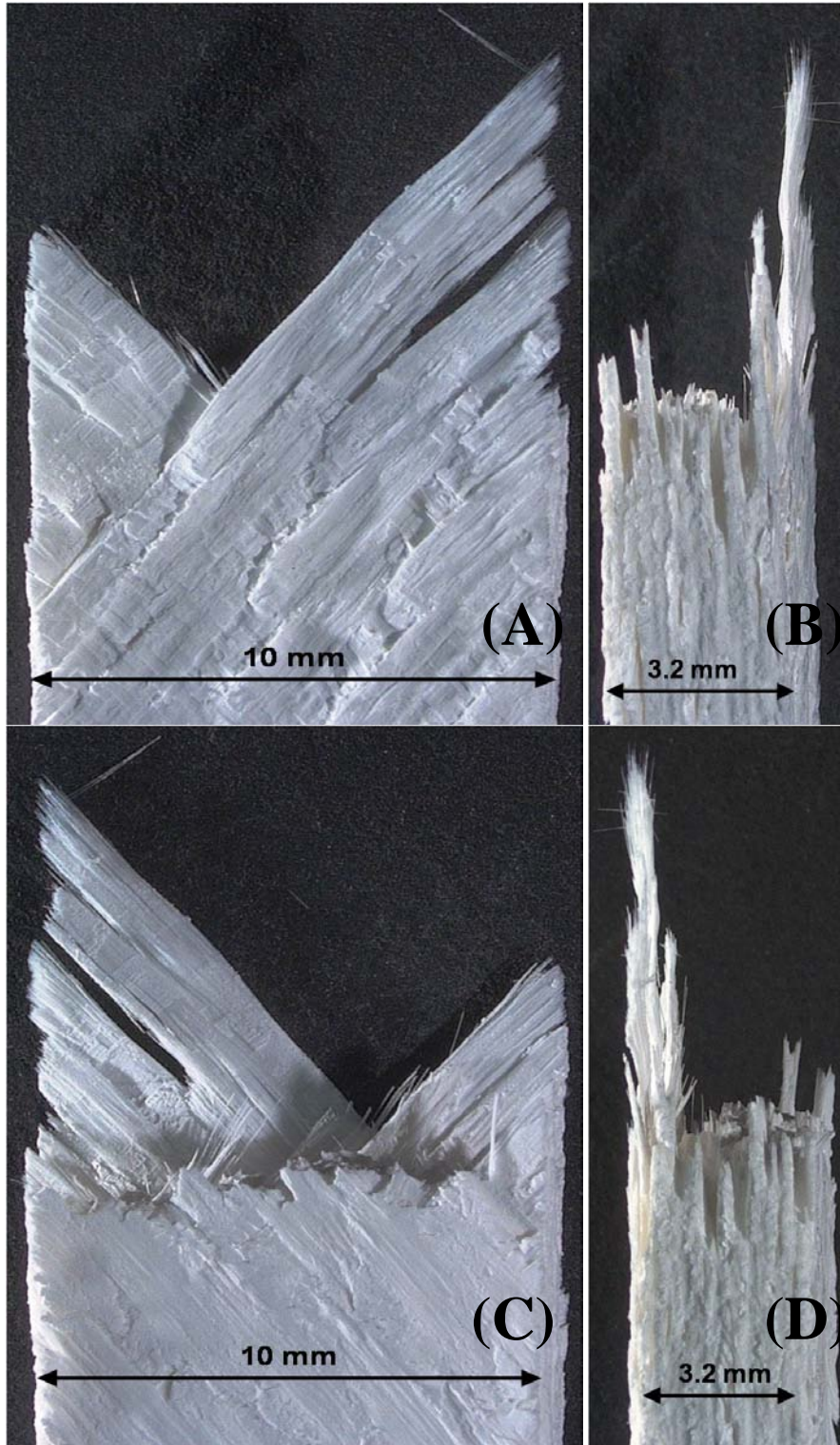


Figure 672. Fracture surface of the N720/AM specimen subjected to tensile test to failure following 100 h at 20 MPa at 1200°C in steam. (a)-(c): front view, (b)-(d): side view

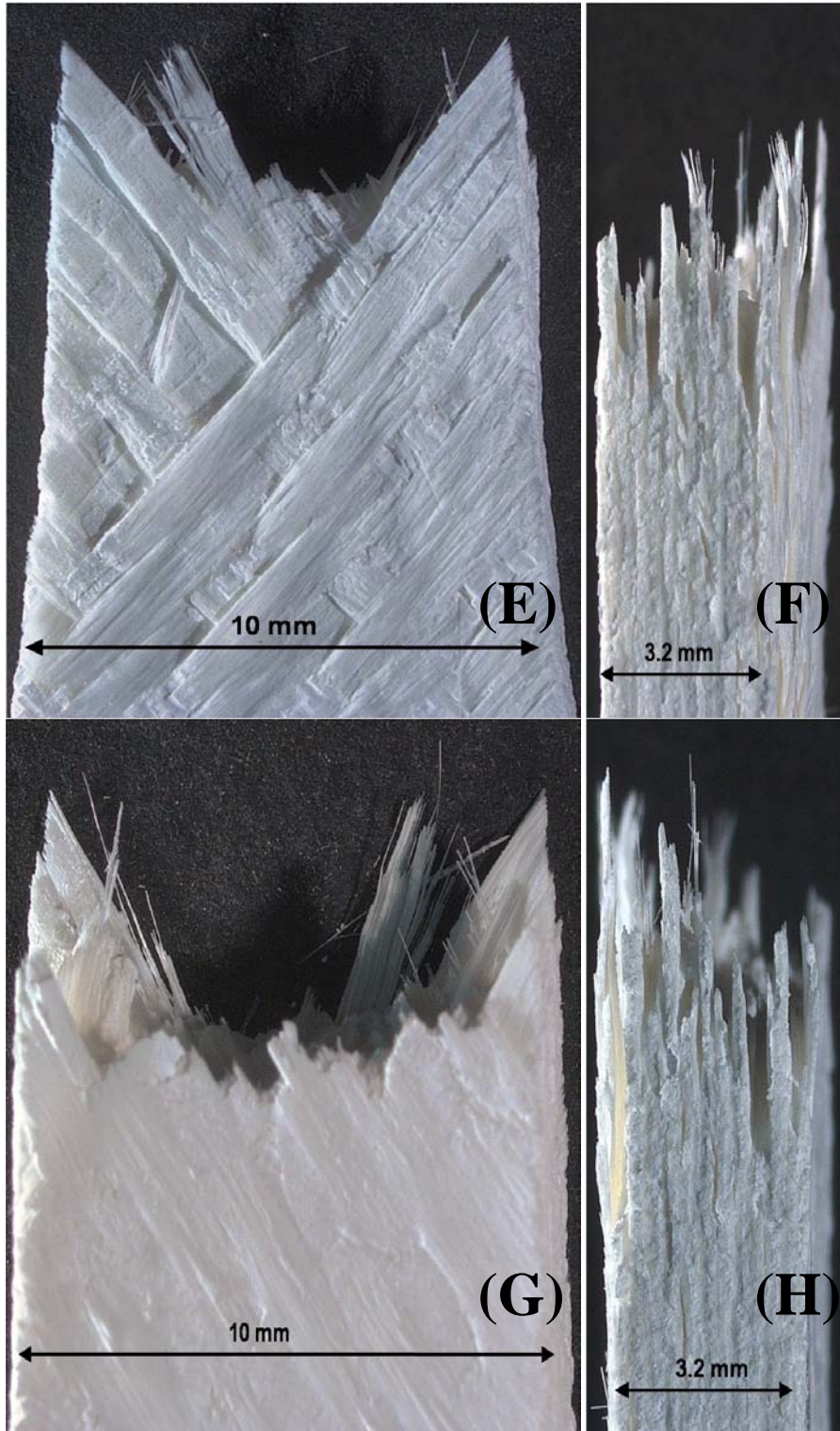


Figure 673. Fracture surface of the N720/AM specimen subjected to tensile test to failure following 100 h at 20 MPa at 1200°C in steam. (e)-(g): front view, (f)-(h): side view

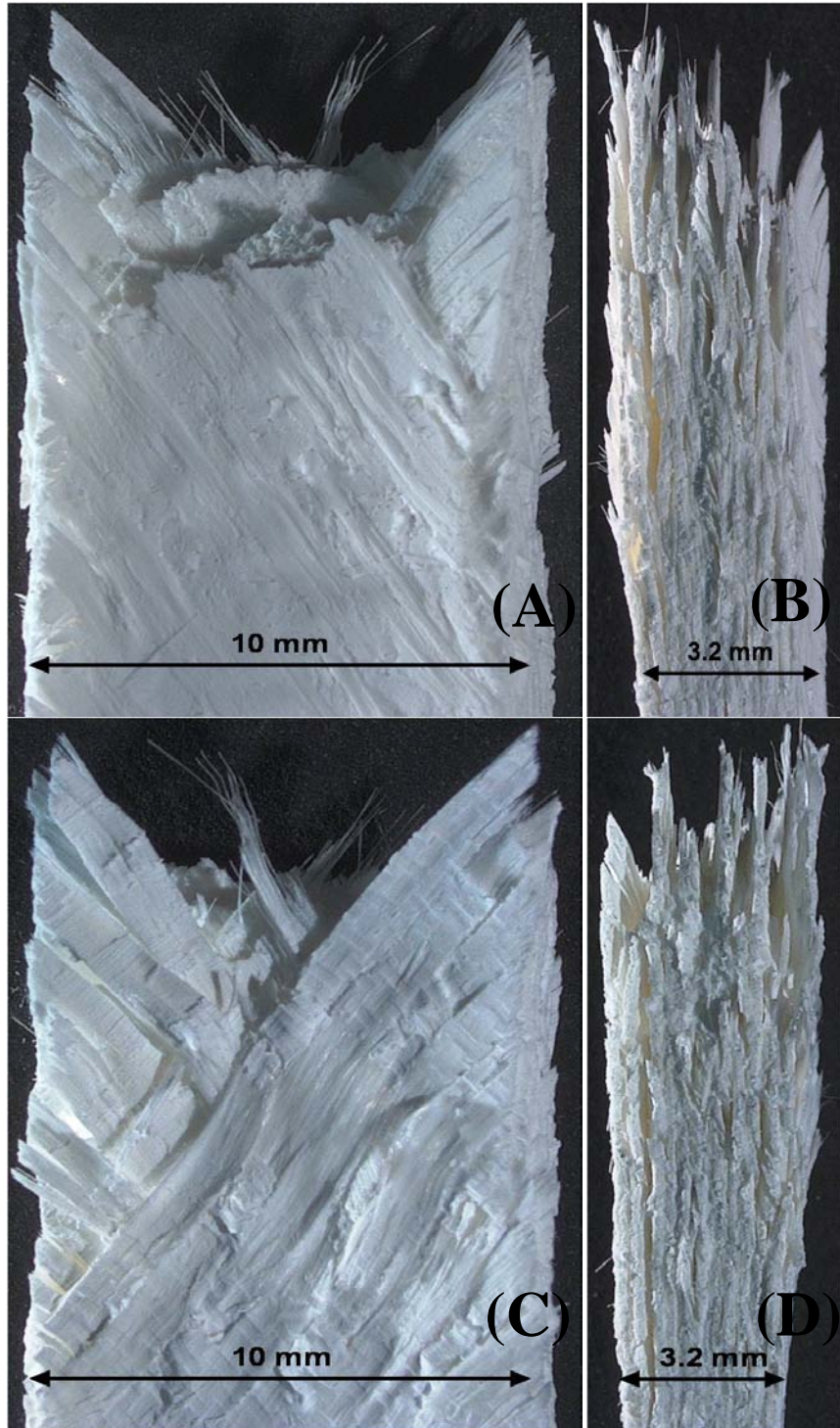


Figure 674. Fracture surface of the N720/AM specimen with  $\pm 45^\circ$  fiber orientation obtained in creep test conducted at 26 MPa at  $1200^\circ\text{C}$  in steam. Creep lifetime  $t_f = 99.4$  h. (a)-(c): front view, (b)-(d): side view

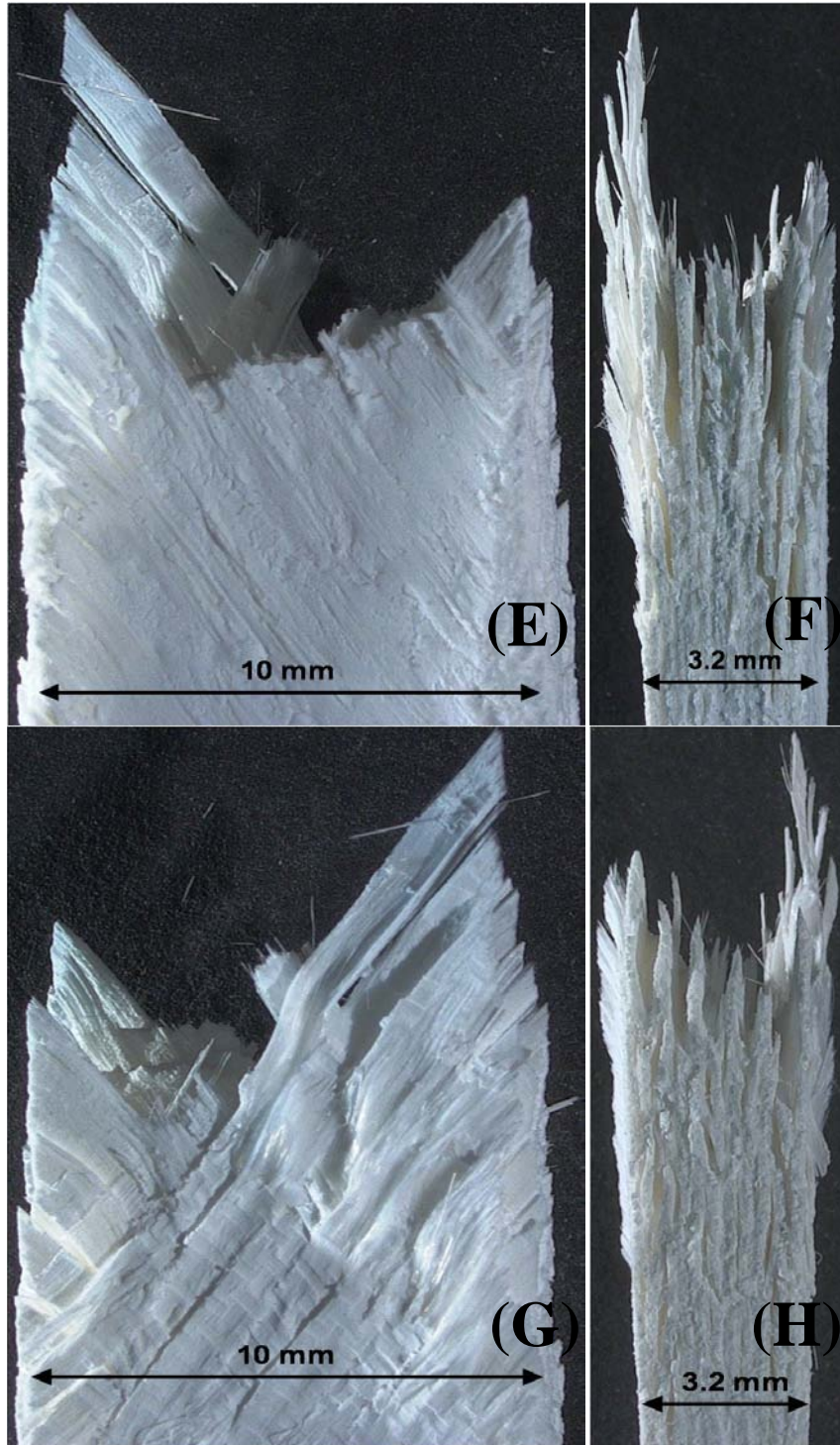


Figure 675. Fracture surface of the N720/AM specimen with  $\pm 45^\circ$  fiber orientation obtained in creep test conducted at 26 MPa at  $1200^\circ\text{C}$  in steam. Creep lifetime  $t_f = 99.4$  h.  
(e)-(g): front view, (f)-(h): side view

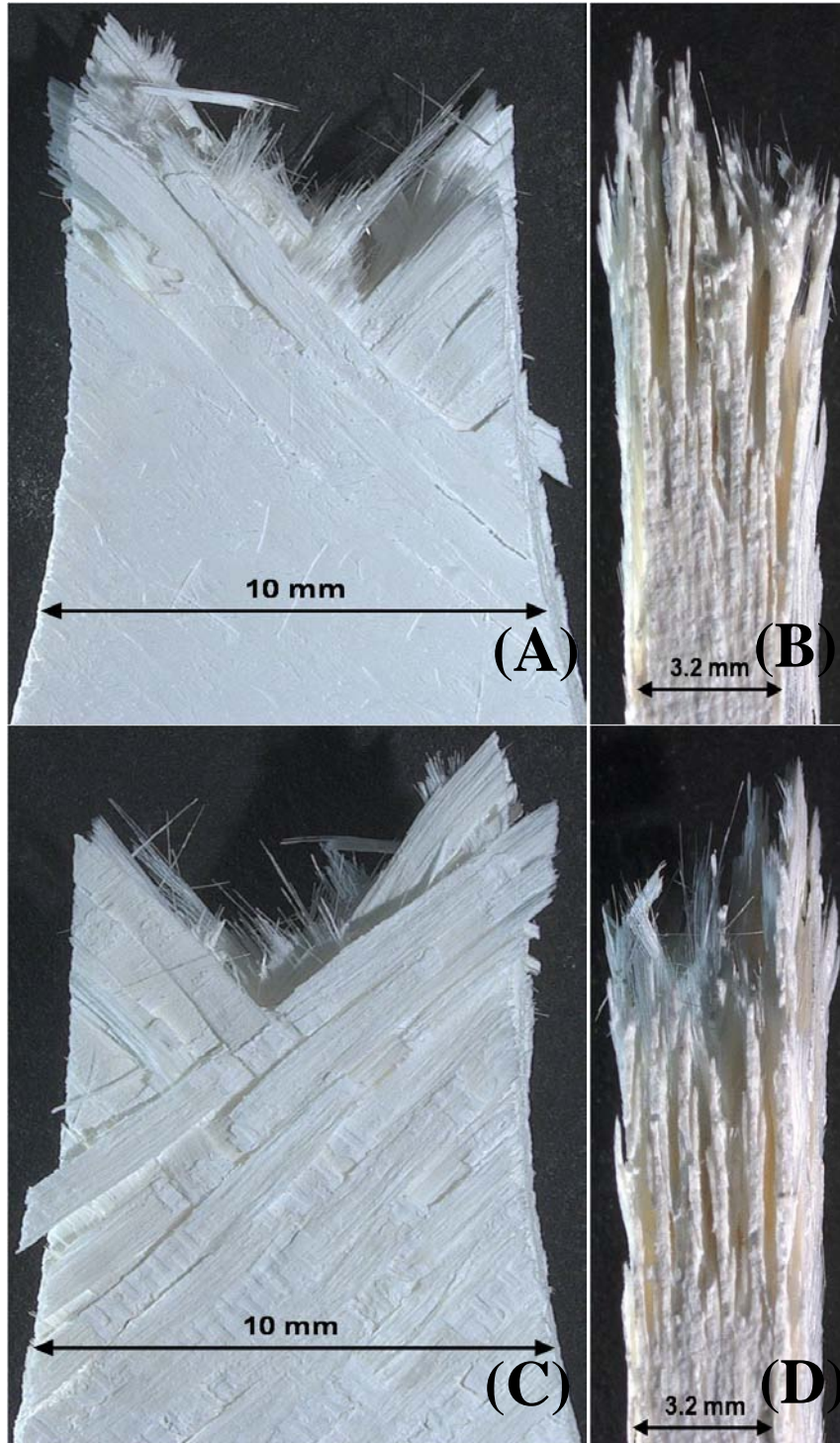


Figure 676. Fracture surface of the N720/AM specimen with  $\pm 45^\circ$  fiber orientation obtained in creep test conducted at 30 MPa at  $1200^\circ\text{C}$  in steam. Creep lifetime  $t_f = 1.08$  h. (a)-(c): front view, (b)-(d): side view

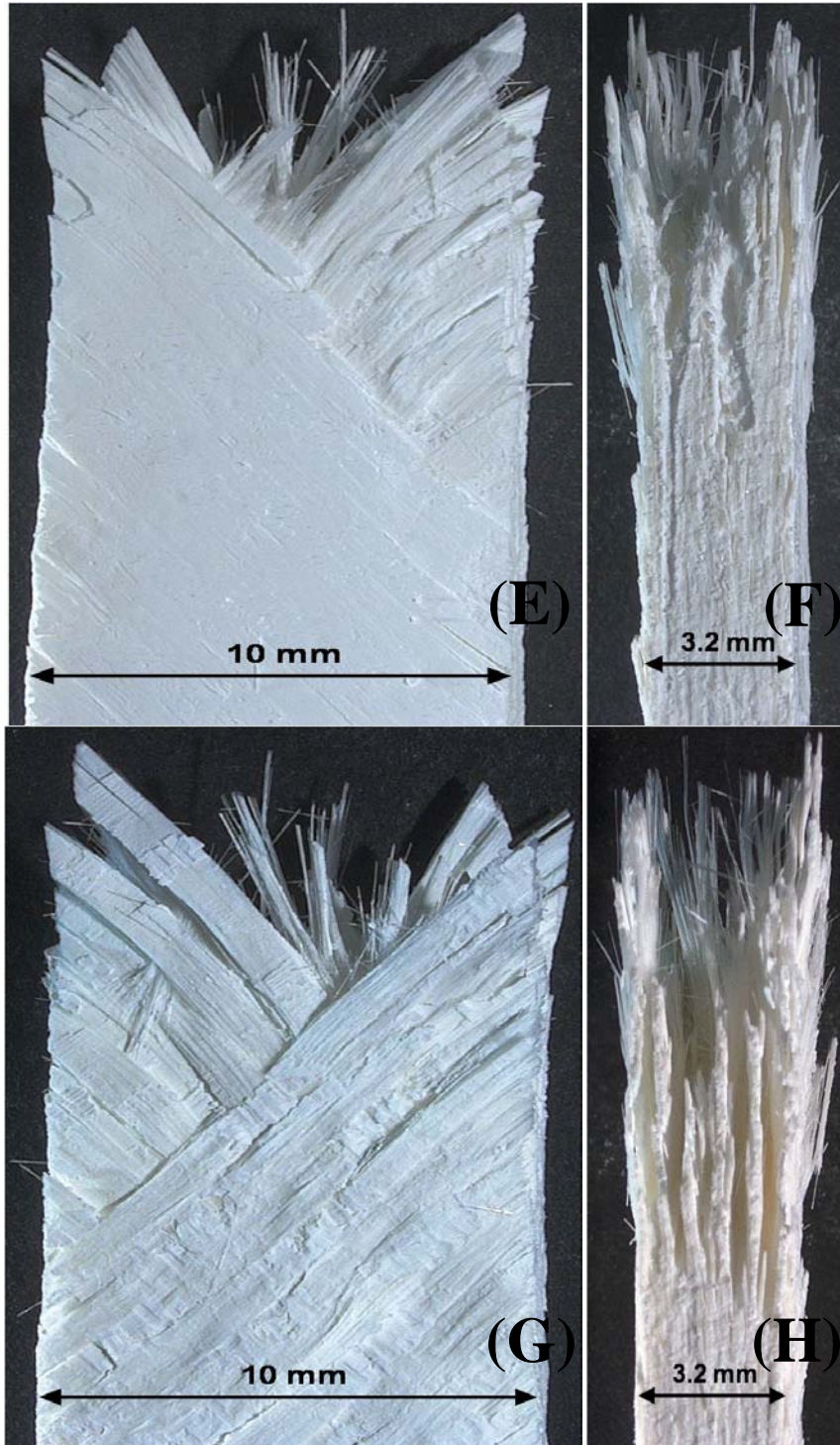


Figure 677. Fracture surface of the N720/AM specimen with  $\pm 45^\circ$  fiber orientation obtained in creep test conducted at 30 MPa at  $1200^\circ\text{C}$  in steam. Creep lifetime  $t_f = 1.08$  h. (e)-(g): front view, (f)-(h): side view

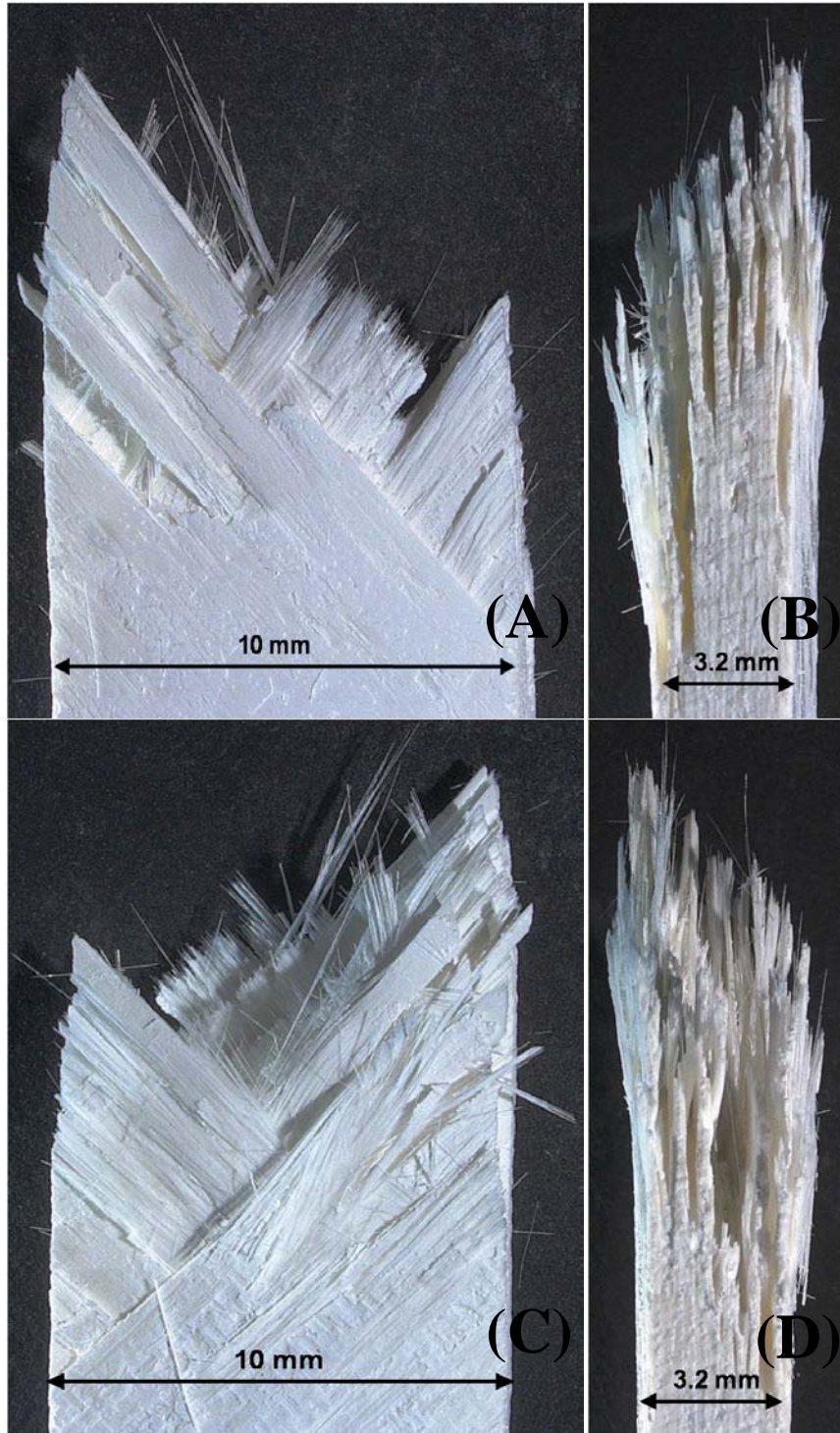


Figure 678. Fracture surface of the N720/AM specimen with  $\pm 45^\circ$  fiber orientation obtained in creep test conducted at 32 MPa at  $1200^\circ\text{C}$  in steam. Creep lifetime  $t_f = 0.02$  h. (a)-(c): front view, (b)-(d): side view

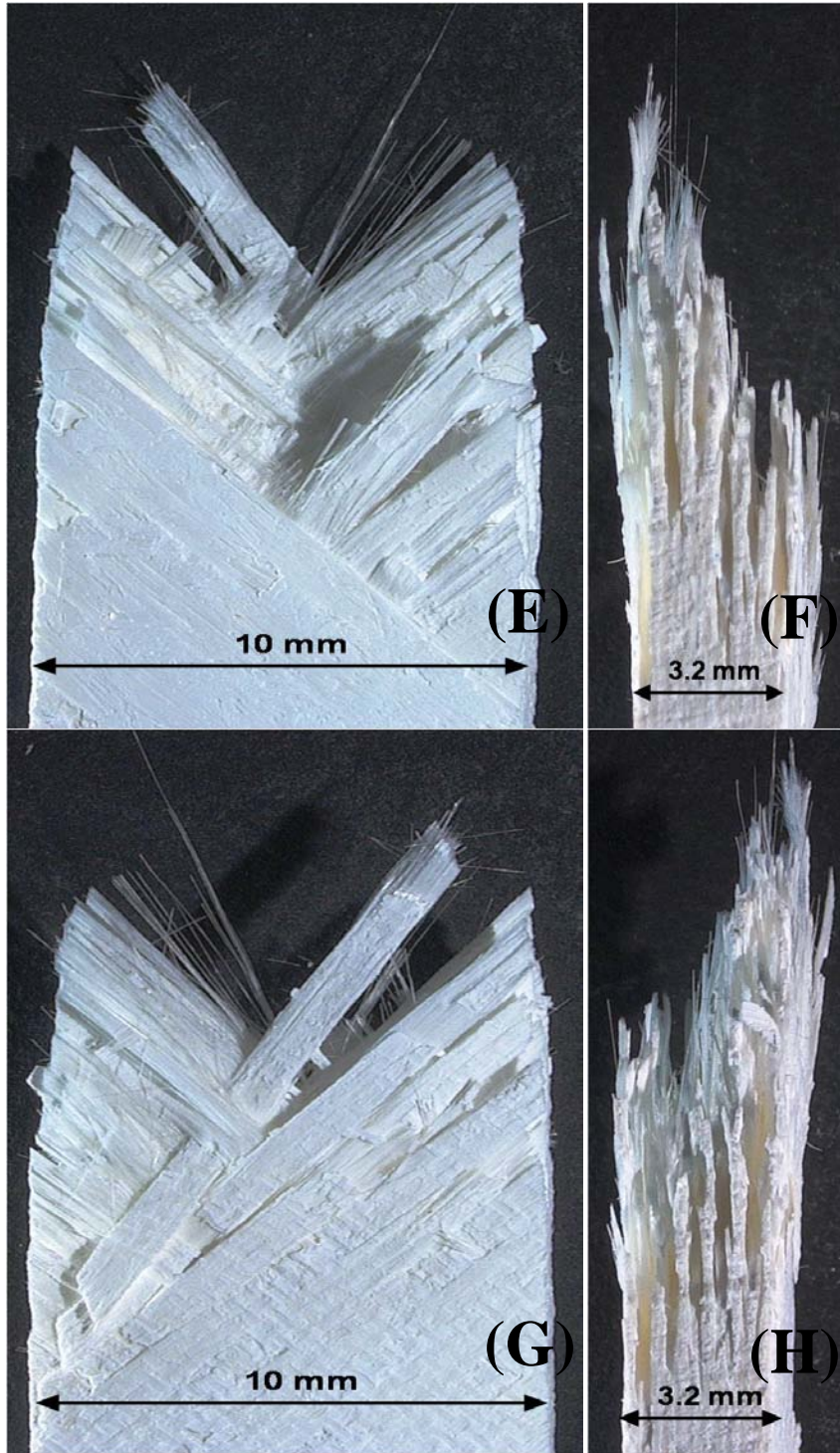


Figure 679. Fracture surface of the N720/AM specimen with  $\pm 45^\circ$  fiber orientation obtained in creep test conducted at 32 MPa at  $1200^\circ\text{C}$  in steam. Creep lifetime  $t_f = 0.02$  h.  
(e)-(g): front view, (f)-(h): side view

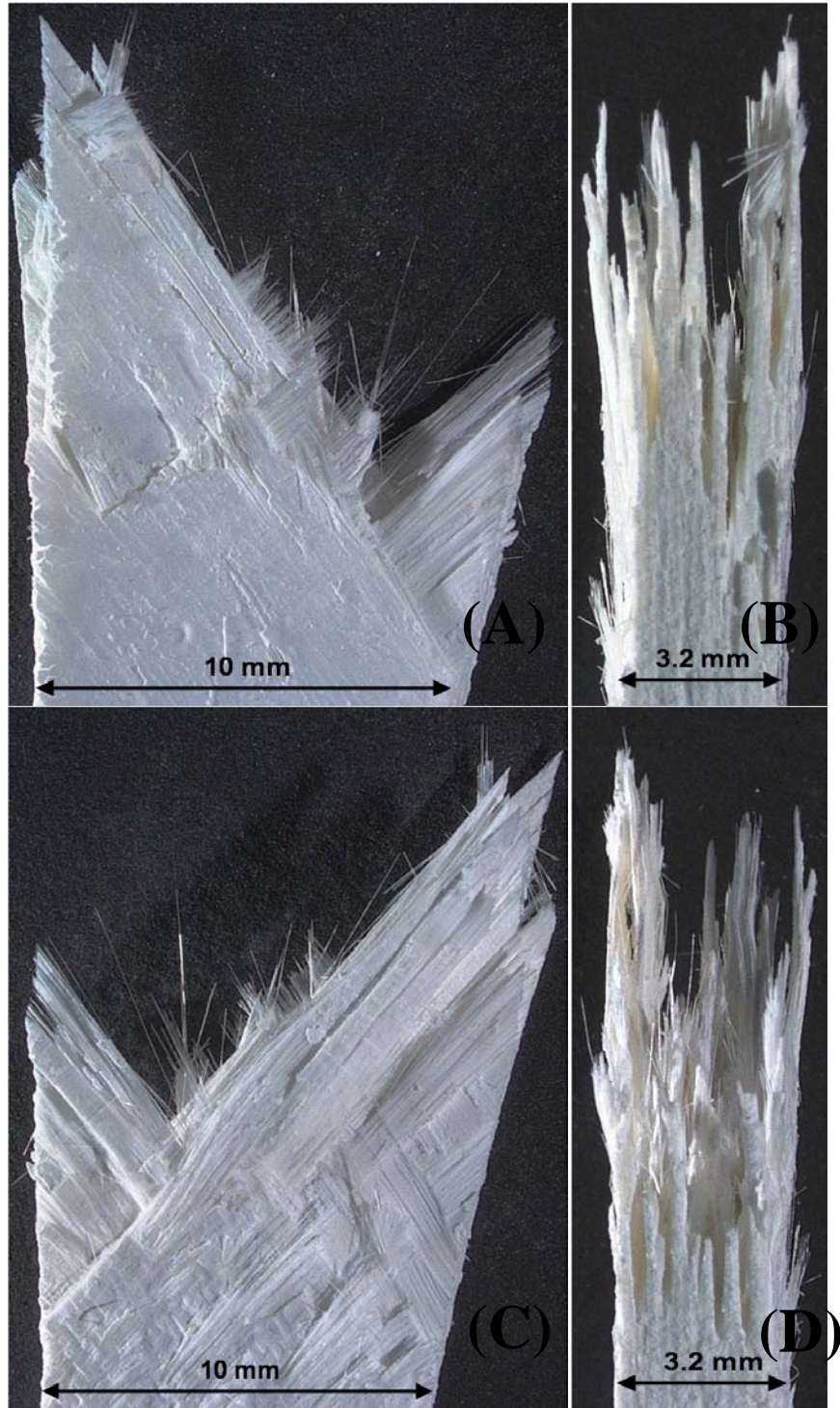


Figure 680. Fracture surface of the N720/AM specimen subjected to tensile test to failure following 100 h at 20 MPa at 1200°C in argon. (a)-(c): front view, (b)-(d): side view

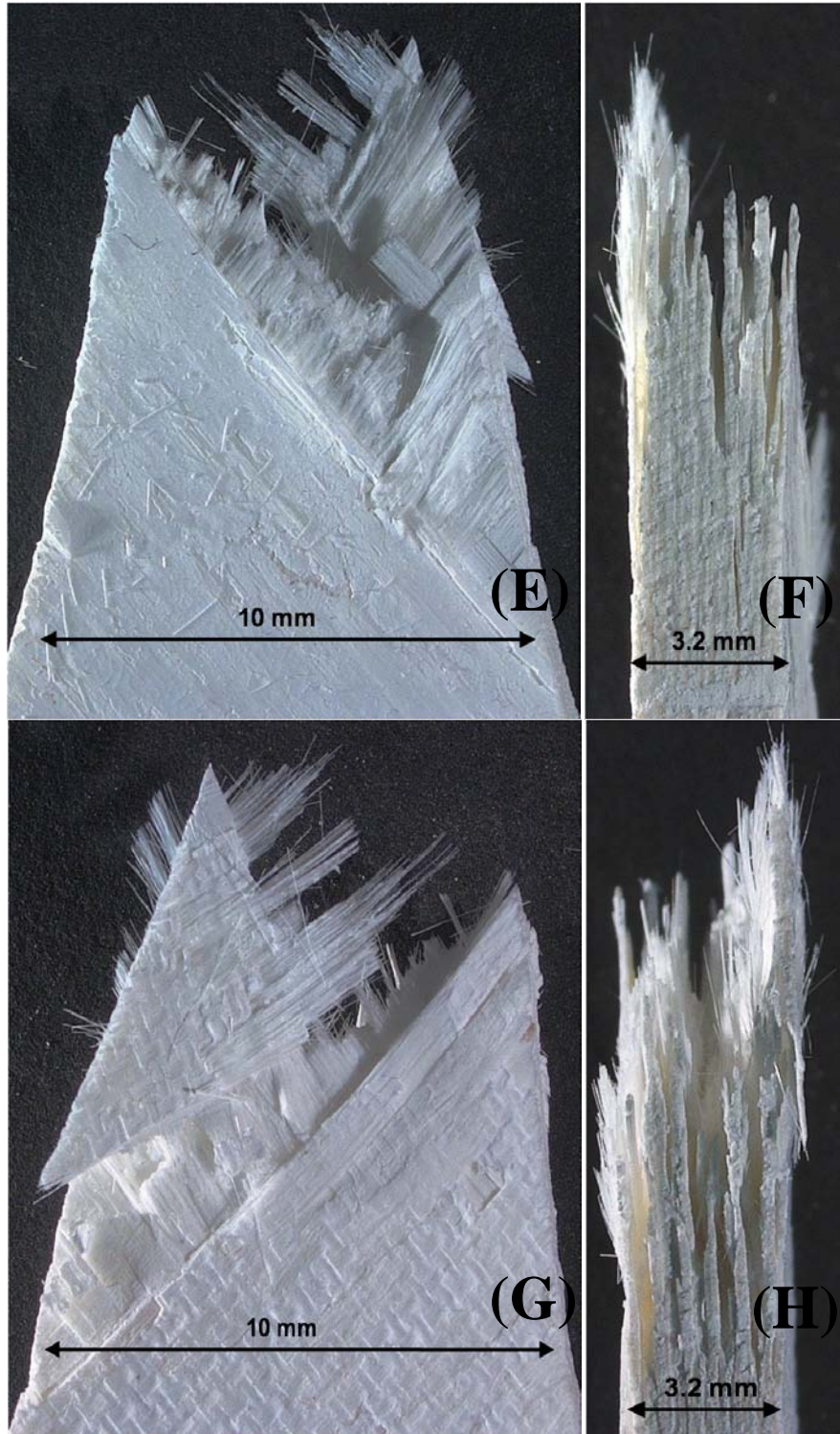


Figure 681. Fracture surface of the N720/AM specimen subjected to tensile test to failure following 100 h at 20 MPa at 1200°C in argon. (e)-(g): front view, (f)-(h): side view

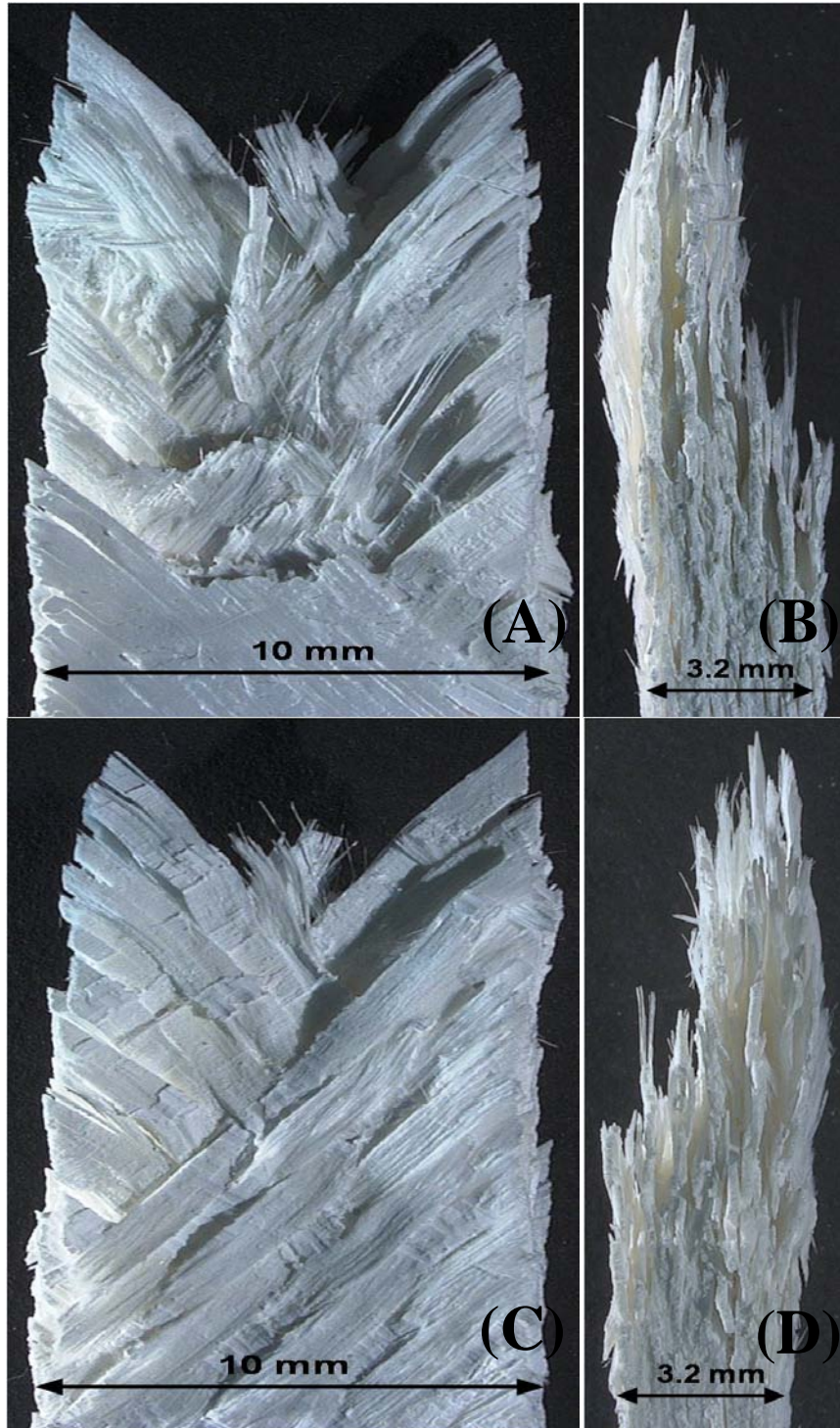


Figure 682. Fracture surface of the N720/AM specimen with  $\pm 45^\circ$  fiber orientation obtained in creep test conducted at 26 MPa at  $1200^\circ\text{C}$  in argon. Creep lifetime  $t_f = 76$  h. (a)-(c): front view, (b)-(d): side view

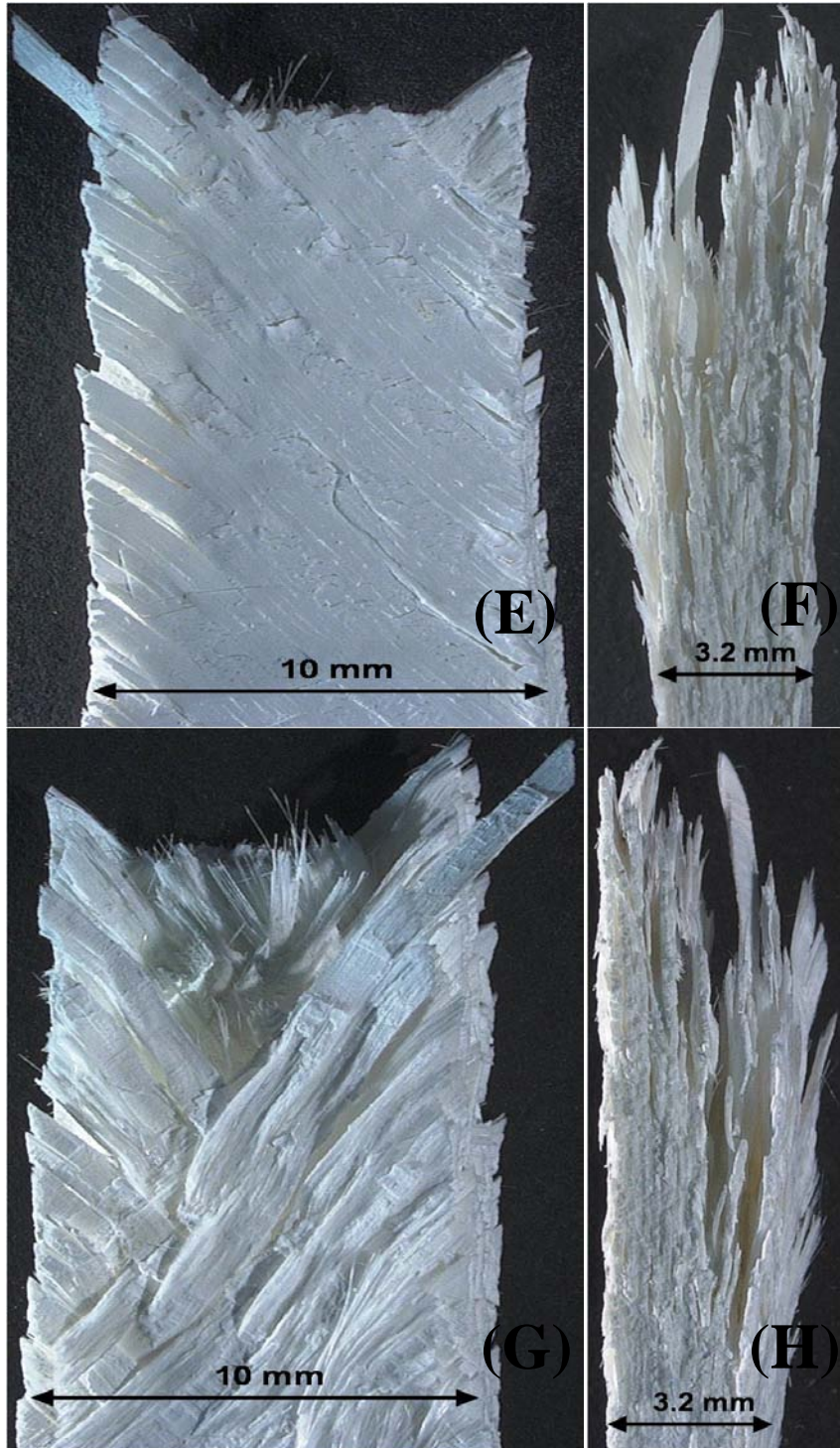


Figure 683. Fracture surface of the N720/AM specimen with  $\pm 45^\circ$  fiber orientation obtained in creep test conducted at 26 MPa at 1200°C in argon. Creep lifetime  $t_f = 76$  h.  
(e)-(g): front view, (f)-(h): side view

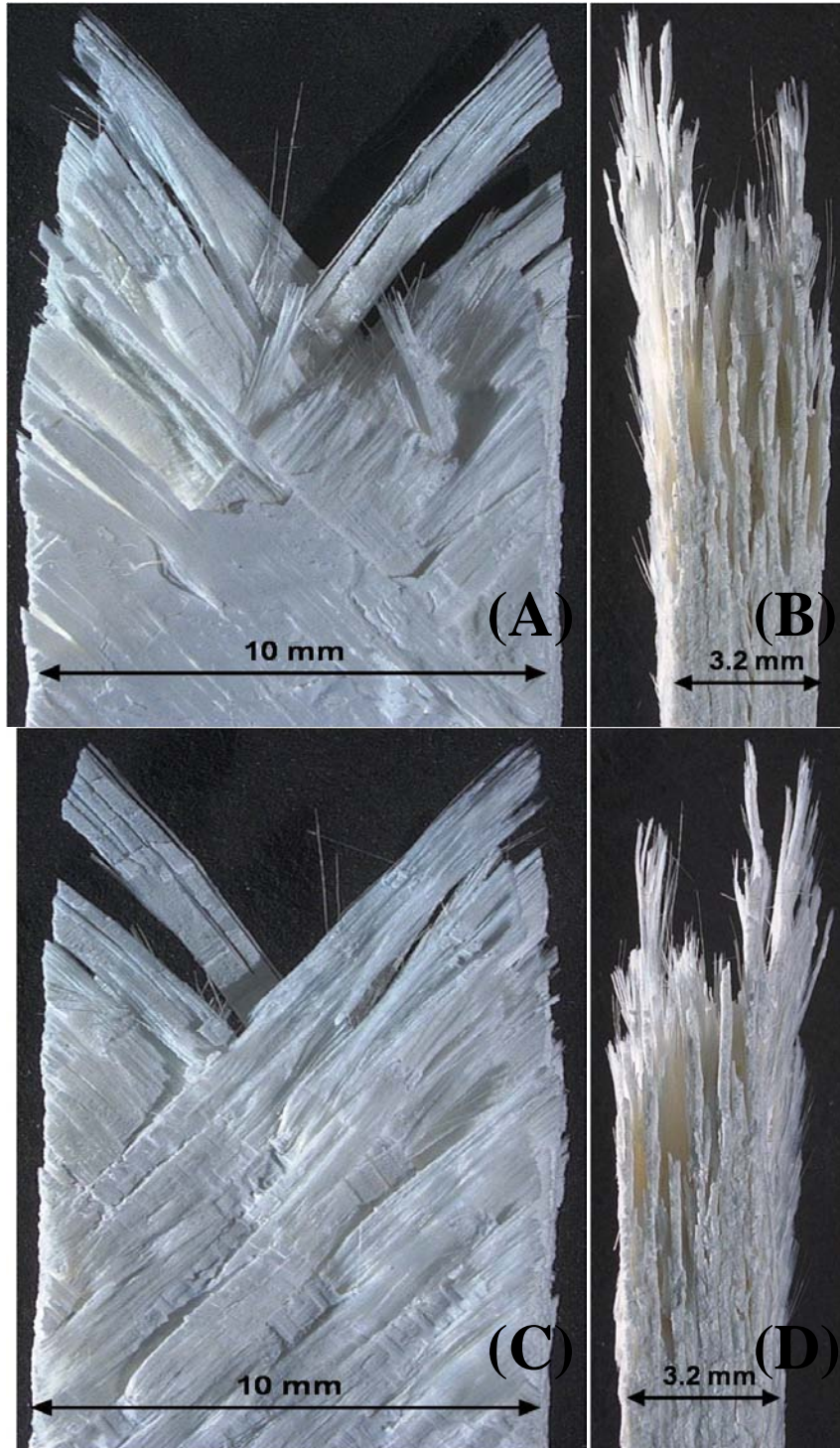


Figure 684. Fracture surface of the N720/AM specimen with  $\pm 45^\circ$  fiber orientation obtained in creep test conducted at 30 MPa at  $1200^\circ\text{C}$  in argon. Creep lifetime  $t_f = 3.42$  h. (a)-(c): front view, (b)-(d): side view

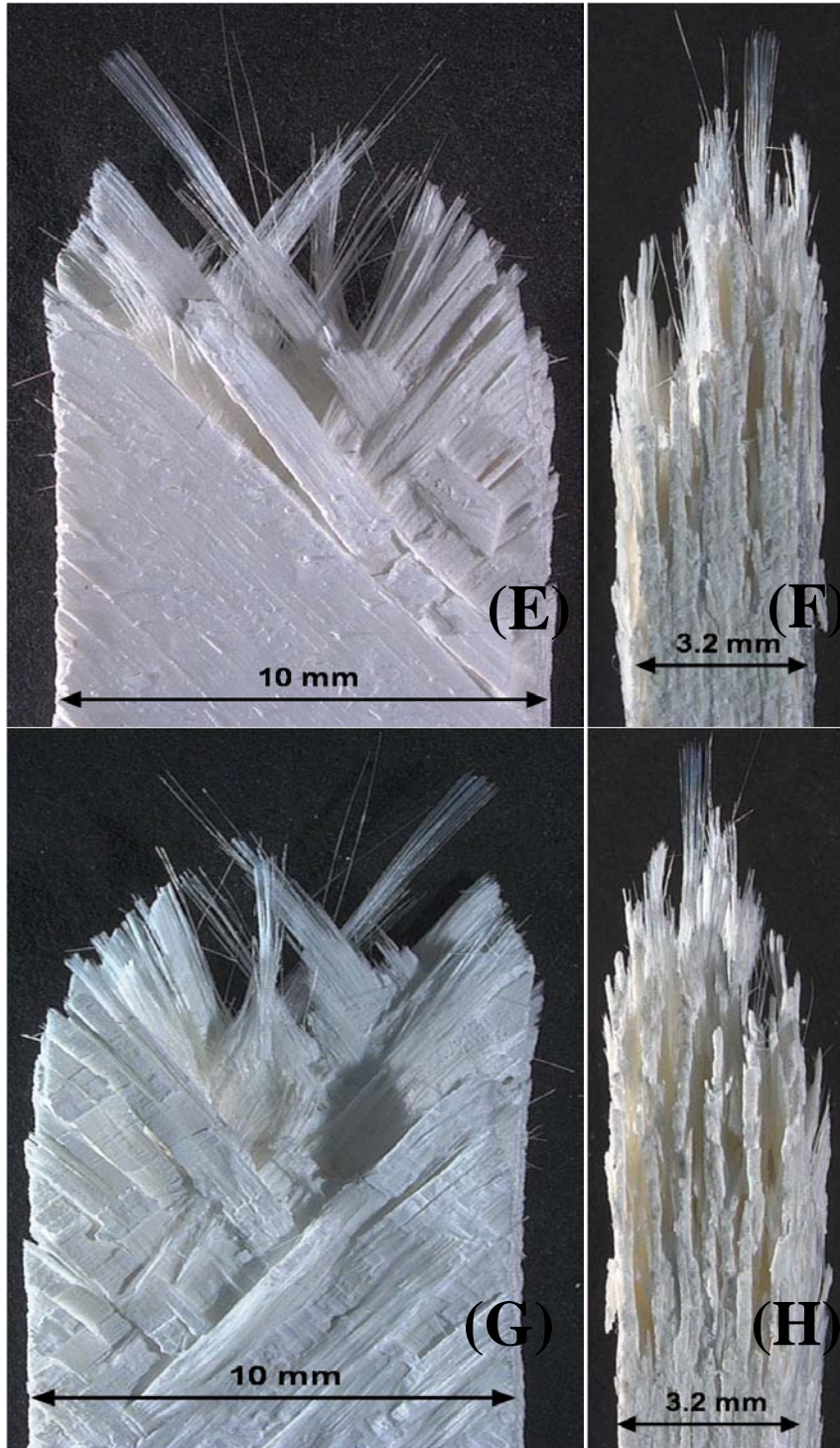


Figure 685. Fracture surface of the N720/AM specimen with  $\pm 45^\circ$  fiber orientation obtained in creep test conducted at 30 MPa at  $1200^\circ\text{C}$  in argon. Creep lifetime  $t_f = 3.42$  h.  
(e)-(g): front view, (f)-(h): side view

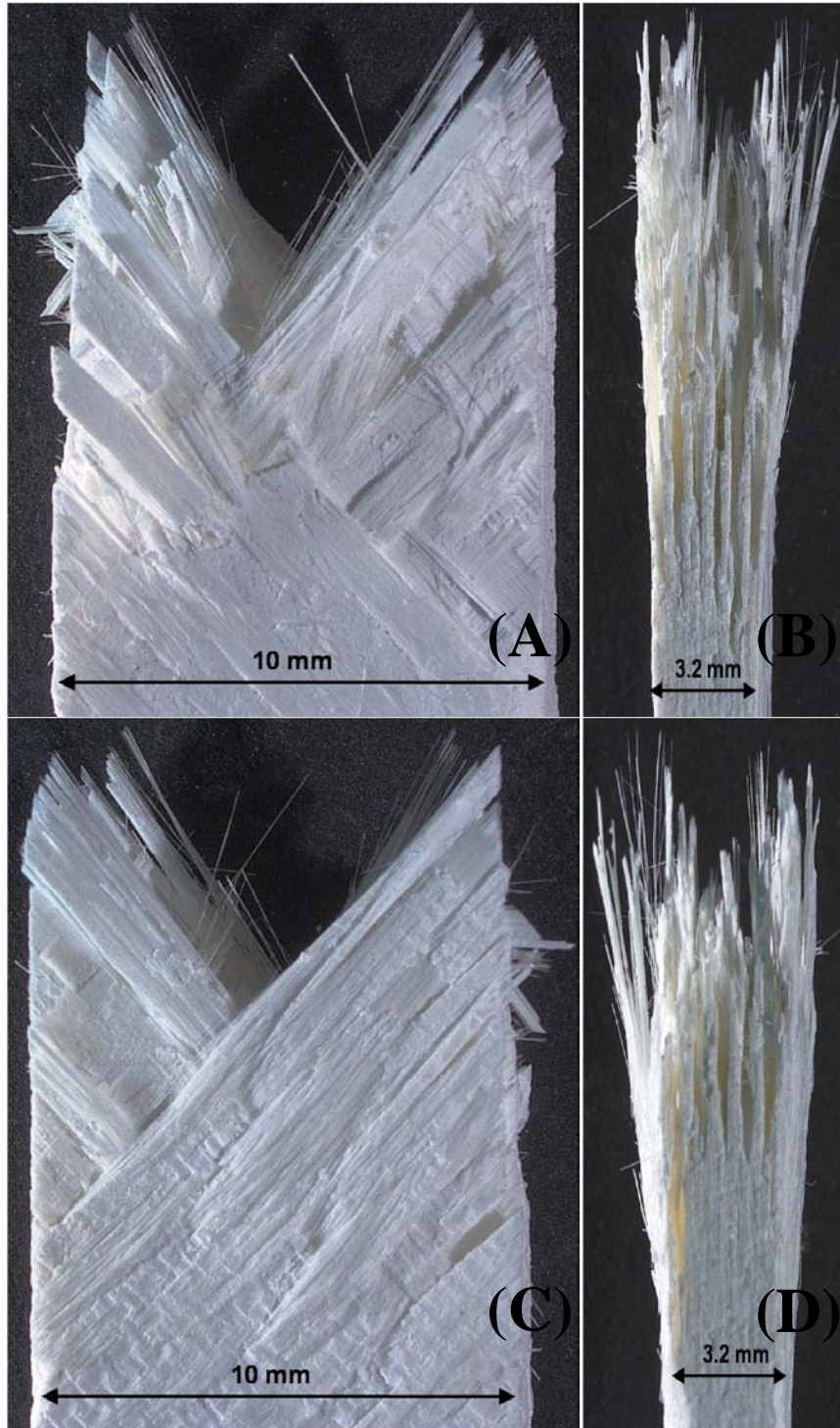


Figure 686. Fracture surface of the N720/AM specimen with  $\pm 45^\circ$  fiber orientation obtained in creep test conducted at 32 MPa at  $1200^\circ\text{C}$  in argon. Creep lifetime  $t_f = 0.08$  h. (a)-(c): front view, (b)-(d): side view

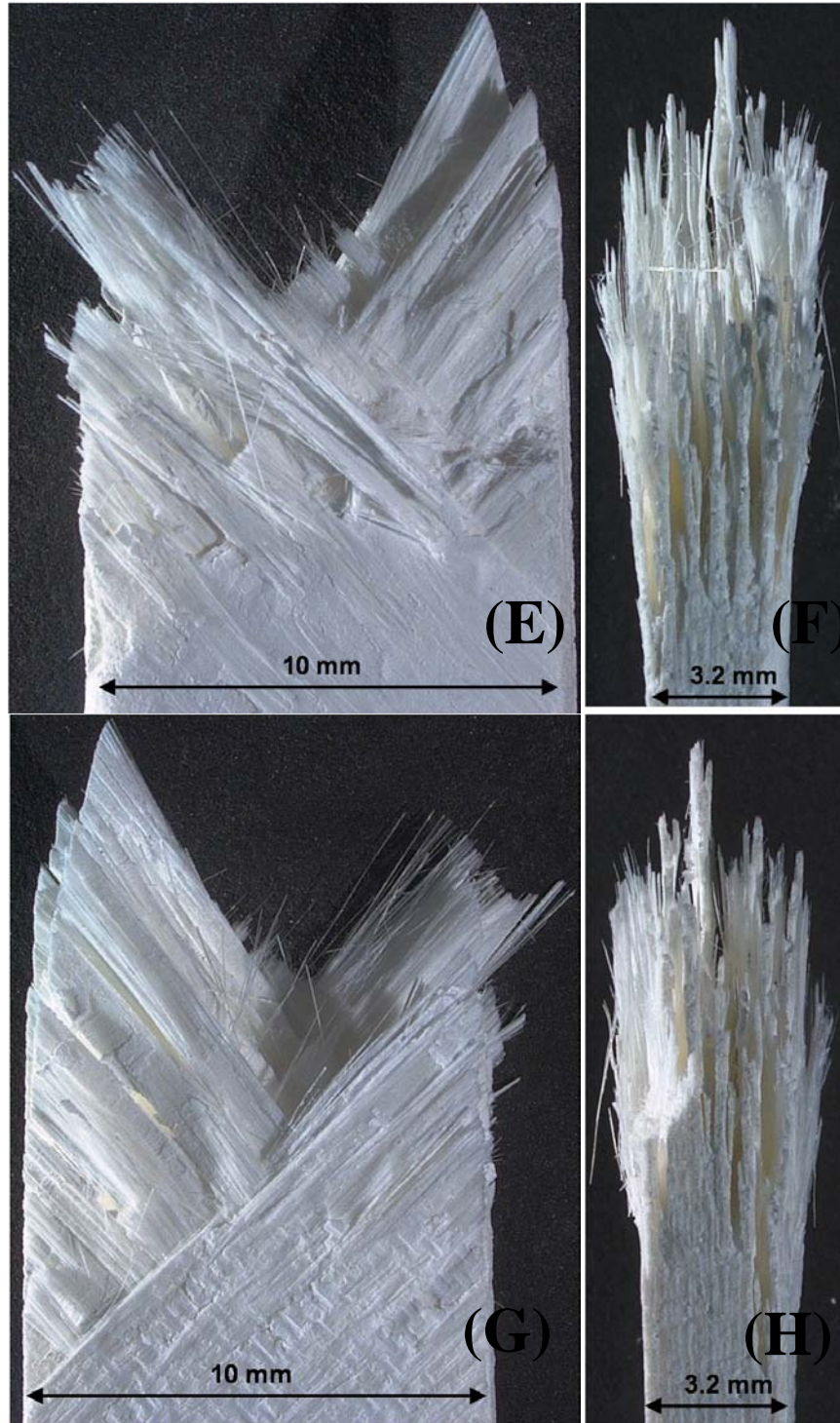


Figure 687. Fracture surface of the N720/AM specimen with  $\pm 45^\circ$  fiber orientation obtained in creep test conducted at 32 MPa at  $1200^\circ\text{C}$  in argon. Creep lifetime  $t_f = 0.08$  h.  
(e)-(g): front view, (f)-(h): side view

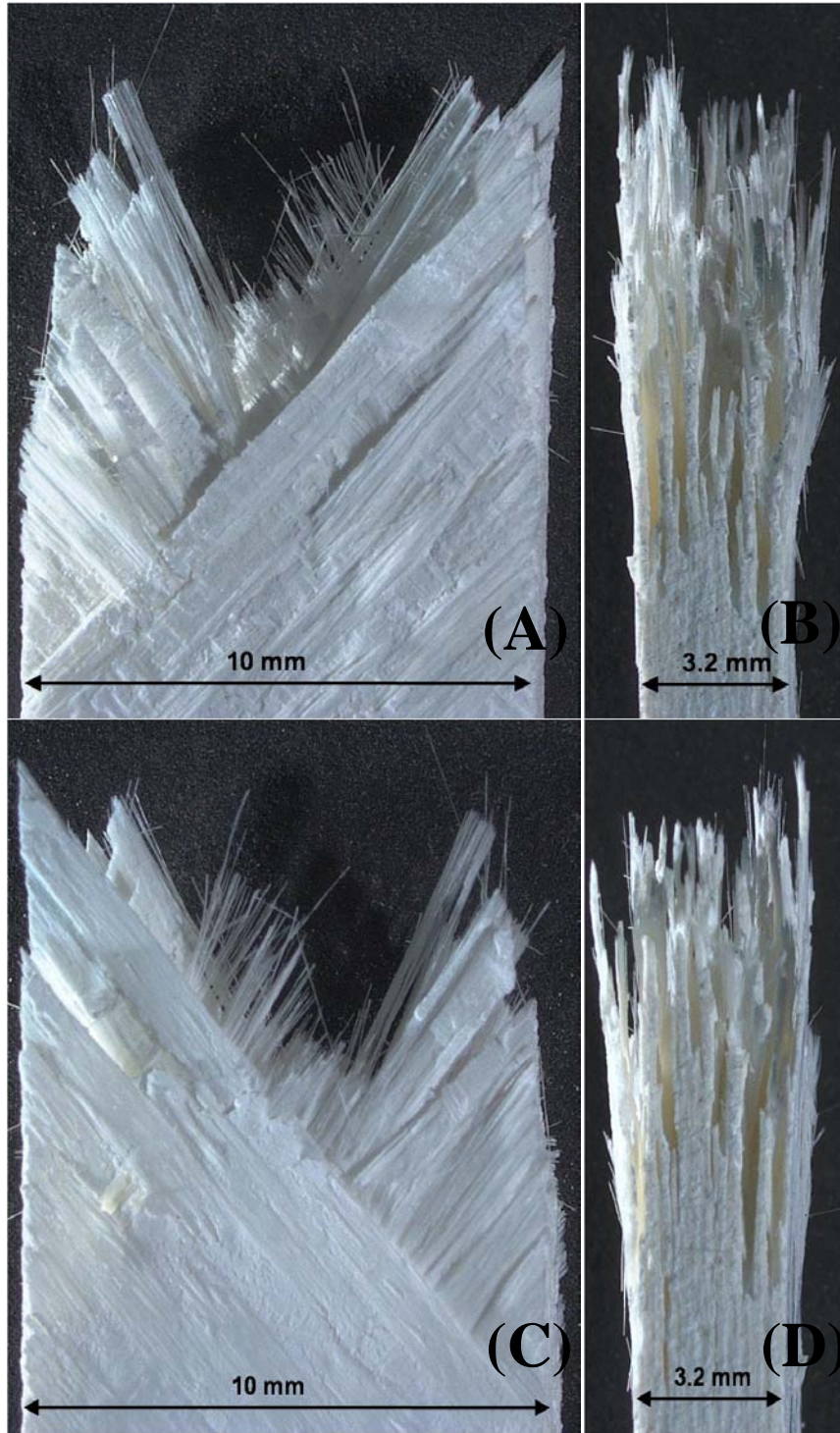


Figure 688. Fracture surface of the N720/AM specimen subjected to tensile test to failure with a constant stress rate of 0.0025 MPa/s at 1200°C in laboratory air. (a)-(c): front view, (b)-(d): side view

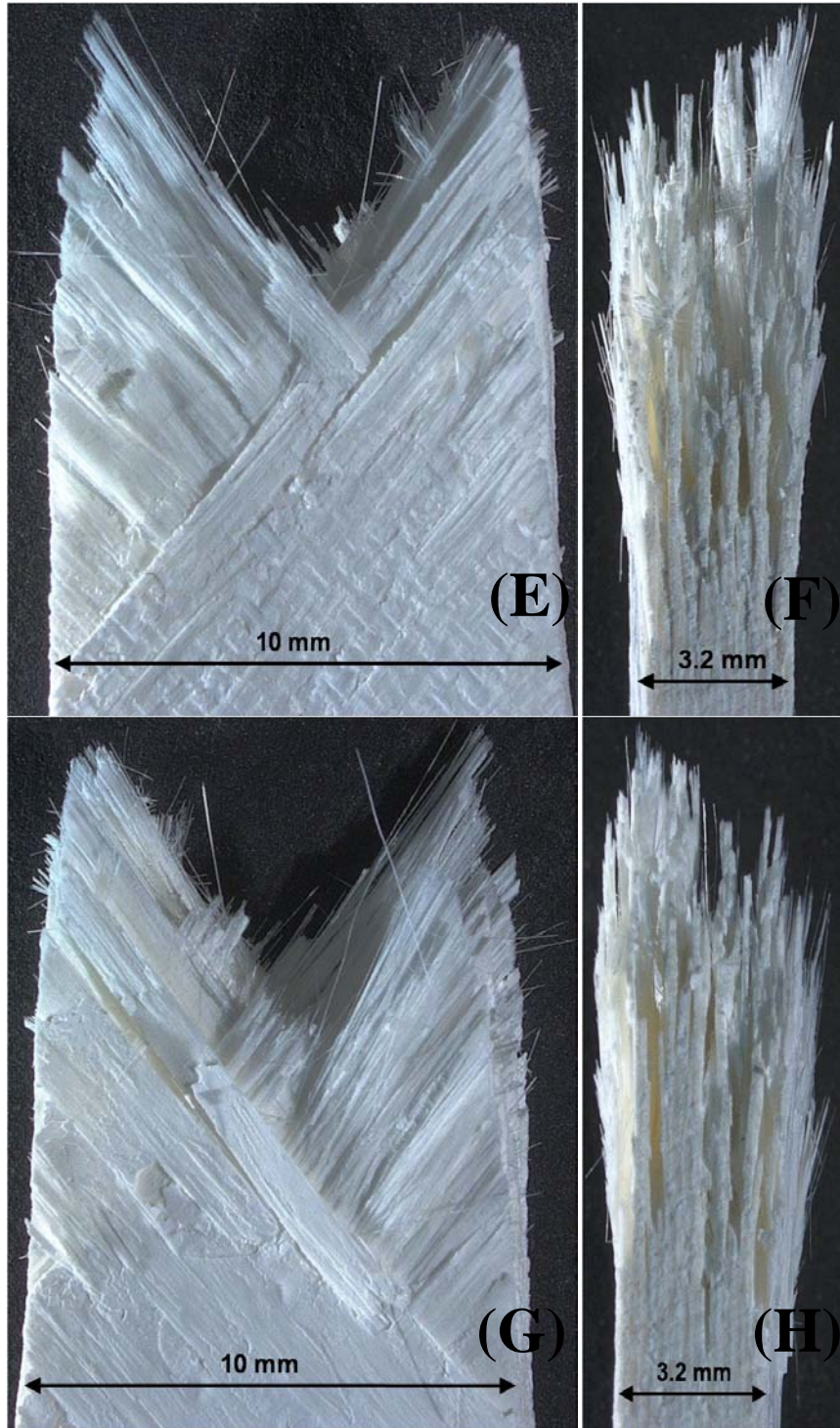


Figure 689. Fracture surface of the N720/AM specimen subjected to tensile test to failure with a constant stress rate of 0.0025 MPa/s at 1200°C in laboratory air. (e)-(g): front view, (f)-(h): side view

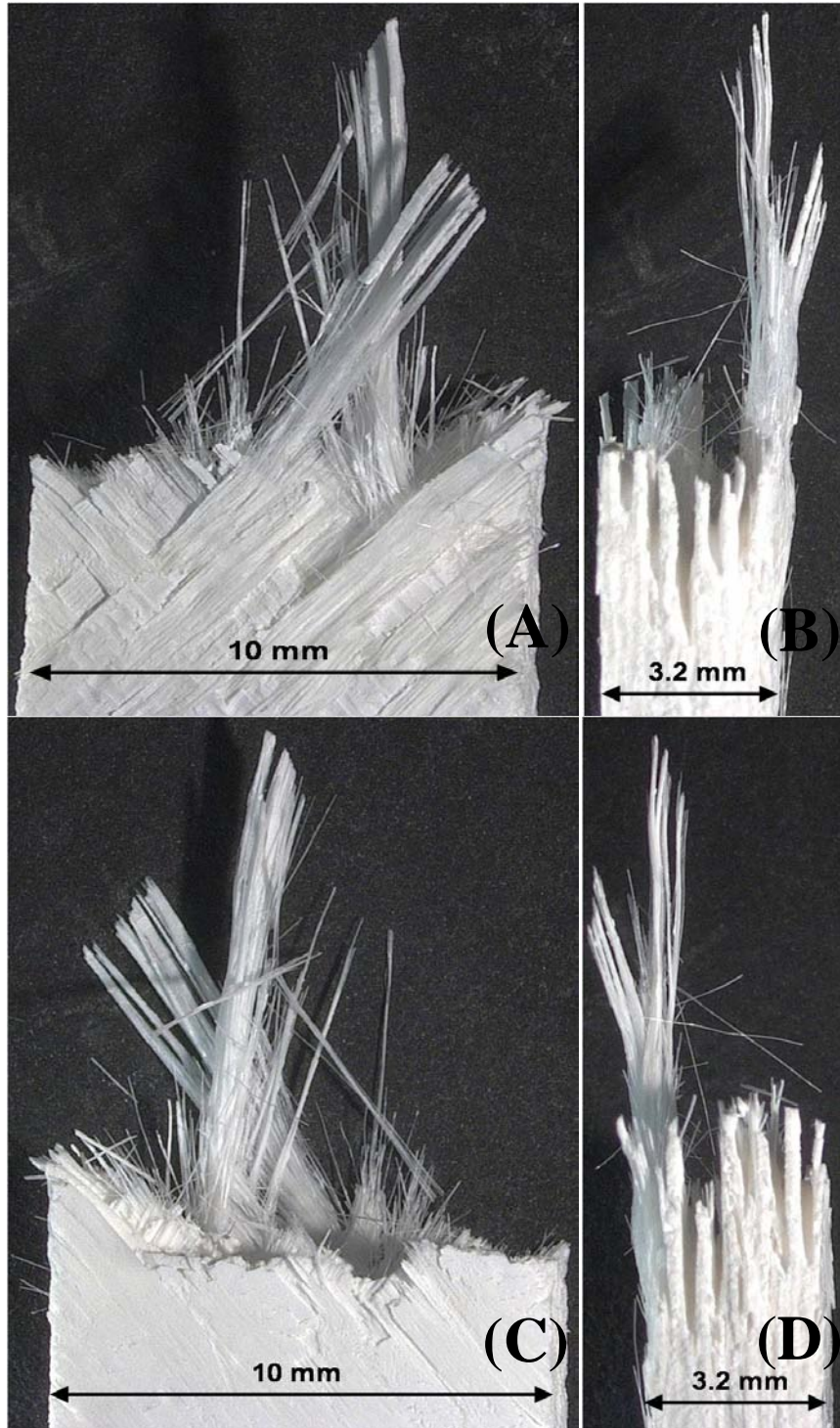


Figure 690. Fracture surface of the N720/AM specimen subjected to tensile test to failure with a constant stress rate of 0.0025 MPa/s at 1200°C in steam. (a)-(c): front view, (b)-(d): side view

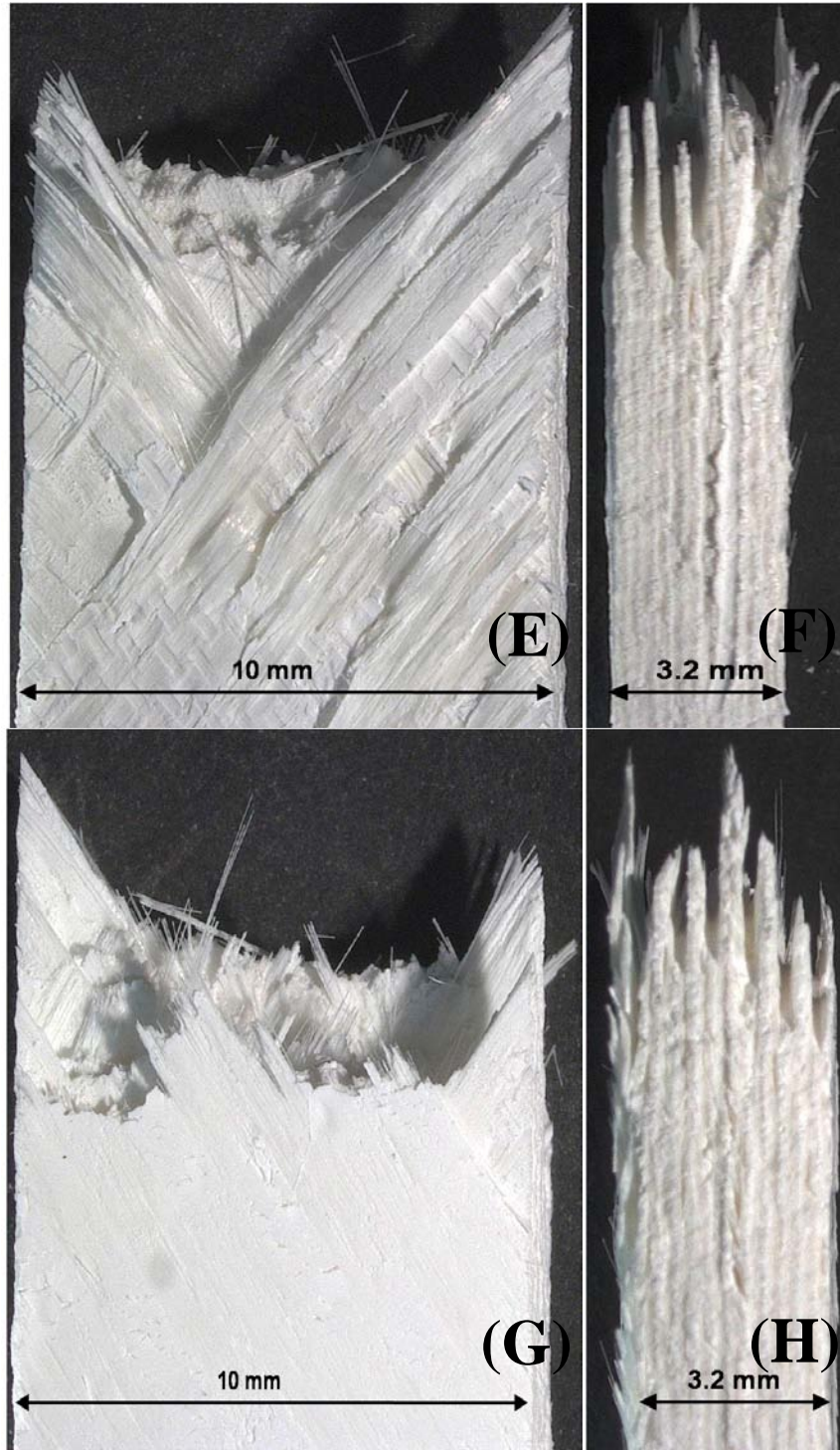


Figure 691. Fracture surface of the N720/AM specimen subjected to tensile test to failure with a constant stress rate of 0.0025 MPa/s at 1200°C in steam. (e)-(g): front view, (f)-(h): side view

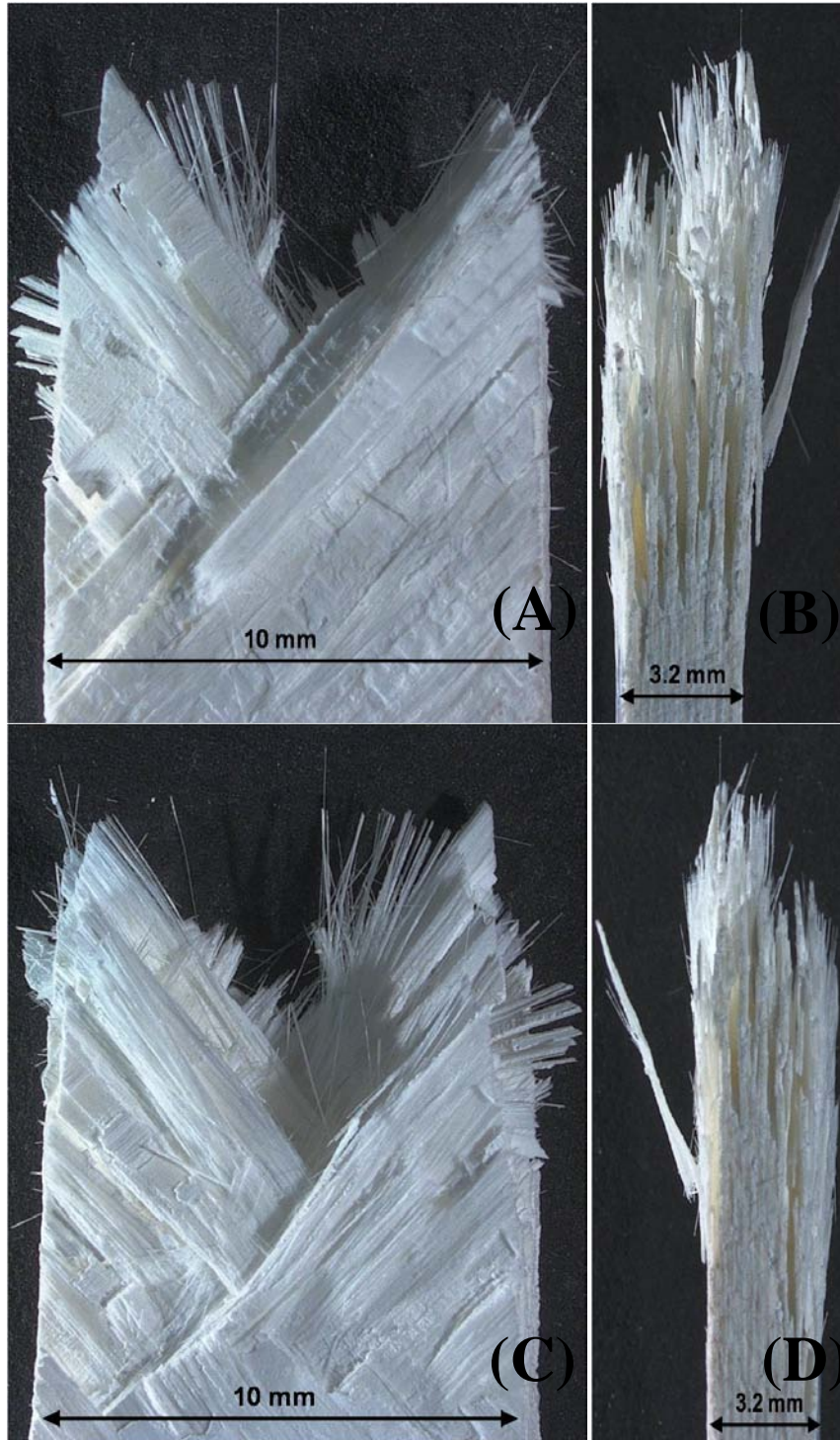


Figure 692. Fracture surface of the N720/AM specimen subjected to tensile test to failure with a constant stress rate of 25 MPa/s at 1200°C in laboratory air. (a)-(c): front view, (b)-(d): side view

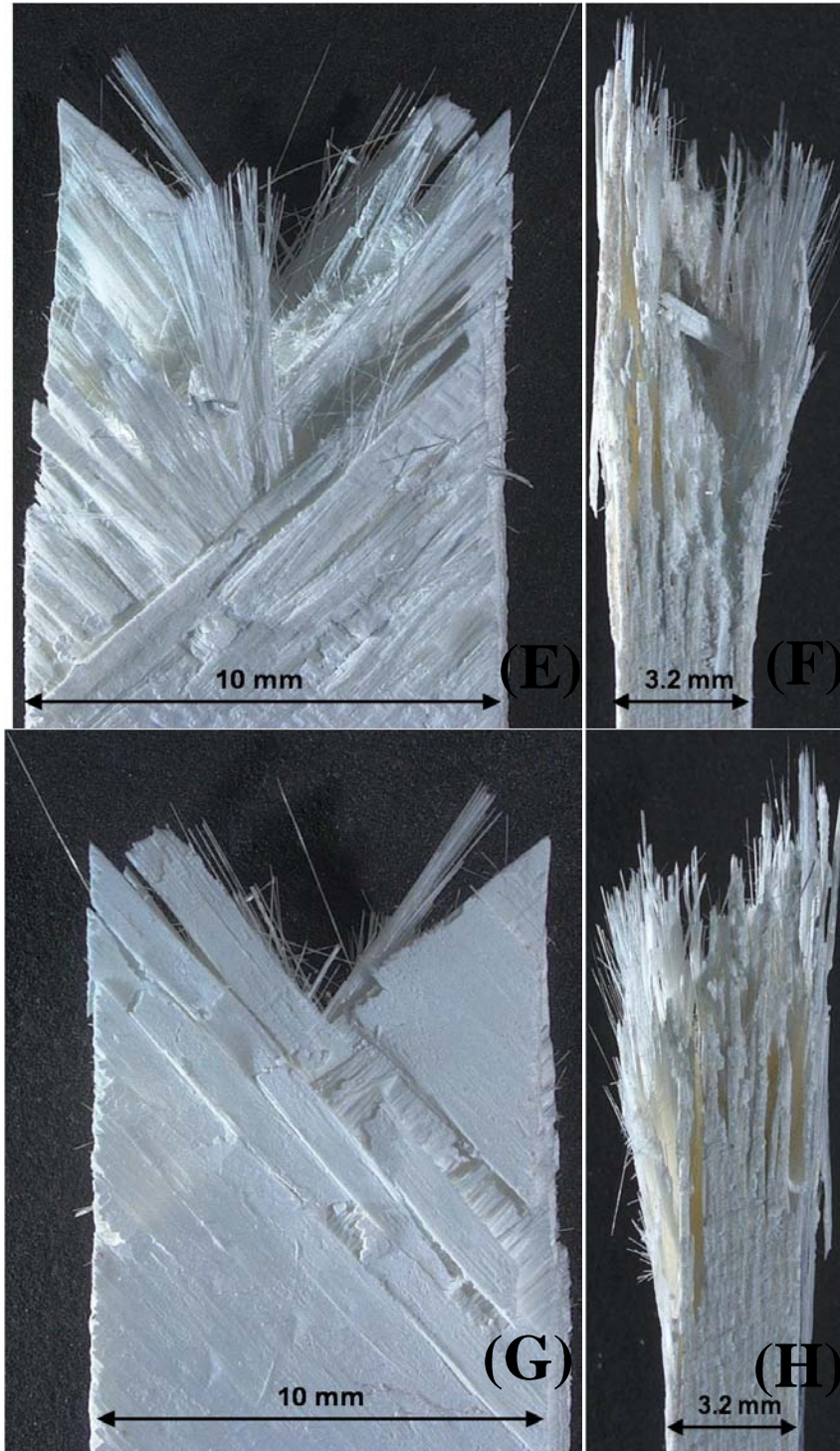


Figure 693. Fracture surface of the N720/AM specimen subjected to tensile test to failure with a constant stress rate of 25 MPa/s at 1200°C in laboratory air. (e)-(g): front view, (f)-(h): side view

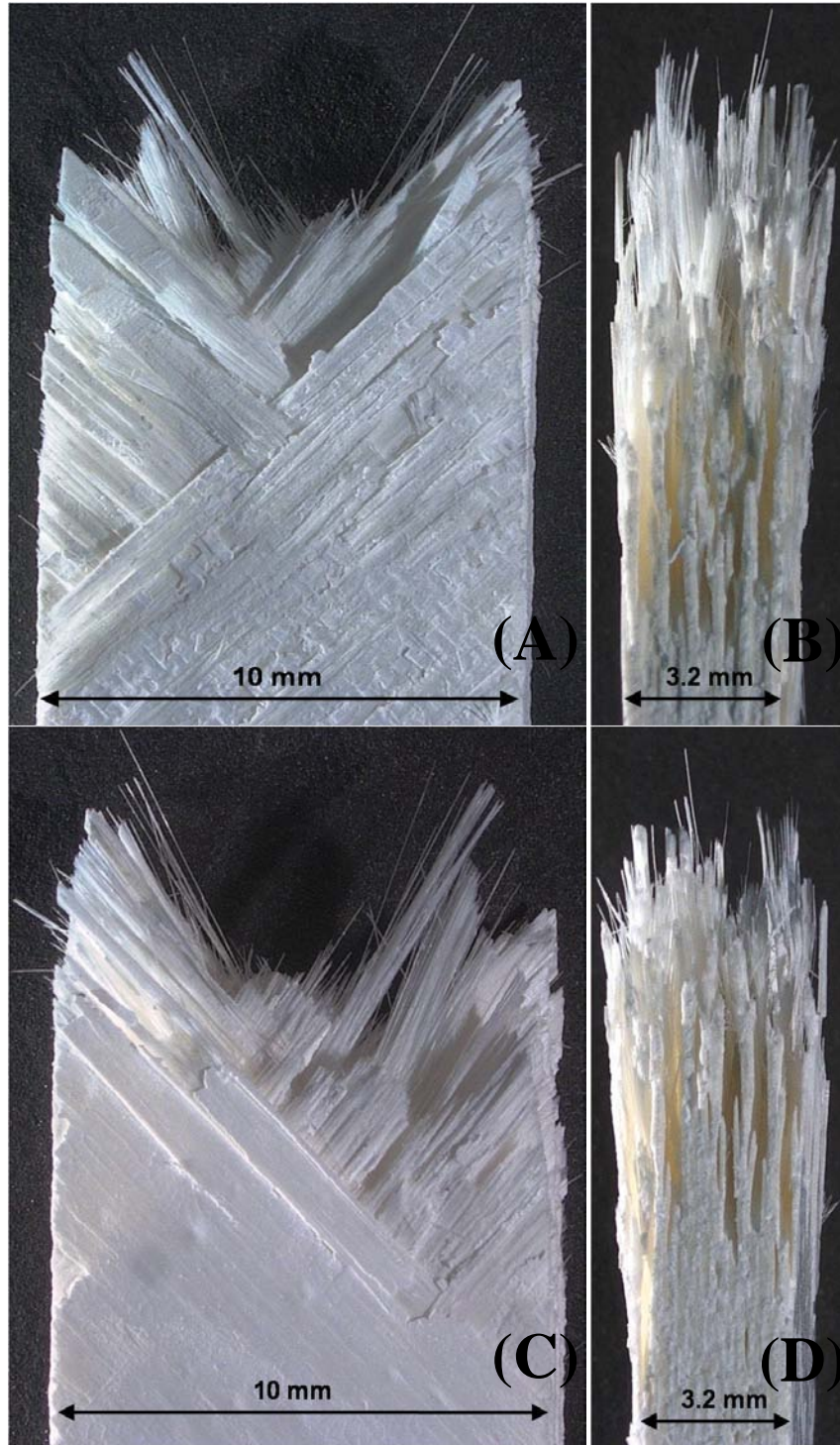


Figure 694. Fracture surface of the N720/AM specimen subjected to tensile test to failure with a constant stress rate of 25 MPa/s at 1200°C in steam. (a)-(c): front view, (b)-(d): side view

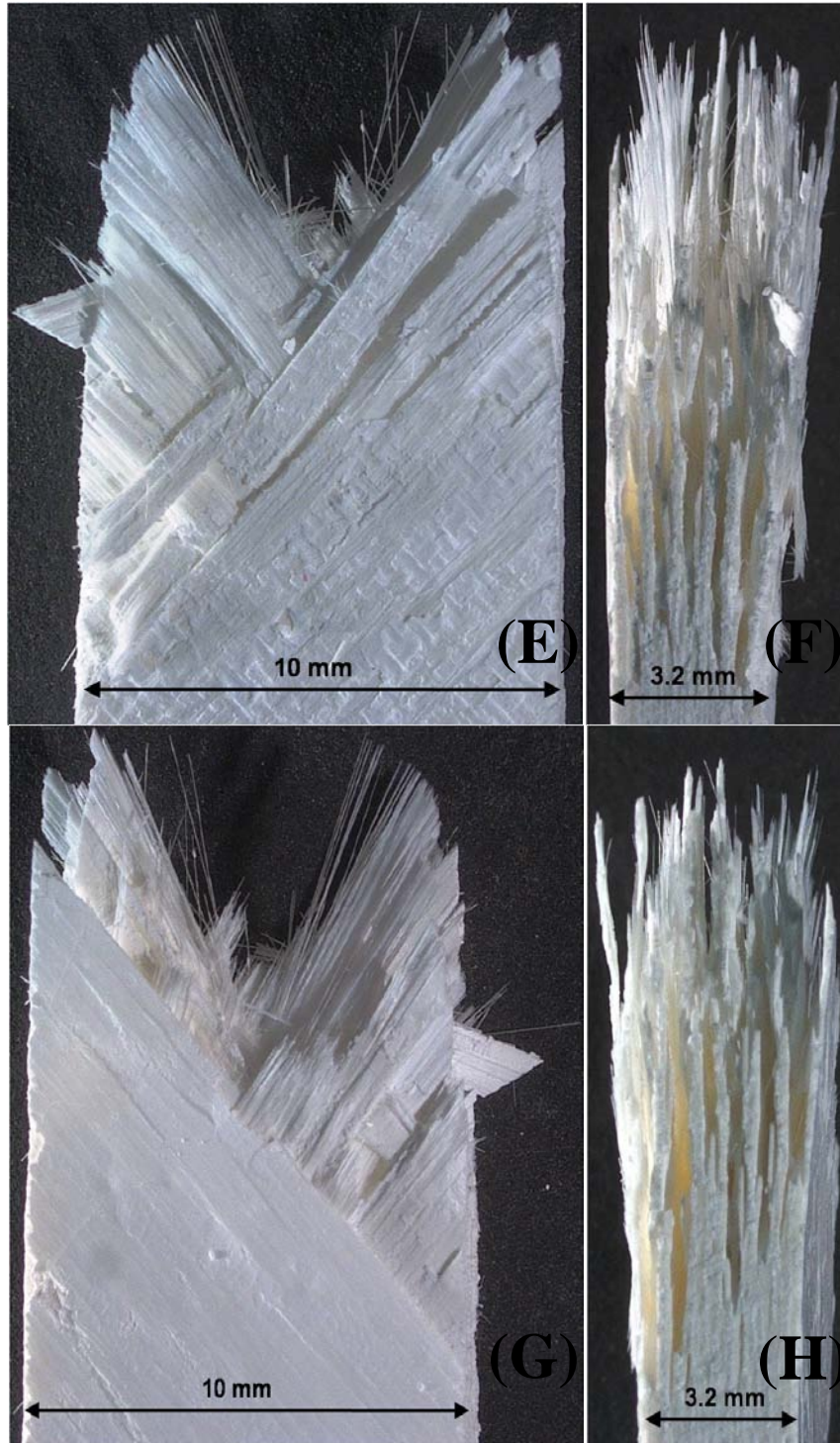


Figure 694. Fracture surface of the N720/AM specimen subjected to tensile test to failure with a constant stress rate of 25 MPa/s at 1200°C in steam. (e)-(g): front view, (f)-(h): side view

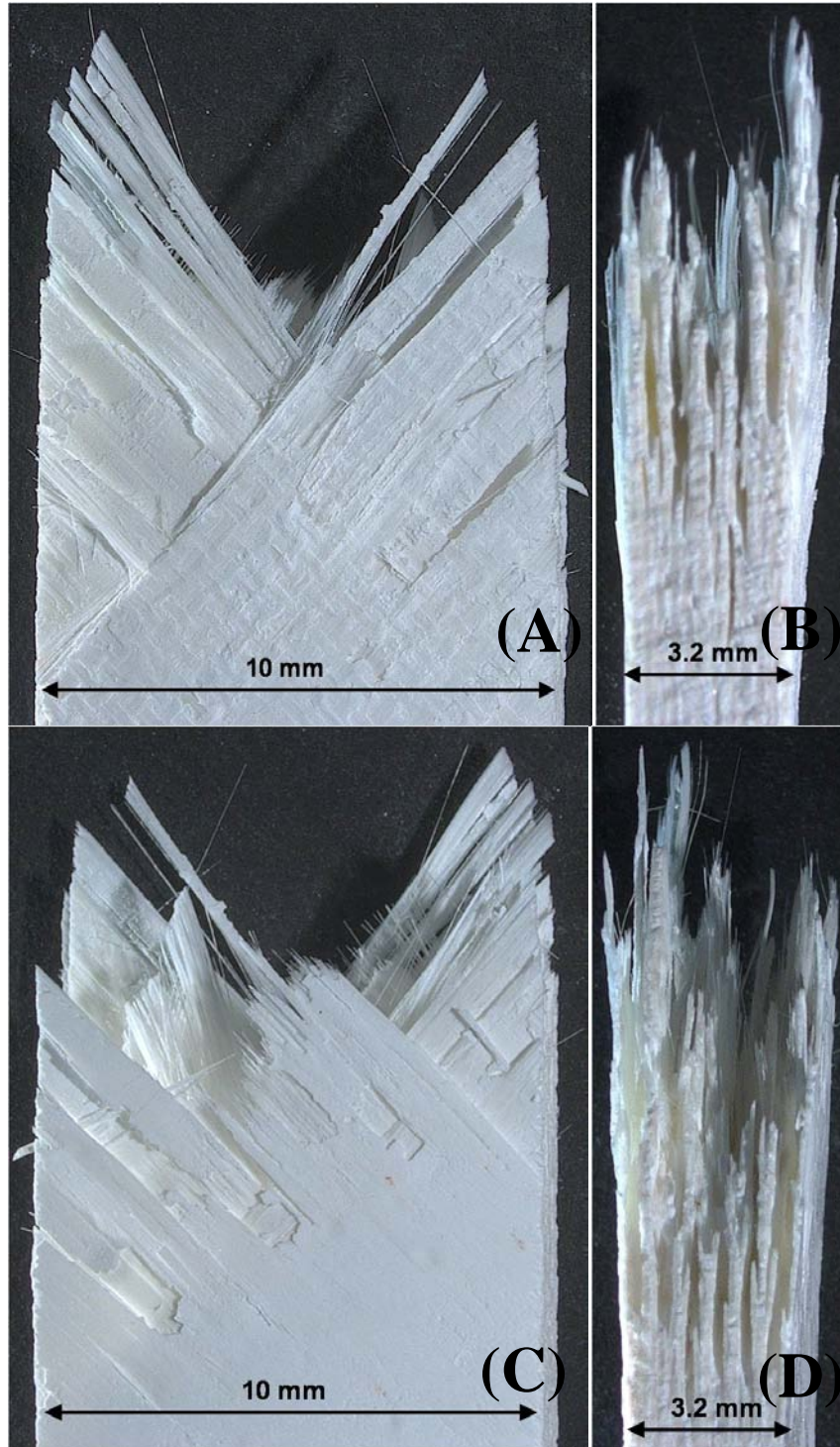


Figure 696. Fracture surface of the N720/AM specimen subjected to monotonic tensile test to failure at 1200°C in laboratory air. (a)-(c): front view, (b)-(d): side view

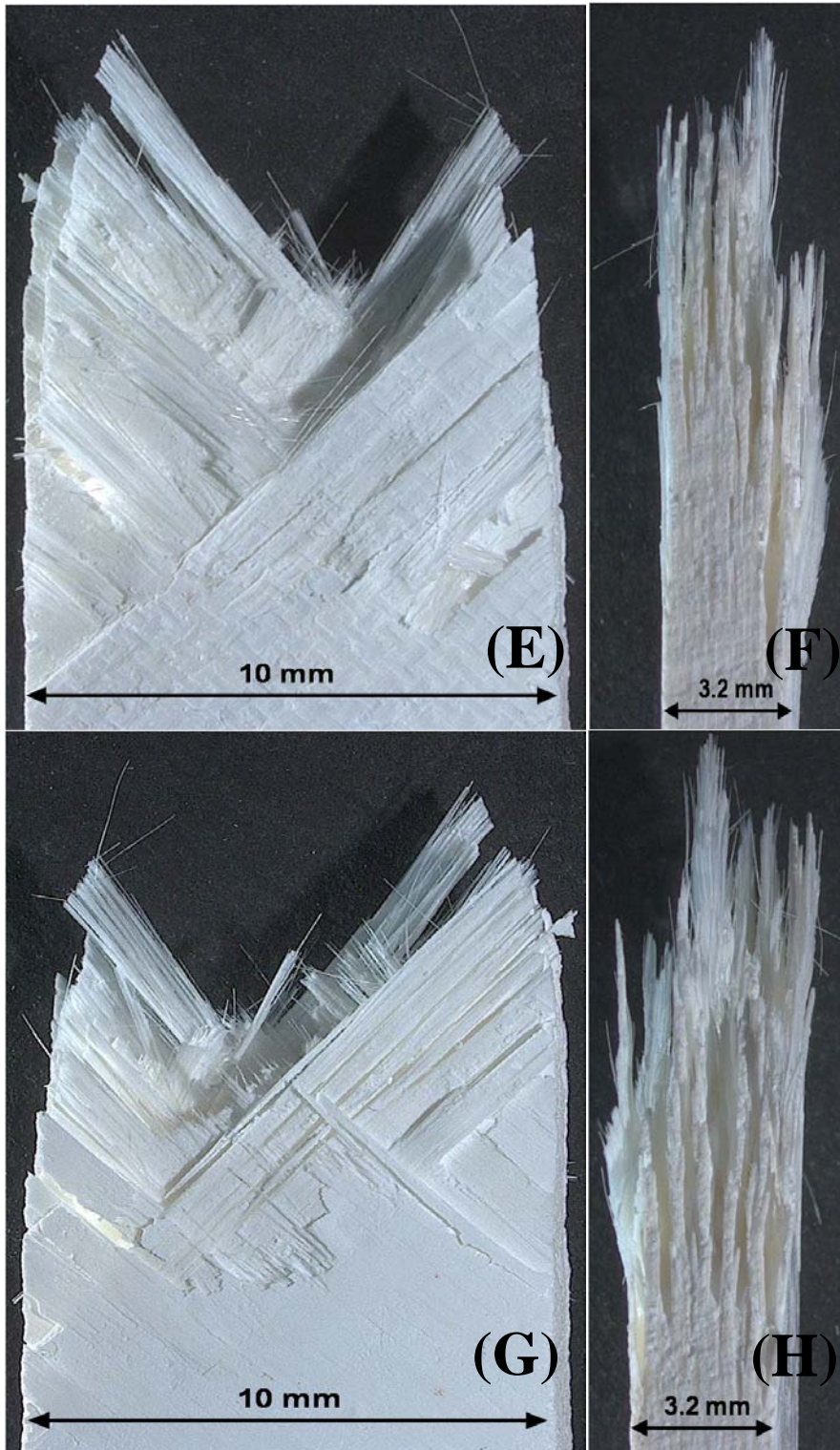


Figure 697. Fracture surface of the N720/AM specimen subjected to monotonic tensile test to failure at 1200°C in laboratory air. (e)-(g): front view, (f)-(h): side view

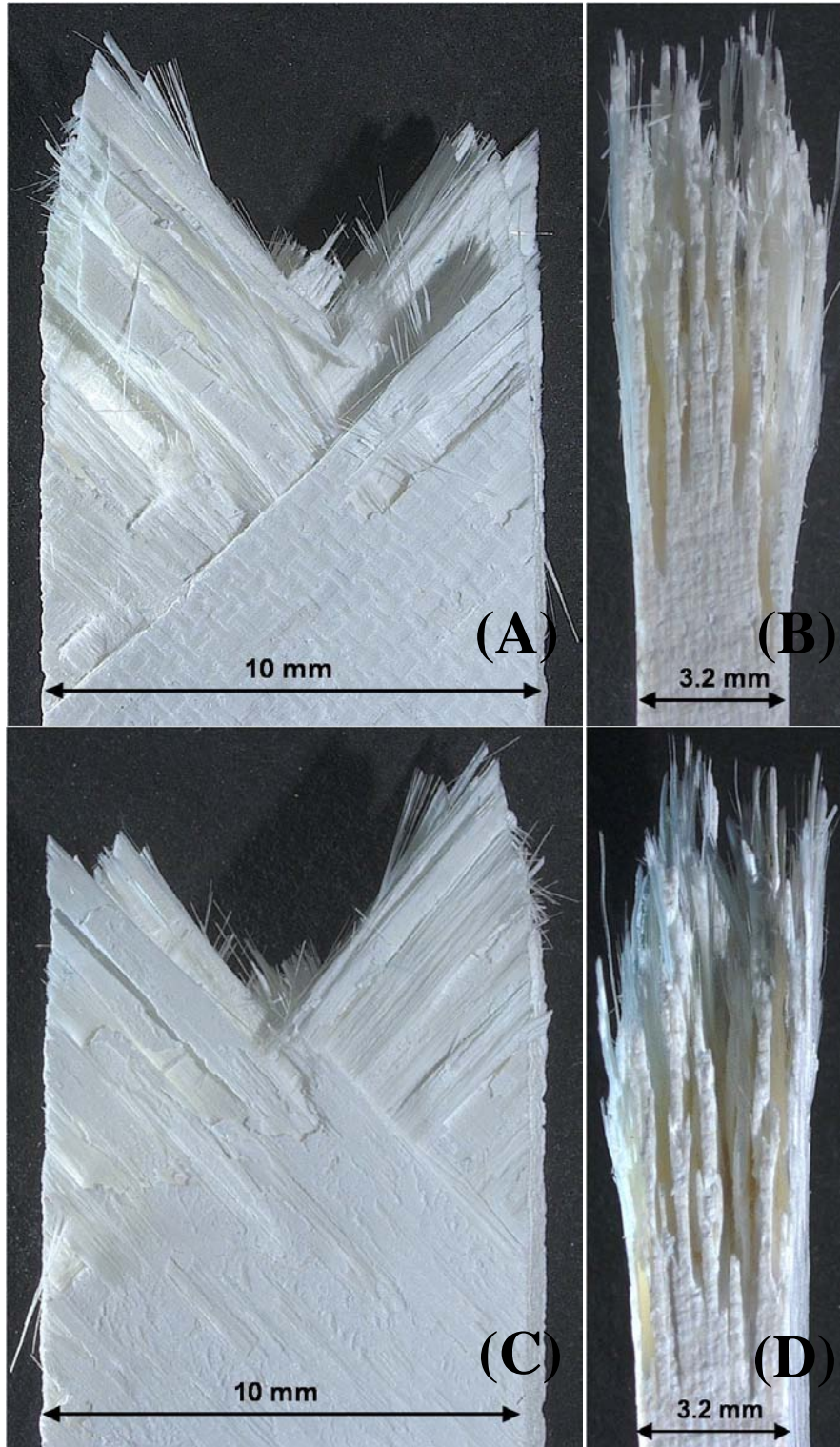


Figure 698. Fracture surface of the N720/AM specimen subjected to monotonic tensile test to failure at 1200°C in laboratory air. (a)-(c): front view, (b)-(d): side view

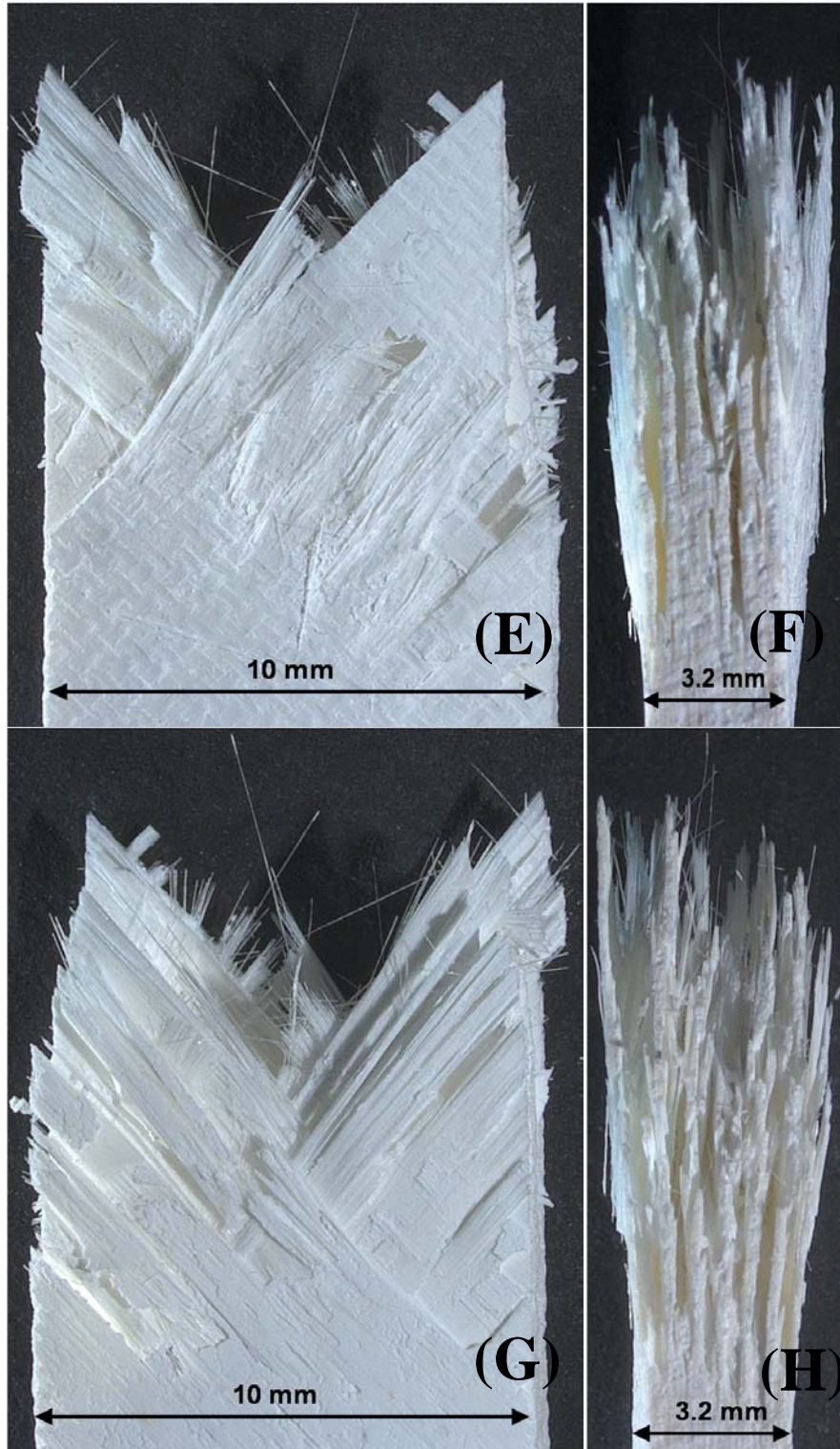


Figure 699. Fracture surface of the N720/AM specimen subjected to monotonic tensile test to failure at 1200°C in laboratory air. (e)-(g): front view, (f)-(h): side view

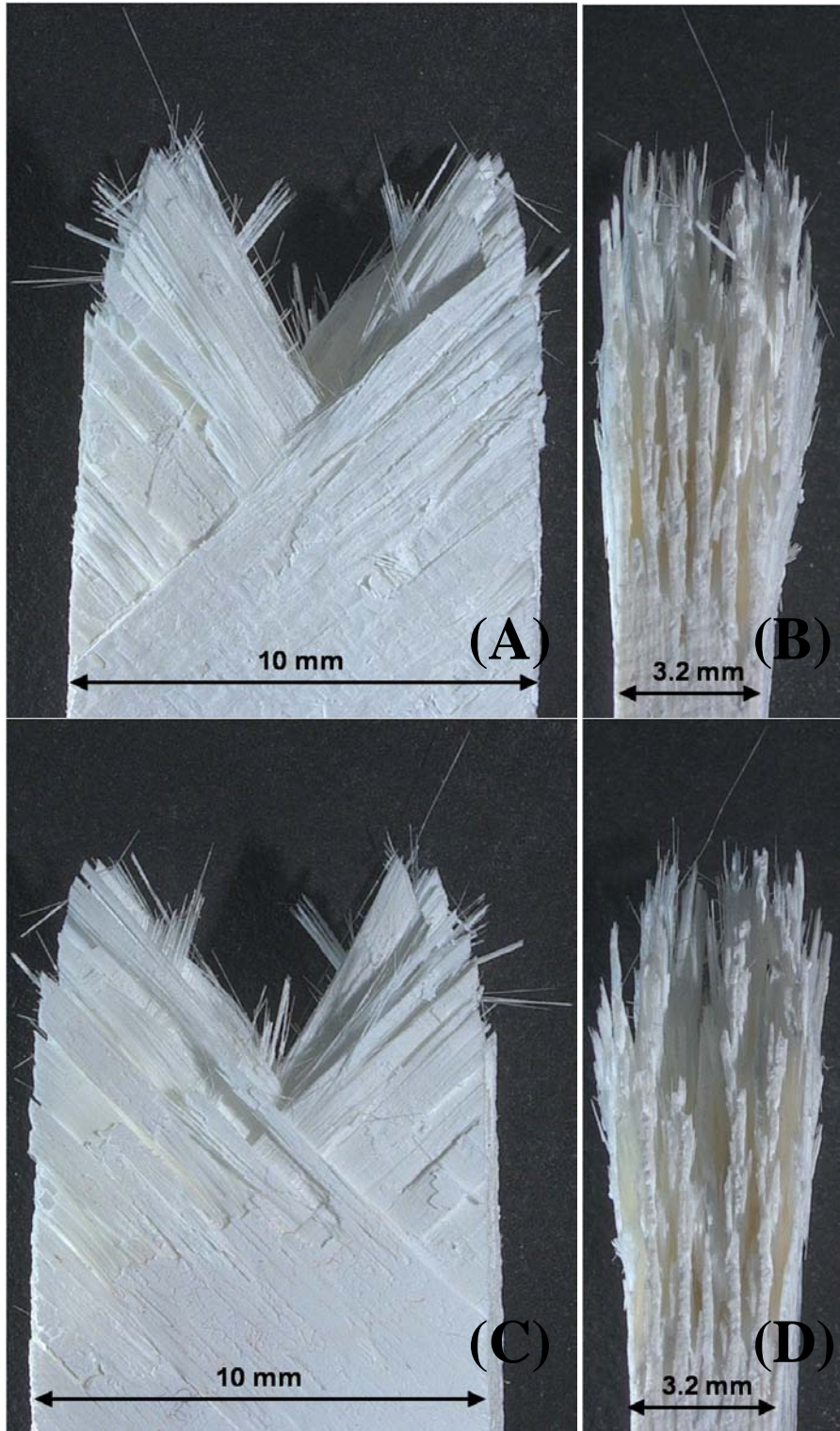


Figure 700. Fracture surface of the N720/AM specimen subjected to monotonic tensile test to failure at 1200°C in laboratory air. (a)-(c): front view, (b)-(d): side view

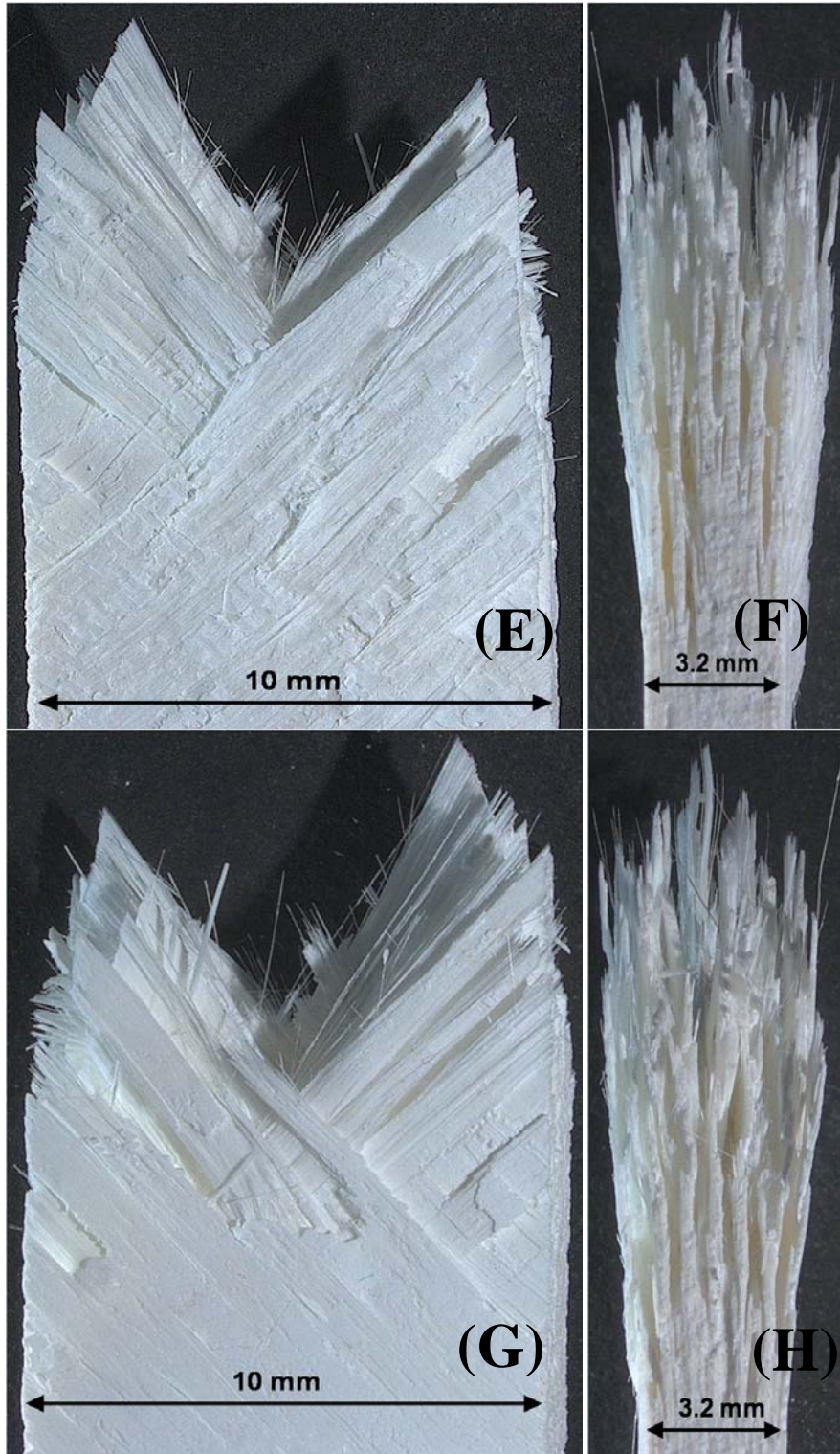


Figure 701. Fracture surface of the N720/AM specimen subjected to monotonic tensile test to failure at 1200°C in laboratory air. (e)-(g): front view, (f)-(h): side view

## Bibliography

1. Daniel, I.M., Ishai, O., *Engineering Mechanics of Composite Materials*. New York: Oxford University Press, 2006
2. [www.boeing.com](http://www.boeing.com), “Boeing 787 Family”, Website, January 2009
3. Chawla, K.K. *Ceramic Matrix Composites* (2nd Edition). Boston: Kluwer Academic Publishers, 2003.
4. Szweda A, Millard ML, Harrison MG. Fiber-reinforced ceramic-matrix composite member and method for making. U. S. Pat. No. 5 601 674, 1997.
5. Sim SM, Kerans RJ. Slurry infiltration and 3-D woven composites. *Ceram Eng Sci Proc* 1992; 13(9-10):632-41.
6. Moore EH, Mah T, and Keller KA. 3D composite fabrication through matrix slurry pressure infiltration. *Ceram Eng Sci. Proc* 1994; 15(4): 113-20.
7. Lange FF, Tu WC, Evans AG. Processing of damage-tolerant, oxidation-resistant ceramic matrix composites by a precursor infiltration and pyrolysis method. *Mater Sci Eng A* 1995; A195:145–50.
8. Mouchon E, Colomban P. Oxide ceramic matrix/oxide fiber woven fabric composites exhibiting dissipative fracture behavior. *Composites* 1995; 26:175–82.
9. Tu WC, Lange FF, Evans AG. Concept for a damage-tolerant ceramic composite with strong interfaces. *J Am Ceram Soc* 1996; 79(2): 417–24.
10. Zok, F.W., Levi, C.G. “Mechanical Properties of Porous-Matrix Ceramic Composites,” *Advanced Engineering Materials*, 3(1-2):15-23 (2001).
11. M. B. Ruggles-Wrenn and N. R. Szymczak, “Effects of Steam Environment on Compressive Creep Behavior of Nextel™720/Alumina Ceramic Composite at 1200 °C”, *Composites Part A: Applied Science and Manufacturing*, in press.

12. M. B. Ruggles-Wrenn, P. Koutsoukos, S. S. Baek, "Effects of Environment on Creep Behavior of Two Oxide-Oxide Ceramic Matrix Composites at 1200 °C", Journal of Materials Science, Vol. 43, No. 20, 2008, pp. 6734-6746.
13. M. B. Ruggles-Wrenn and J. C. Braun, "Effects of Steam Environment on Creep Behavior of Nextel™720/Alumina Ceramic Composite at Elevated Temperature", Materials Science and Engineering A, Vol. 497, No. 1-2, 2008, pp. 101-110.
14. M. B. Ruggles-Wrenn, A. T. Radzicki, S. S. Baek, K. A. Keller, "Effect of Loading Rate on the Monotonic Tensile Behavior and Tensile Strength of Oxide-Oxide Ceramic Matrix Composite at 1200 °C", Materials Science and Engineering A, Vol. 492, No. 1-2, 2008, pp. 88-94.
15. M. B. Ruggles-Wrenn and P. D. Laffey, "Creep Behavior in Interlaminar Shear of Nextel™720/ Alumina Ceramic Composite at Elevated Temperature in Air and in Steam", Composites Science and Technology, Vol. 68, No. 10-11, 2008, pp. 2260-2266.
16. Siegert, Gregory T. *Effect of Environment on Creep Behavior of an Oxide/Oxide CFCC with ±45° Fiber Orientation*, MS thesis, AFIT/GAE/ENY/06-J15, School of Engineering and Management, Air Force Institute of Technology (AU), Wright-Patterson AFB, OH, June 2006..
17. M. B. Ruggles-Wrenn, G. T. Siegert, S. S. Baek, "Creep Behavior of Nextel™720/Alumina Ceramic Composite with ±45° Fiber Orientation at 1200 °C", Composites Science and Technology, Vol. 68, No. 6, 2008, pp. 1588-1595.
18. M. B. Ruggles-Wrenn, G. Hetrick, S. S. Baek, "Effects of Frequency and Environment on Fatigue Behavior of an Oxide-Oxide Ceramic Composite at 1200 °C", International Journal of Fatigue, Vol. 30, No. 3, 2008, pp. 502-516.
19. J. M. Mehrman, M. B. Ruggles-Wrenn, S. S. Baek, "Influence of Hold Times on the Elevated-Temperature Fatigue Behavior of an Oxide-Oxide Ceramic Composite in Air and in Steam Environment", Composites Science and Technology, Vol. 67, No. 7-8, 2007, pp. 1425-1438.
20. M. B. Ruggles-Wrenn, S. Mall, C. A. Eber, L. B. Harlan, "Effects of Steam Environment on High-Temperature Mechanical Behavior of Nextel™720/ Alumina (N720/A) Continuous Fiber Ceramic Composite", Composites Part A: Applied Science and Manufacturing, Vol. 37, No. 11, 2006, pp. 2029-2040.

21. Genelin, Christopher L. *Effect of Environment on Creep Behavior of Nextel™720/Alumina-Mullite Ceramic Composite at 1200 °C*, MS thesis, AFIT/GAE/ENY/08-M11, School of Engineering and Management, Air Force Institute of Technology (AU), Wright-Patterson AFB, OH, March 2008.
22. Deleglise, F., Berger, M.H., Bunsell, A.R. “Microstructural evolution under load and high temperature deformation mechanisms of a mullite/alumina fibre,” *Journal of the European Ceramic Society*, 22:1501-1512 (2002).
23. Fujita, H., Jefferson, G., McMeeking, R.M., Zok, F.W. “Mullite/Alumina Mixtures for Use as Porous Matrices in Oxide Fiber Composites,” *Journal of the American Ceramic Society*, 87[2]:261-67 (2004).
24. Mattoni, M.A., Yang, J.Y., Levi, C.G., Zok, F.W. “Effects of Matrix Porosity on the Mechanical Properties of a Porous-Matrix, All-Oxide Ceramic Composite,” *Journal of the American Ceramic Society*, 84[11]:2594-602 (2001).
25. Zok, F.W., Levi, C.G., McMeeking, R.M. “Matrix-Enabled Damage Tolerance in Oxide CFFs,” AFOSR Contract F49620-02-1-0128.
26. Jurf RA, Butner SC. Advances in oxide-oxide CMC. *Trans ASME J Eng Gas Turbines Power* 1999;122(2):202-205.

## **Vita**

1<sup>ST</sup> Lt. Muzaffer OZER is an officer in Turkish Air Force. He graduated from Maltepe Military High School in 1997. Same year he attended Turkish Air Force Academy and graduated as a 2<sup>nd</sup> Lt. with a Bachelor of Science degree in Aeronautical Engineering in 2001. After graduation, he started the pilot training in Cigli, Izmir then continued in Euro Nato Joint Jet Pilot Training School at Sheppard AFB, Texas. He graduated as a jet pilot in 2003. He flew with F/NF-5 jet aircraft as a part of combat readiness program. Following that he took F-16 Jet Training Course at Oncel Training Squadron, Ankara. After completing F-16 Training, he was assigned to 8<sup>th</sup> Main Jet Base, Diyarbakir. He flew for almost three years with F-16s before attending Graduate School of Engineering and Management, AFIT for master's degree program. Upon graduation he will be stationed at 8<sup>th</sup> Main Jet Base, Diyarbakir.

<b>REPORT DOCUMENTATION PAGE</b>			<i>Form Approved</i> <i>OMB No. 0704-0188</i>		
The public reporting burden for this collection of information is estimated to average 1 hour per response, including the time for reviewing instructions, searching existing data sources, gathering and maintaining the data needed, and completing and reviewing the collection of information. Send comments regarding this burden estimate or any other aspect of this collection of information, including suggestions for reducing this burden to Department of Defense, Washington Headquarters Services, Directorate for Information Operations and Reports (0704-0188), 1215 Jefferson Davis Highway, Suite 1204, Arlington, VA 22202-4302. Respondents should be aware that notwithstanding any other provision of law, no person shall be subject to any penalty for failing to comply with a collection of information if it does not display a currently valid OMB control number. PLEASE DO NOT RETURN YOUR FORM TO THE ABOVE ADDRESS.					
1. REPORT DATE (DD-MM-YYYY) 26-03-2009		2. REPORT TYPE Master's Thesis		3. DATES COVERED (From — To) JAN 2008-MAR 2009	
4. TITLE AND SUBTITLE Effects of Environment On Creep Behavior of Nextel720/Alumina-mullite Ceramic Composite With $\pm 45^\circ$ Fiber Orientation at 1200°C				5a. CONTRACT NUMBER	
				5b. GRANT NUMBER	
				5c. PROGRAM ELEMENT NUMBER	
6. AUTHOR(S) MUZAFFER OZER, AFIT, 1 <sup>ST</sup> LT, TUAF				5d. PROJECT NUMBER 2008-107	
				5e. TASK NUMBER	
				5f. WORK UNIT NUMBER	
7. PERFORMING ORGANIZATION NAME(S) AND ADDRESS(ES) Air Force Institute of Technology Graduate School of Engineering and Management (AFIT/ENY) 2950 Hobson Way WPAFB OH 45433-7765				8. PERFORMING ORGANIZATION REPORT NUMBER  AFIT/GSS/ENY/09-M05	
9. SPONSORING / MONITORING AGENCY NAME(S) AND ADDRESS(ES) Dr. Geoff E. Fair Air Force Research Laboratories (AFRL/RXLN) 2230 Tenth Street, Bldg 655 WPAFB OH 45433-7817				10. SPONSOR/MONITOR'S ACRONYM(S) AFRL/RXLN	
				11. SPONSOR/MONITOR'S REPORT NUMBER(S)	
12. DISTRIBUTION / AVAILABILITY STATEMENT APPROVED FOR PUBLIC RELEASE; DISTRIBUTION UNLIMITED					
13. SUPPLEMENTARY NOTES					
14. ABSTRACT The present effort will investigate the off-axis creep behavior of the Nextel720/Alumina-Mullite CMC, a material system which relies on a porous alumina/mullite matrix for damage tolerance as compared to the pure alumina matrix in earlier studies. This research evaluated the creep behavior of N720/AM with a $\pm 45^\circ$ fiber orientation at 1200°C in: laboratory air, steam, and argon environments. Creep-rupture tests at the creep stress levels of: 32, 30, 26, and 20 MPa were conducted in each environment. Additionally 35 MPa stress level examined in air and 13 MPa stress level examined both in air and steam. The N720/AM with a $\pm 45^\circ$ fiber orientation survived creep run-out (100 h of creep stress) for stress levels $\leq 20$ MPa in all environments. Retained tensile strength was evaluated for all specimens achieving run-out. The creep-rupture results showed a decrease in creep life with increasing creep stress. The presence of steam had negative effect on the creep rates. Following the tests Optical and Scanning Electron Microscope (SEM) micrographs were used to examine damage zones.					
15. SUBJECT TERMS Ceramic Matrix Composite (CMC), Oxide-Oxide, Nextel 720, Creep, Air, Steam, Argon					
16. SECURITY CLASSIFICATION OF:			17. LIMITATION OF ABSTRACT  UU	18. NUMBER OF PAGES  501	19a. NAME OF RESPONSIBLE PERSON Dr. Marina B. Ruggles-Wrenn
a. REPORT U	b. ABSTRACT U	c. THIS PAGE U			19b. TELEPHONE NUMBER (Include Area Code) (937)255-3636, ext4641; marina.ruggles-wrenn@afit.edu